Volume 72A
Number 6
Nov.–Dec. 1968

Physics and Chemistry

U.S. DEPARTMENT OF COMMERCE

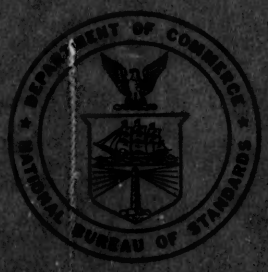

SECTION A

JOURNAL OF RESEARCH

NATIONAL BUREAU OF STANDARDS

Journal of Research

of the

National Bureau of Standards

A. Physics and Chemistry

Nov.-Dec. • 1968

VOLUME • 72A

NUMBER • 6

Editor: C. W. Beckett

Associate Editors: D. D. Wagman
J. M. Richardson

Publication dates:
Feb. 1, Apr. 1, June 1, Aug. 1, Oct. 1, Dec. 1, 1968

JOURNAL OF RESEARCH

The National Bureau of Standards Journal of Research reports research and development in the fields of activity shown at right. Also included from time to time are survey articles on topics closely related to the Bureau's scientific and technical program.

The Journal is published in three separate sections as follows:

A. Physics and Chemistry

Contains papers of interest primarily to scientists working in these fields. Issued six times a year. Annual subscription: domestic, $6.00; foreign, $7.25. Single copy, $1.00.

B. Mathematical Sciences

Presents studies and compilations designed mainly for the mathematician and the theoretical physicist. Issued quarterly. Annual subscription: domestic, $2.25; foreign, $2.75. Single copy, 75c.

C. Engineering and Instrumentation

Reports research and development results of interest chiefly to the engineer and the applied scientist. Issued quarterly. Annual subscription: domestic, $2.75; foreign, $3.50. Single copy, 75c.

NATIONAL BUREAU OF STANDARDS

The National Bureau of Standards[1] was established by an act of Congress March 3, 1901. Today, in addition to serving as the Nation's central measurement laboratory, the Bureau is a principal focal point in the Federal Government for assuring maximum application of the physical and engineering sciences to the advancement of technology in industry and commerce. To this end the Bureau conducts research and provides central national services in three broad program areas and provides central national services in a fourth. These are: (1) basic measurements and standards, (2) materials measurements and standards, (3) technological measurements and standards, and (4) transfer of technology.

The Bureau comprises the Institute for Basic Standards, the Institute for Materials Research, the Institute for Applied Technology, and the Center for Radiation Research.

THE INSTITUTE FOR BASIC STANDARDS provides the central basis within the United States of a complete and consistent system of physical measurement, coordinates that system with the measurement systems of other nations, and furnishes essential services leading to accurate and uniform physical measurements throughout the Nation's scientific community, industry, and commerce. The Institute consists of an Office of Standard Reference Data and a group of divisions organized by the following areas of science and engineering:

Applied Mathematics—Electricity—Metrology—Mechanics—Heat—Atomic Physics—Cryogenics[2]—Radio Physics[2]—Radio Engineering[2]—Astrophysics[2]—Time and Frequency.[3]

THE INSTITUTE FOR MATERIALS RESEARCH conducts materials research leading to methods, standards of measurement, and data needed by industry, commerce, educational institutions, and government. The Institute also provides advisory and research services to other government agencies. The institute consists of an Office of Standard Reference Materials and a group of divisions organized by the following areas of materials research:

Analytical Chemistry—Polymers—Metallurgy—Inorganic Materials—Physical Chemistry.

THE INSTITUTE FOR APPLIED TECHNOLOGY provides for the creation of appropriate opportunities for the use and application of technology within the Federal Government and within the civilian sector of American industry. The primary functions of the Institute may be broadly classified as programs relating to technological measurements and standards and techniques for the transfer of technology. The Institute consists of a Clearinghouse for Scientific and Technical Information,[3] a Center for Computer Sciences and Technology, and a group of technical divisions and offices organized by the following fields of technology:

Building Research—Electronic Instrumentation—Technical Analysis—Product Evaluation—Invention and Innovation—Weights and Measures—Engineering Standards—Vehicle Systems Research.

THE CENTER FOR RADIATION RESEARCH engages in research, measurement, and application of radiation to the solution of Bureau mission problems and the problems of other agencies and institutions. The Center for Radiation Research consists of the following divisions:

Reactor Radiation—Linac Radiation—Applied Radiation—Nuclear Radiation.

[1] Headquarters and Laboratories at Gaithersburg, Maryland, unless otherwise noted; mailing address Washington, D.C. 20234.
[2] Located at Boulder, Colorado 80302.
[3] Located at 5285 Port Royal Road, Springfield, Virginia 22151.

U.S. DEPARTMENT OF COMMERCE
C. R. Smith, Secretary
NATIONAL BUREAU OF STANDARDS
A. V. Astin, Director

Order all publications from the Superintendent of Documents
U.S. Government Printing Office, Washington, D.C. 20402

Use of funds for printing this publication approved by the Director of the Bureau of the Budget June 22, 1966).

JOURNAL OF RESEARCH of the National Bureau of Standards—A. Physics and Chemistry
Vol. 72A, No. 6, November–December 1968

Interaction Energy Surfaces for Li(2^2S) and Li (2^2P) With H_2*

M. Krauss

Institute for Materials Research, National Bureau of Standards, Washington, D.C. 20234

(August 2, 1968)

Interaction energy surfaces for the interaction of Li(2^2S) and Li(2^2P) with H_2 are calculated using approximate Hartree-Fock trial functions. The crossing of energy curves is observed for C_{2v} conformations if the H_2 internuclear distance is sufficiently large. No crossing is observed for colinear collissions for any H_2 distance.

The wave function of the strongly attractive state involved in the crossing is related to the metastable negative-ion states that are postulated to account for resonant electron-molecule scattering. Such a charge-transfer state can only be bound for C_{2v} conformations for the H_2 molecule. The likelihood and geometry of the crossing complexes for other molecules interacting with alkalis is discussed in terms of the formation of these resonance charge-transfer states.

Key Words: Energy surface; Li(2^2S); Li(2^2P); $H_2(X^1\Sigma_g^+)$; Hartree-Fock; energy transfer; resonance state; charge-transfer.

1. Introduction

Fundamental to the understanding of electronic-vibrational energy transfer involving alkali atoms and diatomic molecules is an accurate representation of the energy of interaction. The qualitative features of these surfaces was first considered with semi-empirical techniques [1].[1] To this date there are no ab initio calculations. Accurate energy calculations utilizing correlated wave functions are not yet possible but these systems can be investigated immediately with available Hartree-Fock (H.F.) programs [2]. This is of value for two reasons. First, the approximate H.F. energy surface is considerably more reliable than the earlier results to the extent that the qualitative features of the surfaces can be fixed. In particular, the question of the angular distribution of the interaction energy can be settled and an estimate given given of the activation energy, if any, of the excitation of alkali D radiation by vibrationally excited diatomics. Second, the molecular orbital description is more natural to the discussion of these reactions in the light of recent studies of electron-diatomic molecule resonant scattering [3].

This note will examine the qualitative behavior of the Li(2^2S) and Li(2^2P) interaction with the H_2 molecule without chemical reaction as the simplest example of the alkali-diatomic system. There is a total of four curves, two repulsive ones, and one weakly, and one strongly attractive curve which are depicted in figure 1. Except for the strongly attractive state there is little overlap of the alkali and diatomic charge distributions. It is our contention that the H.F. surfaces are qualitatively correct and of semiquantitative accuracy for this type of surface. The near constancy of the correlation energy over a wide range of geometries is presumed here [4].

The correlation situation is quite different for the strongly attractive curve. This curve has long been characterized as a charge transfer state [1]. The H.F. function does, in fact, describe a charge transfer state and is related to the ionic valence bond configurations. The negative ion H_2^- state formed here is also related to the lowest energy resonance state of H_2^- considered responsible for enhanced vibrational excitation at low incident electron energies [3]. Three electrons are now interpenetrating and the correlation [5] is similar to that in He_2^+ and H_3. However, there are offsetting H.F. and correlation errors that are strongly dependent on the geometry. The depth of the H.F. attractive well should approximate the correlated one.

Since even an accurate H.F. calculation of the strongly attractive curve can only be considered qualitative, we have contented ourselves with self-consistent-field solutions far from the H.F. limit. More accurate solutions will be considered when they are needed as a base for a correlated calculation. The H.F. techniques are briefly described and the results for a rather small but meaningful basis are

*This work was supported in part by the Advanced Research Projects Agency of the Department of Defense under Project DEFENDER.

[1] Figures in brackets indicate the literature references at the end of this paper.

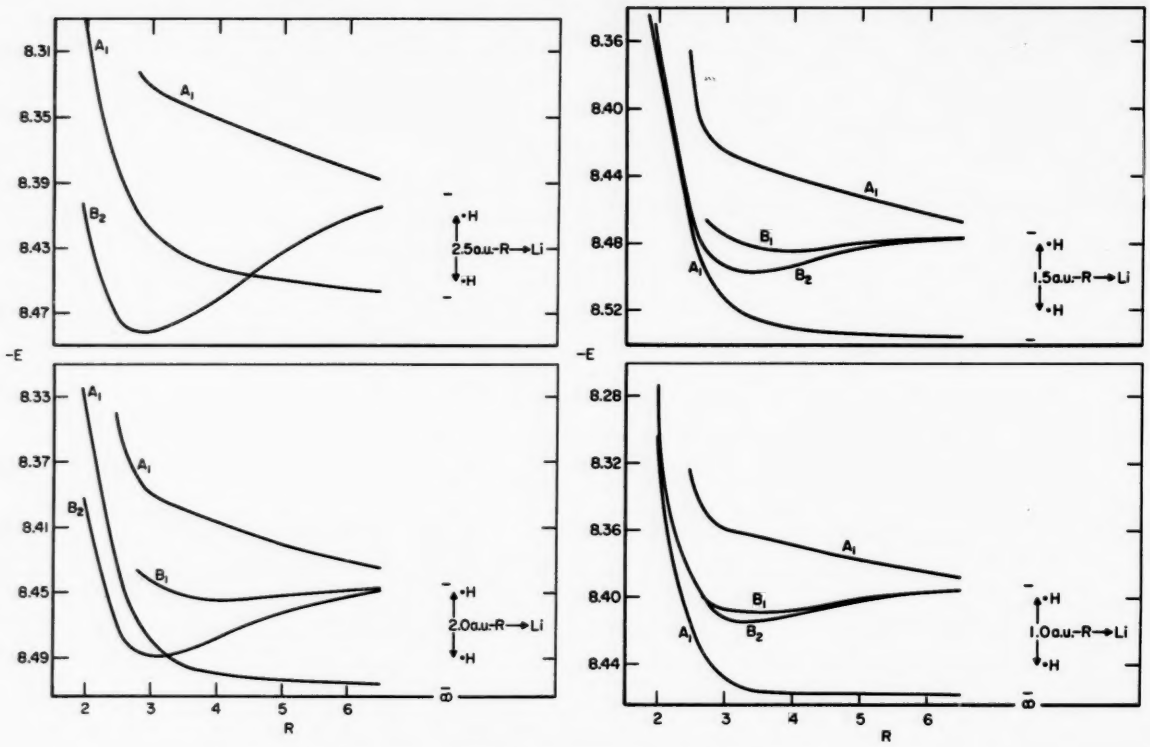

FIGURE 1a. *Interaction energies for* Li(²S *and* ²P) *with the ground state of* H_2 *for* C_{2v} *geometries as a function of the* H_2 *internuclear distance.*

Energies in a.u.

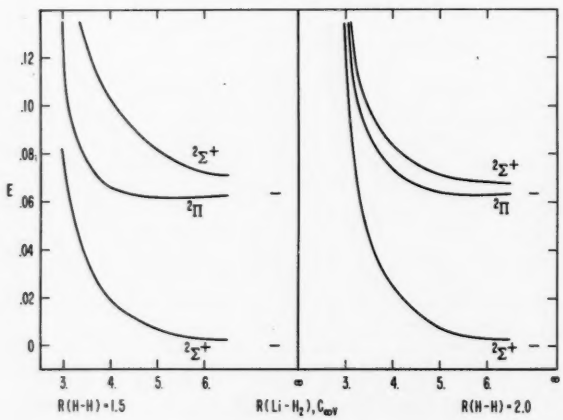

FIGURE 1b. *Interaction energies for* Li(²S *and* ²P) *with the ground state of* H_2 *for* $C_{\infty v}$ *geometries as a function of the* H_2 *internuclear distance*

Energies in a.u.

given in the next section. Similar calculations were completed for the isoelectronic LiHe system at the same level of accuracy. This permits some calibration of the approximate H.F. values since limited configuration interaction results [6] exist for LiHe.

In the final section the H.F. results are compared to the earlier semiempirical calculations. The angular distribution and the position of the crossing in the interaction curves are particularly examined and earlier deductions on the linear surface are questioned. Comparison of the H.F. wave functions for the charge-transfer state to the assumed resonance states in electron scattering is pursued to the point of speculation with regard to other systems.

2. Hartree-Fock Calculation

For doublet systems with one open-shell orbital outside of a closed shell core, the H.F. solutions satisfy a variant of the Brillouin theorem that was noted by Davidson [7]. If the vectors are designated $C_{i,\alpha}$ where α designates the open-shell vector for which self-consistency is achieved then

$$C_{i,\alpha} S C_{j,\alpha} = \delta_{ij}$$

and

$$\langle \Psi_{i,\alpha} H \Psi_{j,\alpha} \rangle = E_i \delta_{ij}$$

where S is the basis function overlap matrix and H is the total electronic Hamiltonian. $\Psi_{i,\alpha}$ is the H.F. function where the excited φ_i orbital replaces the φ_α orbital in $\Psi_{\alpha,\alpha}$. Calculation of any one state will yield upper bounds to higher Rydberg states. The accuracy of the bounds depends upon the size of the basis set and its ability to fit the higher Rydbergs and the extent to which the core orbitals relax for different $\Psi_{\alpha,\alpha}$. As noted in the introduction no special effort will be made to achieve the H.F. limit. But a reasonably large set must be used to insure correct qualitative behavior. Both the Li(^{2}S) and H(^{2}S) bases are chosen from the smallest of the accurate Gaussian-type functions (GTF) sets given by Huzinaga [8]. The $2s_H$, $2p_{Li}$, $2p_H$, $3s_{Li}$, and $3p_{Li}$ orbitals are approximated by choosing effective Slater exponents for the appropriate atomic Rydberg orbitals and using the large coefficient Gaussian fits to the Slater orbitals [9]. This procedure is very rough since not all the GTF required can be used because of computer time limitations so that compromise exponents must be chosen. This set has been contracted severely with the resultant H_2 and Li energies in table 1. The Li(^{2}S-^{2}P) interval is 0.11 eV larger than the H.F. value and 0.12 eV larger than the experimental value [10]. The error is almost entirely in the $2s_{Li}$ due to the use of $1s_{Li}$ coefficients to severely contract the s_{Li} set. For H_2 the error in the H.F. energy is about 0.6 eV at 1.5 a.u. compared to an accurate H.F. energy. This large discrepancy is due to the contraction of the H_2 basis using the Huzinaga expansion coefficients without scaling the orbital exponents. Since the contracted function is equivalent to a single Slater-type function (STF) the 1s function exponents determined by Fraga and Ransil [11] can be used as a guide. The larger exponent would improve the energy significantly but would effect improvements mainly in the H_2 binding and not in the interaction region between the Li and H_2 which is the main concern here. More flexible bases will be used when the correlation is calculated in subsequent work. The errors due to the small basis considerably exceed those that arise from the use of orbital energies to compute the total energies. The general shapes of all curves can be found in figure 1 for the neutral states and in figure 2 for the $Li^+ + H_2$ interaction.

TABLE 1. *Energies of asymptotic atoms and molecule*

Atom/molecule	$-E^a$	
	Present calculation	Accurate H.F.
He	2.86113	[b] 2.86168
Li^+	7.23597	[b] 7.23641
Li(^{2}S)	7.42714	[c] 7.432724
Li(^{2}P)	7.36342	[c] 7.365068
H_2(1.0)[d]	1.02984	
H_2(1.5)	1.11010	
H_2(2.0)	1.08197	
H_2(2.5)	1.03299	
H_2(1.4)		[e] 1.13354

[a] Energy in atomic units: a.u. of energy $= e^2/a_0 = 27.210$ eV.
[b] T. Gilbert and P. Bagus, unpublished results.
[c] A. W. Weiss, Astrophys. J. **138**, 1262 (1963).
[d] $H_2(R)$ where the distance R is in atomic units: 1 a.u. of length $= a_0 = 0.52793 \cdot 10^{-8}$ cm.
[e] W. Kolos and C. C. J. Roothan, Revs. Modern Phys. **32**, 205 (1960).

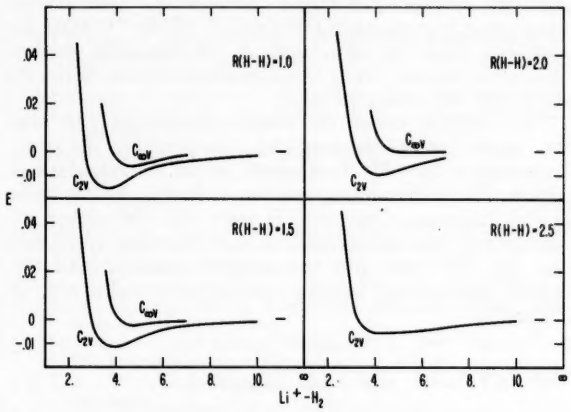

FIGURE 2. *Interaction energies for* $Li^+(^1S)$ *with the ground state of* H_2 *for* (a) C_{2v} *and* (b) $C_{\infty v}$ *geometries as a function of the* H_2 *internuclear distance.*

Energies in a.u.

The quantitative value of the B_2 curves is limited by an uncertain correlation error. Correlation effects will be considered in two categories. The first type are terms which correlate the asymptotic fragments. The K shell of the Li atom is, of course, essentially unaffected by the interaction. It is presumed that for all but the B_2 state the correlation of the H_2 bond is only slightly changed for moderate interaction energies. The correlation energy curve for H_2 is quite constant to about 1.5 a.u. and then starts to rise rapidly [14]. For the B_2 state the separation of the two hydrogen atoms in the presence of the Li atom does not lead to a large increase in the correlation energy as $R(H-H)$ exceeds 1.5 a.u. Since a $b_2(1\sigma_u)$ orbital is occupied, the asymptotic fragments would be $H+H^-$ with Li^+ for electrical neutrality. The correlation energy [15] for H^- is only a little less than that for H_2 and the usual large asymptotic correlation error is avoided. For H_2 separations less than about 1.5 a.u. the correlation energy in the H_2 pair should be comparable for the A_1, B_1, and B_2 states.

At $R(H-H)=2.5$ a.u. the B_2 state would be about 0.01 a.u. lower in energy than the A_1 and B_1 states due to the difference in correlation energy in the H_2 electron-pair for the two categories of states. Offsetting this error would be the increase in the second category of the correlation energy due to the three interpenetrating electrons in the B_2 state. For He_2^+ the correlation energy at equilibrium exceeds that for the He atom by about 0.025 a.u. It is not expected that the additional correlation energy in LiH_2 $^2B_2$ will be that large since the charge is not completely transferred from the Li atom in the range of conformations of interest. Assuming a direct proportionality of the excess correlation energy to the

amount of charge transferred, the value is 0.008 a.u. for the curve where $R(H-H)$ is 1.5 a.u. On this basis it is felt that the calculated surfaces are semiquantitatively correct. For these surfaces the zero activation energy crossing for activation of the ^2P state by colliding the ^2S atom with a vibrationally excited molecule occurs at a conformation where $R(H-H)$ is a little less than 2.0 a.u.

An oblique check on tnese calculations can also be made by considering the isoelectronic diatomic interaction Li+He for which accurate calculations exist. The asymptotic error is still due to the poor Li(^2S) function. Only the $^2\Pi$ state was calculated directly and the well depth and spectroscopic constants for the $^2\Pi$ states are compared in table 2. All the LiHe interaction energy curves are exhibited in figure 3.

TABLE 2. *Spectroscopic constants and dissociation energy,* LiHe

	$^2\Pi$	
Molecular state	This work	Ref. [6]
D_e(eV)	0.037.	0.06267
$r_e(10^{-8}$cm)	2.04	1.964
ω_e(cm^{-1})	261.9	285.7
$\omega_e X_e$(cm^{-1})	28.66	39.68
α_e(cm^{-1})	0.144	0.183

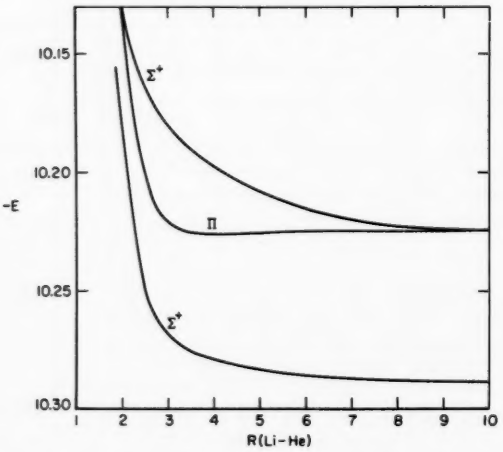

FIGURE 3. *Interaction energies for* Li(^2S *and* ^2P) *with the ground state of* He.
Energies in a.u.

3. Discussion

The present results confirm the early Heitler-London predictions of crossings in the energy curves for triangular geometries [1a]. There are no crossings in the colinear cases. In fact the linear curves strongly resemble the LiHe interaction energy curve. Laidler [1b] has discussed the Na(^2P) quenching in terms of the linear complex and has argued that the conclusions would not be affected by the shape of the complex. For the Li reactions the portion of the surface calculated here would argue quite the opposite. It is improbable that colinear collissions of vibrationally excited or dissociated H_2 with Li(^2S) would lead to excitation to Li(^2P) or the converse. But crossings are available in the C_{2v} configuration and there is no classical activation energy. The curves indicate a very rapid change in crossing position and well depth as a function of the internuclear H_2 distance. This would permit the strong coupling of the electronic and vibrational degrees of freedom which is in accord with both past [1b] and present [12] interpretations of these reactions. In particular deactivation of alkali resonance radiation will occur predominantly by vibrational excitation.

Two features of the curves are worth specia. mention. First, the crossing in the Hartree-Fock approximation is a kind of conical intersection [13] of energy curves. The doublet open-shell configurations have all off-diagonal energy matrix elements zero even if the symmetries are identical. $^2A'$ states would exhibit a conical intersection in the H.F. approximation. However, it is difficult to see how the degeneracy could be maintained when the full correlation interaction is introduced although the splitting is probably small. The second feature is the almost congruence of the H.F. $^2B_1$ or $^2\Pi$ neutral curves and the ion curve for the same geometry. The well depth in the Π-type states is not due, in this approximation, to any slight binding in the π orbital but predominately to the ion core interaction with a polarizable, unshielded atom. Similar results are found for LiHe. Although the well depths are about 40 percent smaller than those of Schneiderman and Michels or an accurate H.F. result, the qualitative behavior is similar. The $^2\Pi$ and $^1\Sigma^+$ well depths are quite comparable with the $^2\Pi$ dissociation energy greater by 0.01 eV.

The large H_2 separations required for the crossing were previously linked to the $^2\Sigma_u^+$ state [1] of H_2^-. H.F. wave functions can be similarly interpreted. For the B_2 state the p orbital is oriented along the H_2 molecule. As the Li(^2P) approaches H_2, a fraction of the charge transfers to the H_2 in a charge distribution very much like that of an isolated $1\sigma_u H_2$ orbital. This is a penetrating valence orbital with strong antibonding characteristics which determines both the deep well and the large H_2 equilibrium separations. The picture that develops is that of a charge-transfer state arising from a low ionization potential atom and a diatomic molecule that can support a valencelike negative-ion resonance state. Those molecules which have no available low-lying valence-type orbitals will not have deep attractive interactions with excited alkali atoms. In this category would fall the Ne-isoelectronic molecules and saturated hydrocarbons. Quenching cross-sections are small for such molecules [16]. On the other hand the diatomics like N_2 have the π_g and σ_u type valence orbitals available. The Π_g state can arise from a p orbital in a co-

linear collision for an orientation perpendicular to the line of centers. The C_{2v} geometry requires a d orbital on the alkali since the π_g orbital correlates with an A_2 representation. But the σ_u antibonding valence-type orbital plays the same role in N_2 as it does in H_2. The relative well depths with angular orientation should provide another measure of the kind of one-particle resonance involved in low energy electron excitation of vibrations. Contrary to H_2 there will probably be a crossing for colinear as well as C_{2v} collisions which could, in part, account for the higher N_2 cross section [17]. The character of the negative-ion should change as a function of angle and as a result so should the vibrational-electronic coupling.

4. References

[1] (a) Magee, J. L., and Ri, T., J. Chem. Phys. **9,** 638 (1941); (b) Laidler, K. J., ibid **10,** 34 (1942). (c) Mori, Y., Bull. Chem. Soc. Japan **35,** 1584 (1962).

[2] The present calculations were made with a modified version of an open-shell Hartree-Fock program using Gaussian-type-functions that was written by Clementi, E., and Veillard, A., of the IBM Research Laboratories, San Jose, Calif.

[3] Bardsley, J. N., Herzenberg, A., and Mandl, F., Proc. Intern. Conf. Phys. Electron Atomic Collisions 4th 1964, 359 (1965) for analysis of $e+H_2$; J. C. Y. Chen, to be published in Advances in Radiation Chemistry (John Wiley & Sons, N. Y., 1968) Vol. 1 for review of all experimental and theoretical information on resonant scattering.

[4] The basis of this assumption is reviewed in a paper describing H. F. interaction energy: Krauss, M., and Mies, F., J. Chem. Phys. **42,** 2703 (1965).

[5] Edmiston, C., and Krauss, M., J. Chem. Phys. **45,** 1833 (1966).

[6] Schneiderman, S. B., and Michels, H. H., J. Chem. Phys. **42,** 3706 (1965).

[7] Davidson, E. R., J. Chem. Phys. **41,** 656 (1964).

[8] Huzinaga, S., J. Chem. Phys. **42,** 1293 (1965).

[9] Oohata, K., Taketa, H., and Huzinaga, S., J. Phys. Soc. Japan **21,** 2306 (1966).

[10] Moore, C. E., Atomic Energy Levels, National Bureau of Standards Circ. 467, Vol. **1** (Washington, D.C., Government Printing Office, 1949).

[11] Fraga, S., and Ransil, B. J., J. Chem. Phys. **35,** 1967 (1961).

[12] Bauer, E., Proc. Intern. Conf. Phys. Electron Atomic Collisions 5th 1967, 236 (1967).

[13] Herzberg, G., and Longuet-Higgins, H. C., Dis. Faraday Soc. **35,** 77 (1963).

[14] Kolos, W., and Roothaan, C. C. J., Revs. Modern Phys. **32,** 219 (1960).

[15] Roothaan, C. C. J., and Weiss, A. W., Revs. Modern Phys. **32,** 194 (1960).

[16] Callear, A. B., Appl. Optica-Supplement **2,** 145 (1965).

[17] Kibble, B. P., Copley, G., and Krause, L., Phys. Rev. **159,** 11 (1967).

(Paper 72A6–520)

JOURNAL OF RESEARCH of the National Bureau of Standards—A. Physics and Chemistry
Vol. 72A, No. 6, November–December 1968

Energy Levels and Classified Lines in the First Spectrum of Technetium (Tc I)

W. R. Bozman, C. H. Corliss, and J. L. Tech

Institute for Basic Standards, National Bureau of Standards, Washington, D.C. 20234

(August 6, 1968)

Progress in the classification of Tc I lines is reported. About 2200 of the known Tc I lines between 2154 and 8918 Å are now classified as transitions between 108 even and 147 odd energy levels. Tables of levels and classified lines are given.

Key Words: Atomic spectra; energy levels, Tc I; spectrum of technetium; technetium.

1. Introduction

The analysis of the first spectrum of technetium has progressed in three separate stages. The first useful description of the spectrum was made by Meggers and Scribner [1].[1] The initial advances in the analysis, made by Meggers [2] from that line list, resulted in the classification of 200 lines of Tc I as combinations between 19 even and 44 odd energy levels, arising from 5 even and 2 odd configurations. A striking result of Meggers' analysis was that the lowest level of the $4d^6 5s$ configuration, a $^6D_{4\frac{1}{2}}$, occurs only 2573 cm^{-1} above the $4d^5 5s^2\ ^6S$ ground level. This may be compared with the value 17052 cm^{-1} for the lowest $3d^6 4s$ level in Mn I relative to the $3d^5 4s^2\ ^6S$ ground level, and with the value 11754 cm^{-1} for the position of the lowest $5d^6 6s$ level above $5d^5 6s^2\ ^6S$ in Re I.

The second step in the analysis of Tc I was taken by Bozman [3, 4], making use of the new and more extensive description of technetium spectra prepared in 1952 and recently published by Bozman, Meggers and Corliss [5]. In that step of the analysis Bozman made one of the first applications of electronic digital computers to the hitherto tedious work of searching out new energy levels. He found 37 new even and 42 odd energy levels, and classified about 900 lines.

In 1955 and 1956 Bozman observed the Zeeman Effect in Tc I by use of electrodeless lamps [6] containing technetium iodide. Hundreds of patterns were measured by him in the region between 2400 and 7000 Å and a number of them were reduced to determine the magnetic splitting factors (g-values). Bozman used some of these g-values to interpret most of the Tc I levels published in Vol. III of "Atomic Energy Levels," compiled by C. E. Moore [7].

In the dozen years that have elapsed since the initial applications of digital computers to energy level searches, significant advances in programming this problem have been made, notably by G. Racah while visiting NBS and recently by one of the present authors [8]. In the currently undertaken third phase of the analysis of Tc I, Corliss and Tech have applied this latest program to a search for new energy levels.

2. Search for New Energy Levels

As the first step in discovering new energy levels in Tc I a special search was made with 61 even and 92 odd levels already known. These levels provided classifications for 914 lines which were then removed from the complete list of 3336 Tc I lines. A search with the remaining unclassified lines yielded 21 new odd levels. With these added to the odd level list, 29 new even levels were found. At this point, 623 more classified lines were removed from the line list. From a second pair of searches 35 odd and 20 even levels were found, classifying 569 lines. A third pair of searches revealed only 2 odd and 7 even levels, whereupon the systematic numerical searches were discontinued.

3. Results

The present lists of even and odd levels are given in tables 1 and 2. The term designations assigned by Meggers or Bozman are given in the first column, the J-values in the second, and the level values in cm^{-1} in the third. The number of combinations with each level and the discoverer are given in the last column. Here "M" refers to Meggers (1951), "B" to Bozman

[1] Figures in brackets indicate the literature references at the end of this paper.

and "C" to the levels recently found with the computer. "A" indicates that the level appears in AEL [7].

The list of classified lines with the wavelengths, wavenumbers, intensities, and energy levels is given in table 3. A doubly classified line is indicated by duplicate entries of the line in table 3.

The intensity numbers are in some cases accompanied by literal symbols indicating characteristic features of the lines as follows:

c—complex
d—double
h—hazy
l—shaded to longer waves
s—shaded to shorter waves
w—wide
tr—intensity < 1.

About 2200 or two-thirds of the known Tc I lines are now classified.

The assignment of the Tc I energy levels to configurations and terms is proceeding with the reduction of the Zeeman patterns. This analysis, together with the results of theoretical calculations in progress, will appear in a later paper.

TABLE 1. *Even levels of* Tc I

Config.	Desig.	J	Level	No. Comb.	Config.	Desig.	J	Level	No. Comb.
$4d^5 5s^2$	a^6S	2 1/2	0.00	36 MA			2 1/2	22265.46	40 C
							1 1/2	22503.10	18 C
$4d^6(a^5D)5s$	a^6D	4 1/2	2572.89	36 MA			3 1/2	22615.94	32 C
		3 1/2	3250.91	40 MA			3 1/2	23460.03	10 C
		2 1/2	3700.54	48 MA			3 1/2	23957.76	22 C
		1 1/2	4002.57	37 MA					
		0 1/2	4178.75	19 MA			4 1/2	24147.13	18 C
							5 1/2	24564.76	13 C
$4d^6(a^5D)5s$	a^4D	3 1/2	10516.53	31 MA			3 1/2	25058.56	25 C
		2 1/2	11063.07	49 MA			2 1/2	25174.13	27 C
		1 1/2	11578.60	34 MA			1 1/2	25405.69	15 C
		0 1/2	11890.94	17 MA					
							2 1/2	25598.30	22 C
$4d^6(^3P)5s$	a^4P	2 1/2	13252.74	47 BA			2 1/2	26788.59	12 C
		1 1/2	14169.75	35 BA			2 1/2	26883.58	18 C
		0 1/2	14679.90	22 BA			5 1/2	26917.97	13 C
							3 1/2	26950.98	23 C
$4d^6(^3F)5s$	a^4F	4 1/2	14733.14	46 BA					
		3 1/2	15298.46	50 BA			6 1/2	27274.11	7 C
		2 1/2	15624.25	47 BA			2 1/2	27517.24	16 C
		1 1/2	15770.42	31 BA			4 1/2	27971.36	22 C
							5 1/2	28839.40	12 C
$4d^6(^3G)5s$	a^4G	5 1/2	16025.15	28 BA			3 1/2	29233.90	19 C
		4 1/2	16133.98	45 BA					
		3 1/2	16287.79	46 BA			4 1/2	29539.00	28 C
		2 1/2	16415.64	44 BA			2 1/2	30060.66	10 C
$4d^6(^3H)5s$	a^4H	6 1/2	16553.39	9 C					
		5 1/2	17146.80	26 B	$4d^5 5s(a^7S)6s$	e^8S	3 1/2	37612.40	5 MA
		4 1/2	17328.02	46 B					
		3 1/2	17282.63	42 B	$4d^5 5s(a^7S)6s$	e^6S	2 1/2	39598.86	5 MA
		1 1/2	19702.77	29 B	$4d^6(a^5D)6s$	e^6D	4 1/2	42855.24	7 BA
		4 1/2	19791.94	42 B			3 1/2	43391.76	11 BA
		0 1/2	19827.50	11 C			2 1/2	43796.70	15 BA
		2 1/2	19895.41	36 B			1 1/2	44028.92	10 BA
		3 1/2	19903.57	45 C			0 1/2	44149.50	7 BA
		1 1/2	20231.22	25 C	$4d^6(a^5D)6s$	e^4D	3 1/2	44101.99	12 BA
		3 1/2	20384.74	42 C			2 1/2	44804.35	10 BA
		2 1/2	20523.34	46 B			1 1/2	45267.82	11 BA
		5 1/2	20639.36	18 B			0 1/2	45497.77	5 BA
		2 1/2	20686.26	34 C					
		3 1/2	20783.83	39 C	$4d^5 5s(a^7S)5d$	e^8D	1 1/2	44333.21	2 MA
		4 1/2	21204.96	35 B			2 1/2	44337.54	5 MA
		2 1/2	21206.34	33 C			3 1/2	44343.90	3 MA
		1 1/2	21447.45	17 C			4 1/2	44352.65	2 MA
		4 1/2	21450.48	35 B			5 1/2	44365.30	1 MA
		5 1/2	21719.83	27 B	$4d^5 5s(a^7S)5d$	f^8D	4 1/2	44919.08	4 BA
		3 1/2	21752.14	32 C			3 1/2	44985.53	7 BA
		2 1/2	21920.15	32 C			2 1/2	45071.05	10 BA
		2 1/2	21926.79	24 C			1 1/2	45108.64	9 BA
		4 1/2	22180.10	33 B			0 1/2	45189.70	5 BA

TABLE 1. *Even levels of* Tc I—Continued

Config.	Desig.	J	Level	No. Comb.	Config.	Desig.	J	Level	No. Comb.
		4 1/2	48418.21	7 C			2 1/2	49813.62	10 C
		3 1/2	48462.94	5 C			2 1/2	49938.69	10 C
		3 1/2	48784.86	10 C			2 1/2	53945.19	6 C
		2 1/2	48944.13	11 C			5 1/2	56118.36	5 C
		4 1/2	48977.03	9 C			5 1/2	59315.30	7 C
		3 1/2	49245.93	9 C			3 1/2	62038.26	7 C
		2 1/2	49337.51	7 C			3 1/2	62501.78	8 C
		2 1/2	49565.96	8 C			4 1/2	62599.48	7 C
		3 1/2	49573.35	5 M			2 1/2	63926.66	7 C
		1 1/2	49735.08	11 C			3 1/2	64785.90	7 C

TABLE 2. *Odd levels of* Tc I

Config.	Desig.	J	Level	No. Comb.	Config.	Desig.	J	Level	No. Comb.
$4d^5 5s(a^7S)5p$	$z\,^8P^\circ$	2 1/2	16428.71	9 MA			3 1/2	39567.76	25 B
		3 1/2	16874.51	9 MA			1 1/2	39576.54	18 B
		4 1/2	17522.92	8 MA			4 1/2	39763.38	18 B
							1 1/2	39844.02	6 B
$4d^5 5s(a^7S)5p$	$z\,^6P^\circ$	3 1/2	23265.32	17 MA			3 1/2	39849.33	7 B
		2 1/2	23455.21	15 MA					
		1 1/2	23588.40	13 MA			2 1/2	39891.05	15 M
							2 1/2	39977.39	24 B
$4d^6(a^5D)5p$	$z\,^6D^\circ$	4 1/2	27369.79	14 MA			1 1/2	40096.61	19 C
		3 1/2	27660.10	26 MA			3 1/2	40236.26	12 C
		2 1/2	27940.73	20 MA			5 1/2	40241.58	12 B
		1 1/2	28151.28	16 MA			2 1/2	40299.14	13 C
		0 1/2	28296.67	12 MA			4 1/2	40403.19	19 C
							3 1/2	40406.40	18 C
$4d^6(a^5D)5p$	$z\,^6F^\circ$	5 1/2	30067.29	4 MA			2 1/2	40821.29	12 C
		4 1/2	30133.26	17 MA			0 1/2	40829.39	9 B
		3 1/2	30382.06	21 MA					
		2 1/2	30528.86	19 MA			1 1/2	41073.16	15 C
		1 1/2	30630.62	17 MA			3 1/2	41088.50	20 C
		0 1/2	30689.12	8 MA			2 1/2	41100.21	21 C
							1 1/2	41250.90	6 B
$4d^6(a^5D)5p$	$z\,^4F^\circ$	4 1/2	31114.08	20 MA			3 1/2	41529.11	22 C
		3 1/2	31605.00	30 MA					
		2 1/2	32014.81	27 MA			5 1/2	41580.75	11 C
		1 1/2	32253.65	21 MA			1 1/2	41625.52	11 C
							4 1/2	41703.59	22 B
$4d^6(a^5D)5p$	$y\,^6P^\circ$	3 1/2	31414.05	26 MA			3 1/2	41729.87	24 C
		2 1/2	31406.74	18 MA			2 1/2	41764.26	11 C
		1 1/2	31503.93	15 MA					
							1 1/2	41788.77	12 B
$4d^6(a^5D)5p$	$z\,^4P^\circ$	2 1/2	31927.01	23 MA			4 1/2	41896.99	23 B
		1 1/2	32258.06	24 MA			2 1/2	41922.68	23 B
		0 1/2	32403.06	7 BA			3 1/2	41993.08	20 B
							5 1/2	42032.57	18 B
$4d^6(a^5D)5p$	$z\,^4D^\circ$	3 1/2	32620.38	26 MA					
		2 1/2	33085.69	30 MA			2 1/2	42102.82	22 B
		1 1/2	33343.18	27 MA			4 1/2	42217.08	27 B
		0 1/2	33480.47	12 MA			1 1/2	42217.33	11 B
							3 1/2	42246.21	17 B
$4d^5 5s(a^5S)5p$	$y\,^4P^\circ$	2 1/2	34515.88	17 MA			2 1/2	42250.66	15 C
		1 1/2	34942.64	16 MA					
		0 1/2	35276.45	5 MA			2 1/2	42294.46	22 B
							5 1/2	42444.33	16 B
$4d^5 5s(a^5S)5p$	$x\,^6P^\circ$	3 1/2	38240.73	9 MA			6 1/2	42474.75	8 C
		2 1/2	38216.75	12 MA			3 1/2	42523.12	14 B
		1 1/2	38319.60	8 MA			4 1/2	42545.01	19 B
		1 1/2	38556.71	5 B			5 1/2	42600.59	12 B
		2 1/2	38600.58	4 M			4 1/2	42613.90	21 C
		3 1/2	38766.20	6 M			2 1/2	42696.45	17 C
		4 1/2	39185.01	6 M			3 1/2	42771.82	27 B
		2 1/2	39459.89	15 C			5 1/2	42773.99	6 C

TABLE 2. *Odd levels of* Tc I—Continued

Config.	Desig.	J	Level	No. Comb.	Config.	Desig.	J	Level	No. Comb.
		4 1/2	42817.00	18 B			2 1/2	44872.37	16 C
		1 1/2	42901.59	14 C			1 1/2	44876.75	15 B
		2 1/2	42905.60	15 C			1 1/2	44955.88	9 B
		2 1/2	43011.14	21 C			4 1/2	45708.77	15 C
		3 1/2	43077.33	25 C			4 1/2	46068.86	13 C
		4 1/2	43097.77	15 C			2 1/2	46104.89	15 C
		5 1/2	43172.19	15 B			3 1/2	46396.17	14 C
		6 1/2	43197.60	5 B			3 1/2	46608.86	16 C
		4 1/2	43265.51	21 B			3 1/2	46656.07	17 C
		3 1/2	43267.16	27 B			1 1/2	47030.68	9 C
		5 1/2	43512.49	14 C			2 1/2	47232.38	14 C
		2 1/2	43546.50	15 C			2 1/2	47281.86	11 C
		4 1/2	43649.73	21 B			5 1/2	47294.35	8 C
		3 1/2	43805.25	13 C			4 1/2	47343.91	8 C
		6 1/2	43857.24	8 C			3 1/2	47389.74	11 C
		3 1/2	43905.73	25 B			2 1/2	47452.27	16 C
		4 1/2	43971.81	10 C			0 1/2	47670.53	5 B
		2 1/2	44007.00	18 C			4 1/2	47819.66	16 C
		3 1/2	44090.55	18 B			3 1/2	47864.34	13 C
		2 1/2	44107.18	23 C			2 1/2	48142.76	11 C
		1 1/2	44110.04	15 C			4 1/2	48213.49	12 C
		5 1/2	44138.17	15 C			3 1/2	48217.35	11 B
		2 1/2	44241.57	18 C			5 1/2	48287.79	11 C
		3 1/2	44266.89	26 B			4 1/2	48881.75	17 C
		1 1/2	44313.57	16 C			4 1/2	49098.66	10 C
		2 1/2	44537.79	17 B			3 1/2	49130.01	8 C
		4 1/2	44576.08	20 C			4 1/2	49815.88	12 C
		3 1/2	44687.20	16 C			5 1/2	51221.24	6 C
		1 1/2	44722.27	14 B			3 1/2	51423.70	10 C
		3 1/2	44839.20	18 C			4 1/2	52350.24	8 C

TABLE 3. *Classified lines of* Tc I

Wavelength A	Wavenumber cm^{-1}	Intensity		Energy levels cm^{-1}
		Arc	Spark	
2154.668	46396.27	2		$0\ ^2D_{3/2}$–$46396^o\ ^3D_{3/2}$
2271.662	44007.03	3		$0\ ^2D_{3/2}$–$44007^o\ ^2D_{3/2}$
2272.976	43981.59	2		$3250\ ^3D_{3/2}$–$47232^o\ ^2D_{3/2}$
2282.121	43805.36	10		$0\ ^2D_{3/2}$–$43805^o\ ^3D_{3/2}$
2405.128	41565.18	8		$2572\ ^4D_{3/2}$–$44138^o\ ^3D_{3/2}$
2412.610	41436.29	6		$3250\ ^3D_{3/2}$–$44687^o\ ^3D_{3/2}$
2418.647	41332.87	5		$2572\ ^4D_{3/2}$–$43905^o\ ^3D_{3/2}$
2418.647	41332.87	5		$2572\ ^4D_{3/2}$–$43905^o\ ^3D_{3/2}$
2424.538	41232.45	20	1	$2572\ ^4D_{3/2}$–$43805^o\ ^3D_{3/2}$
2427.848	41176.24	3		$3700\ ^2D_{3/2}$–$44876^o\ ^1D_{3/2}$
2432.337	41100.25	2		$0\ ^2D_{3/2}$–$41100^o\ ^2D_{3/2}$
2433.728	41076.76	8		$2572\ ^4D_{3/2}$–$43649^o\ ^4D_{3/2}$
2436.994	41021.71	10		$3700\ ^2D_{3/2}$–$44722^o\ ^1D_{3/2}$
2439.081	40986.62	5		$3700\ ^2D_{3/2}$–$44687^o\ ^3D_{3/2}$
2446.049	40869.87	3		$4002\ ^1D_{3/2}$–$44872^o\ ^2D_{3/2}$
2446.864	40856.26	4		$3250\ ^3D_{3/2}$–$44107^o\ ^2D_{3/2}$
2447.860	40839.63	3		$3250\ ^3D_{3/2}$–$44090^o\ ^3D_{3/2}$
2456.386	40697.89	2		$4178\ ^0D_{3/2}$–$44876^o\ ^1D_{3/2}$
2458.994	40654.73	10		$3250\ ^3D_{3/2}$–$43905^o\ ^3D_{3/2}$
2461.523	40612.96	9		$3700\ ^2D_{3/2}$–$44313^o\ ^1D_{3/2}$
2465.086	40554.27	20	1	$3250\ ^3D_{3/2}$–$43805^o\ ^3D_{3/2}$
2465.740	40543.51	10	1	$4178\ ^0D_{3/2}$–$44722^o\ ^1D_{3/2}$
2466.873	40524.89	30	1	$2572\ ^4D_{3/2}$–$43097^o\ ^4D_{3/2}$
2468.114	40504.52	3		$2572\ ^4D_{3/2}$–$43077^o\ ^3D_{3/2}$
2473.915	40409.55	8		$3700\ ^2D_{3/2}$–$44110^o\ ^1D_{3/2}$
2474.570	40398.85	2		$3250\ ^3D_{3/2}$–$43649^o\ ^4D_{3/2}$
2475.107	40390.09	20		$3700\ ^2D_{3/2}$–$44090^o\ ^3D_{3/2}$
2480.699	40299.05	50		$0\ ^2D_{3/2}$–$40299^o\ ^2D_{3/2}$
2484.080	40244.20	4		$2572\ ^4D_{3/2}$–$42817^o\ ^4D_{3/2}$
2484.572	40236.23	8	8	$0\ ^2D_{3/2}$–$40236^o\ ^3D_{3/2}$
2486.496	40205.10	20		$3700\ ^2D_{3/2}$–$43905^o\ ^3D_{3/2}$
2486.884	40198.83	2		$2572\ ^4D_{3/2}$–$42771^o\ ^3D_{3/2}$
2490.854	40134.76	10		$4178\ ^0D_{3/2}$–$44313^o\ ^1D_{3/2}$
2492.721	40104.70	25	3	$3700\ ^2D_{3/2}$–$43805^o\ ^3D_{3/2}$
2492.721	40104.70	25	3	$4002\ ^1D_{3/2}$–$44107^o\ ^2D_{3/2}$
2500.654	39977.48	2		$0\ ^2D_{3/2}$–$39977^o\ ^2D_{3/2}$
2500.990	39972.11	15	1	$2572\ ^4D_{3/2}$–$42545^o\ ^4D_{3/2}$
2502.363	39950.18	7	1	$2572\ ^4D_{3/2}$–$42523^o\ ^3D_{3/2}$
2503.550	39931.24	6		$4178\ ^0D_{3/2}$–$44110^o\ ^1D_{3/2}$
2508.853	39846.85	10		$3250\ ^3D_{3/2}$–$43097^o\ ^4D_{3/2}$
2521.679	39644.19	2		$2572\ ^4D_{3/2}$–$42217^o\ ^4D_{3/2}$
2526.548	39567.79	3		$0\ ^2D_{3/2}$–$39567^o\ ^3D_{3/2}$
2529.550	39520.84	2		$3250\ ^3D_{3/2}$–$42771^o\ ^3D_{3/2}$
2533.467	39459.74	10	1	$2572\ ^4D_{3/2}$–$42032^o\ ^5D_{3/2}$
2538.804	39376.79	2		$3700\ ^2D_{3/2}$–$43077^o\ ^3D_{3/2}$
2544.144	39294.15	2		$3250\ ^3D_{3/2}$–$42545^o\ ^4D_{3/2}$
2545.565	39272.21	15	1	$3250\ ^3D_{3/2}$–$42523^o\ ^3D_{3/2}$
2562.818	39007.85	10		$2572\ ^4D_{3/2}$–$41580^o\ ^5D_{3/2}$
2563.349	38999.77	2		$3250\ ^3D_{3/2}$–$42250^o\ ^2D_{3/2}$
2565.560	38966.16	4		$3250\ ^3D_{3/2}$–$42217^o\ ^4D_{3/2}$

TABLE 3. *Classified lines of* Tc I

Wavelength A	Wavenumber cm^{-1}	Intensity		Energy levels cm^{-1}
		Arc	Spark	
2578.791	38766.25	300*h l*	100*h l*	$0\ ^2{}_{1/2}$–$38766^0{}_{3/2}$
2589.861	38600.56	200	3	$0\ ^2{}_{1/2}$–$38600^0{}_{2/2}$
2592.816	38556.57	100	5	$0\ ^2{}_{1/2}$–$38556^0{}_{1/2}$
2593.247	38550.16	10		$3700\ ^2{}_{1/2}$–$42250^0{}_{2/2}$
2605.753	38365.16	4		$10516\ ^3{}_{1/2}$–$48881^0{}_{4/2}$
2608.855	38319.54	500	15	$0\ ^2{}_{1/2}$–$38319^0{}_{1/2}$
2614.233	38240.72	1500	30	$0\ ^2{}_{1/2}$–$38240^0{}_{3/2}$
2615.873	38216.74	1000	20	$0\ ^2{}_{1/2}$–$38216^0{}_{2/2}$
2642.372	37833.51	100		$2572\ ^4{}_{1/2}$–$40406^0{}_{3/2}$
2654.306	37663.42	100	3	$2572\ ^4{}_{1/2}$–$40236^0{}_{3/2}$
2657.572	37617.13	1	1	$14733\ ^4{}_{1/2}$–$52350^0{}_{4/2}$
2660.884	37570.31	120	30 *l*	$3250\ ^3{}_{1/2}$–$40821^0{}_{2/2}$
2662.296	37550.39	100	2	$3700\ ^2{}_{1/2}$–$41250^0{}_{1/2}$
2669.654	37446.90	1		$4178\ ^0{}_{1/2}$–$41625^0{}_{1/2}$
2673.024	37399.69	6		$3700\ ^2{}_{1/2}$–$41100^0{}_{2/2}$
2683.886	37248.34	80	1	$4002\ ^1{}_{1/2}$–$41250^0{}_{1/2}$
2688.059	37190.52	20		$2572\ ^4{}_{1/2}$–$39763^0{}_{4/2}$
2690.673	37154.39	12		$11063\ ^2{}_{1/2}$–$48217^0{}_{3/2}$
2693.112	37120.74	80	2	$3700\ ^2{}_{1/2}$–$40821^0{}_{2/2}$
2694.780	37097.77	10		$4002\ ^1{}_{1/2}$–$41100^0{}_{2/2}$
2696.636	37072.23	50		$4178\ ^0{}_{1/2}$–$41250^0{}_{1/2}$
2696.755	37070.60	15	1	$4002\ ^1{}_{1/2}$–$41073^0{}_{1/2}$
2702.271	36994.93	70		$2572\ ^4{}_{1/2}$–$39567^0{}_{3/2}$
2714.600	36826.92	2		$4002\ ^1{}_{1/2}$–$40829^0{}_{1/2}$
2715.205	36818.72	30		$4002\ ^1{}_{1/2}$–$40821^0{}_{2/2}$
2723.550	36705.91	30		$3700\ ^2{}_{1/2}$–$40406^0{}_{3/2}$
2730.529	36612.10	500	10	$2572\ ^4{}_{1/2}$–$39184^0{}_{4/2}$
2736.231	36535.81	150		$3700\ ^2{}_{1/2}$–$40236^0{}_{3/2}$
2737.973	36512.56	100	1	$3250\ ^3{}_{1/2}$–$39763^0{}_{4/2}$
2739.819	36487.96	3		$14733\ ^4{}_{1/2}$–$51221^0{}_{3/2}$
2755.761	36276.89	100	8	$3700\ ^2{}_{1/2}$–$39977^0{}_{2/2}$
2760.380	36216.19	7		$16133\ ^4{}_{1/2}$–$52350^0{}_{4/2}$
2762.134	36193.19	100	3	$2572\ ^4{}_{1/2}$–$38766^0{}_{3/2}$
2762.337	36190.53	200	8	$3700\ ^2{}_{1/2}$–$39891^0{}_{2/2}$
2763.957	36169.32	8		$11063\ ^2{}_{1/2}$–$47232^0{}_{2/2}$
2769.714	36094.15	5		$4002\ ^1{}_{1/2}$–$40096^0{}_{1/2}$
2778.908	35974.74	150	9	$4002\ ^1{}_{1/2}$–$39977^0{}_{2/2}$
2782.052	35934.08	1000	15	$3250\ ^3{}_{1/2}$–$39184^0{}_{4/2}$
2785.586	35888.50	500	10	$4002\ ^1{}_{1/2}$–$39891^0{}_{2/2}$
2787.234	35867.28	15	2	$3700\ ^2{}_{1/2}$–$39567^0{}_{3/2}$
2789.246	35841.41	500		$4002\ ^1{}_{1/2}$–$39844^0{}_{1/2}$
2795.650	35759.31	80		$3700\ ^2{}_{1/2}$–$39459^0{}_{2/2}$
2802.810	35667.96	1000	8	$2572\ ^4{}_{1/2}$–$38240^0{}_{3/2}$
2803.018	35665.32	150	3	$4178\ ^0{}_{1/2}$–$39844^0{}_{1/2}$
2803.921	35653.83	8		$11578\ ^1{}_{1/2}$–$47232^0{}_{2/2}$
2810.225	35573.86	15		$4002\ ^1{}_{1/2}$–$39576^0{}_{1/2}$
2812.447	35545.75	3		$11063\ ^2{}_{1/2}$–$46608^0{}_{3/2}$
2814.860	35515.28	30		$3250\ ^3{}_{1/2}$–$38766^0{}_{3/2}$
2819.460	35457.34	40	1	$4002\ ^1{}_{1/2}$–$39459^0{}_{2/2}$
2828.042	35349.75	200	10	$3250\ ^3{}_{1/2}$–$38600^0{}_{2/2}$

TABLE 3. *Classified lines of* Tc I

Wavelength A	Wavenumber cm^{-1}	Intensity		Energy levels cm^{-1}
		Arc	Spark	
2829.375	35333.09	5		$11063\ ^{2}{}_{1/2}$–$46396^{o}{}_{3/2}$
2849.196	35087.30	60	3	$16133\ ^{4}{}_{1/2}$–$51221^{o}{}_{3/2}$
2850.956	35065.64	150	10	$3700\ ^{2}{}_{1/2}$–$38766^{o}{}_{3/2}$
2855.637	35008.17	10	1	$16415\ ^{2}{}_{1/2}$–$51423^{o}{}_{3/2}$
2857.128	34989.90	500*h*	7	$3250\ ^{3}{}_{1/2}$–$38240^{o}{}_{3/2}$
2859.110	34965.64	2000*c*	200*c*	$3250\ ^{3}{}_{1/2}$–$38216^{o}{}_{2_{1/2}}$
2860.988	34942.69	15		$0\ ^{2}{}_{1/2}$–$34942^{o}{}_{1/2}$
2864.486	34900.03	500	8	$3700\ ^{2}{}_{1/2}$–$38600^{o}{}_{2_{1/2}}$
2868.087	34856.21	100	3	$3700\ ^{2}{}_{1/2}$–$38556^{o}{}_{1/2}$
2869.283	34841.68	20		$27660^{o}{}_{3/2}$–$62501\ ^{3}{}_{1/2}$
2883.670	34667.86	5		$16553\ ^{6}{}_{1/2}$–$51221^{o}{}_{3/2}$
2887.734	34619.07	1000	8	$3700\ ^{2}{}_{1/2}$–$38319^{o}{}_{1/2}$
2889.487	34598.07	3		$4002\ ^{1}{}_{1/2}$–$38600^{o}{}_{2_{1/2}}$
2893.160	34554.15	200	2	$4002\ ^{1}{}_{1/2}$–$38556^{o}{}_{1/2}$
2894.322	34540.28	200	2	$3700\ ^{2}{}_{1/2}$–$38240^{o}{}_{3/2}$
2896.340	34516.21	1000	10	$3700\ ^{2}{}_{1/2}$–$38216^{o}{}_{2_{1/2}}$
2896.340	34516.21	1000	10	$0\ ^{2}{}_{1/2}$–$34515^{o}{}_{2_{1/2}}$
2907.982	34378.03	15		$4178\ ^{0}{}_{1/2}$–$38556^{o}{}_{1/2}$
2909.036	34365.58	7		$14733\ ^{4}{}_{1/2}$–$49098^{o}{}_{4_{1/2}}$
2909.852	34355.94	5		$10516\ ^{3}{}_{1/2}$–$44872^{o}{}_{2_{1/2}}$
2913.147	34317.08	1000	7	$4002\ ^{1}{}_{1/2}$–$38319^{o}{}_{1/2}$
2921.912	34214.15	500	2	$4002\ ^{1}{}_{1/2}$–$38216^{o}{}_{2_{1/2}}$
2923.155	34199.60	5		$13252\ ^{2}{}_{1/2}$–$47452^{o}{}_{2_{1/2}}$
2928.198	34140.70	1000	2	$4178\ ^{0}{}_{1/2}$–$38319^{o}{}_{1/2}$
2932.062	34095.71	4		$17328\ ^{4}{}_{1/2}$–$51423^{o}{}_{3/2}$
2933.888	34074.49	80		$17146\ ^{5}{}_{1/2}$–$51221^{o}{}_{3/2}$
2937.801	34029.11	6		$13252\ ^{2}{}_{1/2}$–$47281^{o}{}_{2_{1/2}}$
2942.082	33979.60	30	1	$13252\ ^{2}{}_{1/2}$–$47232^{o}{}_{2_{1/2}}$
2949.580	33893.22	25	1	$17328\ ^{4}{}_{1/2}$–$51221^{o}{}_{3/2}$
2964.287	33725.07	20		$10516\ ^{3}{}_{1/2}$–$44241^{o}{}_{2_{1/2}}$
2973.179	33624.21	18		$11063\ ^{2}{}_{1/2}$–$44687^{o}{}_{3/2}$
2979.338	33554.71	100	3	$14733\ ^{4}{}_{1/2}$–$48287^{o}{}_{3/2}$
2984.137	33500.75	20	1	$14169\ ^{1}{}_{1/2}$–$47670^{o}{}_{1/2}$
2985.046	33490.55	15		$10516\ ^{3}{}_{1/2}$–$44007^{o}{}_{2_{1/2}}$
2985.601	33484.32	8		$14733\ ^{4}{}_{1/2}$–$48217^{o}{}_{3/2}$
2986.453	33474.77	15		$11063\ ^{2}{}_{1/2}$–$44537^{o}{}_{2_{1/2}}$
2994.097	33389.31	15	8	$10516\ ^{3}{}_{1/2}$–$43905^{o}{}_{3/2}$
2997.076	33356.12	20		$13252\ ^{2}{}_{1/2}$–$46608^{o}{}_{3/2}$
2998.235	33343.23	6		$0\ ^{2}{}_{1/2}$–$33343^{o}{}_{1/2}$
3003.698	33282.59	30	1	$14169\ ^{1}{}_{1/2}$–$47452^{o}{}_{2_{1/2}}$
3010.831	33203.74	100	2	$11063\ ^{2}{}_{1/2}$–$44266^{o}{}_{3/2}$
3016.298	33143.56	12		$11578\ ^{1}{}_{1/2}$–$44722^{o}{}_{1/2}$
3017.232	33133.30	300	7	$10516\ ^{3}{}_{1/2}$–$43649^{o}{}_{4_{1/2}}$
3021.555	33085.90	150	2	$0\ ^{2}{}_{1/2}$–$33085^{o}{}_{2_{1/2}}$
3023.680	33062.65	200	3	$14169\ ^{1}{}_{1/2}$–$47232^{o}{}_{2_{1/2}}$
3026.887	33027.62	300*w*	200*w*	$11063\ ^{2}{}_{1/2}$–$44090^{o}{}_{3/2}$
3030.276	32990.69	6		$14679\ ^{0}{}_{1/2}$–$47670^{o}{}_{1/2}$
3030.718	32985.87	2		$11890\ ^{0}{}_{1/2}$–$44876^{o}{}_{1/2}$
3034.568	32944.03	80		$11063\ ^{2}{}_{1/2}$–$44007^{o}{}_{2_{1/2}}$
3036.878	32918.97	40	2	$15298\ ^{3}{}_{1/2}$–$48217^{o}{}_{3/2}$

TABLE 3. *Classified lines of* Tc I

Wavelength A	Wavenumber cm^{-1}	Intensity		Energy levels cm^{-1}
		Arc	Spark	
3042.643	32856.60	40	2	$16025\ ^{5}_{1/2}$–$48881^{o}\ ^{4}_{1/2}$
3043.049	32852.22	12	1	$13252\ ^{2}_{1/2}$–$46104^{o}\ ^{2}_{1/2}$
3043.774	32844.39	8		$15298\ ^{3}_{1/2}$–$48142^{o}\ ^{2}_{1/2}$
3043.938	32842.62	8		$11063\ ^{2}_{1/2}$–$43905^{o}\ ^{3}_{1/2}$
3044.978	32831.40	10		$11890\ ^{0}_{1/2}$–$44722^{o}\ ^{1}_{1/2}$
3057.327	32698.80	30	2	$16874^{o}\ ^{3}_{1/2}$–$49573\ ^{3}_{1/2}$
3060.103	32669.14	4		$17146\ ^{5}_{1/2}$–$49815^{o}\ ^{4}_{1/2}$
3060.672	32663.06	30	1	$11578\ ^{1}_{1/2}$–$44241^{o}\ ^{2}_{1/2}$
3061.283	32656.54	3		$14733\ ^{4}_{1/2}$–$47389^{o}\ ^{3}_{1/2}$
3064.667	32620.49	300	3	$0\ ^{2}_{1/2}$–$32620^{o}\ ^{3}_{1/2}$
3070.241	32561.27	30		$14733\ ^{4}_{1/2}$–$47294^{o}\ ^{3}_{1/2}$
3073.046	32531.55	10		$11578\ ^{1}_{1/2}$–$44110^{o}\ ^{1}_{1/2}$
3073.326	32528.58	12		$11578\ ^{1}_{1/2}$–$44107^{o}\ ^{2}_{1/2}$
3074.270	32518.60	20	1	$15624\ ^{2}_{1/2}$–$48142^{o}\ ^{2}_{1/2}$
3076.528	32494.73	10		$10516\ ^{3}_{1/2}$–$43011^{o}\ ^{2}_{1/2}$
3077.591	32483.51	3		$11063\ ^{2}_{1/2}$–$43546^{o}\ ^{2}_{1/2}$
3081.075	32446.78	15	1	$19903\ ^{3}_{1/2}$–$52350^{o}\ ^{4}_{1/2}$
3083.354	32422.79	20		$31503^{o}\ ^{1}_{1/2}$–$63926\ ^{2}_{1/2}$
3098.657	32262.68	20		$16025\ ^{5}_{1/2}$–$48287^{o}\ ^{3}_{1/2}$
3099.098	32258.09	1000	10	$0\ ^{2}_{1/2}$–$32258^{o}\ ^{1}_{1/2}$
3099.517	32253.73	200	2	$0\ ^{2}_{1/2}$–$32253^{o}\ ^{1}_{1/2}$
3104.293	32204.11	30	1	$11063\ ^{2}_{1/2}$–$43267^{o}\ ^{3}_{1/2}$
3109.151	32153.79	40		$16133\ ^{4}_{1/2}$–$48287^{o}\ ^{3}_{1/2}$
3115.977	32083.35	60	2	$16133\ ^{4}_{1/2}$–$48217^{o}\ ^{3}_{1/2}$
3119.171	32050.50	80	6	$17522^{o}\ ^{4}_{1/2}$–$49573\ ^{3}_{1/2}$
3119.662	32045.46	40	1	$15298\ ^{3}_{1/2}$–$47343^{o}\ ^{4}_{1/2}$
3121.306	32028.58	10*h*		$10516\ ^{3}_{1/2}$–$42545^{o}\ ^{4}_{1/2}$
3122.642	32014.88	700	3	$0\ ^{2}_{1/2}$–$32014^{o}\ ^{2}_{1/2}$
3127.464	31965.52	2		$20384\ ^{3}_{1/2}$–$52350^{o}\ ^{4}_{1/2}$
3131.233	31927.04	1500	20	$0\ ^{2}_{1/2}$–$31927^{o}\ ^{2}_{1/2}$
3138.322	31854.93	20		$16287\ ^{3}_{1/2}$–$48142^{o}\ ^{2}_{1/2}$
3139.936	31838.55	25		$11063\ ^{2}_{1/2}$–$42901^{o}\ ^{1}_{1/2}$
3143.561	31801.84	4		$16415\ ^{2}_{1/2}$–$48217^{o}\ ^{3}_{1/2}$
3144.291	31794.46	20		$16025\ ^{5}_{1/2}$–$47819^{o}\ ^{4}_{1/2}$
3145.937	31777.82	6		$10516\ ^{3}_{1/2}$–$42294^{o}\ ^{2}_{1/2}$
3147.160	31765.48	15	1	$15624\ ^{2}_{1/2}$–$47389^{o}\ ^{3}_{1/2}$
3150.265	31734.17	40 *c*	5 *c*	$10516\ ^{3}_{1/2}$–$42250^{o}\ ^{2}_{1/2}$
3150.650	31730.29	8		$16133\ ^{4}_{1/2}$–$47864^{o}\ ^{3}_{1/2}$
3152.779	31708.86	3		$11063\ ^{2}_{1/2}$–$42771^{o}\ ^{3}_{1/2}$
3153.353	31703.09	20		$13252\ ^{2}_{1/2}$–$44955^{o}\ ^{1}_{1/2}$
3155.079	31685.75	2		$16133\ ^{4}_{1/2}$–$47819^{o}\ ^{4}_{1/2}$
3155.476	31681.76	5		$15770\ ^{1}_{1/2}$–$47452^{o}\ ^{2}_{1/2}$
3157.339	31663.07	5		$14733\ ^{4}_{1/2}$–$46396^{o}\ ^{3}_{1/2}$
3160.463	31631.77	2		$19791\ ^{4}_{1/2}$–$51423^{o}\ ^{3}_{1/2}$
3161.674	31619.66	300	8	$13252\ ^{2}_{1/2}$–$44872^{o}\ ^{2}_{1/2}$
3163.140	31605.00	12		$0\ ^{2}_{1/2}$–$31605^{o}\ ^{3}_{1/2}$
3165.003	31586.40	6		$10516\ ^{3}_{1/2}$–$42102^{o}\ ^{2}_{1/2}$
3166.993	31566.55	3		$20783\ ^{3}_{1/2}$–$52350^{o}\ ^{4}_{1/2}$
3168.271	31553.82	1		$17328\ ^{4}_{1/2}$–$48881^{o}\ ^{4}_{1/2}$
3170.484	31531.80	1		$16287\ ^{3}_{1/2}$–$47819^{o}\ ^{4}_{1/2}$

TABLE 3. *Classified lines of* Tc I

Wavelength A	Wavenumber cm^{-1}	Intensity		Energy levels cm^{-1}
		Arc	Spark	
3170.833	31528.33	3		$19895\ ^{2}_{1/2}$–$51423^{o}_{3/2}$
3173.295	31503.87	3000	100	$0\ ^{2}_{1/2}$–$31503^{o}_{1/2}$
3177.714	31460.06	6		$11063\ ^{2}_{1/2}$–$42523^{o}_{3/2}$
3180.305	31434.43	200	3	$13252\ ^{2}_{1/2}$–$44687^{o}_{3/2}$
3182.367	31414.06	2000	60	$0\ ^{2}_{1/2}$–$31414^{o}_{3/2}$
3183.108	31406.75	2000	60	$0\ ^{2}_{1/2}$–$31406^{o}_{2/2}$
3191.620	31322.99	10		$11578\ ^{1}_{1/2}$–$42901^{o}_{1/2}$
3192.051	31318.76	20		$16025\ ^{5}_{1/2}$–$47343^{o}_{4/2}$
3192.905	31310.38	2		$15298\ ^{3}_{1/2}$–$46608^{o}_{3/2}$
3195.485	31285.11	20		$13252\ ^{2}_{1/2}$–$44537^{o}_{2/2}$
3197.530	31265.10	40*w*		$3250\ ^{3}_{1/2}$–$34515^{o}_{2/2}$
3198.497	31255.65	15	3	$16133\ ^{4}_{1/2}$–$47389^{o}_{3/2}$
3200.980	31231.40	8		$11063\ ^{2}_{1/2}$–$42294^{o}_{2/2}$
3202.831	31213.35	300 *c*	6 *c*	$10516\ ^{3}_{1/2}$–$41729^{o}_{3/2}$
3205.474	31187.62	4		$11063\ ^{2}_{1/2}$–$42250^{o}_{2/2}$
3207.866	31164.36	4		$16287\ ^{3}_{1/2}$–$47452^{o}_{2/2}$
3208.270	31160.44	6		$16133\ ^{4}_{1/2}$–$47294^{o}_{3/2}$
3208.904	31154.28	5		$11063\ ^{2}_{1/2}$–$42217^{o}_{1/2}$
3209.838	31145.22	1		$21204\ ^{4}_{1/2}$–$52350^{o}_{4/2}$
3214.738	31097.75	3		$4178\ ^{0}_{1/2}$–$35276^{o}_{0/2}$
3215.764	31087.83	3		$31414^{o}_{3/2}$–$62501\ ^{3}_{1/2}$
3217.956	31066.65	2		$17146\ ^{5}_{1/2}$–$48213^{o}_{4/2}$
3218.559	31060.83	10		$13252\ ^{2}_{1/2}$–$44313^{o}_{1/2}$
3219.052	31056.07	3		$16287\ ^{3}_{1/2}$–$47343^{o}_{4/2}$
3220.737	31039.83	40	2	$11063\ ^{2}_{1/2}$–$42102^{o}_{2/2}$
3221.573	31031.77	1		$15624\ ^{2}_{1/2}$–$46656^{o}_{3/2}$
3223.762	31010.70	3		$11890\ ^{0}_{1/2}$–$42901^{o}_{1/2}$
3225.500	30993.99	2		$16287\ ^{3}_{1/2}$–$47281^{o}_{2/2}$
3226.044	30988.77	15		$13252\ ^{2}_{1/2}$–$44241^{o}_{2/2}$
3227.412	30975.63	4		$14733\ ^{4}_{1/2}$–$45708^{o}_{4/2}$
3230.640	30944.68	1		$16287\ ^{3}_{1/2}$–$47232^{o}_{2/2}$
3231.114	30940.14	15		$4002\ ^{1}_{1/2}$–$34942^{o}_{1/2}$
3236.439	30889.24	5		$17328\ ^{4}_{1/2}$–$48217^{o}_{3/2}$
3239.789	30857.30	5		$13252\ ^{2}_{1/2}$–$44110^{o}_{1/2}$
3241.837	30837.81	100	5	$13252\ ^{2}_{1/2}$–$44090^{o}_{3/2}$
3244.193	30815.41	500	15	$3700\ ^{2}_{1/2}$–$34515^{o}_{2/2}$
3249.600	30764.14	10		$4178\ ^{0}_{1/2}$–$34942^{o}_{1/2}$
3250.638	30754.32	10		$13252\ ^{2}_{1/2}$–$44007^{o}_{2/2}$
3252.048	30740.98	300	10	$16553\ ^{6}_{1/2}$–$47294^{o}_{2/2}$
3254.700	30715.93	10		$11578\ ^{1}_{1/2}$–$42294^{o}_{2/2}$
3256.102	30702.71	40	2	$14169\ ^{1}_{1/2}$–$44872^{o}_{2/2}$
3259.261	30672.95	3	1	$17146\ ^{5}_{1/2}$–$47819^{o}_{4/2}$
3259.910	30666.85	10	5	$11063\ ^{2}_{1/2}$–$41729^{o}_{3/2}$
3261.370	30653.12	20	3	$13252\ ^{2}_{1/2}$–$43905^{o}_{3/2}$
3262.896	30638.78	6	2 *h*	$11578\ ^{1}_{1/2}$–$42217^{o}_{1/2}$
3272.111	30552.50	10	2	$14169\ ^{1}_{1/2}$–$44722^{o}_{1/2}$
3276.29	30513.54	5		$4002\ ^{1}_{1/2}$–$34515^{o}_{2/2}$
3281.392	30466.09	6		$11063\ ^{2}_{1/2}$–$41529^{o}_{3/2}$
3291.960	30368.29	20	1	$16287\ ^{3}_{1/2}$–$46656^{o}_{3/2}$
3296.504	30326.43	10		$11890\ ^{0}_{1/2}$–$42217^{o}_{1/2}$

TABLE 3. *Classified lines of* Tc I

Wavelength A	Wavenumber cm^{-1}	Intensity		Energy levels cm^{-1}
		Arc	Spark	
3297.074	30321.19	3		$16287\ ^{3}_{1/2}$–$46608^{o}\ ^{3}_{1/2}$
3301.990	30276.05	20		$14679\ ^{0}_{1/2}$–$44955^{o}\ ^{1}_{1/2}$
3303.510	30262.12	6		$16133\ ^{4}_{1/2}$–$46396^{o}\ ^{3}_{1/2}$
3305.891	30240.32	80	10	$16415\ ^{2}_{1/2}$–$46656^{o}\ ^{3}_{1/2}$
3310.646	30196.89	200	15	$14679\ ^{0}_{1/2}$–$44876^{o}\ ^{1}_{1/2}$
3311.051	30193.20	20	2	$16415\ ^{2}_{1/2}$–$46608^{o}\ ^{3}_{1/2}$
3313.652	30169.50	150	5	$17282\ ^{3}_{1/2}$–$47452^{o}\ ^{2}_{1/2}$
3327.102	30047.54	150 *cw*	1 *c*	$2572\ ^{4}_{1/2}$–$32620^{o}\ ^{3}_{1/2}$
3327.665	30042.46	1		$14679\ ^{0}_{1/2}$–$44722^{o}\ ^{1}_{1/2}$
3328.252	30037.16	5		$11063\ ^{2}_{1/2}$–$41100^{o}\ ^{2}_{1/2}$
3330.766	30014.49	100	2	$13252\ ^{2}_{1/2}$–$43267^{o}\ ^{3}_{1/2}$
3332.468	29999.16	50	2	$17282\ ^{3}_{1/2}$–$47281^{o}\ ^{2}_{1/2}$
3337.486	29954.05	10	2 *h l*	$14733\ ^{4}_{1/2}$–$44687^{o}\ ^{3}_{1/2}$
3337.977	29949.65			$17282\ ^{3}_{1/2}$–$47232^{o}\ ^{2}_{1/2}$
3339.332	29937.50	6		$14169\ ^{1}_{1/2}$–$44107^{o}\ ^{2}_{1/2}$
3342.141	29912.34	3		$19903\ ^{3}_{1/2}$–$49815^{o}\ ^{4}_{1/2}$
3343.770	29897.76	10		$11890\ ^{0}_{1/2}$–$41788^{o}\ ^{1}_{1/2}$
3345.016	29886.63	15 *w*		$10516\ ^{3}_{1/2}$–$40403^{o}\ ^{4}_{1/2}$
3350.563	29837.15	60	3	$14169\ ^{1}_{1/2}$–$44007^{o}\ ^{2}_{1/2}$
3350.830	29834.77	50 *c*	1 *h*	$3250\ ^{3}_{1/2}$–$33085^{o}\ ^{2}_{1/2}$
3351.985	29824.49	1		$13252\ ^{2}_{1/2}$–$43077^{o}\ ^{3}_{1/2}$
3356.884	29780.97	8		$16287\ ^{3}_{1/2}$–$46068^{o}\ ^{4}_{1/2}$
3358.038	29770.73	12		$21450\ ^{4}_{1/2}$–$51221^{o}\ ^{3}_{1/2}$
3362.156	29734.27	1		$22615\ ^{3}_{1/2}$–$52350^{o}\ ^{4}_{1/2}$
3371.402	29652.73	5		$13252\ ^{2}_{1/2}$–$42905^{o}\ ^{2}_{1/2}$
3372.543	29642.70	8		$3700\ ^{2}_{1/2}$–$33343^{o}\ ^{1}_{1/2}$
3373.572	29633.66	25	1	$14679\ ^{0}_{1/2}$–$44313^{o}\ ^{1}_{1/2}$
3386.387	29521.52	20		$11578\ ^{1}_{1/2}$–$41100^{o}\ ^{2}_{1/2}$
3386.674	29519.02	40	1	$13252\ ^{2}_{1/2}$–$42771^{o}\ ^{3}_{1/2}$
3388.459	29503.47	8		$21920\ ^{2}_{1/2}$–$51423^{o}\ ^{3}_{1/2}$
3389.492	29494.47	12		$11578\ ^{1}_{1/2}$–$41073^{o}\ ^{1}_{1/2}$
3396.903	29430.13	60	1	$14679\ ^{0}_{1/2}$–$44110^{o}\ ^{1}_{1/2}$
3398.327	29417.80	300	6	$32620^{o}\ ^{3}_{1/2}$–$62038\ ^{3}_{1/2}$
3401.681	29388.79	25	1	$15298\ ^{3}_{1/2}$–$44687^{o}\ ^{3}_{1/2}$
3402.105	29385.13	200	4	$3700\ ^{2}_{1/2}$–$33085^{o}\ ^{2}_{1/2}$
3403.330	29374.55	3		$10516\ ^{3}_{1/2}$–$39891^{o}\ ^{2}_{1/2}$
3403.931	29369.37	200 *c*	2	$3250\ ^{3}_{1/2}$–$32620^{o}\ ^{3}_{1/2}$
3405.328	29357.32	80	5	$14733\ ^{4}_{1/2}$–$44090^{o}\ ^{3}_{1/2}$
3406.964	29343.22	10		$11063\ ^{2}_{1/2}$–$40406^{o}\ ^{3}_{1/2}$
3407.281	29340.49	80		$4002\ ^{1}_{1/2}$–$33343^{o}\ ^{1}_{1/2}$
3411.804	29301.60	40		$4178\ ^{0}_{1/2}$–$33480^{o}\ ^{0}_{1/2}$
3414.600	29277.60	10		$15298\ ^{3}_{1/2}$–$44576^{o}\ ^{4}_{1/2}$
3415.448	29270.34	15	1	$13252\ ^{2}_{1/2}$–$42523^{o}\ ^{3}_{1/2}$
3417.738	29250.72	10		$11578\ ^{1}_{1/2}$–$40829^{o}\ ^{0}_{1/2}$
3418.053	29248.03	20	1	$15624\ ^{2}_{1/2}$–$44872^{o}\ ^{2}_{1/2}$
3418.203	29246.75	40 *cw*	1	$10516\ ^{3}_{1/2}$–$39763^{o}\ ^{4}_{1/2}$
3418.581	29243.51	15		$22180\ ^{4}_{1/2}$–$51423^{o}\ ^{3}_{1/2}$
3419.451	29236.07	15		$11063\ ^{2}_{1/2}$–$40299^{o}\ ^{2}_{1/2}$
3420.583	29226.40	2		$19903\ ^{3}_{1/2}$–$49130^{o}\ ^{3}_{1/2}$
3425.382	29185.45	20		$15770\ ^{1}_{1/2}$–$44955^{o}\ ^{1}_{1/2}$

TABLE 3. *Classified lines of* Tc I

Wavelength A	Wavenumber cm^{-1}	Intensity		Energy levels cm^{-1}
		Arc	Spark	
3426.414	29176.66	3		$20639\ ^{5}_{1/2}-49815^{o}\ ^{4}_{1/2}$
3427.853	29164.41	60		$4178\ ^{0}_{1/2}-33343^{o}\ ^{1}_{1/2}$
3434.701	29106.27	200	4	$15770\ ^{1}_{1/2}-44876^{o}\ ^{1}_{1/2}$
3435.213	29101.93	20		$15770\ ^{1}_{1/2}-44872^{o}\ ^{2}_{1/2}$
3435.679	29097.98	40	1	$15624\ ^{2}_{1/2}-44722^{o}\ ^{1}_{1/2}$
3436.644	29089.81	3		$19791\ ^{4}_{1/2}-48881^{o}\ ^{4}_{1/2}$
3437.439	29083.08	150	1	$4002\ ^{1}_{1/2}-33085^{o}\ ^{2}_{1/2}$
3438.729	29072.18	80	1	$14733\ ^{4}_{1/2}-43805^{o}\ ^{3}_{1/2}$
3439.217	29068.05	3		$17328\ ^{4}_{1/2}-46396^{o}\ ^{3}_{1/2}$
3439.819	29062.96	12		$15624\ ^{2}_{1/2}-44687^{o}\ ^{3}_{1/2}$
3441.217	29051.16	3*w*		$10516\ ^{3}_{1/2}-39567^{o}\ ^{3}_{1/2}$
3442.337	29041.70	10		$13252\ ^{2}_{1/2}-42294^{o}\ ^{2}_{1/2}$
3443.472	29032.13	200 *c*	2	$2572\ ^{4}_{1/2}-31605^{o}\ ^{3}_{1/2}$
3449.897	28978.07	15		$19903\ ^{3}_{1/2}-48881^{o}\ ^{4}_{1/2}$
3451.050	28968.38	200	8	$15298\ ^{3}_{1/2}-44266^{o}\ ^{3}_{1/2}$
3451.507	28964.55	3		$13252\ ^{2}_{1/2}-42217^{o}\ ^{1}_{1/2}$
3453.020	28951.86	30	1	$15770\ ^{1}_{1/2}-44722^{o}\ ^{1}_{1/2}$
3454.073	28943.03	30	1	$15298\ ^{3}_{1/2}-44241^{o}\ ^{2}_{1/2}$
3454.623	28938.42	8		$11890\ ^{0}_{1/2}-40829^{o}\ ^{0}_{1/2}$
3456.849	28919.79	200	5	$3700\ ^{2}_{1/2}-32620^{o}\ ^{3}_{1/2}$
3457.243	28916.49	400	20	$14733\ ^{4}_{1/2}-43649^{o}\ ^{4}_{1/2}$
3457.603	28913.48	40	3	$15624\ ^{2}_{1/2}-44537^{o}\ ^{2}_{1/2}$
3465.212	28850.00	5		$13252\ ^{2}_{1/2}-42102^{o}\ ^{2}_{1/2}$
3466.278	28841.12	5000 *cw*	500 *cw*	$2572\ ^{4}_{1/2}-31414^{o}\ ^{3}_{1/2}$
3470.188	28808.63	10		$15298\ ^{3}_{1/2}-44107^{o}\ ^{2}_{1/2}$
3470.299	28807.71	5		$22615\ ^{3}_{1/2}-51423^{o}\ ^{3}_{1/2}$
3472.165	28792.23	30	6	$15298\ ^{3}_{1/2}-44090^{o}\ ^{3}_{1/2}$
3472.896	28786.17	15		$11063\ ^{2}_{1/2}-39849^{o}\ ^{3}_{1/2}$
3473.726	28779.29	20		$14733\ ^{4}_{1/2}-43512^{o}\ ^{3}_{1/2}$
3475.178	28767.26	80	2	$15770\ ^{1}_{1/2}-44537^{o}\ ^{2}_{1/2}$
3475.592	28763.84	1000	10	$3250\ ^{3}_{1/2}-32014^{o}\ ^{2}_{1/2}$
3477.838	28745.26	1		$20384\ ^{3}_{1/2}-49130^{o}\ ^{3}_{1/2}$
3478.432	28740.35	10		$13252\ ^{2}_{1/2}-41993^{o}\ ^{3}_{1/2}$
3479.452	28731.93	10		$14169\ ^{1}_{1/2}-42901^{o}\ ^{1}_{1/2}$
3482.288	28708.53	2*h*		$15298\ ^{3}_{1/2}-44007^{o}\ ^{2}_{1/2}$
3484.620	28689.32	60	1	$15624\ ^{2}_{1/2}-44313^{o}\ ^{1}_{1/2}$
3486.226	28676.10	1000 *c*	30 *c*	$3250\ ^{3}_{1/2}-31927^{o}\ ^{2}_{1/2}$
3490.299	28642.64	100	2	$15624\ ^{2}_{1/2}-44266^{o}\ ^{3}_{1/2}$
3493.394	28617.26	400	5	$15624\ ^{2}_{1/2}-44241^{o}\ ^{2}_{1/2}$
3494.168	28610.92	20	1	$21204\ ^{4}_{1/2}-49815^{o}\ ^{4}_{1/2}$
3494.623	28607.20	500	4	$15298\ ^{3}_{1/2}-43905^{o}\ ^{3}_{1/2}$
3500.161	28561.94	6		$17146\ ^{5}_{1/2}-45708^{o}\ ^{4}_{1/2}$
3500.704	28557.51	1000	20	$3700\ ^{2}_{1/2}-32258^{o}\ ^{1}_{1/2}$
3501.241	28553.13	200	2	$3700\ ^{2}_{1/2}-32253^{o}\ ^{1}_{1/2}$
3501.507	28550.96	20	10*h*	$16025\ ^{5}_{1/2}-44576^{o}\ ^{4}_{1/2}$
3502.467	28543.13	80	2	$15770\ ^{1}_{1/2}-44313^{o}\ ^{1}_{1/2}$
3502.704	28541.20	800 *c*	20 *c*	$2572\ ^{4}_{1/2}-31114^{o}\ ^{4}_{1/2}$
3503.336	28536.05	30	20*hw*	$13252\ ^{2}_{1/2}-41788^{o}\ ^{1}_{1/2}$
3503.586	28534.02	30		$14733\ ^{4}_{1/2}-43267^{o}\ ^{3}_{1/2}$
3503.786	28532.39	40		$14733\ ^{4}_{1/2}-43265^{o}\ ^{4}_{1/2}$

318-092 O-69—2

TABLE 3. *Classified lines of* Tc I

Wavelength A	Wavenumber cm^{-1}	Intensity		Energy levels cm^{-1}
		Arc	Spark	
3505.558	28517.97	3		$11578\ ^{1}_{1/2}-40096^{o}_{1/2}$
3506.114	28513.44	50	1	$11063\ ^{2}_{1/2}-39576^{o}_{1/2}$
3506.931	28506.80	10		$15298\ ^{3}_{1/2}-43805^{o}_{3/2}$
3507.187	28504.72	100 *c*	1	$11063\ ^{2}_{1/2}-39567^{o}_{3/2}$
3508.271	28495.91	100	1	$19791\ ^{4}_{1/2}-48287^{o}_{5/2}$
3509.519	28485.78	4		$15624\ ^{2}_{1/2}-44110^{o}_{1/2}$
3509.869	28482.94	2		$15624\ ^{2}_{1/2}-44107^{o}_{2/2}$
3510.594	28477.06	10		$13252\ ^{2}_{1/2}-41729^{o}_{3/2}$
3511.328	28471.11	20		$15770\ ^{1}_{1/2}-44241^{o}_{2/2}$
3511.919	28466.31	20	1	$15624\ ^{2}_{1/2}-44090^{o}_{3/2}$
3512.546	28461.23	5		$16415\ ^{2}_{1/2}-44876^{o}_{1/2}$
3512.768	28459.44	6		$20639\ ^{5}_{1/2}-49098^{o}_{4/2}$
3514.700	28443.79	2		$20686\ ^{2}_{1/2}-49130^{o}_{3/2}$
3515.174	28439.96	12	1	$19702\ ^{1}_{1/2}-48142^{o}_{2/2}$
3517.206	28423.53	40	1	$16415\ ^{2}_{1/2}-44839^{o}_{3/2}$
3517.442	28421.62	10		$19791\ ^{4}_{1/2}-48213^{o}_{4/2}$
3520.054	28400.53	30 *c*		$4002\ ^{1}_{1/2}-32403^{o}_{0/2}$
3520.276	28398.74	20		$11578\ ^{1}_{1/2}-39977^{o}_{2/2}$
3520.514	28396.82	30 *c*		$11063\ ^{2}_{1/2}-39459^{o}_{2/2}$
3522.275	28382.62	30		$15624\ ^{2}_{1/2}-44007^{o}_{2/2}$
3522.516	28380.68	15		$17328\ ^{4}_{1/2}-45708^{o}_{4/2}$
3524.523	28364.52	20	1	$14733\ ^{4}_{1/2}-43097^{o}_{4/2}$
3525.828	28354.02	800	15	$3250\ ^{3}_{1/2}-31605^{o}_{3/2}$
3526.178	28351.21	300	5	$15298\ ^{3}_{1/2}-43649^{o}_{4/2}$
3527.626	28339.57	50	2	$15770\ ^{1}_{1/2}-44110^{o}_{1/2}$
3527.976	28336.76	30		$15770\ ^{1}_{1/2}-44107^{o}_{2/2}$
3529.829	28321.88	100	2	$19895\ ^{2}_{1/2}-48217^{o}_{3/2}$
3530.813	28313.99	10		$3700\ ^{2}_{1/2}-32014^{o}_{2/2}$
3531.002	28312.480	3		$11578\ ^{1}_{1/2}-39891^{o}_{2/2}$
3531.318	28309.94	15		$19903\ ^{3}_{1/2}-48213^{o}_{4/2}$
3531.733	28306.62	3		$16415\ ^{2}_{1/2}-44722^{o}_{1/2}$
3534.878	28281.43	150	3	$15624\ ^{2}_{1/2}-43905^{o}_{3/2}$
3535.506	28276.41	500	12	$13252\ ^{2}_{1/2}-41529^{o}_{3/2}$
3538.119	28255.53	300		$4002\ ^{1}_{1/2}-32258^{o}_{1/2}$
3538.678	28251.06	800	3	$4002\ ^{1}_{1/2}-32253^{o}_{1/2}$
3539.148	28247.31	20		$19895\ ^{2}_{1/2}-48142^{o}_{2/2}$
3539.759	28242.44	12		$20639\ ^{5}_{1/2}-48881^{o}_{4/2}$
3540.174	28239.12	1		$19903\ ^{3}_{1/2}-48142^{o}_{2/2}$
3541.772	28226.38	2000 *c*	20 *c*	$3700\ ^{2}_{1/2}-31927^{o}_{2/2}$
3544.382	28205.60	20	1	$11890\ ^{0}_{1/2}-40096^{o}_{1/2}$
3549.725	28163.15	6000 *c*	60 *c*	$3250\ ^{3}_{1/2}-31414^{o}_{3/2}$
3550.645	28155.85	4000 *c*	40 *c*	$3250\ ^{3}_{1/2}-31406^{o}_{2/2}$
3551.206	28151.40	30		$0\ ^{2}_{1/2}-28151^{o}_{1/2}$
3553.539	28132.92	60	1	$16133\ ^{4}_{1/2}-44266^{o}_{3/2}$
3554.580	28124.68	30		$14169\ ^{1}_{1/2}-42294^{o}_{2/2}$
3554.919	28122.00	2		$16415\ ^{2}_{1/2}-44537^{o}_{2/2}$
3556.056	28113.01	40	2 *h*	$16025\ ^{5}_{1/2}-44138^{o}_{5/2}$
3558.209	28096.00	2		$21719\ ^{5}_{1/2}-49815^{o}_{4/2}$
3559.754	28083.80	300	5	$14733\ ^{4}_{1/2}-42817^{o}_{4/2}$
3560.319	28079.35	800	15	$4178\ ^{0}_{1/2}-32258^{o}_{1/2}$

TABLE 3. *Classified lines of* Tc I

Wavelength A	Wavenumber cm^{-1}	Intensity		Energy levels cm^{-1}
		Arc	Spark	
3560.876	28074.95	50		$4178\ ^{0}{}_{1/2}-32253^{o}{}_{1/2}$
3561.192	28072.46	50	1	$19791\ ^{4}{}_{1/2}-47864^{o}{}_{3/2}$
3562.303	28063.71	4		$21752\ ^{3}{}_{1/2}-49815^{o}{}_{4/2}$
3564.359	28047.52	5		$14169\ ^{1}{}_{1/2}-42217^{o}{}_{1/2}$
3565.217	28040.77	100	1	$14733\ ^{4}{}_{1/2}-42773^{o}{}_{3/2}$
3565.490	28038.62	80	1	$14733\ ^{4}{}_{1/2}-42771^{o}{}_{3/2}$
3566.883	28027.67	3		$19791\ ^{4}{}_{1/2}-47819^{o}{}_{4/2}$
3568.853	28012.20	800	5	$4002\ ^{1}{}_{1/2}-32014^{o}{}_{2/2}$
3570.654	27998.08	100	1	$11578\ ^{1}{}_{1/2}-39576^{o}{}_{1/2}$
3570.654	27998.08	100	1	$13252\ ^{2}{}_{1/2}-41250^{o}{}_{1/2}$
3573.083	27979.04	50		$16287\ ^{3}{}_{1/2}-44266^{o}{}_{3/2}$
3574.410	27968.66	25		$15298\ ^{3}{}_{1/2}-43267^{o}{}_{3/2}$
3574.610	27967.09	80	1	$15298\ ^{3}{}_{1/2}-43265^{o}{}_{4/2}$
3575.420	27960.76	100	1	$19903\ ^{3}{}_{1/2}-47864^{o}{}_{3/2}$
3575.964	27956.50	20		$16133\ ^{4}{}_{1/2}-44090^{o}{}_{3/2}$
3576.324	27953.69	50		$16287\ ^{3}{}_{1/2}-44241^{o}{}_{2/2}$
3577.228	27946.62	6		$16025\ ^{5}{}_{1/2}-43971^{o}{}_{4/2}$
3577.986	27940.70	15		$0\ ^{2}{}_{1/2}-27940^{o}{}_{2/2}$
3578.969	27933.03	60		$14169\ ^{1}{}_{1/2}-42102^{o}{}_{2/2}$
3580.059	27924.52	1000	10 *c*	$4002\ ^{1}{}_{1/2}-31927^{o}{}_{2/2}$
3581.258	27915.18	1000	10 *c*	$16428^{o}{}_{2/2}-44343\ ^{3}{}_{1/2}$
3581.744	27911.39	10		$20231\ ^{1}{}_{1/2}-48142^{o}{}_{2/2}$
3582.075	27908.81	800	4	$16428^{o}{}_{2/2}-44337\ ^{2}{}_{1/2}$
3582.628	27904.50	2000	10	$3700\ ^{2}{}_{1/2}-31605^{o}{}_{3/2}$
3582.628	27904.50	2000	10	$16428^{o}{}_{2/2}-44333\ ^{1}{}_{1/2}$
3583.464	27897.99	12		$16415\ ^{2}{}_{1/2}-44313^{o}{}_{1/2}$
3584.005	27893.78	1		$21204\ ^{4}{}_{1/2}-49098^{o}{}_{4/2}$
3585.684	27880.72	30	1	$14733\ ^{4}{}_{1/2}-42613^{o}{}_{4/2}$
3587.386	27867.49	1		$14733\ ^{4}{}_{1/2}-42600^{o}{}_{3/2}$
3587.942	27863.17	4000	40	$3250\ ^{3}{}_{1/2}-31114^{o}{}_{4/2}$
3589.471	27851.31	15		$16415\ ^{2}{}_{1/2}-44266^{o}{}_{3/2}$
3591.222	27837.73	50	1	$16133\ ^{4}{}_{1/2}-43971^{o}{}_{4/2}$
3591.483	27835.70	80	4	$13252\ ^{2}{}_{1/2}-41088^{o}{}_{3/2}$
3591.942	27832.15	8 *cw*		$16025\ ^{5}{}_{1/2}-43857^{o}{}_{6/2}$
3593.580	27819.46	10		$16287\ ^{3}{}_{1/2}-44107^{o}{}_{2/2}$
3594.573	27811.78	300	4	$14733\ ^{4}{}_{1/2}-42545^{o}{}_{4/2}$
3594.908	27809.18	50 *cw*		$2572\ ^{4}{}_{1/2}-30382^{o}{}_{3/2}$
3595.661	27803.36	1000 *cw*	10 *cw*	$3700\ ^{2}{}_{1/2}-31503^{o}{}_{1/2}$
3596.181	27799.34	4		$15298\ ^{3}{}_{1/2}-43097^{o}{}_{4/2}$
3597.401	27789.91	12		$14733\ ^{4}{}_{1/2}-42523^{o}{}_{3/2}$
3598.830	27778.88	30		$15298\ ^{3}{}_{1/2}-43077^{o}{}_{3/2}$
3599.750	27771.78	50	1	$16133\ ^{4}{}_{1/2}-43905^{o}{}_{3/2}$
3602.191	27752.96	20	1	$14169\ ^{1}{}_{1/2}-41922^{o}{}_{2/2}$
3602.639	27749.51	1		$19702\ ^{1}{}_{1/2}-47452^{o}{}_{2/2}$
3605.938	27724.12	15		$10516\ ^{3}{}_{1/2}-38240^{o}{}_{3/2}$
3607.321	27713.49	1000 *c*	30 *c*	$3700\ ^{2}{}_{1/2}-31414^{o}{}_{3/2}$
3607.625	27711.16	200	5	$14733\ ^{4}{}_{1/2}-42444^{o}{}_{3/2}$
3608.271	27706.20	2000 *c*	80 *c*	$3700\ ^{2}{}_{1/2}-31406^{o}{}_{2/2}$
3609.045	27700.26	60		$10516\ ^{3}{}_{1/2}-38216^{o}{}_{2/2}$
3609.843	27694.13	6		$20523\ ^{2}{}_{1/2}-48217^{o}{}_{3/2}$

TABLE 3. *Classified lines of* Tc I

Wavelength A	Wavenumber cm^{-1}	Intensity		Energy levels cm^{-1}
		Arc	Spark	
3611.156	27684.06	50		$16287\ ^{3}_{1/2}-43971^{o}_{4_{1/2}}$
3612.108	27676.77	60		$21204\ ^{4}_{1/2}-48881^{o}_{4_{1/2}}$
3612.346	27674.94	3		$16415\ ^{2}_{1/2}-44090^{o}_{3_{1/2}}$
3612.833	27671.21	4	3*h*	$16133\ ^{4}_{1/2}-43805^{o}_{3_{1/2}}$
3614.282	27660.12	15		$0\ ^{2}_{1/2}-27660^{o}_{3_{1/2}}$
3615.814	27648.40	50	1	$20639\ ^{5}_{1/2}-48287^{o}_{3_{1/2}}$
3616.528	27642.94	30		$15624\ ^{2}_{1/2}-43267^{o}_{3_{1/2}}$
3618.943	27624.50	200	3	$16025\ ^{5}_{1/2}-43649^{o}_{4_{1/2}}$
3619.664	27618.99	20		$14169\ ^{1}_{1/2}-41788^{o}_{4_{1/2}}$
3622.453	27597.73	1		$19791\ ^{4}_{1/2}-47389^{o}_{3_{1/2}}$
3623.508	27589.69	5		$17282\ ^{3}_{1/2}-44872^{o}_{2_{1/2}}$
3625.555	27574.12	150	3	$20639\ ^{5}_{1/2}-48213^{o}_{4_{1/2}}$
3626.294	27568.50	10		$13252\ ^{2}_{1/2}-40821^{o}_{2_{1/2}}$
3627.364	27560.37	1000 *c*	10 *c*	$2572\ ^{4}_{1/2}-30133^{o}_{4_{1/2}}$
3627.858	27556.61	100	2	$17282\ ^{3}_{1/2}-44839^{o}_{3_{1/2}}$
3628.476	27551.92	2		$19791\ ^{4}_{1/2}-47343^{o}_{4_{1/2}}$
3628.901	27548.69	30	1	$19903\ ^{3}_{1/2}-47452^{o}_{2_{1/2}}$
3630.388	27537.41	200	2	$14679\ ^{0}_{1/2}-42217^{o}_{1_{1/2}}$
3631.227	27531.05	2		$20686\ ^{2}_{1/2}-48217^{o}_{3_{1/2}}$
3633.244	27515.76	150	2	$16133\ ^{4}_{1/2}-43649^{o}_{4_{1/2}}$
3635.146	27501.37	3000 *c*	50 *c*	$4002\ ^{1}_{1/2}-31503^{o}_{1_{1/2}}$
3636.070	27494.38	10000 *c*	500 *c*	$2572\ ^{4}_{1/2}-30067^{o}_{3_{1/2}}$
3637.447	27483.97	8		$14733\ ^{4}_{1/2}-42217^{o}_{4_{1/2}}$
3638.012	27479.70	1		$20384\ ^{3}_{1/2}-47864^{o}_{3_{1/2}}$
3638.220	27478.13	1000	15	$16874^{o}_{3_{1/2}}-44352\ ^{4}_{1/2}$
3638.848	27473.39	200	4	$15298\ ^{3}_{1/2}-42771^{o}_{3_{1/2}}$
3639.379	27469.38	900	15	$16874^{o}_{3_{1/2}}-44343\ ^{3}_{1/2}$
3640.226	27462.99	400	10	$16874^{o}_{3_{1/2}}-44337\ ^{2}_{1/2}$
3641.093	27456.45	6	1	$20686\ ^{2}_{1/2}-48142^{o}_{2_{1/2}}$
3641.183	27455.77	15	1	$14169\ ^{1}_{1/2}-41625^{o}_{1_{1/2}}$
3641.534	27453.13	30	1	$15624\ ^{2}_{1/2}-43077^{o}_{3_{1/2}}$
3643.376	27439.25	10		$20231\ ^{1}_{1/2}-47670^{o}_{0_{1/2}}$
3643.950	27434.92	8		$20384\ ^{3}_{1/2}-47819^{o}_{4_{1/2}}$
3644.134	27433.54	50	2	$20783\ ^{3}_{1/2}-48217^{o}_{3_{1/2}}$
3644.427	27431.33	3		$21450\ ^{4}_{1/2}-48881^{o}_{4_{1/2}}$
3648.040	27404.17	1000 *c*	50 *c*	$4002\ ^{1}_{1/2}-31406^{o}_{2_{1/2}}$
3648.860	27398.01	10		$15298\ ^{3}_{1/2}-42696^{o}_{2_{1/2}}$
3650.344	27386.87	60	2	$15624\ ^{2}_{1/2}-43011^{o}_{2_{1/2}}$
3651.467	27378.45	600	20	$16133\ ^{4}_{1/2}-43512^{o}_{3_{1/2}}$
3654.054	27359.07	10	1	$17328\ ^{4}_{1/2}-44687^{o}_{3_{1/2}}$
3656.458	27341.08	1		$20523\ ^{2}_{1/2}-47864^{o}_{3_{1/2}}$
3658.588	27325.16	1000 *c*	60 *c*	$4178\ ^{0}_{1/2}-31503^{o}_{1_{1/2}}$
3659.882	27315.50	3		$15298\ ^{3}_{1/2}-42613^{o}_{4_{1/2}}$
3661.452	27303.79	400 *c*	30 *c*	$16553\ ^{6}_{1/2}-43857^{o}_{6_{1/2}}$
3662.032	27299.46	6		$14733\ ^{4}_{1/2}-42032^{o}_{3_{1/2}}$
3662.838	27293.46	30	1	$17282\ ^{3}_{1/2}-44576^{o}_{4_{1/2}}$
3663.091	27291.57	8		$25058\ ^{3}_{1/2}-52350^{o}_{4_{1/2}}$
3664.455	27281.41	6		$15624\ ^{2}_{1/2}-42905^{o}_{2_{1/2}}$
3664.916	27277.98	200	2	$3250\ ^{3}_{1/2}-30528^{o}_{2_{1/2}}$
3667.349	27259.88	10		$14733\ ^{4}_{1/2}-41993^{o}_{3_{1/2}}$

TABLE 3. *Classified lines of* Tc I

Wavelength A	Wavenumber cm^{-1}	Intensity		Energy levels cm^{-1}
		Arc	Spark	
3667.510	27258.69	30	1	$16287\ ^{3}_{1/2}-43546^{o}\ _{2_{1/2}}$
3667.794	27256.58	10		$11063\ ^{2}_{1/2}-38319^{o}\ _{1_{1/2}}$
3667.991	27255.11	10		$17282\ ^{3}_{1/2}-44537^{o}\ _{2_{1/2}}$
3668.940	27248.06	20	1	$17328\ ^{4}_{1/2}-44576^{o}\ _{4_{1/2}}$
3669.152	27246.49	40	2	$15298\ ^{3}_{1/2}-42545^{o}\ _{4_{1/2}}$
3669.918	27240.80	40	1*h*	$15770\ ^{1}_{1/2}-43011^{o}\ _{2_{1/2}}$
3672.087	27224.71	8		$15298\ ^{3}_{1/2}-42523^{o}\ _{3_{1/2}}$
3675.003	27203.11	3		$19827\ ^{0}_{1/2}-47030^{o}\ _{1_{1/2}}$
3675.003	27203.11	3		$21926\ ^{2}_{1/2}-49130^{o}\ _{3_{1/2}}$
3675.429	27199.96	30		$22615\ ^{3}_{1/2}-49815^{o}\ _{4_{1/2}}$
3678.089	27180.29	80	2	$20639\ ^{5}_{1/2}-47819^{o}\ _{4_{1/2}}$
3678.388	27178.08	70	2	$20686\ ^{2}_{1/2}-47864^{o}\ _{3_{1/2}}$
3679.146	27172.48	1000	30	$16025\ ^{5}_{1/2}-43197^{o}\ _{6_{1/2}}$
3680.318	27163.83	300	6	$14733\ ^{4}_{1/2}-41897^{o}\ _{4_{1/2}}$
3680.575	27161.93	50		$21719\ ^{5}_{1/2}-48881^{o}\ _{4_{1/2}}$
3681.683	27153.76	40		$11063\ ^{2}_{1/2}-38216^{o}\ _{2_{1/2}}$
3682.592	27147.05	100	2	$16025\ ^{5}_{1/2}-43172^{o}\ _{5_{1/2}}$
3684.744	27131.20	5000	100	$3250\ ^{3}_{1/2}-30382^{o}\ _{3_{1/2}}$
3687.772	27108.92	20	1	$14679\ ^{0}_{1/2}-41788^{o}\ _{1_{1/2}}$
3691.324	27082.84	1		$21204\ ^{4}_{1/2}-48287^{o}\ _{3_{1/2}}$
3692.759	27072.31	300	4	$15624\ ^{2}_{1/2}-42696^{o}\ _{2_{1/2}}$
3693.400	27067.62	8		$20384\ ^{3}_{1/2}-47452^{o}\ _{2_{1/2}}$
3695.734	27050.52	1		$20231\ ^{1}_{1/2}-47281^{o}\ _{2_{1/2}}$
3696.297	27046.40	150	3	$13252\ ^{2}_{1/2}-40299^{o}\ _{2_{1/2}}$
3697.415	27038.22	100	1	$16133\ ^{4}_{1/2}-43172^{o}\ _{5_{1/2}}$
3697.736	27035.88	30	1	$20783\ ^{3}_{1/2}-47819^{o}\ _{4_{1/2}}$
3701.478	27008.54	5	1	$21204\ ^{4}_{1/2}-48213^{o}\ _{4_{1/2}}$
3701.966	27004.98	1		$20384\ ^{3}_{1/2}-47389^{o}\ _{3_{1/2}}$
3703.830	26991.39	800	20	$17146\ ^{5}_{1/2}-44138^{o}\ _{5_{1/2}}$
3704.797	26984.35	300	5	$17282\ ^{3}_{1/2}-44266^{o}\ _{3_{1/2}}$
3705.481	26979.37	100	2	$16287\ ^{3}_{1/2}-43267^{o}\ _{3_{1/2}}$
3705.712	26977.69	80	1	$16287\ ^{3}_{1/2}-43265^{o}\ _{4_{1/2}}$
3706.705	26970.46	200	4	$14733\ ^{4}_{1/2}-41703^{o}\ _{4_{1/2}}$
3707.627	26963.75	200	5	$16133\ ^{4}_{1/2}-43097^{o}\ _{4_{1/2}}$
3708.261	26959.14	200	3	$16553\ ^{6}_{1/2}-43512^{o}\ _{5_{1/2}}$
3709.226	26952.13	2		$15298\ ^{3}_{1/2}-42250^{o}\ _{2_{1/2}}$
3709.527	26949.94	15		$22180\ ^{4}_{1/2}-49130^{o}\ _{3_{1/2}}$
3709.831	26947.73	80	1	$15298\ ^{3}_{1/2}-42246^{o}\ _{3_{1/2}}$
3710.126	26945.59	90	2	$14679\ ^{0}_{1/2}-41625^{o}\ _{1_{1/2}}$
3710.428	26943.40	4		$16133\ ^{4}_{1/2}-43077^{o}\ _{3_{1/2}}$
3711.048	26938.90	2		$17328\ ^{4}_{1/2}-44266^{o}\ _{3_{1/2}}$
3711.388	26936.43	80	1	$21206\ ^{2}_{1/2}-48142^{o}\ _{2_{1/2}}$
3712.256	26930.13	1000	10	$3700\ ^{2}_{1/2}-30630^{o}\ _{1_{1/2}}$
3712.819	26926.05	300	3	$15770\ ^{1}_{1/2}-42696^{o}\ _{2_{1/2}}$
3713.838	26918.66	25		$15298\ ^{3}_{1/2}-42217^{o}\ _{4_{1/2}}$
3715.944	26903.41	500	5	$14169\ ^{1}_{1/2}-41073^{o}\ _{1_{1/2}}$
3716.809	26897.14	20	2	$20384\ ^{3}_{1/2}-47281^{o}\ _{2_{1/2}}$
3718.861	26882.30	10000	300	$3250\ ^{3}_{1/2}-30133^{o}\ _{4_{1/2}}$
3721.056	26866.45	3		$20523\ ^{2}_{1/2}-47389^{o}\ _{3_{1/2}}$
3723.132	26851.47	40		$16415\ ^{2}_{1/2}-43267^{o}\ _{3_{1/2}}$

TABLE 3. *Classified lines of* Tc I

Wavelength A	Wavenumber cm^{-1}	Intensity		Energy levels cm^{-1}
		Arc	Spark	
3723.674	26847.56	1500	15	$14733\ ^{4}_{1/2}-41580^{o}_{5/2}$
3724.176	26843.94	10		$13252\ ^{2}_{1/2}-40096^{o}_{1/2}$
3724.395	26842.36	2000	20	$17522^{o}_{4/2}-44365\ ^{5}_{1/2}$
3725.082	26837.41	20		$21450\ ^{4}_{1/2}-48287^{o}_{5/2}$
3726.152	26829.70	100	2	$17522^{o}_{4/2}-44352\ ^{4}_{1/2}$
3726.351	26828.27	5000	40	$3700\ ^{2}_{1/2}-30528^{o}_{2/2}$
3727.364	26820.98	200		$17522^{o}_{4/2}-44343\ ^{3}_{1/2}$
3728.886	26810.03	30		$16287\ ^{3}_{1/2}-43097^{o}_{4/2}$
3728.886	26810.03	30		$17328\ ^{4}_{1/2}-44138^{o}_{5/2}$
3729.177	26807.94	400 *c*	5 *c*	$17282\ ^{3}_{1/2}-44090^{o}_{3/2}$
3730.358	26799.45	10		$20231\ ^{1}_{1/2}-47030^{o}_{1/2}$
3730.836	26796.02	60	1	$14733\ ^{4}_{1/2}-41529^{o}_{3/2}$
3731.412	26791.88	8		$16025\ ^{5}_{1/2}-42817^{o}_{4/2}$
3731.735	26789.56	500	3	$16287\ ^{3}_{1/2}-43077^{o}_{3/2}$
3735.501	26762.56	30		$17328\ ^{4}_{1/2}-44090^{o}_{3/2}$
3735.753	26760.75	4		$19895\ ^{2}_{1/2}-46656^{o}_{3/2}$
3737.420	26748.82	300	2	$16025\ ^{5}_{1/2}-42773^{o}_{5/2}$
3738.501	26741.08	20		$11578\ ^{1}_{1/2}-38319^{o}_{1/2}$
3740.988	26723.30	2		$16287\ ^{3}_{1/2}-43011^{o}_{2/2}$
3742.789	26710.45	150	3	$17146\ ^{5}_{1/2}-43857^{o}_{6/2}$
3743.508	26705.32	1		$19903\ ^{3}_{1/2}-46608^{o}_{3/2}$
3743.610	26704.59	2		$20639\ ^{5}_{1/2}-47343^{o}_{4/2}$
3744.026	26701.62	150	2	$22180\ ^{4}_{1/2}-48881^{o}_{4/2}$
3745.012	26694.59	400	5	$15298\ ^{3}_{1/2}-41993^{o}_{3/2}$
3746.148	26686.50	1000	10	$4002\ ^{1}_{1/2}-30689^{o}_{0/2}$
3746.640	26682.99	100	2	$16133\ ^{4}_{1/2}-42817^{o}_{4/2}$
3746.845	26681.53	5000	150	$3700\ ^{2}_{1/2}-30382^{o}_{3/2}$
3749.634	26661.69	10		$16415\ ^{2}_{1/2}-43077^{o}_{3/2}$
3749.928	26659.60	60	4	$14169\ ^{1}_{1/2}-40829^{o}_{0/2}$
3750.566	26655.06	6		$20639\ ^{5}_{1/2}-47294^{o}_{5/2}$
3751.056	26651.58	6		$14169\ ^{1}_{1/2}-40821^{o}_{2/2}$
3752.134	26643.92	1000	10	$17328\ ^{4}_{1/2}-43971^{o}_{4/2}$
3752.944	26638.17	20		$11578\ ^{1}_{1/2}-38216^{o}_{2/2}$
3754.368	26628.07	4000	40	$4002\ ^{1}_{1/2}-30630^{o}_{1/2}$
3755.221	26622.02	80	3	$15624\ ^{2}_{1/2}-42246^{o}_{3/2}$
3757.722	26604.30	3		$19791\ ^{4}_{1/2}-46396^{o}_{3/2}$
3758.535	26598.55	1000	10	$15298\ ^{3}_{1/2}-41897^{o}_{4/2}$
3758.948	26595.63	5		$20686\ ^{2}_{1/2}-47281^{o}_{2/2}$
3758.948	26595.63	5		$16415\ ^{2}_{1/2}-43011^{o}_{2/2}$
3759.305	26593.10	5		$15624\ ^{2}_{1/2}-42217^{o}_{1/2}$
3759.553	26591.35	20	1	$13252\ ^{2}_{1/2}-39844^{o}_{1/2}$
3761.481	26577.72	8		$17328\ ^{4}_{1/2}-43905^{o}_{3/2}$
3761.807	26575.41	2000	20	$16025\ ^{5}_{1/2}-42600^{o}_{3/2}$
3762.880	26567.84	6		$21719\ ^{5}_{1/2}-48287^{o}_{5/2}$
3763.974	26560.11	40	1	$20783\ ^{3}_{1/2}-47343^{o}_{4/2}$
3765.962	26546.09	2		$20686\ ^{2}_{1/2}-47232^{o}_{2/2}$
3768.365	26529.17	30		$16287\ ^{3}_{1/2}-42817^{o}_{4/2}$
3768.774	26526.29	5000	100	$4002\ ^{1}_{1/2}-30528^{o}_{2/2}$
3769.680	26519.91	3		$16025\ ^{5}_{1/2}-42545^{o}_{4/2}$
3770.498	26514.16	15		$22615\ ^{3}_{1/2}-49130^{o}_{3/2}$

TABLE 3. *Classified lines of* Tc I

Wavelength A	Wavenumber cm^{-1}	Intensity		Energy levels cm^{-1}
		Arc	Spark	
3771.031	26510.41	3000	50	$4178\ ^{0}_{1/2}-30689^{o}\ _{0_{1/2}}$
3771.467	26507.35	4		$20523\ ^{2}_{1/2}-47030^{o}\ _{1_{1/2}}$
3772.088	26502.98	60	2	$17146\ ^{5}_{1/2}-43649^{o}\ _{4_{1/2}}$
3772.388	26500.88	40	2	$19895\ ^{2}_{1/2}-46396^{o}\ _{3_{1/2}}$
3772.782	26498.11	20	1	$20783\ ^{3}_{1/2}-47281^{o}\ _{2_{1/2}}$
3773.413	26493.68	50	4	$21719\ ^{5}_{1/2}-48213^{o}\ _{4_{1/2}}$
3773.930	26490.05	1		$16415\ ^{2}_{1/2}-42905^{o}\ _{2_{1/2}}$
3774.783	26484.06	15		$16287\ ^{3}_{1/2}-42771^{o}\ _{3_{1/2}}$
3774.970	26482.75	10		$22615\ ^{3}_{1/2}-49098^{o}\ _{4_{1/2}}$
3775.355	26480.05	50 *c*	1	$16133\ ^{4}_{1/2}-42613^{o}\ _{4_{1/2}}$
3775.560	26478.61	15		$15624\ ^{2}_{1/2}-42102^{o}\ _{2_{1/2}}$
3777.274	26466.60	500	10	$16133\ ^{4}_{1/2}-42600^{o}\ _{5_{1/2}}$
3779.373	26451.90	2000	40	$4178\ ^{0}_{1/2}-30630^{o}\ _{1_{1/2}}$
3779.693	26449.66	40	1	$16025\ ^{5}_{1/2}-42474^{o}\ _{6_{1/2}}$
3782.299	26431.43	15		$15298\ ^{3}_{1/2}-41729^{o}\ _{3_{1/2}}$
3784.057	26419.16	500	6	$16025\ ^{5}_{1/2}-42444^{o}\ _{5_{1/2}}$
3784.802	26413.96	1		$21450\ ^{4}_{1/2}-47864^{o}\ _{3_{1/2}}$
3785.222	26411.02	20	1	$16133\ ^{4}_{1/2}-42545^{o}\ _{4_{1/2}}$
3785.560	26408.67	6		$16287\ ^{3}_{1/2}-42696^{o}\ _{2_{1/2}}$
3786.064	26405.15	200	3	$15298\ ^{3}_{1/2}-41703^{o}\ _{4_{1/2}}$
3786.494	26402.15	10		$19702\ ^{1}_{1/2}-46104^{o}\ _{2_{1/2}}$
3787.772	26393.24	1		$14679\ ^{0}_{1/2}-41073^{o}\ _{1_{1/2}}$
3788.154	26390.58	2		$21752\ ^{3}_{1/2}-48142^{o}\ _{2_{1/2}}$
3788.370	26389.08	1		$16133\ ^{4}_{1/2}-42523^{o}\ _{3_{1/2}}$
3791.282	26368.81	500	8	$15624\ ^{2}_{1/2}-41993^{o}\ _{3_{1/2}}$
3791.524	26367.13	3		$17282\ ^{3}_{1/2}-43649^{o}\ _{4_{1/2}}$
3791.734	26365.67	300	7	$17146\ ^{5}_{1/2}-43512^{o}\ _{3_{1/2}}$
3792.774	26358.44	1		$23455^{o}\ _{2_{1/2}}-49813\ ^{2}_{1/2}$
3793.087	26356.26	3		$16415\ ^{2}_{1/2}-42771^{o}\ _{3_{1/2}}$
3793.207	26355.43	1		$14733\ ^{4}_{1/2}-41088^{o}\ _{3_{1/2}}$
3794.800	26344.36	60	1	$20686\ ^{2}_{1/2}-47030^{o}\ _{1_{1/2}}$
3796.522	26332.42	12		$15770\ ^{1}_{1/2}-42102^{o}\ _{2_{1/2}}$
3797.435	26326.09	200	5	$16287\ ^{3}_{1/2}-42613^{o}\ _{4_{1/2}}$
3797.767	26323.78	1000	10	$1+252\ ^{2}_{1/2}-39576^{o}\ _{1_{1/2}}$
3798.055	26321.79	40	1	$17328\ ^{4}_{1/2}-43649^{o}\ _{4_{1/2}}$
3799.692	26310.45	80	2	$16133\ ^{4}_{1/2}-42444^{o}\ _{5_{1/2}}$
3803.976	26280.82	40	1	$16415\ ^{2}_{1/2}-42696^{o}\ _{2_{1/2}}$
3804.534	26276.96	2		$19791\ ^{4}_{1/2}-46068^{o}\ _{4_{1/2}}$
3806.144	26265.85	15		$22615\ ^{3}_{1/2}-48881^{o}\ _{4_{1/2}}$
3806.424	26263.92	5		$17282\ ^{3}_{1/2}-43546^{o}\ _{2_{1/2}}$
3807.381	26257.32	10		$16287\ ^{3}_{1/2}-42545^{o}\ _{4_{1/2}}$
3810.568	26235.36	30		$16287\ ^{3}_{1/2}-42523^{o}\ _{3_{1/2}}$
3811.253	26230.64	80	2	$15298\ ^{3}_{1/2}-41529^{o}\ _{3_{1/2}}$
3814.339	26209.42	6	2 *h*	$19895\ ^{2}_{1/2}-46104^{o}\ _{2_{1/2}}$
3814.667	26207.17	200	3	$13252\ ^{2}_{1/2}-39459^{o}\ _{2_{1/2}}$
3815.509	26201.38	80	1	$19903\ ^{3}_{1/2}-46104^{o}\ _{2_{1/2}}$
3816.888	26191.92	300	4	$16025\ ^{5}_{1/2}-42217^{o}\ _{4_{1/2}}$
3817.967	26184.51	150	3	$17328\ ^{4}_{1/2}-43512^{o}\ _{3_{1/2}}$
3818.119	26183.47	100	2	$21206\ ^{2}_{1/2}-47389^{o}\ _{3_{1/2}}$
3820.761	26165.37	50	2	$19903\ ^{3}_{1/2}-46068^{o}\ _{4_{1/2}}$

TABLE 3. *Classified lines of* Tc I

Wavelength A	Wavenumber cm^{-1}	Intensity		Energy levels cm^{-1}
		Arc	Spark	
3822.672	26152.29	80		$15770\ ^{1}_{1/2}$–$41922^{o}_{2_{1/2}}$
3823.066	26149.59	1		$14679\ ^{0}_{1/2}$–$40829^{o}_{0_{1/2}}$
3824.467	26140.01	300	4	$15624\ ^{2}_{1/2}$–$41764^{o}_{2_{1/2}}$
3825.531	26132.74	5		$20523\ ^{2}_{1/2}$–$46656^{o}_{3_{1/2}}$
3826.013	26129.45	20		$14169\ ^{1}_{1/2}$–$40299^{o}_{2_{1/2}}$
3827.593	26118.66	60	1	$17146\ ^{5}_{1/2}$–$43265^{o}_{4_{1/2}}$
3828.537	26112.22	500	4	$16133\ ^{4}_{1/2}$–$42246^{o}_{3_{1/2}}$
3828.750	26110.77	3		$23455^{o}_{2_{1/2}}$–$49565\ ^{2}_{1/2}$
3829.220	26107.57	150		$16415\ ^{2}_{1/2}$–$42523^{o}_{3_{1/2}}$
3830.352	26099.85	200	3	$21719\ ^{5}_{1/2}$–$47819^{o}_{4_{1/2}}$
3831.883	26089.42	20		$21204\ ^{4}_{1/2}$–$47294^{o}_{5_{1/2}}$
3832.448	26085.58	200	1	$20523\ ^{2}_{1/2}$–$46608^{o}_{3_{1/2}}$
3832.817	26083.07	600	5	$16133\ ^{4}_{1/2}$–$42217^{o}_{4_{1/2}}$
3837.559	26050.84	1500	15	$17146\ ^{5}_{1/2}$–$43197^{o}_{6_{1/2}}$
3839.577	26037.15	1		$22180\ ^{4}_{1/2}$–$48217^{o}_{3_{1/2}}$
3840.137	26033.35	60		$22180\ ^{4}_{1/2}$–$48213^{o}_{4_{1/2}}$
3841.307	26025.42	800	8	$17146\ ^{5}_{1/2}$–$43172^{o}_{5_{1/2}}$
3842.342	26018.41	80		$15770\ ^{1}_{1/2}$–$41788^{o}_{1_{1/2}}$
3843.968	26007.40	100	2	$16025\ ^{5}_{1/2}$–$42032^{o}_{5_{1/2}}$
3844.061	26006.77	20		$16287\ ^{3}_{1/2}$–$42294^{o}_{2_{1/2}}$
3844.347	26004.84	60	1	$21447\ ^{1}_{1/2}$–$47452^{o}_{2_{1/2}}$
3845.974	25993.84	800	8	$15770\ ^{1}_{1/2}$–$41764^{o}_{2_{1/2}}$
3847.351	25984.54	100	1	$17282\ ^{3}_{1/2}$–$43267^{o}_{3_{1/2}}$
3847.596	25982.88	500	3	$17282\ ^{3}_{1/2}$–$43265^{o}_{4_{1/2}}$
3849.519	25969.90	1		$20686\ ^{2}_{1/2}$–$46656^{o}_{3_{1/2}}$
3850.553	25962.93	5		$16287\ ^{3}_{1/2}$–$42250^{o}_{2_{1/2}}$
3851.222	25958.42	300	3	$16287\ ^{3}_{1/2}$–$42246^{o}_{3_{1/2}}$
3852.328	25950.97	80	1	$17146\ ^{5}_{1/2}$–$43097^{o}_{4_{1/2}}$
3853.323	25944.26	2		$21920\ ^{2}_{1/2}$–$47864^{o}_{3_{1/2}}$
3854.074	25939.21	8		$17328\ ^{4}_{1/2}$–$43267^{o}_{3_{1/2}}$
3854.326	25937.51	50		$17328\ ^{4}_{1/2}$–$43265^{o}_{4_{1/2}}$
3855.555	25929.25	20		$16287\ ^{3}_{1/2}$–$42217^{o}_{4_{1/2}}$
3855.914	25926.83	1		$14169\ ^{1}_{1/2}$–$40096^{o}_{1_{1/2}}$
3856.543	25922.60	20		$20686\ ^{2}_{1/2}$–$46608^{o}_{3_{1/2}}$
3856.734	25921.32	500 *c*	5 *h*	$16553\ ^{6}_{1/2}$–$42474^{o}_{6_{1/2}}$
3857.388	25916.93	20		$19791\ ^{4}_{1/2}$–$45708^{o}_{4_{1/2}}$
3860.129	25898.52	8		$16133\ ^{4}_{1/2}$–$42032^{o}_{5_{1/2}}$
3861.259	25890.94	25 *c*		$16553\ ^{6}_{1/2}$–$42444^{o}_{5_{1/2}}$
3863.068	25878.82	200	3	$16415\ ^{2}_{1/2}$–$42294^{o}_{2_{1/2}}$
3863.830	25873.72	100	1	$20231\ ^{1}_{1/2}$–$46104^{o}_{2_{1/2}}$
3864.106	25871.87	400	4	$16025\ ^{5}_{1/2}$–$41897^{o}_{4_{1/2}}$
3866.012	25859.11	30		$16133\ ^{4}_{1/2}$–$41993^{o}_{3_{1/2}}$
3866.608	25855.13	5		$15770\ ^{1}_{1/2}$–$41625^{o}_{1_{1/2}}$
3868.240	25844.22	1000	8	$17328\ ^{4}_{1/2}$–$43172^{o}_{5_{1/2}}$
3870.292	25830.52	10		$16415\ ^{2}_{1/2}$–$42246^{o}_{3_{1/2}}$
3871.055	25825.43	12		$25598\ ^{2}_{1/2}$–$51423^{o}_{3_{1/2}}$
3871.223	25824.31	12		$21206\ ^{2}_{1/2}$–$47030^{o}_{1_{1/2}}$
3874.609	25801.74	12		$16415\ ^{2}_{1/2}$–$42217^{o}_{1_{1/2}}$
3875.658	25794.75	200	2	$17282\ ^{3}_{1/2}$–$43077^{o}_{3_{1/2}}$
3876.366	25790.04	80	1	$15298\ ^{3}_{1/2}$–$41088^{o}_{3_{1/2}}$

TABLE 3. *Classified lines of* Tc I

Wavelength A	Wavenumber cm^{-1}	Intensity		Energy levels cm^{-1}
		Arc	Spark	
3877.139	25784.90	30		$21447\ ^{1}_{1/2}-47232^{o}_{2}{}_{1/2}$
3882.497	25749.32	10		$17328\ ^{4}_{1/2}-43077^{o}_{3}{}_{1/2}$
3885.638	25728.50	3		$17282\ ^{3}_{1/2}-43011^{o}_{2}{}_{1/2}$
3886.896	25720.18	2		$20384\ ^{3}_{1/2}-46104^{o}_{2}{}_{1/2}$
3888.177	25711.70	1*h*		$23265^{o}_{3}{}_{1/2}-48977\ ^{4}_{1/2}$
3888.440	25709.96	80	1	$20686\ ^{2}_{1/2}-46396^{o}_{3}{}_{1/2}$
3889.130	25705.40	150	2	$16287\ ^{3}_{1/2}-41993^{o}_{3}{}_{1/2}$
3892.332	25684.26	100	1	$20384\ ^{3}_{1/2}-46068^{o}_{4}{}_{1/2}$
3892.332	25684.26	100	1	$22180\ ^{4}_{1/2}-47864^{o}_{3}{}_{1/2}$
3893.220	25678.40	200	2	$16025\ ^{5}_{1/2}-41703^{o}_{4}{}_{1/2}$
3893.837	25674.33	4		$14169\ ^{1}_{1/2}-39844^{o}_{4}{}_{1/2}$
3894.482	25670.08	15		$14733\ ^{4}_{1/2}-40403^{o}_{4}{}_{1/2}$
3894.482	25670.08	15		$17146\ ^{5}_{1/2}-42817^{o}_{4}{}_{1/2}$
3894.688	25668.72	2		$24147\ ^{4}_{1/2}-49815^{o}_{4}{}_{1/2}$
3899.120	25639.54	100	1	$22180\ ^{4}_{1/2}-47819^{o}_{4}{}_{1/2}$
3899.827	25634.90	600	5	$16287\ ^{3}_{1/2}-41922^{o}_{2}{}_{1/2}$
3901.473	25624.08	5		$21719\ ^{5}_{1/2}-47343^{o}_{4}{}_{1/2}$
3903.740	25609.20	60		$16287\ ^{3}_{1/2}-41897^{o}_{4}{}_{1/2}$
3905.322	25598.83	8		$22265\ ^{2}_{1/2}-47864^{o}_{3}{}_{1/2}$
3905.517	25597.55	30		$22615\ ^{3}_{1/2}-48213^{o}_{4}{}_{1/2}$
3905.774	25595.86	100	1	$16133\ ^{4}_{1/2}-41729^{o}_{3}{}_{1/2}$
3906.400	25591.76	20		$21752\ ^{3}_{1/2}-47343^{o}_{4}{}_{1/2}$
3907.681	25583.37	1		$21447\ ^{1}_{1/2}-47030^{o}_{4}{}_{1/2}$
3907.958	25581.56	30		$20523\ ^{2}_{1/2}-46104^{o}_{2}{}_{1/2}$
3908.596	25577.39	20		$16415\ ^{2}_{1/2}-41993^{o}_{3}{}_{1/2}$
3909.038	25574.49	8		$21719\ ^{5}_{1/2}-47294^{o}_{3}{}_{1/2}$
3909.782	25569.63	20		$16133\ ^{4}_{1/2}-41703^{o}_{4}{}_{1/2}$
3911.921	25555.65	3		$16025\ ^{5}_{1/2}-41580^{o}_{5}{}_{1/2}$
3915.174	25534.41	2		$17282\ ^{3}_{1/2}-42817^{o}_{4}{}_{1/2}$
3915.889	25529.75	10		$21752\ ^{3}_{1/2}-47281^{o}_{2}{}_{1/2}$
3916.536	25525.53	60	1	$21926\ ^{2}_{1/2}-47452^{o}_{2}{}_{1/2}$
3916.941	25522.89	5		$15298\ ^{3}_{1/2}-40821^{o}_{2}{}_{1/2}$
3917.443	25519.62	10*c*		$23265^{o}_{3}{}_{1/2}-48784\ ^{3}_{1/2}$
3919.148	25508.52	50		$14733\ ^{4}_{1/2}-40241^{o}_{5}{}_{1/2}$
3919.375	25507.04	300	3	$16415\ ^{2}_{1/2}-41922^{o}_{2}{}_{1/2}$
3922.134	25489.10	100	1	$17282\ ^{3}_{1/2}-42771^{o}_{3}{}_{1/2}$
3922.134	25489.10	100	1	$17328\ ^{4}_{1/2}-42817^{o}_{4}{}_{1/2}$
3923.663	25479.17	300*c*	3*c*	$16553\ ^{6}_{1/2}-42032^{o}_{5}{}_{1/2}$
3925.143	25469.56	10		$21920\ ^{2}_{1/2}-47389^{o}_{3}{}_{1/2}$
3925.953	25464.31	20		$15624\ ^{2}_{1/2}-41088^{o}_{3}{}_{1/2}$
3927.573	25453.80	200	2	$17146\ ^{5}_{1/2}-42600^{o}_{3}{}_{1/2}$
3928.323	25448.95	10		$15624\ ^{2}_{1/2}-41073^{o}_{1}{}_{1/2}$
3928.770	25446.05	30		$17328\ ^{4}_{1/2}-42773^{o}_{3}{}_{1/2}$
3929.113	25443.83	10		$17328\ ^{4}_{1/2}-42771^{o}_{3}{}_{1/2}$
3929.378	25442.11	40		$16287\ ^{3}_{1/2}-41729^{o}_{3}{}_{1/2}$
3931.319	25429.55	3		$20639\ ^{5}_{1/2}-46068^{o}_{4}{}_{1/2}$
3933.438	25415.85	150	2	$16287\ ^{3}_{1/2}-41703^{o}_{4}{}_{1/2}$
3934.832	25406.85	30		$14169\ ^{1}_{1/2}-39576^{o}_{4}{}_{1/2}$
3936.175	25398.18	1		$17146\ ^{5}_{1/2}-42545^{o}_{4}{}_{1/2}$
3936.648	25395.13	70		$16133\ ^{4}_{1/2}-41529^{o}_{3}{}_{1/2}$

TABLE 3. *Classified lines of* Tc I

Wavelength A	Wavenumber cm^{-1}	Intensity		Energy levels cm^{-1}
		Arc	Spark	
3940.054	25373.18	70		$16415\ ^{2}_{1/2}$–$41788^{o}_{1/2}$
3942.866	25355.08	30		$21926\ ^{2}_{1/2}$–$47281^{o}_{2/2}$
3943.868	25348.64	120	1	$16415\ ^{2}_{1/2}$–$41764^{o}_{2/2}$
3946.571	25331.28	4000 *c*	20 *c*	$17282\ ^{3}_{1/2}$–$42613^{o}_{4/2}$
3947.087	25327.97	2000	10	$17146\ ^{5}_{1/2}$–$42474^{o}_{6/2}$
3948.151	25321.14	1		$20783\ ^{3}_{1/2}$–$46104^{o}_{2/2}$
3949.224	25314.26	9		$16415\ ^{2}_{1/2}$–$41729^{o}_{3/2}$
3951.016	25302.78	7		$15770\ ^{1}_{1/2}$–$41073^{o}_{1/2}$
3951.831	25297.56	180		$17146\ ^{5}_{1/2}$–$42444^{o}_{5/2}$
3953.651	25285.92	100	1	$17328\ ^{4}_{1/2}$–$42613^{o}_{4/2}$
3955.734	25272.60	200	3	$17328\ ^{4}_{1/2}$–$42600^{o}_{5/2}$
3958.793	25253.07	15		$19702\ ^{1}_{1/2}$–$44955^{o}_{1/2}$
3959.090	25251.18	80 *c*	1 *c*	$24564\ ^{5}_{1/2}$–$49815^{o}_{4/2}$
3959.520	25248.44	150	2	$22615\ ^{3}_{1/2}$–$47864^{o}_{3/2}$
3960.770	25240.47	20*w*		$17282\ ^{3}_{1/2}$–$42523^{o}_{3/2}$
3964.266	25218.21	30		$39567^{o}_{3/2}$–$64785\ ^{3}_{1/2}$
3964.467	25216.93	20		$17328\ ^{4}_{1/2}$–$42545^{o}_{4/2}$
3965.619	25209.61	3		$22180\ ^{4}_{1/2}$–$47389^{o}_{3/2}$
3967.500	25197.66	100 *c*		$23265^{o}_{3/2}$–$48462\ ^{3}_{1/2}$
3967.912	25195.04	2		$17328\ ^{4}_{1/2}$–$42523^{o}_{3/2}$
3969.207	25186.82	10		$22265\ ^{2}_{1/2}$–$47452^{o}_{2/2}$
3971.232	25173.98	8		$19702\ ^{1}_{1/2}$–$44876^{o}_{1/2}$
3971.503	25172.26	80	1	$23957\ ^{3}_{1/2}$–$49130^{o}_{3/2}$
3971.914	25169.65	40		$19702\ ^{1}_{1/2}$–$44872^{o}_{2/2}$
3972.264	25167.44	20		$22503\ ^{1}_{1/2}$–$47670^{o}_{0/2}$
3974.554	25152.94	30*h*		$23265^{o}_{3/2}$–$48418\ ^{4}_{1/2}$
3979.095	25124.23	20		$22265\ ^{2}_{1/2}$–$47389^{o}_{3/2}$
3980.354	25116.28	500	3	$14733\ ^{4}_{1/2}$–$39849^{o}_{3/2}$
3980.354	25116.28	500	3	$17328\ ^{4}_{1/2}$–$42444^{o}_{5/2}$
3981.279	25110.45	6		$21920\ ^{2}_{1/2}$–$47030^{o}_{1/2}$
3981.688	25107.87	8		$15298\ ^{3}_{1/2}$–$40406^{o}_{3/2}$
3982.171	25104.83	100	1	$15298\ ^{3}_{1/2}$–$40403^{o}_{4/2}$
3984.967	25087.21	10000 *c*	100 *c*	$2572\ ^{4}_{1/2}$–$27660^{o}_{3/2}$
3987.780	25069.51	400	3	$20639\ ^{5}_{1/2}$–$45708^{o}_{4/2}$
3989.216	25060.49	20		$19895\ ^{2}_{1/2}$–$44955^{o}_{1/2}$
3989.449	25059.03	8		$15770\ ^{1}_{1/2}$–$40829^{o}_{0/2}$
3991.320	25047.28	20		$19791\ ^{4}_{1/2}$–$44839^{o}_{3/2}$
3994.038	25030.24	300	1	$14733\ ^{4}_{1/2}$–$39763^{o}_{4/2}$
3994.509	25027.28	2000	10	$16553\ ^{6}_{1/2}$–$41580^{o}_{5/2}$
3995.741	25019.57	3		$19702\ ^{1}_{1/2}$–$44722^{o}_{1/2}$
3996.974	25011.85	200	1	$17282\ ^{3}_{1/2}$–$42294^{o}_{2/2}$
3998.755	25000.71	40		$15298\ ^{3}_{1/2}$–$40299^{o}_{2/2}$
4001.843	24981.42	20		$19895\ ^{2}_{1/2}$–$44876^{o}_{1/2}$
4003.867	24968.79	4		$19903\ ^{3}_{1/2}$–$44872^{o}_{2/2}$
4003.976	24968.11	4		$17282\ ^{3}_{1/2}$–$42250^{o}_{2/2}$
4004.182	24966.83	15		$22265\ ^{2}_{1/2}$–$47232^{o}_{2/2}$
4004.689	24963.67	300	2	$17282\ ^{3}_{1/2}$–$42246^{o}_{3/2}$
4006.161	24954.49	30		$16133\ ^{4}_{1/2}$–$41088^{o}_{3/2}$
4006.631	24951.57	30 *c*		$24147\ ^{4}_{1/2}$–$49098^{o}_{4/2}$
4007.874	24943.83	40		$19895\ ^{2}_{1/2}$–$44839^{o}_{3/2}$

TABLE 3. *Classified lines of* Tc I

Wavelength A	Wavenumber cm^{-1}	Intensity		Energy levels cm^{-1}
		Arc	Spark	
4008.837	24937.84	50		$15298\ ^3{}_{1/2}$–$40236^o{}_{3/2}$
4009.179	24935.71	15		$19903\ ^3{}_{1/2}$–$44839^o{}_{3/2}$
4010.897	24925.03	1		$20783\ ^3{}_{1/2}$–$45708^o{}_{4/2}$
4011.043	24924.12	10		$23957\ ^3{}_{1/2}$–$48881^o{}_{4/2}$
4011.996	24918.20	1000	5	$17328\ ^4{}_{1/2}$–$42246^o{}_{3/2}$
4014.293	24903.94	20		$21752\ ^3{}_{1/2}$–$46656^o{}_{3/2}$
4015.474	24896.62	30		$14679\ ^0{}_{1/2}$–$39576^o{}_{1/2}$
4015.760	24894.85	20		$19827\ ^0{}_{1/2}$–$44722^o{}_{1/2}$
4015.760	24894.85	20		$39891^o{}_{2/2}$–$64785\ ^3{}_{1/2}$
4016.683	24889.12	400	2	$17328\ ^4{}_{1/2}$–$42217^o{}_{4/2}$
4017.223	24885.78	600	4	$17146\ ^5{}_{1/2}$–$42032^o{}_{3/2}$
4020.755	24863.92	2000	10	$21204\ ^4{}_{1/2}$–$46068^o{}_{4/2}$
4029.108	24812.37	80	1	$16287\ ^3{}_{1/2}$–$41100^o{}_{2/2}$
4031.626	24796.88	20000 *cw*	300 *cw*	$2572\ ^4{}_{1/2}$–$27369^o{}_{4/2}$
4033.677	24784.27	1		$19791\ ^4{}_{1/2}$–$44576^o{}_{4/2}$
4034.014	24782.20	80		$15624\ ^2{}_{1/2}$–$40406^o{}_{3/2}$
4036.787	24765.17	3		$22265\ ^2{}_{1/2}$–$47030^o{}_{1/2}$
4039.246	24750.10	1000	8	$17146\ ^5{}_{1/2}$–$41897^o{}_{4/2}$
4041.559	24735.93	100		$21920\ ^2{}_{1/2}$–$46656^o{}_{3/2}$
4041.781	24734.58	200		$24147\ ^4{}_{1/2}$–$48881^o{}_{4/2}$
4042.657	24729.22	10		$21926\ ^2{}_{1/2}$–$46656^o{}_{3/2}$
4042.657	24729.22	10		$22503\ ^1{}_{1/2}$–$47232^o{}_{2/2}$
4043.401	24724.67	8		$20231\ ^1{}_{1/2}$–$44955^o{}_{1/2}$
4046.697	24704.53	80		$17328\ ^4{}_{1/2}$–$42032^o{}_{3/2}$
4049.108	24689.82	10000 *c*	150 *c*	$3250\ ^3{}_{1/2}$–$27940^o{}_{2/2}$
4050.888	24678.97	60	1	$15298\ ^3{}_{1/2}$–$39977^o{}_{2/2}$
4051.569	24674.82	2		$15624\ ^2{}_{1/2}$–$40299^o{}_{2/2}$
4051.949	24672.51	500	4	$19903\ ^3{}_{1/2}$–$44576^o{}_{4/2}$
4053.177	24665.03	200	3	$17328\ ^4{}_{1/2}$–$41993^o{}_{3/2}$
4054.415	24657.50	30		$16415\ ^2{}_{1/2}$–$41073^o{}_{1/2}$
4057.283	24640.07	60	2 *h*	$17282\ ^3{}_{1/2}$–$41922^o{}_{2/2}$
4058.232	24634.31	30	1	$19903\ ^3{}_{1/2}$–$44537^o{}_{2/2}$
4060.853	24618.41	40	1	$21450\ ^4{}_{1/2}$–$46068^o{}_{4/2}$
4061.516	24614.39	20		$17282\ ^3{}_{1/2}$–$41897^o{}_{4/2}$
4062.095	24610.88	8		$19702\ ^1{}_{1/2}$–$44313^o{}_{1/2}$
4069.023	24568.98	100	1	$17328\ ^4{}_{1/2}$–$41897^o{}_{4/2}$
4071.059	24556.69	100	1	$17146\ ^5{}_{1/2}$–$41703^o{}_{4/2}$
4073.802	24540.16	1		$26883\ ^2{}_{1/2}$–$51423^o{}_{3/2}$
4074.034	24538.76	6		$19702\ ^1{}_{1/2}$–$44241^o{}_{2/2}$
4074.857	24533.81	20		$24564\ ^5{}_{1/2}$–$49098^o{}_{4/2}$
4081.966	24491.08	3		$20231\ ^1{}_{1/2}$–$44722^o{}_{1/2}$
4082.800	24486.08	10		$19827\ ^0{}_{1/2}$–$44313^o{}_{1/2}$
4083.537	24481.66	400	3	$17282\ ^3{}_{1/2}$–$41764^o{}_{2/2}$
4084.500	24475.89	6 *h*		$21920\ ^2{}_{1/2}$–$46396^o{}_{3/2}$
4084.500	24475.89	6 *h*		$22180\ ^4{}_{1/2}$–$46656^o{}_{3/2}$
4084.650	24474.99	10		$19791\ ^4{}_{1/2}$–$44266^o{}_{3/2}$
4085.085	24472.38	20		$15624\ ^2{}_{1/2}$–$40096^o{}_{1/2}$
4086.325	24464.96	18		$15298\ ^3{}_{1/2}$–$39763^o{}_{3/2}$
4088.707	24450.70	10000	100	$3700\ ^2{}_{1/2}$–$28151^o{}_{1/2}$
4089.285	24447.25	60		$17282\ ^3{}_{1/2}$–$41729^o{}_{3/2}$

TABLE 3. *Classified lines of* Tc I

Wavelength A	Wavenumber cm^{-1}	Intensity		Energy levels cm^{-1}
		Arc	Spark	
4092.373	24428.80	12		$22180\ ^4_{1/2}-46608^\circ_{3/2}$
4093.694	24420.92	200	2	$17282\ ^3_{1/2}-41703^\circ_{4/2}$
4094.163	24418.12	80	1	$19895\ ^2_{1/2}-44313^\circ_{1/2}$
4095.668	24409.15	15000	500	$3250\ ^3_{1/2}-27660^\circ_{3/2}$
4098.784	24390.59	100	1	$22265\ ^2_{1/2}-46656^\circ_{3/2}$
4100.114	24382.68	150 *cw*		$40403^\circ_{4/2}-64785\ ^3_{1/2}$
4100.902	24377.99	20		$16025\ ^5_{1/2}-40403^\circ_{4/2}$
4101.312	24375.56	100	1	$17328\ ^4_{1/2}-41703^\circ_{4/2}$
4101.989	24371.54	30		$19895\ ^2_{1/2}-44266^\circ_{3/2}$
4103.368	24363.34	10		$19903\ ^3_{1/2}-44266^\circ_{3/2}$
4103.987	24359.67	3		$23460\ ^3_{1/2}-47819^\circ_{4/2}$
4105.089	24353.13	80		$15624\ ^2_{1/2}-39977^\circ_{2/2}$
4106.246	24346.27	60		$19791\ ^4_{1/2}-44138^\circ_{3/2}$
4106.246	24346.27	60		$19895\ ^2_{1/2}-44241^\circ_{2/2}$
4106.723	24343.44	80	1	$22265\ ^2_{1/2}-46608^\circ_{3/2}$
4107.644	24337.98	20		$19903\ ^3_{1/2}-44241^\circ_{2/2}$
4109.646	24326.13	40		$15770\ ^1_{1/2}-40096^\circ_{1/2}$
4111.199	24316.94	6		$24564\ ^5_{1/2}-48881^\circ_{4/2}$
4111.386	24315.83	150	1	$20523\ ^2_{1/2}-44839^\circ_{3/2}$
4113.341	24304.28	30		$19702\ ^1_{1/2}-44007^\circ_{2/2}$
4115.077	24294.02	10000	300	$4002\ ^1_{1/2}-28296^\circ_{0/2}$
4117.021	24282.55	4		$19827\ ^0_{1/2}-44110^\circ_{1/2}$
4118.740	24272.42	6		$16133\ ^4_{1/2}-40406^\circ_{3/2}$
4119.274	24269.27	600	5	$15298\ ^3_{1/2}-39567^\circ_{3/2}$
4121.576	24255.72	100		$23957\ ^3_{1/2}-48213^\circ_{4/2}$
4124.217	24240.18	8000	200	$3700\ ^2_{1/2}-27940^\circ_{2/2}$
4128.268	24216.40	1000	20	$16025\ ^5_{1/2}-40241^\circ_{3/2}$
4128.557	24214.70	80	1	$19895\ ^2_{1/2}-44110^\circ_{1/2}$
4129.862	24207.05	6		$15770\ ^1_{1/2}-39977^\circ_{2/2}$
4130.453	24203.59	150	2	$19903\ ^3_{1/2}-44107^\circ_{2/2}$
4130.877	24201.10	30		$17328\ ^4_{1/2}-41529^\circ_{3/2}$
4132.530	24191.42	40		$20384\ ^3_{1/2}-44576^\circ_{4/2}$
4133.276	24187.06	20		$19903\ ^3_{1/2}-44090^\circ_{3/2}$
4133.679	24184.70	2		$21920\ ^2_{1/2}-46104^\circ_{2/2}$
4134.490	24179.96	3		$19791\ ^4_{1/2}-43971^\circ_{4/2}$
4134.813	24178.07	300	3	$21926\ ^2_{1/2}-46104^\circ_{2/2}$
4137.234	24163.92	15		$20523\ ^2_{1/2}-44687^\circ_{3/2}$
4137.660	24161.43	4		$15298\ ^3_{1/2}-39459^\circ_{2/2}$
4139.116	24152.93	300	3	$20384\ ^3_{1/2}-44537^\circ_{2/2}$
4139.849	24148.66	800	8	$4002\ ^1_{1/2}-28151^\circ_{1/2}$
4142.917	24130.77	20		$22265\ ^2_{1/2}-46396^\circ_{3/2}$
4144.950	24118.94	6000	30	$3250\ ^3_{1/2}-27369^\circ_{4/2}$
4145.080	24118.18	3000	15	$4178\ ^0_{1/2}-28296^\circ_{0/2}$
4146.202	24111.65	80	1	$19895\ ^2_{1/2}-44007^\circ_{2/2}$
4146.882	24107.70	20		$16133\ ^4_{1/2}-40241^\circ_{3/2}$
4147.615	24103.44	200	2	$19903\ ^3_{1/2}-44007^\circ_{2/2}$
4150.200	24088.43	15		$20783\ ^3_{1/2}-44872^\circ_{2/2}$
4151.241	24082.39	10		$20231\ ^1_{1/2}-44313^\circ_{1/2}$
4153.672	24068.29	150	1	$19903\ ^3_{1/2}-43971^\circ_{4/2}$
4158.547	24040.08	10		$22615\ ^3_{1/2}-46656^\circ_{3/2}$

TABLE 3. *Classified lines of* Tc I

Wavelength A	Wavenumber cm^{-1}	Intensity		Energy levels cm^{-1}
		Arc	Spark	
4158.547	24040.08	10		$25058\ ^{3}_{1/2}$–$49098^{o}\ ^{4}_{1/2}$
4159.319	24035.62	20		$39891^{o}\ ^{2}_{1/2}$–$63926\ ^{2}_{1/2}$
4162.970	24014.54	1		$20523\ ^{2}_{1/2}$–$44537^{o}\ ^{2}_{1/2}$
4163.702	24010.32	20		$19895\ ^{2}_{1/2}$–$43905^{o}\ ^{3}_{1/2}$
4165.609	23999.32	10000	100	$10516\ ^{3}_{1/2}$–$34515^{o}\ ^{2}_{1/2}$
4167.424	23988.87	500	6	$21719\ ^{5}_{1/2}$–$45708^{o}\ ^{4}_{1/2}$
4170.274	23972.48	4000	40	$4178\ ^{0}_{1/2}$–$28151^{o}\ ^{1}_{1/2}$
4172.532	23959.50	5000	60	$3700\ ^{2}_{1/2}$–$27660^{o}\ ^{3}_{1/2}$
4174.462	23948.43	70		$16287\ ^{3}_{1/2}$–$40236^{o}\ ^{3}_{1/2}$
4176.276	23938.03	1000	50	$4002\ ^{1}_{1/2}$–$27940^{o}\ ^{2}_{1/2}$
4182.629	23901.67	5		$19903\ ^{3}_{1/2}$–$43805^{o}\ ^{3}_{1/2}$
4185.815	23883.48	3		$16415\ ^{2}_{1/2}$–$40299^{o}\ ^{2}_{1/2}$
4186.506	23879.53	800	30	$11063\ ^{2}_{1/2}$–$34942^{o}\ ^{1}_{1/2}$
4189.609	23861.85	50		$23957\ ^{3}_{1/2}$–$47819^{o}\ ^{4}_{1/2}$
4190.306	23857.88	2		$19791\ ^{4}_{1/2}$–$43649^{o}\ ^{4}_{1/2}$
4190.477	23856.90	4		$20384\ ^{3}_{1/2}$–$44241^{o}\ ^{2}_{1/2}$
4191.415	23851.57	10		$20686\ ^{2}_{1/2}$–$44537^{o}\ ^{2}_{1/2}$
4193.557	23839.38	1		$22265\ ^{2}_{1/2}$–$46104^{o}\ ^{2}_{1/2}$
4194.224	23835.59	3		$15624\ ^{2}_{1/2}$–$39459^{o}\ ^{2}_{1/2}$
4199.466	23805.84	30	1	$17282\ ^{3}_{1/2}$–$41088^{o}\ ^{3}_{1/2}$
4201.850	23792.33	20	1	$20783\ ^{3}_{1/2}$–$44576^{o}\ ^{4}_{1/2}$
4211.430	23738.21	20	1	$16025\ ^{5}_{1/2}$–$39763^{o}\ ^{4}_{1/2}$
4214.220	23722.50	5		$20384\ ^{3}_{1/2}$–$44107^{o}\ ^{2}_{1/2}$
4215.510	23715.24	10	1	$16133\ ^{4}_{1/2}$–$39849^{o}\ ^{3}_{1/2}$
4218.609	23697.82	300	20	$11578\ ^{1}_{1/2}$–$35276^{o}\ ^{0}_{1/2}$
4220.346	23688.06	50*h*	1	$16553\ ^{6}_{1/2}$–$40241^{o}\ ^{5}_{1/2}$
4221.619	23680.92	10		$16415\ ^{2}_{1/2}$–$40096^{o}\ ^{1}_{1/2}$
4229.948	23634.29	6		$21204\ ^{4}_{1/2}$–$44839^{o}\ ^{3}_{1/2}$
4230.207	23632.85	10	1	$21206\ ^{2}_{1/2}$–$44839^{o}\ ^{3}_{1/2}$
4230.832	23629.35	150	5	$16133\ ^{4}_{1/2}$–$39763^{o}\ ^{4}_{1/2}$
4231.195	23627.33	5		$20686\ ^{2}_{1/2}$–$44313^{o}\ ^{1}_{1/2}$
4232.096	23622.30	40	1	$20384\ ^{3}_{1/2}$–$44007^{o}\ ^{2}_{1/2}$
4238.191	23588.33	5000 *c*	100 *c*	$0\ ^{2}_{1/2}$–$23588^{o}\ ^{1}_{1/2}$
4238.991	23583.87	5		$20523\ ^{2}_{1/2}$–$44107^{o}\ ^{2}_{1/2}$
4239.567	23580.67	20	1	$20686\ ^{2}_{1/2}$–$44266^{o}\ ^{3}_{1/2}$
4241.996	23567.17	8		$20523\ ^{2}_{1/2}$–$44090^{o}\ ^{3}_{1/2}$
4242.979	23561.71	40	1	$16415\ ^{2}_{1/2}$–$39977^{o}\ ^{2}_{1/2}$
4248.953	23528.58	30	1	$22180\ ^{4}_{1/2}$–$45708^{o}\ ^{4}_{1/2}$
4252.756	23507.54	2*h*		$14733\ ^{4}_{1/2}$–$38240^{o}\ ^{3}_{1/2}$
4256.134	23488.88	10		$22615\ ^{3}_{1/2}$–$46104^{o}\ ^{2}_{1/2}$
4257.338	23482.24	30	1	$21204\ ^{4}_{1/2}$–$44687^{o}\ ^{3}_{1/2}$
4258.587	23475.35	20	1	$16415\ ^{2}_{1/2}$–$39891^{o}\ ^{2}_{1/2}$
4258.587	23475.35	20	1	$19791\ ^{4}_{1/2}$–$43267^{o}\ ^{3}_{1/2}$
4262.270	23455.07	10000	400	$0\ ^{2}_{1/2}$–$23455^{o}\ ^{2}_{1/2}$
4262.687	23452.78	1000	20	$11063\ ^{2}_{1/2}$–$34515^{o}\ ^{2}_{1/2}$
4266.158	23433.69	80	1	$16133\ ^{4}_{1/2}$–$39567^{o}\ ^{3}_{1/2}$
4266.158	23433.69	80	1	$16415\ ^{2}_{1/2}$–$39849^{o}\ ^{3}_{1/2}$
4266.983	23429.16	2		$21447\ ^{1}_{1/2}$–$44876^{o}\ ^{1}_{1/2}$
4267.978	23423.70	8		$20686\ ^{2}_{1/2}$–$44110^{o}\ ^{1}_{1/2}$
4268.503	23420.82	30	1	$20686\ ^{2}_{1/2}$–$44107^{o}\ ^{2}_{1/2}$

TABLE 3. *Classified lines of* Tc I

Wavelength A	Wavenumber cm^{-1}	Intensity		Energy levels cm^{-1}
		Arc	Spark	
4269.660	23414.47	4		$39185^{o}_{4\frac{1}{2}}$–$62599_{4\frac{1}{2}}$
4274.971	23385.39	800	100	$11890_{0\frac{1}{2}}$–$35276^{o}_{0\frac{1}{2}}$
4275.504	23382.47	18	2	$20523_{2\frac{1}{2}}$–$43905^{o}_{3\frac{1}{2}}$
4275.906	23380.27	20	2	$19791_{4\frac{1}{2}}$–$43172^{o}_{3\frac{1}{2}}$
4278.895	23363.94	800	100	$11578_{1\frac{1}{2}}$–$34942^{o}_{1\frac{1}{2}}$
4279.263	23361.93	18	2	$19903_{3\frac{1}{2}}$–$43265^{o}_{4\frac{1}{2}}$
4286.353	23323.29	4	1	$20783_{3\frac{1}{2}}$–$44107^{o}_{2\frac{1}{2}}$
4286.843	23320.62	1		$20686_{2\frac{1}{2}}$–$44007^{o}_{2\frac{1}{2}}$
4289.115	23308.27	5	1	$19702_{1\frac{1}{2}}$–$43011^{o}_{2\frac{1}{2}}$
4289.563	23305.84	20	2	$19791_{4\frac{1}{2}}$–$43097^{o}_{4\frac{1}{2}}$
4294.351	23279.85	80	12	$16287_{3\frac{1}{2}}$–$39567^{o}_{3\frac{1}{2}}$
4297.058	23265.19	10000	1000	$0_{2\frac{1}{2}}$–$23265^{o}_{3\frac{1}{2}}$
4302.319	23236.74	1		$21450_{4\frac{1}{2}}$–$44687^{o}_{3\frac{1}{2}}$
4304.848	23223.09	4	1	$20783_{3\frac{1}{2}}$–$44007^{o}_{2\frac{1}{2}}$
4305.516	23219.48	15	2	$20686_{2\frac{1}{2}}$–$43905^{o}_{3\frac{1}{2}}$
4305.819	23217.85	80	8	$20639_{5\frac{1}{2}}$–$43857^{o}_{6\frac{1}{2}}$
4308.615	23202.78	15	2	$19702_{1\frac{1}{2}}$–$42905^{o}_{2\frac{1}{2}}$
4309.370	23198.72	2		$19702_{1\frac{1}{2}}$–$42901^{o}_{1\frac{1}{2}}$
4309.858	23196.09	1		$23460_{3\frac{1}{2}}$–$46656^{o}_{3\frac{1}{2}}$
4310.222	23194.13	60	6	$19903_{3\frac{1}{2}}$–$43097^{o}_{4\frac{1}{2}}$
4311.376	23187.92	3		$20783_{3\frac{1}{2}}$–$43971^{o}_{4\frac{1}{2}}$
4312.504	23181.86	10	1	$19895_{2\frac{1}{2}}$–$43077^{o}_{3\frac{1}{2}}$
4314.021	23173.71	9	1	$19903_{3\frac{1}{2}}$–$43077^{o}_{3\frac{1}{2}}$
4314.679	23170.17	1		$16428^{o}_{2\frac{1}{2}}$–$39598_{2\frac{1}{2}}$
4318.061	23152.03	6	1	$16415_{2\frac{1}{2}}$–$39567^{o}_{3\frac{1}{2}}$
4318.983	23147.08	5	1	$24147_{4\frac{1}{2}}$–$47294^{o}_{5\frac{1}{2}}$
4323.016	23125.49	2		$21450_{4\frac{1}{2}}$–$44576^{o}_{4\frac{1}{2}}$
4323.356	23123.67	80	7	$17282_{3\frac{1}{2}}$–$40406^{o}_{3\frac{1}{2}}$
4323.958	23120.45	12	2	$17282_{3\frac{1}{2}}$–$40403^{o}_{4\frac{1}{2}}$
4324.867	23115.59	12	2	$19895_{2\frac{1}{2}}$–$43011^{o}_{2\frac{1}{2}}$
4326.393	23107.44	3	1	$19903_{3\frac{1}{2}}$–$43011^{o}_{2\frac{1}{2}}$
4328.778	23094.71	60	6	$17146_{5\frac{1}{2}}$–$40241^{o}_{5\frac{1}{2}}$
4330.231	23086.96	2		$21752_{3\frac{1}{2}}$–$44839^{o}_{3\frac{1}{2}}$
4331.866	23078.25	1		$17328_{4\frac{1}{2}}$–$40406^{o}_{3\frac{1}{2}}$
4332.452	23075.13	150	10	$17328_{4\frac{1}{2}}$–$40403^{o}_{4\frac{1}{2}}$
4335.187	23060.57	4	1	$21206_{2\frac{1}{2}}$–$44266^{o}_{3\frac{1}{2}}$
4336.855	23051.70	400 *cw*	40 *cw*	$11890_{0\frac{1}{2}}$–$34942^{o}_{1\frac{1}{2}}$
4338.248	23044.30	2 *h*		$16415_{2\frac{1}{2}}$–$39459^{o}_{2\frac{1}{2}}$
4341.109	23029.11	2		$21926_{2\frac{1}{2}}$–$44955^{o}_{1\frac{1}{2}}$
4342.242	23023.10	20	2	$20523_{2\frac{1}{2}}$–$43546^{o}_{2\frac{1}{2}}$
4342.570	23021.36	4	1	$20783_{3\frac{1}{2}}$–$43805^{o}_{3\frac{1}{2}}$
4345.442	23006.15	10		$19895_{2\frac{1}{2}}$–$42901^{o}_{1\frac{1}{2}}$
4350.013	22981.97	5 *h*		$19791_{4\frac{1}{2}}$–$42773^{o}_{5\frac{1}{2}}$
4350.415	22979.85	1	1	$19791_{4\frac{1}{2}}$–$42771^{o}_{3\frac{1}{2}}$
4354.823	22956.59	2		$21920_{2\frac{1}{2}}$–$44876^{o}_{1\frac{1}{2}}$
4355.398	22953.56	15 *w*	2	$17282_{3\frac{1}{2}}$–$40236^{o}_{3\frac{1}{2}}$
4356.093	22949.90	3	1	$21926_{2\frac{1}{2}}$–$44876^{o}_{1\frac{1}{2}}$
4358.491	22937.27	400	40	$11578_{1\frac{1}{2}}$–$34515^{o}_{2\frac{1}{2}}$
4359.257	22933.24	200	30	$21204_{4\frac{1}{2}}$–$44138^{o}_{5\frac{1}{2}}$
4361.959	22919.03	20	2	$21920_{2\frac{1}{2}}$–$44839^{o}_{3\frac{1}{2}}$

TABLE 3. *Classified lines of* Tc I

Wavelength A	Wavenumber cm^{-1}	Intensity		Energy levels cm^{-1}
		Arc	Spark	
4363.014	22913.49	80	8	$17328\ ^{4}_{1/2}-40241^{o}\ ^{3}_{1/2}$
4364.017	22908.23	1		$17328\ ^{4}_{1/2}-40236^{o}\ ^{3}_{1/2}$
4364.889	22903.65	1		$21206\ ^{2}_{1/2}-44110^{o}\ ^{1}_{1/2}$
4365.425	22900.84	1		$21206\ ^{2}_{1/2}-44107^{o}\ ^{2}_{1/2}$
4365.999	22897.83	4		$26917\ ^{5}_{1/2}-49815^{o}\ ^{4}_{1/2}$
4368.340	22885.55	2		$21204\ ^{4}_{1/2}-44090^{o}\ ^{3}_{1/2}$
4368.616	22884.11	1		$21206\ ^{2}_{1/2}-44090^{o}\ ^{3}_{1/2}$
4368.940	22882.41	30	4	$20384\ ^{3}_{1/2}-43267^{o}\ ^{3}_{1/2}$
4369.255	22880.76	25	3	$20384\ ^{3}_{1/2}-43265^{o}\ ^{4}_{1/2}$
4370.094	22876.37	70	7	$19895\ ^{2}_{1/2}-42771^{o}\ ^{3}_{1/2}$
4370.717	22873.11	60	7	$20639\ ^{5}_{1/2}-43512^{o}\ ^{5}_{1/2}$
4371.661	22868.17	1		$19903\ ^{3}_{1/2}-42771^{o}\ ^{3}_{1/2}$
4372.086	22865.95	10	1	$20783\ ^{3}_{1/2}-43649^{o}\ ^{4}_{1/2}$
4373.181	22860.22	15	2	$20686\ ^{2}_{1/2}-43546^{o}\ ^{2}_{1/2}$
4373.952	22856.19	70	7	$21719\ ^{5}_{1/2}-44576^{o}\ ^{4}_{1/2}$
4380.132	22823.94	2		$21752\ ^{3}_{1/2}-44576^{o}\ ^{4}_{1/2}$
4381.583	22816.39	4	1	$21450\ ^{4}_{1/2}-44266^{o}\ ^{3}_{1/2}$
4383.075	22808.62	60	6	$19791\ ^{4}_{1/2}-42600^{o}\ ^{3}_{1/2}$
4384.317	22802.16	1		$21920\ ^{2}_{1/2}-44722^{o}\ ^{1}_{1/2}$
4385.626	22795.35	1		$21926\ ^{2}_{1/2}-44722^{o}\ ^{1}_{1/2}$
4385.881	22794.03	1		$21447\ ^{1}_{1/2}-44241^{o}\ ^{2}_{1/2}$
4387.501	22785.61	15	1	$21752\ ^{3}_{1/2}-44537^{o}\ ^{2}_{1/2}$
4388.605	22779.88	3	1	$20231\ ^{1}_{1/2}-43011^{o}\ ^{2}_{1/2}$
4391.923	22762.67	3	1	$20783\ ^{3}_{1/2}-43546^{o}\ ^{2}_{1/2}$
4393.787	22753.01	7		$19791\ ^{4}_{1/2}-42545^{o}\ ^{4}_{1/2}$
4395.571	22743.78	2		$20523\ ^{2}_{1/2}-43267^{o}\ ^{3}_{1/2}$
4398.003	22731.20	1		$19791\ ^{4}_{1/2}-42523^{o}\ ^{3}_{1/2}$
4399.337	22724.31	4		$16874^{o}\ ^{3}_{1/2}-39598\ ^{2}_{1/2}$
4401.518	22713.05	10		$20384\ ^{3}_{1/2}-43097^{o}\ ^{4}_{1/2}$
4402.054	22710.28	1*h*		$19903\ ^{3}_{1/2}-42613^{o}\ ^{4}_{1/2}$
4403.905	22700.74	6	1	$21204\ ^{4}_{1/2}-43905^{o}\ ^{3}_{1/2}$
4404.176	22699.34	2		$21206\ ^{2}_{1/2}-43905^{o}\ ^{3}_{1/2}$
4404.403	22698.17	1		$23957\ ^{3}_{1/2}-46656^{o}\ ^{3}_{1/2}$
4405.081	22694.68	7	1	$17282\ ^{3}_{1/2}-39977^{o}\ ^{2}_{1/2}$
4405.485	22692.60	2		$20384\ ^{3}_{1/2}-43077^{o}\ ^{3}_{1/2}$
4405.922	22690.35	3		$22265\ ^{2}_{1/2}-44955^{o}\ ^{1}_{1/2}$
4406.427	22687.75	1		$21450\ ^{4}_{1/2}-44138^{o}\ ^{3}_{1/2}$
4407.346	22683.02	7	1	$42102^{o}\ ^{2}_{1/2}-64785\ ^{3}_{1/2}$
4409.034	22674.33	3	1	$20231\ ^{1}_{1/2}-42905^{o}\ ^{2}_{1/2}$
4409.815	22670.32	2		$20231\ ^{1}_{1/2}-42901^{o}\ ^{1}_{1/2}$
4412.004	22659.07	100	7	$22180\ ^{4}_{1/2}-44839^{o}\ ^{3}_{1/2}$
4413.322	22652.30	1		$19791\ ^{4}_{1/2}-42444^{o}\ ^{5}_{1/2}$
4415.452	22641.37	20*c*	1	$19903\ ^{3}_{1/2}-42545^{o}\ ^{4}_{1/2}$
4415.718	22640.01	5	1	$21450\ ^{4}_{1/2}-44090^{o}\ ^{3}_{1/2}$
4418.412	22626.21	7	1	$20639\ ^{5}_{1/2}-43265^{o}\ ^{4}_{1/2}$
4420.302	22616.53	80	6	$17146\ ^{5}_{1/2}-39763^{o}\ ^{4}_{1/2}$
4421.430	22610.76	2*h*		$39891^{o}\ ^{2}_{1/2}-62501\ ^{3}_{1/2}$
4421.878	22608.47	3*h*		$17282\ ^{3}_{1/2}-39891^{o}\ ^{2}_{1/2}$
4425.139	22591.81	1*h*		$19702\ ^{1}_{1/2}-42294^{o}\ ^{2}_{1/2}$
4427.294	22580.82	10	1	$20686\ ^{2}_{1/2}-43267^{o}\ ^{3}_{1/2}$

TABLE 3. *Classified lines of* Tc I

Wavelength A	Wavenumber cm^{-1}	Intensity		Energy levels cm^{-1}
		Arc	Spark	
4428.702	22573.64	2	1	$22265\ ^{2}_{1/2}-44839^{o}\ ^{3}_{1/2}$
4429.592	22569.10	1000	200	$10516\ ^{3}_{1/2}-33085^{o}\ ^{2}_{1/2}$
4431.716	22558.28	15	2	$20639\ ^{5}_{1/2}-43197^{o}\ ^{3}_{1/2}$
4432.571	22553.93	12	2	$20523\ ^{2}_{1/2}-43077^{o}\ ^{3}_{1/2}$
4433.783	22547.77	1 *h*		$19702\ ^{1}_{1/2}-42250^{o}\ ^{2}_{1/2}$
4436.731	22532.79	2		$20639\ ^{5}_{1/2}-43172^{o}\ ^{3}_{1/2}$
4437.056	22531.14	1 *h*		$31414^{o}\ ^{3}_{1/2}-53945\ ^{2}_{1/2}$
4438.999	22521.27	5		$17328\ ^{4}_{1/2}-39849^{o}\ ^{3}_{1/2}$
4441.418	22509.01	2 *h*		$24147\ ^{4}_{1/2}-46656^{o}\ ^{3}_{1/2}$
4446.502	22483.27	8	2	$20783\ ^{3}_{1/2}-43267^{o}\ ^{3}_{1/2}$
4447.015	22480.68	12 *c*		$17282\ ^{3}_{1/2}-39763^{o}\ ^{4}_{1/2}$
4450.790	22461.61	5 *c*	1	$24147\ ^{4}_{1/2}-46608^{o}\ ^{3}_{1/2}$
4451.433	22458.37	1		$20639\ ^{5}_{1/2}-43097^{o}\ ^{4}_{1/2}$
4452.078	22455.11	6		$21450\ ^{4}_{1/2}-43905^{o}\ ^{3}_{1/2}$
4452.273	22454.13	60	6	$19791\ ^{4}_{1/2}-42246^{o}\ ^{3}_{1/2}$
4454.142	22444.71	3		$21204\ ^{4}_{1/2}-43649^{o}\ ^{4}_{1/2}$
4454.811	22441.34	1		$31503^{o}\ ^{1}_{1/2}-53945\ ^{2}_{1/2}$
4456.621	22432.22	20	3	$20384\ ^{3}_{1/2}-42817^{o}\ ^{4}_{1/2}$
4458.057	22425.00	3		$19791\ ^{4}_{1/2}-42217^{o}\ ^{4}_{1/2}$
4459.395	22418.27	10	2	$21719\ ^{5}_{1/2}-44138^{o}\ ^{3}_{1/2}$
4463.038	22399.97	20	2	$19702\ ^{1}_{1/2}-42102^{o}\ ^{2}_{1/2}$
4463.535	22397.48	1		$41529^{o}\ ^{3}_{1/2}-63926\ ^{2}_{1/2}$
4463.852	22395.89	60	6	$22180\ ^{4}_{1/2}-44576^{o}\ ^{4}_{1/2}$
4464.277	22393.75	15	1	$25058\ ^{3}_{1/2}-47452^{o}\ ^{2}_{1/2}$
4464.864	22390.81	6		$19903\ ^{3}_{1/2}-42294^{o}\ ^{2}_{1/2}$
4465.090	22389.68	20	2	$19827\ ^{0}_{1/2}-42217^{o}\ ^{4}_{1/2}$
4465.613	22387.06	80	8	$20384\ ^{3}_{1/2}-42771^{o}\ ^{3}_{1/2}$
4466.575	22382.23	3	1	$20523\ ^{2}_{1/2}-42905^{o}\ ^{2}_{1/2}$
4467.384	22378.18	3	1	$20523\ ^{2}_{1/2}-42901^{o}\ ^{1}_{1/2}$
4468.309	22373.55	1 *h*		$22503\ ^{1}_{1/2}-44876^{o}\ ^{1}_{1/2}$
4469.173	22369.22	10	1	$22503\ ^{1}_{1/2}-44872^{o}\ ^{2}_{1/2}$
4470.369	22363.24	1		$40236^{o}\ ^{3}_{1/2}-62599\ ^{4}_{1/2}$
4471.986	22355.15	3		$19895\ ^{2}_{1/2}-42250^{o}\ ^{2}_{1/2}$
4473.662	22346.78	15 *c*	2	$21920\ ^{2}_{1/2}-44266^{o}\ ^{3}_{1/2}$
4474.506	22342.56	8	1	$19903\ ^{3}_{1/2}-42246^{o}\ ^{3}_{1/2}$
4475.003	22340.08	7	1	$21926\ ^{2}_{1/2}-44266^{o}\ ^{3}_{1/2}$
4478.673	22321.77	4	1	$19895\ ^{2}_{1/2}-42217^{o}\ ^{1}_{1/2}$
4480.251	22313.91	100	10	$20783\ ^{3}_{1/2}-43097^{o}\ ^{4}_{1/2}$
4481.533	22307.53	1000	100	$21204\ ^{4}_{1/2}-43512^{o}\ ^{3}_{1/2}$
4484.351	22293.51	10	1	$20783\ ^{3}_{1/2}-43077^{o}\ ^{3}_{1/2}$
4486.050	22285.07	6 *c*	1	$17282\ ^{3}_{1/2}-39567^{o}\ ^{3}_{1/2}$
4487.061	22280.05	3000	300	$11063\ ^{2}_{1/2}-33343^{o}\ ^{1}_{1/2}$
4488.624	22272.29	3		$22265\ ^{2}_{1/2}-44537^{o}\ ^{2}_{1/2}$
4490.128	22264.83	1		$25405\ ^{1}_{1/2}-47670^{o}\ ^{0}_{1/2}$
4492.735	22251.91	10	1	$21719\ ^{5}_{1/2}-43971^{o}\ ^{4}_{1/2}$
4493.388	22248.68	8 *h*	7 *h*	$23460\ ^{3}_{1/2}-45708^{o}\ ^{4}_{1/2}$
4495.027	22240.56	400	50	$19791\ ^{4}_{1/2}-42032^{o}\ ^{5}_{1/2}$
4495.213	22239.64	20		$17328\ ^{4}_{1/2}-39567^{o}\ ^{3}_{1/2}$
4497.337	22229.14	2 *w*		$20384\ ^{3}_{1/2}-42613^{o}\ ^{4}_{1/2}$
4497.713	22227.28	5		$20783\ ^{3}_{1/2}-43011^{o}\ ^{2}_{1/2}$

TABLE 3. *Classified lines of* Tc I

Wavelength A	Wavenumber cm^{-1}	Intensity		Energy levels cm^{-1}
		Arc	Spark	
4498.529	22223.25	60	8	$22615\ ^{3}_{1/2}$–$44839^{o}_{3/2}$
4498.529	22223.25	60	8	$25058\ ^{3}_{1/2}$–$47281^{o}_{2/2}$
4499.295	22219.47	7*h*	1*h*	$20686\ ^{2}_{1/2}$–$42905^{o}_{2/2}$
4501.743	22207.38	60	6	$19895\ ^{2}_{1/2}$–$42102^{o}_{2/2}$
4503.399	22199.22	100	10	$21450\ ^{4}_{1/2}$–$43649^{o}_{4/2}$
4505.473	22189.00	2		$39849^{o}_{3/2}$–$62038\ ^{3}_{1/2}$
4505.881	22186.99	3		$21920\ ^{2}_{1/2}$–$44107^{o}_{2/2}$
4506.640	22183.25	2		$21926\ ^{2}_{1/2}$–$44110^{o}_{1/2}$
4507.177	22180.61	4		$26917\ ^{5}_{1/2}$–$49098^{o}_{4/2}$
4507.775	22177.67	3		$20639\ ^{5}_{1/2}$–$42817^{o}_{4/2}$
4508.719	22173.03	8	1	$20523\ ^{2}_{1/2}$–$42696^{o}_{2/2}$
4511.312	22160.28	3*h*		$20384\ ^{3}_{1/2}$–$42545^{o}_{4/2}$
4512.691	22153.51	8		$27660^{o}_{3/2}$– $49813\ ^{2}_{1/2}$
4514.019	22146.99	2*h*		$23957\ ^{3}_{1/2}$–$46104^{o}_{2/2}$
4515.978	22137.38	1000	100	$21719\ ^{5}_{1/2}$–$43857^{o}_{6/2}$
4522.841	22103.79	10000	1000	$10516\ ^{3}_{1/2}$–$32620^{o}_{3/2}$
4525.760	22089.54	2		$19903\ ^{3}_{1/2}$–$41993^{o}_{3/2}$
4526.321	22086.80	10	2	$22180\ ^{4}_{1/2}$–$44266^{o}_{3/2}$
4526.507	22085.89	8	1	$19702\ ^{1}_{1/2}$–$41788^{o}_{1/2}$
4531.157	22063.23	30	4	$20231\ ^{1}_{1/2}$–$42294^{o}_{2/2}$
4531.391	22062.09	8	1	$21204\ ^{4}_{1/2}$–$43267^{o}_{3/2}$
4531.391	22062.09	8	1	$21450\ ^{4}_{1/2}$–$43512^{o}_{3/2}$
4531.703	22060.57	20	3	$21204\ ^{4}_{1/2}$–$43265^{o}_{4/2}$
4534.236	22048.25	1		$22265\ ^{2}_{1/2}$–$44313^{o}_{1/2}$
4537.052	22034.56	2		$22503\ ^{1}_{1/2}$–$44537^{o}_{2/2}$
4537.347	22033.13	100	10	$20783\ ^{3}_{1/2}$–$42817^{o}_{4/2}$
4538.556	22027.26	3	1	$19895\ ^{2}_{1/2}$–$41922^{o}_{2/2}$
4539.530	22022.53	2000	500	$11063\ ^{2}_{1/2}$–$33085^{o}_{2/2}$
4541.247	22014.21	5		$42771^{o}_{3/2}$–$64785\ ^{3}_{1/2}$
4542.090	22010.12	400	40	$20686\ ^{2}_{1/2}$–$42696^{o}_{2/2}$
4543.900	22001.35	5	1	$22265\ ^{2}_{1/2}$–$44266^{o}_{3/2}$
4544.609	21997.92	3		$27940^{o}_{2/2}$–$49938\ ^{2}_{1/2}$
4545.546	21993.39	50	5	$19903\ ^{3}_{1/2}$–$41896^{o}_{4/2}$
4546.672	21987.94	2		$20783\ ^{3}_{1/2}$–$42771^{o}_{3/2}$
4549.439	21974.57	80	8	$20639\ ^{5}_{1/2}$–$42613^{o}_{4/2}$
4552.204	21961.22	400	40	$20639\ ^{5}_{1/2}$–$42600^{o}_{3/2}$
4552.854	21958.09	800	80	$22180\ ^{4}_{1/2}$–$44138^{o}_{3/2}$
4557.046	21937.89	1000	100	$19791\ ^{4}_{1/2}$–$41729^{o}_{3/2}$
4558.711	21929.87	40	4	$21719\ ^{5}_{1/2}$–$43649^{o}_{4/2}$
4560.205	21922.69	15	2	$19702\ ^{1}_{1/2}$–$41625^{o}_{1/2}$
4560.421	21921.65	20*c*	2	$24147\ ^{4}_{1/2}$–$46068^{o}_{4/2}$
4562.522	21911.56	8	1	$19791\ ^{4}_{1/2}$–$41703^{o}_{4/2}$
4562.913	21909.68	30	3	$20384\ ^{3}_{1/2}$–$42294^{o}_{2/2}$
4563.741	21905.70	25	2	$20639\ ^{5}_{1/2}$–$42545^{o}_{4/2}$
4564.539	21901.87	2000	300	$11578\ ^{1}_{1/2}$–$33480^{o}_{0/2}$
4565.436	21897.57	4	1	$21752\ ^{3}_{1/2}$–$43649^{o}_{4/2}$
4566.421	21892.85	7	1	$21204\ ^{4}_{1/2}$–$43097^{o}_{4/2}$
4568.135	21884.63	3		$29539\ ^{4}_{1/2}$–$51423^{o}_{3/2}$
4570.599	21872.84	15		$27940^{o}_{2/2}$–$49813\ ^{2}_{1/2}$
4570.861	21871.58	60	10	$20231\ ^{1}_{1/2}$–$42102^{o}_{2/2}$

318-092 O-69—3

TABLE 3. *Classified lines of* Tc I

Wavelength A	Wavenumber cm^{-1}	Intensity		Energy levels cm^{-1}
		Arc	Spark	
4571.453	21868.75	2		$19895\ ^{2}_{1/2}$–41764^{o}_{2}
4572.062	21865.84	5	1	$20384\ ^{3}_{1/2}$–42250^{o}_{2}
4573.977	21856.68	8	1	$25174\ ^{2}_{1/2}$–47030^{o}_{1}
4576.521	21844.53	2		$27971\ ^{4}_{1/2}$–49815^{o}_{4}
4576.521	21844.53	2		$22265\ ^{2}_{1/2}$–44110^{o}_{1}
4577.129	21841.63	20	3	$22265\ ^{2}_{1/2}$–44107^{o}_{2}
4578.447	21835.34	1000	100	$20639\ ^{5}_{1/2}$–42474^{o}_{6}
4579.559	21830.04	3		$20783\ ^{3}_{1/2}$–42613^{o}_{4}
4580.291	21826.55	3*w*		$25405\ ^{1}_{1/2}$–47232^{o}_{2}
4580.613	21825.02	7	1	$16415\ ^{2}_{1/2}$–38240^{o}_{3}
4582.377	21816.62	25	3	$21450\ ^{4}_{1/2}$–43267^{o}_{3}
4582.726	21814.96	4	1	$21450\ ^{4}_{1/2}$–43265^{o}_{4}
4583.246	21812.48	1		23455^{o}_{2}–$45267\ ^{1}_{1/2}$
4583.686	21810.39	2		$22503\ ^{1}_{1/2}$–44313^{o}_{1}
4584.851	21804.85	50	4	$20639\ ^{5}_{1/2}$–42444^{o}_{5}
4585.884	21799.93	150	15	$19903\ ^{3}_{1/2}$–41703^{o}_{4}
4586.309	21797.91	4	1	$19827\ ^{0}_{1/2}$–41625^{o}_{1}
4587.037	21794.45	6	1	27940^{o}_{2}–$49735\ ^{1}_{1/2}$
4587.628	21791.65	4	1	$22180\ ^{4}_{1/2}$–43971^{o}_{4}
4588.232	21788.78	30	3	$19791\ ^{4}_{1/2}$–41580^{o}_{5}
4588.536	21787.33	2	2	28151^{o}_{1}–$49938\ ^{2}_{1/2}$
4591.988	21770.96	1		$20523\ ^{2}_{1/2}$–42294^{o}_{2}
4593.346	21764.52	1000	100	$11578\ ^{1}_{1/2}$–33343^{o}_{1}
4594.059	21761.14	100	10	$20783\ ^{3}_{1/2}$–42545^{o}_{4}
4598.217	21741.46	10	1	$22265\ ^{2}_{1/2}$–44007^{o}_{2}
4601.231	21727.22	3		$20523\ ^{2}_{1/2}$–42250^{o}_{2}
4601.586	21725.55	2		$22180\ ^{4}_{1/2}$–43905^{o}_{3}
4602.408	21721.67	30	3	$21450\ ^{4}_{1/2}$–43172^{o}_{3}
4602.721	21720.19	100	10	23265^{o}_{3}–$44985\ ^{3}_{1/2}$
4603.162	21718.11	15	2	$20384\ ^{3}_{1/2}$–42102^{o}_{2}
4607.170	21699.22	3		$21206\ ^{2}_{1/2}$–42905^{o}_{2}
4608.005	21695.28	80	8	$21206\ ^{2}_{1/2}$–42901^{o}_{1}
4608.314	21693.83	20	2	$20523\ ^{2}_{1/2}$–42217^{o}_{1}
4608.833	21691.39	8	1	$20231\ ^{1}_{1/2}$–41922^{o}_{2}
4609.159	21689.85	300 *c*	30 *c*	$13252\ ^{2}_{1/2}$–34942^{o}_{1}
4611.171	21680.39	40		40821^{o}_{2}–$62501\ ^{3}_{1/2}$
4611.171	21680.39	40		42246^{o}_{3}–$63926\ ^{2}_{1/2}$
4611.386	21679.38	2		23588^{o}_{1}–$45267\ ^{1}_{1/2}$
4611.811	21677.38	3		27660^{o}_{3}–$49337\ ^{2}_{1/2}$
4616.857	21653.69	1000	100	23265^{o}_{3}–$44919\ ^{4}_{1/2}$
4617.447	21650.92	20	2	$22615\ ^{3}_{1/2}$–44266^{o}_{3}
4619.725	21640.24	1		$22265\ ^{2}_{1/2}$–43905^{o}_{3}
4621.129	21633.67	30		$19895\ ^{2}_{1/2}$–41529^{o}_{3}
4621.458	21632.13	40		42294^{o}_{2}–$63926\ ^{2}_{1/2}$
4622.691	21626.36	200 *c*	20 *c*	$21920\ ^{2}_{1/2}$–43546^{o}_{2}
4622.950	21625.15	30 *c*	1 *c*	27940^{o}_{2}–$49565\ ^{2}_{1/2}$
4622.950	21625.15	30 *c*	1 *c*	$22180\ ^{4}_{1/2}$–43805^{o}_{3}
4624.122	21619.67	3	1	$21926\ ^{2}_{1/2}$–43546^{o}_{2}
4624.961	21615.75	300	30	23455^{o}_{2}–$45071\ ^{2}_{1/2}$
4625.628	21612.63	5	1	$27517\ ^{2}_{1/2}$–49130^{o}_{3}

TABLE 3. *Classified lines of* Tc I

Wavelength A	Wavenumber cm^{-1}	Intensity		Energy levels cm^{-1}
		Arc	Spark	
4625.753	21612.04	5	1	$21204\ ^{4}_{1/2}$–$42817^{o}\ ^{4}_{1/2}$
4626.557	21608.29	20		$20384\ ^{3}_{1/2}$–$41993^{o}\ ^{3}_{1/2}$
4626.557	21608.29	20		$20686\ ^{2}_{1/2}$–$42294^{o}\ ^{2}_{1/2}$
4626.803	21607.14	2		$27369^{o}\ ^{4}_{1/2}$–$48977\ ^{4}_{1/2}$
4628.063	21601.26	60	4	$23588^{o}\ ^{1}_{1/2}$–$45189\ ^{0}_{1/2}$
4630.572	21589.55	1000		$11890\ ^{0}_{1/2}$–$33480^{o}\ ^{0}_{1/2}$
4631.378	21585.80	80	3	$27660^{o}\ ^{3}_{1/2}$–$49245\ ^{3}_{1/2}$
4631.815	21583.76	10	1	$28151^{o}\ ^{1}_{1/2}$–$49735\ ^{1}_{1/2}$
4632.740	21579.45	30	3	$20523\ ^{2}_{1/2}$–$42102^{o}\ ^{2}_{1/2}$
4635.433	21566.91	1		$21204\ ^{4}_{1/2}$–$42771^{o}\ ^{3}_{1/2}$
4635.752	21565.43	150	15	$21206\ ^{2}_{1/2}$–$42771^{o}\ ^{3}_{1/2}$
4637.500	21557.30	3000	300	$11063\ ^{2}_{1/2}$–$32620^{o}\ ^{3}_{1/2}$
4640.015	21545.62	2		$21719\ ^{5}_{1/2}$–$43265^{o}\ ^{4}_{1/2}$
4641.296	21539.67	6	1	$22265\ ^{2}_{1/2}$–$43805^{o}\ ^{3}_{1/2}$
4641.669	21537.94	1		$20384\ ^{3}_{1/2}$–$41922^{o}\ ^{2}_{1/2}$
4645.490	21520.22	150 *c*	5 *c*	$23588^{o}\ ^{1}_{1/2}$–$45108\ ^{1}_{1/2}$
4646.620	21514.99	80	8	$21752\ ^{3}_{1/2}$–$43267^{o}\ ^{3}_{1/2}$
4647.573	21510.58	120	10	$20783\ ^{3}_{1/2}$–$42294^{o}\ ^{2}_{1/2}$
4648.332	21507.07	2000	200	$11578\ ^{1}_{1/2}$–$33085^{o}\ ^{2}_{1/2}$
4652.005	21490.09	2		$21206\ ^{2}_{1/2}$–$42696^{o}\ ^{2}_{1/2}$
4653.609	21482.68	100	1	$23588^{o}\ ^{1}_{1/2}$–$45071\ ^{2}_{1/2}$
4654.658	21477.84	120	10	$21719\ ^{5}_{1/2}$–$43197^{o}\ ^{6}_{1/2}$
4655.363	21474.59	1		$22615\ ^{3}_{1/2}$–$44090^{o}\ ^{3}_{1/2}$
4656.440	21469.62	1		$20523\ ^{2}_{1/2}$–$41993^{o}\ ^{3}_{1/2}$
4656.440	21469.62	1		$22180\ ^{4}_{1/2}$–$43649^{o}\ ^{4}_{1/2}$
4658.934	21458.13	2		$21447\ ^{1}_{1/2}$–$42905^{o}\ ^{2}_{1/2}$
4659.798	21454.15	30	3	$21447\ ^{1}_{1/2}$–$42901^{o}\ ^{1}_{1/2}$
4660.212	21452.24	2000 *c*	200	$11890\ ^{0}_{1/2}$–$33343^{o}\ ^{1}_{1/2}$
4663.237	21438.33	2 *h*		$28296^{o}\ ^{0}_{1/2}$–$49735\ ^{1}_{1/2}$
4664.337	21433.27	100	10	$20783\ ^{3}_{1/2}$–$42217^{o}\ ^{4}_{1/2}$
4668.879	21412.42	100	10	$23460\ ^{3}_{1/2}$–$44872^{o}\ ^{2}_{1/2}$
4669.305	21410.47	2000	200	$10516\ ^{3}_{1/2}$–$31927^{o}\ ^{2}_{1/2}$
4671.749	21399.26	10	1	$20523\ ^{2}_{1/2}$–$41922^{o}\ ^{2}_{1/2}$
4672.170	21397.34	400	40	$19702\ ^{1}_{1/2}$–$41100^{o}\ ^{2}_{1/2}$
4672.545	21395.62	3		$21204\ ^{4}_{1/2}$–$42600^{o}\ ^{5}_{1/2}$
4672.824	21394.34	40	4	$20231\ ^{1}_{1/2}$–$41625^{o}\ ^{1}_{1/2}$
4673.077	21393.18	45	4	$20639\ ^{5}_{1/2}$–$42032^{o}\ ^{5}_{1/2}$
4678.073	21370.34	3		$19702\ ^{1}_{1/2}$–$41073^{o}\ ^{1}_{1/2}$
4678.903	21366.55	200	20	$21450\ ^{4}_{1/2}$–$42817^{o}\ ^{4}_{1/2}$
4682.732	21349.08	20 *c*	1	$23455^{o}\ ^{2}_{1/2}$–$44804\ ^{2}_{1/2}$
4683.599	21345.12	150	15	$20384\ ^{3}_{1/2}$–$41729^{o}\ ^{3}_{1/2}$
4684.716	21340.03	2		$21204\ ^{4}_{1/2}$–$42545^{o}\ ^{4}_{1/2}$
4686.406	21332.34	150	15	$22180\ ^{4}_{1/2}$–$43512^{o}\ ^{5}_{1/2}$
4687.978	21325.19	100	15	$21752\ ^{3}_{1/2}$–$43077^{o}\ ^{3}_{1/2}$
4688.365	21323.43	3 *h*		$21450\ ^{4}_{1/2}$–$42773^{o}\ ^{5}_{1/2}$
4689.359	21318.91	400	40	$20384\ ^{3}_{1/2}$–$41703^{o}\ ^{4}_{1/2}$
4689.359	21318.91	400	40	$20783\ ^{3}_{1/2}$–$42102^{o}\ ^{2}_{1/2}$
4689.810	21316.86	150	5	$21206\ ^{2}_{1/2}$–$42523^{o}\ ^{3}_{1/2}$
4689.810	21316.86	150	5	$27660^{o}\ ^{3}_{1/2}$–$48977\ ^{4}_{1/2}$
4692.384	21305.16	60	2	$27940^{o}\ ^{2}_{1/2}$–$49245\ ^{3}_{1/2}$

TABLE 3. *Classified lines of* Tc I

Wavelength A	Wavenumber cm^{-1}	Intensity		Energy levels cm^{-1}
		Arc	Spark	
4694.282	21296.55	300	30	$19791\ ^4{}_{1/2}$–$41088^o{}_{3/2}$
4695.788	21289.72	15	3	$22615\ ^3{}_{1/2}$–$43905^o{}_{3/2}$
4697.047	21284.01	3		$27660^o{}_{3/2}$–$48944\ ^2{}_{1/2}$
4701.169	21265.35	2		$20523\ ^2{}_{1/2}$–$41788^o{}_{1/2}$
4701.814	21262.43	5	1	$26950\ ^3{}_{1/2}$–$48213^o{}_{4/2}$
4702.586	21258.94	1		$21752\ ^3{}_{1/2}$–$43011^o{}_{2/2}$
4702.880	21257.61	50	5	$20639\ ^5{}_{1/2}$–$41897^o{}_{4/2}$
4704.802	21248.93	15	2	$21447\ ^1{}_{1/2}$–$42696^o{}_{2/2}$
4705.542	21245.59	5	1	$19827\ ^0{}_{1/2}$–$41073^o{}_{1/2}$
4706.918	21239.38	1000	100	$21204\ ^4{}_{1/2}$–$42444^o{}_{5/2}$
4707.575	21236.41	20	2	$20686\ ^2{}_{1/2}$–$41922^o{}_{2/2}$
4712.120	21215.93	8 *c*		$23588^o{}_{1/2}$–$44804\ ^2{}_{1/2}$
4713.610	21209.22	3		$20783\ ^3{}_{1/2}$–$41993^o{}_{3/2}$
4714.222	21206.47	200	20	$20523\ ^2{}_{1/2}$–$41729^o{}_{3/2}$
4714.605	21204.75	40	4	$19895\ ^2{}_{1/2}$–$41100^o{}_{2/2}$
4716.787	21194.94	80	8	$11063\ ^2{}_{1/2}$–$32258^o{}_{1/2}$
4717.766	21190.54	2000	200	$11063\ ^2{}_{1/2}$–$32253^o{}_{1/2}$
4719.018	21184.92	500 *c*	50 *c*	$19903\ ^3{}_{1/2}$–$41088^o{}_{3/2}$
4719.281	21183.74	4000 *c*	400 *c*	$16428^o{}_{2/2}$–$37612\ ^3{}_{1/2}$
4723.828	21163.35	3	1	$21450\ ^4{}_{1/2}$–$42613^o{}_{4/2}$
4725.202	21157.19	1		$21920\ ^2{}_{1/2}$–$43077^o{}_{3/2}$
4726.798	21150.05	10	1	$21450\ ^4{}_{1/2}$–$42600^o{}_{5/2}$
4728.082	21144.31	50	5	$20384\ ^3{}_{1/2}$–$41529^o{}_{3/2}$
4729.302	21138.85	15	2	$20783\ ^3{}_{1/2}$–$41922^o{}_{2/2}$
4731.918	21127.17	10	1	$27971\ ^4{}_{1/2}$–$49098^o{}_{4/2}$
4732.044	21126.60	10	1	$19702\ ^1{}_{1/2}$–$40829^o{}_{0/2}$
4732.469	21124.71	25	1	$27660^o{}_{3/2}$–$48784\ ^3{}_{1/2}$
4733.869	21118.46	20 *c*	2 *c*	$19702\ ^1{}_{1/2}$–$40821^o{}_{2/2}$
4735.058	21113.16	8	1	$20783\ ^3{}_{1/2}$–$41896^o{}_{4/2}$
4736.515	21106.66	200 *cd*	20 *cd*	$14169\ ^1{}_{1/2}$–$35276^o{}_{0/2}$
4737.434	21102.57	1		$20686\ ^2{}_{1/2}$–$41788^o{}_{1/2}$
4738.652	21097.14	2		$21719\ ^5{}_{1/2}$–$42817^o{}_{4/2}$
4739.551	21093.14	100 *c*	10 *c*	$27369^o{}_{4/2}$–$48462\ ^3{}_{1/2}$
4740.608	21088.44	10000	000	$10516\ ^3{}_{1/2}$–$31605^o{}_{3/2}$
4741.284	21085.43	50	5	$22180\ ^4{}_{1/2}$–$43265^o{}_{4/2}$
4741.532	21084.33	6	1	$21926\ ^2{}_{1/2}$–$43011^o{}_{2/2}$
4742.940	21078.07	8	1	$20686\ ^2{}_{1/2}$–$41764^o{}_{2/2}$
4744.250	21072.25	1 *h*		$23265^o{}_{3/2}$–$44337\ ^2{}_{1/2}$
4749.614	21048.45	500	20	$27369^o{}_{4/2}$–$48418\ ^4{}_{1/2}$
4750.552	21044.30	3		$21206\ ^2{}_{1/2}$–$42250^o{}_{2/2}$
4750.759	21043.38	8	1	$22503\ ^1{}_{1/2}$–$43546^o{}_{2/2}$
4751.548	21039.88	15	2	$21206\ ^2{}_{1/2}$–$42246^o{}_{3/2}$
4756.111	21019.70	100	10	$20231\ ^1{}_{1/2}$–$41250^o{}_{1/2}$
4756.111	21019.70	100	10	$21752\ ^3{}_{1/2}$–$42771^o{}_{3/2}$
4757.502	21013.55	40 *c*	2	$27274\ ^6{}_{1/2}$–$48287^o{}_{5/2}$
4757.840	21012.06	2		$21204\ ^4{}_{1/2}$–$42217^o{}_{4/2}$
4758.094	21010.94	80	6	$21206\ ^2{}_{1/2}$–$42217^o{}_{1/2}$
4759.280	21005.70	40	3	$20523\ ^2{}_{1/2}$–$41529^o{}_{3/2}$
4759.806	21003.38	50	3	$27940^o{}_{2/2}$–$48944\ ^2{}_{1/2}$
4760.160	21001.82	2		$22265\ ^2{}_{1/2}$–$43267^o{}_{3/2}$

TABLE 3. *Classified lines of* Tc I

Wavelength A	Wavenumber cm^{-1}	Intensity		Energy levels cm^{-1}
		Arc	Spark	
4761.968	20993.85	40	3	$21450\ ^4_{1/2}$–$42444^0_{3/2}$
4762.362	20992.11	200	20	$22180\ ^4_{1/2}$–$43172^0_{3/2}$
4764.796	20981.39	5		$21920\ ^2_{1/2}$–$42901^0_{1/2}$
4764.987	20980.55	3		$20783\ ^3_{1/2}$–$41764^0_{2/2}$
4764.987	20980.55	3		$43805^0_{3/2}$–$64785\ ^3_{1/2}$
4765.381	20978.81	8	1	$21926\ ^2_{1/2}$–$42905^0_{2/2}$
4766.305	20974.74	7	1	$21926\ ^2_{1/2}$–$42901^0_{1/2}$
4771.543	20951.72	4000	400	$11063\ ^2_{1/2}$–$32014^0_{2/2}$
4773.237	20944.28	5	1	$21752\ ^3_{1/2}$–$42696^0_{2/2}$
4773.890	20941.42	200	20	$20639\ ^5_{1/2}$–$41580^0_{3/2}$
4776.355	20930.61	120	12	$25174\ ^2_{1/2}$–$46104^0_{2/2}$
4776.355	20930.61	120	12	$22615\ ^3_{1/2}$–$43546^0_{2/2}$
4783.925	20897.49	200	20	$10516\ ^3_{1/2}$–$31414^0_{3/2}$
4784.137	20896.57	20	2	$21206\ ^2_{1/2}$–$42102^0_{2/2}$
4784.720	20894.02	100	10	$21719\ ^5_{1/2}$–$42613^0_{4/2}$
4785.597	20890.19	500	50	$10516\ ^3_{1/2}$–$31406^0_{2/2}$
4787.589	20881.50	40	2	$23957\ ^3_{1/2}$–$44839^0_{3/2}$
4787.758	20880.76	100	8	$21719\ ^5_{1/2}$–$42600^0_{3/2}$
4790.482	20868.89	200 *c*	20 *c*	$20231\ ^1_{1/2}$–$41100^0_{2/2}$
4791.623	20863.92	250	20	$11063\ ^2_{1/2}$–$31927^0_{2/2}$
4792.120	20861.75	5	1	$21752\ ^3_{1/2}$–$42613^0_{4/2}$
4796.176	20844.11	3		$27940^0_{2/2}$–$48784\ ^3_{1/2}$
4796.480	20842.79	10	1	$20686\ ^2_{1/2}$–$41529^0_{3/2}$
4797.895	20836.64	6 *h*		$23265^0_{3/2}$–$44102\ ^3_{1/2}$
4799.978	20827.60	300	30	$21204\ ^4_{1/2}$–$42032^0_{3/2}$
4800.700	20824.47	80 *c*	5 *c*	$11578\ ^1_{1/2}$–$32403^0_{1/2}$
4803.623	20811.80	2		$22265\ ^2_{1/2}$–$43077^0_{3/2}$
4804.777	20806.80	1 *h*		$23460\ ^3_{1/2}$–$44266^0_{3/2}$
4805.688	20802.86	100	10	$27660^0_{3/2}$–$48462\ ^3_{1/2}$
4807.349	20795.67	8	1	$21450\ ^4_{1/2}$–$42246^0_{3/2}$
4807.988	20792.91	1 *h*		$28151^0_{1/2}$–$48944\ ^2_{1/2}$
4809.094	20788.12	1		$21204\ ^4_{1/2}$–$41993^0_{3/2}$
4809.416	20786.73	100	10	$21206\ ^2_{1/2}$–$41993^0_{3/2}$
4810.633	20781.47	2		$23460\ ^3_{1/2}$–$44241^0_{2/2}$
4811.842	20776.25	60	6	$21920\ ^2_{1/2}$–$42696^0_{2/2}$
4812.630	20772.85	3		$14169\ ^1_{1/2}$–$34942^0_{1/2}$
4813.324	20769.85	50	5	$21447\ ^1_{1/2}$–$42217^0_{4/2}$
4814.073	20766.62	60	6	$21450\ ^4_{1/2}$–$42217^0_{4/2}$
4816.062	20758.05	30 *c*	1	$27660^0_{3/2}$–$48418\ ^4_{1/2}$
4816.794	20754.89	500	80	$21719\ ^5_{1/2}$–$42474^0_{6/2}$
4819.024	20745.29	1 *h*		$20783\ ^3_{1/2}$–$41529^0_{3/2}$
4820.739	20737.91	10000	000	$16874^0_{3/2}$–$37612\ ^3_{1/2}$
4825.748	20716.38	20	2	$21206\ ^2_{1/2}$–$41922^0_{2/2}$
4828.698	20703.73	2		$20384\ ^3_{1/2}$–$41088^0_{3/2}$
4831.347	20692.38	300	30	$2572\ ^4_{1/2}$–$23265^0_{3/2}$
4834.367	20679.45	1000	100	$11578\ ^1_{1/2}$–$32258^0_{1/2}$
4835.394	20675.06	1000	100	$11578\ ^1_{1/2}$–$32253^0_{1/2}$
4838.034	20663.77	1		$26788\ ^2_{1/2}$–$47452^0_{2/2}$
4839.017	20659.58	1		$43267^0_{3/2}$–$63926\ ^2_{1/2}$
4840.974	20651.23	20	2	$22615\ ^3_{1/2}$–$43267^0_{3/2}$

TABLE 3. *Classified lines of* Tc I

Wavelength A	Wavenumber cm^{-1}	Intensity		Energy levels cm^{-1}
		Arc	Spark	
4841.364	20649.56	100	10	$22615\ ^3{}_{1/2}-43265\ ^4{}_{1/2}$
4842.022	20646.76	10 *h*	1 *h*	$23455\ ^2{}_{1/2}-44102\ ^3{}_{1/2}$
4843.559	20640.20	6	1	$22265\ ^2{}_{1/2}-42905\ ^2{}_{1/2}$
4844.326	20636.94	2		$22180\ ^4{}_{1/2}-42817\ ^4{}_{1/2}$
4848.716	20618.25	3		$23957\ ^3{}_{1/2}-44576\ ^4{}_{1/2}$
4849.608	20614.46	40	2	$19791\ ^4{}_{1/2}-40406\ ^3{}_{1/2}$
4850.368	20611.23	4		$19791\ ^4{}_{1/2}-40403\ ^4{}_{1/2}$
4853.588	20597.56	20000	2000	$10516\ ^3{}_{1/2}-31114\ ^4{}_{1/2}$
4855.343	20590.11	1		$20231\ ^1{}_{1/2}-40821\ ^2{}_{1/2}$
4857.211	20582.19	100	10	$21450\ ^4{}_{1/2}-42032\ ^3{}_{1/2}$
4858.446	20576.96	2		$20523\ ^2{}_{1/2}-41100\ ^2{}_{1/2}$
4859.216	20573.70	40 *c*	2 *c*	$23455\ ^2{}_{1/2}-44028\ ^1{}_{1/2}$
4860.424	20568.59	1		$26883\ ^2{}_{1/2}-47452\ ^2{}_{1/2}$
4861.232	20565.17	20	2	$20523\ ^2{}_{1/2}-41088\ ^3{}_{1/2}$
4862.193	20561.10	100 *c*	8 *c*	$23588\ ^1{}_{1/2}-44149\ ^0{}_{1/2}$
4862.931	20557.98	40	4	$21206\ ^2{}_{1/2}-41764\ ^2{}_{1/2}$
4866.733	20541.92	10000	1000	$11063\ ^2{}_{1/2}-31605\ ^3{}_{1/2}$
4869.240	20531.35	3 *c*		$23265\ ^3{}_{1/2}-43796\ ^2{}_{1/2}$
4870.772	20524.89	200	20	$21204\ ^4{}_{1/2}-41729\ ^3{}_{1/2}$
4873.799	20512.14	10 *c*		$11890\ ^0{}_{1/2}-32403\ ^1{}_{1/2}$
4874.768	20508.06	30	1	$22503\ ^1{}_{1/2}-43011\ ^2{}_{1/2}$
4875.142	20506.49	1		$22265\ ^2{}_{1/2}-42771\ ^3{}_{1/2}$
4876.768	20499.65	12 *c*	1	$19903\ ^3{}_{1/2}-40403\ ^4{}_{1/2}$
4877.016	20498.61	30	3	$21204\ ^4{}_{1/2}-41703\ ^4{}_{1/2}$
4877.344	20497.23	15	2	$21719\ ^5{}_{1/2}-42217\ ^4{}_{1/2}$
4878.094	20494.08	12	1	$21752\ ^3{}_{1/2}-42246\ ^3{}_{1/2}$
4882.586	20475.23	8	1	$21447\ ^1{}_{1/2}-41922\ ^2{}_{1/2}$
4885.044	20464.93	30	3	$21752\ ^3{}_{1/2}-42217\ ^4{}_{1/2}$
4885.889	20461.39	12	1	$22615\ ^3{}_{1/2}-43077\ ^3{}_{1/2}$
4888.695	20449.64	100	10	$19791\ ^4{}_{1/2}-40241\ ^3{}_{1/2}$
4889.444	20446.51	50	5	$21450\ ^4{}_{1/2}-41897\ ^4{}_{1/2}$
4890.884	20440.49	150 *c*	10 *c*	$23588\ ^1{}_{1/2}-44028\ ^1{}_{1/2}$
4890.884	20440.49	150 *c*	10 *c*	$11063\ ^2{}_{1/2}-31503\ ^1{}_{1/2}$
4891.918	20436.17	8000	800	$11578\ ^1{}_{1/2}-32014\ ^2{}_{1/2}$
4892.490	20433.78	150	15	$22180\ ^4{}_{1/2}-42613\ ^4{}_{1/2}$
4893.153	20431.01	1 *h*		$22265\ ^2{}_{1/2}-42696\ ^2{}_{1/2}$
4893.651	20428.93	10 *c*	1 *c*	$24147\ ^4{}_{1/2}-44576\ ^4{}_{1/2}$
4895.977	20419.23	2		$21206\ ^2{}_{1/2}-41625\ ^1{}_{1/2}$
4897.251	20413.91	8	1	$20686\ ^2{}_{1/2}-41100\ ^2{}_{1/2}$
4900.046	20402.27	30	3	$20686\ ^2{}_{1/2}-41088\ ^3{}_{1/2}$
4900.955	20398.49	10	1	$22503\ ^1{}_{1/2}-42901\ ^1{}_{1/2}$
4902.085	20393.78	1		$19702\ ^1{}_{1/2}-40096\ ^1{}_{1/2}$
4903.747	20386.87	2		$20686\ ^2{}_{1/2}-41073\ ^1{}_{1/2}$
4906.410	20375.81	50	5	$21204\ ^4{}_{1/2}-41580\ ^3{}_{1/2}$
4906.791	20374.23	10	1	$21920\ ^2{}_{1/2}-42294\ ^2{}_{1/2}$
4908.509	20367.09	1000	100	$11890\ ^0{}_{1/2}-32258\ ^1{}_{1/2}$
4909.053	20364.84	5	1	$22180\ ^4{}_{1/2}-42545\ ^4{}_{1/2}$
4909.566	20362.71	2000	200	$11890\ ^0{}_{1/2}-32253\ ^1{}_{1/2}$
4912.422	20350.87	5 *c*		$11063\ ^2{}_{1/2}-31414\ ^3{}_{1/2}$
4913.020	20348.39	500	50	$11578\ ^1{}_{1/2}-31927\ ^2{}_{1/2}$

TABLE 3. *Classified lines of* Tc I

Wavelength A	Wavenumber cm^{-1}	Intensity		Energy levels cm^{-1}
		Arc	Spark	
4914.166	20343.65	10	1	$11063\ ^{2}{}_{1/2}-31406^{o}{}_{2_{1/2}}$
4914.699	20341.44	150 *c*	15 *c*	$23455^{o}{}_{2_{1/2}}-43796\ ^{2}{}_{1/2}$
4918.917	20324.00	3		$21204\ ^{4}{}_{1/2}-41529^{o}{}_{3_{1/2}}$
4918.917	20324.00	3		$21926\ ^{2}{}_{1/2}-42250^{o}{}_{2_{1/2}}$
4919.229	20322.71	5		$21206\ ^{2}{}_{1/2}-41529^{o}{}_{3_{1/2}}$
4920.668	20316.77	200 *c l*	20 *c*	$21447\ ^{1}{}_{1/2}-41764^{o}{}_{2_{1/2}}$
4921.646	20312.73	20	2	$21719\ ^{5}{}_{1/2}-42032^{o}{}_{3_{1/2}}$
4923.601	20304.67	300	3	$20783\ ^{3}{}_{1/2}-41088^{o}{}_{3_{1/2}}$
4925.412	20297.20	2		$21920\ ^{2}{}_{1/2}-42217^{o}{}_{1_{1/2}}$
4927.031	20290.53	5	1	$21926\ ^{2}{}_{1/2}-42217^{o}{}_{1_{1/2}}$
4928.676	20283.76	3		$23957\ ^{3}{}_{1/2}-44241^{o}{}_{2_{1/2}}$
4929.749	20279.34	25	2	$21450\ ^{4}{}_{1/2}-41729^{o}{}_{3_{1/2}}$
4930.360	20276.83	20	2	$29539\ ^{4}{}_{1/2}-49815^{o}{}_{4_{1/2}}$
4930.904	20274.59	15		$19702\ ^{1}{}_{1/2}-39977^{o}{}_{2_{1/2}}$
4933.430	20264.21	10		$22180\ ^{4}{}_{1/2}-42444^{o}{}_{3_{1/2}}$
4933.798	20262.70	25 *c*	2	$14679\ ^{0}{}_{1/2}-34942^{o}{}_{1_{1/2}}$
4936.132	20253.12	40	3	$21450\ ^{4}{}_{1/2}-41703^{o}{}_{4_{1/2}}$
4939.112	20240.90	2		$21752\ ^{3}{}_{1/2}-41993^{o}{}_{3_{1/2}}$
4947.078	20208.31	50 *c*	5 *c*	$23588^{o}{}_{1_{1/2}}-43796\ ^{2}{}_{1/2}$
4948.064	20204.28	400	40	$3250\ ^{3}{}_{1/2}-23455^{o}{}_{2_{1/2}}$
4948.839	20201.12	20	2	$19895\ ^{2}{}_{1/2}-40096^{o}{}_{1_{1/2}}$
4950.743	20193.35	2		$22503\ ^{1}{}_{1/2}-42696^{o}{}_{2_{1/2}}$
4953.351	20182.72	1 *h*		$21920\ ^{2}{}_{1/2}-42102^{o}{}_{2_{1/2}}$
4954.508	20178.00	2 *h*		$21447\ ^{1}{}_{1/2}-41625^{o}{}_{1_{1/2}}$
4954.713	20177.17	10	1	$21719\ ^{5}{}_{1/2}-41897^{o}{}_{4_{1/2}}$
4954.985	20176.06	20	2	$21926\ ^{2}{}_{1/2}-42102^{o}{}_{2_{1/2}}$
4956.337	20170.56	40	4	$21752\ ^{3}{}_{1/2}-41922^{o}{}_{2_{1/2}}$
4959.942	20155.90	4		$22615\ ^{3}{}_{1/2}-42771^{o}{}_{3_{1/2}}$
4961.532	20149.44	1		$23957\ ^{3}{}_{1/2}-44107^{o}{}_{2_{1/2}}$
4962.654	20144.88	10	1	$21752\ ^{3}{}_{1/2}-41896^{o}{}_{4_{1/2}}$
4966.255	20130.28	10	1	$21450\ ^{4}{}_{1/2}-41580^{o}{}_{3_{1/2}}$
4966.255	20130.28	10	1	$39185^{o}{}_{4_{1/2}}-59315\ ^{5}{}_{1/2}$
4967.200	20126.45	60 *cw*	6	$23265^{o}{}_{3_{1/2}}-43391\ ^{3}{}_{1/2}$
4968.854	20119.75	5 *c*		$24147\ ^{4}{}_{1/2}-44266^{o}{}_{3_{1/2}}$
4976.340	20089.48	5000	500	$17522^{o}{}_{4_{1/2}}-37612\ ^{3}{}_{1/2}$
4978.569	20080.49	20	2	$22615\ ^{3}{}_{1/2}-42696^{o}{}_{2_{1/2}}$
4979.028	20078.64	8	1	$21450\ ^{4}{}_{1/2}-41529^{o}{}_{3_{1/2}}$
4980.214	20073.85	3		$19903\ ^{3}{}_{1/2}-39977^{o}{}_{2_{1/2}}$
4980.448	20072.91	50	4	$21920\ ^{2}{}_{1/2}-41993^{o}{}_{3_{1/2}}$
4991.346	20029.08	1 *h*		$22265\ ^{2}{}_{1/2}-42294^{o}{}_{2_{1/2}}$
4993.978	20018.53	80 *c*		$20384\ ^{3}{}_{1/2}-40403^{o}{}_{4_{1/2}}$
4994.997	20014.44	400	40	$3250\ ^{3}{}_{1/2}-23265^{o}{}_{3_{1/2}}$
4999.120	19997.94	30	2	$22615\ ^{3}{}_{1/2}-42613^{o}{}_{4_{1/2}}$
5000.831	19991.10	50 *c*	3	$24147\ ^{4}{}_{1/2}-44138^{o}{}_{5_{1/2}}$
5002.674	19983.73	200	20	$21719\ ^{5}{}_{1/2}-41703^{o}{}_{4_{1/2}}$
5003.405	19980.81	2		$22265\ ^{2}{}_{1/2}-42246^{o}{}_{3_{1/2}}$
5005.737	19971.50	100	5	$19791\ ^{4}{}_{1/2}-39763^{o}{}_{4_{1/2}}$
5010.766	19951.46	30	2	$21752\ ^{3}{}_{1/2}-41703^{o}{}_{4_{1/2}}$
5014.517	19936.53	200 *cw*	20 *cw*	$23455^{o}{}_{2_{1/2}}-43391\ ^{3}{}_{1/2}$
5017.324	19925.38	1 *h*		$11578\ ^{1}{}_{1/2}-31503^{o}{}_{1_{1/2}}$

TABLE 3. *Classified lines of* Tc I

Wavelength A	Wavenumber cm^{-1}	Intensity		Energy levels cm^{-1}
		Arc	Spark	
5026.793	19887.85	300	30	$3700\ ^{2}_{1/2}$–$23588^{o}\ _{1/2}$
5027.894	19883.49	150	15	$21204\ ^{4}_{1/2}$–$41088^{o}\ _{3/2}$
5031.663	19868.60	4		$21920\ ^{2}_{1/2}$–$41788^{o}\ _{1/2}$
5032.107	19866.85	10	1	$21206\ ^{2}_{1/2}$–$41073^{o}\ _{1/2}$
5032.446	19865.51	80	8	$10516\ ^{3}_{1/2}$–$30382^{o}\ _{3/2}$
5033.613	19860.90	5	1	$21719\ ^{5}_{1/2}$–$41580^{o}\ _{3/2}$
5035.760	19852.44	3		$22180\ ^{4}_{1/2}$–$42032^{o}\ _{3/2}$
5036.002	19851.48	4		$20384\ ^{3}_{1/2}$–$40236^{o}\ _{3/2}$
5036.833	19848.21	5	1	$27971\ ^{4}_{1/2}$–$47819^{o}\ _{4/2}$
5039.572	19837.42	10	1	$22265\ ^{2}_{1/2}$–$42102^{o}\ _{2/2}$
5041.905	19828.24	1 *h*		$11578\ ^{1}_{1/2}$–$31406^{o}\ _{2/2}$
5043.699	19821.19	2		$42217^{o}\ _{4/2}$–$62038\ ^{3}_{1/2}$
5045.580	19813.80	2 *h*		$25058\ ^{3}_{1/2}$–$44872^{o}\ _{2/2}$
5046.622	19809.71	3 *h*		$21920\ ^{2}_{1/2}$–$41729^{o}\ _{3/2}$
5051.303	19791.35	40	4	$22503\ ^{1}_{1/2}$–$42294^{o}\ _{2/2}$
5055.274	19775.80	300	30	$19791\ ^{4}_{1/2}$–$39567^{o}\ _{3/2}$
5058.331	19763.85	60	6	$20639\ ^{5}_{1/2}$–$40403^{o}\ _{4/2}$
5060.686	19754.65	500	50	$3700\ ^{2}_{1/2}$–$23455^{o}\ _{2/2}$
5062.136	19749.00	2		$19827\ ^{0}_{1/2}$–$39576^{o}\ _{1/2}$
5067.632	19727.58	1		$22265\ ^{2}_{1/2}$–$41993^{o}\ _{3/2}$
5069.549	19720.12	50	5	$20686\ ^{2}_{1/2}$–$40406^{o}\ _{3/2}$
5070.378	19716.89	4		$22180\ ^{4}_{1/2}$–$41897^{o}\ _{4/2}$
5074.051	19702.62	3		$25174\ ^{2}_{1/2}$–$44876^{o}\ _{1/2}$
5075.184	19698.22	10	1	$25174\ ^{2}_{1/2}$–$44872^{o}\ _{2/2}$
5079.561	19681.25	2		$19895\ ^{2}_{1/2}$–$39576^{o}\ _{1/2}$
5080.268	19678.51	1 *h*		$22615\ ^{3}_{1/2}$–$42294^{o}\ _{2/2}$
5081.860	19672.35	3		$19895\ ^{2}_{1/2}$–$39567^{o}\ _{3/2}$
5083.969	19664.19	30	3	$19903\ ^{3}_{1/2}$–$39567^{o}\ _{3/2}$
5085.611	19657.84	2		$26950\ ^{3}_{1/2}$–$46608^{o}\ _{3/2}$
5086.922	19652.77	40	4	$21447\ ^{1}_{1/2}$–$41100^{o}\ _{2/2}$
5088.200	19647.84	1		$29233\ ^{3}_{1/2}$–$48881^{o}\ _{4/2}$
5090.743	19638.02	80	8	$21450\ ^{4}_{1/2}$–$41088^{o}\ _{3/2}$
5093.182	19628.62	10	1	$25058\ ^{3}_{1/2}$–$44687^{o}\ _{3/2}$
5095.575	19619.40	2		$20783\ ^{3}_{1/2}$–$40403^{o}\ _{4/2}$
5096.280	19616.68	5000	500	$10516\ ^{3}_{1/2}$–$30133^{o}\ _{4/2}$
5100.033	19602.25	6	1	$20639\ ^{5}_{1/2}$–$40241^{o}\ _{3/2}$
5100.327	19601.12	3	1	$22615\ ^{3}_{1/2}$–$42217^{o}\ _{4/2}$
5102.525	19592.68	30	3	$20384\ ^{3}_{1/2}$–$39977^{o}\ _{2/2}$
5103.240	19589.93	200 *c*	20 *c*	$23265^{o}\ _{3/2}$–$42855\ ^{4}_{1/2}$
5103.531	19588.81	10	1	$23957\ ^{3}_{1/2}$–$43546^{o}\ _{2/2}$
5104.321	19585.78	500	50	$4002\ ^{1}_{1/2}$–$23588^{o}\ _{1/2}$
5107.581	19573.28	8	1	$20523\ ^{2}_{1/2}$–$40096^{o}\ _{1/2}$
5109.079	19567.54	4	1	$11063\ ^{2}_{1/2}$–$30630^{o}\ _{1/2}$
5109.809	19564.75	200	20	$3700\ ^{2}_{1/2}$–$23265^{o}\ _{3/2}$
5111.113	19559.76	1		$29539\ ^{4}_{1/2}$–$49098^{o}\ _{4/2}$
5112.019	19556.29	3		$19903\ ^{3}_{1/2}$–$39459^{o}\ _{2/2}$
5113.370	19551.12	5		$23460\ ^{3}_{1/2}$–$43011^{o}\ _{2/2}$
5113.686	19549.91	30	3	$22180\ ^{4}_{1/2}$–$41729^{o}\ _{3/2}$
5120.605	19523.50	100	10	$22180\ ^{4}_{1/2}$–$41703^{o}\ _{4/2}$
5122.180	19517.49	20	2	$25058\ ^{3}_{1/2}$–$44576^{o}\ _{4/2}$

TABLE 3. *Classified lines of* Tc I

Wavelength A	Wavenumber cm^{-1}	Intensity		Energy levels cm^{-1}
		Arc	Spark	
5122.739	19515.36	6	1	$20783\ ^{3}_{3/2}$–$40299^{o}\ ^{2}_{3/2}$
5125.158	19506.15	6 *c*	1 *c*	$15770\ ^{1}_{1/2}$–$35276^{o}\ ^{0}_{1/2}$
5130.260	19486.76	1 *h*		$22615\ ^{3}_{3/2}$–$42102^{o}\ ^{2}_{3/2}$
5135.789	19465.78	6	1	$11063\ ^{2}_{3/2}$–$30528^{o}\ ^{2}_{3/2}$
5136.156	19464.39	40	4	$22265\ ^{2}_{3/2}$–$41729^{o}\ ^{3}_{3/2}$
5138.886	19454.05	3		$20523\ ^{2}_{3/2}$–$39977^{o}\ ^{2}_{3/2}$
5139.262	19452.62	500	50	$4002\ ^{1}_{3/2}$–$23455^{o}\ ^{2}_{3/2}$
5141.227	19445.19	1		$26950\ ^{3}_{3/2}$–$46396^{o}\ ^{3}_{3/2}$
5147.997	19419.62	4		$22503\ ^{1}_{3/2}$–$41922^{o}\ ^{2}_{3/2}$
5150.630	19409.69	500	50	$4178\ ^{0}_{3/2}$–$23588^{o}\ ^{1}_{3/2}$
5157.991	19381.99	10	1	$21447\ ^{1}_{3/2}$–$40829^{o}\ ^{0}_{3/2}$
5158.858	19378.73	30 *c*	3 *c*	$20384\ ^{3}_{3/2}$–$39763^{o}\ ^{4}_{3/2}$
5160.130	19373.96	1		$28839\ ^{5}_{3/2}$–$48213^{o}\ ^{4}_{3/2}$
5161.810	19367.65	2000	200	$13252\ ^{2}_{3/2}$–$32620^{o}\ ^{3}_{3/2}$
5161.810	19367.65	2000	200	$20523\ ^{2}_{3/2}$–$39891^{o}\ ^{2}_{3/2}$
5162.410	19365.40	5 *h*		$24147\ ^{4}_{3/2}$–$43512^{o}\ ^{5}_{3/2}$
5167.038	19348.05	1		$21752\ ^{3}_{3/2}$–$41100^{o}\ ^{2}_{3/2}$
5167.774	19345.30	8	1	$20231\ ^{1}_{3/2}$–$39576^{o}\ ^{1}_{3/2}$
5168.470	19342.69	2		$29539\ ^{4}_{3/2}$–$48881^{o}\ ^{4}_{3/2}$
5174.812	19318.99	2000	200	$11063\ ^{2}_{3/2}$–$30382^{o}\ ^{3}_{3/2}$
5177.018	19310.76	2		$14169\ ^{1}_{3/2}$–$33480^{o}\ ^{0}_{3/2}$
5177.387	19309.38	3		$23957\ ^{3}_{3/2}$–$43267^{o}\ ^{3}_{3/2}$
5177.746	19308.04	10 *c*		$30630^{o}\ ^{1}_{3/2}$–$49938\ ^{2}_{3/2}$
5178.104	19306.71	10		$22615\ ^{3}_{3/2}$–$41922^{o}\ ^{2}_{3/2}$
5181.930	19292.45	2 *h s*		$24564\ ^{5}_{3/2}$–$43857^{o}\ ^{6}_{3/2}$
5183.999	19284.75	50	2	$30528^{o}\ ^{2}_{3/2}$–$49813\ ^{2}_{3/2}$
5184.994	19281.05	10	1	$22615\ ^{3}_{3/2}$–$41896^{o}\ ^{4}_{3/2}$
5189.687	19263.62	40	4	$22265\ ^{2}_{3/2}$–$41529^{o}\ ^{3}_{3/2}$
5202.152	19217.46	10 *cw*		$15298\ ^{3}_{3/2}$–$34515^{o}\ ^{2}_{3/2}$
5206.862	19200.07	10		$21206\ ^{2}_{3/2}$–$40406^{o}\ ^{3}_{3/2}$
5207.358	19198.25	4		$21204\ ^{4}_{3/2}$–$40403^{o}\ ^{4}_{3/2}$
5208.623	19193.58	25		$20783\ ^{3}_{3/2}$–$39977^{o}\ ^{2}_{3/2}$
5211.262	19183.86	6		$30382^{o}\ ^{3}_{3/2}$–$49565\ ^{2}_{3/2}$
5211.477	19183.07	6		$30630^{o}\ ^{1}_{3/2}$–$49813\ ^{2}_{3/2}$
5214.087	19173.47	20	4	$14169\ ^{1}_{3/2}$–$33343^{o}\ ^{1}_{3/2}$
5220.239	19150.87	15	3	$26917\ ^{5}_{3/2}$–$46068^{o}\ ^{4}_{3/2}$
5221.447	19146.44	10	1	$21926\ ^{2}_{3/2}$–$41073^{o}\ ^{1}_{3/2}$
5223.517	19138.86	2		$27517\ ^{2}_{3/2}$–$46656^{o}\ ^{3}_{3/2}$
5225.360	19132.11	10	1	$25405\ ^{1}_{3/2}$–$44537^{o}\ ^{2}_{3/2}$
5228.648	19120.08	40 *cw*	4 *cw*	$24147\ ^{4}_{3/2}$–$43267^{o}\ ^{3}_{3/2}$
5228.756	19119.68	10		$23957\ ^{3}_{3/2}$–$43077^{o}\ ^{3}_{3/2}$
5230.342	19113.88	12	1	$22615\ ^{3}_{3/2}$–$41729^{o}\ ^{3}_{3/2}$
5231.268	19110.50	15	1	$11578\ ^{1}_{3/2}$–$30689^{o}\ ^{0}_{3/2}$
5232.164	19107.23	5	1	$20783\ ^{3}_{3/2}$–$39891^{o}\ ^{2}_{3/2}$
5232.929	19104.43	1 *h*		$30630^{o}\ ^{1}_{3/2}$–$49735\ ^{1}_{3/2}$
5236.130	19092.75	7	1	$25174\ ^{2}_{3/2}$–$44266^{o}\ ^{3}_{3/2}$
5236.452	19091.58	5	1	$27517\ ^{2}_{3/2}$–$46608^{o}\ ^{3}_{3/2}$
5237.180	19088.93	2		$25598\ ^{2}_{3/2}$–$44687^{o}\ ^{3}_{3/2}$
5237.521	19087.68	2		$22615\ ^{3}_{3/2}$–$41703^{o}\ ^{4}_{3/2}$
5238.247	19085.04	1		$24564\ ^{5}_{3/2}$–$43649^{o}\ ^{4}_{3/2}$

TABLE 3. *Classified lines of* Tc I

Wavelength A	Wavenumber cm^{-1}	Intensity		Energy levels cm^{-1}
		Arc	Spark	
5240.953	19075.19	20 *c*	2 *c*	$20384\ ^{3}_{1/2}$–$39459^{\circ}_{2,1/2}$
5242.641	19069.04	2		$21752\ ^{3}_{1/2}$–$40821^{\circ}_{2,1/2}$
5243.094	19067.40	2		$25174\ ^{2}_{1/2}$–$44241^{\circ}_{2,1/2}$
5247.006	19053.18	20	2	$20523\ ^{2}_{1/2}$–$39576^{\circ}_{1,1/2}$
5249.428	19044.39	20 *c*	2	$20523\ ^{2}_{1/2}$–$39567^{\circ}_{3,1/2}$
5249.428	19044.39	20 *c*	2	$30528^{\circ}_{2,1/2}$–$49573\ ^{3}_{1/2}$
5251.421	19037.16	40 *c*	3 *c*	$30528^{\circ}_{2,1/2}$–$49565\ ^{2}_{1/2}$
5253.052	19031.25	5		$21204\ ^{4}_{1/2}$–$40236^{\circ}_{3,1/2}$
5253.421	19029.91	6		$21206\ ^{2}_{1/2}$–$40236^{\circ}_{3,1/2}$
5254.762	19025.06	20 *c*	2 *c*	$24147\ ^{4}_{1/2}$–$43172^{\circ}_{3,1/2}$
5260.217	19005.33	200 *cw*	20 *c*	$13252\ ^{2}_{1/2}$–$32258^{\circ}_{1,1/2}$
5261.444	19000.90	200 *c*	20 *c*	$13252\ ^{2}_{1/2}$–$32253^{\circ}_{1,1/2}$
5267.350	18979.59	3		$20783\ ^{3}_{1/2}$–$39763^{\circ}_{4,1/2}$
5273.930	18955.91	15	2	$21450\ ^{4}_{1/2}$–$40406^{\circ}_{3,1/2}$
5274.824	18952.70	50	5	$21450\ ^{4}_{1/2}$–$40403^{\circ}_{4,1/2}$
5275.512	18950.23	1000	100	$11578\ ^{1}_{1/2}$–$30528^{\circ}_{2,1/2}$
5279.330	18936.52	30 *c*	2 *c*	$20523\ ^{2}_{1/2}$–$39459^{\circ}_{2,1/2}$
5281.101	18930.17	20 *c*	1 *c*	$24147\ ^{4}_{1/2}$–$43077^{\circ}_{3,1/2}$
5285.067	18915.97	800	80	$14169\ ^{1}_{1/2}$–$33085^{\circ}_{2,1/2}$
5285.838	18913.21	8	1	$22615\ ^{3}_{1/2}$–$41529^{\circ}_{3,1/2}$
5291.060	18894.54	2 *h*		$21926\ ^{2}_{1/2}$–$40821^{\circ}_{2,1/2}$
5291.905	18891.53	3 *h*		$15624\ ^{2}_{1/2}$–$34515^{\circ}_{2,1/2}$
5292.263	18890.25	30 *c*	3 *c*	$20686\ ^{2}_{1/2}$–$39576^{\circ}_{1,1/2}$
5292.263	18890.25	30 *c*	3 *c*	$21206\ ^{2}_{1/2}$–$40096^{\circ}_{1,1/2}$
5299.669	18863.85	20	1	$30382^{\circ}_{3,1/2}$–$49245\ ^{3}_{1/2}$
5305.307	18843.80	100	6	$30133^{\circ}_{4,1/2}$–$48977\ ^{4}_{1/2}$
5307.558	18835.81	5		$25405\ ^{1}_{1/2}$–$44241^{\circ}_{2,1/2}$
5307.875	18834.69	1		$22265\ ^{2}_{1/2}$–$41100^{\circ}_{2,1/2}$
5311.163	18823.03	10	1	$22265\ ^{2}_{1/2}$–$41088^{\circ}_{3,1/2}$
5313.696	18814.05	1 *h*		$23957\ ^{3}_{1/2}$–$42771^{\circ}_{3,1/2}$
5317.509	18800.56	30 *c*	3 *c*	$14679\ ^{0}_{1/2}$–$33480^{\circ}_{0,1/2}$
5318.186	18798.17	15 *c*	1 *c*	$11890\ ^{0}_{1/2}$–$30689^{\circ}_{0,1/2}$
5320.198	18791.06	600	60	$21450\ ^{4}_{1/2}$–$40241^{\circ}_{3,1/2}$
5325.132	18773.65	5		$20686\ ^{2}_{1/2}$–$39459^{\circ}_{2,1/2}$
5325.848	18771.13	4		$21206\ ^{2}_{1/2}$–$39977^{\circ}_{2,1/2}$
5328.406	18762.12	10	1	$13252\ ^{2}_{1/2}$–$32014^{\circ}_{2,1/2}$
5329.620	18757.84	4		$26950\ ^{3}_{1/2}$–$45708^{\circ}_{4,1/2}$
5332.201	18748.76	2		$29539\ ^{4}_{1/2}$–$48287^{\circ}_{3,1/2}$
5334.790	18739.66	200	20	$11890\ ^{0}_{1/2}$–$30630^{\circ}_{1,1/2}$
5335.080	18738.64	6	1	$23957\ ^{3}_{1/2}$–$42696^{\circ}_{2,1/2}$
5337.066	18731.67	5	1	$25174\ ^{2}_{1/2}$–$43905^{\circ}_{3,1/2}$
5345.690	18701.45	8		$25405\ ^{1}_{1/2}$–$44107^{\circ}_{2,1/2}$
5345.890	18700.75	15 *c*	1 *c*	$24564\ ^{5}_{1/2}$–$43265^{\circ}_{4,1/2}$
5350.498	18684.65	4		$21206\ ^{2}_{1/2}$–$39891^{\circ}_{2,1/2}$
5350.873	18683.34	15		$21719\ ^{5}_{1/2}$–$40403^{\circ}_{4,1/2}$
5353.480	18674.24	500 *cw*	50 *cw*	$13252\ ^{2}_{1/2}$–$31927^{\circ}_{2,1/2}$
5355.110	18668.56	6	1	$25598\ ^{2}_{1/2}$–$44266^{\circ}_{3,1/2}$
5356.634	18663.25	200	20	$14679\ ^{0}_{1/2}$–$33343^{\circ}_{1,1/2}$
5358.646	18656.24	300	30	$23957\ ^{3}_{1/2}$–$42613^{\circ}_{4,1/2}$
5359.222	18654.23	40	4	$21752\ ^{3}_{1/2}$–$40406^{\circ}_{3,1/2}$

TABLE 3. *Classified lines of* Tc I

Wavelength A	Wavenumber cm^{-1}	Intensity		Energy levels cm^{-1}
		Arc	Spark	
5360.142	18651.03	200	20	$21752\ ^{3}_{1/2}-40403^{o}\ ^{4}_{1/2}$
5360.690	18649.12	15	1	$21447\ ^{1}_{1/2}-40096^{o}\ ^{1}_{1/2}$
5362.420	18643.11	4*wd*		$21206\ ^{2}_{1/2}-39849^{o}\ ^{3}_{1/2}$
5364.050	18637.44	20	2	$27971\ ^{4}_{1/2}-46608^{o}\ ^{3}_{1/2}$
5366.082	18630.39	10	1	$29233\ ^{3}_{1/2}-47864^{o}\ ^{3}_{1/2}$
5367.090	18626.89	2		$24147\ ^{4}_{1/2}-42773^{o}\ ^{5}_{1/2}$
5372.719	18607.37	1*h*		$24564\ ^{5}_{1/2}-43172^{o}\ ^{5}_{1/2}$
5376.298	18594.98	10*h*	1*h*	$30382^{o}\ ^{3}_{1/2}-48977\ ^{4}_{1/2}$
5377.414	18591.13	20	2	$25058\ ^{3}_{1/2}-43649^{o}\ ^{4}_{1/2}$
5378.457	18587.52	2	1	$27517\ ^{2}_{1/2}-46104^{o}\ ^{2}_{1/2}$
5378.970	18585.75	1*h*		$29233\ ^{3}_{1/2}-47819^{o}\ ^{4}_{1/2}$
5383.509	18570.08	30 *c*	2 *c*	$22503\ ^{1}_{1/2}-41073^{o}\ ^{1}_{1/2}$
5385.832	18562.07	10*h*		$30382^{o}\ ^{3}_{1/2}-48944\ ^{2}_{1/2}$
5386.872	18558.48	10	1	$21204\ ^{4}_{1/2}-39763^{o}\ ^{4}_{1/2}$
5387.630	18555.87	6*h*		$22265\ ^{2}_{1/2}-40821^{o}\ ^{2}_{1/2}$
5390.214	18546.98	1		$21752\ ^{3}_{1/2}-40299^{o}\ ^{2}_{1/2}$
5394.569	18532.00	3*h*		$31406^{o}\ ^{2}_{1/2}-49938\ ^{2}_{1/2}$
5395.149	18530.01	1		$21447\ ^{1}_{1/2}-39977^{o}\ ^{2}_{1/2}$
5395.149	18530.01	1		$43971^{o}\ ^{4}_{1/2}-62501\ ^{3}_{1/2}$
5396.690	18524.72	2		$31414^{o}\ ^{3}_{1/2}-49938\ ^{2}_{1/2}$
5397.539	18521.81	5		$21719\ ^{5}_{1/2}-40241^{o}\ ^{5}_{1/2}$
5400.480	18511.72	20		$25598\ ^{2}_{1/2}-44110^{o}\ ^{1}_{1/2}$
5407.910	18486.29	50 *c*	3 *c*	$21920\ ^{2}_{1/2}-40406^{o}\ ^{3}_{1/2}$
5411.928	18472.56	20	1	$22615\ ^{3}_{1/2}-41088^{o}\ ^{3}_{1/2}$
5413.624	18466.78	2*h*		$24147\ ^{4}_{1/2}-42613^{o}\ ^{4}_{1/2}$
5417.121	18454.86	3		$28839\ ^{5}_{1/2}-47294^{o}\ ^{5}_{1/2}$
5418.934	18448.68	2*h*		$19791\ ^{4}_{1/2}-38240^{o}\ ^{3}_{1/2}$
5422.382	18436.95	2		$23460\ ^{3}_{1/2}-41896^{o}\ ^{4}_{1/2}$
5423.048	18434.69	150 *c*	15 *c*	$31503^{o}\ ^{1}_{1/2}-49938\ ^{2}_{1/2}$
5425.956	18424.81	6	1	$27971\ ^{4}_{1/2}-46396^{o}\ ^{3}_{1/2}$
5430.712	18408.67	2		$25598\ ^{2}_{1/2}-44007^{o}\ ^{2}_{1/2}$
5431.246	18406.86	15*h*	1	$31406^{o}\ ^{2}_{1/2}-49813\ ^{2}_{1/2}$
5432.437	18402.83	5		$30382^{o}\ ^{3}_{1/2}-48784\ ^{3}_{1/2}$
5433.894	18397.89	1		$24147\ ^{4}_{1/2}-42545^{o}\ ^{4}_{1/2}$
5438.774	18381.38	2*h*		$20384\ ^{3}_{1/2}-38766^{o}\ ^{3}_{1/2}$
5441.440	18372.38	2		$21926\ ^{2}_{1/2}-40299^{o}\ ^{2}_{1/2}$
5441.440	18372.38	2		$25174\ ^{2}_{1/2}-43546^{o}\ ^{2}_{1/2}$
5442.071	18370.25	4 *cw*		$21206\ ^{2}_{1/2}-39576^{o}\ ^{1}_{1/2}$
5444.258	18362.87	50	5	$21204\ ^{4}_{1/2}-39567^{o}\ ^{3}_{1/2}$
5447.402	18352.27	200	20	$13252\ ^{2}_{1/2}-31605^{o}\ ^{3}_{1/2}$
5447.800	18350.93	20 *c*		$30067^{o}\ ^{5}_{1/2}-48418\ ^{4}_{1/2}$
5451.900	18337.13	500 *c*	50 *c*	$19903\ ^{3}_{1/2}-38240^{o}\ ^{3}_{1/2}$
5454.124	18329.65	3		$30133^{o}\ ^{4}_{1/2}-48462\ ^{3}_{1/2}$
5455.112	18326.33	20*wd*		$22503\ ^{1}_{1/2}-40829^{o}\ ^{0}_{1/2}$
5458.159	18316.10	30 *cw*		$21920\ ^{2}_{1/2}-40236^{o}\ ^{3}_{1/2}$
5459.118	18312.88	2 *c*		$21450\ ^{4}_{1/2}-39763^{o}\ ^{4}_{1/2}$
5460.747	18307.42	10		$25598\ ^{2}_{1/2}-43905^{o}\ ^{3}_{1/2}$
5467.471	18284.91	10		$30133^{o}\ ^{4}_{1/2}-48418\ ^{4}_{1/2}$
5468.768	18280.57	3		$29539\ ^{4}_{1/2}-47819^{o}\ ^{4}_{1/2}$
5471.962	18269.90	300		$23460\ ^{3}_{1/2}-41729^{o}\ ^{3}_{1/2}$

TABLE 3. *Classified lines of* Tc I

Wavelength A	Wavenumber cm^{-1}	Intensity		Energy levels cm^{-1}
		Arc	Spark	
5477.540	18251.29	20 *cw*		$13252\ ^{2}_{1/2}$–$31503^{o}\ ^{2}_{1/2}$
5480.035	18242.98	3 *c*		$20523\ ^{2}_{1/2}$–$38766^{o}\ ^{2}_{3/2}$
5482.92	18233.37	120 *c*	12 *c*	$14169\ ^{1}_{1/2}$–$32403^{o}\ ^{0}_{1/2}$
5483.012	18233.08	70	7	$43805^{o}\ ^{3}_{1/2}$–$62038\ ^{3}_{1/2}$
5485.026	18226.39	50 *c*	1 *c*	$22180\ ^{4}_{1/2}$–$40406^{o}\ ^{3}_{1/2}$
5485.373	18225.23	60	3	$21752\ ^{3}_{1/2}$–$39977^{o}\ ^{2}_{1/2}$
5486.028	18223.06	2		$22180\ ^{4}_{1/2}$–$40403^{o}\ ^{4}_{1/2}$
5490.391	18208.58	30 *c*	2	$31605^{o}\ ^{3}_{1/2}$–$49813\ ^{2}_{1/2}$
5490.903	18206.88	5		$25058\ ^{3}_{1/2}$–$43265^{o}\ ^{4}_{1/2}$
5500.096	18176.45	20	2	$21920\ ^{2}_{1/2}$–$40096^{o}\ ^{1}_{1/2}$
5502.110	18169.79	5		$21926\ ^{2}_{1/2}$–$40096^{o}\ ^{1}_{1/2}$
5504.608	18161.55	2*h*		$13252\ ^{2}_{1/2}$–$31414^{o}\ ^{3}_{1/2}$
5505.274	18159.35	30*h*	2*h*	$31414^{o}\ ^{3}_{1/2}$–$49573\ ^{3}_{1/2}$
5506.890	18154.02	80 *cw*	5 *c*	$13252\ ^{2}_{1/2}$–$31406^{o}\ ^{2}_{1/2}$
5510.866	18140.92	10	1	$22265\ ^{2}_{1/2}$–$40406^{o}\ ^{3}_{1/2}$
5511.478	18138.91	2		$21752\ ^{3}_{1/2}$–$39891^{o}\ ^{2}_{1/2}$
5513.630	18131.83	10*h*		$31114^{o}\ ^{4}_{1/2}$–$49245\ ^{3}_{1/2}$
5514.216	18129.90	20*h*		$46656^{o}\ ^{3}_{1/2}$–$64785\ ^{3}_{1/2}$
5518.051	18117.30	30	3	$21450\ ^{4}_{1/2}$–$39567^{o}\ ^{3}_{1/2}$
5524.107	18097.44	150	15	$27971\ ^{4}_{1/2}$–$46068^{o}\ ^{4}_{1/2}$
5526.878	18088.37	6		$14169\ ^{1}_{1/2}$–$32258^{o}\ ^{1}_{1/2}$
5528.233	18083.94	100	10	$14169\ ^{1}_{1/2}$–$32253^{o}\ ^{1}_{1/2}$
5532.793	18069.03	1		$23460\ ^{3}_{1/2}$–$41529^{o}\ ^{3}_{1/2}$
5535.098	18061.51	10		$22180\ ^{4}_{1/2}$–$40241^{o}\ ^{3}_{1/2}$
5536.394	18057.28	20	1	$21920\ ^{2}_{1/2}$–$39977^{o}\ ^{2}_{1/2}$
5538.875	18049.19	10 *cw*	1 *c*	$24564\ ^{5}_{1/2}$–$42613^{o}\ ^{4}_{1/2}$
5540.596	18043.58	10	1	$21719\ ^{5}_{1/2}$–$39763^{o}\ ^{4}_{1/2}$
5541.939	18039.21	200	20	$25058\ ^{3}_{1/2}$–$43097^{o}\ ^{4}_{1/2}$
5543.627	18033.72	80	8	$22265\ ^{2}_{1/2}$–$40299^{o}\ ^{2}_{1/2}$
5548.227	18018.77	2		$25058\ ^{3}_{1/2}$–$43077^{o}\ ^{3}_{1/2}$
5554.516	17998.37	1*h*		$29233\ ^{3}_{1/2}$–$47232^{o}\ ^{2}_{1/2}$
5556.110	17993.20	2		$26883\ ^{2}_{1/2}$–$44876^{o}\ ^{1}_{1/2}$
5563.006	17970.90	10 *cw*		$21920\ ^{2}_{1/2}$–$39891^{o}\ ^{2}_{1/2}$
5564.840	17964.98	3*h*		$23957\ ^{3}_{1/2}$–$41922^{o}\ ^{2}_{1/2}$
5565.140	17964.01	1		$44537^{o}\ ^{2}_{1/2}$–$62501\ ^{3}_{1/2}$
5566.102	17960.90	4*hd*		$31605^{o}\ ^{3}_{1/2}$–$49565\ ^{2}_{1/2}$
5567.748	17955.59	2*h*		$26883\ ^{2}_{1/2}$–$44839^{o}\ ^{3}_{1/2}$
5568.700	17952.52	5		$25058\ ^{3}_{1/2}$–$43011^{o}\ ^{2}_{1/2}$
5570.032	17948.23	3		$25598\ ^{2}_{1/2}$–$43546^{o}\ ^{2}_{1/2}$
5572.858	17939.13	20	1	$23957\ ^{3}_{1/2}$–$41896^{o}\ ^{4}_{1/2}$
5575.438	17930.83	10*h*		$31406^{o}\ ^{2}_{1/2}$–$49337\ ^{2}_{1/2}$
5577.649	17923.72	15*w*		$21920\ ^{2}_{1/2}$–$39844^{o}\ ^{1}_{1/2}$
5581.931	17909.97	2 *c*		$24564\ ^{5}_{1/2}$–$42474^{o}\ ^{4}_{1/2}$
5584.031	17903.23	20	2	$25174\ ^{2}_{1/2}$–$43077^{o}\ ^{3}_{1/2}$
5589.019	17887.26	3000 *cw*	300 *cw*	$14733\ ^{4}_{1/2}$–$32620^{o}\ ^{3}_{1/2}$
5591.400	17879.64	1*h*		$24564\ ^{5}_{1/2}$–$42444^{o}\ ^{5}_{1/2}$
5596.614	17862.98	2*h*		$31114^{o}\ ^{4}_{1/2}$–$48977\ ^{4}_{1/2}$
5602.229	17845.08	200	20	$14169\ ^{1}_{1/2}$–$32014^{o}\ ^{2}_{1/2}$
5604.069	17839.22	2*h*		$31406^{o}\ ^{2}_{1/2}$–$49245\ ^{3}_{1/2}$
5604.762	17837.01	1*h*		$25174\ ^{2}_{1/2}$–$43011^{o}\ ^{2}_{1/2}$

TABLE 3. *Classified lines of* Tc I

Wavelength A	Wavenumber cm^{-1}	Intensity		Energy levels cm^{-1}
		Arc	Spark	
5606.376	17831.88	10 *h*		$20384\ ^{3}_{1/2}$–38216^{o}_{2}
5606.376	17831.88	10 *h*		31414^{o}_{4}–$49245\ ^{3}_{2}$
5611.482	17815.65	20	2	$21752\ ^{3}_{2}$–39567^{o}_{3}
5613.863	17808.10	2 *h*		31927^{o}_{2}–$49735\ ^{1}_{2}$
5615.272	17803.63	8	1	$26883\ ^{2}_{2}$–44687^{o}_{3}
5615.272	17803.63	8	1	$30060\ ^{2}_{2}$–47864^{o}_{3}
5616.795	17798.80	10		32014^{o}_{2}–$49813\ ^{2}_{2}$
5617.651	17796.09	7	1	$20523\ ^{2}_{2}$–38319^{o}_{1}
5620.450	17787.23	2000 *c*	200	$15298\ ^{3}_{2}$–33085^{o}_{2}
5625.232	17772.11	6		$23957\ ^{3}_{2}$–41729^{o}_{3}
5628.956	17760.35	1		44839^{o}_{3}–$62599\ ^{4}_{2}$
5629.568	17758.42	5		$25058\ ^{3}_{2}$–42817^{o}_{4}
5629.937	17757.25	300	30	$14169\ ^{1}_{2}$–31927^{o}_{2}
5636.253	17737.36	30	3	$27971\ ^{4}_{2}$–45708^{o}_{4}
5637.792	17732.51	8 *h*	1	31605^{o}_{3}–$49337\ ^{2}_{2}$
5640.782	17723.11	40 *c*	2 *c*	$14679\ ^{0}_{2}$–32403^{o}_{0}
5642.132	17718.87	1500	150	$15624\ ^{2}_{2}$–33343^{o}_{1}
5643.940	17713.20	6		$25058\ ^{3}_{2}$–42771^{o}_{3}
5644.357	17711.89	12	1	$22265\ ^{2}_{2}$–39977^{o}_{2}
5644.944	17710.05	800	80	$15770\ ^{1}_{2}$–33480^{o}_{0}
5645.694	17707.70	2		$21752\ ^{3}_{2}$–39459^{o}_{2}
5650.259	17693.39	1		$20523\ ^{2}_{2}$–38216^{o}_{2}
5652.909	17685.09	1		32253^{o}_{1}–$49938\ ^{2}_{2}$
5654.338	17680.62	6		32258^{o}_{1}–$49938\ ^{2}_{2}$
5657.490	17670.77	3		31114^{o}_{4}–$48784\ ^{3}_{2}$
5658.106	17668.85	8	1	$25598\ ^{2}_{2}$–43267^{o}_{3}
5661.557	17658.08	20	2	$26917\ ^{5}_{2}$–44576^{o}_{4}
5662.104	17656.37	10	1	$21920\ ^{2}_{2}$–39576^{o}_{1}
5664.232	17649.74	4		$21926\ ^{2}_{2}$–39576^{o}_{1}
5664.900	17647.66	40 *cw*	2 *cw*	$21920\ ^{2}_{2}$–39567^{o}_{3}
5667.058	17640.94	15		$21926\ ^{2}_{2}$–39567^{o}_{3}
5667.058	17640.94	15		31605^{o}_{3}–$49245\ ^{3}_{2}$
5672.153	17625.09	60	6	$26950\ ^{3}_{2}$–44576^{o}_{4}
5675.178	17615.70	5 *h s*		27369^{o}_{4}–$44985\ ^{3}_{2}$
5678.478	17605.46	50	2	$25405\ ^{1}_{2}$–43011^{o}_{2}
5680.973	17597.73	15		$25174\ ^{2}_{2}$–42771^{o}_{3}
5682.298	17593.63	1 *h*		$22503\ ^{1}_{2}$–40096^{o}_{1}
5687.301	17578.15	200	20	$14679\ ^{0}_{2}$–32258^{o}_{1}
5688.730	17573.74	20	2	$14679\ ^{0}_{2}$–32253^{o}_{1}
5689.046	17572.76	200	20	$15770\ ^{1}_{2}$–33343^{o}_{1}
5692.212	17562.99	15 *h*	1	31414^{o}_{4}–$48977\ ^{4}_{2}$
5694.330	17556.45	15 *c*	2 *c*	$24147\ ^{4}_{2}$–41703^{o}_{4}
5696.056	17551.13	20 *h*	2	32014^{o}_{2}–$49565\ ^{2}_{2}$
5696.626	17549.38	18 *cw*	2 *c*	27369^{o}_{4}–$44919\ ^{4}_{2}$
5702.894	17530.09	5 *h*		31414^{o}_{3}–$48944\ ^{2}_{2}$
5705.403	17522.38	1 *h*		$25174\ ^{2}_{2}$–42696^{o}_{2}
5718.775	17481.41	1 *h*		32253^{o}_{1}–$49735\ ^{1}_{2}$
5719.542	17479.06	10	1	$25598\ ^{2}_{2}$–43077^{o}_{3}
5720.205	17477.04	1 *h*		32258^{o}_{1}–$49735\ ^{1}_{2}$
5721.090	17474.339	10 *h*	1 *h*	$22503\ ^{1}_{2}$–39977^{o}_{2}

TABLE 3. *Classified lines of* Tc I

Wavelength A	Wavenumber cm^{-1}	Intensity		Energy levels cm^{-1}
		Arc	Spark	
5723.255	17467.72	2*h*		$24564\ ^{5}_{1/2}$–$42032^{o}\ ^{5}_{1/2}$
5725.314	17461.44	700	70	$15624\ ^{2}_{1/2}$–$33085^{o}\ ^{2}_{1/2}$
5732.791	17438.67	3		$27517\ ^{2}_{1/2}$–$44955^{o}\ ^{1}_{1/2}$
5734.691	17432.89	2*h*		$20783\ ^{3}_{1/2}$–$38216^{o}\ ^{2}_{1/2}$
5734.691	17432.89	2*h*		$21752\ ^{3}_{1/2}$–$39185^{o}\ ^{4}_{1/2}$
5735.636	17430.02	3		$26883\ ^{2}_{1/2}$–$44313^{o}\ ^{1}_{1/2}$
5737.543	17424.23	5*w*		$10516\ ^{3}_{1/2}$–$27940^{o}\ ^{2}_{1/2}$
5739.479	17418.35	1*h*		$41896^{o}\ ^{4}_{1/2}$–$59315\ ^{5}_{1/2}$
5741.301	17412.82	5		$25598\ ^{2}_{1/2}$–$43011^{o}\ ^{2}_{1/2}$
5741.943	17410.87	10*hw*	1*h*	$27660^{o}\ ^{3}_{1/2}$–$45071\ ^{2}_{1/2}$
5748.307	17391.60	3		$30060\ ^{2}_{1/2}$–$47452^{o}\ ^{2}_{1/2}$
5749.542	17387.86	10*c*		$22503\ ^{1}_{1/2}$–$39891^{o}\ ^{2}_{1/2}$
5751.050	17383.30	1*h*		$26883\ ^{2}_{1/2}$–$44266^{o}\ ^{3}_{1/2}$
5754.775	17372.05	20*h*		$31605^{o}\ ^{3}_{1/2}$–$48977\ ^{4}_{1/2}$
5755.199	17370.77	3*h*		$31414^{o}\ ^{3}_{1/2}$–$48784\ ^{3}_{1/2}$
5758.298	17361.42	1*h*		$22615\ ^{3}_{1/2}$–$39977^{o}\ ^{2}_{1/2}$
5760.389	17355.12	2		$27517\ ^{2}_{1/2}$–$44872^{o}\ ^{2}_{1/2}$
5761.734	17351.07	1		$44687^{o}\ ^{3}_{1/2}$–$62038\ ^{3}_{1/2}$
5762.449	17348.92	5		$25174\ ^{2}_{1/2}$–$42523^{o}\ ^{3}_{1/2}$
5765.698	17339.14	5*h*		$31605^{o}\ ^{3}_{1/2}$–$48944\ ^{2}_{1/2}$
5767.232	17334.53	4 *hc*		$14169\ ^{1}_{1/2}$–$31503^{o}\ ^{1}_{1/2}$
5767.546	17333.58	6		$47452^{o}\ ^{2}_{1/2}$–$64785\ ^{3}_{1/2}$
5768.002	17332.21	2		$24564\ ^{5}_{1/2}$–$41896^{o}\ ^{4}_{1/2}$
5769.704	17327.10	3		$27940^{o}\ ^{2}_{1/2}$–$45267\ ^{1}_{1/2}$
5770.249	17325.47	4		$27660^{o}\ ^{3}_{1/2}$–$44985\ ^{3}_{1/2}$
5771.468	17321.81	500 *c*	50 *c*	$15298\ ^{3}_{1/2}$–$32620^{o}\ ^{3}_{1/2}$
5772.500	17318.71	1*h*		$26788\ ^{2}_{1/2}$–$44107^{o}\ ^{2}_{1/2}$
5773.656	17315.24	20	2	$15770\ ^{1}_{1/2}$–$33085^{o}\ ^{2}_{1/2}$
5775.069	17311.01	10 *cw*	1 *c*	$22265\ ^{2}_{1/2}$–$39576^{o}\ ^{1}_{1/2}$
5777.360	17304.14	1		$31114^{o}\ ^{4}_{1/2}$–$48418\ ^{4}_{1/2}$
5777.976	17302.30	6	1	$22265\ ^{2}_{1/2}$–$39567^{o}\ ^{3}_{1/2}$
5792.474	17258.99	10 *cw*		$27660^{o}\ ^{3}_{1/2}$–$44919\ ^{4}_{1/2}$
5799.850	17237.04	80 *c*	8 *c*	$14169\ ^{1}_{1/2}$–$31406^{o}\ ^{2}_{1/2}$
5802.433	17229.37	10	1	$28839\ ^{5}_{1/2}$–$46068^{o}\ ^{4}_{1/2}$
5805.214	17221.11	20	2	$30060\ ^{2}_{1/2}$–$47281^{o}\ ^{2}_{1/2}$
5805.525	17220.19	10	1	$26917\ ^{5}_{1/2}$–$44138^{o}\ ^{5}_{1/2}$
5806.126	17218.41	2*h*		$26788\ ^{2}_{1/2}$–$44007^{o}\ ^{2}_{1/2}$
5814.241	17194.38	100 *cw*	10 *c*	$22265\ ^{2}_{1/2}$–$39459^{o}\ ^{2}_{1/2}$
5814.639	17193.20	2		$32620^{o}\ ^{3}_{1/2}$–$49813\ ^{2}_{1/2}$
5815.038	17192.02	1*h*		$25058\ ^{3}_{1/2}$–$42250^{o}\ ^{2}_{1/2}$
5819.176	17179.80	15*h l*		$31605^{o}\ ^{3}_{1/2}$–$48784\ ^{3}_{1/2}$
5821.310	17173.50	10	1	$25598\ ^{2}_{1/2}$–$42771^{o}\ ^{3}_{1/2}$
5823.196	17167.94	8	1	$27940^{o}\ ^{2}_{1/2}$–$45108\ ^{1}_{1/2}$
5827.189	17156.17	10	1	$26950\ ^{3}_{1/2}$–$44107^{o}\ ^{2}_{1/2}$
5831.477	17143.56	200	20	$10516\ ^{3}_{1/2}$–$27660^{o}\ ^{3}_{1/2}$
5831.858	17142.44	2		$23957\ ^{3}_{1/2}$–$41100^{o}\ ^{2}_{1/2}$
5832.836	17139.56	2		$26950\ ^{3}_{1/2}$–$44090^{o}\ ^{3}_{1/2}$
5835.865	17130.67	6	1	$23957\ ^{3}_{1/2}$–$41088^{o}\ ^{3}_{1/2}$
5836.329	17129.30	150 *c*	15 *c*	$13252\ ^{2}_{1/2}$–$30382^{o}\ ^{3}_{1/2}$
5838.366	17123.33	10	1	$26883\ ^{2}_{1/2}$–$44007^{o}\ ^{2}_{1/2}$

TABLE 3. *Classified lines of* Tc I

Wavelength A	Wavenumber cm^{-1}	Intensity		Energy levels cm^{-1}
		Arc	Spark	
5846.973	17098.12	1		$42217^{o}_{4\,1/2}$–$59315_{5\,1/2}$
5850.364	17088.21	6	1	$11063_{2\,1/2}$–$28151^{o}_{1\,1/2}$
5853.376	17079.42	25 *h*	2 *h*	$32258^{o}_{1\,1/2}$–$49337_{2\,1/2}$
5855.439	17073.40	7 *cw*		$22503_{1\,1/2}$–$39576^{o}_{1\,1/2}$
5855.898	17072.06	1		$25174_{2\,1/2}$–$42246^{o}_{3\,1/2}$
5856.656	17069.85	5		$29539_{4\,1/2}$–$46608^{o}_{3\,1/2}$
5863.865	17048.87	30 *h*		$31414^{o}_{3\,1/2}$–$48462_{3\,1/2}$
5865.826	17043.17	10 *cw*	1	$25174_{2\,1/2}$–$42217^{o}_{1\,1/2}$
5867.484	17038.35	10 *cw*	1	$28151^{o}_{1\,1/2}$–$45189_{0\,1/2}$
5873.635	17020.51	7	1	$27517_{2\,1/2}$–$44537^{o}_{2\,1/2}$
5874.804	17017.12	20	1	$31927^{o}_{2\,1/2}$–$48944_{2\,1/2}$
5879.288	17004.14	18 *h*		$31414^{o}_{3\,1/2}$–$48418_{4\,1/2}$
5882.067	16996.11	25	2	$15624_{2\,1/2}$–$32620^{o}_{3\,1/2}$
5890.704	16971.19	1		$28296^{o}_{0\,1/2}$–$45267_{1\,1/2}$
5896.406	16954.78	6		$26950_{3\,1/2}$–$43905^{o}_{3\,1/2}$
5897.420	16951.86	3		$22615_{3\,1/2}$–$39567^{o}_{3\,1/2}$
5903.415	16934.65	3		$25058_{3\,1/2}$–$41993^{o}_{3\,1/2}$
5905.477	16928.74	8 *h*		$25174_{2\,1/2}$–$42102^{o}_{2\,1/2}$
5905.904	16927.51	10	1	$16415_{2\,1/2}$–$33343^{o}_{1\,1/2}$
5908.577	16919.86	15 *cw*	1 *c*	$28151^{o}_{1\,1/2}$–$45071_{2\,1/2}$
5917.963	16893.02	2 *h*		$28296^{o}_{0\,1/2}$–$45189_{0\,1/2}$
5918.780	16890.69	1		$45708^{o}_{4\,1/2}$–$62599_{4\,1/2}$
5919.462	16888.74	5	1	$25405_{1\,1/2}$–$42294^{o}_{2\,1/2}$
5923.357	16877.64	150	10	$11063_{2\,1/2}$–$27940^{o}_{2\,1/2}$
5924.468	16874.47	1000 *cw*	100 *cw*	$0_{2\,1/2}$–$16874^{o}_{3\,1/2}$
5925.384	16871.86	20 *c*	1 *c*	$14733_{4\,1/2}$–$31605^{o}_{3\,1/2}$
5925.714	16870.92	10	1	$42444^{o}_{5\,1/2}$–$59315_{5\,1/2}$
5926.286	16869.30	200	20	$28839_{5\,1/2}$–$45708^{o}_{4\,1/2}$
5928.111	16864.10	2		$25058_{3\,1/2}$–$41922^{o}_{2\,1/2}$
5928.111	16864.10	2		$27274_{6\,1/2}$–$44138^{o}_{5\,1/2}$
5930.310	16857.85	20		$31927^{o}_{2\,1/2}$–$48784_{3\,1/2}$
5930.544	16857.18	2		$29539_{4\,1/2}$–$46396^{o}_{3\,1/2}$
5931.929	16853.25	600 *c*	60 *c*	$10516_{3\,1/2}$–$27369^{o}_{4\,1/2}$
5937.136	16838.47	5 *h*		$25058_{3\,1/2}$–$41896^{o}_{4\,1/2}$
5938.394	16834.90	20	2	$29233_{3\,1/2}$–$46068^{o}_{4\,1/2}$
5942.259	16823.95	20 *cw*	1	$14679_{0\,1/2}$–$31503^{o}_{1\,1/2}$
5946.514	16811.91	10 *cw*		$28296^{o}_{0\,1/2}$–$45108_{1\,1/2}$
5951.484	16797.87	40 *c*	3 *c*	$16287_{3\,1/2}$–$33085^{o}_{2\,1/2}$
5961.256	16770.34	2		$42545^{o}_{4\,1/2}$–$59315_{5\,1/2}$
5969.013	16748.54	6	1	$25174_{2\,1/2}$–$41922^{o}_{2\,1/2}$
5974.845	16732.20	8	1	$27369^{o}_{4\,1/2}$–$44102_{3\,1/2}$
5977.678	16724.27	1		$27517_{2\,1/2}$–$44241^{o}_{2\,1/2}$
5979.893	16718.07	4		$11578_{1\,1/2}$–$28296^{o}_{0\,1/2}$
5980.512	16716.34	20 *c*	1 *c*	$15298_{3\,1/2}$–$32014^{o}_{2\,1/2}$
5980.694	16715.83	10		$27971_{4\,1/2}$–$44687^{o}_{3\,1/2}$
5986.820	16698.73	6		$26950_{3\,1/2}$–$43649^{o}_{4\,1/2}$
5988.406	16694.31	1 *h*		$47232^{o}_{2\,1/2}$–$63926_{2\,1/2}$
5993.208	16680.93	10 *cw*		$14733_{4\,1/2}$–$31414^{o}_{3\,1/2}$
5996.700	16671.22	15 *c*	1 *c*	$25058_{3\,1/2}$–$41729^{o}_{3\,1/2}$
5997.130	16670.02	5		$16415_{2\,1/2}$–$33085^{o}_{2\,1/2}$

TABLE 3. *Classified lines of* Tc I

Wavelength A	Wavenumber cm^{-1}	Intensity		Energy levels cm^{-1}
		Arc	Spark	
5999.701	16662.88	3 *c*		$26883\ ^{2}D_{3/2}$–$43546^{o}\ ^{2}D_{3/2}$
6003.496	16652.34	1		$25598\ ^{2}D_{3/2}$–$42250^{o}\ ^{2}D_{3/2}$
6004.566	16649.38	3 *h*		$33085^{o}\ ^{2}D_{3/2}$–$49735\ ^{1}D_{3/2}$
6005.099	16647.90	1 *h*	1 *h*	$25598\ ^{2}D_{3/2}$–$42246^{o}\ ^{3}D_{3/2}$
6006.099	16645.13	2 *h*		$25058\ ^{3}D_{3/2}$–$41703^{o}\ ^{4}D_{3/2}$
6010.191	16633.80	20 *c*	2 *c*	$15624\ ^{2}D_{3/2}$–$32258^{o}\ ^{1}D_{3/2}$
6011.790	16629.37	4		$15624\ ^{2}D_{3/2}$–$32253^{o}\ ^{1}D_{3/2}$
6012.104	16628.50	15 *cw*	1 *cw*	$15298\ ^{3}D_{3/2}$–$31927^{o}\ ^{2}D_{3/2}$
6013.183	16625.52	10 *h*		$32620^{o}\ ^{3}D_{3/2}$–$49245\ ^{3}D_{3/2}$
6020.726	16604.69	10	1	$27971\ ^{4}D_{3/2}$–$44576^{o}\ ^{4}D_{3/2}$
6023.500	16597.04	50	5	$11063\ ^{2}D_{3/2}$–$27660^{o}\ ^{3}D_{3/2}$
6024.046	16595.54	2 *h*		$33343^{o}\ ^{1}D_{3/2}$–$49938\ ^{2}D_{3/2}$
6024.423	16594.50	10	1	$26917\ ^{5}D_{3/2}$–$43512^{o}\ ^{3}D_{3/2}$
6026.085	16589.92	2		$27517\ ^{2}D_{3/2}$–$44107^{o}\ ^{2}D_{3/2}$
6028.542	16583.16	6	1	$27274\ ^{6}D_{3/2}$–$43857^{o}\ ^{6}D_{3/2}$
6032.355	16572.68	60	6	$11578\ ^{1}D_{3/2}$–$28151^{o}\ ^{1}D_{3/2}$
6038.504	16555.80	4 *h*		$25174\ ^{2}D_{3/2}$–$41729^{o}\ ^{3}D_{3/2}$
6047.992	16529.83	60	6	$29539\ ^{4}D_{3/2}$–$46068^{o}\ ^{4}D_{3/2}$
6052.685	16517.02	1 *h*		$25405\ ^{1}D_{3/2}$–$41922^{o}\ ^{2}D_{3/2}$
6057.249	16504.57	20	2	$25598\ ^{2}D_{3/2}$–$42102^{o}\ ^{2}D_{3/2}$
6063.473	16487.63	30	3	$15770\ ^{1}D_{3/2}$–$32258^{o}\ ^{1}D_{3/2}$
6063.473	16487.63	30	3	$33085^{o}\ ^{2}D_{3/2}$–$49573\ ^{3}D_{3/2}$
6063.930	16486.39	20 *c*	2	$16133\ ^{4}D_{3/2}$–$32620^{o}\ ^{3}D_{3/2}$
6065.090	16483.23	200	20	$15770\ ^{1}D_{3/2}$–$32253^{o}\ ^{1}D_{3/2}$
6066.182	16480.27	5 *h*		$33085^{o}\ ^{2}D_{3/2}$–$49565\ ^{2}D_{3/2}$
6069.785	16470.48	30	3	$33343^{o}\ ^{1}D_{3/2}$–$49813\ ^{2}D_{3/2}$
6077.819	16448.71	1		$23957\ ^{3}D_{3/2}$–$40406^{o}\ ^{3}D_{3/2}$
6080.327	16441.93	1		$27660^{o}\ ^{3}D_{3/2}$–$44102\ ^{3}D_{3/2}$
6085.229	16428.68	800	80	$0\ ^{2}D_{3/2}$–$16428^{o}\ ^{2}D_{3/2}$
6093.741	16405.73	20 *c*	2 *c*	$11890\ ^{0}D_{3/2}$–$28296^{o}\ ^{0}D_{3/2}$
6097.790	16394.84	1		$25598\ ^{2}D_{3/2}$–$41993^{o}\ ^{3}D_{3/2}$
6098.891	16391.88	3 *h*		$33343^{o}\ ^{1}D_{3/2}$–$49735\ ^{1}D_{3/2}$
6099.387	16390.55	300	30	$15624\ ^{2}D_{3/2}$–$32014^{o}\ ^{2}D_{3/2}$
6102.961	16380.95	500 *cw*	50 *c*	$14733\ ^{4}D_{3/2}$–$31114^{o}\ ^{4}D_{3/2}$
6111.120	16359.08	20	1	$14169\ ^{1}D_{3/2}$–$30528^{o}\ ^{2}D_{3/2}$
6112.030	16356.64	20 *h*	1 *h*	$32620^{o}\ ^{3}D_{3/2}$–$48977\ ^{4}D_{3/2}$
6112.630	16355.04	1		$25174\ ^{2}D_{3/2}$–$41529^{o}\ ^{3}D_{3/2}$
6112.630	16355.04	1		$39763^{o}\ ^{4}D_{3/2}$–$56118\ ^{5}D_{3/2}$
6115.490	16347.39	4 *h*		$26917\ ^{5}D_{3/2}$–$43265^{o}\ ^{4}D_{3/2}$
6120.684	16333.52	1000	100	$23265^{o}\ ^{3}D_{3/2}$–$39598\ ^{2}D_{3/2}$
6122.196	16329.48	1		$45708^{o}\ ^{4}D_{3/2}$–$62038\ ^{3}D_{3/2}$
6124.339	16323.77	5		$32620^{o}\ ^{3}D_{3/2}$–$48944\ ^{2}D_{3/2}$
6127.167	16316.24	8	1	$26950\ ^{3}D_{3/2}$–$43267^{o}\ ^{3}D_{3/2}$
6127.791	16314.57	1		$26950\ ^{3}D_{3/2}$–$43265^{o}\ ^{4}D_{3/2}$
6130.805	16306.55	1000	100	$15298\ ^{3}D_{3/2}$–$31605^{o}\ ^{3}D_{3/2}$
6132.230	16302.76	150 *c*	10 *c*	$15624\ ^{2}D_{3/2}$–$31927^{o}\ ^{2}D_{3/2}$
6150.522	16254.28	2		$26917\ ^{5}D_{3/2}$–$43172^{o}\ ^{3}D_{3/2}$
6151.460	16251.80	7 *h*		$33085^{o}\ ^{2}D_{3/2}$–$49337\ ^{2}D_{3/2}$
6154.274	16244.37	5	1	$15770\ ^{1}D_{3/2}$–$32014^{o}\ ^{2}D_{3/2}$
6156.540	16238.39	1 *h*		$27274\ ^{6}D_{3/2}$–$43512^{o}\ ^{3}D_{3/2}$

TABLE 3. *Classified lines of* Tc I

Wavelength A	Wavenumber cm^{-1}	Intensity		Energy levels cm^{-1}
		Arc	Spark	
6163.603	16219.788	8	1	$25405\ ^{1}_{1/2}$–$41625^{o}\ ^{1}_{1/2}$
6174.723	16190.578	1 *h*		$25598\ ^{2}_{1/2}$–$41788^{o}\ ^{1}_{1/2}$
6182.668	16169.773	20	2	$29539\ ^{4}_{1/2}$–$45708^{o}\ ^{4}_{1/2}$
6183.771	16166.889	10	1	$27971\ ^{4}_{1/2}$–$44138^{o}\ ^{5}_{1/2}$
6184.698	16164.465	100	2	$32620^{o}\ ^{3}_{1/2}$–$48784\ ^{3}_{1/2}$
6185.908	16161.304	5		$27940^{o}\ ^{2}_{1/2}$–$44102\ ^{3}_{1/2}$
6187.702	16156.618	3		$15770\ ^{1}_{1/2}$–$31927^{o}\ ^{2}_{1/2}$
6192.665	16143.670	800	80	$23455^{o}\ ^{2}_{1/2}$–$39598\ ^{2}_{1/2}$
6195.384	16136.585	40	2	$27660^{o}\ ^{3}_{1/2}$–$43796\ ^{2}_{1/2}$
6197.312	16131.565	1		$25598\ ^{2}_{1/2}$–$41729^{o}\ ^{3}_{1/2}$
6198.853	16127.554	4 *h*		$26883\ ^{2}_{1/2}$–$43011^{o}\ ^{2}_{1/2}$
6202.630	16117.734	5		$43197^{o}\ ^{6}_{1/2}$–$59315\ ^{5}_{1/2}$
6202.902	16117.027	3		$26788\ ^{2}_{1/2}$–$42905^{o}\ ^{2}_{1/2}$
6204.446	16113.016	4		$26788\ ^{2}_{1/2}$–$42901^{o}\ ^{1}_{1/2}$
6214.032	16088.160	30	2	$27940^{o}\ ^{2}_{1/2}$–$44028\ ^{1}_{1/2}$
6218.473	16076.671	2		$25174\ ^{2}_{1/2}$–$41250^{o}\ ^{1}_{1/2}$
6232.076	16041.580	2 *h*		$25058\ ^{3}_{1/2}$–$41100^{o}\ ^{2}_{1/2}$
6236.621	16029.889	3 *c*		$25058\ ^{3}_{1/2}$–$41088^{o}\ ^{3}_{1/2}$
6236.865	16029.262	8	1	$27517\ ^{2}_{1/2}$–$43546^{o}\ ^{2}_{1/2}$
6239.698	16021.984	20	1	$27369^{o}\ ^{4}_{1/2}$–$43391\ ^{3}_{1/2}$
6244.178	16010.489	600 *cw*	50 *c*	$23588^{o}\ ^{1}_{1/2}$–$39598\ ^{2}_{1/2}$
6248.971	15998.209	15	1	$28151^{o}\ ^{1}_{1/2}$–$44149\ ^{0}_{1/2}$
6255.807	15980.728	5	1	$15624\ ^{2}_{1/2}$–$31605^{o}\ ^{3}_{1/2}$
6266.102	15954.472	2*w*		$26950\ ^{3}_{1/2}$–$42905^{o}\ ^{2}_{1/2}$
6267.598	15950.664	2*w*		$14679\ ^{0}_{1/2}$–$30630^{o}\ ^{1}_{1/2}$
6274.014	15934.352	1		$27971\ ^{4}_{1/2}$–$43905^{o}\ ^{3}_{1/2}$
6275.425	15930.769	4		$25598\ ^{2}_{1/2}$–$41529^{o}\ ^{3}_{1/2}$
6277.250	15926.138	2 *cw*		$25174\ ^{2}_{1/2}$–$41100^{o}\ ^{2}_{1/2}$
6287.962	15899.007	4 *cw*		$26917\ ^{5}_{1/2}$–$42817^{o}\ ^{4}_{1/2}$
6288.358	15898.006	1 *h*		$27274\ ^{6}_{1/2}$–$43172^{o}\ ^{5}_{1/2}$
6290.397	15892.852	5		$46608^{o}\ ^{3}_{1/2}$–$62501\ ^{3}_{1/2}$
6292.239	15888.200	1 *h*		$26883\ ^{2}_{1/2}$–$42771^{o}\ ^{3}_{1/2}$
6296.423	15877.642	2		$28151^{o}\ ^{1}_{1/2}$–$44028\ ^{1}_{1/2}$
6296.765	15876.780	6 *h*		$40241^{o}\ ^{5}_{1/2}$–$56118\ ^{5}_{1/2}$
6304.048	15858.438	6		$33085^{o}\ ^{2}_{1/2}$–$48944\ ^{2}_{1/2}$
6305.028	15855.973	30	3	$27940^{o}\ ^{2}_{1/2}$–$43796\ ^{2}_{1/2}$
6306.260	15852.875	8		$28296^{o}\ ^{0}_{1/2}$–$44149\ ^{0}_{1/2}$
6310.420	15842.425	40 *c*	3 *c*	$16415\ ^{2}_{1/2}$–$32258^{o}\ ^{1}_{1/2}$
6312.179	15838.010	100	10	$16415\ ^{2}_{1/2}$–$32253^{o}\ ^{1}_{1/2}$
6319.033	15820.831	1		$26950\ ^{3}_{1/2}$–$42771^{o}\ ^{3}_{1/2}$
6321.099	15815.660	1		$15298\ ^{3}_{1/2}$–$31114^{o}\ ^{4}_{1/2}$
6326.116	15803.118	1		$17282\ ^{3}_{1/2}$–$33085^{o}\ ^{2}_{1/2}$
6347.458	15749.983	1		$27517\ ^{2}_{1/2}$–$43267^{o}\ ^{3}_{1/2}$
6354.632	15732.203	50 *cw*	2 *c*	$28296^{o}\ ^{0}_{1/2}$–$44028\ ^{1}_{1/2}$
6354.860	15731.638	100	10	$27660^{o}\ ^{3}_{1/2}$–$43391\ ^{3}_{1/2}$
6356.732	15727.005	100	10	$16287\ ^{3}_{1/2}$–$32014^{o}\ ^{2}_{1/2}$
6369.313	15695.941	4		$26917\ ^{5}_{1/2}$–$42613^{o}\ ^{4}_{1/2}$
6380.889	15667.466	5 *c*		$25405\ ^{1}_{1/2}$–$41073^{o}\ ^{1}_{1/2}$
6382.724	15662.962	3		$26950\ ^{3}_{1/2}$–$42613^{o}\ ^{4}_{1/2}$
6388.426	15648.982	30 *cw*	1	$14733\ ^{4}_{1/2}$–$30382^{o}\ ^{3}_{1/2}$

318-092 O-69—4

TABLE 3. *Classified lines of* Tc I

Wavelength A	Wavenumber cm^{-1}	Intensity		Energy levels cm^{-1}
		Arc	Spark	
6389.871	15645.44	80	6	$28151^{o}{}_{1\frac{1}{2}}$–$43796\ {}_{2\frac{1}{2}}$
6392.408	15639.23	30 *c*	2 *c*	$16287\ {}_{3\frac{1}{2}}$–$31927^{o}{}_{2\frac{1}{2}}$
6392.716	15638.48	3		$29233\ {}_{3\frac{1}{2}}$–$44872^{o}{}_{2\frac{1}{2}}$
6408.830	15599.16	100	8	$16415\ {}_{2\frac{1}{2}}$–$32014^{o}{}_{2\frac{1}{2}}$
6419.353	15573.58	2		$19702\ {}_{1\frac{1}{2}}$–$35276^{o}{}_{1\frac{1}{2}}$
6432.774	15541.09	5		$27971\ {}_{4\frac{1}{2}}$–$43512^{o}{}_{3\frac{1}{2}}$
6445.100	15511.37	30 *cw*	1 *cw*	$16415\ {}_{2\frac{1}{2}}$–$31927^{o}{}_{2\frac{1}{2}}$
6449.026	15501.93	4		$25598\ {}_{2\frac{1}{2}}$–$41100^{o}{}_{2\frac{1}{2}}$
6453.925	15490.16	3		$25598\ {}_{2\frac{1}{2}}$–$41088^{o}{}_{3\frac{1}{2}}$
6455.896	15485.43	1000	30	$27369^{o}{}_{4\frac{1}{2}}$–$42855\ {}_{4\frac{1}{2}}$
6460.338	15474.79	5 *h*		$25598\ {}_{2\frac{1}{2}}$–$41073^{o}{}_{1\frac{1}{2}}$
6461.928	15470.98	600 *c*	20 *c*	$16133\ {}_{4\frac{1}{2}}$–$31605^{o}{}_{3\frac{1}{2}}$
6467.570	15457.48	2 *h*		$26788\ {}_{2\frac{1}{2}}$–$42246^{o}{}_{3\frac{1}{2}}$
6470.270	15451.03	100	6	$27940^{o}{}_{2\frac{1}{2}}$–$43391\ {}_{3\frac{1}{2}}$
6479.620	15428.74	1 *h*		$26788\ {}_{2\frac{1}{2}}$–$42217^{o}{}_{4\frac{1}{2}}$
6491.676	15400.08	200 *cw*	5	$14733\ {}_{4\frac{1}{2}}$–$30133^{o}{}_{4\frac{1}{2}}$
6496.606	15388.40	10		$38556^{o}{}_{1\frac{1}{2}}$–$53945\ {}_{2\frac{1}{2}}$
6496.606	15388.40	10		$27517\ {}_{2\frac{1}{2}}$–$42905^{o}{}_{2\frac{1}{2}}$
6515.160	15344.57	20		$25058\ {}_{3\frac{1}{2}}$–$40403^{o}{}_{4\frac{1}{2}}$
6515.660	15343.40	2 *h*		$26950\ {}_{3\frac{1}{2}}$–$42294^{o}{}_{2\frac{1}{2}}$
6516.192	15342.14	2		$29233\ {}_{3\frac{1}{2}}$–$44576^{o}{}_{4\frac{1}{2}}$
6519.740	15333.79	1		$26883\ {}_{2\frac{1}{2}}$–$42217^{o}{}_{4\frac{1}{2}}$
6526.817	15317.17	200	20	$16287\ {}_{3\frac{1}{2}}$–$31605^{o}{}_{3\frac{1}{2}}$
6528.038	15314.30	5 *c*		$26788\ {}_{2\frac{1}{2}}$–$42102^{o}{}_{2\frac{1}{2}}$
6532.494	15303.86	2		$29233\ {}_{3\frac{1}{2}}$–$44537^{o}{}_{2\frac{1}{2}}$
6534.063	15300.18	6		$29539\ {}_{4\frac{1}{2}}$–$44839^{o}{}_{3\frac{1}{2}}$
6534.659	15298.79	10		$28839\ {}_{5\frac{1}{2}}$–$44138^{o}{}_{5\frac{1}{2}}$
6535.947	15295.77	3 *h*		$27971\ {}_{4\frac{1}{2}}$–$43267^{o}{}_{3\frac{1}{2}}$
6536.633	15294.17	5		$27971\ {}_{4\frac{1}{2}}$–$43265^{o}{}_{4\frac{1}{2}}$
6537.425	15292.31	2 *c*		$17328\ {}_{4\frac{1}{2}}$–$32620^{o}{}_{3\frac{1}{2}}$
6563.197	15232.26	4		$25174\ {}_{2\frac{1}{2}}$–$40406^{o}{}_{3\frac{1}{2}}$
6564.004	15230.39	50 *w*		$15298\ {}_{3\frac{1}{2}}$–$30528^{o}{}_{2\frac{1}{2}}$
6568.820	15219.23	2 *h*		$34515^{o}{}_{2\frac{1}{2}}$–$49735\ {}_{1\frac{1}{2}}$
6576.820	15200.71	50 *w l*		$27274\ {}_{6\frac{1}{2}}$–$42474^{o}{}_{6\frac{1}{2}}$
6576.820	15200.71	50 *w l*		$27971\ {}_{4\frac{1}{2}}$–$43172^{o}{}_{5\frac{1}{2}}$
6579.243	15195.12	150		$27660^{o}{}_{3\frac{1}{2}}$–$42855\ {}_{4\frac{1}{2}}$
6581.747	15189.33	8		$16415\ {}_{2\frac{1}{2}}$–$31605^{o}{}_{3\frac{1}{2}}$
6586.147	15179.19	3		$27517\ {}_{2\frac{1}{2}}$–$42696^{o}{}_{2\frac{1}{2}}$
6590.039	15170.22	15		$27274\ {}_{6\frac{1}{2}}$–$42444^{o}{}_{5\frac{1}{2}}$
6598.037	15151.83	10		$26950\ {}_{3\frac{1}{2}}$–$42102^{o}{}_{2\frac{1}{2}}$
6609.746	15124.99	3 *h s*		$25174\ {}_{2\frac{1}{2}}$–$40299^{o}{}_{2\frac{1}{2}}$
6614.304	15114.57	3		$26917\ {}_{5\frac{1}{2}}$–$42032^{o}{}_{5\frac{1}{2}}$
6618.080	15105.95	2		$27971\ {}_{4\frac{1}{2}}$–$43077^{o}{}_{3\frac{1}{2}}$
6625.573	15088.86	500 *cw*	10 *cw*	$16025\ {}_{5\frac{1}{2}}$–$31114^{o}{}_{4\frac{1}{2}}$
6627.896	15083.57	50 *c*	1 *c*	$15298\ {}_{3\frac{1}{2}}$–$30382^{o}{}_{3\frac{1}{2}}$
6646.143	15042.16	1		$26950\ {}_{3\frac{1}{2}}$–$41993^{o}{}_{3\frac{1}{2}}$
6647.489	15039.12	4		$26883\ {}_{2\frac{1}{2}}$–$41922^{o}{}_{2\frac{1}{2}}$
6648.383	15037.09	30	1	$29539\ {}_{4\frac{1}{2}}$–$44576^{o}{}_{4\frac{1}{2}}$
6650.177	15033.04	2		$29233\ {}_{3\frac{1}{2}}$–$44266^{o}{}_{3\frac{1}{2}}$
6656.906	15017.84	2		$28839\ {}_{5\frac{1}{2}}$–$43857^{o}{}_{6\frac{1}{2}}$

TABLE 3. *Classified lines of* Tc I

Wavelength A	Wavenumber cm^{-1}	Intensity		Energy levels cm^{-1}
		Arc	Spark	
6661.433	15007.64	5		$29233\ ^{3}_{1/2}$–44241^{o}_{2}
6662.015	15006.33	20		$15624\ ^{2}_{1/2}$–30630^{o}_{1}
6664.722	15000.23	2		$26788\ ^{2}_{1/2}$–41788^{o}_{1}
6673.656	14980.15	300 *c*	5 *c*	$16133\ ^{4}_{1/2}$–31114^{o}_{4}
6687.099	14950.04	100	1	$2572\ ^{4}_{1/2}$–17522^{o}_{4}
6699.464	14922.44	2		$25174\ ^{2}_{1/2}$–40096^{o}_{1}
6701.142	14918.71	5		$15770\ ^{1}_{1/2}$–30689^{o}_{0}
6707.478	14904.61	8		$15624\ ^{2}_{1/2}$–30528^{o}_{2}
6710.202	14898.56	10		$13252\ ^{2}_{1/2}$–28151^{o}_{1}
6712.512	14893.44	4		$25405\ ^{1}_{1/2}$–40299^{o}_{2}
6718.327	14880.55	1 *h*		$26883\ ^{2}_{1/2}$–41764^{o}_{2}
6721.629	14873.24	3		$29233\ ^{3}_{1/2}$–44107^{o}_{2}
6731.187	14852.12	50		30133^{o}_{4}–$44985\ ^{3}_{1/2}$
6733.847	14846.25	7		$26883\ ^{2}_{1/2}$–41729^{o}_{3}
6738.066	14836.95	1		$26788\ ^{2}_{1/2}$–41625^{o}_{1}
6742.901	14826.31	5		$16287\ ^{3}_{1/2}$–31114^{o}_{4}
6745.042	14821.61	6		34515^{o}_{2}–$49337\ ^{2}_{1/2}$
6747.530	14816.14	7 *h*		$30060\ ^{2}_{1/2}$–44876^{o}_{1}
6748.838	14813.27	5		$26950\ ^{3}_{1/2}$–41764^{o}_{2}
6753.399	14803.27	10		$25174\ ^{2}_{1/2}$–39977^{o}_{2}
6758.326	14792.48	20		34942^{o}_{1}–$49735\ ^{1}_{1/2}$
6761.469	14785.60	30	1	$26917\ ^{5}_{1/2}$–41703^{o}_{4}
6764.101	14779.85	2		47819^{o}_{4}–$62599\ ^{4}_{1/2}$
6764.574	14778.81	5		$26950\ ^{3}_{1/2}$–41729^{o}_{3}
6764.758	14778.41	8		$30060\ ^{2}_{1/2}$–44839^{o}_{3}
6767.183	14773.12	2		$29233\ ^{3}_{1/2}$–44007^{o}_{2}
6773.899	14758.47	4		$15770\ ^{1}_{1/2}$–30528^{o}_{2}
6776.580	14752.63	8		$26950\ ^{3}_{1/2}$–41703^{o}_{4}
6786.003	14732.14	80	2	$17282\ ^{3}_{1/2}$–32014^{o}_{2}
6786.965	14730.06	10		34515^{o}_{2}–$49245\ ^{3}_{1/2}$
6787.951	14727.92	2		$29539\ ^{4}_{1/2}$–44266^{o}_{3}
6795.564	14711.42	2		$20231\ ^{1}_{1/2}$–34942^{o}_{1}
6798.629	14704.79	70	2	$25058\ ^{3}_{1/2}$–39763^{o}_{4}
6800.793	14700.11	2		$27517\ ^{2}_{1/2}$–42217^{o}_{4}
6805.049	14690.91	5		$25405\ ^{1}_{1/2}$–40096^{o}_{1}
6805.942	14688.98	15		30382^{o}_{3}–$45071\ ^{2}_{1/2}$
6813.340	14673.04	5		$28839\ ^{5}_{1/2}$–43512^{o}_{3}
6818.126	14662.74	10		$26917\ ^{5}_{1/2}$–41580^{o}_{3}
6826.146	14645.51	5		$26883\ ^{2}_{1/2}$–41529^{o}_{3}
6826.686	14644.35	5		$17282\ ^{3}_{1/2}$–31927^{o}_{2}
6830.007	14637.23	8		30630^{o}_{1}–$45267\ ^{1}_{1/2}$
6833.736	14629.24	3		$27971\ ^{4}_{1/2}$–42600^{o}_{3}
6837.906	14620.32	4 *hw*		$19895\ ^{2}_{1/2}$–34515^{o}_{2}
6837.906	14620.32	4 *hw*		$24564\ ^{5}_{1/2}$–39185^{o}_{4}
6856.902	14579.82	60	1	30528^{o}_{2}–$45108\ ^{1}_{1/2}$
6860.726	14571.69	30	1	$25405\ ^{1}_{1/2}$–39977^{o}_{2}
6866.677	14559.06	25		30630^{o}_{1}–$45189\ ^{0}_{1/2}$
6874.626	14542.23	10		30528^{o}_{2}–$45071\ ^{2}_{1/2}$
6894.386	14500.55	20		30689^{o}_{0}–$45189\ ^{0}_{1/2}$
6901.620	14485.35	2		39459^{o}_{2}–$53945\ ^{2}_{1/2}$

TABLE 3. *Classified lines of* Tc I

Wavelength A	Wavenumber cm^{-1}	Intensity		Energy levels cm^{-1}
		Arc	Spark	
6905.117	14478.02	10		$30630^{\circ}_{1/2}$–$45108_{1/2}$
6907.514	14472.99	30		$27971_{4/2}$–$42444^{\circ}_{3/2}$
6924.055	14438.42	15		$25405_{1/2}$–$39844^{\circ}_{1/2}$
6928.934	14428.25	3 *h*		$34515^{\circ}_{2/2}$–$48944_{2/2}$
6931.795	14422.29	30		$30382^{\circ}_{3/2}$–$44804_{2/2}$
6933.236	14419.30	30		$20523_{2/2}$–$34942^{\circ}_{1/2}$
6939.892	14405.47	4		$27517_{2/2}$–$41922^{\circ}_{2/2}$
6944.988	14394.90	2		$34942^{\circ}_{1/2}$–$49337_{2/2}$
6945.597	14393.64	15		$25174_{2/2}$–$39567^{\circ}_{3/2}$
6949.320	14385.92	7 *h*		$48213^{\circ}_{4/2}$–$62599_{4/2}$
6952.625	14379.09	3		$25598_{2/2}$–$39977^{\circ}_{2/2}$
6958.593	14366.75	4		$29539_{4/2}$–$43905^{\circ}_{3/2}$
6968.151	14347.05	30		$23265^{\circ}_{3/2}$–$37612_{3/2}$
6975.067	14332.82	7		$28839_{5/2}$–$43172^{\circ}_{3/2}$
6980.153	14322.38	10		$17282_{3/2}$–$31605^{\circ}_{3/2}$
6985.402	14311.62	30		$26788_{2/2}$–$41100^{\circ}_{2/2}$
6985.402	14311.62	30		$48287^{\circ}_{3/2}$–$62599_{4/2}$
6990.300	14301.59	40		$2572_{4/2}$–$16874^{\circ}_{3/2}$
6998.037	14285.78	8		$25174_{2/2}$–$39459^{\circ}_{2/2}$
6998.653	14284.52	15		$20231_{1/2}$–$34515^{\circ}_{2/2}$
7002.375	14276.93	150		$17328_{4/2}$–$31605^{\circ}_{3/2}$
7004.781	14272.02	6		$3250_{3/2}$–$17522^{\circ}_{4/2}$
7006.293	14268.94	20 *c*		$34515^{\circ}_{2/2}$–$48784_{3/2}$
7011.448	14258.45	2		$28839_{5/2}$–$43097^{\circ}_{4/2}$
7014.108	14253.05	10 *c*		$30060_{2/2}$–$44313^{\circ}_{1/2}$
7016.574	14248.04	100		$16133_{4/2}$–$30382^{\circ}_{3/2}$
7020.025	14241.03	20		$16287_{3/2}$–$30528^{\circ}_{2/2}$
7029.723	14221.39	8		$41896^{\circ}_{4/2}$–$56118_{5/2}$
7032.894	14214.97	10		$16415_{2/2}$–$30630^{\circ}_{1/2}$
7054.800	14170.83	10		$25405_{1/2}$–$39576^{\circ}_{1/2}$
7061.633	14157.12	7		$23455^{\circ}_{2/2}$–$37612_{3/2}$
7065.596	14149.18	10		$26950_{3/2}$–$41100^{\circ}_{2/2}$
7071.442	14137.48	30		$26950_{3/2}$–$41088^{\circ}_{3/2}$
7076.770	14126.84	15		$14169_{1/2}$–$28296^{\circ}_{1/2}$
7083.599	14113.22	15		$16415_{2/2}$–$30528^{\circ}_{2/2}$
7084.871	14110.69	1		$29539_{4/2}$–$43649^{\circ}_{4/2}$
7086.180	14108.08	560 *cw*		$16025_{5/2}$–$30133^{\circ}_{4/2}$
7093.120	14094.28	60		$16287_{3/2}$–$30382^{\circ}_{3/2}$
7097.242	14086.09	3		$17328_{4/2}$–$31414^{\circ}_{3/2}$
7109.813	14061.19	8		$27971_{4/2}$–$42032^{\circ}_{3/2}$
7115.781	14049.39	8		$30060_{2/2}$–$44110^{\circ}_{1/2}$
7117.170	14046.65	4		$30060_{2/2}$–$44107^{\circ}_{2/2}$
7123.974	14033.24	4		$29233_{3/2}$–$43267^{\circ}_{3/2}$
7124.784	14031.64	30		$29233_{3/2}$–$43265^{\circ}_{4/2}$
7134.829	14011.89	1		$27517_{2/2}$–$41529^{\circ}_{3/2}$
7140.187	14001.37	3		$34942^{\circ}_{1/2}$–$48944_{2/2}$
7141.286	13999.22	200		$16133_{4/2}$–$30133^{\circ}_{4/2}$
7144.678	13992.57	15		$20523_{2/2}$–$34515^{\circ}_{2/2}$
7156.874	13968.73	20		$30133^{\circ}_{4/2}$–$44102_{3/2}$
7157.626	13967.26	200 *c*		$17146_{5/2}$–$31114^{\circ}_{4/2}$

TABLE 3. *Classified lines of* Tc I

Wavelength A	Wavenumber cm^{-1}	Intensity		Energy levels cm^{-1}
		Arc	Spark	
7179.043	13925.59	10		$27971\ ^{4}_{1/2}$–$41896^{o}\ ^{4}_{1/2}$
7191.591	13901.29	3		$42217^{o}\ ^{4}_{1/2}$–$56118\ ^{5}_{1/2}$
7194.656	13895.37	2		$48142^{o}\ ^{2}_{1/2}$–$62038\ ^{3}_{1/2}$
7207.026	13871.52	8		$31114^{o}\ ^{4}_{1/2}$–$44985\ ^{3}_{1/2}$
7220.543	13845.55	2		$16287\ ^{3}_{1/2}$–$30133^{o}\ ^{4}_{1/2}$
7251.685	13786.09	15		$17328\ ^{4}_{1/2}$–$31114^{o}\ ^{4}_{1/2}$
7256.089	13777.73	70		$19702\ ^{1}_{1/2}$–$33480^{o}\ ^{0}_{1/2}$
7264.840	13761.13	3		$28839\ ^{5}_{1/2}$–$42600^{o}\ ^{5}_{1/2}$
7283.164	13726.51	15		$29539\ ^{4}_{1/2}$–$43265^{o}\ ^{4}_{1/2}$
7296.248	13701.89	5*wd*		$31406^{o}\ ^{2}_{1/2}$–$45108\ ^{1}_{1/2}$
7320.300	13656.88	5*w*		$31414^{o}\ ^{3}_{1/2}$–$45071\ ^{2}_{1/2}$
7322.382	13652.99	100		$19827\ ^{0}_{1/2}$–$33480^{o}\ ^{0}_{1/2}$
7329.148	13640.39	80		$19702\ ^{1}_{1/2}$–$33343^{o}\ ^{1}_{1/2}$
7331.895	13635.28	5		$28839\ ^{5}_{1/2}$–$42474^{o}\ ^{6}_{1/2}$
7338.202	13623.56	50		$3250\ ^{3}_{1/2}$–$16874^{o}\ ^{3}_{1/2}$
7340.134	13619.97	4		$48881^{o}\ ^{4}_{1/2}$–$62501\ ^{3}_{1/2}$
7341.852	13616.79	2		$14679\ ^{0}_{1/2}$–$28296^{o}\ ^{0}_{1/2}$
7345.819	13609.43	4		$27971\ ^{4}_{1/2}$–$41580^{o}\ ^{5}_{1/2}$
7360.063	13583.09	10		$29233\ ^{3}_{1/2}$–$42817^{o}\ ^{4}_{1/2}$
7362.460	13578.67	5*w*		$31406^{o}\ ^{2}_{1/2}$–$44985\ ^{3}_{1/2}$
7366.336	13571.53	40 *cw*		$31414^{o}\ ^{3}_{1/2}$–$44985\ ^{3}_{1/2}$
7395.066	13518.80	50		$30630^{o}\ ^{1}_{1/2}$–$44149\ ^{0}_{1/2}$
7402.619	13505.01	100 *cw*		$31414^{o}\ ^{3}_{1/2}$–$44919\ ^{4}_{1/2}$
7405.363	13500.00	200		$30528^{o}\ ^{2}_{1/2}$–$44028\ ^{1}_{1/2}$
7421.120	13471.34	8		$14679\ ^{0}_{1/2}$–$28151^{o}\ ^{1}_{1/2}$
7424.011	13466.09	20		$31605^{o}\ ^{3}_{1/2}$–$45071\ ^{2}_{1/2}$
7427.154	13460.40	60		$30689^{o}\ ^{0}_{1/2}$–$44149\ ^{0}_{1/2}$
7431.650	13452.25	2		$26950\ ^{3}_{1/2}$–$40403^{o}\ ^{4}_{1/2}$
7434.122	13447.78	150		$19895\ ^{2}_{1/2}$–$33343^{o}\ ^{1}_{1/2}$
7452.496	13414.62	600		$30382^{o}\ ^{3}_{1/2}$–$43796\ ^{2}_{1/2}$
7461.594	13398.27	60		$30630^{o}\ ^{1}_{1/2}$–$44028\ ^{1}_{1/2}$
7470.148	13382.93	50		$19702\ ^{1}_{1/2}$–$33085^{o}\ ^{2}_{1/2}$
7471.776	13380.01	20		$29233\ ^{3}_{1/2}$–$42613^{o}\ ^{4}_{1/2}$
7494.288	13339.82	6		$30689^{o}\ ^{0}_{1/2}$–$44028\ ^{1}_{1/2}$
7512.280	13307.87	3		$26788\ ^{2}_{1/2}$–$40096^{o}\ ^{1}_{1/2}$
7534.952	13267.83	80		$30528^{o}\ ^{2}_{1/2}$–$43796\ ^{2}_{1/2}$
7540.265	13258.48	800		$30133^{o}\ ^{4}_{1/2}$–$43391\ ^{3}_{1/2}$
7543.391	13252.98	80		$32014^{o}\ ^{2}_{1/2}$–$45267\ ^{1}_{1/2}$
7545.510	13249.26	30		$20231\ ^{1}_{1/2}$–$33480^{o}\ ^{0}_{1/2}$
7547.268	13246.18	5		$17282\ ^{3}_{1/2}$–$30528^{o}\ ^{2}_{1/2}$
7548.442	13244.12	50		$32253^{o}\ ^{1}_{1/2}$–$45497\ ^{0}_{1/2}$
7550.991	13239.65	10*w*		$32258^{o}\ ^{1}_{1/2}$–$45497\ ^{0}_{1/2}$
7574.026	13199.38	200		$31605^{o}\ ^{3}_{1/2}$–$44804\ ^{2}_{1/2}$
7577.614	13193.13	2		$28839\ ^{5}_{1/2}$–$42032^{o}\ ^{5}_{1/2}$
7579.267	13190.25	500		$19895\ ^{2}_{1/2}$–$33085^{o}\ ^{2}_{1/2}$
7583.935	13182.13	5		$19903\ ^{3}_{1/2}$–$33085^{o}\ ^{2}_{1/2}$
7583.935	13182.13	5		$25058\ ^{3}_{1/2}$–$38240^{o}\ ^{3}_{1/2}$
7586.447	13177.77	5		$3250\ ^{3}_{1/2}$–$16428^{o}\ ^{2}_{1/2}$
7588.611	13174.01	7		$3700\ ^{2}_{1/2}$–$16874^{o}\ ^{3}_{1/2}$
7593.152	13166.13	7		$30630^{o}\ ^{1}_{1/2}$–$43796\ ^{2}_{1/2}$

TABLE 3. *Classified lines of* Tc I

Wavelength A	Wavenumber cm^{-1}	Intensity		Energy levels cm^{-1}
		Arc	Spark	
7624.538	13111.93	90		$20231\ ^{1}_{1/2}-33343^{o}_{1/2}$
7631.825	13099.42	4		$17282\ ^{3}_{1/2}-30382^{o}_{3/2}$
7634.531	13094.77	7		$32403^{o}_{1/2}-45497\ ^{0}_{1/2}$
7635.083	13093.83	4		$32014^{o}_{2/2}-45108\ ^{1}_{1/2}$
7657.044	13056.27	2		$32014^{o}_{2/2}-45071\ ^{2}_{1/2}$
7658.374	13054.00	30 *c*		$17328\ ^{4}_{1/2}-30382^{o}_{3/2}$
7676.957	13022.41	4		$21920\ ^{2}_{1/2}-34942^{o}_{1/2}$
7681.790	13014.21	15		$32253^{o}_{1/2}-45267\ ^{1}_{1/2}$
7684.458	13009.69	100		$30382^{o}_{3/2}-43391\ ^{3}_{1/2}$
7684.458	13009.69	100		$32258^{o}_{1/2}-45267\ ^{1}_{1/2}$
7697.370	12987.87	500		$31114^{o}_{4/2}-44102\ ^{3}_{1/2}$
7698.190	12986.49	80 *cw*		$17146\ ^{5}_{1/2}-30133^{o}_{4/2}$
7719.592	12950.48	2 *h*		$30060\ ^{2}_{1/2}-43011^{o}_{2/2}$
7722.199	12946.11	3		$43172^{o}_{5/2}-56118\ ^{5}_{1/2}$
7733.630	12926.98	5 *c*		$14733\ ^{4}_{1/2}-27660^{o}_{3/2}$
7737.368	12920.73	50 *c*		$17146\ ^{5}_{1/2}-30067^{o}_{5/2}$
7746.605	12905.32	10		$29539\ ^{4}_{1/2}-42444^{o}_{3/2}$
7777.220	12854.52	40		$20231\ ^{1}_{1/2}-33085^{o}_{2/2}$
7779.594	12850.60	6 *c*		$17282\ ^{3}_{1/2}-30133^{o}_{4/2}$
7779.594	12850.60	6 *c*		$32258^{o}_{1/2}-45108\ ^{1}_{1/2}$
7782.993	12844.99	15		$41100^{o}_{2/2}\ 53945\ ^{2}_{1/2}$
7782.993	12844.99	15		$30060\ ^{2}_{1/2}-42905^{o}_{2/2}$
7793.046	12828.42	800 *cw*		$19791\ ^{4}_{1/2}-32620^{o}_{3/2}$
7798.280	12819.81	60		$20523\ ^{2}_{1/2}-33343^{o}_{1/2}$
7807.200	12805.16	10		$17328\ ^{4}_{1/2}-30133^{o}_{4/2}$
7816.741	12789.53	60		$32014^{o}_{2/2}-44804\ ^{2}_{1/2}$
7817.728	12787.92	800		$30067^{o}_{5/2}-42855\ ^{4}_{1/2}$
7854.400	12728.21	10		$3700\ ^{2}_{1/2}-16428^{o}_{2/2}$
7856.380	12725.00	100		$19895\ ^{2}_{1/2}-32620^{o}_{3/2}$
7858.250	12721.97	10		$30133^{o}_{4/2}-42855\ ^{4}_{1/2}$
7861.440	12716.81	200		$19903\ ^{3}_{1/2}-32620^{o}_{3/2}$
7871.250	12700.96	400 *l d*		$20384\ ^{3}_{1/2}-33085^{o}_{2/2}$
7874.760	12695.30	60 *cw*		$31406^{o}_{2/2}-44102\ ^{3}_{1/2}$
7876.190	12693.00	2		$26883\ ^{2}_{1/2}-39576^{o}_{1/2}$
7879.370	12687.87	8 *c*		$31414^{o}_{3/2}-44102\ ^{3}_{1/2}$
7881.630	12684.24	5		$26883\ ^{2}_{1/2}-39567^{o}_{3/2}$
7885.980	12677.24	40 *cw*		$22265\ ^{2}_{1/2}-34942^{o}_{1/2}$
7894.750	12663.16	2		$29233\ ^{3}_{1/2}-41896^{o}_{4/2}$
7898.567	12657.04	3		$20686\ ^{2}_{1/2}-33343^{o}_{1/2}$
7905.729	12645.57	20 *c*		$31503^{o}_{1/2}-44149\ ^{0}_{1/2}$
7911.290	12636.68	4 *c*		$14733\ ^{4}_{1/2}-27369^{o}_{4/2}$
7920.371	12622.19	10 *h*		$31406^{o}_{2/2}-44028\ ^{1}_{1/2}$
7949.716	12575.60	15 *c*		$19827\ ^{0}_{1/2}-32403^{o}_{0/2}$
7958.092	12562.37	5		$20523\ ^{2}_{1/2}-33085^{o}_{2/2}$
7965.452	12550.76	70		$32253^{o}_{1/2}-44804\ ^{2}_{1/2}$
7968.304	12546.27	50		$32258^{o}_{1/2}-44804\ ^{2}_{1/2}$
7981.805	12525.04	50 *cw*		$31503^{o}_{1/2}-44028\ ^{1}_{1/2}$
7999.730	12496.98	500		$31605^{o}_{3/2}-44102\ ^{3}_{1/2}$
8001.889	12493.61	10		$29539\ ^{4}_{1/2}-42032^{o}_{3/2}$
8017.229	12469.70	8		$29233\ ^{3}_{1/2}-41703^{o}_{4/2}$

TABLE 3. *Classified lines of* Tc I

Wavelength A	Wavenumber cm^{-1}	Intensity		Energy levels cm^{-1}
		Arc	Spark	
8029.468	12450.70	8 *c*		$32620^{a}_{3\frac{1}{2}}$–$45071\ _{2\frac{1}{2}}$
8042.473	12430.56	30		$19827\ _{0\frac{1}{2}}$–$32258^{a}_{1\frac{1}{2}}$
8045.330	12426.15	25		$4002\ _{1\frac{1}{2}}$–$16428^{a}_{2\frac{1}{2}}$
8068.794	12390.01	40 *c*		$31406^{a}_{2\frac{1}{2}}$–$43796\ _{2\frac{1}{2}}$
8073.665	12382.54	10 *c*		$31414^{a}_{3\frac{1}{2}}$–$43796\ _{2\frac{1}{2}}$
8112.776	12322.84	1		$32014^{a}_{2\frac{1}{2}}$–$44337\ _{2\frac{1}{2}}$
8116.919	12316.55	5		$15624\ _{2\frac{1}{2}}$–$27940^{a}_{2\frac{1}{2}}$
8119.869	12312.08	40		$19702\ _{1\frac{1}{2}}$–$32014^{a}_{2\frac{1}{2}}$
8126.557	12301.95	200		$20783\ _{3\frac{1}{2}}$–$33085^{a}_{2\frac{1}{2}}$
8132.651	12292.73	5 *h*		$31503^{a}_{1\frac{1}{2}}$–$43796\ _{2\frac{1}{2}}$
8142.630	12277.66	30		$31114^{a}_{4\frac{1}{2}}$–$43391\ _{3\frac{1}{2}}$
8170.558	12235.70	200		$20384\ _{3\frac{1}{2}}$–$32620^{a}_{3\frac{1}{2}}$
8200.050	12191.69	3		$31605^{a}_{3\frac{1}{2}}$–$43796\ _{2\frac{1}{2}}$
8205.276	12183.93	150		$32620^{a}_{3\frac{1}{2}}$–$44804\ _{2\frac{1}{2}}$
8206.495	12182.12	100		$33085^{a}_{2\frac{1}{2}}$–$45267\ _{1\frac{1}{2}}$
8211.310	12174.97	150		$31927^{a}_{2\frac{1}{2}}$–$44102\ _{3\frac{1}{2}}$
8225.074	12154.60	50		$33343^{a}_{1\frac{1}{2}}$–$45497\ _{0\frac{1}{2}}$
8237.089	12136.87	500 *cw*		$21206\ _{2\frac{1}{2}}$–$33343^{a}_{1\frac{1}{2}}$
8248.960	12119.40	40		$19895\ _{2\frac{1}{2}}$–$32014^{a}_{2\frac{1}{2}}$
8254.505	12111.26	30		$19903\ _{3\frac{1}{2}}$–$32014^{a}_{2\frac{1}{2}}$
8264.138	12097.15	10		$20523\ _{2\frac{1}{2}}$–$32620^{a}_{3\frac{1}{2}}$
8276.202	12079.51	1 *h*		$32253^{a}_{1\frac{1}{2}}$–$44333\ _{1\frac{1}{2}}$
8276.202	12079.51	1 *h*		$32258^{a}_{1\frac{1}{2}}$–$44337\ _{2\frac{1}{2}}$
8306.220	12035.86	2		$15624\ _{2\frac{1}{2}}$–$27660^{a}_{3\frac{1}{2}}$
8308.158	12033.05	200		$21447\ _{1\frac{1}{2}}$–$33480^{a}_{0\frac{1}{2}}$
8309.161	12031.60	200		$19895\ _{2\frac{1}{2}}$–$31927^{a}_{2\frac{1}{2}}$
8315.502	12022.42	60		$53945\ _{2\frac{1}{2}}$–$41922^{a}_{2\frac{1}{2}}$
8319.074	12017.26	20 *cw*		$33480^{a}_{0\frac{1}{2}}$–$45497\ _{0\frac{1}{2}}$
8346.576	11977.66	40		$31414^{a}_{3\frac{1}{2}}$–$43391\ _{3\frac{1}{2}}$
8383.670	11924.67	40		$33343^{a}_{1\frac{1}{2}}$–$45267\ _{1\frac{1}{2}}$
8404.004	11895.82	7		$32253^{a}_{1\frac{1}{2}}$–$44149\ _{0\frac{1}{2}}$
8415.550	11879.50	50 *cw*		$21206\ _{2\frac{1}{2}}$–$33085^{a}_{2\frac{1}{2}}$
8422.434	11869.79	5		$31927^{a}_{2\frac{1}{2}}$–$43796\ _{2\frac{1}{2}}$
8462.808	11813.16	10 *c*		$19791\ _{4\frac{1}{2}}$–$31605^{a}_{3\frac{1}{2}}$
8477.918	11792.10	2		$27971\ _{4\frac{1}{2}}$–$39763^{a}_{4\frac{1}{2}}$
8481.348	11787.34	50 *c*		$33480^{a}_{0\frac{1}{2}}$–$45267\ _{1\frac{1}{2}}$
8484.000	11783.65	40		$20231\ _{1\frac{1}{2}}$–$32014^{a}_{2\frac{1}{2}}$
8497.126	11765.45	5 *h*		$33343^{a}_{1\frac{1}{2}}$–$45108\ _{1\frac{1}{2}}$
8514.700	11741.16	30		$31114^{a}_{4\frac{1}{2}}$–$42855\ _{4\frac{1}{2}}$
8522.539	11730.37	20		$20523\ _{2\frac{1}{2}}$–$32253^{a}_{1\frac{1}{2}}$
8531.062	11718.65	100		$33085^{a}_{2\frac{1}{2}}$–$44804\ _{2\frac{1}{2}}$
8537.653	11709.60	30		$19895\ _{2\frac{1}{2}}$–$31605^{a}_{3\frac{1}{2}}$
8543.616	11701.43	100		$19903\ _{3\frac{1}{2}}$–$31605^{a}_{3\frac{1}{2}}$
8595.933	11630.21	10		$20384\ _{3\frac{1}{2}}$–$32014^{a}_{2\frac{1}{2}}$
8604.090	11619.18	3		$38319^{a}_{1\frac{1}{2}}$–$49938\ _{2\frac{1}{2}}$
8639.395	11571.70	4		$20686\ _{2\frac{1}{2}}$–$32258^{a}_{1\frac{1}{2}}$
8664.128	11538.67	6		$32258^{a}_{1\frac{1}{2}}$–$43796\ _{2\frac{1}{2}}$
8673.629	11526.03	8		$16133\ _{4\frac{1}{2}}$–$27660^{a}_{3\frac{1}{2}}$
8707.215	11481.57	100 *cw*		$32620^{a}_{3\frac{1}{2}}$–$44102\ _{3\frac{1}{2}}$
8719.950	11464.80	30		$31927^{a}_{2\frac{1}{2}}$–$43391\ _{3\frac{1}{2}}$

TABLE 3. *Classified lines of* Tc I

Wavelength A	Wavenumber cm^{-1}	Intensity		Energy levels cm^{-1}
		Arc	Spark	
8722.680	11461.21	25		$33343^{o}_{1\,1/2}$–$44804\,_{2\,1/2}$
8737.936	11441.20	100 *cw*		$31414^{o}_{3\,1/2}$–$42855\,_{4\,1/2}$
8751.779	11423.11	20		$21920\,_{2\,1/2}$–$33343^{o}_{1\,1/2}$
8756.861	11416.48	15		$21926\,_{2\,1/2}$–$33343^{o}_{1\,1/2}$
8766.685	11403.68	6		$20523\,_{2\,1/2}$–$31927^{o}_{2\,1/2}$
8787.243	11377.00	3		$32014^{o}_{2\,1/2}$–$43391\,_{3\,1/2}$
8790.906	11372.26	2		$16287\,_{3\,1/2}$–$27660^{o}_{3\,1/2}$
8808.817	11349.14	2 *h*		$38216^{o}_{2\,1/2}$–$49565\,_{2\,1/2}$
8812.420	11344.50	5 *c*		$16025\,_{5\,1/2}$–$27369^{o}_{4\,1/2}$
8820.915	11333.58	10 *c*		$21752\,_{3\,1/2}$–$33085^{o}_{2\,1/2}$
8829.829	11322.13	200 *cw*		$19791\,_{4\,1/2}$–$31114^{o}_{4\,1/2}$
8897.645	11235.84	2 *c*		$16133\,_{4\,1/2}$–$27369^{o}_{4\,1/2}$
8901.474	11231.01	30 *c*		$20783\,_{3\,1/2}$–$32014^{o}_{2\,1/2}$
8909.930	11220.35	2		$20384\,_{3\,1/2}$–$31605^{o}_{3\,1/2}$
8917.736	11210.53	8		$19903\,_{3\,1/2}$–$31114^{o}_{4\,1/2}$

4. References

[1] Meggers, W. F., and Scribner, B. F., J. Res. NBS **45,** 476 (1950).
[2] Meggers, W. F., J. Res. NBS **47,** 7 (1951) RP2221.
[3] Bozman, W. R., J. Opt. Soc. Am. **44,** 828(A) (1954).
[4] Bozman, W. R., J. Opt. Soc. Am. **46,** 383(A) (1956).
[5] Bozman, W. R., Meggers, W. F., and Corliss, C. H., J. Res. NBS **71A** (Phys. and Chem.) No. 6, 547 (1967).
[6] Corliss, C. H., Bozman, W. R., and Westfall, F. O., J. Opt. Soc. Am. **43,** 398 (1953).
[7] Moore, C. E., Atomic Energy Levels, Vol. **III,** NBS Circ. 467, p. 18 (Washington, U.S. Gov't Printing Office, 1958).
[8] Tech, J. L., NBS Publication in preparation.

(Paper 72A6–521)

JOURNAL OF RESEARCH of the National Bureau of Standards—A. Physics and Chemistry
Vol. 72A, No. 6, November–December 1968

The First Spectrum of Tungsten (W I)

Donald D. Laun [1] and C. H. Corliss

Institute for Basic Standards, National Bureau of Standards, Washington, D.C. 20234

(August 6, 1968)

The first spectrum of tungsten (W i) has been observed in the region between 2000 Å and 10500 Å. Of the 6800 spectral lines reported here, about 5500 have been classified as transitions between 91 even and 365 odd levels.

Key Words: Atomic spectra; energy levels; spectroscopy; spectrum of tungsten; tungsten; wavelengths.

1. Introduction

The analysis of the first spectrum of tungsten (or wolfram), W I, was initiated by Otto Laporte [1][2] in 1925 during his stay in the NBS Spectroscopy Section. By using mainly the wavelengths measured by Belke [2] in Kayser's laboratory at Bonn and existing Zeeman effect data, he identified the low $4d^46s^2\ ^5D$ and $4d^56s\ ^7S$ terms. Over the next two decades this work was greatly extended by Laporte and Julian Mack [3] who in 1943 reported 50 even and 250 odd levels. That report incorporated, in addition to their own work, contributions from Catalán and Poggio [4] and from Laun [5].

In 1955 Laun contributed over 50 new levels to C. E. Moore for inclusion in her compilation "Atomic Energy Levels" [6]. Since that time the work has been extended. The entire spectrum has been remeasured and the results are reported in this paper.

Gilbert Gluck [7] has described the hyperfine isotopic structure of tungsten. He found that the relative isotopic shifts in natural tungsten, between isotope 186 and the isotopes 184, 183, 182, and 180 are respectively (1), (1.54), (2.13), and (2.92). Gluck then measured by interferometer the separation of the strong 184 and 186 components of 578 lines. He verified the level 397°_7, which has only two combinations and unresolved Zeeman patterns. The hyperfine separations of its combinations with 19_6 and $^3H_6$ are -68 and $+08$ millikaysers which values agree with those found for other lines. Gluck used an electronic computer to look for new levels. Eight of these had been found independently by Laun, or are adopted from Gluck with assigned J-values, but eight others are apparently spurious due to the use of spark lines. The level 41637°_3 which Gluck believed to be the first level of the configuration d^5p to be identified, because it might explain the line 4466.74 Å with isotope displacement -63, is, however, not confirmed with any other combinations.

From his observations Gluck assigned 150 odd levels to d^4sp or d^3s^2p and 36 even levels to d^4s^2 or d^5s configurations. Some of these lead to designations different from those in AEL. The designations in this paper are the same as those in AEL. Gluck's associate Bauche is working on the configuration assignment of more levels.

Yehuda Shadmi of Jerusalem reports that his calculations account for all the low even levels. His work is presented in this issue of the NBS Journal of Research [8]. Spin-orbit interaction is strong enough to mix states with different term assignments; hence many of the levels, especially those with small J-values do not have definite LS designations. Shadmi is also making calculations on the odd levels.

2. Experiments

The observations of the arc spectrum presented here were carried out with those of the spark spectrum, which were reported in 1964 [9]. The list of W II lines in that paper is not complete, since, with the exception of a few of the stronger lines, only classified lines were reported there. The spectrum described here, on the other hand, contains all the lines attributable to the neutral atom, including one or two observed only by Belke or Gluck. The lines at 4645.72 and 5796.49 Å are due to Gluck.

The making of the spectrograms is described in the paper on W II. The d-c arc in air between tungsten electrodes has a beautiful white color. The spark spectrum was photographed alongside the arc ex-

[1] Formerly with the Spectroscopy Section, NBS; present address: Kiel, Wisconsin 53042.
[2] Figures in brackets indicate references on page 614.

posure. Since most of the lines appear in both sources, visual estimates of the intensities in each source were made. Ninety lines in the W II paper were marked "*A*" to indicate that a calculated arc line coincided with a calculated spark line. These coincidences are marked with an "*s*" in the spark column in this table. About 50 more of the "*s*" lines will be found in this table than "*a*" lines in the spark table [9].

Very few impurity lines were detected, but it is possible that in such a rich spectrum band lines were measured, especially in the region beyond 6350 Å where the arc in air was troubled by band lines. To eliminate these, the spectrum was excited in an electrodeless lamp containing tungsten iodide and photographed and measured in 1967 at NBS. In this case, thorium standards were used. The observations beyond 10 000 Å were made by C. C. Kiess. No arc lines were positively identified below 2000 Å.

3. Results

The results of this investigation are presented in three tables. Table 1 contains the levels of even parity and table 2, those of odd parity. The configurations and term designations (where assigned) are followed by the total angular momentum quantum number, J, in column 3, the numerical value of the level in cm^{-1} in column 4, intervals between levels of terms in column 5; and magnetic splitting factors, g, in column 6, measured by other observers.

TABLE 1. *Even levels of* W I

Configuration	Desig.	J	Level	Interval	Obs. g	Configuration	Desig.	J	Level	Interval	Obs. g
$5d^4\ 6s^2$	^5D	0	0.00			$5d^5\ 6s$	^5S	2	18280.48		1.43
				1670.29							
		1	1670.29		1.51			3	19827.68		1.28
				1655.24				0	20174.20		
		2	3325.53		1.48			1	20427.84		2.1
				1504.47				2	20983.02		
		3	4830.00		1.50			4	22476.68		1.48
				1389.33				0	22773.78		
		4	6219.33		1.49			4	22852.80		1.2
								1	23455.02		
$5d^5\ 6s$	^7S	3	2951.29		1.98			6	23484.78		
								3	23930.08		1.4
$5d^4\ 6s^2$	^3P	0	9528.06					2	23982.80		
				3779.04				3	24610.88		
		1	13307.10		1.32			2	24789.66		
				5946.46				2	26861.64		
		2	19253.56		1.18			4	27213.82		
								1	27670.48		
$5d^4\ 6s^2$	^3H	4	12161.96		0.99			5	27849.80		
				2907.97				2	28204.20		
		5	15069.93		1.05			5	28233.44		
				1938.57				3	28291.88		
		6	17008.50		1.4			3	28347.60		
								6	28392.70		
$5d^4\ 6s^2$	^3G	3	13348.56		0.92			1	28720.88		
				3082.75				2	28898.96		
		4	16431.31		1.02			7	29460.98		
				3394.73				4	29479.32		
		5	19826.04		1.20			4	29853.66		
								2	30374.20		
$5d^4\ 6s^2$	^3F	2	13777.71		1.09			5	31389.08		
				3923.47				4	32135.94		
		3	17701.18		1.02			1	32378.40		
				−594.17				5	33291.80		
		4	17107.01		1.19			4	34302.04		
$5d^4\ 6s^2$	^3D	3	15460.01		1.17	$5d^4\ 6s\ 7s$	^7D	1	43451.98		2.83
				483.83						1467.86	
		2	14976.18		1.06			2	44919.84		1.9
				−3106.65						1576.78	
		1	18082.83		0.7			3	46496.62		1.74
										1478.92	
$5d^5\ 6s$	^5G	2	18116.84		1.08			4	47975.54		1.68
				857.67						1379.14	
		3	18974.51		1.06			5	49354.68		1.7
				281.73							
		4	19256.24		1.20	$5d^4\ 6s\ 7s$	$e\ ^5D$	0	45225.22		
				278.77						1233.08	
		5	19535.01		1.21			1	46458.30		
				113.53						1620.02	
		6	19648.54		1.32			2	48078.32		1.55

TABLE 1. *Even levels of* W I (cont'd).

Configuration	Desig.	J	Level	Interval	Obs. g	Configuration	Desig.	J	Level	Interval	Obs. g
				1577.72				3	52284.76		
		3	49656.04		1.66			4	52378.22		
				1467.10				1	52956.92		
		4	51123.14		1.4			4	53786.00		
								3	53916.90		
		2	50525.35					5	53974.10		
		1	50906.20					3	54657.56		
		1	50949.07					4	55333.12		1.45
		0	51285.46					5	55381.00		
		2	51936.84					6	55420.88		
		3	52002.25					5	56573.54		
		1	52057.80					5	56768.06		
		2	52183.20					6	56832.90		

TABLE 2. *Odd levels of* W I

Configuration	Desig.	J	Level	Interval	Obs. g	Configuration	Desig.	J	Level	Interval	Obs. g
$5d^4\ 6s\ 6p$	$^7F°$	0	19389.43			$5d^4\ 6s\ 6p$	$^5P°$	1	28198.90		
				674.87						1194.50	
		1	20064.30		1.54			2	29393.40		1.83
				1384.46						1193.24	
		2	21448.76		1.48			3	30586.64		1.64
				1598.55							
		3	23047.31		1.53			1	30683.54		1.39
				1716.08				1	31323.48		0.86
		4	24763.39		1.50			2	31817.63		1.52
				1913.09				3	32238.02		1.3
		5	26676.48		1.46			0	32386.56		
				2966.58				3	32957.58		1.43
		6	29643.06					2	33141.38		1.51
								2	33944.06		
$5d^4\ 6s\ 6p$	$^7D°$	1	21453.90		2.51			4	34121.68		1.5
				2510.77				3	34228.60		
		2	23964.67		1.93			1	34342.44		1.56
				2224.53				3	34354.08		0.71
		3	26189.20		1.80			2	34485.86		0.82
				2608.04				4	34632.60		0.89
		4	28797.24		1.61			1	34719.33		0.15
				976.10				4	35116.78		1.2
		5	29773.34		1.55			2	35311.56		1.0
								3	35499.15		1.0
$5d^4\ 6s\ 6p$	$^5F°$	1	25983.60		0.54			5	35507.07		
				1678.92				2	35731.96		1.5
		2	27662.52		1.21			3	35943.17		1.4
				1476.60				4	36082.30		1.24
		3	29139.12		1.06			1	36190.49		1.62
				2293.79				5	36275.10		1.27
		4	31432.91		1.32			0	36588.32		
				1937.13				2	36673.70		1.50
		5	33370.04		1.39			3	36874.36		1.50
								2	36904.16		1.57
$5d^5(^6S)6p$	$^7P°$	2	26229.77		1.84			4	37146.36		1.1
				1258.34				5	37309.16		1.25
		3	27488.11		1.72			2	37466.30		1.28
				401.57				3	37674.08		1.13
		4	27889.68		1.71			1	37773.96		
								4	38001.12		1.1
		2	26367.28		0.87			3	38053.05		1.11
								6	38203.12		
$5d^4\ 6s\ 6p$	^5D	0	26629.46					3	38206.38		
				1149.04				4	38259.40		
		1	27778.50		1.25			1	38355.84		
				1417.34				0	38576.14		
		2	29195.84		1.28			4	38748.44		
				717.01				2	39030.25		
		3	29912.85		1.31			1	39183.20		1.01
				2915.27				5	39361.01		1.13
		4	32828.12		1.7			5	39614.05		1.20

TABLE 2. *Odd levels of* W I—Continued

Configuration	Desig.	J	Level	Interval	Obs. g	Configuration	Desig.	J	Level	Interval	Obs. g
		1	39636.62		1.44			5	45451.65		1.16
		3	39646.41		1.46			3	45551.32		1.30
		2	39707.02		1.00			3	45677.69		1.24
		7	39709.04					1	45760.80		
		4	39719.96		1.17			5	45789.14		1.19
		2	40011.50		1.0			4	45869.10		1.36
		4	40233.97		1.53			2	45902.48		0.5
		3	40269.35		1.03			3	46068.02		1.46
		1	40411.12		1.58			1	46104.62		
		5	40476.42		1.04			6	46106.20		
		4	40583.07					1	46291.63		
		3	40665.85		0.96			2	46327.75		0.8
		1	40770.78		1.28			3	46385.46		1.4
		2	40868.40		1.26			5	46506.37		1.38
		5	40911.98		1.03			0	46613.70		
		3	40923.83		1.32			4	46625.05		1.14
		2	41104.52		1.5			6	46672.22		1.18
		0	41127.38					2	46806.45		1.1
		6	41171.44					5	46854.80		1.21
		4	41198.14		1.22			4	46931.84		1.0
		6	41417.52		1.23			2	47079.40		1.3
		3	41499.43		1.11			1	47255.55		
		2	41583.20		1.06			2	47337.79		0.9
		3	41694.34		1.28			4	47360.19		
		2	41734.13		1.1			3	47361.74		1.3
		4	41871.94		1.11			2	47442.53		
		0	41965.24					3	47483.68		1.29
		2	41978.62		0.8			6	47541.56		1.23
		6	42239.06					3	47593.44		1.2
		3	42251.51		1.32			4	47689.33		1.4
		1	42262.30		1.5			1	47819.94		
		2	42449.60					5	47850.84		
		4	42450.24					4	47968.62		1.23
		3	42514.14		1.22			5	48138.38		1.2
		4	42532.62					3	48170.55		
		1	42573.49		1.3			2	48244.29		1.4
		3	42601.19		1.12			7	48250.70		
		5	42866.00		1.11			0	48264.62		
		4	42910.74		1.18			2	48318.84		1.4
		5	43034.10					3	48326.41		
		0	43053.88					1	48389.96		
		1	43217.33		1.3			0	48603.44		
		2	43227.66		1.3			4	48676.08		1.20
		4	43251.00		1.14			6	48684.68		
		7	43411.50		1.20			1	48788.06		
		3	43478.58		1.3			3	49072.14		1.26
		2	43514.68		0.9			5	49073.88		
		4	43720.87					4	49147.95		
		5	43741.37		1.09			2	49151.94		
		3	43850.84		1.17			5	49187.92		1.25
		1	43892.62		1.05			2	49270.16		
		5	43924.25		1.2			3	49417.90		
		2	43975.22		1.15			1	49443.70		
		4	43985.41		1.24			3	49514.34		1.3
		3	44021.00		1.2			2	49517.26		
		1	44353.46		1.02			4	49636.52		
		2	44367.50		1.1			2	49699.56		1.9
		6	44390.42		1.28			4	49788.58		
		3	44447.02		1.38			0	49798.48		
		5	44546.76		1.3			3	49966.03		
		2	44596.28		1.11			5	50137.55		1.11
		1	44737.21		1.1			3	50185.70		
		6	44923.90		1.23			4	50284.64		1.03
		4	44940.57		1.20			3	50303.78		
		7	44970.82		1.20			6	50429.18		
		3	45014.54		1.3			2	50494.54		
		2	45019.02					1	50533.55		
		4	45116.77		1.2			2	50718.90		
		4	45262.55		1.1			3	50800.44		1.0
		0	45306.89					5	50806.07		
		1	45374.00					3	50894.12		
		2	45422.26		0.63			4	50909.47		1.2

TABLE 2. *Odd levels of* W I—Continued

Configuration	Desig.	J	Level	Interval	Obs. g	Configuration	Desig.	J	Level	Interval	Obs. g
		6	50951.86					2	55619.66		
		3	51072.18					7	55690.82		
		2	51182.38					5	55795.48		
		1	51260.68					2	55835.12		
		5	51290.73					6	55847.68		
		7	51296.92					1	55859.32		
		4	51473.04					4	55867.24		
		3	51600.52					4	55955.36		
		2	51606.78					5	55987.90		
		2	51693.85					2	56037.28		
		1	51763.44					3	56108.44		
		4	51856.10					4	56174.63		
		6	51978.68					4	56255.65		
		3	52015.28					5	56280.45		
		4	52059.78					3	56332.00		
		2	52064.08					3	56484.33		
		5	52081.09					4	56502.10		
		2	52152.62					6	56526.57		
		0	52233.10					7	56557.20		
		3	52255.80					3	56717.13		
		5	52395.50					7	56790.60		
		4	52436.44					4	56831.67		
		1	52477.57					2	56999.30		
		2	52503.41					3	57131.78		
		2	52653.58					5	57143.48		
		5	52774.10					6	57148.98		
		3	52806.56					4	57315.25		
		6	52855.98					3	57352.32		
		2	52885.50					4	57471.80		
		3	52943.48					5	57560.83		
		4	52992.69					3	57619.36		
		2	53003.72					6	57702.30		
		1	53042.00					3	57732.46		
		4	53118.29					4	57803.66		
		5	53194.25		1.3			6	57919.17		
		1	53227.03					3	58091.58		
		6	53228.42					5	58179.38		
		4	53238.41					3	58206.00		
		2	53284.92					1	58290.18		
		3	53345.52					4	58316.46		
		3	53390.42					4	58330.13		
		2	53669.36					3	58487.52		
		4	53848.63					5	58562.68		
		5	53862.72					2	58595.42		
		1	53875.26					3	58644.10		
		2	53912.55					2	58655.72		
		2	53959.28					6	58760.96		
		3	54117.36					4	58777.80		
		4	54118.78					4	58848.90		
		3	54269.77					5	58903.98		
		0	54295.64					6	59128.80		
		5	54310.30					5	59149.60		
		1	54374.80					4	59171.71		
		1	54419.67					2	59211.47		
		3	54556.43					5	59263.63		
		6	54733.38					7	59346.98		
		2	54859.15					3	59399.74		
		6	54895.96					6	59410.52		
		3	54900.90					2	59422.00		
		4	54911.61					5	59673.32		
		1	54941.01					2	59999.10		
		5	55009.22					4	60158.32		
		2	55032.67					5	60229.18		
		4	55043.34					4	60385.09		
		2	55084.02					6	60414.83		
		4	55346.20					5	60741.40		
		1	55384.38					7	61180.86		
		3	55389.30					5	61476.60		
		2	55390.16					4	61535.50		
		5	55455.35					5	62154.50		
		5	55492.22					6	62524.02		
		3	55546.06					6	62687.50		
		4	55596.90					6	63532.78		

There are 91 even levels of which 37 are new. There are 365 odd levels, 64 of them new. As an aid in checking the reality of the levels, a square array showing all the predicted combinations between even and odd levels was prepared on the NBS electronic computer by W. R. Bozman and Jack Sugar.

Table 3 contains about 6800 observed lines of the arc spectrum of tungsten. Approximately 5500 of these are classified, compared with the table of 2400 lines classified by Laporte and Mack [2] 25 years ago. In table 3, wavelengths in air in Ångstroms are followed by intensity estimates of the lines as observed on the exposures of arc and spark. Between 6359 and 10000 Å the arc intensities are taken from the electrodeless lamp exposures and no spark exposure was made. The symbols in the intensity columns are as follows:

a air line coincident
b broadened
bb very broad
d double
g possible ghost
v shaded to short wavelength
l shaded to long wavelength
r reversed
s classified in spark spectrum

Vacuum wavenumbers in cm^{-1} are derived from the observed wavelengths with the aid of the Table of Wavenumbers by Coleman, Bozman, and Meggers [10].

The column "o-c" of differences between the observed wave numbers and those calculated from the term combinations is an index of the accuracy of the measurements. The "o-c" is greater at short wavelengths and, also, where lines are too close together for precise measurement. The corresponding levels between which the transition occurs are given in the next column. A few term designations are used where unambiguous, but in most cases the even levels are indicated by the first two digits of the level value and the odd levels by the first three digits as was done by Laporte and Mack. Where the levels are too close together, all five digits are given. *J*-values are given as subscripts and the odd symbol as a superscript.

The number of doubly classified lines in table 3 has been severely reduced by limiting the tolerance "o−c" and especially by casting out the higher combinations if they fall on a low combination. The higher combinations are usually masked by the lower ones. A further check is given in the last column by indicating the type of Zeeman pattern. The symbols in the last column describe the Zeeman patterns as follows:

Res resolved Zeeman pattern in apparent agreement with the classification
1 type 1 pattern ($g_x < g_y$, $J_x > J_y$)
2 type 2 pattern ($g_x > g_y$, $J_x > J_y$)
3 type 3 pattern ($J_x = J_y$)
7 type 7 pattern (indeterminate)
(b) *p*-components broadened
(0) *p*-components unchanged from the zero-field position
zd two superimposed patterns

An explanation and illustrations of the types are given in ref. [11].

We acknowledge the encouragement of the late W. F. Meggers in this work and the assistance of the late C. C. Kiess who made most of the spectrograms.

4. References

[1] Laporte, O., Naturwiss. **13,** 627–628 (1925).
[2] Belke, M., Z. Wiss. Photographie **17,** 132 and 145 (1918).
[3] Laporte, O., and Mack, J. E., Phys. Rev. **63,** 246–297 (1943).
[4] Catalán, M. A., and Poggio, F., Ann. Soc. Espan. Fisica y Quimica **32,** 255 (1934); Poggio, F., ibid. **33,** 171–202 (1935).
[5] Laun, D. D., J. Res. NBS **21,** 207–224 (1938) RP1125.
[6] Moore, C. E., Atomic Energy Levels, NBS Circ. 467, Vol. **III,** 156–161 Washington (1958).
[7] Gluck, G., Ann. Phys. **10,** 673–696 (1965).
[8] Shadmi, Y., and Caspi, E., J. Res. NBS **72A** (Phys. and Chem.) No. 6, 757 (1968).
[9] Laun, D. D., J. Res. NBS **68A,** 207–252 (1964).
[10] Coleman, C. D., Bozman, W. R., and Meggers, W. F., Table of Wave numbers, NBS Mono. 3, Washington (1960).
[11] Corliss, C. H., Meggers, W. F., J. Res. NBS **61** No. 4, 269 (1958) RP2904.

TABLE 3. *Observed and classified lines of* W I

Wavelength Å	Intensity		Wavenumber (cm^{-1})		Classification	Zeeman effect
	Arc	Spark	Observed	o−c		
2000.40	3		49973.8			
2000.97	3		49959.6	+0.21	$^5D_2$− 532°$_2$	
2001.15	1		49955.1	−0.20	$^5D_4$− 561°$_4$	
2002.47	5		49922.2			
2006.93	3		49811.3			
2008.63	1		49769.1	+0.53	$^5D_4$− 559°$_5$	
2008.91	3		49762.2			
2014.72	1		49618.7	+0.75	$^5D_2$− 529°$_3$	
2016.40	3		49577.4	+1.25	$^5D_4$− 557°$_5$	
2020.11	5		49486.3	+1.15	$^7S_3$− 524°$_4$	
2021.81	3		49444.7	+1.0	$^5D_0$− 494°$_1$	
2022.04	2	4	49439.1	−0.67	$^5D_3$− 542°$_3$	
2023.87	5		49394.4			
2030.19	2		49240.6			
2030.36	2		49236.5	+0.48	$^5D_4$–55455°$_5$	
2034.77	4		49129.8	+0.52	$^5D_3$− 539°$_2$	
2035.46	2		49113.3	+0.51	$^7S_3$− 520°$_2$	
2036.92	3	1	49078.0			
2039.38	3		49018.9	+0.27	$^5D_3$− 538°$_4$	
2044.16	1		48904.2	−0.61	$^7S_3$− 518°$_4$	
2045.74	3		48866.4			
2047.48	3		48824.9	+0.65	$^5D_1$− 504°$_2$	
				+0.89	$^5D_4$− 550°$_4$	
2049.03	3	8	48788.0	−0.06	$^5D_0$− 487°$_1$	
2051.04	3	8	48740.1			
2051.94	3		48718.8			
2053.514	3	20	48681.4	−0.17	$^5D_4$− 549°$_3$	
2058.616	10	2	48560.8	+0.38	$^5D_3$–53390°$_3$	
2060.53	3	2 *s*	48515.7	+0.18	$^5D_3$–53345°$_3$	
2061.31	2		48497.4			
2062.754	4		48463.4	+0.54	$^3H_5$− 635°$_6$	
2063.10	6		48455.3	+0.38	$^5D_3$− 532°$_2$	
2064.51	2		48422.2			
2065.056	6	3 *s*	48409.4	+0.99	$^5D_3$− 532°$_4$	
2065.86	4		48390.5	+0.54	$^5D_0$− 483°$_1$	
2066.604	6		48373.1			
2070.23	3		48288.4	+0.11	$^5D_3$− 531°$_4$	
2070.55	6	1	48280.9	+0.35	$^5D_2$–51606°$_2$	
2070.80	3	1	48275.1	+0.11	$^5D_2$− 516°$_3$	
2077.10	8		48128.7	+0.51	$^5D_1$− 497°$_0$	
2077.732	1	2	48114.1	+0.62	$^5D_3$− 529°$_3$	
2080.45	4		48051.2	+0.76	$^5D_4$− 542°$_3$	
2081.37	12		48030.0	+0.73	$^5D_1$− 496°$_2$	
2082.806	8		47996.9	+0.54	$^3H_4$− 601°$_4$	
2085.46	8	1	47935.8	+0.65	$^5D_2$− 512°$_1$	
2087.10	80 *d*	2 *l*	47898.1	−1.35	$^5D_4$− 541°$_4$	
2087.933	3		47879.0			
2088.90	2	2	47856.9	+0.05	$^5D_2$− 511°$_2$	
2089.30	30		47847.7	+0.73	$^5D_1$− 495°$_2$	
2090.48	60		47820.7	+0.76	$^5D_0$− 478°$_1$	

TABLE 3. *Observed and classified lines of* W I

Wavelength Å	Intensity		Wavenumber (cm^{-1})		Classification	Zeeman effect
	Arc	Spark	Observed	o−c		
2092.516	10	1	47774.2	+0.79	$^5D_1$— 494°$_1$	
2093.66	15		47748.1	+1.45	$^5D_2$— 510°$_3$	
2094.06	15		47739.0			
2095.03	2		47716.9			
2095.56	25	12	47704.8			
2097.52	1	1	47660.2			
2098.22	60	30 *s*	47644.2	+0.81	$^5D_4$— 538°$_5$	
2098.846	25		47630.1	+0.80	$^5D_4$— 538°$_4$	
2099.85	50	1	47607.3	+0.86	$^5D_3$— 524°$_4$	
2101.538	50		47569.1	+0.51	$^5D_2$–50894°$_3$	
2102.65	8	1	47544.0	+0.75	$^7S_3$— 504°$_2$	
2102.977	3	1	47536.6			
2103.37	5		47527.7			
2104.08	15		47511.7	+0.34	$^3H_4$— 596°$_5$	
2105.40	50	1	47481.9	+0.25	$^5D_1$— 491°$_2$	
2105.75	25	12	47474.0	−0.91	$^5D_2$— 508°$_3$	
2106.57	15	2	47455.5	+1.41	$^3H_5$— 625°$_6$	
2106.94	8		47447.16			
2107.86	15		47426.4	+0.60	$^5D_3$— 522°$_3$	
2109.31	60	2	47393.8	+0.43	$^5D_2$— 507°$_2$	
2109.89	12		47380.8			
2111.13	15	1	47353.0	+0.51	$^7S_3$— 503°$_3$	
2112.47	6		47323.0	+0.38	$^5D_3$— 521°$_2$	
2114.82	8	1	47270.4			
2115.49	3		47255.4	−0.15	$^5D_0$— 472°$_1$	
2116.30	40	8	47237.3	−0.48	$^3H_4$— 593°$_3$	
2116.44	30		47234.2	+0.12	$^5D_3$— 520°$_2$	
				−0.21	$^7S_3$— 501°$_3$	
2116.63	20		47230.0	+0.22	$^5D_3$— 520°$_4$	
2117.59	30	1	47208.6	+0.58	$^5D_2$— 505°$_1$	
2118.62	25		47185.6	+0.32	$^5D_3$— 520°$_3$	
2119.30	120	6	47170.5	−0.59	$^5D_4$–53390°$_3$	
				+1.49	$^5D_2$— 504°$_2$	
2120.74	12		47138.4			
2121.27	3		47126.7	+0.51	$^5D_4$–53345°$_3$	
2121.60	100 *d*	25 *s*	47119.3	+1.53	$^5D_1$— 487°$_1$	
2122.37	20	4	47102.2	+0.53	$^3H_4$— 592°$_5$	
2123.15	30		47084.9	+0.33	$^3H_5$— 621°$_5$	
2124.86	20 *b*		47047.1			
2124.95	6		47045.1			
2125.36	3		47036.0	−0.53	$^3G_3$— 603°$_4$	
2125.79	15		47026.5	+0.40	$^5D_3$— 518°$_4$	
2126.114	25		47019.31	+0.23	$^5D_4$— 532°$_4$	
2126.544	6	1	47009.81	+0.06	$^3H_4$— 591°$_4$	
2127.55	3		46987.6	−0.04	$^3H_4$— 591°$_5$	
2127.957	15	5	46978.59	+0.34	$^5D_2$— 503°$_3$	
2128.122	50	5	46974.95	+0.03	$^5D_4$— 531°$_5$	
2129.00	10	2 *s*	46955.58			
2130.05	20	2 *s*	46932.4	−0.75	$^5D_1$— 486°$_0$	
2131.526	8	2	46899.9	+0.94	$^5D_4$— 531°$_4$	

TABLE 3. *Observed and classified lines of* W I

Wavelength Å	Intensity		Wavenumber (cm^{-1})		Classification	Zeeman effect
	Arc	Spark	Observed	o−c		
2133.17	1	2	46863.8	−0.05	$^5D_3$–51693°$_2$	
2133.32	3		46860.5	+0.33	$^5D_2$– 501°$_3$	
2133.65	30		46853.3			
2135.625	6		46809.94	+0.18	$^3G_3$– 601°$_4$	
2135.875	8		46804.46			
2137.135	20	10 *s*	46776.87	+0.09	$^5D_3$–51606°$_2$	
2137.400	10		46771.07	+0.55	$^5D_3$– 516°$_3$	
2138.71	10		46742.4	+0.38	$^3H_4$– 589°$_5$	
2139.53	8		46724.51	+0.36	$^5D_4$– 529°$_3$	
2139.73	15		46720.14	+0.47	$^5D_1$– 483°$_1$	
2141.222	15		46687.59	+0.65	$^3H_4$– 588°$_4$	
2141.307	6	3	46685.74	+0.51	$^7S_3$– 496°$_4$	
2142.92	2		46650.60	+0.06	$^3G_3$– 599°$_2$	
2143.00	20		46648.86	+0.31	$^5D_1$– 483°$_2$	
2143.257	15	3 *s*	46643.27	+0.23	$^5D_3$– 514°$_4$	
2143.36	10		46641.03	+0.53	$^5D_2$– 499°$_3$	
2144.50	12	5	46616.24	+0.40	$^3H_4$– 587°$_4$	
2145.49	6	3	46594.73	+0.40	$^5D_1$– 482°$_0$	
2146.43	35 *r*		46574.33	+0.33	$^5D_1$– 482°$_2$	
2147.31	35	3 *s*	46555.24	−0.47	$^5D_4$– 527°$_5$	
2147.53	12		46550.47			
2148.716	6		46524.78	+0.50	$^3H_6$– 635°$_6$	
2150.68	2		46482.30	+0.16	$^3H_4$– 586°$_3$	
2151.075	8		46473.76			
2151.44	8		46465.88	+0.31	$^3H_5$– 615°$_4$	
2151.92	5		46455.52			
2154.86	5		46392.14			
2155.690	20		46374.28	+0.25	$^5D_2$– 496°$_2$	
2156.69	2	8	46352.78	+0.40	$^5D_3$– 511°$_2$	
2157.68	10		46331.52	+0.26	$^3P_0$– 558°$_1$	
2157.95	6		46325.72	+0.16	$^3H_4$– 584°$_3$	
2159.53	12		46291.83	+0.20	$^5D_0$– 462°$_1$	
2162.816	6		46221.50	+0.11	$^3F_2$– 599°$_2$	
2163.004	15	2	46217.49	+0.38	$^5D_4$– 524°$_4$	
2163.795	8		46200.59	−0.06	$^7S_3$– 491°$_2$	
2164.20	15		46191.95	+0.22	$^5D_2$– 495°$_2$	
2164.340	25 *r*		46188.96	+0.15	$^5D_2$– 495°$_3$	
2164.534	12		46184.82			
2164.928	25 *r*		46176.42	+0.25	$^5D_4$– 523°$_5$	
2165.686	8		46160.26			
2165.940	12		46154.85	+0.35	$^3H_4$–58316°$_4$	
2166.165	2		46150.05	+0.40	$^5D_1$– 478°$_1$	
2167.654	25	12	46118.36	+0.19	$^5D_2$– 494°$_1$	
2167.806	5		46115.12	+0.22	$^3P_1$– 594°$_2$	
2168.290	25	5	46104.83	+0.21	$^5D_0$– 461°$_1$	
2168.856	10		46092.80	+0.43	$^5D_2$– 494°$_3$	
2169.474	100 *r*	4	46079.67	+0.20	$^5D_3$– 509°$_4$	
2169.660	4		46075.72	+0.23	$^3D_3$– 615°$_4$	
2169.760	2		46073.60	+0.16	$^3G_3$– 594°$_2$	
2170.196	40	1	46064.34	+0.22	$^5D_3$–50894°$_3$	

318-092 O-69—5

TABLE 3. *Observed and classified lines of* W I

Wavelength Å	Intensity		Wavenumber (cm^{-1})		Classification	Zeeman effect
	Arc	Spark	Observed	o−c		
2170.632	3		46055.09			
2171.086	4 *b*		46045.46			
2171.14	1		46044.31	+0.27	$^3H_4$— 582°$_3$	
2171.51	3		46036.47	0.00	$^5D_4$— 522°$_3$	
2172.984	12		46005.24			
2174.620	60	1	45970.64	+0.20	$^5D_3$—50800°$_3$	
2175.08	3		45960.9			
2175.842	80 *r*	2	45944.82	+0.19	$^5D_2$— 492°$_2$	
2176.558	6		45929.71	+0.09	$^3H_4$— 580°$_3$	
2176.938	10		45921.69			
2177.760	30		45904.36	−0.05	$^3P_1$— 592°$_2$	
2178.474	80 *r*	1	45889.32	+0.42	$^5D_3$— 507°$_2$	
2178.886	3		45880.65			
2179.764	100 *r*	3	45862.17	+0.41	$^5D_4$— 520°$_5$	
2180.026	4		45856.65	+0.33	$^3P_0$— 553°$_1$	
2180.778	40	1	45840.84	+0.39	$^5D_4$— 520°$_4$	
2181.49	15	3 *s*	45825.9	−0.51	$^5D_2$— 491°$_2$	
2181.603	2		45823.51	+0.36	$^3G_3$— 591°$_4$	
2181.946	10		45816.31			
2182.90	150 *r*		45796.29	+0.34	$^5D_4$— 520°$_3$	
2183.47	12		45784.34			
2184.204	35	10	45768.95			
2184.56	6		45761.49	+0.69	$^5D_0$— 457°$_1$	
2185.256	40		45746.92	+0.31	$^5D_2$— 490°$_3$	
2186.300	8		45725.08	+0.29	$^7S_3$— 486°$_4$	
2186.374	25		45723.53	+0.34	$^3G_4$— 621°$_5$	
2187.70	3		45695.82			
2188.49	10		45679.33	+0.33	$^3H_6$— 626°$_6$	
2188.86	5		45671.60	+0.13	$^3H_5$— 607°$_5$	
2189.05	15		45667.64	+0.14	$^5D_1$— 473°$_2$	
2189.19	30	30 *s*	45664.72	+0.18	$^5D_3$— 504°$_2$	
2190.28	1	1	45642.0	+0.30	$^3H_4$— 578°$_4$	
2190.52	40	1	45637.0	+0.23	$^5D_4$— 518°$_4$	
2191.225	4		45622.32	+0.29	13$_2$— 593°$_3$	
2191.446	4		45617.72			
2191.80	4		45610.35			
2192.36	60	8	45598.7			
2192.615	30		45593.40			
2193.016	50	125	45585.06	−0.20	$^5D_1$— 472°$_1$	
2193.707	30		45570.70	+0.20	$^3H_4$— 577°$_3$	
2194.78	10		45548.42			
2196.354	4		45515.79	+0.27	$^3H_6$— 625°$_6$	
2197.080	80	4	45500.74	+0.40	$^3G_3$— 588°$_4$	
2198.367	150	6	45474.11	+0.33	$^5D_3$— 503°$_3$	
2198.915	200 *r*	3	45462.78	+0.25	$^5D_2$— 487°$_1$	
2199.166	40	2 *s*	45457.59	+0.19	$^3H_4$— 576°$_3$	
2199.300	50	3	45454.82	+0.18	$^5D_3$— 502°$_4$	
2199.88	12	1	45442.84			
2200.316	25		45433.84	+0.07	13$_2$— 592°$_2$	
2200.532	20		45429.38	+0.14	$^3G_3$— 587°$_4$	

TABLE 3. *Observed and classified lines of* W I

Wavelength Å	Intensity		Wavenumber (cm^{-1})		Classification	Zeeman effect
	Arc	Spark	Observed	o−c		
2201.504	60		45409.32	+0.21	$^5D_1$ — 470°$_2$	
2202.856	50	1	45381.45	+0.26	$^5D_4$ — 516°$_3$	
2203.188	40		45374.61	−0.51	$^7S_3$ — 483°$_3$	
				+0.61	$^5D_0$ — 453°$_1$	
2203.518	6		45367.82	+0.27	$^7S_3$ — 483°$_2$	
2204.092	50		45356.01	+0.31	$^5D_3$ — 501°$_3$	
2204.610	15		45345.35	+0.45	$^3H_5$ — 604°$_6$	
2205.368	20		45329.77			
2206.456	4		45307.42	+0.26	$^3G_3$ — 586°$_2$	
2207.028	20		45295.67	+0.13	$^3G_3$ — 586°$_3$	
2207.160	30	1	45292.97	−0.03	$^7S_3$ — 482°$_2$	
2207.373	40	3 *s*	45288.60	+0.28	$^3P_1$ — 585°$_2$	
2207.542	20		45285.13			
2208.314	25		45269.30			
2208.382	15		45267.91			
2209.064	35	12	45253.93	+0.22	$^5D_4$ — 514°$_4$	
2209.422	20	25	45246.60	−0.26	$^3G_3$ — 585°$_2$	
2210.745	15	3	45219.53	+0.27	$^7S_3$ — 481°$_3$	
2211.644	30		45201.15			
2212.170	75	3	45190.40	+0.04	$^3H_4$ — 573°$_3$	
2212.606	20	2	45181.50			
2213.460	8		45164.07			
2213.696	40		45159.25	0.00	$^3H_5$ — 602°$_5$	
2214.340	50		45146.12	+0.12	$^3H_6$ — 621°$_5$	
2214.708	20	30	45138.62	−0.38	$^3G_3$ — 584°$_3$	
2214.830	40	15	45136.13	−0.03	$^5D_1$ — 468°$_2$	
2215.354	12	3	45125.46			
2216.414	30	20	45103.88	−0.31	$^3G_4$ — 615°$_4$	
2217.176	30		45088.38	−0.01	$^3H_5$ — 601°$_4$	
2218.02	3		45071.2	−0.20	$^5D_4$ — 512°$_5$	
2218.352	40	10	45064.48	+0.05	$^5D_2$ — 483°$_1$	
2219.192	25		45047.43	−0.06	17$_4$ — 621°$_5$	
2219.295	6 *d*		45045.34	+0.05	$^3G_4$ — 614°$_5$	
2220.09	3		45029.2			
2220.40	35		45022.92	0.00	14$_2$ — 599°$_2$	
2220.675	8 *d*		45017.34	+0.01	$^7S_3$ — 479°$_4$	
2221.852	40	4	44993.50	+0.19	$^5D_2$ — 483°$_2$	
2222.363	6		44983.15	+0.07	$^3P_1$ — 582°$_1$	
2222.444	10	1	44981.52	0.00	$^3H_4$ — 571°$_5$	
2222.90	10		44972.3			
2223.01	12		44970.06	+0.24	$^3H_4$ — 571°$_3$	
2223.574	80 *r*	2	44958.66	+0.08	$^5D_3$ — 497°$_4$	
2224.314	25		44943.70	+0.29	$^5D_1$ — 466°$_0$	
2225.230	15	5 *s*	44925.2	+0.12	$^3D_3$ — 603°$_4$	
2225.544	100	2 *d*	44918.87	+0.11	$^5D_2$ — 482°$_2$	
2226.98	10		44889.9			
2227.98	80 *r*	3	44869.75	+0.19	$^5D_3$ — 496°$_2$	
2228.14	20	12	44866.53	+0.14	13$_2$ — 586°$_3$	
2228.58	30		44857.68	+0.24	$^3G_3$ — 582°$_3$	
2228.80	40		44853.25	+0.40	$^5D_4$ — 510°$_3$	

TABLE 3. *Observed and classified lines of* W I

Wavelength Å	Intensity		Wavenumber (cm^{-1})		Classification	Zeeman effect
	Arc	Spark	Observed	o−c		
2229.11	15	2	44847.01	+0.21	$^3P_0$− 543°$_1$	
2229.196	50	2	44845.28	+0.26	$^5D_2$− 481°$_3$	
2230.734	50		44814.37			
2231.12	6		44806.6	+0.08	$^5D_3$− 496°$_4$	
2234.30	5		44742.85	−0.17	$^3G_3$− 580°$_3$	
2234.58	40		44737.24	+0.03	$^5D_0$− 447°$_1$	
2235.28	4		44723.24			
2235.954	5		44709.75	−0.06	13$_2$− 584°$_3$	
2236.525	8		44698.34	+0.03	$^3D_3$− 601°$_4$	
2236.566	8		44697.52			
2236.932	12		44690.21	+0.07	$^5D_4$− 509°$_4$	
2237.09	15		44687.05	−0.21	$^5D_3$− 495°$_2$	
2237.222	30	3	44684.42	+0.08	$^5D_3$− 495°$_3$	
2237.39	4		44681.06			
2237.70	25	3	44674.87	+0.08	$^5D_4$–50894°$_3$	
2237.953	35	1	44669.82	+0.11	$^3H_4$− 568°$_4$	
2238.567	10		44657.57	+0.11	$^5D_1$− 463°$_2$	
2239.039	8		44648.16			
2239.333	7		44642.30	+0.15	$^7S_3$− 475°$_3$	
2240.01	7		44628.8			
2240.376	35	2	44621.52	+0.18	$^5D_1$− 462°$_1$	
2240.587	30	6	44617.32			
2241.282	50	10 *s*	44603.48	+0.09	$^3H_5$− 596°$_5$	
2242.06	25		44588.0	+0.10	$^5D_3$− 494°$_3$	
2242.115	5		44586.91	+0.17	$^5D_4$− 508°$_5$	
2242.40	25	2	44581.25	+0.14	$^5D_4$–50800°$_3$	
2243.70	6		44555.42	+0.25	$^3H_4$− 567°$_3$	
2244.52	4	2	44539.14	+0.05	$^3D_3$− 599°$_2$	
2244.85	4		44532.6	+0.21	$^7S_3$− 474°$_3$	
2245.86	5		44512.57	+0.10	13$_2$− 582°$_1$	
2246.77	45 *r*	5	44494.54	+0.13	$^5D_2$− 478°$_1$	
2246.92	6		44491.57	+0.33	$^7S_3$− 474°$_2$	
2248.096	5	1	44468.30	+0.20	$^3H_6$− 614°$_5$	
2248.750	60 *r*	100 *s*	44455.37	+0.27	$^3G_3$− 578°$_4$	z d
2249.22	1		44446.08	+0.26	14$_2$− 594°$_2$	
2249.508	30	3	44440.39	+0.23	$^5D_3$− 492°$_2$	
2249.804	20	*s*	44434.54	+0.21	$^5D_1$− 461°$_1$	
2250.11	3		44428.50	+0.01	17$_4$− 615°$_4$	
2250.31	10		44424.55			
2250.35	5		44423.76	+0.20	14$_2$− 593°$_3$	
2251.02	8		44410.54	+0.09	$^7S_3$− 473°$_3$	
2252.236	6	8	44386.57	+0.07	$^7S_3$− 473°$_2$	
2252.30	8		44385.31			
2252.36	25	1	44384.12	+0.22	$^3G_3$− 577°$_3$	
2253.093	10		44369.68	+0.09	17$_4$− 614°$_5$	
2253.91	25 *r*	4	44353.60	+0.14	$^5D_0$− 443°$_1$	
2254.224	20		44347.43	+0.23	$^3P_0$− 538°$_1$	
2254.574	30	2	44340.54	−0.05	$^3H_5$− 594°$_6$	
2255.505	20	1	44322.24	−0.13	$^3H_4$− 564°$_3$	
2255.584	8		44320.69			

TABLE 3. *Observed and classified lines of* W I

Wavelength Å	Intensity		Wavenumber (cm^{-1})		Classification	Zeeman effect
	Arc	Spark	Observed	o−c		
2255.715	10	10 *s*	44318.12	+0.17	$^5D_3$— 491°$_4$	
2256.12	15		44310.16	+0.07	$^3G_4$— 607°$_5$	
2256.56	3		44301.52			
2258.12	40	30 *s*	44270.92	+0.12	$^3G_3$— 576°$_3$	
2258.276	2		44267.86	−0.05	$^5D_2$— 475°$_3$	
2259.585	30		44242.22	+0.08	$^5D_3$— 490°$_3$	
2259.81	3		44237.82			
2260.10	35 *r*	5	44232.14	−0.05	$^5D_1$— 459°$_2$	
2260.98	5	2	44214.92			
2261.39	8		44206.91			
2262.06	12		44193.82	+0.12	$^3H_5$— 592°$_5$	
2262.18	8		44191.47			
2263.158	15	1	44172.38	+0.02	$^3H_6$— 611°$_7$	
2263.274	15		44170.11	+0.07	$^3H_4$— 563°$_3$	
2263.88	35 *r*		44158.3	+0.15	$^5D_2$— 474°$_3$	
2264.45	4		44147.2			
2265.42	7	3	44128.3	+0.19	$^7S_3$— 470°$_2$	
2265.67	35	20 *s*	44123.4	+0.16	$^3G_3$— 574°$_4$	
2265.915	6		44118.64	+0.15	$^3H_4$— 562°$_5$	
2265.994	12		44117.10	+0.10	$^5D_2$— 474°$_2$	
2266.78	2		44101.80	+0.02	$^3H_5$— 591°$_4$	
2266.90	15		44099.5			
2267.19	15		44093.8	+0.11	$^3H_4$— 562°$_4$	
2267.36	4	2	44090.5	−0.01	$^5D_1$— 457°$_1$	
2268.60	4	1	44066.4			
2268.646	35	1	44065.53	+0.22	$^5D_4$— 502°$_4$	
2268.98	20		44059.0	+0.13	$^3H_5$— 591°$_6$	
2269.71	4		44044.9			
2270.15	15		44036.3	+0.09	$^5D_2$— 473°$_3$	
2271.374	40	2	44012.61	−0.06	12$_4$— 561°$_4$	
2272.135	15		43997.87	+0.10	19535$_5$— 635°$_6$	
2273.02	40		43980.74	+0.19	$^7S_3$— 469°$_4$	
2273.75	30		43966.6	−0.09	$^3G_3$— 573°$_4$	
				+0.23	$^5D_4$— 501°$_3$	
2273.984	10		43962.10	+0.11	15$_3$— 594°$_2$	
2274.405	40		43953.96	+0.18	$^3G_4$— 603°$_4$	
2274.782	20		43946.68	+0.20	$^3H_4$— 561°$_3$	
2275.138	8		43939.80	+0.07	15$_3$— 593°$_3$	
2275.645	25	4	43930.02	0.00	$^5D_2$— 472°$_1$	
2276.253	15	30	43918.28	+0.06	$^5D_4$— 501°$_5$	
2277.583	60 *r*	20 *s*	43892.64	+0.02	$^5D_0$— 438°$_1$	
2280.00	2	1	43846.1	+0.02	$^5D_3$— 486°$_4$	
2280.226	20		43841.77	+0.12	13$_2$— 576°$_3$	
2280.621	30	12 *s*	43834.18	+0.13	$^3H_5$— 589°$_5$	
				−0.14	17$_3$— 615°$_4$	
2280.85	25		43829.8			
2281.050	35	12	43825.93	−0.01	$^3H_4$— 559°$_5$	
2281.95	30		43808.6			
2282.508	30		43797.94	+0.07	$^3G_4$— 602°$_5$	
2282.75	35	2	43793.3	−0.10	$^3H_4$— 559°$_4$	

TABLE 3. *Observed and classified lines of* W I

Wavelength Å	Intensity		Wavenumber (cm^{-1})		Classification	Zeeman effect
	Arc	Spark	Observed	o−c		
2283.266	25	5 *s*	43783.40	+0.18	$^3G_3$— 571°_3	
2283.496	15		43778.99	+0.02	$^3H_5$— 588°_4	
2283.771	20		43773.72			
2284.794	40	3	43754.12	+0.25	$^5D_2$— 470°_2	
2284.909	40		43751.92	−0.05	$^5D_1$— 454°_2	
2285.17	100 *r*	8	43746.92	+0.22	$^5D_4$— 499°_3	
2285.90	20		43732.95	+0.05	$^3H_6$— 607°_5	
2286.21	40		43727.0	−0.01	$^3G_4$— 601°_4	
2287.012	15		43711.69	−0.01	15_3— 591°_4	
2287.212	20	2	43707.87	0.00	$^3H_5$— 587°_4	
2287.344	18		43705.35	+0.07	$^3H_4$— 558°_4	
2287.46	8	5 *s*	43703.1	−0.61	$^5D_1$— 453°_1	
2287.68	30	1	43698.9	−0.07	$^3P_0$— 532°_1	
2288.10	20		43690.9	−0.13	$^3H_5$— 587°_6	
2288.695	20		43679.55	+0.01	14_2— 586°_2	
2289.01	12	8 *s*	43673.54	−0.22	$^7S_3$— 466°_4	
2289.31	15	9	43667.82	−0.10	14_2— 586°_3	
2289.864	20		43657.26			
2290.206	2		43650.74	0.00	$^3G_3$— 569°_2	
2290.73	6		43640.75			
2290.95	30	4	43636.56	−0.04	$^5D_1$— 453°_0	
2291.09	35		43633.9	+0.38	$^3H_4$— 557°_5	
				−0.49	17_4— 607°_5	
2291.63	6	1	43623.6			
2291.724	6		43621.83			
2291.86	5		43619.24	0.00	14_2— 585°_2	
2292.43	5	1	43608.4			
2294.494	80 *r*	8	43569.17	−0.08	$^5D_4$— 497°_4	3
2297.402	12	4	43514.03	+0.09	$^3P_0$— 530°_1	
2297.546	4		43511.30	−0.04	14_2— 584°_3	
2298.332	25	6	43496.42	+0.01	$^5D_3$— 483°_3	
2298.521	20		43492.85	+0.10	$^3H_5$— 585°_5	
2298.727	20	2	43488.95	+0.11	$^5D_3$— 483°_2	
2299.032	20	1	43483.18	+0.07	$^3G_3$— 568°_4	
2299.15	25	3	43480.94	+0.02	$^5D_2$— 468°_2	
2299.55	8		43473.4			
2299.97	3		43465.4			
2300.70	2	3	43451.7			
2300.906	10	3	43447.76			
2301.072	6		43444.63			
2301.568	6		43435.27	+0.33	$^3H_4$— 555°_4	
2301.642	20	30 *s*	43433.87	−0.30	$^7S_3$— 463°_3	
2302.282	25	6	43421.8			
2302.514	4		43417.42	+0.23	$^5D_4$— 496°_4	
2302.676	20	1	43414.37	+0.08	$^5D_3$— 482°_2	
2303.102	30	6	43406.34	+0.01	$^3H_6$— 604°_6	7
2304.036	3	2	43388.74	−0.15	15_3— 588°_4	
2304.587	4		43378.37			
2305.087	20		43368.96	+0.37	$^3G_3$— 567°_3	
2305.876	12		43354.13	+0.06	13_2— 571°_3	

TABLE 3. *Observed and classified lines of* W I

Wavelength Å	Intensity		Wavenumber (cm^{-1})		Classification	Zeeman effect
	Arc	Spark	Observed	o−c		
2306.160	10		43348.79	+0.06	$^5D_1$— 450°$_2$	
2306.593	35 *r*	5	43340.65	+0.10	$^5D_3$— 481°$_3$	
2307.148	3		43330.23	−0.03	$^3H_4$–55492°$_5$	
2307.826	4	10	43317.50	−0.29	15$_3$— 587°$_4$	
2308.012	1		43314.0	0.00	14$_2$— 582°$_1$	
2309.018	25 *r*	6	43295.14	+0.13	$^5D_4$— 495°$_3$	
2309.11	15		43293.4	+0.01	$^3H_4$–55455°$_5$	
2309.93	3		43278.05	−0.03	17$_4$— 603°$_4$	
2310.88	20	3	43260.25	+0.05	$^3H_5$–58330°$_4$	
2311.46	8		43249.4			
2311.608	8		43246.6	+0.07	$^3H_5$–58316°$_4$	
2311.734	6		43244.28			
2311.854	15	1	43242.03	+0.02	$^3G_4$— 596°$_5$	
2312.373	12	1	43232.33			
2312.50	8		43229.9	+0.08	14$_2$— 582°$_3$	
2312.638	5		43227.37	+0.03	$^3H_4$— 553°$_3$	
2313.012	25	2	43220.38	−0.30	$^3H_6$— 602°$_5$	
2313.170	30 *r*	6	43217.43	+0.10	$^5D_0$— 432°$_1$	7
2314.174	20 *r*	5	43198.68	+0.11	$^5D_4$— 494°$_3$	
2314.332	8		43195.74	+0.03	15$_3$— 586°$_2$	
2314.83	5		43186.4			
2314.946	15		43184.28	+0.04	$^3H_4$— 553°$_4$	
2315.474	5		43174.44			
2316.587	12		43153.70	+0.16	$^3G_3$— 565°$_4$	
2316.644	6		43152.63	+0.14	19$_5$— 626°$_6$	
2317.392	15	8	43138.71	+0.09	$^5D_3$— 479°$_4$	
2317.554	12	8	43135.68	−0.09	$^3G_3$— 564°$_3$	
2318.28	8		43122.2	+0.03	17$_4$— 602°$_5$	
2318.565	12		43116.88	+0.15	$^7S_3$— 460°$_3$	
2318.643	12		43115.43	+0.03	14$_2$— 580°$_3$	
2318.96	25	4	43109.5	+0.05	$^3H_5$— 581°$_5$	
2321.25	15	1	43067.0	+0.08	$^5D_1$— 447°$_1$	
2321.629	40 *r*	10	43059.98	+0.05	$^5D_2$— 463°$_3$	
2322.098	4		43051.29	−0.02	17$_4$— 601°$_4$	
2322.134	5		43050.62			
2323.380	20		43027.53	+0.02	15$_3$— 584°$_3$	
2324.750	12		43002.18	−0.04	$^5D_2$— 463°$_2$	
2325.462	3		42989.01	0.00	19$_5$— 625°$_6$	
2325.761	10		42983.48	+0.04	$^3G_3$— 563°$_3$	
2326.564	25 *r*	8	42968.65	+0.06	$^5D_4$— 491°$_5$	(0)
2326.698	15 *r*	4	42966.17	+0.07	$^5D_2$— 462°$_1$	
2326.786	12		42964.55			
2327.505	8		42951.28	+0.09	$^7S_3$— 459°$_2$	
2327.592	8	5 *s*	42949.67	+0.16	$^3P_0$— 524°$_1$	
2328.144	2		42939.49	+0.07	13$_2$— 567°$_3$	
2328.732	6	2	42928.65	+0.03	$^5D_4$— 491°$_4$	
2328.872	15		42926.07	+0.08	$^5D_1$— 445°$_2$	
2329.316	12	3	42917.88	+0.07	$^7S_3$— 458°$_4$	
2329.896	8		42907.20	+0.11	$^3G_3$— 562°$_4$	
2331.292	30 *r*	3	42881.51	+0.13	$^3H_4$— 550°$_4$	

TABLE 3. *Observed and classified lines of* W I

Wavelength Å	Intensity		Wavenumber (cm^{-1})		Classification	Zeeman effect
	Arc	Spark	Observed	o−c		
2331.909	15	2	42870.16	+0.04	15_3–58330°_4	
2332.378	5		42861.55	+0.09	19826_5– 626°_6	
2332.493	15	1	42859.44	+0.11	$^5D_3$– 476°_4	
2332.646	5		42856.63	+0.18	15_3–58316°_4	
2332.758	8	2	42854.57	+0.02	$^5D_4$– 490°_5	
2332.848	8		42852.92	+0.11	$^5D_4$– 490°_3	
2333.055	1		42849.11	−0.13	$^3H_5$– 579°_6	
2333.146	25	12 *s*	42847.44	+0.18	$^3H_4$– 550°_5	
2333.967	12		42832.37	+0.05	$^3G_4$– 592°_5	
2334.301	20		42826.24	+0.17	$^3G_3$– 561°_4	
2335.787	4		42799.00			
2336.866	8		42779.24	+0.15	$^5D_2$– 461°_1	
2337.17	25	1	42773.68			
2337.724	10	1	42763.54	+0.10	$^5D_3$– 475°_3	
2337.918	8		42759.99	+0.11	$^3G_3$– 561°_3	
2338.155	15		42755.66			
2338.478	20	2	42749.75	+0.10	$^3H_4$– 549°_4	
2338.681	2	1	42746.04	+0.05	15_3– 582°_3	
2338.871	12		42742.57	+0.08	$^5D_2$– 460°_3	
2338.983	10	3	42740.53	+0.13	$^3G_4$– 591°_4	3
2339.348	15		42733.86	+0.13	$^3H_5$– 578°_4	
2339.543	15		42730.30	+0.12	$^3P_1$– 560°_2	
2340.837	12	4	42706.68	+0.06	13_2– 564°_3	
2340.99	4	2	42703.89			
2341.368	25	35 *s*	42696.99	−0.22	$^5D_1$– 443°_2	
2341.816	20		42688.82	+0.10	$^3G_3$– 560°_2	
2342.122	12		42683.25	+0.08	$^5D_1$– 443°_1	
2342.469	35	2	42676.92			
2342.995	5		42667.34			
2343.125	15	7	42664.98	+0.16	$^3H_6$– 596°_5	
2343.74	10		42653.78	+0.10	$^5D_3$– 474°_3	
2344.32	1		42643.23	+0.05	14_2– 576°_3	
2344.918	8		42632.36	−0.01	$^3H_5$– 577°_6	
2344.958	2		42631.63	+0.06	15_3– 580°_3	
2345.622	4		42619.56	+0.07	19535_5– 621°_5	
2346.007	8	1	42612.57	+0.04	$^5D_3$– 474°_2	
2346.32	5		42606.89	+0.09	$^3G_3$– 559°_4	
2346.693	10		42600.11	+0.08	$^7S_3$– 455°_3	
2347.97	10		42576.95	0.00	$^5D_2$– 459°_2	
2348.16	8		42573.50	+0.01	$^5D_0$– 425°_1	
2348.557	5	1	42566.30	−0.01	17_4– 596°_5	
2348.847	3	1	42561.05	+0.06	18_3– 615°_4	
2349.328	12		42552.33	+0.11	$^3P_1$– 558°_1	
2350.461	10	1	42531.83	+0.09	$^5D_3$– 473°_3	
2350.546	8	1	42530.29	+0.10	$^5D_3$– 473°_4	
2351.792	10	1	42507.76	−0.03	$^5D_3$– 473°_2	
2351.895	1		42505.90	−0.06	19_6– 621°_5	
2352.734	4		42490.74	−0.16	$^3H_5$– 575°_5	
2352.962	12		42486.62	+0.06	$^3G_3$– 558°_2	
2353.38	4		42479.08			

TABLE 3. *Observed and classified lines of* W I

Wavelength Å	Intensity		Wavenumber (cm^{-1})		Classification	Zeeman effect
	Arc	Spark	Observed	o−c		
2353.737	7		42472.64	−0.03	$^3G_4$ − 589°$_5$	
2353.827	7		42471.01	+0.04	$^7S_3$ − 454°$_2$	
2354.614	15 *r*	8	42456.82	+0.07	$^5D_4$ − 486°$_4$	
2356.087	4	1	42430.28			
2356.789	8	1	42417.64	+0.05	$^3G_4$ − 588°$_4$	
2357.078	3		42412.44			
2357.657	10	1	42402.02	0.00	$^3H_6$ − 594°$_6$	
2358.068	15	1	42394.63	+0.16	$^3H_4$ − 545°$_3$	
2359.098	2		42376.12	−0.02	14$_2$ − 573°$_3$	
2360.44	15 *r*	5	42352.03	−0.13	$^5D_2$ − 456°$_3$	
2360.753	3		42346.42	−0.07	$^3G_4$ − 587°$_4$	
2360.91	5		42343.60	−0.05	15$_3$ − 578°$_4$	
2361.194	12	10 *s*	42338.51	+0.03	$^3H_6$ − 593°$_7$	3
2361.622	10		42330.84	+0.11	13$_2$ − 561°$_3$	
2361.755	4		42328.45	−0.01	19826$_5$ − 621°$_5$	
2362.641	6		42312.59	+0.03	$^3P_1$ − 556°$_2$	
2363.072	18 *r*	8	42304.87	−0.06	$^5D_1$ − 439°$_2$	
2363.464	8	14 *s*	42297.85	−0.07	17$_3$ − 599°$_2$	
2363.752	2		42292.70	−0.03	17$_4$ − 593°$_3$	
2364.884	5		42272.46	+0.01	15$_3$ − 577°$_3$	
2364.958	8		42271.13	+0.03	$^3G_3$ − 556°$_2$	
2365.452	12	4	42262.30	0.00	$^5D_0$ − 422°$_1$	
2365.853	20		42255.14	+0.01	$^3H_6$ − 592°$_5$	
2366.177	15	3	42249.36	−0.04	$^5D_3$ − 470°$_2$	
2366.236	5	2	42248.30	−0.04	$^3G_3$ − 555°$_4$	
2366.958	25	4	42235.42	+0.04	$^3P_0$ − 517°$_1$	
2367.374	3		42228.00			
2367.504	4		42225.68	−0.11	$^5D_2$ − 455°$_3$	
2367.693	10	4	42222.31	−0.02	$^5D_1$ − 438°$_1$	
2368.216	2	2	42212.98	+0.19	$^3G_4$ − 586°$_3$	
2369.088	6		42197.45	−0.05	$^3G_3$ − 555°$_3$	
2369.552	4		42189.19			
2370.888	15	2	42165.40	−0.08	$^7S_3$ − 451°$_4$	
2371.387	12	1	42156.54	−0.08	17$_4$ − 592°$_5$	
2371.849	8		42148.33	−0.01	$^3H_4$ − 543°$_5$	
2372.804	14		42131.37	0.00	$^3G_4$ − 585°$_5$	
2373.43	10		42120.26	−0.04	$^3H_6$ − 591°$_6$	
2374.127	10	1	42107.89	+0.08	$^3H_4$ − 542°$_3$	
2374.176	7	1	42107.02	−0.06	$^5D_4$ − 483°$_3$	
2374.468	30 *r*		42101.85	+0.01	$^5D_3$ − 469°$_4$	
2374.756	10	3	42096.74	+0.01	$^5D_2$ − 454°$_2$	
2375.536	4		42082.92	−0.14	$^3P_1$ − 553°$_2$	
2375.61	3		42081.61	0.00	13$_2$ − 558°$_1$	
2375.753	10		42079.08	+0.04	$^3H_5$ − 571°$_6$	
2376.064	20	8	42073.57	+0.02	$^3H_5$ − 571°$_5$	
2376.394	6		42067.73	0.00	$^7S_3$ − 450°$_2$	
2376.566	15	2	42064.68	−0.02	17$_4$ − 591°$_4$	
2376.644	3		42063.30	+0.05	$^7S_3$ − 450°$_3$	
2376.975	10	1	42057.44	+0.03	13$_2$ − 558°$_2$	
2377.048	15	1	42056.15	−0.06	$^3G_4$ − 584°$_3$	

TABLE 3. *Observed and classified lines of* W I

Wavelength Å	Intensity		Wavenumber (cm^{-1})		Classification	Zeeman effect
	Arc	Spark	Observed	o−c		
2377.484	1		42048.44	−0.03	$^5D_2$— 453°$_1$	
2377.916	10	1	42040.80	+0.06	$^3G_3$— 553°$_3$	
2378.916	7		42023.13	+0.01	14$_2$— 569°$_2$	
2379.066	12		42020.48			
2379.556	7	8	42011.83	+0.04	15$_3$— 574°$_4$	
2379.65	12		42010.17			
2380.194	2		42000.57	+0.08	19535$_5$— 615°$_4$	
2380.356	3		41997.71	+0.07	$^3G_3$— 553°$_4$	
2380.832	7	1	41989.32	+0.04	$^7S_3$— 449°$_4$	
2381.559	15	1	41976.50	+0.05	$^5D_3$— 468°$_2$	
2382.673	10		41956.88	+0.06	$^3H_4$— 541°$_4$	
2382.99	20 *r*	4	41951.29	+0.07	$^5D_4$— 481°$_3$	
2383.39	4		41944.25			
2383.548	4		41941.47	−0.12	19535$_5$— 614°$_5$	
2384.824	25 *r*	30	41919.04	−0.01	$^5D_4$— 481°$_5$	
2384.982	2		41916.26	−0.01	18$_1$— 599°$_2$	
2386.162	20	2	41895.53	+0.05	$^3H_6$— 589°$_5$	
2386.348	9		41892.27	−0.04	15$_3$— 573°$_3$	
2386.75	3		41885.21	+0.06	$^3G_4$–58316°$_4$	
2386.918	1		41882.26	0.00	18$_2$— 599°$_2$	
2387.212	3		41877.10			
2389.078	15 *r*	4	41844.40	+0.01	$^5D_1$— 435°$_2$	
2389.21	2		41842.1	+0.15	13$_2$— 556°$_2$	
2391.794	2		41796.89	−0.08	17$_4$— 589°$_5$	
2391.896	10		41795.10	+0.05	$^5D_3$— 466°$_4$	
2392.932	20	60 *s*	41777.01	+0.09	$^3P_1$–55084°$_2$	
2393.063	15		41774.72	+0.03	$^3G_4$— 582°$_3$	
2393.424	25	5	41768.42	+0.07	13$_2$— 555°$_3$	
2393.808	8		41761.72	−0.02	$^3H_5$— 568°$_4$	
2394.444	12	7 *s*	41750.63			
2394.522	3		41749.27	−0.02	$^5D_4$— 479°$_4$	
2394.59	8		41748.09	+0.02	$^3G_4$— 581°$_5$	
2394.947	10	1	41741.86	−0.03	17$_4$— 588°$_4$	
2395.313	15 *r*	2	41735.49	+0.03	$^3G_3$–55084°$_2$	
2395.476	30 *r*	3	41732.65	+0.03	$^3P_0$— 512°$_1$	
2395.878	10		41725.63	+0.06	$^3P_1$–55032°$_2$	
2396.153	1		41720.85	+0.03	17$_3$— 594°$_2$	
2396.287	2		41718.51	−0.11	$^5S_2$— 599°$_2$	
2396.902	4		41707.81	−0.01	19$_3$— 615°$_4$	
2397.304	9	1	41700.81	+0.05	$^3H_4$— 538°$_5$	
2397.434	9		41698.54	−0.02	17$_3$— 593°$_3$	
2397.652	2		41694.77	−0.01	$^3G_3$— 550°$_4$	
2397.726	20 *r*	5	41693.48	−0.01	$^5D_2$— 450°$_2$	Res
2397.984	25 *r*		41689.00	−0.01	$^5D_2$— 450°$_3$	Res
2398.118	8		41686.67	0.00	$^3H_4$— 538°$_4$	
2398.260	10		41684.20	+0.09	$^3G_3$–55032°$_2$	
2399.037	15	2	41670.70	−0.09	17$_4$— 587°$_4$	
2400.198	3		41650.54	−0.02	19826$_5$— 614°$_5$	
2400.519	5	8 *s*	41644.98	−0.01	$^7S_3$— 445°$_2$	
2401.155	18	1	41633.94	+0.03	$^3P_1$— 549°$_1$	

TABLE 3. *Observed and classified lines of* W I

Wavelength Å	Intensity		Wavenumber (cm^{-1})		Classification	Zeeman effect
	Arc	Spark	Observed	o−c		
2401.298	12	4	41631.46	−0.05	$^5D_4$— 478°$_5$	
2402.394	6		41612.47	+0.02	13$_2$— 553°$_2$	
2402.446	15	2	41611.57	−0.02	13$_2$— 553°$_3$	
2402.733	7	2	41606.60	−0.07	13$_2$— 553°$_1$	
2402.924	3	1	41603.30			
2404.244	25	20	41580.47			
2405.257	35		41562.95	−0.10	$^3G_3$— 549°$_4$	
2405.580	30 *r*	8	41557.36	−0.01	$^5D_1$— 432°$_2$	
2405.689	20 *r*	6	41555.48	+0.02	$^5D_3$— 463°$_3$	
2405.764	15		41554.20	+0.02	$^3H_6$— 585°$_5$	
2406.180	15 *r*	3	41547.01	−0.03	$^5D_1$— 432°$_1$	
2406.632	2		41539.20	−0.09	15$_3$— 569°$_2$	
2406.760	10		41537.00	−0.09	17$_4$— 586°$_3$	
2407.039	2		41532.18	−0.14	19$_6$— 611°$_7$	
2408.282	12	15 *s*	41510.73	+0.14	$^3G_3$— 548°$_2$	
2408.444	5		41507.95	−0.20	14$_2$— 564°$_3$	
2409.034	15	3	41497.78	+0.03	$^5D_3$— 463°$_2$	
2409.155	8		41495.70	−0.03	$^7S_3$— 444°$_3$	
2409.776	1		41485.01	−0.15	19$_4$— 607°$_5$	
2410.620	15	1	41470.50	−0.03	17$_3$— 591°$_4$	
2411.427	7		41456.60	−0.04	$^3H_5$— 565°$_6$	
2411.483	7		41455.64	−0.03	17$_4$— 585°$_5$	
2412.847	1		41432.22	+0.05	$^3H_5$— 565°$_4$	
2413.782	15	2	41416.17	−0.04	$^7S_3$— 443°$_2$	
2414.039	20 *r*	4	41411.75	+0.07	$^5D_2$— 447°$_1$	
2414.118	4	7 *s*	41410.40	−0.18	18$_3$— 603°$_4$	
2414.417	4		41405.27			
2414.627	5	2	41401.67			
2415.685	35 *r*	8	41383.54	−0.05	$^5D_1$— 430°$_0$	
2415.871	6	1	41380.36	−0.15	17$_4$— 584°$_3$	
2416.237	15	1	41374.08	−0.11	$^5D_4$— 475°$_3$	
2416.339	10		41372.34	−0.01	$^3G_4$— 578°$_4$	
2417.290	2		41356.06	+0.24	14$_2$— 563°$_3$	
2418.360	5		41337.78			
2418.822	3		41329.87			
2420.202	20	2	41306.31	0.00	13$_2$–55084°$_2$	
2420.504	8	15	41301.16	+0.01	$^3G_4$— 577°$_3$	
2422.292	30	20 *s*	41270.67	−0.08	$^5D_2$— 445°$_2$	
2422.662	12		41264.37	+0.02	$^5D_4$— 474°$_3$	
2423.214	1		41254.97	+0.01	13$_2$–55032°$_2$	
2424.206	80 *r*	8	41238.10	+0.08	$^5D_3$— 460°$_3$	Res
2424.770	15		41228.51	+0.05	$^3H_4$–53390°$_3$	
2425.086	1		41223.13	+0.01	17$_4$–58330°$_4$	
2425.850	3	3	41210.15	−0.37	$^3H_5$— 562°$_5$	
2425.888	5		41209.50	+0.05	17$_4$–58316°$_4$	
2425.975	10	6 *s*	41208.02	+0.15	$^3G_3$— 545°$_3$	
2426.076	9		41206.31	−0.08	19535$_5$— 607°$_5$	
2426.805	5		41193.94			
2427.156	2		41187.97	−0.08	$^3G_4$— 576°$_3$	
2427.282	15	2	41185.84	+0.12	$^3H_5$— 562°$_4$	

TABLE 3. *Observed and classified lines of* W I

Wavelength Å	Intensity		Wavenumber (cm^{-1})		Classification	Zeeman effect
	Arc	Spark	Observed	o−c		
2427.408	7		41183.70	+0.16	$^3H_4$–53345°$_3$	
2428.158	8		41170.98	+0.10	$^3H_6$– 581°$_5$	
2428.600	6		41163.49	+0.19	13$_2$– 549°$_1$	
2429.838	15	3	41142.50	+0.09	$^5D_4$– 473°$_3$	
2429.930	5		41140.96	+0.10	$^5D_4$– 473°$_4$	
2430.440	20	2	41132.33	+0.07	14$_2$– 561°$_3$	
2430.604	5		41129.56	+0.04	$^3G_4$– 575°$_5$	
2430.647	3		41128.82	−0.03	19$_4$– 603°$_4$	
2430.976	6		41123.26	+0.07	13$_2$– 549°$_3$	
2431.081	25 *r*	5	41121.49	0.00	$^5D_2$– 444°$_3$	
2431.604	4		41112.64	+0.07	$^3P_1$– 544°$_1$	
2431.811	3		41109.14			
2432.670	2		41094.63			
2432.776	4		41092.83	−0.03	19$_6$– 607°$_5$	
2433.442	10	1	41081.59	+0.15	13$_2$– 548°$_2$	
2433.739	12	2	41076.57	+0.12	$^3H_4$– 532°$_4$	
				−0.05	17$_3$– 587°$_4$	
2433.982	25	20 *s*	41072.47	−0.01	$^5D_3$– 459°$_2$	
2434.140	6		41069.81	+0.10	$^7S_3$– 440°$_3$	
2434.254	10	12 *s*	41067.88	+0.18	$^3P_1$– 543°$_1$	
2434.658	5		41061.07	−0.03	14$_2$– 560°$_2$	
2435.782	12	3	41042.13	+0.16	$^5D_2$– 443°$_2$	
				+0.04	15$_3$– 565°$_4$	
2435.874	6		41040.58	+0.09	$^3G_4$– 574°$_4$	
2435.957	80	20	41039.18	+0.08	$^5D_3$– 458°$_4$	
2436.255	10	2	41034.16	+0.04	$^7S_3$– 439°$_4$	
2436.363	3		41032.34	+0.05	$^3H_4$– 531°$_5$	
2436.624	25 *r*	6	41027.94	+0.01	$^5D_2$– 443°$_1$	
2436.838	5		41024.34	+0.02	15$_3$– 564°$_3$	
2437.952	10	1	41005.60	0.11	$^3P_0$– 505°$_1$	
2438.964	8		40988.58	+0.04	$^3P_1$– 542°$_0$	
2439.200	12		40984.62	+0.05	17$_4$– 580°$_3$	
2440.880	5		40956.42	+0.09	$^3H_4$– 531°$_4$	
2440.993	3	1	40954.51	−0.03	17$_3$– 586°$_2$	
2441.690	2		40942.83	−0.09	17$_3$– 586°$_3$	
2442.391	2		40931.07	+0.08	$^5S_2$– 592°$_2$	
2442.976	25	1	40921.27	+0.06	$^3G_3$– 542°$_3$	
2443.171	10	3	40918.01	+0.04	$^3H_5$– 559°$_5$	
2443.326	12	1	40915.41	+0.05	19826$_5$– 607°$_5$	
2443.612	40	5	40910.62	−0.05	$^3H_6$– 579°$_6$	
2444.056	60 *r*	12	40903.20	0.00	$^5D_1$– 425°$_1$	Res
2444.170	3	1	40901.29			
2444.272	2		40899.58	+0.03	$^7S_3$– 438°$_3$	
2444.590	2		40894.26	+0.02	17$_3$– 585°$_2$	
2445.119	2		40885.41	−0.02	$^3H_5$– 559°$_4$	
2445.255	4		40883.14	0.00	14$_2$– 558°$_1$'	
2445.455	8	1	40879.80	−0.02	19535$_5$– 604°$_6$	
2445.918	5		40872.05	+0.06	15$_3$– 563°$_3$	
2446.704	4		40858.92	−0.02	14$_2$– 558°$_2$	
2446.800	5		40857.33			

TABLE 3. *Observed and classified lines of* W I

Wavelength Å	Intensity		Wavenumber (cm^{-1})		Classification	Zeeman effect
	Arc	Spark	Observed	o−c		
2447.375	10		40847 ..	+0.04	$^5D_3$— 456°$_3$	
2448.390	25 *r*	3	40830.80	+0.07	$^3H_4$— 529°$_4$	Res
2450.398	4		40797.34	+0.03	$^3H_5$— 558°$_4$	
2450.50	6	1	40795.64	0.00	15$_3$— 562°$_4$	
2451.346	30 *r*	4	40781.56	+0.04	$^3H_4$— 529°$_3$	
2451.484	70 *r*		40779.26	−0.05	$^5D_1$— 424°$_2$	
2451.576	4		40777.73	−0.02	$^3H_5$— 558°$_6$	
2451.996	100 *r*	15	40770.74	−0.04	$^5D_0$— 407°$_1$	
2452.063	4		40769.64	+0.06	$^7S_3$— 437°$_4$	
2452.107	3	1	40768.90			
2453.232	3		40750.22			
2454.717	40 *r*	5	40725.56	+0.01	$^3H_5$— 557°$_5$	
2454.978	80	10	40721.23	−0.09	$^5D_3$— 455°$_3$	Res
2455.372	10		40714.70	+0.08	15$_3$— 561°$_4$	
2455.506	80 *r*	10 *s*	40712.48	−0.03	$^5D_4$— 469°$_4$	Res
2456.228	15	2	40700.51	+0.04	$^3G_4$— 571°$_3$	
2456.454	5 *b*		40696.77	+0.12	17$_4$— 578°$_4$	
2456.534	150 *r*	8	40695.44	−0.03	$^5D_2$— 440°$_3$	
2456.616	3		40694.08	+0.28	$^3H_6$— 577°$_6$	
2459.146	4		40652.22	+0.04	$^3P_1$— 539°$_2$	
2459.300	140 *r*	20	40649.68	−0.01	$^5D_2$— 439°$_2$	Res
2459.602	20	10 *s*	40644.68	+0.08	$^3H_4$— 528°$_3$	
2459.674	3		40643.50	+0.02	14$_2$— 556°$_2$	
2459.768	3		40641.94	−0.02	13$_2$— 544°$_1$	
2460.160	50 *r*	5	40635.47	0.00	$^5D_4$— 468°$_5$	Res
2460.548	10		40629.06	+0.11	17$_3$—58330°$_4$	
2460.763	6		40625.51	+0.06	17$_4$— 577°$_3$	
2460.894	15	1	40623.34	+0.03	19535$_5$— 601°$_4$	
2461.384	3		40615.26	−0.02	17$_3$—58316°$_4$	
2461.568	30	15	40612.22	+0.08	$^3H_4$— 527°$_5$	
2461.653	5		40610.82	+0.10	$^3G_3$— 539°$_2$	
2462.480	12	1	40597.19	+0.10	13$_2$— 543°$_1$	
2462.793	100 *r*	15	40592.02	+0.01	$^5D_1$— 422°$_1$	
2462.986	10	1	40588.84	+0.05	19826$_5$— 604°$_6$	
2463.486	1	3	40580.61	−0.03	19$_6$— 602°$_5$	
2463.688	8	1	40577.28	+0.01	15$_3$— 560°$_2$	
2463.952	2		40572.93	+0.04	18$_1$— 586°$_2$	
2464.135	8	4	40569.92	+0.04	14$_2$— 555°$_3$	
2464.305	60 *r*	6	40567.12	+0.03	$^5D_2$— 438°$_1$	
2464.489	2		40564.09	+0.10	$^3G_3$—53912°$_2$	
2464.532	2		40563.38	−0.01	$^7S_3$— 435°$_2$	
2464.798	3		40559.01	−0.04	19826$_5$— 603°$_4$	
2464.897	2		40557.38	−0.03	19$_3$— 603°$_4$	
2465.203	35		40552.34	+0.01	$^3H_6$— 575°$_5$	
2466.028	2		40538.78	−0.10	18$_2$— 586°$_2$	
2466.848	100 *r*	15	40525.31	0.00	$^5D_2$— 438°$_3$	
2467.620	12	1	40512.63	+0.04	18$_1$— 585°$_2$	
2468.094	4		40504.85	+0.03	17$_3$— 582°$_3$	
2468.461	3		40498.82			
2468.668	7		40495.43	+0.08	15$_3$— 559°$_4$	

TABLE 3. *Observed and classified lines of* W I

Wavelength Å	Intensity		Wavenumber (cm^{-1})		Classification	Zeeman effect
	Arc	Spark	Observed	o−c		
2468.875	5		40492.03	−0.03	13_2− 542°_3	
2470.260	4		40469.33			
2470.733	4		40461.59			
2471.208	25	3	40453.81	−0.01	17_4− 575°_5	
2471.592	5		40447.53	+0.04	18_3− 594°_2	
2471.956	5	4	40441.58			
2472.127	15	1	40438.77			
2472.506	70 *r*		40432.58	+0.03	$^5D_3$− 452°_4	Res
2473.137	4		40422.26	−0.03	$^3H_5$−55492°_5	
2473.458	1		40417.02	−0.06	19_4− 596°_5	
2473.644	3		40413.98	0.00	14_2− 553°_2	
2473.698	10	1	40413.09	−0.03	14_2− 553°_3	
2473.819	15	2	40411.12	0.00	$^5D_0$− 404°_1	
2474.01	2		40408.0	−0.20	14_2− 553°_1	
2474.149	140 *r*	25	40405.73	+0.01	$^5D_4$− 466°_4	3
2474.316	1		40403.00	−0.14	19826_5− 602°_5	
2474.478	10	2	40400.36	0.00	$^3G_4$− 568°_4	
2474.865	4		40394.04			
2475.088	25		40390.40	0.00	17_3− 580°_3	
2475.392	2		40385.44	+0.02	$^3H_5$−55455°_5	
2476.016	15	1	40375.26	+0.15	15_3− 558°_2	
				+0.02	$^5S_2$− 586°_2	
2476.302	1		40370.60	−0.08	18_2− 584°_3	
2476.656	6		40364.83	+0.04	17_4− 574°_4	
2476.809	10		40362.34	+0.08	$^3P_1$− 536°_2	
2476.992	3		40359.35			
2478.458	4		40335.49			
2478.644	6		40332.46	+0.18	19826_5− 601°_4	
2478.756	5		40330.64	0.00	19_3− 601°_4	
2479.361	4		40320.80	0.00	$^3G_3$− 536°_2	
2479.720	3		40314.96	+0.02	$^5S_2$− 585°_2	
2480.130	100 *r*	15	40308.29	−0.04	$^5D_1$− 419°_2	
2480.658	20	2	40299.71	0.00	$^7S_3$− 432°_4	
2480.955	60 *r*	6	40294.89	−0.06	$^5D_1$− 419°_0	
2481.440	150 *r*	30	40287.02	−0.02	$^5D_4$− 465°_5	
2481.504	5		40285.98	+0.16	$^3G_4$− 567°_3	
2482.10	35 *r*	6	40276.3	−0.07	$^7S_3$− 432°_2	
2482.212	30 *r*	5	40274.49	+0.01	$^3H_4$− 524°_4	Res
2484.741	80 *r*	10	40233.50	−0.04	$^3H_4$− 523°_5	7
2486.302	18	1	40208.24	0.00	17_4− 573°_4	
2486.708	5		40201.67			
2486.988	5		40197.15	−0.05	18_3− 591°_4	
2487.495	50 *r*	7	40188.96	−0.06	$^5D_3$− 450°_2	Res
2487.770	12	1	40184.52	−0.02	$^5D_3$− 450°_3	
2487.945	7		40181.68	+0.11	13_2− 539°_2	
2488.468	3		40173.25	−0.09	18_2− 582°_1	
2488.932	15	7 *s*	40165.76	−0.37	$^5D_4$− 463°_3	
2489.306	2		40159.72	+0.07	15_3− 556°_2	
2489.720	35 *r*	8	40153.04	−0.01	$^5D_2$− 434°_3	Res
2490.309	2		40143.55	+0.05	19_4− 593°_3	

TABLE 3. *Observed and classified lines of* W I

Wavelength Å	Intensity		Wavenumber (cm^{-1})		Classification	Zeeman effect
	Arc	Spark	Observed	o−c		
2490.495	15	1	40140.55	+0.07	$^3H_6$— 571°$_6$	
2490.718	12	25 *s*	40136.95	+0.06	15$_3$— 555°$_4$	
2490.846	25	2	40134.89	+0.05	13$_2$–53912°$_2$	
2491.998	8	1	40116.34			
2492.360	30	3	40110.51	−0.06	$^5D_3$— 449°$_4$	Res
2492.522	5		40107.91	+0.07	14$_2$–55084°$_2$	
2493.160	18	1	40097.65	+0.10	13$_2$— 538°$_1$	
2493.394	30	4	40093.88	+0.04	$^3H_4$— 522°$_3$	
2493.877	4		40086.12	+0.07	15$_3$— 555°$_3$	
2494.831	30	3	40070.79	0.00	$^3G_4$— 565°$_4$	
2495.011	3		40067.90			
2495.264	100 *r*	10	40063.84	0.00	$^5D_1$— 417°$_2$	
2495.72	10		40056.52	+0.02	14$_2$–55032°$_2$	
2495.931	15	1	40053.13	+0.11	$^3G_4$— 564°$_3$	
2496.110	3	1	40050.26			
2496.249	4		40048.03	+0.03	23$_6$— 635°$_6$	
2496.97	25	2	40036.47	0.00	17$_4$— 571°$_5$	
2497.293	18	2	40031.29	+0.01	17$_3$— 577°$_3$	
2497.697	8	2	40024.81	+0.04	17$_4$— 571°$_3$	
				+0.03	19$_6$— 596°$_5$	
2498.638	6		40009.74	+0.04	$^5S_2$— 582°$_1$	
2498.788	3		40007.34	−0.05	19$_4$— 592°$_5$	
2499.432	25	3	39997.04	+0.08	$^3G_3$–53345°$_3$	
2500.638	3		39977.74	−0.08	$^3P_1$— 532°$_2$	
2500.829	1		39974.69	−0.05	18$_2$— 580°$_3$	
2500.905	5		39973.48	+0.07	$^3H_5$— 550°$_4$	
2501.440	5		39964.93	+0.10	14$_2$— 549°$_1$	
2501.780	20	3	39959.5	+0.05	$^7S_3$— 429°$_4$	
2501.896	30		39957.65	−0.24	$^3P_2$— 592°$_2$	
2503.042	12	1	39939.35	+0.06	$^3H_5$–55009°$_5$	
2503.226	4		39936.42	+0.06	$^3G_3$— 532°$_2$	
2503.61	4		39930.3	+0.15	15$_3$— 553°$_2$	
2503.956	30	1	39924.76	+0.04	14$_2$— 549°$_3$	
2504.26	3		39919.9	−0.03	$^3P_1$— 532°$_1$	
2504.305	4		39919.21	+0.08	$^3H_4$— 520°$_5$	
2504.376	4		39918.08	−0.10	17$_3$— 576°$_3$	
2504.526	25	3	39915.69	+0.05	$^3P_0$— 494°$_1$	
2504.698	60 *r*	15	39912.95	0.00	$^5D_1$— 415°$_2$	Res
2505.374	18	1	39902.18	+0.05	$^5D_2$— 432°$_2$	
2505.646	30	3	39897.85	+0.03	$^3H_4$— 520°$_4$	
2506.020	20		39891.89	+0.09	$^5D_2$— 432°$_1$	
2506.146	20		39889.89	+0.04	$^3G_3$— 532°$_4$	
2506.373	4	1	39886.28	+0.09	15$_3$— 553°$_4$	
2506.578	3		39883.02	+0.05	14$_2$— 548°$_2$	
2506.63	3		39882.2			
2507.051	12	2	39875.49	−0.02	19535$_5$— 594°$_6$	
2507.122	3	2	39874.36	−0.03	18$_3$— 588°$_4$	
2508.444	40	4	39853.35	+0.03	$^3H_4$— 520°$_3$	
2508.734	45	4	39848.74	+0.05	$^5D_4$— 460°$_3$	
2508.827	3		39847.26	−0.02	19826$_5$— 596°$_5$	

TABLE 3. *Observed and classified lines of* W I

Wavelength Å	Intensity		Wavenumber (cm^{-1})		Classification	Zeeman effect
	Arc	Spark	Observed	o−c		
2509.178	6	1	39841.69	+0.01	$^3H_5$— 549°$_4$	
2510.166	30	4	39826.01	−0.02	$^3H_5$— 548°$_6$	
2510.211	4		39825.30			
2510.272	6		39824.33	−0.01	$^3G_4$— 562°$_4$	
2510.88	4		39814.7			
2511.103	10		39811.15	+0.05	$^5S_2$— 580°$_3$	
2511.373	3		39806.87			
2511.593	2		39803.38	+0.09	18$_3$— 587°$_4$	
2512.938	25		39782.09	−0.01	$^3H_6$— 567°$_7$	
2513.366	8		39775.31			
2513.664	7		39770.60	−0.02	17$_3$— 574°$_4$	
2513.726	4		39769.61	−0.12	$^3G_3$— 531°$_4$	
2513.934	30	4	39766.32	+0.04	$^5D_3$— 445°$_2$	
2514.206	7		39762.02	+0.04	19$_6$— 594°$_6$	
2515.388	3		39743.34	+0.02	$^3G_4$— 561°$_4$	
2515.922	4		39734.90	0.00	$^3P_1$— 530°$_1$	
2516.16	20		39731.14			
2516.328	3		39728.49	−0.13	19535$_5$— 592°$_5$	
2516.549	10	7	39725.00	+0.34	17$_4$— 568°$_4$	
2516.632	16		39723.69			
2518.235	1		39698.41	−0.03	19$_6$— 593°$_7$	
2518.348	4		39696.63	+0.01	$^3P_1$— 530°$_2$	
2518.504	18		39694.17	+0.03	$^3H_4$— 518°$_4$	
2519.182	18		39683.49			
2519.330	3		39681.16		18$_3$— 586°$_2$	
2519.580	4		39677.22	+0.09	$^3G_4$— 561°$_3$	
2519.874	50	3	39672.59			
2520.455	50	8	39663.45	0.00	$^3H_5$— 547°$_6$	
2520.978	30	2	39655.22	+0.06	$^3G_3$— 530°$_2$	
2521.244	5		39651.03	−0.11	17$_3$— 573°$_3$	
2521.323	100	10	39649.79	+0.02	$^5D_4$— 458°$_4$	
				−0.11	$^7S_3$— 426°$_3$	
2521.686	3	3 *s*	39644.09	−0.04	$^3G_3$— 529°$_4$	
2522.156	12		39636.70	+0.08	$^5D_0$— 396°$_1$	
				0.00	19$_5$— 591°$_4$	
2522.96	10	3	39624.06	+0.05	15$_3$—55084°$_2$	
2523.410	60 *r*	12	39617.00	−0.02	$^5D_3$— 444°$_3$	Res
2523.484	3		39615.84	+0.22	18$_2$— 577°$_3$	
2523.531	5	1	39615.10	+0.01	19$_6$— 592°$_5$	
2523.592	12	2	39614.14	+0.07	17$_3$— 573°$_4$	
2523.686	2		39612.67	−0.04	13$_2$—53390°$_3$	
2523.845	4		39610.18	+0.06	17$_4$— 567°$_3$	
2524.808	16	1	39595.06	+0.14	$^3G_3$— 529°$_3$	
2524.904	3		39593.56	−0.23	19535$_5$— 591°$_6$	
2525.084	3		39590.74			
2525.550	12		39583.43	+0.10	15$_3$— 550°$_4$	
2525.684	18	3	39581.34	+0.01	$^7S_3$— 425°$_4$	
2525.749	1		39580.32	+0.07	14$_2$— 545°$_3$	
2525.873	1		39578.38	−0.02	$^3P_1$— 528°$_2$	
2526.232	5		39572.75	+0.09	15$_3$—55032°$_2$	

TABLE 3. *Observed and classified lines of* W I

Wavelength Å	Intensity		Wavenumber (cm^{-1})		Classification	Zeeman effect
	Arc	Spark	Observed	o−c		
2526.328	5		39571.24	−0.02	20_1— 599°_2	
2526.416	12	3	39569.87	+0.06	$^5D_4$— 457°_5	
2526.542	3		39567.90	+0.09	13_2—53345°_3	
2526.86	4		39562.9	+0.05	$^7S_3$— 425°_3	
2527.262	9		39556.62	+0.03	$^3G_4$— 559°_5	
2527.763	40	6	39548.78	+0.08	$^3H_6$— 565°_7	
2528.486	50	6	39537.47	−0.03	$^5D_3$— 443°_2	
2529.329	12	1	39524.30	+0.25	$^3G_4$— 559°_4	
2529.510	1		39521.47	−0.09	19_4— 587°_4	
2529.722	40	4	39518.16	+0.09	$^3H_6$— 565°_6	3
2530.048	4		39513.07	+0.06	18_3— 584°_3	
2530.417	5		39507.30	+0.09	13_2— 532°_2	
2530.986	5	50 *s*	39498.42	+0.11	$^7S_3$— 424°_2	
2532.148	3		39480.30	+0.04	19_6— 591°_6	
2533.551	25	2	39458.44	+0.08	$^5D_4$— 456°_3	Res
2533.635	35 *r*	5	39457.13	+0.04	$^5D_1$— 411°_0	7
2533.985	25	1	39451.68	+0.08	15_3— 549°_4	
2534.678	30		39440.90	+0.01	15_3— 549°_3	
2534.89	5		39437.6	+0.01	19826_5— 592°_5	
2535.106	35	3	39434.24	+0.01	$^5D_1$— 411°_2	
2535.335	25	1	39430.68	+0.08	17_3— 571°_3	
2537.356	15		39399.27	+0.13	15_3— 548°_2	
2537.621	10		39395.16	+0.07	17_4— 565°_4	
2538.096	6		39387.78	−0.08	19_4— 586°_3	
2538.343	10		39383.95	+0.15	19_3— 592°_2	
2538.76	4		39377.5	+0.18	17_4— 564°_3	
2539.614	10		39364.24	+0.07	$^3G_4$— 557°_5	
2540.303	3	1	39353.57			
2540.755	2		39346.57	+0.09	$^3P_1$— 526°_2	
2540.925	10	4 *s*	39343.93	−0.10	19_3— 591°_4	
2541.063	6	20 *s*	39341.80	−0.06	19_2— 585°_2	
2541.144	8		39340.54			
2541.696	20	2	39332.00	+0.01	$^5D_4$— 455°_3	Res
2541.948	3		39328.10			
2542.237	8		39323.63	+0.07	$^3G_5$— 591°_5	
2543.050	4		39311.06	−0.02	$^3H_4$— 514°_4	
2543.436	40	2	39305.10	+0.08	$^3G_3$— 526°_2	
2543.586	5	1	39302.78	+0.02	19826_5— 591°_6	
2543.656	4		39301.70	0.00	22852_4— 621°_5	
2543.758	1		39300.12	−0.10	$^7S_3$— 422°_3	
2543.903	1		39297.88	−0.24	17_3— 569°_2	
2544.170	15	1	39293.76	+0.17	14_2— 542°_3	
2545.340	50 *r*	12	39275.70	+0.04	$^5D_2$— 426°_3	
2545.583	30	2	39271.95	0.00	$^3H_6$— 562°_5	
2546.077	5		39264.33	+0.04	13_2— 530°_1	
2546.357	4		39260.01	+0.01	$^3P_6$— 487°_1	
2546.649	12		39255.51	+0.07	19_6— 589°_5	
2553.168	70	50 *s*	39155.29	−0.12	$^5D_3$— 439°_4	2
2547.136	100 *r*	25	39248.00	+0.04	$^5D_2$— 425°_1	Res
2547.466	25	1	39242.92	+0.13	19535_5— 587°_4	

318-092 O-69—6

TABLE 3. *Observed and classified lines of* W I

Wavelength Å	Intensity		Wavenumber (cm^{-1})		Classification	Zeeman effect
	Arc	Spark	Observed	o−c		
2547.626	15	1	39240.46	+0.09	$^3H_5$— 543°$_5$	
2547.943	6		39235.58	+0.10	18$_2$— 573°$_3$	
2548.053	1		39233.88	−0.06	19$_2$— 584°$_3$	
2548.148	25	1	39232.42	+0.10	$^5D_4$— 454°$_5$	Res
2548.562	40	2	39226.05	+0.04	13$_2$— 530°$_2$	
				+0.10	19535$_5$— 587°$_6$	
2550.08	20	30 *s*	39202.70	−0.02	23$_6$— 626°$_6$	
2550.131	5		39201.91			
2550.378	60 *r*	8	39198.12	+0.01	$^5D_1$— 408°$_2$	Res
2550.497	12	2	39196.29	−0.02	$^3P_1$— 525°$_2$	
2550.843	4		39190.98	−0.02	$^5D_3$— 440°$_3$	
2551.00	25	4	39188.56	−0.05	$^5D_2$— 425°$_3$	Res
2551.349	200 *r*	30	39183.20	0.00	$^5D_0$— 391°$_1$	
2551.986	25		39173.42	−0.02	17$_4$— 562°$_5$	
2552.489	30		39165.70	−0.07	13$_2$— 529°$_3$	
2553.606	30	2	39148.57	−0.07	17$_4$— 562°$_4$	
2553.824	100 *r*	8	39145.23	+0.01	$^5D_3$— 439°$_2$	
2554.092	30	1	39141.12			
2554.795	2		39130.35	−0.14	17$_3$— 568°$_4$	
2554.906	6		39128.65	−0.12	$^3H_4$— 512°$_5$	
2555.207	40	4	39124.04	−0.03	$^5D_2$— 424°$_2$	3
2555.664	4		39117.05	−0.02	18$_3$— 580°$_3$	
2555.816	2		39114.72	−0.03	$^3G_4$— 555°$_3$	
2555.968	6		39112.40	−0.02	19$_6$— 587°$_6$	
2556.266	20	1	39107.84	+0.05	13$_2$— 528°$_2$	
2556.51	3		39104.1			
2556.749	40 *r*	8	39100.45	−0.04	$^5D_1$— 407°$_1$	3
2557.008	18		39096.49	+0.07	15$_3$— 545°$_3$	
2557.57	20	2	39087.9	+0.02	$^3G_3$— 524°$_4$	
2558.234	2		39077.75	−0.19	19826$_5$— 589°$_5$	
2558.484	20		39073.94	+0.05	19$_4$–58330°$_4$	
2558.90	4	2	39067.58	−0.04	17$_4$— 561°$_4$	
2559.339	15	1	39060.88	−0.03	$^3G_4$–55492°$_5$	
2560.124	40	6	39048.91	+0.06	$^3H_5$— 541°$_4$	
2560.502	8		39043.14	−0.08	$^5D_4$— 452°$_4$	
2560.758	25		39039.24	0.00	23$_6$— 625°$_6$	
2561.445	6	1	39028.77	−0.08	13$_2$— 528°$_3$	
2561.528	20	2	39027.50	+0.17	$^7S_3$— 419°$_2$	
				−0.17	19535$_5$— 585°$_5$	
2561.762	3		39023.94	−0.10	$^3G_4$–55455°$_5$	
2561.846	3		39022.66	−0.20	19826$_5$— 588°$_4$	
2561.968	100 *r*	20	39020.80	−0.04	$^5D_3$— 438°$_3$	3
2562.296	4		39015.81	−0.14	17$_3$— 567°$_3$	
2562.358	10	3	39014.86	−0.08	18$_2$— 571°$_3$	
2563.244	4		39001.38	−0.05	17$_4$— 561°$_3$	
2563.343	6		38999.87	−0.05	22476$_4$— 614°$_5$	
2563.720	6	1	38994.14	−0.02	20$_1$— 594°$_2$	
2564.458	4		38982.92	−0.18	14$_2$— 539°$_2$	
2564.696	45	3	38979.30	−0.10	$^3H_6$— 559°$_5$	
2565.232	2		38971.16			

TABLE 3. *Observed and classified lines of* W I

Wavelength Å	Intensity		Wavenumber (cm^{-1})		Classification	Zeeman effect
	Arc	Spark	Observed	o−c		
2565.806	4		38962.44			
2566.104	7		38957.91	−0.08	$^3G_4$ − 553°$_3$	
2566.206	6		38956.37			
2566.518	6		38951.64	−0.12	19826$_5$ − 587°$_4$	
2566.608	1	1	38950.27	−0.15	19$_3$ − 587°$_4$	
2566.648	6		38949.66	−0.10	19$_4$ − 582°$_3$	
2566.968	6		38944.81			
2567.258	3		38940.40			
2567.506	20	3	38936.64	−0.13	$^5D_2$ − 422°$_1$	
2567.62	10	30 *s*	38934.91	−0.01	19826$_5$ − 587°$_6$	
2568.214	30	4	38925.90	−0.10	$^3P_1$ − 522°$_0$	
				−0.08	$^5D_2$ − 422°$_3$	
2568.401	2	1	38923.08	−0.06	19$_4$ − 581°$_5$	
2568.564	30	4	38920.61	−0.04	$^7S_3$ − 418°$_4$	
2568.85	10	30 *s*	38916.27	−0.20	18$_1$ − 569°$_2$	
2568.992	40	2	38914.12	−0.02	19$_6$ − 585°$_5$	
2569.248	30		38910.25	+0.03	$^3H_4$ − 510°$_3$	
2569.505	6		38906.35			
2569.761	3		38902.48			
2569.986	8		38899.07	−0.01	14$_2$ − 538°$_1$	
2570.099	35	3	38897.36	−0.08	$^5D_4$ − 451°$_4$	Res
2571.181	12	1	38880.99	+0.10	17$_4$ − 559°$_5$	
2571.523	7		38875.83	−0.04	13$_2$ − 526°$_2$	
2572.447	15		38861.86	−0.04	$^3P_0$ − 483°$_1$	
2573.152	12		38851.21	−0.09	$^5S_2$ − 571°$_3$	
2573.346	12		38848.29	−0.06	17$_4$ − 559°$_4$	
2573.531	40	4	38845.49	−0.03	$^3P_1$ − 521°$_2$	
2573.952	15	7 *s*	38839.14	−0.04	$^3H_6$ − 558°$_6$	
2574.048	3		38837.69	−0.33	19$_2$ − 580°$_3$	
2574.206	12		38835.31	−0.03	19$_4$ − 580°$_3$	
2574.684	7		38828.10	+0.06	19$_3$ − 586°$_2$	
2575.468	20	1	38816.28	−0.14	19$_3$ − 586°$_3$	
2575.898	20	2	38809.80	+0.04	15$_3$ − 542°$_3$	
2576.278	5		38804.07	+0.01	$^3G_3$ − 521°$_2$	
2576.507	1		38800.63	−0.29	17$_3$ − 565°$_4$	
2576.87	4		38795.15	−0.06	$^5D_4$ − 450°$_3$	
				+0.03	19535$_5$−58330°$_4$	
2577.029	35	4	38792.76	−0.03	$^3H_5$ − 538°$_5$	
2577.411	30	2	38787.01	+0.03	$^3H_6$ − 557°$_5$	
2577.69	18	1	38782.81	−0.03	$^7S_3$ − 417°$_2$	
2577.781	5		38781.45	0.00	19535$_5$−58316°$_4$	
2577.96	9		38778.76	+0.06	$^3H_5$ − 538°$_4$	
2578.695	8	3 *s*	38767.70	−0.04	19$_3$ − 585°$_2$	
2579.192	3		38760.24	+0.01	17$_4$ − 558°$_4$	
2579.357	4		38757.75	−0.20	18$_3$ − 577°$_3$	
2579.409	20	5	38756.98	0.00	$^3P_1$ − 520°$_2$	
2580.040	12		38747.49	−0.02	$^3H_4$ − 509°$_4$	
2580.337	30	5	38743.04	−0.01	$^7S_3$ − 416°$_3$	
2580.487	125 *r*	20	38740.78	−0.05	$^5D_1$ − 404°$_1$	
2580.76	3		38736.68	+0.04	19826$_5$ − 585°$_5$	

TABLE 3. *Observed and classified lines of* W I

Wavelength Å	Intensity		Wavenumber (cm^{-1})		Classification	Zeeman effect
	Arc	Spark	Observed	o−c		
2581.062	35	2	38732.16	0.00	$^3H_4$–50894°$_3$	
2581.490	15	1	38725.73	+0.03	13$_2$– 525°$_2$	
2581.954	2		38718.77	−0.05	$^5S_2$– 569°$_2$	
2582.039	3		38717.49			
2582.156	2		38715.74	+0.22	$^3G_3$– 520°$_2$	
2582.460	5		38711.18	−0.04	$^3G_3$– 520°$_4$	
2583.222	30	4	38699.76	−0.10	13$_2$– 524°$_1$	
2583.664	15		38693.14	−0.04	14$_2$– 536°$_2$	
2584.236	12	5 *s*	38684.58	−0.09	$^5D_3$– 435°$_2$	
2584.386	70	10	38682.33	+0.01	$^3H_6$– 556°$_7$	2
2584.932	3		38674.16			
2585.235	50	4	38669.63	−0.09	23$_6$– 621°$_5$	
2585.431	45	3	38666.70	−0.02	$^3G_3$– 520°$_3$	
2585.508	20		38665.55			
2585.970	10		38658.64	−0.13	15$_3$– 541°$_4$	
2586.048	2		38657.48			
2586.350	8	25 *s*	38652.96	−0.12	$^5D_2$– 419°$_2$	
2586.644	25	1	38648.57	−0.01	$^5D_3$– 434°$_3$	
2586.894	8	1	38644.83	−0.02	18$_3$– 576°$_3$	
2586.944	40	4	38644.08	−0.03	$^3H_4$– 508°$_5$	
2587.324	15		38638.41	−0.07	$^3H_4$– 508°$_3$	
2587.766	30	3	38631.81	−0.10	$^7S_3$– 415°$_2$	
2588.304	10		38623.78	−0.02	22852$_4$– 614°$_5$	
2589.088	25		38612.09	+0.06	$^3G_4$– 550°$_4$	
2589.727	5		38602.56			
2591.174	7		38581.01			
2591.386	40	4	38577.85	−0.06	$^3G_4$– 550°$_5$	
2593.388	25		38548.07	−0.07	$^7S_3$– 414°$_3$	
2593.44	2		38547.3	−0.12	19$_4$– 578°$_4$	
2594.43	5		38532.6			
2594.549	7	7	38530.82	−0.02	19$_6$– 581°$_5$	
2595.04	3		38523.53			
2596.118	8		38507.54	0.00	$^3G_3$– 518°$_4$	
2596.348	35	2	38504.13	+0.04	19826$_5$–58330°$_4$	
2596.666	25	5	38499.41	+0.14	15$_3$– 539°$_2$	
2597.29	7 *b*	2	38490.16	−0.26	19826$_5$–58316°$_4$	
				+0.29	17$_4$– 555°$_4$	
2597.384	2		38488.77	−0.01	19$_3$–58316°$_4$	
2597.726	25	3	38483.70	−0.02	$^3H_6$–55492°$_5$	
2597.954	15		38480.32	+0.02	$^3G_4$– 549°$_4$	
2598.104	15	1	38478.11	+0.02	13$_2$– 522°$_3$	
2598.234	4		38476.18	−0.04	19$_4$– 577°$_3$	
2598.416	30	2	38473.49	+0.04	17$_3$– 561°$_4$	
2598.672	7	7 *s*	38469.70	+0.11	$^3G_4$– 549°$_3$	
2599.126	2		38462.97			
2599.316	4		38460.16			
2599.568	4		38456.43	+0.09	$^3P_1$– 517°$_1$	
2600.209	20	2	38446.96	+0.01	$^3H_6$–55455°$_5$	
2600.734	30	3	38439.20	+0.15	17$_4$– 555°$_3$	
2600.904	6	1	38436.70	+0.05	$^5S_2$– 567°$_3$	

TABLE 3. *Observed and classified lines of* W I

Wavelength Å	Intensity		Wavenumber (cm^{-1})		Classification	Zeeman effect
	Arc	Spark	Observed	o−c		
2601.052	6		38434.50			
2601.963	40 *r*	4	38421.04	+0.04	$^5D_3$− 432°$_4$	Res
2602.42	12		38414.3	+0.06	14$_2$–53390°$_3$	
2602.804	25	2	38408.63	+0.03	$^5D_2$− 417°$_2$	
2603.170	5		38403.23			
2603.544	40 *r*	5	38397.71	+0.05	$^5D_3$− 432°$_2$	Res
2604.156	15	1	38388.69	+0.07	15$_3$− 538°$_4$	
2604.282	6	1	38386.83	+0.08	$^3P_1$–51693°$_2$	
2604.385	18	3	38385.32	+0.11	17$_4$–55492°$_5$	
2604.464	12	1	38384.15	−0.01	19535$_5$− 579°$_6$	
2604.902	6		38377.70	−0.11	18$_3$− 573°$_3$	
2605.462	10	1	38369.45	+0.11	14$_2$–53345°$_3$	
2605.508	8	2	38368.77	−0.04	$^5D_2$− 416°$_3$	
2605.597	2		38367.46	−0.03	18$_2$− 564°$_3$	
2605.708	10		38365.83	+0.03	19$_2$− 576°$_3$	
2605.884	15	3	38363.24	+0.12	19$_4$− 576°$_3$	
2606.388	35 *r*	5	38355.82	−0.02	$^5D_0$− 383°$_1$	
2606.556	4		38353.35	+0.01	19826$_5$− 581°$_5$	
2606.892	15	1	38348.40	+0.06	17$_4$–55455°$_5$	
2607.103	12		38345.30	+0.01	$^3G_3$–51693°$_2$	
2607.378	35 *r*	6	38341.26	+0.05	$^5D_1$− 400°$_2$	Res
2607.724	12	1	38336.17	+0.07	17$_3$− 560°$_2$	
2607.808	4		38334.94			
2608.222	3		38328.85			
2608.32	50 *r*	8	38327.41	−0.02	$^5D_4$− 445°$_5$	Res
2609.592	8		38308.74	0.00	14$_2$− 532°$_2$	
2609.874	15	1	38304.59	0.00	19$_4$− 575°$_5$	
2610.208	20	1	38299.69	+0.01	$^3P_1$–51606°$_2$	
2610.495	3		38295.47			
2610.744	20	3	38291.82	−0.06	$^3P_0$− 478°$_1$	
2611.113	10		38286.41	+0.04	13$_2$− 520°$_2$	
2611.392	20	1	38282.32	+0.03	17$_4$− 553°$_3$	
2612.188	30	4	38270.66	+0.03	19$_6$− 579°$_6$	
2613.076	80 *r*	20	38257.65	−0.02	$^5D_2$− 415°$_2$	Res
2613.315	15		38254.16	−0.02	17$_3$− 559°$_4$	
2613.443	4		38252.28	+0.32	$^3G_3$− 516°$_3$	
2613.547	4		38250.76	−0.09	14$_2$− 532°$_1$	
2613.818	50 *r*	12	38246.80	−0.05	$^7S_3$− 411°$_4$	Res
2614.452	15		38237.52	−0.05	13$_2$− 520°$_3$	
2615.124	40	4	38227.69	0.00	$^5D_4$− 444°$_3$	Res
2615.980	2		38215.2	+0.04	18$_2$− 563°$_3$	
2616.353	10	3	38209.74			
2616.666	15	1	38205.17			
2616.760	6		38203.8	−0.05	$^5S_2$− 564°$_3$	
2617.652	5		38190.78			
2618.416	4		38179.64			
2618.808	25	3	38173.92	+0.02	$^5D_2$− 414°$_3$	
2619.178	40	15 *s*	38168.53	+0.05	$^3H_5$− 532°$_4$	
2619.254	3		38167.42	+0.13	19535$_5$− 577°$_6$	
2619.342	2		38166.14	+0.08	17$_3$− 558°$_4$	

TABLE 3. *Observed and classified lines of* W I

Wavelength Å	Intensity		Wavenumber (cm^{-1})		Classification	Zeeman effect
	Arc	Spark	Observed	o−c		
2619.717	8		38160.67			
2619.868	6		38158.47	−0.02	$^3H_5$− 532°$_6$	
2619.954	15	2	38157.22	−0.05	18$_3$− 571°$_3$	
2620.215	50	60 *s*	38153.42	+0.19	$^7S_3$− 411°$_2$	
2620.516	3		38149.04			
2620.996	6		38142.05	+0.23	$^3H_4$− 503°$_3$	
2621.542	16		38134.11	+0.17	17$_3$− 558°$_2$	
2622.16	30 *d*		38125.12	0.00	16$_4$− 545°$_3$	
2622.214	35	5	38124.34	+0.02	$^3H_5$− 531°$_5$	
2622.328	30	2	38122.68	0.00	$^3H_4$− 502°$_4$	
2623.463	2		38106.2			
2623.988	2		38098.57	−0.19	19$_2$− 573°$_3$	
2624.154	20	1	38096.16	+0.08	19$_4$− 573°$_3$	
2624.366	9		38093.08	−0.05	19826$_5$− 579°$_6$	
2624.996	20		38083.94			
2625.220	60 *r*	10	38080.69	−0.05	$^5D_3$− 429°$_4$	Res
2625.742	2	1	38073.12			
2626.244	40	3	38065.84	+0.02	14$_2$− 530°$_1$	
2626.456	3		38062.77			
2626.717	12	1	38058.99	−0.02	19$_4$− 573°$_4$	
2627.225	1		38051.63	+0.11	$^5S_2$− 563°$_3$	
2627.451	18	1	38048.36	0.00	$^3H_5$− 531°$_4$	
2628.255	40	5	38036.73	0.00	$^5D_1$− 397°$_2$	
2628.89	25	1	38027.53	−0.01	14$_2$− 530°$_2$	
2629.086	7		38024.70	−0.09	18$_3$− 569°$_2$	
2629.152	15	2	38023.74	0.00	$^3H_4$− 501°$_3$	
2629.30	3		38021.6			
2630.568	5		38003.28			
2630.742	10		38000.76	+0.04	$^3H_6$− 550°$_5$	
2631.357	7		37991.88	+0.06	23$_6$− 614°$_5$	
2631.780	25	1	37985.77	+0.04	13$_2$− 517°$_1$	
2632.344	2		37977.63	+0.01	19826$_5$− 578°$_4$	
2632.485	35 *r*	7 *s*	37975.60	+0.01	$^3H_4$− 501°$_5$	
2632.695	80 *r*	6	37972.57	+0.03	$^7S_3$− 409°$_3$	Res
2633.129	150 *r*	15	37966.32	−0.01	$^5D_1$− 396°$_1$	3
2633.42	6		37962.12			
2634.012	15		37953.59	+0.01	$^3P_1$− 512°$_1$	
2634.864	20	9	37941.32			
2635.205	5		37936.41	+0.08	17$_4$− 550°$_4$	
2635.618	45	1	37930.47	+0.06	15$_3$−53390°$_3$	
2636.326	3		37920.28	−0.16	18$_2$− 560°$_2$	
2636.544	30	3	37917.14	+0.03	$^7S_3$− 408°$_2$	
2636.616	12	1	37916.11	−0.03	13$_2$−51693°$_2$	Res
2636.885	5		37912.24	−0.05	19$_6$− 575°$_5$	
2637.085	9		37909.36	+0.04	14$_2$− 528°$_2$	
2637.161	5		37908.27	−0.14	22476$_4$− 603°$_4$	
2637.406	10		37904.75	−0.03	19$_3$− 577°$_3$	
2637.576	15	25 *s*	37902.31	+0.10	17$_4$− 550°$_5$	
2638.032	6		37895.75	+0.03	17$_3$− 555°$_4$	
2638.615	45	9	37887.38	+0.14	19$_4$− 571°$_5$	
				−0.08	17$_6$− 548°$_6$	

TABLE 3. *Observed and classified lines of* W I

Wavelength λ_A	Intensity		Wavenumber (cm^{-1})		Classification	Zeeman effect
	Arc	Spark	Observed	o−c		
2638.746	30	3	37885.50	−0.01	15_3–53345°$_3$	Res
2639.20	7	1	37878.98	−0.01	$^3G_4$– 543°$_5$	
2639.406	3		37876.03	−0.23	19826_5– 577°$_6$	
2639.896	5 *b*		37869.0			
2640.364	6		37862.29	−0.05	20_1– 582°$_1$	
2640.724	8	1	37857.13	−0.03	18_3– 568°$_4$	
2641.116	3	3	37851.51			
2641.581	4		37844.84	−0.04	17_3– 555°$_3$	
2642.024	15		37838.50	+0.04	$^3G_4$– 542°$_3$	
2642.349	12		37833.85	+0.03	$^3G_3$– 511°$_2$	
2642.681	15		37829.10	+0.03	13_2–51606°$_2$	
2642.758	6		37828.00	+0.04	$^5S_2$– 561°$_3$	
2642.974	3		37824.91	0.00	$^3D_3$– 532°$_2$	
2643.122	25		37822.78	−0.03	13_2– 516°$_3$	Res
2643.920	2		37811.38			
2644.396	20		37804.56	−0.04	17_4– 549°$_4$	
2644.600	30	3	37801.64	−0.03	$^5D_4$– 440°$_3$	Res
2645.143	20	4	37793.88	−0.01	17_4– 549°$_3$	
2645.302	9	2	37791.62	−0.06	19_3– 576°$_3$	
2645.692	25	7 *s*	37786.04	−0.01	$^3H_5$– 528°$_6$	
2646.185	70	12	37779.00	+0.01	$^5D_2$– 411°$_2$	7
2646.365	2		37776.44	−0.05	18_1– 558°$_1$	
2646.536	15	1	37774.00	−0.04	$^5D_0$– 377°$_1$	
2646.730	80	8	37771.22	+0.05	$^5D_3$– 426°$_3$	3
2647.091	60	5	37766.07	−0.01	$^5D_4$– 439°$_4$	
2648.043	12		37752.49	+0.20	18_1– 558°$_2$	
				−0.01	22476_4– 602°$_5$	
2648.325	3 *b*		37748.47			
2648.524	3		37745.64	−0.10	$^3P_2$– 569°$_2$	
2648.730	15		37742.70	+0.08	18_3– 567°$_3$	
2649.024	3		37738.51			
2649.284	15		37734.81	+0.02	19826_5– 575°$_5$	
2649.792	6		37727.58	+0.11	$^3P_0$– 472°$_1$	
2649.98	30	3	37724.90	+0.02	$^3H_6$– 547°$_6$	
2650.071	10		37723.60	−0.02	$^3G_3$– 510°$_3$	
2650.452	40	2	37718.18	+0.10	18_2– 558°$_2$	
2650.707	2		37714.55	+0.01	$^7S_3$– 406°$_3$	
2651.388	6	1	37704.86	−0.06	$^5D_4$– 439°$_5$	
2651.439	10	1	37704.14	−0.03	$^3H_5$– 527°$_5$	3
2651.546	5		37702.62	0.00	$^5D_3$– 425°$_4$	
2652.007	25	1	37696.07	−0.01	23_6– 611°$_7$	
2652.507	4		37688.96	−0.02	17_3– 553°$_2$	
2652.592	50		37687.76	−0.36	17_3– 553°$_3$	
				+0.29	$^3G_4$– 541°$_4$	
2652.71	5		37686.08			
2652.844	8		37684.18	+0.04	$^5D_3$– 425°$_3$	
2653.015	10	8 *s*	37681.75	+0.11	22476_4– 601°$_4$	
2653.314	20		37677.50	+0.10	14_2– 526°$_2$	
2654.499	10 *b*		37660.68	−0.40	20_2– 586°$_3$	

TABLE 3. *Observed and classified lines of* W I

Wavelength Å	Intensity		Wavenumber (cm⁻¹)		Classification	Zeeman effect
	Arc	Spark	Observed	o−c		
2654.659	60	6	37658.40	+0.12	$^3D_3$— 531°$_4$	
2655.558	15		37645.66	−0.10	19826$_5$— 574°$_4$	
2655.667	15	20 *s*	37644.12	0.00	19$_3$— 574°$_4$	
2656.171	20		37636.98			
2656.540	300 *r*	30	37631.75	−0.03	$^7S_3$— 405°$_4$	Res
2656.896	20	1	37626.70	+0.08	$^3H_4$— 497°$_4$	
2657.361	60	5	37620.12	−0.12	$^5D_3$— 424°$_4$	
2657.399	40	4	37619.58	−0.02	$^5D_3$— 424°$_2$	
2657.794	1		37614.00	+0.03	19535$_5$— 571°$_6$	
2657.906	15		37612.42	+0.02	20$_2$— 585°$_2$	
2658.178	30	3	37608.56	+0.09	19535$_5$— 571°$_5$	
2658.393	10		37605.52	+0.10	23$_3$— 615°$_4$	
2658.555	12		37603.24			
2658.898	25		37598.38	+0.08	$^5D_2$— 409°$_3$	
2659.836	3 *b*		37585.12			
2660.283	2		37578.80	−0.04	$^5S_2$— 558°$_1$	
2660.526	40	3	37575.38	−0.05	19$_4$— 568°$_4$	
2661.552	40	7	37560.90	−0.01	$^3G_3$— 509°$_4$	
2661.793	4		37557.48			
2661.987	1		37554.76	+0.12	$^5S_2$— 558°$_2$	
2662.644	20	2	37545.48	−0.08	$^3G_3$–50894°$_3$	
2662.835	200 *r*	20	37542.80	−0.07	$^5D_2$— 408°$_2$	Res
2663.259	12		37536.82	−0.01	18$_1$— 556°$_2$	
2663.556	50	4	37532.64	−0.04	15$_3$— 529°$_4$	
2663.945	18		37527.16	−0.07	14$_2$— 525°$_2$	
2664.321	80		37521.86	−0.18	$^5D_4$— 437°$_5$	
2664.966	100	10	37512.78	−0.13	$^5D_1$— 391°$_1$	3
2665.779	30	4	37501.34	−0.20	$^5D_4$— 437°$_4$	
2665.852	15	4	37500.30	−0.14	19$_6$— 571°$_6$	
2666.238	7		37494.89	−0.05	19$_6$— 571°$_5$	
2666.638	8		37489.26	+0.05	19826$_5$— 573°$_4$	
2666.765	7		37487.46	−0.11	19$_3$— 573°$_4$	
2667.054	3		37483.40	−0.07	15$_3$— 529°$_3$	
2667.206	3		37481.28			
2667.684	2	20	37474.56	0.00	$^3H_4$— 496°$_4$	
2668.473	50	1	37463.48	−0.09	19$_2$— 567°$_3$	
2668.661	6		37460.84	−0.05	19$_4$— 567°$_3$	
2669.301	20		37451.86	−0.02	$^3G_3$— 508°$_3$	
2669.473	5		37449.44	+0.02	17$_4$— 545°$_3$	
2669.777	40	2	37445.18	−0.07	$^5D_2$— 407°$_1$	
2670.766	5		37431.32	−0.09	$^3G_4$— 538°$_5$	
2670.916	7		37429.22	0.00	18$_2$— 555°$_3$	
2671.181	18		37425.50	+0.01	15$_3$— 528°$_2$	
2671.472	200	20	37421.42	−0.09	$^5D_3$— 422°$_3$	Res
2671.763	40 *d*	15	37417.34	+0.02	$^3G_4$— 538°$_4$	
2672.158	25		37411.82	+0.02	$^3P_1$— 507°$_2$	
2672.665	20		37404.72	+0.05	13$_2$— 511°$_2$	
2673.172	8		37397.62			
2674.232	8		37382.80	−0.04	17$_3$–55084°$_2$	
2674.692	50	1	37376.38	0.00	22852$_4$— 602°$_5$	

TABLE 3. *Observed and classified lines of* W I

Wavelength Å	Intensity		Wavenumber (cm^{-1})		Classification	Zeeman effect
	Arc	Spark	Observed	o−c		
2675.126	40		37370.30	−0.04	$^3G_3$− 507°$_2$	
2675.398	35	2	37366.52	+0.01	$^3H_5$− 524°$_4$	
2675.598	2		37363.72			
2675.867	60		37359.96	0.00	$^5D_1$− 390°$_2$	
2676.415	25		37352.32	−0.06	$^3H_4$− 495°$_3$	
2676.832	12		37346.50	−0.05	15$_3$− 528°$_3$	
2677.149	18		37342.07	−0.09	17$_3$− 550°$_4$	
2677.276	100	20	37340.30	−0.02	$^5D_2$− 406°$_3$	Res
2677.913	25	1	37331.42	−0.07	17$_3$–55032°$_2$	
2678.34	10		37325.47	−0.10	$^3H_5$− 523°$_5$	
2678.532	35	3	37322.80	−0.14	19826$_5$− 571°$_6$	
2678.878	150	8	37317.98	−0.08	$^7S_3$− 402°$_3$	
2678.924	20	2	37317.34	−0.10	19826$_5$− 571°$_5$	
2679.884	20		37303.96	−0.14	19$_3$− 571°$_3$	
2680.046	60	6	37301.72	−0.08	$^3H_6$− 543°$_5$	
2680.344	12		37297.56			
2680.412	3		37296.61	−0.05	19535$_5$− 568°$_4$	
2680.57	15		37294.42	−0.05	13$_2$− 510°$_3$	
2681.422	400 *r*	50	37282.57	−0.11	$^7S_3$− 402°$_4$	Res
2681.638	30	2	37279.56	−0.06	14$_2$− 522°$_3$	
2681.883	5		37276.15			
2682.146	7		37272.50	+0.04	18$_2$− 553°$_3$	
2682.219	4		37271.49			
2682.50	4		37267.59	+0.05	18$_2$− 553°$_1$	
2682.648	20		37265.52	−0.06	$^5S_2$− 555°$_3$	
2683.105	5		37259.19	−0.06	$^5D_4$− 434°	
2683.347	100	8	37255.82	−0.12	$^3H_4$− 494°$_3$	
2684.072	25		37245.76	−0.10	19$_4$− 565°$_4$	
2685.160	20		37230.67	−0.10	19$_2$− 564°$_3$	
2685.366	6	12 *s*	37227.82	−0.27	19$_4$− 564°$_3$	
2685.472	8		37226.34	−0.11	$^3P_1$− 505°$_1$	
2685.722	30		37222.88	−0.10	20$_2$− 582°$_3$	
2686.628	20		37210.33	−0.10	17$_3$− 549°$_4$	
2687.141	20		37203.23	−0.06	17$_4$− 543°$_5$	
2687.369	80	2	37200.07	−0.05	18$_3$− 561°$_4$	
2687.624	12		37196.54	−0.10	22476$_4$− 596°$_5$	
2687.84	10	3	37193.55	−0.02	15$_3$− 526°$_2$	
2688.002	30		37191.30			
2688.29	25		37187.33	−0.11	$^3P_1$− 504°$_2$	
2689.077	1		37176.44	0.00	14$_2$− 521°$_2$	
2689.435	4	1	37171.50	−0.12	19$_3$− 569°	
2689.656	25		37168.44			
2690.069	10		37162.74	−0.02	17$_4$− 542°$_3$	
2690.416	20		37157.95	−0.02	17$_3$− 548°$_2$	
2690.577	15		37155.71			
2691.094	100	8	37148.58	−0.04	$^5D_3$− 419°$_2$	
2691.289	70	1	37145.90	−0.08	$^3G_3$− 504°$_2$	
2691.566	30	1	37142.06	0.00	19$_6$− 567°$_7$	
2692.159	40	1	37133.88	−0.05	18$_3$− 561°$_3$	
2692.43	10		37130.15			

TABLE 3. *Observed and classified lines of* W I

Wavelength Å	Intensity		Wavenumber (cm^{-1})		Classification	Zeeman effect
	Arc	Spark	Observed	o−c		
2692.968	3		37122.72			
2693.918	15		37109.63	−0.05	$^5S_2$— 553°$_2$	
2694.006	10	15	37108.42	−0.14	20$_2$— 580°$_3$	
2694.338	6		37103.86	−0.04	$^5S_2$— 553°$_1$	
2694.442	5		37102.42			
2694.873	3		37096.48			
2695.22	3		37091.71			
2695.50	4		37087.86	−0.04	14$_2$— 520°$_2$	
2695.67	150 *r*	15	37085.52	−0.07	$^5D_2$— 404°$_1$	7
2696.198	2		37078.26	−0.18	19$_2$— 563°$_3$	
2696.384	16		37075.70	−0.06	19$_4$— 563°$_3$	
2697.514	60	3	37060.17	−0.04	$^7S_3$— 400°$_2$	
2698.735	3		37043.40	0.00	15$_3$— 525°$_2$	
2698.844	80	6	37041.90	−0.04	$^5D_3$— 418°$_4$	Res
2699.041	8	12 *s*	37039.21	+0.11	14$_2$— 520°$_3$	
2699.594	150 *r*	20	37031.62	−0.05	$^5D_4$— 432°$_4$	Res
2700.012	100	15	37025.89	−0.07	$^3H_4$— 491°$_5$	Res
2700.141	6		37024.11	−0.10	19$_4$— 562°$_5$	
2700.244	20		37022.71	−0.02	13$_2$— 508°$_3$	
2701.036	8	10 *s*	37011.85	+0.08	17$_4$— 541°$_4$	
2701.091	6		37011.10	−0.06	$^3H_5$— 520°$_5$	
2701.485	20	60 *s*	37005.70	+0.07	19826$_5$— 568°$_4$	
2701.814	25		37001.20	+0.01	18$_1$—55084°$_2$	
2701.95	10		36999.33	−0.08	19$_4$— 562°$_4$	
2702.366	8		36993.64			
2702.524	50	5	36991.47	−0.09	19535$_5$— 565°$_6$	
2702.649	10	1	36989.76	−0.09	$^3H_5$— 520°$_4$	
2702.934	8		36985.85	−0.14	$^3H_4$— 491°$_4$	
2703.306	8		36980.77	−0.08	18$_3$— 559°$_4$	
2703.625	25		36976.40	-0.03	15$_3$— 524°$_4$	
2703.974	4	1	36971.64			
2704.040	6		36970.74			
2704.308	30	1	36967.07	−0.02	19$_5$— 565°$_4$	
2705.174	60	2	36955.24	+0.02	$^3G_3$— 503°$_3$	3
2705.599	10	35 *s*	36949.43	−0.41	18$_1$—55032°$_2$	
2706.017	50	3	36943.73	−0.09	$^5D_2$— 402°$_3$	
2706.204	25	1	36941.18	−0.01	13$_2$— 507°$_2$	
2706.579	100	10	36936.07	−0.01	$^3G_3$— 502°$_4$	
2707.026	25		36929.96	−0.09	23$_6$— 604°$_6$	
2707.42	6		36924.58	−0.04	24$_3$— 615°$_4$	
2707.877	80	3	36918.35	−0.04	19$_4$— 561°$_4$	3
2708.064	6		36915.80	−0.03	18$_2$—55032°$_2$	
2708.188	50	3	36914.11	−0.10	$^3G_4$—53345°$_3$	
2708.36	4	2 *s*	36911.77	−0.15	$^3H_4$— 490°$_5$	
2708.493	2		36909.96	−0.22	$^3H_4$— 490°$_3$	
2708.592	100	15	36908.61	−0.14	$^3H_5$— 519°$_6$	
				−0.05	19$_6$— 565°$_7$	
2708.797	30	3	36905.82	−0.03	$^5D_1$— 385°$_0$	
2708.927	80	8	36904.04	−0.09	$^5D_3$— 417°$_2$	
2709.118	3 *b*		36901.44			

TABLE 3. *Observed and classified lines of* W I

Wavelength Å	Intensity		Wavenumber (cm^{-1})		Classification	Zeeman effect
	Arc	Spark	Observed	o−c		
2709.76	30		36892.70	−0.03	18_3− 558°_4	
2710.004	35	2	36889.38	−0.07	19_3− 567°_3	
2710.842	10		36877.98	−0.05	19_6− 565°_6	
2711.846	8	1	36864.33	−0.01	$^5D_3$− 416°_3	
2711.949	3 *b*		36862.92			
2712.128	4	2	36860.48	−0.13	18_3− 558°_2	
2712.302	12	2	36858.12	−0.06	18_1− 549°_1	
2712.516	6		36855.22	−0.03	17_3− 545°_3	
2712.549	2		36854.77	−0.11	19_2− 561°_3	
2712.591	15		36854.20	−0.02	$^3H_6$− 538°_5	
2712.743	1		36852.13	−0.07	19_4− 561°_3	
2713.718	12 *b*		36838.90			
2713.856	16		36837.02	−0.12	$^3G_3$− 501°_3	
2714.82	12		36823.94	−0.23	18_2− 549°_1	
2715.086	4		36820.33	−0.19	22852_4− 596°_5	
2715.503	75	7	36814.68	−0.09	$^5D_4$− 430°_5	(b)
2716.064	10		36807.08	−0.02	$^3G_4$− 532°_4	
2716.178	3		36805.53			
2716.322	30	80 *s*	36803.58	+0.04	$^5S_2$−55084°_2	
2716.89	35	35 *s*	36795.90	+0.11	$^3G_3$− 522°_3	
2717.53	30	1	36787.22	−0.04	14_2− 517°_1	
2717.612	30	1	36786.11	−0.06	$^3H_5$− 518°_4	
2717.795	5		36783.62	−0.10	$^3P_2$− 560°_2	
2718.55	3		36773.42			
2718.906	250 *r*	30	36768.60	−0.07	$^7S_3$− 397°_4	Res
2719.284	30	1	36763.50	−0.07	$^3P_0$− 462°_1	
2719.331	50	6	36762.86	−0.08	$^3G_4$− 531°_5	
2719.858	50	6	36755.73	0.00	$^7S_3$− 397°_2	
2720.046	30	3	36753.20	0.00	$^5D_3$− 415°_2	
2720.118	10		36752.22	+0.03	$^5S_2$−55032°_2	
2720.326	8		36749.42	−0.02	20_2− 577°_3	
2720.616	25		36745.50	+0.06	19535_5− 562°_5	
2720.701	18		36744.34	−0.06	23_6− 602°_5	
2720.856	10		36742.26	−0.05	18_2− 548°_2	
2720.906	35	3	36741.58	−0.04	17_4− 538°_4	
2721.65	50		36731.53	−0.13	19_4− 559°_5	
2722.243	10		36723.53			
2722.456	50	8	36720.66	+0.02	19535_5− 562°_4	
2722.674	30	2	36717.72	+0.05	14_2−51693°_2	
2722.739	3		36716.85	+0.02	13_2− 504°_2	
2723.946	35	2	36700.58	+0.05	19826_5− 565°_6	
2724.352	300 *r*	50	36695.10	−0.02	$^7S_3$− 396°_3	
2724.536	20	2	36692.62	+0.01	15_3− 521°_2	
2724.624	35	7	36691.44	+0.03	$^5D_4$− 429°_4	
2725.033	60	6	36685.94	−0.03	$^5D_2$− 400°_2	
2725.062	60	6	36685.55	0.00	$^5D_1$− 383°_1	
2725.765	12	1	36676.08	+0.02	19826_5− 565°_4	
2725.892	25	1	36674.38	−0.04	19_3− 565°_4	
2726.26	30	1	36669.43	0.00	$^5D_3$− 414°_3	
2726.496	4		36666.26			

TABLE 3. *Observed and classified lines of* W I

Wavelength Å	Intensity		Wavenumber (cm^{-1})		Classification	Zeeman effect
	Arc	Spark	Observed	o−c		
2726.918	8		36660.58	+0.05	$^5S_2$— 549°$_1$	
2727.208	6		36656.68	+0.03	19$_3$— 564°$_3$	
2727.954	40	4	36646.65	−0.02	$^5D_4$— 428°$_5$	Res
2728.064	20	1	36645.18	+0.03	18$_3$— 556°$_2$	
2728.321	20	2	36641.73			
2729.052	20		36631.91	0.00	19$_6$— 562°$_5$	
2729.157	12		36630.50	−0.10	14$_2$—51606°$_2$	
2729.336	10	1	36628.10			
2729.62	25	75 *s*	36624.29	−0.05	14$_2$— 516°$_3$	
2729.761	35		36622.41	+0.02	18$_3$— 555°$_4$	
2730.05	3		36618.53			
2730.146	6		36617.24	−0.23	$^3G_3$— 499°$_3$	
2730.279	3		36615.46			
2730.61	2		36611.02	+0.02	19$_4$— 558°$_4$	
2731.006	8	1	36605.71	−0.05	19$_2$— 558°$_1$	
2731.125	30	1	36604.12	+0.05	15$_3$— 520°$_2$	
2731.451	7		36599.74	−0.03	15$_3$— 520°$_4$	
2732.809	25	2	36581.56	0.00	19$_2$— 558°$_2$	
2733.026	4		36578.65	−0.02	$^5S_2$— 548°$_2$	
2733.178	50	5	36576.61	+0.05	$^3P_0$— 461°$_1$	
2733.562	15		36571.48	−0.07	18$_3$— 555°$_3$	
2733.775	40	2	36568.63	+0.04	17$_3$— 542°$_3$	
2734.316	4	3	36561.40	+0.02	$^3G_4$— 529°$_4$	
2734.409	4	2	36560.16			
2734.771	40		36555.31	+0.04	15$_3$— 520°$_3$	
2735.402	15		36546.88	−0.06	22852$_4$— 593°$_3$	
2735.618	6		36544.00	−0.08	23$_1$— 599°$_2$	
2735.975	50	3	36539.22	−0.02	19$_4$— 557°$_5$	
2736.888	4	2	36527.04			
2737.426	5		36519.86			
2738.002	40	4	36512.18	+0.01	$^3G_4$— 529°$_3$	
2738.562	6		36504.71			
2738.769	10		36501.95			
2739.564	40	2	36491.36	−0.02	$^3P_1$— 497°$_0$	
2739.903	3		36486.84			
2741.129	3		36470.53			
2742.306	8		36454.88	−0.13	23$_3$— 603°$_4$	
2742.471	15	30 *s*	36452.68	−0.21	19535$_5$— 559°$_5$	
2743.068	4		36444.75			
2743.426	50	5	36440.00	−0.02	$^3G_3$— 497°$_4$	
2744.209	20	1	36429.60	−0.01	19826$_5$— 562°$_4$	
2744.338	20	1	36427.88	−0.09	19$_3$— 562°$_4$	
2744.386	25	1	36427.25	−0.05	22476$_4$— 589°$_5$	
2744.910	15		36420.30	−0.05	19535$_5$— 559°$_4$	
2745.113	12		36417.60	0.00	17$_3$— 541°$_4$	
2745.268	1		36415.54	−0.11	18$_3$— 553°$_2$	
2745.325	10		36414.80	+0.01	18$_3$— 553°$_3$	
2745.626	12	1	36410.80	−0.03	22852$_4$— 592°$_5$	
2745.837	20	2	36408.00	+0.01	13$_2$— 501°$_3$	
2746.206	40	3	36403.11	0.00	$^3H_5$— 514°$_4$	

TABLE 3. *Observed and classified lines of* W I

Wavelength Å	Intensity		Wavenumber (cm^{-1})		Classification	Zeeman effect
	Arc	Spark	Observed	o−c		
2746.734	40		36396.11	+0.02	15_3— 518°_4	
2747.005	50	2	36392.52	+0.06	$^3P_1$— 496°_2	
2747.155	15	3	36390.54			
2747.826	40	2	36381.65	−0.21	$^5D_4$— 426°_3	
				+0.16	$^5D_2$— 397°_2	
2748.312	20	15 *s*	36375.21	−0.04	$^3G_4$— 528°_3	
2748.577	30	3	36371.71	+0.02	18_3— 553°_4	
2748.767	5		36369.20	−0.10	20_2— 573°_3	
2748.844	80	20	36368.17	+0.03	$^5D_3$— 411°_4	
2748.997	25	2	36366.15	+0.15	19_2— 556°_2	
2749.538	1	2	36359.01			
2749.641	10		36357.65			
2750.145	40	4	36350.98	−0.02	$^3G_3$— 496°_2	
2750.325	10	20 *s*	36348.60	+0.01	19826_5— 561°_4	
2750.444	10		36347.03	+0.08	19_3— 561°_4	
2750.763	15		36342.82	+0.03	$^3G_4$— 527°_5	
2750.948	3		36340.38	−0.28	19_4— 555°_4	
2751.027	3		36339.32	−0.04	19_6— 559°_5	
2751.210	15		36336.90	+0.06	18_1— 544°_1	
2751.559	8		36332.30	+0.07	19535_5— 558°_4	
2751.691	5		36330.55			
2752.051	9		36325.80			
2752.172	10		36324.20			
2752.418	10		36320.95	+0.07	$^5D_2$— 396°_3	
2752.570	6		36318.95	+0.04	22852_4— 591°_4	
2752.996	30	3	36313.33	+0.04	$^5D_4$— 425°_4	
2753.049	15	2	36312.63	−0.04	19535_5— 558°_6	
2753.159	20		36311.18	+0.09	$^5D_2$— 396°_1	
2753.648	3		36304.72			
2753.793	3		36302.81	−0.02	18_2— 544°_1	
2753.940	1		36300.88	−0.24	22476_4— 587°_4	
2754.258	3		36296.69			
2754.402	12		36294.80	−0.01	$^5D_4$— 425°_3	
2754.58	5		36292.45	−0.05	19_2— 555°_3	
2754.78	3		36289.81	−0.01	19_4— 555°_3	
2754.915	30	3	36288.03	+0.07	$^3G_3$— 496°_4	
2755.266	40	3	36283.41	0.00	17_4—53390°_3	
2755.465	8		36280.79	+0.03	19_3— 561°_3	
2755.584	15		36279.22			
2755.830	3		36275.99	+0.04	$^5S_2$— 545°_3	
2755.942	40	4	36274.51	−0.01	$^5D_3$— 411°_2	
2756.360	12		36269.01			
2756.694	12		36264.62			
2757.008	8		36260.49	+0.02	19535_5— 557°_5	
2757.201	8	10	36257.95	−0.01	18_2— 543°_1	
2758.683	20	1	36238.47	−0.04	17_4—53345°_3	
2758.876	20	1	36235.93	−0.05	19_4—55492°_5	
2759.035	25	2	36233.85	+0.01	15_3—51693°_2	
2759.122	6		36232.71	−0.03	$^3P_0$— 457°_1	
2759.257	10		36230.93	+0.02	$^5D_4$— 424°_4	

TABLE 3. *Observed and classified lines of* W I

Wavelength Å	Intensity		Wavenumber (cm^{-1})		Classification	Zeeman effect
	Arc	Spark	Observed	o−c		
2759.904	5		36222.44			
2760.036	30	5	36220.71	−0.09	$^3H_5$ − 512°$_5$	
2760.100	8		36219.87	−0.05	$^3H_6$ − 532°$_6$	
2760.409	7		36215.81			
2760.742	12	10 *s*	36211.44	+0.07	17$_3$ − 53912°$_2$	
2760.84	40	1	36210.16	0.00	$^3P_1$ − 495°$_2$	
2761.142	30		36206.20	0.00	14$_2$ − 511°$_2$	
2761.685	12		36199.08	−0.03	19$_4$ − 55455°$_5$	
				−0.06	19$_6$ − 55847°$_6$	
2762.339	150	15	36190.51	+0.02	$^5D_0$ − 361°$_1$	
2762.499	6	15 *s*	36188.42	+0.10	13$_2$ − 499°$_3$	
				−0.12	23$_6$ − 596°$_5$	
2762.70	35	2	36185.78	0.00	$^3H_6$ − 531°$_5$	
2763.55	4	1	36174.66			
2763.614	5		36173.82			
2764.004	30	2	36168.72	+0.02	$^3G_3$ − 495°$_2$	
2764.344	10		36164.27	−0.18	$^3H_4$ − 483°$_3$	
2764.638	4		36160.42			
2765.131	4		36153.97			
2765.211	12	3	36152.93	0.00	18$_2$ − 542°$_3$	
2765.535	2		36148.69	−0.07	20$_2$ − 571°$_3$	
2765.642	50 *l*	1	36147.30	−0.15	17$_3$ − 538°$_4$	
				+0.36	19$_6$ − 557°$_5$	
				+0.53	15$_3$ − 51606°$_2$	
2766.268	3		36139.11	−0.08	$^5S_2$ − 544°$_1$	
2766.464	8	4	36136.56	−0.04	19$_2$ − 553°$_2$	
2766.531	3		36135.68	−0.06	19$_2$ − 553°$_3$	
2766.731	20		36133.07	+0.01	19$_4$ − 553°$_3$	
2766.861	4		36131.37	−0.03	17$_4$ − 532°$_4$	
2766.898	6		36130.89	+0.07	19$_2$ − 553°$_1$	
2767.144	50	1	36127.68	0.00	19$_3$ − 559°$_4$	
2767.472	5		36123.39			
2768.534	12		36109.54	+0.03	18$_3$ − 55084°$_2$	
2768.848	6	2	36105.44			
2768.982	100	12	36103.70	+0.03	$^5D_1$ − 377°$_1$	Res
2769.576	10		36095.95	−0.05	14$_2$ − 510°$_3$	
2769.741	80	8	36093.80	−0.03	$^5D_3$ − 409°$_3$	
2770.042	15	8	36089.88	−0.08	19$_4$ − 553°$_4$	
2770.215	30		36087.61			
2770.349	6		36085.88	−0.12	22476$_4$ − 585°$_5$	
2770.880	200 *r*	20	36078.96	0.00	$^7S_3$ − 390°$_2$	
2771.628	50	1	36069.23	−0.11	$^3G_3$ − 494°$_3$	
2772.188	30		36061.94	+0.05	19535$_5$ − 555°$_4$	
2772.485	30		36058.08	−0.08	18$_3$ − 55032°$_2$	
2773.022	6		36051.10	−0.08	22852$_4$ − 589°$_5$	
2773.702	80	4	36042.26	−0.02	19$_6$ − 556°$_7$	
2773.918	8		36039.45	−0.11	19$_3$ − 558°$_4$	
2773.999	200 *r*	20	36038.40	0.00	$^5D_3$ − 408°$_2$	
2774.476	300 *r*	50	36032.20	+0.02	$^5D_4$ − 422°$_3$	
2775.290	4		36021.64	0.00	19826$_5$ − 558°$_6$	

TABLE 3. *Observed and classified lines of* W I

Wavelength Å	Intensity		Wavenumber (cm^{-1})		Classification	Zeeman effect
	Arc	Spark	Observed	o−c		
2775.71	1		36016.19	−0.11	23_2− 599°_2	
				−0.09	20_2− 569°_2	
2775.988	8*d*	6	36012.58	−0.45	15_3− 514°_4	
2776.095	40	2	36011.19	−0.09	17_4− 531°_4	
2776.30	5		36008.53	−0.06	$^3H_4$− 481°_3	
2776.392	6		36007.35	−0.09	19_3− 558°_2	
2776.564	10		36005.12	−0.01	$^3G_4$− 524°_4	
2776.916	3		36000.55			
2777.269	15		35995.97	−0.13	22852_4− 588°_4	
2777.786	10		35989.27	−0.02	$^5S_2$− 542°_3	
2778.787	1		35976.31	−0.11	$^3H_4$− 481°_5	
2779.321	15	1	35969.39	−0.05	19826_5− 557°_5	
2779.52	1		35966.82	−0.16	23_1− 594°_2	
2779.642	15	1	35965.24			
2779.733	30	4	35964.07	−0.12	$^3G_4$− 523°_5	
2779.824	8		35962.89	−0.16	$^3P_1$− 492°_2	
2780.285	60	40 *s*	35956.94	−0.27	19535_5–55492°_5	
2781.376	4*b*		35942.82			
2781.820	15		35937.09	−0.01	18_3− 549°_4	
2782.658	12		35926.26	−0.13	18_3− 549°_3	
2782.692	1		35925.82	+0.08	23_6− 594°_6	
2782.763	3	5	35924.90	−0.10	22852_4− 587°_4	
2783.022	10		35921.57	−0.03	$^3G_3$− 492°_2	
2783.131	40	12	35920.16	−0.18	19535_5–55455°_5	
2783.679	20		35913.09			
2785.806	15	1	35885.67	−0.01	17_4− 529°_4	
2785.896	25	2	35884.51	−0.13	18_3− 548°_2	
2786.102	8		35881.86	−0.07	$^3H_5$− 509°_6	
2786.52	30		35876.48	+0.03	18_1− 539°_2	
2787.131	6		35868.61			
2787.632	10		35862.16	−0.04	23_6− 593°_7	
2787.984	50	5	35857.63	−0.04	$^5D_2$− 391°_1	Res
2788.778	10	3	35847.43	−0.05	$^3H_6$− 528°_6	
2788.906	6		35845.78	−0.16	$^3P_0$− 453°_1	
2789.074	30	2	35843.62	−0.06	19_6–55492°_5	
2789.170	10		35842.39	−0.05	18_2− 539°_2	
2789.380	25		35839.69	+0.14	$^3H_5$− 509°_4	
2789.623	5		35836.56	+0.09	17_4− 529°_3	
2789.684	25	2	35835.78	−0.07	$^5D_3$− 406°_3	
2790.103	3		35830.41	−0.05	19_2–55084°_2	
2790.210	2		35829.03			
2790.576	25		35824.33	−0.16	$^3G_4$− 522°_3	
				+0.07	14_2–50800°_3	
2791.604	4		35811.14	−0.05	19_2− 553°_4	
2791.961	80	8	35806.56	−0.10	$^3H_4$− 479°_4	3
2792.216	20	1	35803.29	−0.09	$^3G_3$− 491°_2	
2792.526	25	4	35799.32	−0.07	$^3G_3$− 491°_4	
2792.696	60 *r*	20	35797.14	−0.01	$^7S_3$− 387°_4	Res
2792.781	35	3	35796.05	+0.04	$^5D_1$− 374°_2	
2793.105	12	1	35791.90	−0.08	19_3− 556°_2	

TABLE 3. *Observed and classified lines of* W I

Wavelength Å	Intensity		Wavenumber (cm^{-1})		Classification	Zeeman effect
	Arc	Spark	Observed	o−c		
2793.496	8	1	35786.89	−0.21	19_4− 550°_4	
2794.127	12		35778.81	−0.04	23_6− 592°_5	
2794.278	3		35776.87			
2794.506	8		35773.96	−0.25	24_3− 603°_4	
2794.752	6		35770.81	−0.05	19826_5− 555°_4	
2794.882	5		35769.14	−0.08	19_3− 555°_4	
2795.165	10		35765.52	−0.08	$^3H_6$− 527°_5	
2795.723	3		35758.38	−0.04	18_2− 538°_1	
2795.906	2		35756.04			
2796.153	30	3	35752.88	−0.19	$^5D_3$− 405°_4	
				−0.10	19_4− 550°_5	
2796.958	4		35742.60	−0.12	14_2− 507°_2	
2797.201	25	2	35739.49	−0.06	13_2− 495°_2	
2797.464	25	2	35736.13	−0.01	$^3H_5$− 508°_5	
2797.633	10		35733.97	−0.14	20_2− 567°_3	
2798.005	6		35729.22	−0.10	22476_4− 582°_3	
2798.286	3		35725.63			
2798.455	12		35723.47	−0.11	$^3G_3$− 490°_3	
2798.544	6		35722.34	−0.03	15_3− 511°_2	
2798.860	5		35718.30	−0.08	19_3− 555°_3	
2799.688	15	1	35707.74			
2799.928	50	10	35704.68	−0.04	$^5D_2$− 390°_2	Res
2800.097	8		35702.53	−0.17	22476_4− 581°_5	
2800.333	8		35699.52	−0.03	17_4− 528°_3	
2800.886	10		35692.47			
2801.172	25	4	35688.83	−0.05	$^3H_4$− 478°_5	
2801.410	6		35685.80			
2801.469	5		35685.04	−0.08	20_0− 558°_1	
2801.644	8		35682.81	−0.17	27_5− 635°_6	
2801.848	3		35680.22			
2801.958	15	1	35678.81	+0.01	$^5S_2$− 539°_2	
2802.884	15	2	35667.03	−0.06	17_4− 527°_3	
2802.958	20	3	35666.09	−0.09	19826_5−55492°_3	
				+0.10	13_2− 494°_1	
2803.800	7		35655.38	+0.01	19_4− 549°_4	
2804.020	30	4	35652.58	−0.03	$^5D_4$− 418°_4	
2804.243	30	6	35649.75	−0.03	$^3G_4$− 520°_5	
2804.676	40	6	35644.24	−0.10	17_3−53345°_3	
				+0.22	23_6− 591°_6	
2804.996	6		35640.18	−0.01	13_2− 494°_3	
2805.427	4		35634.70	−0.02	22852_4− 584°_3	
2805.632	30	2	35632.10	+0.03	$^5S_2$−53912°_2	
2806.787	4		35617.44			
2805.874	10		35629.02	−0.29	19826_5−55455°_5	
2807.208	6		35612.09	−0.08	15_3− 510°_3	
2807.725	35	2	35605.54	−0.05	19_2− 548°_2	
2807.938	12	3	35602.84			
2808.574	20		35594.78	0.00	$^5S_2$− 538°_1	
2809.231	10	2	35586.45	−0.08	18_1− 536°_2	
2809.430	3		35583.93	−0.04	$^3G_4$− 520°_3	

TABLE 3. *Observed and classified lines of* W I

Wavelength Å	Intensity		Wavenumber (cm^{-1})		Classification	Zeeman effect
	Arc	Spark	Observed	o−c		
2809.594	15	1	35581.85	−0.07	18_3− 545°_3	
2811.122	10	1	35562.51	+0.03	19_3− 553°_2	
2811.185	2		35561.71	+0.09	19_3− 553°_3	
2811.534	12		35557.30	−0.07	14_2− 505°_1	
2811.911	4		35552.53	+0.01	18_2− 536°_2	
2812.324	10		35547.31	−0.13	24_3− 601°_4	
2813.128	35	4	35537.16	−0.07	17_3− 532°_4	
2813.902	3		35527.38	+0.01	$^3H_4$− 476°_4	
2814.478	6		35520.11	−0.05	19826_5− 553°_4	
2814.604	8		35518.52	0.00	19_3− 553°_4	
2815.416	40	4	35508.28	−0.05	19535_5− 550°_4	
2815.880	6		35502.43			
2815.975	4		35501.23	−0.08	20_2− 564°_3	
2816.326	8		35496.80			
2816.685	12		35492.28	−0.17	13_2− 492°_2	
2817.590	10	1	35480.88	−0.08	$^3P_1$− 487°_1	
2818.060	250 *r*	40	35474.96	−0.05	$^5D_4$− 416°_3	Res
2818.138	40		35473.98	−0.23	19535_5− 550°_5	
2818.480	4		35469.68	+0.02	23_3− 593°_3	
2818.957	2		35463.68	+0.02	22852_4−58316°_4	
2819.108	4		35461.78			
2819.330	3		35458.98			
2820.092	12		35449.40	−0.06	15_3− 509°_4	
2820.702	20	2	35441.74			
2820.900	3		35439.25	−0.10	$^5D_3$− 402°_3	
				+0.05	23_2− 594°_2	
2821.310	20	2	35434.10	−0.10	15_3−50894°_3	
2821.522	15		35431.44	−0.04	$^3H_4$− 475°_3	
2821.629	6	1	35430.09			
2822.054	7		35424.76	−0.03	$^3G_4$− 518°_4	
2822.597	30		35417.95			
2822.659	5		35417.17	+0.06	17_3− 531°_4	
2823.460	1		35407.12	−0.16	20_1− 558°_2	
2823.710	30	2	35403.98	+0.01	$^5D_3$− 402°_4	
2824.467	5		35394.50			
2824.983	3		35388.03	−0.19	24_3− 599°_2	
2825.072	6		35386.92	−0.08	$^3H_6$− 523°_5	
2825.248	3		35384.71			
2825.366	3		35383.24			
2825.891	3		35376.66	+0.06	19535_5− 549°_4	
2826.084	15	1	35374.25	+0.02	13_2− 491°_2	
2826.598	5		35367.82			
2826.861	3		35364.52			
2827.149	12	2	35360.92	−0.03	19535_5− 548°_6	
2827.286	18	6	35359.21	−0.04	$^3H_5$− 504°_6	
2827.651	4		35354.64			
2828.117	3		35348.82	−0.16	20_2− 563°_3	
2828.796	15		35340.34	−0.09	15_3− 508°_3	
2828.958	5		35338.32			
2829.158	3		35335.82			

318-092 O-69—7

TABLE 3. *Observed and classified lines of* W I

Wavelength Å	Intensity		Wavenumber (cm^{-1})		Classification	Zeeman effect
	Arc	Spark	Observed	o−c		
2829.668	2		35329.45	+0.02	17_4 — 524°_4	
2829.821	50	10	35327.54	+0.02	$^3G_3$ — 486°_4	
				−0.06	14_2 — 503°_3	
2829.898	8		35326.58	0.00	22852_4 — 581°_5	
2830.286	30	2	35321.73	+0.01	$^3H_4$ — 474°_3	
2831.379	250 *r*	40	35308.10	−0.01	$^7S_3$ — 382°_4	Res
2831.828	6	6	35302.50	−0.04	17_3 — 530°_2	
2832.073	1		35299.44	+0.10	28_5 — 635°_6	
2832.322	10	3	35296.34	0.00	$^3P_1$ — 486°_0	
2832.478	30	3	35294.40	−0.03	13_2 — 490°_3	
2832.710	5		35291.50	−0.01	17_3 — 529°_4	
2832.954	20	2	35288.47	−0.02	17_4 — 523°_5	
2833.630	120 *r*	30	35280.05	−0.05	$^5D_4$ — 414°_3	
2834.155	15		35273.51	−0.07	18_2—53390$^\circ_3$	
2834.495	6	4	35269.28			
2835.334	8	5 *s*	35258.85	−0.04	15_3 — 507°_2	
2835.544	5		35256.24	−0.10	19_3—55084$^\circ_2$	
2835.638	60	6	35255.07	−0.02	$^7S_3$ — 382°_3	
2836.057	3		35249.86			
2836.254	30	3	35247.41	−0.01	19_6 — 548°_6	
2836.426	3		35245.27			
2836.663	3		35242.33	+0.03	17_3 — 529°_3	
2836.718	1		35241.64	+0.01	23_3 — 591°_4	
2837.345	60	5	35233.86	−0.01	$^5D_1$ — 369°_2	
2837.768	40	4	35228.60	−0.08	18_2—53345$^\circ_3$	
2838.682	20	2	35217.26	−0.04	19826_5 — 550°_4	
2838.819	10		35215.56	0.00	19_3 — 550°_4	
2838.894	20	2	35214.63	−0.08	$^3H_5$ — 502°_4	
2839.120	5		35211.83			
2839.340	50	5	35209.10	−0.05	$^3P_0$ — 447°_1	
2840.104	15	1	35199.63	−0.15	$^3H_4$ — 473°_3	
2840.222	15	2	35198.17	−0.06	$^3H_4$ — 473°_4	
2840.738	10	1	35191.78	−0.04	20_1 — 556°_2	
2841.128	8		35186.95			
2841.345	5		35184.26	−0.06	17_3 — 528°_2	
2841.570	80 *r*	10	35181.47	−0.03	$^5D_3$ — 400°_2	
2841.752	4		35179.22			
2841.843	2		35178.10			
2842.566	25	1	35169.15	−0.06	$^3G_4$ — 516°_3	
2842.818	12		35166.03	−0.08	$^3P_2$ — 544°_1	
2843.780	30	2	35154.13			
2844.220	2		35148.70	−0.09	17_4 — 522°_3	
2844.578	5		35144.27	0.00	18_3 — 541°_4	
				+0.07	18_1 — 532°_1	
2844.711	4		35142.63	−0.05	22476_4 — 576°_3	
2844.922	50	2	35140.02	−0.06	28_6 — 635°_6	
2845.392	6		35134.22			
2846.446	10		35121.21	−0.03	$^3P_2$ — 543°_1	
2847.366	25	3	35109.86	−0.08	$^5S_2$—53390$^\circ_3$	
2847.736	5		35105.30	−0.08	17_3 — 528°_3	

TABLE 3. *Observed and classified lines of* W I

Wavelength Å	Intensity		Wavenumber (cm^{-1})		Classification	Zeeman effect
	Arc	Spark	Observed	o−c		
2847.832	20	10	35104.12			
2848.022	180 *r*	50	35101.78	+0.02	$^7S_3$ — 380°$_3$	
2849.333	8		35085.63	+0.06	19826$_5$ — 549°$_4$	
2849.395	8		35084.86	+0.02	19$_6$ — 547°$_6$	
2849.468	10	2	35083.97	+0.04	19$_3$ — 549°$_4$	
2849.560	12	2	35082.83	−0.03	$^3P_1$ — 483°$_1$	
2849.961	6		35077.90	0.00	23$_6$ — 585°$_5$	
2850.399	15	1	35072.51	−0.08	$^3H_6$ — 520°$_5$	
2850.610	3	1	35069.91	−0.01	19826$_5$ — 548°$_6$	
2850.808	35	8 *s*	35067.48	−0.14	$^3H_5$ — 501°$_5$	
2851.009	5		35065.00	−0.04	$^5S_2$—53345°$_3$	
2851.456	3		35059.51			
2851.901	18	2	35054.04	−0.02	19$_4$ — 543°$_5$	
2852.250	6		35049.74	−0.09	$^7S_3$ — 380°$_4$	
2852.914	15	3	35041.59	−0.14	$^3G_4$ — 514°$_4$	
2853.023	3		35040.25			
2853.143	8		35038.78			
2853.502	50	5	35034.37	−0.16	15$_3$ — 504°$_2$	
2853.841	30	2	35030.20	−0.11	$^5D_2$ — 383°$_1$	Res
2854.998	8		35016.02	−0.19	$^3P_2$ — 542°$_3$	
2855.354	25	2	35011.65	−0.09	$^3P_1$ — 483°$_2$	
2855.470	8		35010.22	−0.13	13$_2$ — 487°$_1$	
2856.030	150 *r*	15	35003.36	−0.05	$^5D_1$ — 366°$_2$	
2856.202	10		35001.25			
2856.720	6		34994.90	−0.22	22476$_4$ — 574°$_4$	
2857.145	50	5	34989.70	−0.15	14$_2$ — 499°$_3$	Res
2857.549	4		34984.76	−0.01	18$_3$ — 539°$_2$	
2858.042	60	6	34978.72	−0.09	$^5D_4$ — 411°$_4$	Res
2858.430	25	2	34973.97	−0.11	17$_4$ — 520°$_5$	
2858.742	30	2	34970.16	−0.02	$^3H_6$ — 519°$_6$	
2859.647	8		34959.08	−0.09	18$_1$ — 530°$_1$	
2859.780	10	1	34957.46	−0.06	$^3P_1$ — 482°$_0$	
2859.870	10	1	34956.36	−0.18	20$_1$ — 553°$_1$	
2860.170	12	3	34952.69	−0.08	17$_4$ — 520°$_4$	
2860.316	1		34950.90	+0.04	22852$_4$ — 578°$_4$	
2860.668	10		34946.60	+0.05	$^5S_2$ — 532°$_1$	
2860.736	7		34945.78			
2861.149	2		34940.74	+0.06	27$_4$ — 621°$_5$	
2861.443	12	2	34937.15	−0.04	$^3P_1$ — 482°$_2$	
2862.432	10		34925.08	−0.08	18$_2$ — 530°$_1$	
2862.781	8		34920.82	−0.07	18$_1$ — 530°$_2$	
2863.012	50	5	34918.00	−0.03	$^5D_1$ — 365°$_0$	
2863.892	35	7	34907.27	−0.07	19826$_5$ — 547°$_6$	1
2864.858	3	10 *s*	34895.51	−0.22	$^3G_3$ — 482°$_2$	
2865.318	10	1	34889.90	−0.06	$^5D_3$ — 397°$_4$	
2865.568	12		34886.86	−0.02	18$_2$ — 530°$_2$	
2866.062	200 *r*	40	34880.84	−0.01	$^5D_2$ — 382°$_3$	
2866.387	25	3	34876.89	−0.13	$^5D_3$ — 397°$_2$	
2866.600	4	8 *s*	34874.30	+0.18	18$_3$ — 538°$_4$	
2867.564	20		34862.58	+0.04	19$_4$ — 541°$_4$	

TABLE 3. *Observed and classified lines of* W I

Wavelength Å	Intensity		Wavenumber (cm^{-1})		Classification	Zeeman effect
	Arc	Spark	Observed	o−c		
2867.814	3		34859.54	+0.12	$^3G_4$— 512°$_5$	
2868.436	3		34851.98	−0.12	20$_2$— 558°$_2$	
2868.796	8		34847.61	−0.11	23$_3$— 587°$_4$	
2869.117	50	2	34843.71	−0.06	15$_3$— 503°$_3$	
2869.552	4		34838.42	−0.15	22476$_4$— 573°$_4$	
2869.625	10	10	34837.54	−0.16	27$_5$— 626°$_6$	
2869.826	6		34835.10	−0.06	23$_1$— 582°$_1$	
2870.416	5	3	34827.94			
2870.528	6		34826.58	−0.06	18$_2$— 529°$_3$	
2870.630	4		34825.34	−0.06	$^3P_0$— 443°$_1$	
2870.690	3		34824.62	−0.01	15$_3$— 502°$_4$	
2870.786	2		34823.45			
2870.855	4		34822.61			
2870.906	18	10 *s*	34822.00	+0.01	$^3G_3$— 481°$_3$	
2871.363	30	6	34816.45	+0.04	$^5D_3$— 396°$_3$	
2872.505	12		34802.60	−0.07	18$_1$— 528°$_2$	
2873.40	7		34791.77			
2873.643	2		34788.83	−0.03	24$_3$— 593°$_3$	
2874.418	6		34779.44			
2874.762	1		34775.29	0.00	19535$_5$— 543°$_5$	
2874.845	3		34774.28			
2875.208	30	3	34769.89	+0.01	$^3H_4$— 469°$_4$	
2875.314	5		34768.61	−0.05	18$_2$— 528°$_2$	
2875.474	10	3	34766.68	−0.13	20$_0$— 549°$_1$	
2875.906	2		34761.46	−0.06	$^5S_2$— 530°$_1$	
2876.934	20	10 *s*	34749.01	−0.01	17$_4$— 518°$_4$	
2878.083	10	8 *s*	34735.16	−0.10	17$_3$— 524°$_4$	
2878.721	50	5	34727.47	−0.05	$^5D_2$— 380°$_3$	
2878.882	1		34725.53	−0.11	23$_3$— 586°$_2$	
2879.112	150 *r*	25	34722.75	−0.04	$^7S_3$— 376°$_3$	Res
2879.396	140 *r*	20	34719.33	0.00	$^5D_0$— 347°$_1$	
2880.349	2		34707.84	−0.19	22852$_4$— 575°$_5$	
2880.521	3		34705.77	+0.05	$^3P_2$— 539°$_2$	
2880.634	25	3	34704.40	−0.10	$^5D_4$— 409°$_3$	
2881.080	4		34699.03			
2881.438	4		34694.72	−0.13	18$_3$— 536°$_2$	
				+0.12	23$_6$— 581°$_5$	
2881.606	80	12	34692.70	+0.05	$^5D_4$— 409°$_5$	
				−0.14	$^3H_4$— 468°$_5$	
2881.847	2		34689.80	+0.08	18$_2$— 528°$_3$	
2882.196	10		34685.60			
2883.152	3	3 *s*	34674.10	−0.12	27$_5$— 625°$_6$	
2883.247	6	4 *s*	34672.95	+0.03	23$_2$— 586°$_2$	
2883.367	3		34671.50			
2883.569	10		34669.08			
2884.084	3		34662.89	−0.11	$^5S_2$— 529°$_3$	
2884.180	25	3	34661.74	−0.02	19$_6$— 543°$_5$	
2884.233	2		34661.10	−0.20	23$_2$— 586°$_3$	
2884.412	4		34658.96	−0.03	$^3P_2$—53912°$_2$	
2884.641	15		34656.20	+0.02	20$_1$—55084°$_2$	

TABLE 3. *Observed and classified lines of* W I

Wavelength Å	Intensity		Wavenumber (cm⁻¹)		Classification	Zeeman effect
	Arc	Spark	Observed	o−c		
2884.888	4		34653.24			
2885.058	5	2	34651.20			
2885.921	12	2	34640.83	−0.04	$^3G_4$ — 510°_3	
2886.280	2		34636.52	−0.12	20_2 — 556°_2	
2886.645	6		34632.14	−0.20	24_2 — 594°_2	
2887.518	4		34621.67	−0.03	$^3P_2$ — 538°_1	
2887.662	20	3	34619.94	−0.12	$^3G_3$ — 479°_4	
2887.743	2		34618.97	−0.03	22852_4 — 574°_4	
2888.318	15	8 *s*	34612.08	−0.17	13_2 — 483°_1	
2888.788	6		34606.45	−0.03	19_4 — 538°_5	
2888.924	4		34604.82	−0.01	20_1 — 55032°_2	
2889.968	25	1	34592.32	−0.07	19_4 — 538°_4	
2890.314	5 *b*		34588.18			
2890.687	3		34583.72	−0.05	19535_5 — 541°_4	
2891.76	3		34570.88	+0.13	18_1 — 526°_2	
2892.120	8	2	34566.58	−0.01	$^3H_5$ — 496°_4	
2892.413	7		34563.08	+0.04	20_2 — 555°_3	
2892.608	12		34560.75	−0.08	24_3 — 591°_4	
2893.124	25	2	34554.59	−0.03	17_3 — 522°_3	
2893.616	20	2	34548.72	+0.02	13_2 — 483°_3	
2894.257	20	3	34541.06	−0.07	13_2 — 483°_2	z d
				−0.02	14_2 — 495°_2	
2894.500	10		34538.16	0.00	14_2 — 495°_3	
2894.624	15	1	34536.68	−0.06	18_2 — 526°_2	
2895.143	3		34530.49			
2895.525	1		34525.94	−0.14	$^5S_2$ — 528°_3	
2896.009	150 *r*	30	34520.16	−0.04	$^5D_1$ — 361°_1	
2896.442	400 *r*	80	34515.00	−0.01	$^7S_3$ — 374°_2	
2896.918	6		34509.32			
2897.062	1		34507.62			
2897.202	15	2	34505.95	−0.07	15_3 — 499°_3	
2897.726	2	3 *s*	34499.70	+0.18	22852_4 — 573°_3	
2898.248	20	2	34493.50	−0.01	17_4 — 516°_3	
2899.029	1		34484.20	−0.06	19826_5 — 543°_5	
2899.193	3		34482.26			
2899.723	8	2	34475.96			
2900.442	15		34467.40	−0.12	14_2 — 494°_1	
2900.518	25	4	34466.51	+0.01	13_2 — 482°_2	
2900.812	15	2	34463.01	−0.08	$^3H_4$ — 466°_4	
2900.866	8	1	34462.36	−0.09	22852_4 — 573°_4	
2901.789	35	5	34451.40	−0.04	17_3 — 521°_2	
2902.040	15	2	34448.43	0.00	$^5D_2$ — 377°_1	
2902.201	30	20 *s*	34446.52	0.00	$^5D_4$ — 406°_3	
2902.429	5		34443.82			
2902.602	12	20	34441.76	+0.04	14_2 — 494°_3	Res
2903.230	4		34434.31	−0.08	23_6 — 579°_6	
2904.788	40	2	34415.84	−0.07	18_3 — 53390°_3	
				+0.04	$^3P_2$ — 536°_2	
2905.182	35	2	34411.18			
2905.545	2		34406.88	−0.26	20_2 — 553°_2	

TABLE 3. *Observed and classified lines of* W I

Wavelength Å	Intensity		Wavenumber (cm⁻¹)		Classification	Zeeman effect
	Arc	Spark	Observed	o−c		
2905.602	8	12 *s*	34406.20	−0.08	20_2— 553°_3	
2906.022	2		34401.23	−0.13	20_2— 553°_1	
2906.134	3		34399.90	−0.15	23_3–58330°_4	
2906.576	20	2	34394.68	−0.06	18_1— 524°_1	
2906.734	15	2	34392.81	−0.03	13_2— 481°_3	
2907.260	35	4	34386.58	+0.01	18_2— 525°_2	Res
2907.660	8		34381.85			
2907.848	6		34379.63			
2908.266	20	2	34374.69	−0.08	$^3G_4$— 508°_5	
2908.403	30	3	34373.07	−0.03	$^5S_2$— 526°_2	
2909.120	50	6	34364.59	+0.03	$^3P_0$— 438°_1	
2909.188	5		34363.79	+0.05	$^5D_4$— 405°_4	
2909.274	5		34362.77	−0.13	17_3— 520°_2	
2909.460	6		34360.58	−0.15	18_2— 524°_1	
2909.633	10		34358.53	−0.07	17_3— 520°_4	
2909.930	3		34355.03	+0.04	22476_4— 568°_4	
2910.483	100	25	34348.50	−0.05	$^5D_2$— 376°_3	
2910.607	3		34347.04			
2910.834	6	2	34344.36	−0.05	$^3H_4$— 465°_5	
2910.997	100	20	34342.43	−0.01	$^5D_0$— 343°_1	
2911.142	10		34340.73	−0.04	$^3G_3$— 476°_4	
2912.034	3		34330.20			
2912.187	4	12 *l*	34328.40	−0.17	15_3— 497°_4	
2912.251	10	3	34327.66	−0.05	19535_5— 538°_5	
2912.756	15		34321.70	+0.02	27_4— 615°_4	
2913.412	3		34313.96	−0.14	17_3— 520°_3	
2913.973	7		34307.37	−0.01	23_2— 582°_1	
2914.204	6		34304.65	−0.05	27_5— 621°_5	
2915.040	10		34294.81	+0.01	28_6— 626°_6	
2915.118	12	2	34293.89	−0.09	14_2— 492°_2	
2915.210	5		34292.81	+0.07	19826_5— 541°_4	
2915.356	5		34291.10	0.00	19_3— 541°_4	
2915.395	1		34290.64	−0.04	22852_4— 571°_5	
2915.587	50	8	34288.38	−0.04	$^3H_6$— 512°_7	
2916.108	15	2	34282.25	+0.02	$^3H_6$— 512°_5	
2916.388	7		34278.96	−0.02	22852_4— 571°_3	
2917.295	20	1	34268.30			
2917.668	20	2	34263.92	+0.02	18_3— 532°_4	
2917.768	10	1	34262.74	−0.04	27_4— 614°_5	
2918.254	100	20	34257.03	−0.06	$^5D_4$— 404°_5	Res
2918.419	4		34255.10			
2919.288	30	2	34244.90	+0.02	$^3G_3$— 475°_3	
2919.685	6		34240.25	−0.20	22476_4— 567°_3	
2919.749	6		34239.50	−0.05	15_3— 496°_2	
2919.849	3		34238.33	+0.31	24_3— 588°_4	
2920.381	4		34232.09			
2921.13	20	3	34223.34	−0.16	$^3H_4$— 463°_3	
				+0.14	23_2— 582°_3	
2921.17	20	3	34222.87	−0.06	$^5S_2$— 525°_2	3
2921.633	4		34217.43	−0.08	23_6— 577°_6	

TABLE 3. *Observed and classified lines of* W I

Wavelength Å	Intensity		Wavenumber (cm^{-1})		Classification	Zeeman effect
	Arc	Spark	Observed	o−c		
2921.908	10	12 *s*	34214.21	+0.03	19_6— 538°_5	
2923.103	150	10	34200.23	−0.02	$^5D_3$— 390°_2	Res
2923.382	5	10 *s*	34196.95	−0.14	$^5S_2$— 524°_1	
2923.539	60	6	34195.12	+0.05	$^7S_3$— 371°_4	
2924.038	4		34189.28			
2924.515	2		34183.70	−0.02	17_4— 512°_5	
2924.664	3		34181.96			
2925.134	40	6	34176.47	−0.04	15_3— 496°_4	
2925.205	10		34175.64	−0.12	14_2— 491°_2	
2925.963	4	2	34166.79	−0.13	24_3— 587°_4	
2926.436	8	1	34161.27	−0.23	23_3— 580°_3	
2926.662	3		34158.62			
2926.990	40	10 *s*	34154.80	−0.12	17_3— 518°_4	
2927.378	3		34150.27	0.00	18_1— 522°_0	
2927.538	10	1	34148.40			
2927.812	3		34145.20			
2927.932	20	5	34143.80	+0.02	18_3— 531°_4	
2928.194	50	5	34140.75	−0.02	$^5D_2$— 374°_2	
2928.348	2		34138.95	−0.01	18_2— 522°_3	
2928.536	5		34136.76	−0.10	$^3P_2$—53390°_3	
2928.662	30	3	34135.29	+0.17	$^3G_3$— 474°_3	
				−0.14	$^3P_1$— 474°_2	
2928.762	2		34134.13	−0.05	19_4—53390°_3	
2928.986	20		34131.52	−0.08	19_3— 539°_2	
2930.154	40	4	34117.91	−0.08	$^3H_5$— 491°_5	
2930.931	3	1	34108.86	+0.08	23_2— 580°_3	
2932.044	12	1	34095.92	−0.04	14_2— 490°_3	
2932.215	10		34093.93	−0.04	$^3G_3$— 474°_2	
2932.669	6		34088.65			
2932.994	8		34084.87	0.00	19_3—53912°_2	
2933.592	2		34077.93	−0.09	$^3H_5$— 491°_4	
2933.769	2		34075.88	−0.17	23_6— 575°_5	
2934.129	7		34071.70	−0.10	29_7— 635°_6	
2934.297	2		34069.75	−0.04	18_1— 521°_2	
2934.996	250 *r*	50	34061.63	−0.04	$^5D_1$— 357°_2	
2935.358	8	25 *s*	34057.43	+0.18	15_3— 495°_2	
2935.629	30	3	34054.29	−0.04	15_3— 495°_3	
2936.009	50	5	34049.88	−0.14	$^5D_4$— 402°_3	
				+0.23	20_2—55032°_2	Res
2936.468	4		34044.56			
2936.66	40	12 *s*	34042.34	+0.11	13_2— 478°_1	
2937.142	60	15	34036.75	+0.07	19826_5— 538°_5	3
2937.20	8	15 *s*	34036.08	+0.30	18_2— 521°_2	
2937.464	2		34033.01	−0.21	24_3— 586°_3	
2937.606	10	12 *s*	34031.37	+0.01	$^3P_2$— 532°_2	
2937.677	8		34030.55	−0.14	$^3P_1$— 473°_2	
2937.774	2	4 *s*	34029.42	+0.21	18_3— 530°_2	
2938.104	2		34025.60	+0.18	22476_4— 565°_4	
2938.364	3		34022.59	0.00	19826_5— 538°_4	
2938.506	20	3	34020.95	0.00	19_3— 538°_4	

TABLE 3. *Observed and classified lines of* W I

Wavelength Å	Intensity		Wavenumber (cm^{-1})		Classification	Zeeman effect
	Arc	Spark	Observed	o−c		
2938.746	6	2	34018.17	−0.01	18_3— 529°_4	
2939.047	30 *r*	6	34014.68	+0.04	$^5D_4$— 402°_4	
2939.180	15	2	34013.15	−0.03	$^3G_3$— 473°_3	
2939.318	6		34011.55	−0.08	$^3G_3$— 473°_4	
2939.54	4 *b*		34008.98			
2940.954	12		33992.63	−0.04	17_3—51693°_2	
2941.023	3		33991.83	0.00	20_1— 544°_1	
2941.246	30	3	33989.26	+0.03	$^3G_3$— 473°_2	
2941.665	4		33984.42	−0.12	24_3— 585°_2	
2941.854	1		33982.23	+0.06	19_4— 532°_4	
2941.938	1		33981.26	+0.01	18_1— 520°_2	
2942.128	12	10 *s*	33979.07	+0.20	22852_4— 568°_4	
2942.452	25	3	33975.33	+0.01	$^5S_2$— 522°_3	
2942.618	3	10 *s*	33973.41	−0.06	$^3P_2$— 532°_1	
2943.006	4		33968.93	−0.04	18_3— 529°_3	
2943.326	20	2	33965.24	+0.07	17_4— 510°_3	
2943.966	12	1	33957.85	−0.04	15_3— 494°_3	
2944.398	300 *r*	60	33952.87	0.00	$^7S_3$— 369°_2	
2944.784	1		33948.42	−0.03	$^3P_1$— 472°_1	
2944.916	7	2	33946.90	−0.06	20_1— 543°_1	
2945.064	3		33945.20			
2945.224	6		33943.35	−0.01	$^3H_6$— 509°_6	
2945.691	8		33937.97	−0.04	19_4— 531°_5	
2946.344	8		33930.45			
2946.522	20		33928.40			
2946.782	5		33925.41			
2946.989	300 *r*	60	33923.02	−0.05	$^7S_3$— 368°_3	Res
2947.388	150 *r*	25	33918.43	−0.01	$^5D_3$— 387°_4	Res
2948.470	5		33905.98	−0.08	$^3H_4$— 460°_3	
2948.660	6		33903.80			
2948.921	5		33900.80			
2949.122	15	2	33898.49	+0.05	18_2— 520°_3	
2950.703	15 *b*		33880.33			
2951.076	5		33876.04	−0.09	20_2— 548°_2	
2951.226	4		33874.32			
2951.416	10	1	33872.14	0.00	$^5S_2$— 521°_2	
2951.795	20	2	33867.79	−0.01	20_1— 542°_0	
2951.950	1		33866.01	−0.05	24_2— 586°_2	
2952.091	1		33864.40	+0.07	22852_4— 567°_3	
2952.262	75	100 *s*	33862.44	+0.39	19_4— 531°_4	z d
2952.880	5		33855.35	+0.03	22476_4— 563°_3	
2952.974	4	4 *s*	33854.27	−0.17	24_2— 586°_3	
2953.788	4		33844.93			
2954.070	4	3 *s*	33841.71	+0.03	19_3— 536°_2	
2954.262	4		33839.51			
2954.904	35	5	33832.16	+0.11	18_3— 528°_3	(0)
2955.910	6		33820.65			
2956.076	4		33818.75			
2956.338	2		33815.76	+0.03	13_2— 475°_3	
2956.67	20	10 *s*	33811.96	+0.08	14_2— 487°_1	

TABLE 3. *Observed and classified lines of* W I

Wavelength Å	Intensity		Wavenumber (cm⁻¹)		Classification	Zeeman effect
	Arc	Spark	Observed	o−c		
2956.822	12	1	33810.22	+0.07	15_3 — 492°_2	
2957.501	25	5	33802.45	−0.01	17_4 — 509°_4	
2957.927	20	3	33797.58	+0.01	$^3H_6$ — 508°_5	(0)
2958.73	12		33788.41	−0.03	$^3P_2$ — 530°_1	
2958.846	10		33787.09	−0.02	17_4 — 50894°_3	
2959.40	3		33780.76			
2959.564	6		33778.89	−0.08	22476_4 — 562°_4	
2959.741	3		33776.87			
2960.146	60	6	33772.25	−0.05	$^3P_1$ — 470°_2	Res
2961.712	15		33754.39	0.00	$^3G_4$ — 501°_3	
2962.122	2		33749.72	+0.06	23_2 — 577°_3	
2962.206	3		33748.76			
2962.613	3		33744.13			
2963.284	2		33736.49	+0.04	19_4 — 529°_4	
2963.432	8		33734.80	0.00	$^5S_2$ — 520°_3	
2963.620	3		33732.66			
2963.782	10		33730.82	−0.02	$^3G_3$ — 470°_2	
2964.520	150	20	33722.42	+0.01	$^7S_3$ — 366°_2	Res
2965.860	12	2	33707.19	+0.05	$^3H_4$ — 458°_4	
2965.981	12		33705.81	−0.16	13_2 — 474°_3	
				+0.23	24_3 — 58316°_4	
2966.197	4		33703.36	−0.04	19535_5 — 532°_4	
2966.417	4	2 *s*	33700.86	−0.20	20_0 — 538°_1	
2966.575	35	5	33699.07	+0.01	17_4 — 508°_5	
2966.679	5		33697.88	−0.07	22476_4 — 561°_4	
				+0.02	24_2 — 584°_3	
2967.073	40	6	33693.41	−0.02	17_4 — 508°_3	
				0.00	19535_5 — 532°_6	
2967.438	8 *c*		33689.27	0.00	$^3P_0$ — 432°_1	
				−0.01	23_3 — 576°_3	
2967.554	35	4	33687.95	+0.01	15_3 — 491°_4	
2968.206	10		33680.55	−0.06	18_1 — 517°_1	
2968.358	6		33678.82	−0.25	18_3 — 526°_2	
2968.788	10	1	33673.95			
2969.618	60 *d*	6	33664.53	−0.29	13_2 — 474°_2	
				+0.33	23_6 — 571°_6	
2970.191	3		33658.04			
2970.977	5		33649.14	−0.16	22852_4 — 565°_4	
2971.203	10		33646.57	−0.03	18_2 — 517°_1	
2971.482	3		33643.42			
2971.675	40	6	33641.23	−0.04	$^5D_1$ — 353°_2	Res
2972.498	25	2	33631.92	−0.02	$^3P_2$ — 528°_2	
2972.922	50	8 *s*	33627.17	−0.01	$^3H_4$ — 457°_5	Res
2973.546	3		33620.07			
2973.792	3		33617.29			
2974.019	25	2	33614.72	−0.03	$^3H_5$ — 486°_6	
2974.261	6		33611.99	−0.14	15_3 — 490°_3	
2975.748	5		33595.19	+0.07	24_3 — 582°_3	
2976.074	6		33591.51			
2976.802	40	6	33583.30	+0.02	$^3G_3$ — 469°_4	
				+0.02	19535_5 — 531°_4	

TABLE 3. *Observed and classified lines of* W I

Wavelength Å	Intensity		Wavenumber (cm^{-1})		Classification	Zeeman effect
	Arc	Spark	Observed	o−c		
2977.106	60	12	33579.87	−0.01	19_6− 532°_6	3
2977.214	30	6	33578.65	+0.02	$^5D_2$− 369°_2	
2977.682	10		33573.37	−0.04	20_2− 545°_3	
2978.624	10		33562.76	+0.02	19_3−53390$^\circ_3$	3
2978.868	4		33560.01	−0.07	13_2− 473°_2	
2979.496	5		33552.93	−0.07	$^3P_2$− 528°_3	
2979.714	30	4	33550.47	+0.15	19_4− 528°_3	
2979.860	70 *r*	25	33548.83	0.00	$^5D_2$− 368°_3	7
2980.138	6		33545.70	−0.01	19_6− 531°_5	
2980.283	2		33544.07	−0.21	23_1− 569°_2	
2981.129	10		33524.55	−0.17	$^3G_4$− 499°_3	
2981.407	5		33531.42	−0.02	20_1− 539°_2	
2981.631	15	1	33528.90	0.00	18_3− 525°_2	
2981.762	3		33527.43	−0.15	27_4− 607°_5	
2982.606	40	8	33517.94	+0.08	19_4− 527°_5	Res
2982.810	10		33515.65	−0.08	$^3H_4$− 456°_3	
2984.140	40	4	33500.71	+0.08	$^5D_4$− 397°_4	Res
2984.264	3		33499.32	−0.03	$^3P_1$− 468°_2	
2985.254	2		33488.21			
2985.668	12	1	33483.57	−0.11	18_2−51693$^\circ_2$	
2985.884	12		33481.15	−0.05	17_3− 511°_2	
2986.185	12	2	33477.78	−0.06	13_2− 472°_1	
2987.608	5		33461.83	−0.10	18_3− 524°_4	
2987.960	15		33457.89	0.00	$^3G_3$− 468°_2	
2988.244	6		33454.71			
2988.502	4		33451.82			
2988.898	8		33447.39	−0.03	20_1− 538°_1	
2990.506	40	8	33429.41	+0.01	$^5D_3$− 382°_4	
2990.714	50	2	33427.08	0.00	$^5D_4$− 396°_3	
2991.946	10		33413.32	−0.05	$^5S_2$−51693$^\circ_2$	
2992.178	18	1	33410.73	0.00	19_3− 532°_4	
2992.931	16	1	33402.32	−0.06	19826_5− 528°_6	
2993.157	2		33399.80	−0.22	$^3P_2$− 526°_2	
2993.614	125 *r*	25	33394.70	−0.02	$^5D_4$− 396°_5	
2993.886	5		33391.67	−0.11	20_2− 543°_1	
2993.995	5		33390.45	−0.11	22476_4− 558°_4	
2994.107	5		33389.20	−0.16	$^3H_4$− 455°_3	
2995.258	60	12	33376.37	−0.01	$^5D_3$− 382°_3	
2995.514	10		33373.52			
2995.748	12	2	33370.91	−0.09	17_3− 510°_3	
2995.992	15	5	33368.19	−0.02	19826_5− 531°_5	3
2996.978	20	2	33357.22	−0.05	$^3G_4$− 497°_4	
2997.616	20	3	33350.12	−0.11	14_2− 483°_3	
2997.793	75	15	33348.15	−0.02	$^5D_2$− 366°_2	
2998.288	10	1	33342.64	−0.02	14_2− 483°_2	
2999.117	5		33333.43			
3000.163	5		33321.81	−0.02	22852_4− 561°_4	
3000.242	40	8	33320.93	−0.04	19535_5− 528°_6	
3000.439	30	1	33318.74	−0.06	22476_4− 557°_5	

TABLE 3. *Observed and classified lines of* W I

Wavelength Å	Intensity		Wavenumber (cm^{-1})		Classification	Zeeman effect
	Arc	Spark	Observed	o−c		
3000.882	3		33313.82			
3001.536	6		33306.57	−0.03	$^3P_1$ − 466°_0	
3001.625	1		33305.58	−0.24	23_6 − 567°_7	
3001.982	60	6	33301.62	−0.07	13_2 − 470°_2	Res
3002.418	4		33296.78			
3002.827	35	7	33292.24	−0.01	19826_5 − 531°_4	
3002.981	10		33290.54	−0.07	19_3 − 531°_4	
3003.824	5		33281.20	−0.09	18_3 − 522°_3	
3004.260	7		33276.37	−0.12	$^3G_3$ − 466°_4	
3005.010	35	3	33268.06	−0.05	14_2 − 482°_2	Res
3006.318	50	12	33253.59			
3006.658	20	1	33249.83	−0.02	$^3P_2$ − 525°_2	3
3007.135	5		33244.55			
3007.328	3		33242.42			
3007.411	15	5	33241.50	−0.02	20_1 − 536°_2	
3007.637	12		33239.01	−0.08	19535_5 − 527°_5	
3008.036	12		33234.63			
3008.502	4		33229.45			
3008.768	40	4	33226.52	0.00	29_7 − 626°_6	
3008.987	5		33224.10	+0.09	$^3P_2$ − 524°_1	
3009.086	80		33223.00	−0.05	$^5D_3$ − 380°_3	Res
3009.724	10		33215.96	−0.11	15_3 − 486°_4	
3010.418	20	4	33208.30	+0.01	17_3 − 509°_4	(0)
3010.495	15	3	33207.45	+0.01	19_6 − 528°_6	
3010.693	8		33205.27	+0.06	$^3G_4$ − 496°_4	
3011.682	20	2	33194.36	−0.01	14_2 − 481°_3	(b)
3011.816	3 *c*		33192.89	−0.05	17_3 − 50894°_3	
				+0.11	24_3 − 578°_4	
3013.192	30	3	33177.73	+0.10	17_4 − 502°_4	3
3013.442	1		33176.05	+0.01	19_3 − 530°_2	
3013.788	120	12	33171.17	+0.05	$^5D_3$ − 380°_4	Res
3014.200	6	3 *s*	33166.64	−0.01	19826_5 − 529°_4	
3014.348	2		33165.01	0.00	19_3 − 529°_4	
3016.272	3	1	33143.85	+0.01	18_2 − 512°_1	
3016.466	150	15	33141.72	+0.04	$^5D_4$ − 393°_5	Res
3016.685	8	2	33139.31	+0.05	19_4 − 523°_5	
3017.077	2		33135.01	−0.09	22852_4 − 559°_5	
3017.436	200	20	33131.07	+0.06	$^7S_3$ − 360°_4	Res
3017.617	5		33129.08	+0.03	$^3H_6$ − 501°_5	
3017.936	12		33125.58	+0.02	19_6 − 527°_5	
3018.304	1		33121.54	−0.04	24_3 − 577°_3	
3018.414	3		33120.34	+0.12	22476_4 − 555°_4	
3018.820	3		33115.88	+0.08	19_3 − 529°_3	
3020.040	5		33102.50	−0.06	22852_4 − 559°_4	
3020.214	15	3	33100.59	0.00	$^3H_4$ − 452°_4	3
3020.328	2		33099.35	+0.09	17_3 − 508°_3	
3021.206	3		33089.73	+0.16	18_3 − 520°_2	
3021.614	20	2	33085.26	−0.01	18_3 − 520°_4	
3021.734	4		33083.94	+0.04	28_6 − 614°_5	
3021.823	6		33082.97	−0.06	$^3G_4$ − 495°_3	

TABLE 3. *Observed and classified lines of* W I

Wavelength Å	Intensity		Wavenumber (cm^{-1})		Classification	Zeeman effect
	Arc	Spark	Observed	o−c		
3022.774	2		33072.56	+0.14	23_6— $565°_7$	
3023.152	12		33068.43	−0.02	$^3H_5$— $481°_5$	
3023.410	1		33065.60	+0.06	18_2— $511°_2$	
3023.646	12	3	33063.03	−0.01	29_7— $625°_6$	
3024.124	5		33057.79	−0.03	19_3— $528°_2$	
3024.590	1		33052.71	−0.12	20_6— $532°_1$	
3024.928	100	10	33049.01	−0.03	$^5D_1$— $347°_1$	
3025.263	50	5	33045.36	−0.07	$^3P_0$— $425°_1$	
3025.590	8		33041.72	−0.07	23_6— $565°_6$	
3025.685	6		33040.74	−0.03	18_3— $520°_3$	
3026.039	4		33036.88	−0.02	$^3G_3$— $463°_3$	
3026.672	50	10	33029.97	+0.03	19826_5— $528°_6$	
3026.788	50	10	33028.71	−0.03	13_2— $468°_2$	3
3026.962	10	2	33026.81			
3027.527	6		33020.64	−0.01	$^3P_1$— $463°_2$	
3027.792	30	3	33017.75	+0.03	17_3— $507°_2$	(0)
3027.902	2	1	33016.56	+0.06	23_2— $569°_2$	
3028.008	4		33015.40	+0.04	27_4— $602°_5$	
3028.094	3		33014.46	+0.02	22852_4— $558°_4$	
3028.651	1		33008.39	−0.09	24_3— $576°_3$	
3029.217	10		33002.22	−0.02	$^3P_2$— $522°_3$	
3030.354	12		32989.84			
3030.656	6		32986.55	−0.04	$^3G_4$— $494°_3$	
3030.840	8	1	32984.55	+0.02	$^3P_1$— $462°_1$	
3031.366	25	2	32978.82	−0.06	19_3— $528°_3$	
3031.584	2		32976.45	+0.19	20_2— $539°_2$	
3033.523	20		32955.38	+0.04	18_2— $510°_3$	(0)
3033.558	30		32955.00	+0.19	$^3H_4$— $451°_4$	
3034.054	2	1	32949.61			
3034.188	40	8	32948.16	+0.16	19826_5— $527°_5$	Res
3034.290	6		32947.05			
3034.516	4		32944.59	+0.09	27_4— $601°_4$	
3035.900	5		32929.58	+0.05	20_2—$53912°_2$	
3037.460	12	3	32912.67	+0.05	22476_4— $553°_3$	
3038.488	8	2	32901.53	+0.10	19535_5— $524°_4$	(0)
				−0.06	23_3— $568°_4$	
3038.708	25	3	32899.15	+0.09	$^3P_2$— $521°_2$	3
3039.312	50	10	32892.61			
3040.333	3		32881.56	−0.03	18_3— $518°_4$	
3041.730	25	3	32866.46	+0.06	15_3— $483°_3$	3
3041.863	80	20 *s*	32865.03	+0.07	$^5D_2$— $361°_1$	
3042.282	4		32860.50	+0.01	19535_5— $523°_5$	3
3042.416	15	2	32859.06	+0.04	17_4— $499°_3$	(0)
3042.717	2		32855.80			
3043.010	12	2	32852.64	+0.06	$^3H_4$— $450°_3$	
3043.800	150	25	32844.11	+0.03	$^5D_3$— $376°_3$	Res
3045.052	2		32830.61			
3045.473	2		32826.08	+0.18	19_3— $526°_2$	
3045.576	15	2	32824.96	+0.11	19_4— $520°_5$	(0)
3046.440	120	20	32815.65	+0.08	$^5D_1$— $344°_2$	Res

TABLE 3. *Observed and classified lines of* W I

Wavelength Å	Intensity		Wavenumber (cm^{-1})		Classification	Zeeman effect
	Arc	Spark	Observed	o−c		
3047.556	40	4	32803.63	+0.09	19_4 — 520°_4	3
3048.120	15		32797.57	+0.05	$^3P_1$ — 461°_1	7
3048.502	3		32793.46	+0.10	17_3 — 504°_2	
3048.657	20	4	32791.78	+0.08	$^5S_2$ — 510°_3	
3049.000	20	3	32788.10	−0.06	28_6 — 611°_7	(b)
3049.348	10		32784.36	+0.08	15_3 — 482°_2	
3049.688	120	20	32780.70	−0.03	$^7S_3$ — 357°_2	Res
3049.992	20	8 *s*	32777.43	+0.15	18_2—50894°_3	
3051.452	6		32761.75	+0.03	$^3P_2$ — 520°_3	
3051.838	10	2	32757.61			
3051.925	10	2	32756.68	+0.07	$^3G_4$ — 491°_5	
3052.816	10		32747.12	+0.16	19_6 — 523°_5	
3053.354	6	*s*	32741.34	−0.10	24_3 — 573°_3	
3054.008	50	5	32734.34	+0.. 0	$^3P_0$ — 422°_1	7
3054.376	5		32730.41			
3055.134	4	1	32722.26			
3055.384	30	3	32719.59	+0.13	$^3G_3$ — 460°_3	Res
3056.218	10	1	32710.67	+0.13	15_3 — 481°_3	
3056.787	2		32704.57	+0.20	24_3 — 573°_4	
3057.773	2		32694.01			
3057.836	1		32693.35	+0.09	22852_4 — 555°_3	
3058.104	3		32690.50			
3058.488	4		32686.39	+0.05	20_2 — 536°_2	
3058.733	8		32683.77	+0.17	18_2 — 508°_3	
3058.932	8		32681.65	+0.08	17_4 — 497°_4	
3059.474	4		32675.86	+0.13	19_3 — 525°_2	
3059.818	8		32672.19	+0.04	$^5D_1$ — 343°_1	
3059.990	3		32670.35			
3060.178	3	1	32668.34	−0.03	$^7F^\circ_0$—52057_1	
3060.448	5		32665.45			
3062.600	20	2	32642.51	−0.06	$^3G_4$ — 490°_5	(0)
3062.885	15	2	32639.47	+0.05	22852_4—55492°_5	(b)
3063.174	60	6	32636.39	+0.09	$^5D_3$ — 374°_2	Res
3063.560	15	2	32632.28	+0.01	18_3—51606°_2	
3064.140	10	1	32626.10	+0.09	18_3 — 516°_3	
3064.768	15	2	32619.41	+0.01	$^3H_5$ — 476°_4	
3064.927	60	6	32617.72	+0.08	$^5D_2$ — 359°_3	Res
3065.233	4		32614.47	+0.31	20_1 — 530°_1	
3065.303	5		32613.72	+0.08	$^5S_2$—50894°_3	
3065.606	8		32610.50	−0.10	22_6 — 553°_1	
				+0.10	19826_5 — 524°_4	
3065.861	6		32607.78	+0.03	13_2 — 463°_3	
3066.382	12		32602.25	−0.30	22852_4—55455°_5	
				+0.19	18_2 — 507°_2	
3066.602	5		32599.91	+0.05	19_4 — 518°_4	3
3067.722	6		32588.00			
3068.146	10	2	32583.51	+0.05	17_3 — 502°_4	(0)
3068.256	4	2	32582.33	+0.07	23_1 — 560°_2	
3069.460	20	2	32569.55	+0.09	19826_5 — 523°_5	
3069.720	5		32566.80	+0.14	22476_4 — 550°_4	

TABLE 3. *Observed and classified lines of* W I

Wavelength Å	Intensity		Wavenumber (cm^{-1})		Classification	Zeeman effect
	Arc	Spark	Observed	o−c		
3069.887	3	1	32565.03	0.00	27_5− 604°_6	
3070.910	12	1	32554.18	−0.07	23_3− 564°_3	
3071.302	5		32550.02	−0.02	13_2− 463°_2	
3071.512	3		32547.80	−0.06	$^7S_3$− 354°_3	
3071.678	5		32546.03	−0.05	19535_5− 520°_5	
3072.578	5		32536.50	0.00	22852_4− 553°_3	
3072.956	6		32532.51	−0.03	22476_4− 550°_5	
3073.276	120	6 *s*	32529.12	+0.01	$^5D_4$− 387°_4	Res
3073.692	20	2	32524.71	−0.06	19535_5− 520°_4	
3074.084	50	8 *s*	32520.56	+0.02	$^3G_3$− 458°_4	
3074.713	5		32513.91	−0.01	13_2− 462°_1	
3075.218	6		32508.57	−0.04	15_3− 479°_4	
3075.324	5		32507.45	−0.05	14_2− 474°_3	
3076.170	10		32498.51	−0.02	18_3− 514°_4	
3076.852	12	4	32491.31			
3078.717	3		32471.63	0.00	$^3H_5$− 475°_6	
3078.838	6		32470.36			
3079.032	15		32468.31	+0.17	$^7F^\circ_2$− 53_3	
3079.218	30	3	32466.35	0.00	14_2− 474°_2	3
3080.038	6		32457.70	+0.04	20_1− 528°_2	
3080.416	25		32453.72	+0.02	$^3P_1$− 457°_1	3
3080.696	20		32450.77	+0.05	18_1− 505°_1	3
3080.883	5		32448.80			
3081.368	12	1	32443.69	+0.02	19535_5− 519°_6	(0)
3081.862	30		32438.49	+0.07	$^5S_2$− 507°_2	3
3082.200	6		32434.94	+0.01	22476_4− 549°_4	
3082.417	1		32432.65	+0.10	19_6− 520°_5	
3082.842	5		32428.18	+0.06	19_3− 522°_3	
3083.227	1		32424.14	−0.08	22476_4− 549°_3	
3083.934	6		32416.71	0.00	18_2− 505°_1	
3084.220	12		32413.70			
3084.413	8		32411.67	−0.04	18_1− 504°_2	
3084.826	20	2	32407.33	0.00	17_4− 495°_3	
3084.910	25	2	32406.45	+0.02	$^5D_2$− 357°_2	
3085.113	2		32404.31	+0.01	23_1− 558°_1	
3085.340	10		32401.93	+0.01	23_3− 563°_3	
3086.973	40	4	32384.79	−0.01	$^3H_4$− 445°_5	Res
3087.180	3		32382.62			
3087.640	20		32377.79	+0.09	18_2− 504°_2	
3089.055	25	2	32362.96	+0.06	23_6− 558°_6	
3089.180	30	3	32361.65	+0.04	14_2− 473°_2	
3089.308	25	2	32360.31	+0.04	$^7S_3$− 353°_2	
3089.424	2		32359.10			
3089.974	2		32353.33	+0.11	$^3P_2$–51606°_2	
3090.088	10	1	32352.14			
3090.413	15	3	32348.75	+0.05	28_6− 607°_5	
3090.580	40	2	32347.00	+0.04	$^3P_2$− 516°_3	Res
3090.836	5	1	32344.31	+0.03	19_4− 516°_3	
3091.042	3	2	32342.17	+0.05	24_2− 571°_3	
3092.184	8	1	32330.21	+0.07	19_6− 519°_6	

TABLE 3. *Observed and classified lines of* W I

Wavelength Å	Intensity		Wavenumber (cm^{-1})		Classification	Zeeman effect
	Arc	Spark	Observed	o−c		
3092.280	15	2	32329.21	+0.08	$^3G_3$ — 456°_3	
3092.510	12	1	32326.81	−0.10	13_2 — 461°_1	
3092.676	3		32325.07	+0.13	19_3 — 521°_2	
3093.084	4		32320.81	−0.28	19535_5 — 518°_4	
3093.310	10	1	32318.45			
3093.500	100	10	32316.46	+0.10	$^5D_3$ — 371°_4	Res
3093.62	4		32315.21			
3094.026	15		32310.97	+0.08	17_4 — 494°_3	
3094.05		10	32310.72	+0.02	23_6 — 557°_5	(b)
3094.25	2		32308.63	+0.11	27_5 — 601°_4	
3094.757	5		32303.33	−0.04	20_0 — 524°_1	
3094.887	6		32301.98	+0.08	20_2 — 532°_2	
3094.98	2		32301.01	+0.17	29853_4 — 621°_5	
3095.051	4		32300.28			
3096.00	15		32290.37	+0.06	13_2 — 460°_3	
3096.414	10		32286.05	+0.24	$^7F^\circ_3$ — 55_4	
3096.498	10	1	32285.17	+0.11	$^3H_4$ — 444°_3	
3096.837	20	2	32281.65			
3097.053	4		32279.40	+0.03	14_2 — 472°_1	
3097.574	4		32273.97	+0.20	$^5D_1$ — 339°_2	
3098.436	30		32264.98	+0.13	17_3 — 499°_3	
3099.035	20		32258.75			
3101.427	3		32233.87	+0.13	19826_5 — 520°_4	
3101.580	10	1	32232.27	+0.17	19_3 — 520°_4	
3101.852	5		32229.45	+0.13	15_3 — 476°_4	
3102.654	6		32221.12			
3103.050	15	2	32217.01	+0.21	19_4 — 514°_4	
3103.321	4		32214.20	+0.14	$^5S_2$ — 504°_2	
3103.918	20		32208.00	+0.13	18_3 — 511°_2	
3104.088	8		32206.23	+0.19	23_6 — 556°_7	
3104.413	15		32202.87	+0.11	$^3G_3$ — 455°_3	
3105.876	40	8	32187.70	+0.10	19_3 — 520°_3	Res
3106.49	2		32181.36	−0.03	28_5 — 604°_6	
3107.227	100	10	32173.70	+0.08	$^5D_2$ — 354°_3	Res
3108.018	100	4	32165.51	+0.02	$^7S_3$ — 351°_4	Res
3108.128	3		32164.40	−0.24	23_1 — 556°_2	
3110.116	4		32143.82	+0.12	31_5 — 635°_6	
3111.036	4		32134.31			
3111.116	30	30	32133.49	+0.06	15_3 — 475°_3	
3111.578	3		32128.71			
3111.948	20		32124.89	+0.12	13_2 — 459°_2	
3113.656	5		32107.27	+0.07	23_3 — 560°_2	
3113.746	5	5	32106.35	+0.10	24_3 — 567°_3	
3113.876	8		32105.01			
3114.042	5		32103.29	+0.07	14_2 — 470°_2	
3114.58	15	2	32097.75	+0.08	18_3 — 510°_3	
3115.464	8		32088.64			
3115.59	3		32087.34	−0.06	17_3 — 497°_4	
3116.21	25	2	32080.96	+0.05	17_4 — 491°_5	
3116.333	20	2	32079.69	−0.06	22476_4 — 545°_3	

TABLE 3. *Observed and classified lines of* W I

Wavelength Å	Intensity		Wavenumber (cm^{-1})		Classification	Zeeman effect
	Arc	Spark	Observed	o−c		
3116.864	25	3	32074.23	+0.07	$^5D_3$ — 369°_2	
3117.38	15	1	32068.92	+0.06	18_2 — 501°_3	
3117.572	120	12	32066.95	+0.05	$^3P_1$ — 453°_1	
3118.346	20	2	32058.99	+0.01	20_2 — 530°_1	
3118.776	8		32054.57	+0.09	23_2 — 560°_2	
3119.237	5	12 *s*	32049.83	+0.02	27_4 — 592°_5	
3119.528	4	3	32046.84			
3119.762	50	5	32044.44	+0.08	$^5D_3$ — 368°_3	
3120.098	15	2	32040.99	+0.05	17_4 — 491°_4	
3120.18	60	6	32040.14	+0.07	$^5D_4$ — 382°_4	
3120.718	20	5	32034.62	+0.13	19_4 — 512°_5	
3121.146	2		32030.23	+0.17	19826_5 — 518°_4	
3121.794	8		32023.58	−0.09	15_3 — 474°_3	
3121.99	5		32021.57			
3122.455	4		32016.80			
3123.36	5	1	32007.52	+0.08	23_6—55492°_5	
3123.63	5		32004.76	+0.09	$^7F^\circ_4$—56768_5	
3124.11	4		31999.84	+0.05	$^3P_1$ — 453°_0	
3124.50	12	2	31995.84	+0.10	28_5 — 602°_5	
3124.722	15	2	31993.57	+0.07	$^7F^\circ_1$ — 52_1	
3125.063	3		31990.08			
3125.348	50	5	31987.16	+0.11	$^5D_4$ — 382°_3	Res
3125.46	20	2	31986.02	−0.01	$^5D_2$ — 353°_2	
3127.328	60	6	31966.91	+0.04	17_4 — 490°_5	Res
3127.498	8	1	31965.17	+0.04	17_4 — 490°_3	(0)
3127.946	3		31960.60	+0.14	20_2 — 529°_3	
3130.152	15	2	31938.07	+0.04	19535_5 — 514°_4	
3130.452	30	3	31935.01	+0.05	18_3 — 509°_4	
3130.994	5		31929.48	+0.12	23_1 — 553°_1	
3131.047	2		31928.94	+0.12	$^3P_2$ — 511°_2	
3131.183	4	1	31927.56	+0.09	24_2 — 567°_3	
3132.51	2		31914.03	+0.04	$^3G_3$ — 452°_4	
3132.593	25		31913.19			
3133.37	6		31905.27	+0.05	$^5S_2$ — 501°_3	
3133.633	6	2	31902.60	+0.12	20_2 — 528°_2	
3133.716	12		31901.75	+0.02	15_3 — 473°_3	
3133.884	80	8	31900.04	+0.06	13_2 — 456°_3	Res
3135.028	3		31888.40			
3136.07	40	4	31877.81	+0.03	15_3 — 473°_2	Res
3136.18		2	31876.69	+0.17	23_2 — 558°_1	
3136.584	20		31872.58	+0.04	$^7F^\circ_1$ — 51_2	
3137.224	4	8 *s*	31866.08	−0.09	19_3—51693°_2	
3137.416	4		31864.13			
3137.63	25	5	31861.96	+0.05	$^3H_5$ — 469°_4	
3137.912	15	2	31859.09	+0.05	$^3H_4$ — 440°_3	
3138.88	15		31849.27	+0.08	18_2 — 499°_3	
3139.422	12		31843.77	+0.07	$^5D_3$ — 366°_2	
3140.146	6		31836.43	−0.05	28_6 — 602°_5	
3140.411	30	3	31833.74	+0.02	$^5D_4$ — 380°_3	Res
3140.752	60	6	31830.29	+0.02	14_2 — 468°_2	Res

TABLE 3. *Observed and classified lines of* W I

Wavelength Å	Intensity		Wavenumber (cm⁻¹)		Classification	Zeeman effect
	Arc	Spark	Observed	o−c		
3141.174	12	1	31826.01	+0.08	18_3— 508°_3	
3141.420	100	10	31823.52	+0.07	$^3H_4$— 439°_4	Res
3141.898	5		31818.68	+0.06	$^3P_2$— 510°_3	(0)
3142.147	80	4	31816.16	+0.08	17_3— 495°_2	Res
3142.724	20 *b*		31810.31	+0.16	$^7F^\circ_4$—56573_5	
3143.215	25		31805.35	+0.09	20_1— 522°_0	
3144.415	3		31793.21	+0.12	22476_4— 542°_3	
3145.24	12	2	31784.87	0.00	$^3H_5$— 468°_5	
3145.54	50	5	31781.84	+0.05	$^5D_4$— 380°_4	
3145.804	3		31779.17	+0.07	19_3—51606°_2	
3146.034	3		31776.85			
3146.352	20	2	31773.64	+0.03	13_2— 455°_3	
3146.428	8		31772.87	+0.03	19_3— 516°_3	
3147.176	3		31765.32			
3147.547	4		31761.57			
3148.12	6		31755.79	+0.07	19535_5— 512°_5	
3149.252	2		31744.38	−0.01	18_3— 507°_2	
3149.747	1		31739.39	+0.15	$^3G_4$— 481°_3	
3150.46	2	1	31732.21			
3151.685	6	4 *v*	31719.87	−0.01	29_7— 611°_7	
3151.996	15	2	31716.74	+0.02	17_3— 494°_3	
3152.104	10		31715.66	+0.01	18_1— 497°_0	
3152.484	25	100 *s*	31711.84	−0.08	$^3P_1$— 450°_2	
3152.954	80	4	31707.11	+0.04	$^3G_4$— 481°_5	Res
3153.653	3		31700.08			
3154.172	5	10 *s*	31694.87	+0.20	24_2— 564°_3	
3154.762	8	2	31688.94	+0.06	$^3H_4$— 438°_3	
3155.09	60	6	31685.64	+0.09	$^5S_2$— 499°_3	Res
3155.52	25	5	31681.33	+0.02	$^7S_3$— 346°_4	
3156.59	3		31670.59	+0.13	$^3G_3$— 450°_2	
3158.16	15		31654.84			
3158.32	4		31653.24	+0.01	19_4— 509°_4	
3158.804	30	6	31648.39	+0.01	19_6— 512°_7	
3159.042	5	1	31646.00	+0.11	22_0— 544°_1	
3159.181	60	6	31644.61	+0.06	13_2— 454°_2	3
3159.418	10	2	31642.24	+0.14	22476_4— 541°_4	
3159.572	12	3	31640.70	+0.02	22476_4— 541°_3	
				+0.14	$^3P_2$—50894°_3	
3159.858	2		31637.83	−0.05	19_4— 508°_3	
3160.134	3		31635.07	−0.01	27_4— 588°_4	
3161.715	2		31619.25	−0.14	15_3— 470°_2	
3161.972	15		31616.68	−0.05	18_1— 496°_2	
3162.616	3		31610.24	−0.01	$^7F^\circ_3$— 54_3	
3163.416	80	15	31602.25	−0.04	$^3H_5$— 466°_6	2
3164.008	12	2	31596.34	+0.05	13_2— 453°_1	
3164.44	60	12	31592.03	+0.02	$^3G_3$— 449°_4	Res
3165.375	60	8	31582.69	−0.03	18_2— 496°_2	Res
3165.708	5		31579.37	−0.04	$^3H_4$— 437°_5	
3165.875	4	1	31577.71	+0.06	23_1—55032°_2	
3166.74	10	2	31569.08	+0.01	17_4— 486°_4	

318-092 O-69—8

TABLE 3. *Observed and classified lines of* W I

Wavelength Å	Intensity		Wavenumber (cm^{-1})		Classification	Zeeman effect
	Arc	Spark	Observed	o−c		
3167.272	10		31563.78	+0.03	24_3— 561°_4	
3167.585	30	5	31560.66	−0.06	27_5— 594°_6	
3168.674	1		31549.81	−0.02	19_4— 508°_5	
3168.976	15	2	31546.81	−0.07	$^3P_2$—50800°_3	(b)
3169.242	2		31544.16	−0.04	19_4—50800°_3	
3169.336	1		31543.22	−0.12	24_2— 563°_3	
3169.934	40	4	31537.27	−0.04	$^3G_4$— 479°_4	
3170.206	60	6	31534.57	0.00	$^7S_3$— 344°_2	(b)
3170.342	25	1	31533.21			
3171.643	15	1	31520.28	−0.11	20_2— 525°_2	
3173.114	4		31505.67			
3173.336	4		31503.46			
3176.533	6		31471.76	−0.07	15_3— 469°_4	
3176.601	150	15	31471.09	0.00	$^5D_1$— 331°_2	7
3177.20	30	120 *s*	31465.15	−0.19	$^3P_2$— 507°_2	
3177.25	5		31464.66	−0.03	19826_5— 512°_5	
3177.708	4		31460.12	+0.04	23_3— 553°_2	
3177.97	5		31457.53	+0.03	22852_4— 543°_5	
3178.256	25	2	31454.70	−0.05	$^5D_4$— 376°_3	
3179.06	80	8	31446.74	−0.03	17_3— 491°_4	
3179.17	4		31445.65			
3180.113	4		31436.33	−0.11	$^3H_5$— 465°_5	
3180.198	5		31435.49			
3180.31	20	2	31434.38	−0.05	18_1— 495°_2	
3180.745	60	10	31430.09	−0.02	$^3P_1$— 447°_1	3
3181.125	2	2	31426.33	−0.07	24_3— 560°_2	
3181.816	100	10	31419.51	−0.02	$^3G_4$— 478°_5	Res
3181.868	6		31418.99	−0.05	$^5S_2$— 496°_2	
3182.074	8		31416.96	+0.01	22852_4— 542°_3	
3182.167	4		31416.04	−0.08	23_3— 553°_4	
3182.66	6		31411.17	−0.01	23_6— 548°_6	
3182.86	60	6	31409.20	−0.08	14_2— 463°_3	Res
3183.045	4		31407.37	+0.01	23_2— 553°_2	
3183.514	30	2	31402.75	−0.04	$^7S_3$— 343°_3	
3183.752	20	2	31400.40	−0.02	18_2— 495°_2	
3184.05	50	5	31397.46	−0.04	18_2— 495°_3	
3184.418	120	12	31393.83	+0.03	$^5D_2$— 347°_1	
3185.206	25	3	31386.07	+0.03	22476_4— 538°_5	
3185.402	6	1	31384.14			
3186.743	15	3	31370.93	−0.03	17_3— 490°_3	
3186.971	8		31368.69			
3187.768	20	5	31360.84	−0.03	18_1— 494°_1	
3188.392	12	2	31354.71	+0.01	19_3— 511°_2	
3188.709	3		31351.59	+0.02	14_2— 463°_2	
3189.238	50	100 *s*	31346.39	−0.05	15_3— 468°_2	
3191.228	10	1	31326.84	−0.02	18_2— 494°_1	
3191.572	200	20	31323.47	−0.01	$^5D_0$— 313°_1	7
3191.732	8	2	31321.90	−0.01	27_5— 591°_4	
3192.266	8	1	31316.66	+0.04	$^3H_4$— 434°_3	(0)
3192.39	15	2	31315.44	−0.01	14_2— 462°_1	

TABLE 3. *Observed and classified lines of* W I

Wavelength Å	Intensity		Wavenumber (cm⁻¹)		Classification	Zeeman effect
	Arc	Spark	Observed	o−c		
3192.936	15	3	31310.09	−0.04	18_3— 502°_4	(0)
3193.624	4		31303.34	+0.02	19_6— 509°_6	
3193.856	30		31301.07	+0.01	18_2— 494°_3	(b)
3193.984	20	1	31299.81			
3194.546	25	1	31294.31			
3195.070	25	2	31289.17	−0.01	$^3P_1$— 445°_2	Res
3195.953	6	1	31280.53	−0.09	28_6— 596°_5	
3196.01	6	1	31279.97	−0.02	$^3P_2$— 505°_1	
3196.12	6	1	31278.90	−0.10	27_5— 591°_6	
3196.926	8	2	31271.01	−0.05	19535_5— 508°_5	3
3197.436	6		31266.02	+0.01	20_1—51693°_2	
3198.262	10		31257.95	−0.07	$^3G_4$— 476°_4	
3198.840	200	20	31252.30	0.00	$^5D_3$— 360°_4	Res
3199.314	15	1	31247.67	−0.05	$^3G_3$— 445°_2	
3199.816	4		31242.77	+0.05	$^3P_0$— 407°_1	
3199.877	4		31242.17	−0.03	$^3H_6$— 482°_7	
3199.966	30	6	31241.30	−0.01	13_2— 450°_2	3
3200.428	25		31236.79	+0.01	$^5S_2$— 495°_2	
3200.73	25	2	31233.85	−0.01	$^5S_2$— 495°_3	
3202.030	8		31221.17	+0.01	$^7F^\circ_1$— 51_0	
3202.21	6		31219.41	+0.01	17_4— 483°_3	
3203.055	40	4	31211.17	−0.02	18_3— 501°_3	3
3203.684	10		31205.05			
3205.502	25	2	31187.35	+0.02	18_1— 492°_2	(0)
3206.557	3		31177.09	+0.01	28_5— 594°_6	
3207.25	300	30	31170.35	−0.04	$^7S_3$— 341°_4	Res
3207.80	25	2	31165.01	−0.03	15_3— 466°_4	
3207.988	20	2	31163.18	−0.04	$^5S_2$— 494°_1	
3208.10	40	6	31162.09	−0.07	$^3G_4$— 475°_3	
3208.28	200	20	31160.35	+0.02	$^5D_2$— 344°_2	Res
3208.566	60	12	31157.57	+0.04	19_6— 508°_5	
3208.843	12		31154.88			
3209.008	12	2	31153.28	−0.04	18_2— 492°_2	
3210.31	3		31140.64			
3210.642	20	2	31137.42	0.00	$^5S_2$— 494°_3	
3210.922	1		31134.71	−0.23	31_5— 625°_6	
3211.422	5	1	31129.86	−0.02	$^3H_6$— 481°_5	
3211.837	6	1	31125.84	+0.02	19826_5— 509°_6	
3212.235	5		31121.98			
3213.136	12	3	31113.26	+0.09	$^5D_3$— 359°_3	
3214.23	10		31102.67	+0.03	27_4—58316°_4	
3214.666	6	1	31098.45	−0.01	$^3G_3$— 444°_3	
3215.146	8		31093.81			
3215.354	6		31091.79	−0.05	14_2— 460°_3	
3215.562	200	40	31089.78	−0.05	$^5D_4$— 373°_5	Res
3215.648		30 *s*	31088.95	−0.09	$^3H_4$— 432°_4	
3216.214	20	2	31083.48	+0.05	19826_5— 509°_4	
3216.99	4		31075.98			
3217.70	12		31069.13	+0.02	18_1— 491°_2	
3217.977	2		31066.45	+0.01	19_3—50894°_3	

TABLE 3. *Observed and classified lines of* W I

Wavelength Å	Intensity		Wavenumber (cm^{-1})		Classification	Zeeman effect
	Arc	Spark	Observed	o−c		
3218.444	3		31061.94			
3218.605	60	6	31060.39	−0.01	$^3P_1$ − 443°$_2$	Res
3219.054	10	2	31056.06			
3219.44	4	1	31052.33	−0.04	$^3G_4$ − 474°$_3$	
3220.06	30	3	31046.36	0.00	$^3P_1$ − 443°$_1$	
3221.11	4		31036.24	−0.03	$^3H_5$ − 461°$_6$	
3221.212	75	15	31035.25	+0.15	18$_2$ − 491°$_2$	7
3221.515	3		31032.34	+0.08	20$_2$ − 520°$_3$	
3221.617	25	4	31031.35	−0.02	17$_4$ − 481°$_5$	
3221.914	60	20 *s*	31028.49	−0.06	$^5D_2$ − 343°$_3$	Res
3222.67	8		31021.21			
3223.120	25	3	31016.88	−0.03	$^5D_2$ − 343°$_1$	(0)
3223.83	1		31010.05	+0.13	22852$_4$ − 538°$_5$	
3224.027	4		31008.16			
3224.968	1		30999.11	+0.01	27$_5$ − 588°$_4$	
3225.29	1	1	30996.01	+0.17	22852$_4$ − 538°$_4$	
3225.632	50	5	30992.73	−0.04	$^7S_3$ − 339°$_2$	Res
3225.743	3		30991.66	+0.14	18$_3$ − 499°$_3$	
3225.947	15	3	30989.70	+0.02	$^5S_2$ − 492°$_2$	3
3226.32	2		30986.12	+0.10	24$_3$ − 555°$_4$	
3226.413	2		30985.23	+0.01	27$_1$ − 586°$_2$	
3226.526	4	1	30984.14			
3226.793	4		30981.58	+0.05	23$_3$ − 549°$_4$	
3227.492	30	6	30974.87	−0.03	17$_3$ − 486°$_4$	
3229.227	3		30958.23	+0.02	23$_2$ − 549°$_1$	
3229.530	15	2	30955.32	+0.02	18$_2$ − 490°$_3$	
3229.641	20	10	30954.26	−0.02	28$_6$ − 593°$_7$	
3229.687	5		30953.82	−0.03	29$_7$ − 604°$_6$	
3231.297	2		30938.39	+0.12	28$_5$ − 591°$_4$	
3231.628	4		30935.23	+0.05	24$_3$ − 555°$_3$	
3231.954	6		30932.11	−0.03	$^3P_2$ − 501°$_3$	
3232.132	15	6 *s*	30930.40	−0.03	$^3G_4$ − 473°$_3$	
3232.23	8	1	30929.47	+0.01	19$_4$ − 501°$_3$	
3232.302	2		30928.77	−0.11	$^3G_4$ − 473°$_4$	
3232.487	80	8	30927.01	−0.02	$^5D_4$ − 371°$_4$	Res
3232.57	2		30926.21	−0.09	14$_2$ − 459°$_2$	
3232.654	60	12 *s*	30925.41	−0.04	15$_3$ − 463°$_3$	3
3233.24	4		30919.80	+0.02	23$_1$ − 543°$_1$	
3234.994	30	6	30903.04	−0.03	$^5D_2$ − 342°$_3$	Res
3235.108	15	2	30901.95	−0.01	$^5D_3$ − 357°$_2$	
3235.922	25	5	30894.18	+0.01	19535$_5$ − 504°$_6$	(b)
3236.486	4		30888.79			
3237.087	80	8	30883.06	0.00	$^3P_0$ − 404°$_1$	7
3237.786	10	2	30876.39	+0.04	23$_2$ − 548°$_2$	
3237.91	8		30875.21			
3238.118	5	3	30873.23			
3238.303	2		30871.47	+0.01	$^5S_2$ − 491°$_2$	
3238.496	50	5	30869.62	+0.03	$^7F°_3$ − 53$_3$	3
3238.69	12	2	30867.77	+0.03	15$_3$ − 463°$_2$	
3239.338	10	1	30861.60	−0.01	17$_4$ − 479°$_4$	3

TABLE 3. *Observed and classified lines of* W I

Wavelength Å	Intensity		Wavenumber (cm^{-1})		Classification	Zeeman effect
	Arc	Spark	Observed	o−c		
3240.966	2		30846.1			
3241.114	3	1 *b*	30844.69			
3241.408	20	4	30841.89	−0.01	$^7F^\circ_1$–50906$_1$	
3241.55	3		30840.54	−0.08	23$_1$– 542$^\circ_0$	
3242.026	100	10	30836.01	+0.01	$^7F^\circ_2$– 52$_3$	7
3242.554	3		30830.99			
3242.672	4	1	30829.87	−0.13	24$_2$– 556$^\circ_2$	
3243.122	6		30825.59	+0.07	23$_6$– 543$^\circ_5$	
3244.449	2		30812.99			
3245.01	4		30807.66			
3246.698	4		30791.64	−0.02	$^5S_2$– 490$^\circ_3$	
3247.436	15		30784.64	+0.02	14$_2$– 457$^\circ_1$	
3247.883	2		30780.41	+0.01	20$_2$– 517$^\circ_1$	
3248.031	2 *v*	3	30779.00	−0.28	24$_3$– 553$^\circ_2$	
3248.098	6		30778.37	−0.05	24$_3$– 553$^\circ_3$	3
3249.848	10	30 *s*	30761.80	+0.07	22476$_4$– 532$^\circ_4$	
3251.13	3		30749.67	+0.04	19535$_5$– 502$^\circ_4$	
3251.23	40	40 *s*	30748.72	−0.06	$^3H_4$– 429$^\circ_4$	
3251.744	6	8 *b*	30743.86	+0.03	17$_4$– 478$^\circ_5$	
3252.292	100	10	30738.68	−0.01	$^7F^\circ_3$– 53$_4$	7
3252.566	4	1	30736.09	−0.01	28$_6$– 591$^\circ_6$	
3252.64	15	2	30735.39	+0.07	24$_3$– 553$^\circ_4$	
3252.727	3		30734.57	+0.13	$^7F^\circ_2$– 52$_2$	
3254.360	50	5	30719.15	−0.06	$^3H_5$– 457$^\circ_5$	3
3254.526	12	2	30717.58	+0.01	22476$_4$– 531$^\circ_5$	
3254.660	6		30716.32	+0.05	$^5D_1$– 323$^\circ_0$	
3255.067	20		30712.48	+0.01	$^3P_2$– 499$^\circ_3$	
3255.23	2	2	30710.94	+0.11	20$_2$–51693$^\circ_2$	
3255.35	10	2	30709.81	+0.02	19$_4$– 499$^\circ_3$	
3255.957	60	20 *s*	30704.08	+0.08	$^3H_4$– 428$^\circ_5$	
3256.230	100	10	30701.51	0.00	14$_2$– 456$^\circ_3$	Res
3256.493	25	5	30699.03			
3258.140	12	2	30683.51	−0.03	$^5D_0$– 306$^\circ_1$	(0)
3259.434	60	6	30671.33	+0.11	18$_2$– 487$^\circ_1$	
3259.66	60	8	30669.20	+0.05	$^5D_3$– 354$^\circ_3$	
3259.778	12	2	30668.09	−0.03	$^3P_1$– 439$^\circ_2$	
3259.905	12	2	30666.90	+0.04	19$_3$– 504$^\circ_2$	3
3261.163	40	2	30655.07	+0.04	$^5D_4$– 368$^\circ_3$	
3262.586	1		30641.7	+0.09	22476$_4$– 531$^\circ_4$	
3262.676	3		30640.85			
3263.100	40	4	30636.87	+0.02	$^3G_3$– 439$^\circ_4$	Res
3264.19	6	1	30626.64	−0.02	$^3G_3$– 439$^\circ_2$	
3264.34	15		30625.24	+0.01	17$_3$– 483$^\circ_3$	
3265.06	4	1	30618.48	−0.05	$^5D_2$– 339$^\circ_2$	
3265.152	60	1	30617.62	+0.01	$^7F^\circ_4$– 55$_5$	
				−0.04	17$_3$– 483$^\circ_2$	
3266.073	12	1	30608.99	−0.05	$^7F^\circ_2$– 52$_1$	
3266.182	8		30607.97	−0.04	15$_3$– 460$^\circ_3$	
3266.620	40	4	30603.86	−0.04	$^7D^\circ_1$– 52$_1$	
3266.695	3		30603.16	+0.02	19826$_5$– 504$^\circ_6$	

TABLE 3. *Observed and classified lines of* W I

Wavelength Å	Intensity		Wavenumber (cm^{-1})		Classification	Zeeman effect
	Arc	Spark	Observed	o−c		
3266.766	30	6	30602.49	−0.05	19535_5− 501°_5	7
3266.970	3		30600.58	+0.08	24_2− 553°_2	
3267.603	2		30594.65	−0.07	24_2− 553°_1	
3268.124	12	2	30589.78	−0.01	13_2− 443°_2	
3268.574	25	12	30585.57	+0.05	$^3P_1$− 438°_1	
3268.924	40		30582.29	−0.03	17_4− 476°_4	
3269.622	50	10 *s*	30575.76	+0.01	13_2− 443°_1	
3269.694	4		30575.09	−0.05	14_2− 455°_3	
3270.266	60	6	30569.74	+0.01	$^7F^\circ_4$− 55_4	3
3271.634	8	1	30556.96	−0.06	28291_3− 588°_4	
3272.00	15	1	30553.54	+0.05	$^7F^\circ_2$–52002_3	
3273.12	20	2	30543.09	−0.02	17_3− 482°_2	
3273.154	3		30542.77	+0.02	18_3− 495°_2	
3273.474	15	1	30539.78	−0.05	18_3− 495°_3	
3274.616	10		30529.13			
3275.524	3		30520.67	+0.06	18_1− 486°_0	
3275.74	3		30518.66	+0.02	27_4− 577°_3	
3276.018	6	1	30516.07	+0.06	22476_4− 529°_4	
3276.532	5		30511.28	0.00	28_6− 589°_5	
3276.928	25	2	30507.59	+0.01	$^5S_2$− 487°_1	
3277.50	8		30502.27	−0.01	$^3G_3$− 438°_3	
3277.608	3	3 *v s*	30501.27	−0.03	28347_3− 588°_4	
3278.524	12	1	30492.74	+0.02	22852_4–53345°_3	
3278.924	12	20 *s*	30489.02	+0.01	19_6− 501°_5	
3279.03	30	3	30488.04	−0.04	$^7F^\circ_2$–51936_2	
3279.207	12	1	30486.39	−0.04	17_4− 475°_3	(0)
3279.578	40	4	30482.95	+0.01	$^7D^\circ_1$− 51_2	
3279.724	6		30481.59	+0.03	$^5D_3$− 353°_2	
3280.306	5 *b*		30476.18	+0.08	19_3− 503°_3	
3281.041	3	1	30469.35	−0.02	17_3− 481°_3	
3281.938	120	12	30461.03	−0.02	$^7F^\circ_1$− 50_2	Res
3282.196	15	2	30458.63	+0.03	19826_5− 502°_4	
3282.376	10		30456.96	0.00	19_3− 502°_4	
3283.554	50		30446.03	+0.03	$^3P_2$− 496°_2	
				−0.05	14_2− 454°_2	
3283.94	5		30442.45	−0.02	15_3− 459°_2	
3284.288	25	3	30439.23	0.00	$^3H_4$− 426°_3	(b)
3284.536	3		30436.93	+0.06	23_2− 544°_1	
3284.682	2		30435.58			
3285.02	12	2	30432.45	−0.01	24_3− 550°_4	
3285.992	15	2	30423.45	−0.04	$^3G_4$− 468°_5	
3286.177	1		30421.73	−0.06	24_3–55084°_2	
3287.125	2		30412.96			
3287.915	2		30405.65	+0.11	27_4− 576°_3	
3288.758	10		30397.86	+0.04	14_2− 453°_1	
3289.728	2		30388.90			
3290.043	2 *b*		30386.0	+0.39	22852_4− 532°_4	
3290.51	30	6	30381.68	−0.04	$^3H_5$− 454°_5	
3290.660	20	5	30380.29	+0.01	19_4− 496°_4	
3290.906	2		30378.02	+0.08	23_6− 538°_5	

TABLE 3. *Observed and classified lines of* W I

Wavelength Å	Intensity		Wavenumber (cm⁻¹)		Classification	Zeeman effect
	Arc	Spark	Observed	o−c		
3291.054	25	5	30376.65	−0.02	17_4— 474°_3	
3291.524	12	1	30372.32	+0.01	$^3G_3$— 437°_4	
3291.712	20		30370.58	−0.08	$^3H_4$— 425°_4	
3292.802	60	6	30360.53			
3292.938	20	2	30359.27	−0.08	20_0— 505°_1	
3293.070	6		30358.06	+0.04	19_3— 501°_3	
3293.712	80	12	30352.14	−0.04	$^3H_4$— 425°_3	
3293.946	3		30349.98			
3294.266	2		30347.04	+0.03	27_4— 575°_5	
3295.062	3	1	30339.71	+0.02	23_3— 542°_3	
3295.200	3	1	30338.43			
3295.564	8	1	30335.09			
3296.187	25 *b*	2 *b*	30329.35	−0.23	27_5— 581°_5	
				+0.11	28_5— 585°_5	
3298.130	60	6	30311.48	−0.03	19826_5— 501°_5	3
3298.507	2		30308.02	−0.10	28347_3— 586°_2	
3298.606	12	2	30307.11	−0.02	18_1— 483°_1	3
3298.937	3	4	30304.07			
3299.300	10	1	30300.73	0.00	24_3— 549°_4	
3299.660	6		30297.43	+0.01	22476_4— 527°_5	
3299.858	6		30295.61	−0.04	18_3— 492°_2	
3300.344	5	12 *s*	30291.15	+0.09	20_1— 507°_2	
3300.660	8	1	30288.25	−0.03	$^3H_4$— 424°_4	
3300.822	150	40	30286.77	−0.01	$^5D_3$— 351°_4	Res
3301.81	8		30277.7	+0.04	20_2— 512°_1	
3302.275	2		30273.44	+0.32	18_2— 483°_1	
3302.842	4		30268.24	+0.02	22_0— 530°_1	
3303.338	12	1	30263.70	0.00	$^3P_2$— 495°_2	
3303.660	8	1	30260.75	−0.03	$^3P_2$— 495°_3	
3304.250	3		30255.34			
3304.324	4	3 *s*	30254.66	−0.07	17_4— 473°_3	
3304.45	20		30253.5	−0.07	19535_5— 497°_4	
3304.482	20		30253.22	+0.04	17_4— 473°_4	
3305.570	25	2	30243.26	−0.03	13_2— 440°_3	(0)
3305.825	3		30240.93	−0.05	33_5— 635°_6	
3306.365	30	3	30235.99	−0.02	18_1— 483°_2	Res
3308.358	3	60 *s*	30217.77	+0.09	15_3— 456°_3	
3308.417	2		30217.24			
3308.76	1		30214.1	−0.24	23_1— 536°_2	
3309.258	2		30209.56	−0.01	18_2— 483°_3	
3309.478	30	3	30207.55	−0.03	$^3P_1$— 435°_2	Res
3310.083	5		30202.03	+0.03	18_2— 483°_2	
3310.246	2		30200.54			
3310.38	5 *b*		30199.3	−0.06	20_2— 511°_2	
3310.57	1		30197.6	+0.09	13_2— 439°_2	
3310.72	1		30196.2			
3310.994	1		30193.72	+0.02	$^3G_4$— 466°_4	
3311.118	25	5	30192.59	−0.03	$^3H_5$— 452°_4	
3311.388	200	40	30190.13	+0.04	$^7S_3$— 331°_2	Res
3311.552	5		30188.63	−0.07	23_3— 541°_4	

TABLE 3. *Observed and classified lines of* W I

Wavelength Å	Intensity		Wavenumber (cm^{-1})		Classification	Zeeman effect
	Arc	Spark	Observed	o−c		
3312.303	3		30181.79	0.00	18_1— 482°_0	
3312.776	3		30177.48	+0.05	18_3— 491°_2	
3313.226	6	5*b*	30173.38	−0.06	18_3— 491°_4	
3313.606	4		30169.92	−0.06	28_6— 585°_5	
3314.020	25	2	30166.15	+0.03	$^3G_3$— 435°_2	(b)
3314.538	15	2	30161.44	−0.02	18_1— 482°_2	
3315.090	80	4	30156.42	0.00	$^7F^\circ_5$— 56_6	(b)
3316.088	60	6	30147.34	0.00	$^5D_1$— 318°_2	
3316.91	10	5	30139.9	+0.01	22852_4— 529°_4	
				−0.05	28347_3— 584°_3	
3317.078	15	1	30138.34	−0.01	19_3— 499°_3	
3317.50	3		30134.5	−0.06	23_2— 541°_3	
3317.75	4	1	30132.2			
3317.996	40	4	30130.01	−0.01	$^3G_3$— 434°_3	Res
3319.664	8		30114.87	−0.04	13_2— 438°_1	
3320.257	8	1	30109.48	0.00	$^5S_2$— 483°_1	
3320.364	40	4	30108.52	−0.04	$^3P_0$— 396°_1	7
3320.664	2		30105.8	+0.09	20_1— 505°_1	
3321.140	25		30101.48	−0.03	19535_5— 496°_4	
				+0.05	27_4— 573°_4	
3321.45	2	1	30098.7			
3321.569	35	4	30097.59	−0.04	18_3— 490°_3	3
3322.256	80	8	30091.37	+0.06	15_3— 455°_3	
3322.504	12	1	30089.13	−0.03	20_2— 510°_3	
3322.856	2		30085.94	−0.04	28204_2— 582°_1	
3324.064	30	3	30075.01	−0.05	$^3G_4$— 465°_5	(0)
3324.280	4		30073.05	−0.08	13_2— 438°_3	
3324.696	20	4	30069.29	−0.08	27_5— 579°_6	(0)
3324.984	10		30066.68	−0.02	20_1— 504°_2	
3326.196	120	12	30055.73	−0.04	$^5D_4$— 362°_5	Res
3326.424	20	2	30053.67	−0.04	18_2— 481°_3	
3327.19	12	2	30046.75	−0.09	$^3H_5$— 451°_4	
3327.63	50	5	30042.78	−0.06	14_2— 450°_2	3
3328.124	60	6	30038.32	−0.04	$^5S_2$— 483°_2	3
3328.34	2		30036.4			
3329.135	4		30029.2	0.00	23_3—53912°_2	
3329.650	2		30024.55	−0.03	28291_3—58316°_4	
3330.53	15		30016.6	0.00	$^3P_2$— 492°_2	
3331.687	150	8	30006.19	−0.10	$^7S_3$— 329°_3	Res
3332.175	2		30001.8	0.00	28204_2— 582°_3	
3333.704	6	1	29988.04	−0.11	17_3— 476°_4	(0)
3334.606	5		29979.93			
3336.581	40	4	29962.18	−0.07	15_3— 454°_2	
3336.860	30	2	29959.68	−0.08	22476_4— 524°_4	3
3337.514	15*b*	1	29953.81	+0.05	22852_4— 528°_3	
				−0.05	27_5— 578°_4	
3337.690	60	6	29952.23	0.00	$^7D^\circ_2$— 53_3	(b)
3338.447	1		29945.44	−0.11	24_3— 545°_3	
3339.996	6	1	29931.55	−0.13	19_4— 491°_5	
3340.115	12		29930.48			

TABLE 3. *Observed and classified lines of* W I

Wavelength Å	Intensity		Wavenumber (cm⁻¹)		Classification	Zeeman effect
	Arc	Spark	Observed	o−c		
3340.206	3		29929.67	+0.01	$27_4 - 571^\circ_5$	
3341.146	3	1	29921.25	−0.05	$22852_4 - 527^\circ_5$	
3341.412	3		29918.87	+0.05	$22476_4 - 523^\circ_5$	
3341.446	1		29918.56	+0.01	$23_3 - 538^\circ_4$	
3342.28	2		29911.1	0.00	$20_2 - 50894^\circ_3$	
3343.246	50	2	29902.45	+0.01	$^3G_3 - 432^\circ_4$	
3343.696	3		29898.43	+0.05	$^3P_2 - 491^\circ_2$	
3343.852	20		29897.03	−0.03	$^7F^\circ_5 - 56573_5$	
3344.16	2		29894.3	+0.13	$^7F^\circ_4 - 54_3$	
3344.40	3		29892.1	−0.16	$17_3 - 475^\circ_3$	
3344.450	20	2	29891.69	−0.02	$19_4 - 491^\circ_4$	
3344.63	6		29890.1	+0.03	$^5S_2 - 481^\circ_3$	
3345.088	60	6	29885.99	−0.01	$29_7 - 593^\circ_7$	3
3345.858	100	80 *s*	29879.11	+0.01	$^3G_3 - 432^\circ_2$	
3346.114	40		29876.83	0.00	$^7S_3 - 328^\circ_4$	(0)
3346.66	5	5	29872.0	+0.12	$19_3 - 496^\circ_2$	
3346.81	3		29870.6	−0.04	$^3H_5 - 449^\circ_4$	
3348.496	5		29855.57	+0.08	$26_2 - 567^\circ_3$	
3349.538	6	1	29846.28	−0.02	$^3H_6 - 468^\circ_5$	
3351.202	15	8	29831.47	−0.09	$^7D^\circ_1 - 51_0$	(0)
3351.391	3	4	29829.78	−0.12	$23_1 - 532^\circ_2$	
3351.971	15	3	29824.62	−0.21	$17_4 - 469^\circ_4$	
3352.651	5	1	29818.57	−0.01	$^3P_2 - 490^\circ_3$	
3352.954	20	15 *s*	29815.88	+0.03	$^5D_2 - 331^\circ_2$	z d
				−0.02	$19_4 - 490^\circ_3$	
3353.554	30	3	29810.55	+0.07	$19826_5 - 496^\circ_4$	
3353.738	30	6	29808.91	+0.07	$19_3 - 496^\circ_4$	Res
3354.452	120	12	29802.57	−0.03	$^5D_3 - 346^\circ_4$	Res
				+0.03	$15_3 - 452^\circ_4$	
3356.241	4	2 *s*	29786.68	0.00	$28_6 - 581^\circ_5$	
3356.505	2		29784.33	+0.02	$29479_4 - 592^\circ_5$	
3356.712	15	2	29782.50	0.00	$17_3 - 474^\circ_3$	
3357.086	4		29779.18	+0.06	$22476_4 - 522^\circ_3$	
3357.892	3	2	29772.03	+0.02	$23_1 - 532^\circ_1$	
3360.63	2		29747.8	+0.01	$17_4 - 468^\circ_5$	
3360.740	6	1	29746.81	+0.03	$^3P_1 - 430^\circ_0$	
3361.104	40	100 *s*	29743.58	−0.06	$23_6 - 532^\circ_6$	
3361.364	20	2	29741.28	−0.07	$17_3 - 474^\circ_2$	Res
3361.852	15	2	29736.97	0.00	$13_2 - 435^\circ_2$	
3361.98	4	1	29735.8	−0.08	$20_2 - 507^\circ_2$	
3363.336	80	8	29723.85	+0.01	$^5D_4 - 359^\circ_3$	Res
3364.792	4	1	29710.98	−0.05	$27_5 - 575^\circ_5$	
3364.898	6	1	29710.05	+0.07	$^3H_4 - 418^\circ_4$	
3365.936	40	4	29700.89	+0.02	$13_2 - 434^\circ_3$	(0)
3367.214	15	2	29689.61	+0.03	$19_3 - 495^\circ_2$	(0)
3367.550	15	2	29686.65	−0.01	$19_3 - 495^\circ_3$	
3367.656	8	3	29685.72	−0.01	$28_5 - 579^\circ_6$	(0)
3369.680	20	2	29667.89	+0.02	$29_7 - 591^\circ_6$	(b)
3370.157	10	2	29663.69	−0.03	$^3H_6 - 466^\circ_6$	
3370.508	30	3	29660.60	+0.04	$17_3 - 473^\circ_3$	

TABLE 3. *Observed and classified lines of* W I

Wavelength Å	Intensity		Wavenumber (cm^{-1})		Classification	Zeeman effect
	Arc	Spark	Observed	o−c		
3370.691	12	2	29658.99	−0.02	17_3− 473°_4	
				+0.10	24_3− 542°_3	
3370.94	6	1	29656.8	+0.04	15_3− 451°_4	
3371.044	40	4	29655.88	+0.02	$^5D_3$− 344°_2	
3371.12	20*g*	4	29655.2	+0.06	$^3P_0$− 391°_1	
3371.352	50	5	29653.17	−0.02	$^5D_1$− 313°_1	
3373.231	20	2	29636.66	−0.05	$^3G_4$− 460°_3	
				+0.05	17_3− 473°_2	
3373.752	300	30	29632.08	+0.03	$^5D_2$− 329°_3	1
3374.574	3		29624.86	−0.04	30_2− 599°_2	
3375.112	40	4	29620.14	+0.04	14_2− 445°_2	
3375.361	4	2	29617.95	+0.10	27_4− 568°_4	
3376.898	20	1	29604.47	+0.06	22476_4− 520°_5	(0)
3378.515	40	4	29590.31	+0.09	19_3− 494°_3	Res
3378.728	5		29588.44	−0.12	28898_2− 584°_3	
3379.096	8		29585.22	+0.08	24_2− 543°_1	
3379.264	6		29583.75	+0.11	22852_4− 524°_4	
3380.032	4		29577.03			
3380.406	3		29573.75			
3381.725	40	4	29562.22	+0.04	$^3G_3$− 429°_4	
3382.086	30	3	29559.06	+0.05	15_3− 450°_2	
3382.598	50	40 *s*	29554.59	+0.06	15_3− 450°_3	
3384.332	80	8	29539.45	+0.07	19_6− 491°_5	
				−0.01	$^5S_2$− 478°_1	
3384.888	25	20 *s*	29534.60	+0.10	$^3P_2$− 487°_1	
3385.818	30	15	29526.48	+0.01	28_6− 579°_6	
3386.090	80	8	29524.11	+0.03	$^5D_3$− 343°_3	
3386.778	8	1	29518.11	+0.07	17_4− 466°_4	
3387.492	1		29511.89	+0.11	28291_3− 578°_4	
3387.93	3		29508.1	+0.20	24_3− 541°_4	
3388.116	6		29506.46	−0.02	24_3− 541°_3	
3388.822	150	6	29500.31	0.00	$^7F^\circ_2$−50949_1	
3389.10	5		29497.9	+0.03	$^3H_6$− 465°_5	
3389.82	3		29491.6			
3391.090	80	8	29480.58	+0.02	15_3− 449°_4	(b)
3391.520	80	8	29476.84	+0.01	$^3H_5$− 445°_5	
3392.204	6		29470.90	+0.06	14_2− 444°_3	
3392.25	1		29470.5	+0.14	26_2− 563°_3	
3392.462	2		29468.66	−0.20	28_5− 577°_6	
3392.820	12	3	29465.55	+0.10	27_5− 573°_4	(b)
3393.427	2		29460.28	−0.06	23_3−53390°_3	
3393.748	10	2	29457.49	+0.05	$^7F^\circ_2$−50906_1	3
3394.613	8	2	29449.99	+0.04	13_2− 432°_2	
3395.472	12	2	29442.54	+0.06	19_3− 492°_2	
3395.806	40	4	29439.64	+0.02	13_2− 432°_1	Res
3396.395	3		29434.54			
3396.850	6	1	29430.59	+0.11	23_1− 528°_2	
3397.455	8	1	29425.35	+0.01	19_6− 490°_5	
3398.089	50	5	29419.86	+0.02	19_4− 486°_4	3
3398.585	12	1	29415.57	+0.13	23_3−53345°_3	

TABLE 3. *Observed and classified lines of* W I

Wavelength Å	Intensity		Wavenumber (cm^{-1})		Classification	Zeeman effect
	Arc	Spark	Observed	o−c		
3400.453	5	1	29399.41	+0.05	17_4 − 465°_5	
3400.548	12	1	29398.59	−0.01	$^5D_3$ − 342°_3	
3400.859	6	1	29395.90	+0.20	33_5 − 626°_6	
3401.388	30	3	29391.33	+0.01	14_2 − 443°_2	
3402.758	12	2	29379.50	+0.08	22476_4 − 518°_4	
3402.895	4	1	29378.31	+0.09	17_3 − 470°_2	
3403.010	1		29377.32	+0.04	14_2 − 443°_1	
3403.370	5	1	29374.21			
3403.785	8		29370.63	−0.01	20_1 − 497°_0	
3404.216	30	3	29366.91	+0.07	18_2 − 474°_3	
3404.704	2		29362.70	−0.02	23_2 − 53345°_3	
3404.792	25	5	29361.95	−0.07	19826_5 − 491°_5	
3405.052	4		29359.70	0.00	18_1 − 474°_2	
3405.266	25	3	29357.86	+0.03	$^3G_4$ − 457°_5	
3405.952	25	2	29351.95	+0.05	18_3 − 483°_3	
3406.824	30	40 *s*	29344.43	+0.10	18_3 − 483°_2	z d
3407.244	2		29340.81	+0.15	32_4 − 614°_5	
3407.628	40	4	29337.51	+0.04	$^3H_4$ − 414°_3	(0)
3408.379	150	5	29331.05	+0.14	$^7F^\circ_3$ − 52_4	
3408.770	5		29327.68	−0.02	24_2 − 541°_3	
3409.003	12		29325.67	−0.02	18_2 − 474°_2	
3409.164	5	1	29324.29	+0.03	19_3 − 491°_2	
3409.432	20	3	29321.99	+0.08	19826_5 − 491°_4	
3409.608	12	1	29320.47	−0.02	$^3H_5$ − 443°_6	
3410.483	15	2	29312.95	−0.01	$^5S_2$ − 475°_3	
3410.872	40	4	29309.61	+0.01	28_6 − 577°_6	
3411.008	12	1	29308.44	+0.11	23_3 − 532°_4	
3411.780	2		29301.81	+0.14	24_3 − 53912°_2	
3411.997	5	1	29299.95	−0.03	29_7 − 587°_6	
3412.078	12	2	29299.25	+0.07	27_5 − 571°_6	
3412.736	3	30 *s*	29293.60	−0.08	27_5 − 571°_5	
3412.956	80	8	29291.71	+0.03	$^5D_3$ − 341°_4	
3413.410	4	1	29287.82	+0.08	$^5D_4$ − 355°_5	
3413.528	80	15	29286.80	+0.07	$^7S_3$ − 322°_3	Res
3414.336	5		29279.87	+0.05	$^5D_4$ − 354°_3	
3415.016	3		29274.04			
3415.288	5	1	29271.71	−0.01	20_1 − 496°_2	
				−0.05	28347_3 − 576°_3	
3415.406	4	6 *s*	29270.70	+0.19	27_4 − 564°_3	
3415.548	20	2	29269.48	−0.02	20_0 − 494°_1	(0)
3415.908	5	1	29266.40	+0.01	$^3P_1$ − 425°_1	
3417.508	6		29252.70	+0.07	$^3G_3$ − 426°_3	
3418.07	2		29247.9	+0.06	19826_5 − 490°_5	
3418.241	10		29246.42	+0.04	$^3G_4$ − 456°_3	
3418.456	20	4	29244.59	+0.13	19_3 − 490°_3	Res
3419.170	3		29238.48	+0.12	28_5 − 574°_4	
3419.277	30	4	29237.56	+0.11	$^7F^\circ_3$ − 52_3	7
				−0.19	24_3 − 538°_4	
3420.075	3	2	29230.74	+0.08	17_3 − 469°_4	
3420.348	25	2	29228.41	+0.12	22852_4 − 520°_5	

TABLE 3. *Observed and classified lines of* W I

Wavelength Å	Intensity		Wavenumber (cm^{-1})		Classification	Zeeman effect
	Arc	Spark	Observed	o−c		
3421.216	3		29221.00	+0.05	18_2 — 473°_2	
3422.415	100	10	29210.76	+0.05	$^7F^\circ_4$ — 53_5	(b)
3422.849	8	1	29207.05	+0.07	22852_4 — 520°_4	
3423.110	1		29204.83			
3423.293	20	4	29203.27	+0.07	$^5S_2$ — 474°_3	
3423.834	10	1	29198.65	+0.09	23_1 — 526°_2	
3424.127	3		29196.15	+0.11	18_3 — 481°_3	
3424.816	10	2	29190.28			
3424.909	5	1	29189.49			
3425.044	10	2	29188.34	+0.13	23_3 — 531°_4	
3425.538	25	3	29184.13	+0.07	$^3G_3$ — 425°_4	Res
3426.881	8	1	29172.69	−0.03	18_1 — 472°_1	3
3427.580	20	3	29166.74			
3427.710	80	10	29165.63	+0.05	$^3G_3$ — 425°_3	Res
3428.131	12	1	29162.05	0.00	$^5S_2$ — 474°_2	
3428.530	6		29158.66			
3429.128	2	1	29153.57	+0.06	$^7F^\circ_4$ — 53_3	
3429.592	100	20	29149.63	−0.04	19535_5 — 486°_6	7
3430.255	30	6	29144.00	+0.08	$^7D^\circ_3$ — 55_4	
3430.426	15	1	29142.54	+0.04	$^3P_1$ — 424°_2	
3430.871	15	5	29138.76	+0.05	18_2 — 472°_1	
3432.578	2		29124.27	+0.07	28347_3 — 574°_4	
3432.625	2		29123.87	+0.03	22476_4 — 516°_3	
3433.074	12	1	29120.07	+0.06	$^3G_4$ — 455°_3	
3433.774	40	4	29114.13	+0.07	$^5D_3$ — 339°_2	(0)
3434.814	4		29105.31	+0.04	17_3 — 468°_2	
3435.235	20	2	29101.75	+0.07	$^3G_3$ — 424°_4	(0)
3435.710	30	6 *s*	29097.73	+0.03	$^3H_6$ — 461°_6	z d
3436.716	2		29089.21	−0.21	20_1 — 495°_2	
3437.133	6		29085.68	+0.08	24_2 — 538°_1	
3437.574	4		29081.95	+0.14	28_5 — 573°_4	
3437.654	2		29081.27	+0.01	$^5S_2$ — 473°_2	
3438.191	20	2	29076.73	+0.14	$^7F^\circ_2$ — 50_2	
3438.808	50	5	29071.51	+0.06	$^7D^\circ_1$ — 50_2	(b)
3438.954	15	5	29070.28	+0.11	19_4 — 483°_3	(b)
3439.372	10	1	29066.74	+0.11	27_4 — 562°_5	(b)
3439.542	3		29065.31	+0.03	$^3P_2$ — 483°_2	
3439.991	15	3	29061.51			
3440.340	5		29058.57	+0.09	24_3 — 536°_2	
3440.426	6		29057.84			
3440.482	4		29057.37	+0.06	$^5S_2$ — 473°_2	
3441.31	2		29050.4	+0.08	29853_4 — 589°_5	
3441.962	25	5	29044.87	+0.05	14_2 — 440°_3	Res
3442.311	8	4	29041.93	+0.10	27_4 — 562°_4	
3442.998	80	8	29036.13	−0.01	19_6 — 486°_6	Res
3443.687	3	2	29030.33			
3444.224	3	1	29025.80	+0.05	31_5 — 604°_6	
3444.598	30	3	29022.65	+0.10	23_1 — 524°_1	
				+0.04	$^7F^\circ_4$ — 53_4	
3444.874	1		29020.32	−0.02	$^3G_4$ — 454°_5	

TABLE 3. *Observed and classified lines of* W I

Wavelength Å	Intensity		Wavenumber (cm^{-1})		Classification	Zeeman effect
	Arc	Spark	Observed	o−c		
3445.395	15	2	29015.93	+0.07	20_1 − 494°_1	
3445.710	30	6	29013.28	+0.03	$^5D_1$ − 306°_1	3
3446.888	12	3	29003.37	+0.07	22852_4 − 518°_4	3
3447.566	2		28997.66	−0.02	26_2 − 558°_1	
3447.712	8	1	28996.43	−0.14	18_1 − 470°_2	(b)
3447.984	15	4	28994.15	+0.04	18_3 − 479°_4	(b)
3448.208	40	10	28992.26	+0.01	$^7D^\circ_2$ − 52956_1	
3448.381	4		28990.81	+0.08	$^3P_2$ − 482°_2	
3448.826	50	8	28987.07	+0.06	15_3 − 444°_3	
3449.302	12	2	28983.07	+0.06	20_2 − 499°_3	
3449.437	8	1	28981.93	+0.06	27_5 − 568°_4	
3450.118	2		28976.21			
3450.246	2		28975.14	+0.07	$^5S_2$ − 472°_1	
3450.442	3		28973.49	+0.01	26_2 − 558°_2	
3451.136	6		28967.67	+0.02	28347_3 − 573°_4	
3451.739	50	5	28962.61	+0.05	18_2 − 470°_2	
3451.956	12	1	28960.79	+0.11	23_2 − 529°_3	
				−0.02	27_4 − 561°_4	
3452.616	30	3	28955.25	+0.05	$^3P_1$ − 422°_1	
3455.918	2	1	28927.58	0.00	28204_2 − 571°_3	
3456.358	10	1	28923.90	+0.01	17_3 − 466°_4	
3457.238	3	1	28916.54	+0.10	14_2 − 438°_1	
3457.360	20	3	28915.52	+0.04	$^3H_5$ − 439°_4	
				−0.02	28_5 − 571°_6	
3457.489	5	1	28914.44	+0.13	19_4 − 481°_3	
3457.713	60	12	28912.57	+0.08	$^5D_2$ − 322°_3	1
3457.838	4		28911.52			
3458.006	4	1	28910.12	+0.08	28_5 − 571°_5	
3458.310	25	5	28907.58	+0.09	15_3 − 443°_2	Res
3458.855	3		28903.02	+0.07	$^3G_3$ − 422°_3	
3458.995	8	1	28901.85			
3459.516	30	5	28897.50	+0.05	$^5D_4$ − 351°_4	Res
3460.036	2		28893.16			
3460.460	1		28889.62	+0.09	$^7F^\circ_3$ − 51_2	
3461.012	2		28885.01			
3461.354	15	3	28882.16	+0.02	19_4 − 481°_5	
3461.642	2	2	28879.75	+0.05	24_2 − 536°_2	
3461.802	15		28878.42	+0.04	$^7P^\circ_4$ − 56768_5	
3461.870	2		28877.85			
3462.248	4		28874.70	+0.04	14_2 − 438°_3	
3462.850	2		28869.68			
3463.247	50	5	28866.37	+0.03	$^7S_3$ − 318°_2	Res
3464.668	1		28854.53	+0.21	$^3H_5$ − 439°_5	
3465.114	1		28850.82	+0.01	29479_4 − 58330°_4	
3465.206	2		28850.05	+0.01	19826_5 − 486°_4	
3465.399	6		28848.44	+0.04	19_3 − 486°_4	
3466.136	3	1	28842.31	−0.01	20_1 − 492°_2	
3466.407	6		28840.06	−0.04	31_5 − 602°_5	
3466.650	4	1	28838.03			
3466.741	1		28837.28	+0.14	29479_4 − 58316°_4	

TABLE 3. *Observed and classified lines of* W I

Wavelength Å	Intensity		Wavenumber (cm^{-1})		Classification	Zeeman effect
	Arc	Spark	Observed	o−c		
3467.460	4	1	28831.30	+0.06	$^3G_4$ − 452°$_4$	
3467.663	3		28829.61			
3467.876	15	3	28827.84	+0.06	$^3P_0$ − 383°$_1$	7
3468.398	40	4	28823.50	+0.02	13$_2$ − 426°$_3$	(0)
3469.534	3		28814.06	+0.01	22476$_4$ − 512°$_5$	
3470.932	2		28802.46			
3471.111	3	1	28800.97			
3471.350	8	1	28798.99	+0.07	$^5S_2$ − 470°$_2$	
3472.957	4	1	28785.67			
3474.928	1		28769.34	+0.10	31$_5$ − 601°$_4$	
3475.823	40	8	28761.93	+0.06	$^3H_4$ − 409°$_3$	z d
				−0.16	17$_4$ − 458°$_4$	
3476.496	30	8 *s*	28756.36	+0.08	28$_6$ − 571°$_6$	7
3477.170	4		28750.79	+0.01	28$_6$ − 571°$_5$	
3477.262	8	1	28750.03	+0.01	$^3H_4$ − 409°$_5$	
3477.536	1		28747.76	+0.04	22852$_4$ − 516°$_3$	
3477.943	80	8	28744.40	0.00	$^7F°_5$ − 55$_6$	7
3478.702	4		28738.13			
3478.906	8		28736.44	+0.01	13$_2$ − 425°$_3$	
3479.121	5	1	28734.67	+0.03	24$_3$−53345°$_3$	
3480.405	1		28724.07	−0.03	20$_1$ − 491°$_2$	
3480.453	10	2	28723.67	+0.05	18$_1$ − 468°$_2$	(0)
3481.320	8	2	28716.52	−0.02	20$_2$ − 496°$_2$	3
3481.520	1	3	28714.87	+0.05	18$_3$ − 476°$_4$	
3481.816	40	4	28712.43	+0.05	19$_4$ − 479°$_4$	3
3482.428	2	1	28707.38	−0.04	28291$_3$ − 569°$_2$	
3482.765	20	2	28704.60	+0.08	$^7F°_5$ − 55$_5$	(b)
3483.60	1		28697.7	+0.10	23$_1$ − 521°$_2$	
3484.580	2		28689.65	+0.04	18$_2$ − 468°$_2$	
3485.208	2		28684.48	+0.20	17$_3$ − 463°$_3$	
3485.278	15	1	28683.91	+0.05	$^7P°_4$−56573$_5$	
3485.490	30	3	28682.16	+0.03	17$_4$ − 457°$_5$	7
3486.785	4	1	28671.51	−0.01	$^3P_1$ − 419°$_2$	
				+0.07	$^3H_5$ − 437°$_5$	
3487.142	2		28668.57			
3488.407	4		28658.18	+0.04	$^3P_1$ − 419°$_0$	
3488.590	3	2	28656.67	+0.03	$^7F°_5$ − 55$_4$	
3489.12	1		28652.3	0.00	27$_5$ − 565°$_4$	
3489.280	20	2	28651.01	+0.07	$^3H_5$ − 437°$_4$	7
3491.38	2		28633.8	−0.06	29853$_4$ − 584°$_3$	
3491.827	15	1	28630.11	+0.05	$^3G_3$ − 419°$_2$	
3492.132	3		28627.61	+0.08	24$_3$ − 532°$_4$	
3492.250	4	1	28626.64	+0.07	17$_3$ − 463°$_2$	
3493.025	8	2	28620.29	+0.05	22852$_4$ − 514°$_4$	
3493.187	10	1	28618.96	+0.03	18$_3$ − 475°$_3$	3
3493.803	3	1	28613.92	+0.06	20$_0$ − 487°$_1$	
3494.364	1		28609.33	+0.27	23$_1$ − 520°$_2$	
3494.752	4		28606.15			
3495.082	3		28603.45	+0.08	19535$_5$ − 481°$_5$	
3495.236	75	15	28602.19	+0.03	19$_6$ − 482°$_7$	Res

TABLE 3. *Observed and classified lines of* W I

Wavelength Å	Intensity		Wavenumber (cm^{-1})		Classification	Zeeman effect
	Arc	Spark	Observed	o−c		
3495.683	2		28598.53	+0.30	28_5— 568°_4	
3495.927	3		28596.53	+0.22	23_6— 520°_5	
3496.154	3	1	28594.68	+0.08	19_4— 478°_5	
3498.760	3		28573.38	+0.05	23_3— 525°_2	
3499.620	15	2	28566.36	−0.02	$^3P_2$— 478°_1	
3500.272	40	8	28561.04	+0.05	15_3— 440°_3	Res
3500.905	3		28555.87	+0.01	24_2—53345°_3	
3502.88	2		28539.77	−0.02	28291_3— 568°_4	
3503.030	30		28538.55	+0.05	14_2— 435°_2	3
3503.554	20	1	28534.28	+0.04	20_2— 495°_2	
3503.909	4	1	28531.39	+0.07	20_2— 495°_3	
3504.244	4	1	28528.67	+0.15	26_2— 553°_2	
3504.57	2	2	28526.0	+0.03	$^5S_2$— 468°_2	
3504.643	15	2	28525.42	+0.02	15_3— 439°_4	(0)
3504.886	3		28523.44	+0.06	$^3G_3$— 418°_4	
3505.240	1		28520.56	−0.05	23_2— 525°_2	
3505.897	2		28515.21	0.00	15_3— 439°_2	
3506.634	20	2	28509.22	+0.05	18_3— 474°_3	3
				−0.04	$^3G_4$— 449°_4	
3506.85	3*b*		28507.47	+0.06	24_3— 531°_4	
3507.277	30	3	28503.99	+0.10	$^3H_4$— 406°_3	(0)
3507.918	6		28498.79	+0.06	19_3— 483°_3	
3508.352	2*b*		28495.26	0.00	24_2— 532°_2	
3508.732	40		28492.17	+0.07	$^5D_2$— 318°_2	
3508.849	8		28491.22	+0.06	19_3— 483°_2	
3509.011	20	2	28489.91	+0.07	19_6— 481°_5	
3509.374	3		28486.96	+0.06	22_0— 512°_1	
3509.661	10	1	28484.63	+0.04	13_2— 422°_1	
3510.025	200	20	28481.68	+0.06	$^7S_3$— 314°_4	Res
3511.666	3	2	28468.37		$^7D^\circ_3$— 54_3	
3511.718	3	2	28467.95	−0.07	18_3— 474°_2	
3512.613	8	1	28460.70	+0.02	20_2— 494°_1	
3512.911	3	1	28458.28	+0.09	29_7— 579°_6	
3513.51	2	2	28453.43	+0.07	28898_2— 573°_3	
3514.196	3		28447.88			
3514.633	6	1	28444.34	+0.03	17_4— 455°_3	
3514.775	8	2	28443.19	+0.04	$^3H_6$— 454°_5	(0)
3515.797	6	1	28434.92	+0.04	20_2— 494°_3	
3515.955	12	2	28433.64	+0.03	19535_5— 479°_4	(0)
3516.018	3		28433.13	+0.04	19_4— 476°_4	
3516.352	1		28430.43	−0.22	27_5— 562°_5	
3516.771	10	1	28427.05	+0.02	$^3P_1$— 417°_2	
3517.502	30	3	28421.14	+0.03	$^3H_4$— 405°_4	
3518.055	5	1	28416.67	+0.06	19_3— 482°_2	
3518.473	40	4	28413.30	+0.03	$^5D_4$— 346°_4	
3519.394	3	1	28405.86	+0.01	27_5— 562°_4	
3520.374	1		28397.95	+0.05	28_6— 567°_7	
3521.014	1		28392.80	−0.04	24_3— 530°_2	
3521.706	20	2	28387.21	−0.02	18_3— 473°_3	
3521.907	40	4	28385.59	+0.02	$^3G_3$— 417°_2	Res

TABLE 3. *Observed and classified lines of* W I

Wavelength Å	Intensity		Wavenumber (cm^{-1})		Classification	Zeeman effect
	Arc	Spark	Observed	o−c		
3522.367	3		28381.89	+0.08	24_3 — 529°_4	
3523.446	3		28373.19			
3524.236	15	1	28366.83	−0.01	17_3 — 460°_3	3
3524.674	6		28363.31	+0.03	18_3 — 473°_2	
3525.050	2		28360.28	+0.06	20_1 — 487°_1	
3526.850	30		28345.81	+0.03	$^3G_3$ — 416°_3	
3526.995	30		28344.64	0.00	17_4 — 454°_5	
3527.210	6	2	28342.92	+0.05	19_3 — 481°_3	
3527.588	8	2	28339.88	0.00	$^3P_2$ — 475°_3	
3527.920	10		28337.21	+0.01	19_4 — 475°_3	(0)
3528.490	6	1	28332.64	+0.04	24_3 — 529°_3	
3528.897	5		28329.37	−0.02	22476_4 — 508°_5	
3529.350	6		28325.73	+0.01	23_3 — 522°_3	
				+0.01	29853_4 — 581°_5	
3529.594	10		28323.77	+0.01	22476_4 — 508°_3	
3529.955	3		28320.88			
3530.581	8	1	28315.86	+0.03	19535_5 — 478°_5	
3530.754	20	3	28314.47	+0.01	$^3H_4$ — 404°_5	
3531.018	12	2	28312.35	+0.01	19826_5 — 481°_5	
3531.126	6		28311.49	+0.11	$^5D_3$ — 331°_2	
3533.80	1 *b*		28290.06	+0.22	263°_2 — 54_3	
3533.922	1		28289.09			
3534.165	4		28287.14	0.00	20_2 — 492°_2	
3534.543	1		28284.12	−0.12	31_5 — 596°_5	
3535.254	3	3	28278.43	+0.03	27_4—55492°_5	
				+0.01	28_1 — 569°_2	
3535.539	100	20	28276.15	+0.05	$^3P_1$ — 415°_2	Res
3536.024	2		28272.27			
3536.486	6		28268.58	−0.04	18_2 — 463°_3	
				−0.08	28_5 — 565°_4	
3537.156	2		28263.22			
3537.446	80	15	28260.91	+0.05	15_3 — 437°_4	Res
3538.626	15	1	28251.48	0.00	14_2 — 432°_2	3
3539.323	8	1	28245.92	+0.02	$^3P_0$ — 377°_1	(0)
3539.455	3	4 *s*	28244.87	−0.05	18_1 — 463°_2	
3539.588	5		28243.80	+0.10	33_5 — 615°_4	
3539.88	1		28241.47	−0.06	27_4—55455°_5	
3539.924	10		28241.12	−0.03	14_2 — 432°_1	
3540.206	2		28238.87	+0.04	23_1—51693°_2	
3540.734	20	2	28234.66	+0.02	$^3G_3$ — 415°_2	Res
3540.86	2 *b*		28233.66			
3540.96	1		28232.86	+0.02	28898_2 — 571°_3	
3541.307	2		28230.09	−0.03	$^3P_2$ — 474°_3	
3541.639	25	2	28227.45	+0.01	19_4 — 474°_3	(b)
3542.268	1	3 *b*	28222.44	−0.10	23_3 — 521°_2	
3542.647	6		28219.42	+0.04	22852_4 — 510°_3	
3543.106	8	15 *l*	28215.76	0.00	20_0 — 483°_1	(0)
3543.325	1		28214.02	−0.04	24_2 — 530°_2	
3543.710	12		28210.95	+0.04	18_2 — 463°_2	7
3543.98	4		28208.8	0.00	18_1 — 462°_1	

TABLE 3. *Observed and classified lines of* W I

Wavelength Å	Intensity		Wavenumber (cm^{-1})		Classification	Zeeman effect
	Arc	Spark	Observed	o−c		
3544.16	2		28207.37	+0.09	$^7F^\circ_2$− 49$_3$	
3544.79	12	1	28202.36	+0.06	19$_6$− 478$^\circ_5$	
3544.973	12	1	28200.90	−0.01	13$_2$− 419$^\circ_2$	3
3545.220	200	40	28198.94	+0.04	$^5D_0$− 281$^\circ_1$	7
3545.623	4		28195.73	+0.05	24$_3$− 528$^\circ_3$	
3546.354	4		28189.92			
3546.474	3	3 *s*	28188.97	0.00	$^3P_2$− 474$^\circ_2$	
3547.00	1		28184.79	+0.01	33$_5$− 614$^\circ_5$	
3547.466	15	2	28181.08	+0.01	$^3H_5$− 432$^\circ_4$	
3548.160	3	1	28175.57	−0.03	20$_1$− 486$^\circ_0$	
				+0.09	27$_4$− 553$^\circ_3$	
3548.258	15	12 *s*	28174.79	0.00	18$_2$− 462$^\circ_1$	
3548.75	2 *b*		28170.9	−0.13	26$_2$−55032$^\circ_2$	
3549.60	3		28164.14			
3550.682	20	3	28155.56	+0.02	17$_4$− 452$^\circ_4$	
3550.838	40		28154.32	0.00	19535$_5$− 476$^\circ_4$	Res
3551.024	30		28152.85			
3551.142	2		28151.91	+0.15	23$_1$−51606$^\circ_2$	
3551.268	10		28150.91	+0.04	$^3G_3$− 414$^\circ_3$	
3552.320	8		28142.58	0.00	19826$_5$− 479$^\circ_4$	
3552.883	3 *b*		28138.12	+0.02	27$_5$− 559$^\circ_5$	
3553.303	2		28134.79	+0.04	$^5D_4$− 343$^\circ_3$	
3554.02	2		28129.12			
3554.206	100	3	28127.64	+0.06	$^5D_3$− 329$^\circ_3$	3
3554.325	3		28126.70			
3555.746	15	1	28115.46	+0.01	$^3G_4$− 445$^\circ_5$	(0)
3556.01	1		28113.37	+0.05	30$_2$− 584$^\circ_3$	
3556.676	2	1	28108.11	−0.07	$^3P_2$− 473$^\circ_3$	
3556.764	3	1	28107.42	+0.03	$^3H_4$− 402$^\circ_3$	
3557.008	6		28105.49	−0.01	19$_4$− 473$^\circ_3$	
3557.08	2		28104.92	+0.03	18$_3$− 470$^\circ_2$	
				−0.06	$^5S_2$− 463$^\circ_3$	
3557.203	40	4	28103.95	0.00	19$_4$− 473$^\circ_4$	
3558.226	2		28095.87	+0.03	24$_2$− 528$^\circ_2$	
3558.571	3 *b*	1	28093.14	+0.01	$^7D^\circ_2$− 52$_1$	
3559.080	6		28089.12	0.00	20$_2$− 490$^\circ_3$	
3559.44	3	1	28086.28			
3559.59	*a*	4	28085.10	−0.10	23$_3$− 520$^\circ_3$	
3559.702	25		28084.22	−0.01	$^3P_2$− 473$^\circ_2$	
3560.060	12	1	28081.39	+0.11	23$_2$− 520$^\circ_2$	
				−0.12	29479$_4$− 575$^\circ_5$	
3560.30	2		28079.5	+0.13	26$_2$− 549$^\circ_1$	
3561.244	12	1	28072.06	+0.05	$^3H_4$− 402$^\circ_4$	
3563.444	40	4	28054.73	+0.06	15$_3$− 435$^\circ_2$	
3564.41	2		28047.12	−0.15	$^5S_2$− 463$^\circ_2$	
				+0.11	28$_5$− 562$^\circ_5$	
3565.146	10	1	28041.33	+0.01	22852$_4$− 508$^\circ_3$	
3565.609	12	1	28037.69	+0.06	$^7D^\circ_2$−52002$_3$	
3567.245	10		28024.83	+0.03	19826$_5$− 478$^\circ_5$	(0)
3567.64	3		28021.73	−0.06	18$_1$− 461$^\circ_1$	

318-092 O-69—9

TABLE 3. *Observed and classified lines of* W I

Wavelength Å	Intensity		Wavenumber (cm⁻¹)		Classification	Zeeman effect
	Arc	Spark	Observed	o−c		
3567.68	5		28021.42	−0.02	31_5 — 594°_6	
3568.036	60	6	28018.62	+0.05	15_3 — 434°_3	3
3568.404	12	2	28015.73	+0.02	$^3G_4$ — 444°_3	
3568.618	3		28014.05	+0.03	$^7F^\circ_1$ — e^5D_2	
3568.85	2		28012.23			
3568.983	20		28011.19	+0.04	$^5S_2$ — 462°_1	
3569.16	12	1	28009.80	+0.04	17_4 — 451°_4	7
3569.222	15	1	28009.31	+0.04	$^5D_4$ — 342°_3	
3569.577	20	2	28006.53	−0.02	19535_5 — 475°_6	(0)
3570.17	1		28001.87	−0.12	$^3P_2$ — 472°_1	
3570.648	150	15	27998.13	+0.18	$^5D_2$ — 313°_1	z d
				+0.01	$^5D_3$ — 328°_4	
3571.034	6		27995.10			
3571.166	3		27994.07			
3571.362	2 *b*		27992.53	+0.05	29479_4 — 574°_4	
3571.972	3	8 *s*	27987.75	−0.03	18_2 — 461°_1	
3573.410	50	4	27976.49	−0.02	17_3 — 456°_3	Res
3573.960	8		27972.18	+0.01	$^7D^\circ_2$ — 51_2	
3575.220	80	8	27962.32	0.00	$^3H_6$ — 449°_7	2
3575.34	3		27961.38			
3575.852	15	1	27957.38	+0.05	18_3 — 469°_4	(0)
3575.968	60	6	27956.47	+0.05	13_2 — 417°_2	3
3576.370	10	2	27953.33	+0.06	22852_4 — 508°_5	
3576.87	1		27949.42	+0.24	27_1 — 556°_2	
3577.088	2		27947.72	+0.08	22852_4—50800°_3	
3578.011	2	1	27940.51			
3578.490	3 *b*		27936.77			
3579.86	4		27926.08	+0.06	23_3 — 518°_4	
3580.40	2		27921.9			
3581.062	12	1	27916.71	+0.08	13_2 — 416°_3	
3581.222	30	3	27915.46	+0.06	$^3H_6$ — 449°_6	
3582.233	25		27907.58	+0.05	17_4 — 450°_3	
3582.638	3	2	27904.43	+0.19	28204_2 — 561°_3	
3582.898	10	1	27902.40	+0.05	$^5D_4$ — 341°_4	
3584.094	50	5	27893.09	+0.07	19_6 — 475°_6	Res
3584.333	3 *b*		27891.23	+0.23	20_1 — 483°_2	
3584.771	8	1	27887.82	+0.07	28_6 — 562°_5	
3585.05	2		27885.65			
3585.91	2	2	27879.0	+0.20	29853_4 — 577°_3	
3586.475	1 *b*		27874.57	+0.02	31_5 — 592°_5	
3587.922	8		27863.33	+0.04	19826_5 — 476°_4	
3588.134	5		27861.69	+0.04	19_3 — 476°_4	
3589.624	8		27850.12	−0.02	17_3 — 455°_3	Res
3589.692	10		27849.59	+0.01	$^3G_3$ — 411°_4	Res
3590.822	60	6	27840.83	+0.02	$^3H_5$ — 429°_4	Res
3591.340	6		27836.82	+0.04	20_1 — 482°_0	
3591.45	4		27835.96	+0.03	29479_4 — 573°_4	
3591.765	15	1	27833.52	−0.04	17_4 — 449°_4	
3591.968	15	2	27831.95	+0.01	18_3 — 468°_2	
3592.274	2		27829.58	+0.06	27_4 — 550°_4	

TABLE 3. *Observed and classified lines of* W I

Wavelength Å	Intensity Arc	Intensity Spark	Wavenumber (cm⁻¹) Observed	Wavenumber (cm⁻¹) o−c	Classification	Zeeman effect
3592.79	3		27825.58	+0.02	24_3— 524°_4	
3592.846	8		27825.15	−0.03	19535_5— 473°_4	
3592.975	10		27824.15	+0.01	$^5S_2$— 461°_1	
3593.482	2		27820.22	−0.06	$^3P_1$— 411°_0	
3593.555	8		27819.66	+0.01	18_1— 459°_2	
3593.73	2 *b*		27818.3	+0.13	28898_2— 567°_3	
3593.966	30		27816.48	+0.03	20_1— 482°_2	Res
3594.525	25		27812.15	+0.01	23_6— 512°_7	(b)
3595.055	1 *b*		27808.05	+0.09	22476_4— 502°_4	
3595.32	2		27806.0	+0.05	23_6— 512°_5	
3595.382	15		27805.52	+0.03	13_2— 415°_2	
3595.440	8		27805.07	+0.03	20_2— 487°_1	
3596.428	12		27797.43	+0.01	$^3P_1$— 411°_2	
3596.601	8		27796.10	+0.03	$^3H_5$— 428°_5	
3596.69	2		27795.4	0.00	27_4— 550°_5	
3597.260	40	4	27791.01	+0.02	15_3— 432°_4	(0)
3597.710	15	2	27787.53	−0.01	$^5S_2$— 460°_3	
3597.956	8	1	27785.63	−0.01	18_2— 459°_2	
3598.12	2		27784.4			
3598.874	40	2	27778.54	+0.04	$^5D_0$— 277°_1	(0)
3599.173	3		27776.24	−0.06	$^7D^\circ_4$—56573_5	
3600.287	10		27767.64	−0.01	15_3— 432°_2	
3600.532	2		27765.75	−0.01	19_3— 475°_3	
3600.783	3		27763.82	+0.05	23_3—51693°_2	
3601.164	2		27760.88	+0.04	28347_3— 561°_3	
3601.796	5		27756.01	+0.05	$^3G_3$— 411°_2	
3602.00	1		27754.43	−0.03	28_5— 559°_5	
3603.907	10	1	27739.75	+0.03	31_5— 591°_6	(b)
3606.063	150	15	27723.16	+0.05	$^5D_1$— 293°_2	Res
3606.249	12		27721.74	+0.02	13_2— 414°_3	
3606.333	10		27721.09	+0.01	17_3— 454°_2	
3607.059	80	8	27715.51	−0.01	19826_5— 475°_6	
3607.898	4		27709.07	+0.05	22476_4— 501°_3	
3608.146	2		27707.16	−0.01	29853_4— 575°_5	
3608.904	4		27701.34			
3609.348	2		27697.93	+0.14	27_4— 549°_4	
3609.443	3	4	27697.20			
3609.952	3		27693.30			
3610.421	2		27689.70	+0.02	28347_3— 560°_2	
3610.634	2		27688.07	+0.07	29_7— 571°_6	
3610.75	1		27687.18	+0.05	$^7P^\circ_2$— 53_3	
3611.956	1 *b*	1	27677.93	−0.04	18_1— 457°_1	
3612.27	1		27675.5	−0.10	19_4— 469°_4	
3612.70	2		27672.2			
3612.947	1		27670.34	−0.10	23_3— 516°_3	
3614.24	3		27660.44			
3614.798	15 *b*		27656.17	+0.17	19_3— 474°_3	
3615.124	2	1	27653.68			
3615.536	10		27650.53	−0.01	18_3— 466°_4	
3616.155	5 *b*		27645.80	+0.06	20_6— 478°_1	

TABLE 3. *Observed and classified lines of* W I

Wavelength Å	Intensity		Wavenumber (cm^{-1})		Classification	Zeeman effect
	Arc	Spark	Observed	o−c		
3616.398	8		27643.94	−0.02	18_2— 457°_1	
3616.595	3		27642.43	+0.01	27_5—55492°_5	
3617.104	4 *b*		27639.54			
3617.515	500	50	27635.40	+0.05	$^7S_3$— 305°_3	
3618.103	2		27630.91	−0.01	28204_2— 558°_2	
3618.877	5		27625.00	−0.01	14_2— 426°_3	
3619.269	25	2	27622.01	+0.01	$^5S_2$— 459°_2	3
3620.20	1 *b*		27614.91	+0.06	19_3— 474°_2	
3620.282	1		27614.28	+0.04	28_5— 558°_6	
3621.128	4	2	27607.83	+0.07	28347_3— 559°_4	
3621.422	3		27605.59	+0.04	27_5—55455°_5	
3622.104	3		27600.39			
3622.337	60	12	27598.62	+0.06	19_4— 468°_5	
3622.506	20	1	27597.33	+0.02	14_2— 425°_1	
3622.584	1		27596.74	−0.06	$^7D^\circ_3$— 53_4	
3623.509	30	2	27589.69	0.00	$^3G_4$— 440°_3	
3624.058	2		27585.51	+0.14	28898_2— 564°_3	
3625.059	2		27577.89			
3625.398	60	6	27575.32	+0.05	$^3G_3$— 409°_3	Res
3627.132	2		27562.13	+0.09	28_5— 557°_5	
3627.237	80	8	27561.34	−0.03	17_3— 452°_4	(b)
				+0.04	$^3P_1$— 408°_2	
3627.611	2		27558.49			
3627.673	2		27558.02	+0.02	$^3H_4$— 397°_4	
3628.348	1		27552.90	+0.01	$^3P_2$— 468°_2	
3629.660	2		27542.94	−0.02	23_3— 514°_4	
3629.817	3		27541.75	+0.01	24_3— 521°_2	
3630.317	50	5	27537.95	−0.01	14_2— 425°_3	Res
3630.447	2		27536.97			
3630.819	60	5	27534.15	0.00	19826_5— 473°_4	(b)
3631.038	3		27532.49	−0.02	19_3— 473°_4	
3631.649	2		27527.85			
3631.943	200	20	27525.62	+0.07	$^5D_1$— 291°_2	Res
3632.704	30	3	27519.86	+0.02	$^3G_3$— 408°_2	
3633.569	5		27513.31	+0.15	26_2— 543°_1	
3634.02	1		27509.9	−0.21	19_3— 473°_2	
3634.554	2		27505.85			
3635.256	3 *b*		27500.54			
3636.478	3		27491.30	−0.02	$^7P^\circ_4$— 55_5	
3636.726	10		27489.42	+0.07	22476_4— 499°_3	
3636.962	2		27487.64	+0.12	28347_3— 558°_2	
3637.380	60	3	27484.48	+0.03	$^3H_4$— 396°_3	
3637.932	8		27480.31	−0.01	$^5S_2$— 457°_1	
3638.35	2		27477.15			
3638.53	2		27475.8			
3639.371	2	1	27469.45			
3640.134	40	2	27463.69	+0.01	$^3P_1$— 407°_1	
3640.266	6		27462.69	0.00	$^3H_5$— 425°_4	
3640.412	2		27461.59	0.00	29853_4— 573°_4	
3640.641	2		27459.86	+0.04	31_5— 588°_4	

TABLE 3. *Observed and classified lines of* W I

Wavelength A	Intensity		Wavenumber (cm^{-1})		Classification	Zeeman effect
	Arc	Spark	Observed	o−c		
3641.259	10		27455.20	+0.22	28_6— 558°_6	
3641.664	2		27452.15	+0.06	$^3H_4$— 396°_5	
3641.848	20	2	27450.76	+0.03	15_3— 429°_4	
3642.095	8	1	27448.90	0.00	24_3— 520°_4	
3642.813	20	1	27443.49	+0.05	$^7P^\circ_4$— 55_4	
3643.310	10		27439.75	0.00	17_4— 445°_5	
3644.002	4		27434.54	−0.06	18_2— 455°_3	
3644.360	3		27431.84	0.00	22852_4— 502°_4	
3645.992	3		27419.56	+0.03	$^3G_4$— 438°_3	
3646.517	20		27415.62	+0.03	17_3— 451°_4	
3647.138	8		27410.95	0.00	18_3— 463°_3	
3647.522	40	2	27408.06	+0.04	$^5D_3$— 322°_3	
3647.661	15	1	27407.02	+0.08	20_2— 483°_1	
3648.004	1		27404.44	+0.04	24_3— 520°_3	
3648.213	2		27402.87	+0.09	28_6— 557°_5	
3649.016	15		27396.84	+0.01	19535_5— 469°_4	
3649.230	3 *b*	2 *b*	27395.23			
3650.089	8		27388.79	+0.07	31_5— 587°_4	
3650.997	60	6	27381.98	+0.06	$^3H_6$— 443°_6	3
3651.222	2		27380.29	−0.02	$^3H_5$— 424°_4	
3651.471	2		27378.42			
3652.752	5		27368.82	+0.01	19_4— 466°_4	
3653.05	2		27366.6			
3653.14	2		27365.9			
3653.525	4		27363.03	+0.07	24_2— 521°_2	
3654.194	100	10	27358.02	+0.01	$^5D_2$— 306°_1	(0)
3654.441	2		27356.17			
3654.952	1		27352.35	0.00	29479_4— 568°_4	
3655.128	8 *b*		27351.03			
3655.64	2		27347.2			
3656.150	6 *b*		27343.38	−0.01	20_2— 483°_3	
3656.677	15	1	27339.44	+0.01	18_1— 454°_2	
3657.207	3		27335.48	+0.34	20_2— 483°_2	
3658.07	2		27329.03			
3658.362	10	1	27326.85	+0.04	13_2— 411°_2	
3659.308	10	1	27319.79	0.00	19535_5— 468°_5	
3659.354	3		27319.44			
3659.56	8 *b*		27317.9	+0.06	17_3— 450°_2	
3660.165	25	1	27313.39	+0.03	17_3— 450°_3	
3660.359	20	2	27311.94	+0.04	22476_4— 497°_4	
3660.604	30	6 *s*	27310.12	+0.06	$^3G_4$— 437°_5	
3661.228	5	1	27305.46	+0.04	18_2— 454°_2	
3662.207	1		27298.16	+0.04	28_6— 556°_7	
3662.281	2		27297.61	−0.01	$^7F^\circ_5$— 53_5	
3662.586	3		27295.34			
3662.669	2		27294.72			
3663.144	30	3	27291.18	+0.01	18_1— 453°_1	
3663.353	100	5	27289.62	+0.06	$^3G_4$— 437°_4	
3663.696	3		27287.07			
3663.821	20	2	27286.14	+0.02	14_2— 422°_1	

TABLE 3. *Observed and classified lines of* W I

Wavelength Å	Intensity		Wavenumber (cm^{-1})		Classification	Zeeman effect
	Arc	Spark	Observed	o−c		
3664.821	2		27278.70			
3664.888	1		27278.20	+0.08	29853_4 − 571°_3	
3664.953	2		27277.71	−0.17	23_2 − 512°_1	
3665.273	3		27275.33	0.00	14_2 − 422°_3	
3665.389	3		27274.47	+0.05	24_2 − 520°_2	
3665.875	40	4	27270.85	+0.01	$^5S_2$ − 455°_3	Res
3666.106	2		27269.13			
3666.804	15		27263.94	+0.06	23_1 − 507°_2	
3667.174	50	2	27261.19	+0.08	$^5D_2$ − 305°_3	(0)
3667.486	8		27258.87	+0.09	28_5 − 55492°_5	
3667.711	60	4	27257.20	+0.04	18_2 − 453°_1	
3668.46	1		27251.63	−0.09	19_3 − 470°_2	
3668.658	60	4	27250.16	+0.03	19_4 − 465°_5	Res
3669.323	6	1	27245.22	0.00	24_3 − 518°_4	
3669.64	2		27242.87			
3670.108	2 *b*		27239.40	+0.01	17_3 − 449°_4	
3670.761	20	2	27234.55	+0.04	$^3G_3$ − 405°_4	
3671.766	2		27227.10			
3671.962	3		27225.64	+0.02	24_2 − 520°_3	
3672.173	15		27224.08	+0.02	18_1 − 453°_0	
3672.905	8 *b*		27218.65			
3672.961	1		27218.24			
3673.164	2		27216.73			
3674.131	3		27209.57	+0.09	28898_2 − 561°_3	
3674.19	2		27209.13			
3674.575	50	5	27206.28	+0.02	19_6 − 468°_5	Res
3675.554	80	8	27199.04	−0.01	$^3H_4$ − 393°_5	Res
3676.286	8		27193.62	+0.08	27_5 − 550°_4	
3676.797	40	4	27189.84	0.00	$^7F^\circ_6$ − 56_6	3
3677.112	3		27187.51	−0.02	20_2 − 481°_3	
3679.600	40	4	27169.13	0.00	$^3H_5$ − 422°_6	(0)
3679.892	5 *b*		27166.97			
3680.448	2		27162.87			
3680.710	2		27160.94			
3680.854	4		27159.87	+0.03	22476_4 − 496°_4	
3680.920	4		27159.39	−0.03	27_5 − 550°_5	
3682.084	200	20	27150.80	+0.09	$^5D_4$ − 333°_5	1
3682.538	3		27147.45			
3682.718	6		27146.13	+0.01	13_2 − 409°_3	
3683.296	40	4	27141.87	+0.09	$^5S_2$ − 454°_2	Res
3683.388	30	3	27141.19	+0.01	15_3 − 426°_3	Res
3683.930	60	10	27137.20	−0.01	19535_5 − 466°_6	(b)
3684.650	40	4	27131.89	−0.01	$^3P_2$ − 463°_3	(b)
3685.010	35	3	27129.24	+0.02	19_4 − 463°_3	(0)
3685.586	15	1	27125.00	0.00	$^7F^\circ_6$ − 56768_5	
3686.994	3 *b*		27114.65			
3688.057	200	15	27106.83			
3688.190	5	1	27105.85	+0.05	19826_5 − 469°_4	
3688.414	20	1	27104.21	+0.05	19_3 − 469°_4	
3689.047	12	1	27099.56	+0.04	28_6 − 55492°_5	

TABLE 3. *Observed and classified lines of* W I

Wavelength Å	Intensity		Wavenumber (cm⁻¹)		Classification	Zeeman effect
	Arc	Spark	Observed	o−c		
3689.333	2		27097.46	+0.04	$28291_3 - 553^\circ_3$	
3689.506	5		27096.19	−0.03	$29_7 - 565^\circ_7$	
3689.866	50	3	27093.54	+0.03	$18_3 - 460^\circ_3$	3
3690.248	50	6	27090.74	+0.05	$13_2 - 408^\circ_2$	3
3690.347	3		27090.01	−0.03	$19535_5 - 466^\circ_4$	
3690.45	2		27089.25	−0.13	$23_2 - 510^\circ_3$	
3690.61	3		27088.08			
3691.09	2		27084.56			
3691.546	6		27081.21	−0.14	$20_0 - 472^\circ_1$	
3691.909	3		27078.55	+0.02	$23_1 - 505^\circ_1$	
3692.332	2		27075.45			
3692.49	2		27074.29	+0.10	$^3P_2 - 463^\circ_2$	
3692.715	15		27072.64	+0.03	$15_3 - 425^\circ_4$	
3693.668	2 *b*	3 *b*	27065.65	+0.06	$29_7 - 565^\circ_6$	
3694.07	3		27062.71	+0.06	$28_6 - 55455^\circ_5$	
3694.193	1		27061.81	0.00	$27_5 - 549^\circ_4$	
3694.500	40		27059.56	0.00	$^7D^\circ_5 - 56_6$	
3695.240	10		27054.14	+0.01	$15_3 - 425^\circ_3$	
3695.665	2		27051.03	+0.12	$26_2 - 53912^\circ_2$	
3696.161	3	3 *b*	27047.40	+0.13	$^3G_4 - 434^\circ_3$	
3696.808	3		27042.67	+0.11	$28347_3 - 553^\circ_2$	
3697.431	4		27038.11	+0.04	$^3P_2 - 462^\circ_1$	
3697.483	4		27037.73	+0.07	$22476_4 - 495^\circ_3$	
3698.196	3		27032.52			
3698.712	30	3	27028.75	−0.01	$19826_5 - 468^\circ_5$	Res
3699.406	50	5	27023.67	−0.01	$19_6 - 466^\circ_6$	Res
3700.178	4 *b*		27018.04			
3700.642	8	1	27014.65	−0.04	$20_1 - 474^\circ_2$	
3700.929	2		27012.55			
3702.310	50	5	27002.48	+0.04	$14_2 - 419^\circ_2$	3
3702.832	3		26998.67	+0.07	$28347_3 - 553^\circ_4$	
3703.202	6		26995.97	+0.07	$24_3 - 51606^\circ_2$	
3703.323	10		26995.09	+0.05	$276^\circ_2 - 54_3$	
3703.380	12		26994.68	−0.04	$^7D^\circ_5 - 56768_5$	
3703.597	50	3	26993.10	+0.03	$13_2 - 407^\circ_1$	(0)
3704.080	1		26989.58	−0.01	$15_3 - 424^\circ_2$	
3704.339	8		26987.69	+0.06	$^5D_3 - 318^\circ_2$	
3704.790	60	3	26984.40	0.00	$^7D^\circ_2 - 50949_1$	Res
3705.480	40	4	26979.38	−0.01	$23_3 - 509^\circ_4$	
3705.585	2		26978.61	−0.16	$19_3 - 468^\circ_2$	
3706.578	2		26971.40	+0.04	$19535_5 - 465^\circ_5$	
3707.611	4 *b*		26963.87	−0.17	$23_3 - 508^\circ_3$	
3707.922	300	30	26961.61	+0.05	$^7S_3 - 299^\circ_3$	Res
3710.274	8		26944.52	+0.12	$23_6 - 504^\circ_6$	
3710.504	2		26942.85			
3710.672	2 *b*		26941.63	+0.10	$^7D^\circ_2 - 50906_1$	
3711.418	2		26936.21	+0.02	$18_1 - 450^\circ_2$	
3711.475	10	1	26935.80	+0.02	$22852_4 - 497^\circ_4$	
3712.202	3	12 *s*	26930.53	−0.05	$^7F^\circ_6 - 56573_5$	
3714.232	30	1	26915.81	+0.06	$^3H_6 - 439^\circ_5$	(b)

TABLE 3. *Observed and classified lines of* W I

Wavelength Å	Intensity		Wavenumber (cm^{-1})		Classification	Zeeman effect
	Arc	Spark	Observed	o−c		
3714.842	30	1	26911.39	+0.07	23_2–50894°_3	
3715.034	40	2	26910.00	+0.05	20_1– 473°_2	(0)
3715.696	4		26905.20	+0.24	27_4– 541°_4	
3715.832	5	8 *s*	26904.22	+0.03	24789_2–51693°_2	
3715.912	4		26903.64	+0.10	27_4– 541°_3	
3716.722	30	2	26897.78	+0.08	18_2– 450°_3	
3717.082	30	3	26895.17	+0.07	17_3– 445°_2	
3717.160	20	2	26894.61	+0.02	18_3– 458°_4	
3718.676	4		26883.64	+0.06	27_5– 547°_6	
3718.962	2		26881.57			
3719.391	100	10	26878.47	+0.07	17_4– 439°_4	
3720.504	40	2	26870.43	+0.07	23_3–50800°_3	3
3721.732	4		26861.57			
3722.235	60	12	26857.94	+0.11	19_6– 465°_5	
3723.862	8		26846.20	+0.02	19826_5– 466°_6	
3725.153	15		26836.90	−0.02	20_2– 478°_1	
3726.429	4		26827.71	0.00	20_1– 472°_1	
3726.776	2		26825.21			
3727.528	5		26819.80	+0.11	$^3G_4$– 432°_4	
3727.819	6		26817.71	+0.07	23_2–50800°_3	
3727.882	8		26817.25	+0.01	17_4– 439°_5	
3728.273	15	1	26814.44	−0.02	$^3P_2$– 460°_3	
3729.195	8		26807.81	+0.09	26_2– 536°_2	
3729.990	5		26802.10	+0.09	$^3H_5$– 418°_4	
3730.251	3		26800.22	+0.02	$^7D^\circ_5$–56573_5	
3730.419	60	6	26799.02	+0.01	19826_5– 466°_4	
3730.646	8		26797.39	+0.02	19_3– 466°_4	
3731.461	2		26791.53	+0.03	15_3– 422°_3	
3731.532	3		26791.02			
3731.818	1		26788.97	+0.15	23_3– 507°_2	
3732.093	2		26787.00			
3732.541	20		26783.78	+0.06	22852_4– 496°_4	3
3733.016	2		26780.37			
3733.670	6	1	26775.68	−0.10	28_5– 550°_5	
3734.030	3 *b*		26773.10			
3734.394	5 *b*		26770.50			
3734.757	4 *b*	1	26767.90	+0.02	278°_4– 54_3	(0)
3735.142	4		26765.13			
3735.530	5		26762.35			
3735.938	3		26759.43			
3736.141	8		26757.98	+0.03	14_2– 417°_2	
3736.348	5		26756.49			
3736.762	4		26753.53			
3737.200	4		26750.39			
3737.346	2		26749.35	+0.16	27_1– 544°_1	
3737.636	3		26747.27			
3737.838	10	1	26745.83	−0.01	17_3– 444°_3	
3738.110	20		26743.88	+0.05	17_4– 438°_3	
3738.551	6		26740.73	−0.06	28291_3–55032°_2	
3738.888	25	2	26738.32	+0.07	$^5D_4$– 329°_3	

TABLE 3. *Observed and classified lines of* W I

Wavelength Å	Intensity		Wavenumber (cm^{-1})		Classification	Zeeman effect
	Arc	Spark	Observed	o−c		
3739.024	4		26737.34			
3739.481	40	4	26734.08	+0.02	$^5S_2$— 450°$_3$	
3739.996	3		26730.40			
3740.502	5		26726.78			
3741.016	4		26723.11			
3741.182	8	10	26721.92			
3741.338	2		26720.81	+0.11	28898$_2$— 556°$_2$	
3741.540	2		26719.36			
3741.706	30	12 *s*	26718.18	+0.02	14$_2$— 416°$_3$	z d
3742.076	3		26715.54			
3742.601	15	1	26711.79			
3742.676	20	2	26711.25	+0.01	22476$_4$— 491°$_5$	
3743.177	4 *b*		26707.68			
3743.807	20	2	26703.19	+0.01	18$_3$— 456°$_3$	
3744.047	8		26701.47			
3744.899	6 *b*		26695.40	+0.09	29479$_4$— 561°$_4$	
3745.886	2		26688.37			
3745.961	1		26687.83			
3746.063	4		26687.10			
3746.344	1		26685.10	+0.03	28347$_3$–55032°$_2$	
3746.734	3 *b*		26682.32			
3747.321	3		26678.15	−0.02	28$_5$— 543°$_5$	
3747.448	8	1	26677.24			
3747.581	3		26676.29			
3747.953	1		26673.65			
3748.027	2		26673.12			
3748.285	5	1	26671.28	+0.01	22476$_4$— 491°$_4$	
3748.475	4		26669.93	+0.01	22$_0$— 494°$_1$	
3748.610	2		26668.97	−0.31	28$_1$–55390°$_2$	
3748.981	2		26666.33	+0.01	17$_3$— 443°$_2$	
3749.456	10		26662.95	+0.01	$^3G_3$— 400°$_2$	
3749.531	6		26662.42	−0.01	$^3P_0$— 361°$_1$	
3749.655	50	*b*	26661.54	0.00	22852$_4$— 495°$_3$	Res
3749.935	2		26659.55			
3750.164	2		26657.92			
3750.605	3		26654.80	−0.15	28204$_2$— 548°$_2$	
3750.69	2		26654.18	−0.20	18$_1$— 447°$_1$	
3751.062	3		26651.54	−0.02	20$_1$— 470°$_2$	
3751.422	20	3 *b*	26648.98	+0.08	27$_4$— 538°$_5$	(0)
3751.688	2		26647.09	−0.01	28898$_2$— 555°$_3$	
3752.570	4		26640.83			
3753.480	8		26634.37	+0.01	17$_4$— 437°$_5$	
3754.148	6		26629.63	+0.07	$^7F°_2$— 48$_2$	
3754.872	10 *b*		26624.50	+0.08	$^7D°_1$— 48$_2$	
3755.450	4		26620.40	+0.03	18$_2$— 447°$_1$	
3755.532	4		26619.82	+0.09	28291$_3$— 549°$_4$	
3756.372	10	1	26613.87	+0.01	17$_4$— 437°$_4$	
3756.867	10	6	26610.36	−0.06	20$_2$— 475°$_3$	
3757.082	25	2	26608.84	+0.05	$^5D_4$— 328°$_4$	
				+0.11	$^7F°_3$— 49$_3$	

TABLE 3. *Observed and classified lines of* W I

Wavelength Å	Intensity		Wavenumber (cm⁻¹)		Classification	Zeeman effect
	Arc	Spark	Observed	o−c		
3757.338	6		26607.02	0.00	14_2— 415°_2	
3757.482	2		26606.00			
3757.604	1		26605.14			
3757.736	2		26604.21			
3757.923	200	40	26602.88	−0.03	$^5D_3$— 314°_4	Res
				+0.09	$^3G_4$— 430°_5	
3759.448	2*b*		26592.10			
3759.678	2		26590.46			
3760.126	200	40	26587.30	−0.02	$^5D_2$— 299°_3	Res
3760.630	15	1	26583.73	−0.03	$^7D^\circ_4$— 55_5	
3761.212	2		26579.62			
3761.608	10	1	26576.82	+0.01	18_3— 455°_3	3
3762.183	1		26572.76			
3762.404	1		26571.20	+0.01	19535_5— 461°_6	
3763.256	2		26565.18	+0.08	22852_4— 494°_3	
3763.420	3		26564.03	+0.02	28291_3— 549°_4	
3763.882	2		26560.77	+0.09	$^7D^\circ_2$— 50_2	
3763.974	2		26560.12			
3764.312	20	2	26557.73	−0.05	19_3— 463°_3	3
3765.302	6		26550.75	0.00	23_2— 505°_1	
3766.576	2		26541.77			
3767.418	10	1	26535.84	−0.04	$^7D^\circ_4$— 55_4	
3767.838	30	3	26532.88	−0.02	19_4— 457°_5	
3768.122	2		26530.88			
3768.447	250	50	26528.59	−0.02	$^5D_1$— 281°_1	
3769.207	50	5	26523.24	0.00	14_2— 414°_3	
3769.536	1		26520.93			
3769.860	50	5	26518.65	+0.04	15_3— 419°_2	
3769.992	2		26517.72			
3770.320	2		26515.41			
3770.598	6		26513.46	+0.01	18_1— 445°_2	
3771.492	2		26507.17	−0.07	$^3P_2$— 457°_1	
3772.050	8	3 *l s*	26503.25	−0.01	28_6— 548°_6	
3772.420	10	1	26500.65	−0.01	20_2— 474°_3	
3772.500	6		26500.09	+0.02	19_3— 463°_2	
3773.706	150	30	26491.62	−0.02	13_2— 402°_3	
3774.460	3		26486.33			
3774.800	2		26483.94	+0.06	26_2—53345°_3	
3775.442	15	2	26479.44	0.00	18_2— 445°_2	3
				+0.01	$^3G_4$— 429°_4	
3776.634	3*b*		26471.08	+0.06	24_2— 512°_1	
3776.990	2		26468.59			
3778.144	10	2	26460.50	0.00	27_5— 543°_5	
3778.550	20	2	26457.66	0.00	19_6— 461°_6	
3778.686	30	8 *s*	26456.71	−0.02	$^5S_2$— 447°_1	
3779.966	12		26447.75	0.00	18_3— 454°_2	
3780.340	2		26445.13			
3780.458	2		26444.31			
3780.772	200	40	26442.11	0.00	$^7S_3$— 293°_2	
3780.921	6	4	26441.07			

TABLE 3. *Observed and classified lines of* W I

Wavelength Å	Intensity		Wavenumber (cm^{-1})		Classification	Zeeman effect
	Arc	Spark	Observed	o−c		
3781.837	30	2	26434.67	−0.02	$^3G_4$ — 428°$_5$	
3782.680	15	12 *l*	26428.77	−0.02	$^7P°_3$ — 53$_3$	
3782.966	2		26426.78	−0.01	29853$_4$ — 562°$_5$	
3783.727	40	4	26421.46	+0.01	19$_4$ — 456°$_3$	(b)
3784.550	3		26415.72			
3785.086	6		26411.97	+0.04	15$_3$ — 418°$_4$	
3786.370	25	2	26403.02	+0.02	$^3H_6$ — 434°$_7$	
3786.510	4	1	26402.04	+0.05	29853$_4$ — 562°$_4$	
3786.813	6		26399.93	+0.01	$^3P_1$ — 397°$_2$	
3787.646	2 *b*		26394.12	+0.12	$^7F°_1$ — e^5D_1	
3790.875	4		26371.64	+0.07	17$_4$ — 434°$_3$	
3791.770	2		26365.42	+0.03	26$_2$ — 532°$_1$	
3792.570	3		26359.86	+0.11	$^7F°_4$ — e^5D_4	
3792.759	100	10	26358.54	+0.08	$^3G_3$ — 397°$_2$	Res
3793.311	12		26354.71	−0.06	20$_2$ — 473°$_2$	
3794.13	2		26349.02			
3794.340	50	5	26347.56	−0.03	$^3H_5$ — 414°$_6$	
3796.282	20	2	26334.08	−0.01	19535$_5$ — 458°$_4$	
3796.935	6		26329.55	+0.03	$^3P_1$ — 396°$_1$	
3798.344	30	3	26319.79	−0.03	17$_3$ — 440°$_3$	3
3798.48	2 *g*		26318.85			
3798.915	15	2	26315.83	+0.03	$^5S_2$ — 445°$_2$	3
3801.026	1		26301.22	+0.06	259°$_1$—52284$_3$	
3801.165	2		26300.25			
3801.405	2		26298.59	0.00	24$_3$ — 509°$_4$	
3801.512	30	3	26297.85	+0.09	$^3P_2$ — 455°$_3$	(0)
				−0.02	$^3G_3$ — 396°$_3$	
				−0.04	$^7P°_3$ — 53$_4$	
3801.909	40	4	26295.11	+0.03	19$_4$ — 455°$_3$	(b)
				−0.04	22852$_4$ — 491°$_4$	
3802.053	3 *g*		26294.11			
3802.922	12		26288.10	+0.06	18$_3$ — 452°$_4$	
3803.409	5		26284.74	+0.07	18$_1$ — 443°$_2$	
3803.480	3		26284.25	+0.02	17$_3$ — 439°$_4$	
3803.620	2		26283.28	+0.04	24$_3$—50894°$_3$	
3804.072	15		26280.16	0.00	19826$_5$ — 461°$_6$	
3804.244	6		26278.97			
3804.942	10		26274.15	+0.03	15$_3$ — 417°$_2$	
				+0.11	17$_3$ — 439°$_2$	
3805.446	8		26270.67	+0.04	18$_1$ — 443°$_1$	
3806.308	2		26264.72	+0.17	28291$_3$ — 545°$_3$	
3807.622	6		26255.66	+0.04	23$_3$ — 501°$_3$	
3807.840	5	3 *b*	26254.15	+0.02	19535$_5$ — 457°$_5$	
3808.90	2		26246.85			
3809.220	150	15	26244.64	+0.09	$^7S_3$ — 291°$_2$	Res
3809.848	15		26240.31	−0.03	19$_3$ — 460°$_3$	
3810.380	100	10	26236.65	+0.03	18$_2$ — 443°$_1$	
3810.790	120	12	26233.83	+0.04	13$_2$ — 400°$_2$	
3812.646	10	1	26221.06	−0.02	22852$_4$ — 490°$_5$	
3812.896	4		26219.34	0.00	22852$_4$ — 490°$_3$	

TABLE 3. *Observed and classified lines of* W I

Wavelength Å	Intensity		Wavenumber (cm⁻¹)		Classification	Zeeman effect
	Arc	Spark	Observed	o−c		
3814.418	5	6 *b s*	26208.88	+0.05	$28347_3 - 545^\circ_3$	
3815.026	3		26204.70	−0.08	$27_1 - 538^\circ_1$	
3815.768	15	1	26199.61	+0.01	$259^\circ_1 - 52183_2$	
3816.386	40	4	26195.36	−0.05	$19_4 - 454^\circ_5$	
3817.294	12 *g*		26189.13	−0.03	$^7D^\circ_3 - 52378_4$	
3817.480	400	40	26187.86	+0.03	$^7S_3 - 291^\circ_3$	Res
3817.760	2 *g*		26185.94	+0.08	$20_1 - 466^\circ_0$	
3817.960	6		26184.56			
3818.344	2 *b*		26181.93			
3818.576	4 *b*		26180.34	−0.02	$26_2 - 530^\circ_1$	
3819.040	2		26177.16			
3819.402	2 *b*		26174.68			
3820.110	50	5	26169.83	−0.05	$^3G_4 - 426^\circ_3$	Res
3823.062	3	10 *s*	26149.62	−0.04	$17_3 - 438^\circ_3$	
3824.146	25	3	26142.21	−0.05	$18_3 - 451^\circ_4$	
3824.388	60	6	26140.55	−0.05	$19_6 - 457^\circ_5$	
3826.193	50	5	26128.22	+0.01	$^3H_5 - 411^\circ_4$	
				−0.12	$14_2 - 411^\circ_2$	
3826.667	1		26125.00			
3826.934	8	2 *l*	26123.16	−0.03	$15_3 - 415^\circ_2$	
3827.344	10		26120.37	−0.07	$^3P_2 - 453^\circ_1$	
3827.69	1 *b*		26118.0			
3827.788	2		26117.34	−0.09	$20_0 - 462^\circ_1$	
3828.81	1		26110.36			
3829.128	50	5	26108.20	−0.01	$^5D_1 - 277^\circ_1$	
3829.690	2		26104.37	−0.09	$24_2 - 50894^\circ_3$	
3830.130	12 *b*		26101.37	−0.14	$^3H_5 - 411^\circ_6$	
				+0.06	$^3G_4 - 425^\circ_4$	
3830.714	20		26097.39	−0.05	$^3H_4 - 382^\circ_4$	
3830.99	8 *b*		26095.51	−0.05	$^7D^\circ_3 - 52_3$	
3832.247	8		26086.95	−0.07	$^5S_2 - 443^\circ_2$	
3832.628	4		26084.35	−0.07	$^7P^\circ_4 - 53_5$	
3832.71	2		26083.8			
3832.862	15		26082.76	−0.07	$^3G_4 - 425^\circ_3$	
				+0.04	$31_5 - 574^\circ_4$	
3832.999	3		26081.83	−0.01	$26_2 - 529^\circ_3$	
3834.040	15		26074.75	−0.05	$19_3 - 459^\circ_2$	
3834.312	1		26072.9	−0.08	$^5S_2 - 443^\circ_1$	
3834.612	3		26070.86			
3834.735	4		26070.02	−0.04	$32_4 - 582^\circ_3$	
3835.058	250	25	26067.83	−0.04	$^5D_2 - 293^\circ_2$	Res
3835.31	2		26066.11			
3835.523	2		26064.67			
3835.890	8		26062.17	−0.07	$23_1 - 495^\circ_2$	
3836.952	15		26054.96	−0.03	$^7P^\circ_2 - 52_3$	
3838.511	80	8	26044.38	−0.13	$18_3 - 450^\circ_2$	Res
				−0.06	$^3H_4 - 382^\circ_3$	(0)
3838.96	4		26041.33	−0.09	$19_3 - 458^\circ_4$	
3839.25	15		26039.37	−0.05	$15_3 - 414^\circ_3$	
3839.866	2		26035.19			

TABLE 3. *Observed and classified lines of* W I

Wavelength Å	Intensity		Wavenumber (cm^{-1})		Classification	Zeeman effect
	Arc	Spark	Observed	o−c		
3841.050	3		26027.16	−0.06	$^7P^\circ_4$− 53$_3$	
3841.274	4		26025.64	+0.04	$^3H_6$− 430$^\circ_5$	
3841.31	1		26025.40			
3841.974	2		26020.90			
3842.164	4		26019.62	−0.07	17$_3$− 437$^\circ_4$	
3842.310	50		26018.63	−0.06	$^5D_4$− 322$^\circ_3$	(b)
3843.162	4		26012.86	−0.06	27$_5$− 538$^\circ_5$	
				−0.04	29479$_4$–55492$^\circ_5$	
3843.476	3 *b*		26010.73	−0.05	24$_2$–50800$^\circ_3$	
3845.784	1		25995.12			
3846.218	300	30	25992.19	−0.04	$^5D_1$− 276$^\circ_2$	Res
3847.020	4 *b*		25986.77			
3847.244	4		25985.26			
3847.498	150	15	25983.54	−0.06	$^5D_0$− 259$^\circ_1$	7
3847.958	1		25980.44	+0.01	27$_4$− 531$^\circ_5$	
3848.620	2 *b*		25975.97	−0.06	29479$_4$–55455$^\circ_5$	
3849.222	2		25971.91		33$_5$− 592$^\circ_5$	
3850.090	3 *d*		25966.05	−0.01	18$_3$− 449$^\circ_4$	
3851.954	2		25953.50	+0.07	$^7P^\circ_2$–52183$_2$	
3852.01	3		25953.11	−0.13	259$^\circ_1$− 51$_2$	
3852.835	12		25947.55	−0.10	14$_2$− 409$^\circ_3$	
3853.23	3		25944.89	−0.03	26$_2$− 528$^\circ_3$	
3853.778	8		25941.20			
3854.515	2	3	25936.24			
3855.554	50	5	25929.25	−0.06	13$_2$− 397$^\circ_2$	3
3855.880	3		25927.06	−0.03	17$_4$− 430$^\circ_5$	
				−0.08	34$_4$− 602$^\circ_5$	
3856.023	3		25926.10	−0.07	31$_5$− 573$^\circ_4$	
3857.30	10		25917.52	+0.08	263$^\circ_2$− 52$_3$	(b)
				−0.08	28$_6$− 543$^\circ_5$	
3858.847	5		25907.13			
3859.303	60	6	25904.07	−0.09	18$_2$− 440$^\circ_3$	
3859.929	20		25899.87	−0.04	20$_1$− 463$^\circ_2$	(0)
3861.066	30	3	25892.24	−0.15	18$_1$− 439$^\circ_2$	z d
				+0.02	14$_2$− 408$^\circ_2$	
3861.245	25	2	25891.04	−0.05	$^3H_4$− 380$^\circ_3$	(0)
3862.672	1		25881.47			
3863.480	15		25876.06	−0.04	$^3P_1$− 391$^\circ_1$	3
3864.343	60	6	25870.28	−0.03	$^5D_2$− 291$^\circ_2$	Res
3864.592	5		25868.62	−0.08	13$_2$− 396$^\circ_3$	
3865.326	8		25863.70	−0.09	20$_1$− 462$^\circ_1$	Res
3866.055	25		25858.83	−0.08	13$_2$− 396$^\circ_1$	Res
3866.257	4		25857.47	−0.03	$^3H_6$− 428$^\circ_5$	
3866.849	3		25853.52			
3867.158	3		25851.45			
3867.373	1		25850.01	0.00	19$_3$− 456$^\circ_3$	
3867.422	3		25849.69	−0.04	22476$_4$− 483$^\circ_3$	
3867.544	4		25848.87			
3867.666	5		25848.06			
3867.986	600	60	25845.92	−0.03	$^7S_3$− $^7D^\circ_4$	

TABLE 3. *Observed and classified lines of* W I

Wavelength Å	Intensity		Wavenumber (cm⁻¹)		Classification	Zeeman effect
	Arc	Spark	Observed	o−c		
3868.460	6		25842.75			
3868.578	12		25841.96	−0.09	$^3H_5$— 409°$_5$	
3868.857	2		25840.10			
3869.007	2		25839.10	−0.06	$^3H_4$— 380°$_4$	
3869.312	3		25837.06	+0.06	33$_5$— 591°$_6$	
3869.928	2 *b*		25832.95			
3870.684	3		25827.90	−0.13	$^7P°_2$— 52$_1$	
3870.818	6		25827.01	+0.11	28291$_3$— 541°$_4$	
3871.370	3		25823.33	−0.10	20$_2$— 468°$_2$	
				+0.05	22852$_4$— 486°$_4$	
3871.694	4		25821.17			
3871.845	3		25820.16	−0.04	$^3G_4$— 422°$_3$	
3872.487	12		25815.88	−0.04	263°$_2$—52183$_2$	
3872.840	100	10	25813.52	−0.07	$^5D_2$— 291°$_3$	z d
				+0.02	17$_3$— 435°$_2$	
3873.410	2		25809.73	−0.06	18$_1$— 438°$_1$	
3874.412	50	5	25803.05	−0.06	19$_6$— 454°$_5$	Res
3875.684	40	4	25794.58	−0.02	14$_2$— 407°$_1$	Res
3877.42	3		25783.04			
3877.516	3		25782.40			
3877.838	2 *b*		25780.25			
3878.279	1 *b*		25777.32	−0.08	17$_3$— 434°$_3$	
3878.524	6	1	25775.70	−0.08	18$_2$— 438°$_1$	
3879.002	6	1	25772.52	−0.01	$^7P°_2$—52002$_3$	
3879.20	5	2	25771.07	−0.11	28347$_3$— 541°$_4$	
3879.43	1		25769.68	+0.08	28347$_3$— 541°$_3$	
3879.482	3		25769.33	−0.15	23$_3$— 496°$_2$	
3880.082	12	1	25765.35	−0.11	$^3P_2$— 450°$_2$	
3880.57	2		25762.1			
3880.77	8 *b*	2 *b*	25760.78	−0.20	$^3P_2$— 450°$_3$	
3880.90	3		25759.91	+0.01	31$_5$— 571°$_6$	
3880.951	2		25759.6			
3881.052	5		25758.91	−0.08	17$_4$— 428°$_5$	
3881.15	5 *g*		25758.26	−0.04	19$_4$— 450°$_3$	
3881.405	250	25	25756.56	−0.08	$^5D_3$— 305°$_3$	Res
3881.877	2		25753.43			
3882.170	2		25751.49			
3882.274	2		25750.80			
3882.530	3 *b*		25749.10			
3883.336	2	3 *s*	25743.76	−0.13	24$_2$— 505°$_1$	
3883.832	20		25740.47	−0.05	$^5S_2$— 440°$_3$	(0)
3884.197	4	3	25738.05	−0.08	15$_3$— 411°$_4$	
3885.123	2		25731.92			
3885.456	1		25729.71	+0.05	27$_4$— 529°$_3$	
3885.784	2	1	25727.54	0.00	19535$_5$— 452°$_4$	
3886.452	20	2	25723.12	−0.03	$^3P_1$— 390°$_2$	
3887.405		1 *b*	25716.81	+0.05	23$_2$— 496°$_2$	
3888.886	5		25707.02			
3888.976	4		25706.42	−0.02	23$_3$— 496°$_4$	
3889.207	1		25704.90	+0.02	24$_2$— 504°$_2$	

TABLE 3. *Observed and classified lines of* W I

Wavelength Å	Intensity		Wavenumber (cm^{-1})		Classification	Zeeman effect
	Arc	Spark	Observed	o−c		
3889.470	2		25703.16	+0.02	23_6— 491°_5	
3890.126	1		25698.82	+0.03	28_1— 544°_1	
3890.420	8	2	25696.88	−0.04	23_1— 491°_2	
3890.746	12	1	25694.73	−0.01	$^5S_2$— 439°_2	
3891.252	6		25691.39	+0.02	$^7D^\circ_2$— e^5D_3	
3892.330	10		25684.27	−0.06	19_4— 449°_4	
3892.724	40	4	25681.67	−0.02	$^3G_3$— 390°_2	(0)
3893.473	8	1	25676.73	−0.05	20_1— 461°_1	3
3893.931	8	3	25673.71	−0.05	24_3— 502°_4	
3894.874	1		25667.50	+0.10	28291_3—53959°_2	
3895.758	3		25661.67	−0.03	22476_4— 481°_5	
3896.930	3	20 *s*	25653.95	+0.03	28_1— 543°_1	
3897.912	30	3	25647.49	−0.05	$^7D^\circ_5$— 55_6	
3898.773	2		25641.83	+0.06	26_2— 525°_2	
3899.782	2	3 *s*	25635.19	+0.22	263°_2—52002_3	
3901.250	3	1 *b*	25625.55	−0.06	19826_5— 454°_5	
3901.826	20	1	25621.76	−0.01	18_3— 445°_2	(0)
3902.672	4		25616.21	+0.03	22_0— 483°_1	
3902.730	1		25615.83	−0.10	26_2— 524°_1	
3902.820	2		25615.24	+0.05	28_5— 538°_4	
3903.294	12		25612.13	−0.01	$^5S_2$— 438°_1	
3903.984	20	2	25607.60	−0.06	$^7D^\circ_5$— 55_5	
3904.890	2		25601.66	−0.03	29853_4—55455°_5	
3905.660	1		25596.61	+0.09	32_4— 577°_3	
3905.972	20	4	25594.57	−0.01	19_3— 454°_2	Res
3906.240	4		25592.81	+0.07	27_4— 528°_3	
3907.090	2		25587.25	+0.07	23_3— 495°_2	
3907.190	8		25586.59	−0.01	20_0— 457°_1	
3907.924	1		25581.78	+0.02	19535_5— 451°_4	
3909.790	2	1	25569.57			
3911.280	5		25559.83	+0.05	$^7D^\circ_5$— 55_4	
3911.740	1		25556.83	+0.08	28291_3— 538°_4	
3912.810	10	1	25549.84	+0.02	17_3— 432°_4	
3914.16	2 *b*		25541.03			
3915.15	2		25534.57	+0.11	23_2— 495°_2	
3915.614	3		25531.54	0.00	23_2— 495°_3	
3916.386	4		25526.51	+0.03	17_3— 432°_2	
3917.260	2		25520.82	+0.11	28898_2— 544°_1	
3917.624	6		25518.45	+0.01	291°_3— 54_3	
3918.195	2		25514.73			
3918.266	1 *b*		25514.27	+0.15	24_2— 503°_3	
3918.438	3		25513.14	0.00	$^3H_5$— 405°_4	
3918.587	20		25512.17	+0.05	$^3H_4$— 376°_3	
3920.025	4		25509.32			
3920.646	1		25498.77			
3922.326	8		25487.86	+0.04	23_3— 494°_3	
3922.606	1 *b*		25486.04	+0.04	33_5— 587°_4	
3922.716	1		25485.32	+0.20	30_2— 558°_1	
3924.362	10		25474.63	−0.01	20_1— 459°_2	
3924.687	10		25472.53	+0.02	18_3— 444°_3	3

TABLE 3. *Observed and classified lines of* W I

Wavelength Å	Intensity		Wavenumber (cm^{-1})		Classification	Zeeman effect
	Arc	Spark	Observed	o−c		
3925.058	1		25470.11	+0.09	28_6— 538°_5	
3926.027	10		25463.83	+0.01	15_3— 409°_3	3
3926.35	2 *b*		25461.74	+0.02	291°_2— 54_3	
3926.46	1 *b*		25461.02	+0.12	23_2— 494°_1	
3929.294	3		25442.65	+0.06	31_5— 568°_4	
3929.664	3		25440.26			
3930.232	12	2	25436.58	+0.07	19826_5— 452°_4	Res
3930.474	15	2	25435.02	+0.04	29_7— 548°_6	(b)
3930.96	12	2	25431.81	−0.04	18_1— 435°_2	Res
3931.44	2		25428.77			
3931.926	4		25425.62	+0.01	17_4— 425°_4	
3934.593	4		25408.39	0.00	15_3— 408°_2	
3934.887	5		25406.49	0.00	$^3H_5$— 404°_5	
3935.033	25	2	25405.55	+0.06	13_2— 391°_1	
				−0.01	19535_5— 449°_4	
3935.352	5		25403.50			
3935.912	3		25399.88	0.00	$^3G_3$— 387°_4	
3936.062	4		25398.91			
3936.220	12		25397.89	+0.05	18_2— 435°_2	Res
3936.488	1		25396.16	+0.12	24_2— 501°_3	
3936.782	1		25394.27	+0.11	26_2— 522°_3	
3936.974	25		25393.03	+0.04	18_3— 443°_2	
3937.614	15		25388.90	+0.01	19535_5— 449°_6	
3937.73	1		25388.15			
3938.777	3 *b*		25381.40			
3939.434	8	3 *s*	25377.17			
3939.684	1 *b*		25375.56			
3939.894	5		25374.21	+0.05	22476_4— 478°_5	
3940.415	1		25370.85	+0.04	28898_2— 542°_3	
3941.824	8		25361.78	+0.04	18_2— 434°_3	
3942.338	4 *b*	1 *b*	25358.48			
3944.790	6		25342.71	−0.01	$^3P_2$— 445°_2	
3945.197	5		25340.10	+0.02	23_3— 492°_2	
3945.971	1 *b*		25335.13	−0.02	314°_4—56768_5	
3946.296	8 *b*		25333.04	+0.08	20_1— 457°_1	3
				0.00	23_1— 487°_1	
3947.977	20	2	25322.25	−0.03	19_6— 449°_7	(b)
3948.673	2		25317.79	+0.04	22852_4— 481°_3	
3949.636	2		25311.62			
3950.113	5	3 *l*	25308.56	−0.05	20_2— 462°_1	
3950.384	1		25306.83			
3951.161	4 *b*		25301.86	0.00	259°_1— 51_0	
3951.876	6	1	25297.28			
3952.254	5		25294.85			
3952.517	25	2	25293.17	0.00	14_2— 402°_3	(b)
3952.897	20		25290.74	+0.01	19826_5— 451°_4	(b)
3953.152	30	3	25289.11	+0.02	19_3— 451°_4	(0)
3953.422	5		25287.38	+0.02	23_2— 492°_2	
3953.708	6		25285.55	−0.03	22852_4— 481°_5	
3955.304	40	4	25275.35	−0.01	19_6— 449°_6	3

TABLE 3. *Observed and classified lines of* W I

Wavelength Å	Intensity		Wavenumber (cm^{-1})		Classification	Zeeman effect
	Arc	Spark	Observed	o−c		
3955.763	2		25272.42	+0.02	29_7 — 547°_6	
3956.29	2		25269.05	+0.01	$^3P_1$ — 385°_0	
3957.066	3*b*		25264.09	−0.07	293°_2 — 54_3	
3957.219	1		25263.12	+0.09	$^3G_4$ — 416°_3	
3958.874	20		25252.56	+0.02	13_2 — 390°_2	3
3961.756	4		25234.19	−0.01	$^5S_2$ — 435°_2	
3962.324	15	2	25230.57	+0.01	$^3H_6$ — 422°_6	3
3963.562	1		25222.69	+0.07	27_4 — 524°_4	
3963.695	4		25221.84	−0.02	23_3 — 491°_2	
3964.319	3		25217.87	0.00	23_3 — 491°_4	
3964.798	1*b*		25214.83	−0.19	27_1 — 528°_2	
3964.992	10		25213.59	+0.01	$^5D_4$ — 314°_4	
3965.137	20	1	25212.67	+0.02	22476_4 — 476°_4	Res
3965.483	4*b*		25210.47			
3965.632	3		25209.52	−0.04	17_3 — 429°_4	
3965.905	1		25207.8			
3966.210	3		25205.85	+0.01	15_3 — 406°_3	
3966.754	5*b*		25202.39	−0.05	26_2 — 520°_2	
3967.175	2		25199.72	−0.08	20_0 — 453°_1	
3967.392	1*b*		25198.34	+0.24	$^5S_2$ — 434°_3	
3968.171	6		25193.39	−0.07	$^3P_2$ — 444°_3	
3968.502	6		25191.29	+0.02	$^3P_0$ — 347°_1	
3968.590	20	2	25190.73	−0.05	19_4 — 444°_3	
3969.004	1		25188.11			
3969.195	15	2	25186.89	+0.03	19_3 — 450°_3	
3970.798	30	3	25176.73	−0.13	$^7D^\circ_4$ — 53_5	(b)
3971.539	1		25172.03		30_2 — 555°_3	
3972.002	6		25169.10	−0.04	23_2 — 491°_2	
3972.806	4		25164.00	−0.04	$^3H_5$ — 402°_4	
3973.290	5	50	25160.94	+0.02	$^7F^\circ_1$ — e^5D_0	
3974.15	2		25155.50	−0.06	29853_4 — 550°_5	
3974.306	2		25154.50		28_1 — 538°_1	
3974.451	1		25153.60	−0.04	26_2 — 520°_3	
3974.84	1		25151.13			
3975.470	12		25147.14	−0.06	$^3H_4$ — 373°_5	
3975.896	8		25144.45	−0.05	17_4 — 422°_3	
3976.290	4		25141.95	−0.11	23_3 — 490°_3	
3976.52	2		25140.5	−0.13	314°_4–56573_5	
3977.001	2		25137.46	−0.03	31_5 — 565°_6	
3978.822	2		25125.96			
3979.290	30	3	25123.00	−0.06	15_3 — 405°_4	(b)
3979.519	1		25121.55	−0.05	20_2 — 461°_1	
3979.56	1*b*		25121.29			
3979.84	1*b*	1*b l*	25119.53	−0.13	$^7D^\circ_4$ — 53_3	
3980.298	4		25116.64	−0.12	22476_4 — 475°_3	
3980.644	25	3	25114.46	−0.07	19826_5 — 449°_4	(b)
3980.742	3		25113.84	−0.10	$^3P_2$ — 443°_2	
3980.910	4		25112.77	−0.12	19_3 — 449°_4	
3981.233	6		25110.74	−0.08	18_2 — 432°_2	
3981.578	2		25108.57			

318-092 O-69—10

TABLE 3. *Observed and classified lines of* W I

Wavelength Å	Intensity		Wavenumber (cm^{-1})		Classification	Zeeman effect
	Arc	Spark	Observed	o−c		
3982.45	1		25103.07			
3982.874	6		25100.40	−0.09	18_2 — 432°_1	
3982.968	10	1	25099.80	−0.10	$^3P_2$ — 443°_1	
3983.173	1		25098.51	−0.03	28291_3–53390°_3	
3983.292	50	5 *s*	25097.76	−0.10	19826_5 — 449°_6	z d
3984.634	2		25089.31	−0.03	24_2 — 490°_3	
3984.757	1		25088.53	−0.15	24_3 — 496°_2	
3985.668	5		25082.80	−0.05	$^5D_3$ — 299°_3	
3985.788	4		25082.04			
3987.531	5 *b*		25071.08			
3987.854	3		25069.05			
3988.010	8		25068.07	−0.05	$^3G_4$ — 414°_3	
3990.614	1		25051.71			
3991.227	15	1	25047.86	0.00	$^7F^\circ_2$ — $^7D_3$	
3991.518	4		25046.04	−0.12	22_0 — 478°_1	
3992.018	1 *b*		25042.90	+0.08	28347_3–53390°_3	
3992.756	12		25038.27	−0.06	33_5–58330°_4	
3993.911	8		25031.03	+0.02	$^7F^\circ_3$ — e^5D_2	
3994.774	3		25025.62	−0.02	24_3 — 496°_4	
3996.450	3		25015.13	+0.03	30_2 — 553°_3	
3997.008	1		25011.63	−0.12	19535_5 — 445°_5	
3997.136	8		25010.83	−0.07	18_3 — 439°_4	
3997.341	6		25009.55	+0.01	$^7F^\circ_2$ — e^5D_1	
3997.757	5		25006.95	−0.05	22476_4 — 474°_3	
3997.891	2		25006.11	−0.07	27_5 — 528°_6	
3998.160	10		25004.43	+0.03	$^7D^\circ_1$ — e^5D_1	
3998.756	15	1	25000.70	−0.01	18_3 — 439°_2	
3999.188	3		24998.00	−0.04	22852_4 — 478°_5	
				+0.08	28347_3–53345°_3	
3999.675	2		24994.96	−0.02	28_5 — 532°_6	
3999.76	1		24994.43	+0.01	20_1 — 454°_2	
4000.695	15	1	24988.59	−0.17	$^7D^\circ_4$ — 53_4	3
4001.380	20	2	24984.31	−0.09	$^3H_4$ — 371°_4	3
4002.656	3		24976.34	+0.04	28898_2 — 538°_1	
4002.782	1		24975.56			
4002.956	1		24974.47			
4005.152	1		24960.78	−0.03	28_5 — 531°_5	
4005.404	25		24959.21	+0.04	$^5D_1$ — 266°_0	(0)
4005.688	1		24957.44			
4005.893	8		24956.16			
4007.355	1		24947.06	−0.12	$^5S_2$ — 432°_2	
4007.437	1		24946.55	+0.02	28291_3 — 532°_4	
4008.753	1000	100	24938.36	−0.03	$^7S_3$ — $^7P^\circ_4$	
4009.005	5	2	24936.79	−0.06	$^5S_2$ — 432°_1	
4009.454	3		24934.00	+0.06	$^7D^\circ_3$ — e^5D_4	
4010.377	15	1	24928.26	+0.03	$^7F^\circ_3$ — $^7D_4$	
4011.022	3		24924.25	−0.05	27_5 — 527°_5	
4011.302	4		24922.51	−0.09	259°_1–50906_1	
4011.810	4		24919.35	−0.11	20_2 — 459°_2	
4012.492	1 *b*		24915.12			

TABLE 3. *Observed and classified lines of* W I

Wavelength Å	Intensity		Wavenumber (cm⁻¹)		Classification	Zeeman effect
	Arc	Spark	Observed	o−c		
4012.704	1		24913.81			
4012.988	1		24912.04			
4013.186	10		24910.81	−0.03	$^3G_3$ — 382°_4	
4013.440	1 *b*		14909.23			
4014.935	6		24899.96	−0.05	17_3 — 426°_3	
4015.218	100	40	24898.20	−0.02	19_6 — 445°_5	
4016.108	6		24892.68	+0.03	$^7F^\circ_4$ — e^5D_3	
4016.524	50	3	24890.11	0.0	$^7P^\circ_3$ — 52_4	Res
4016.922	3		24887.64	+0.06	33_5 — 581°_5	
4017.348	5		24885.00	−0.06	22476_4 — 473°_3	
				+0.15	28_5 — 531°_5	
4018.313	3		24879.03	−0.02	20_1 — 453°_0	
4018.750	3		24876.32	−0.01	18_3 — 438°_3	
4018.898	1		24875.41			
4019.123	2		24874.01			
4019.227	60	3	24873.37	0.00	$^5D_2$ — 281°_1	
4020.204	2		24867.33	+0.06	27_4 — 520°_5	
4021.746	3		24857.79	−0.03	$^3G_3$ — 382°_3	
4022.115	15		24855.51	−0.03	$^7F^\circ_1$ — $^7D_2$	(b)
4022.830	4		24851.09			
4022.994	1 *b*		24850.08			
4023.492	2		24847.01			
4023.666	1		24845.93	−0.03	27_4 — 520°_4	
4025.194	5		24836.50	−0.03	22852_4 — 476°_4	
4025.348	1		24835.55	−0.17	28_6 — 532°_6	
4025.888	1		24832.22	+0.01	26_2 — 51693°_2	
4026.028	2		24831.35	−0.09	17_3 — 425°_4	
4026.822	1 *b*		24826.46	+0.05	28291_3 — 531°_4	
4028.786	40	2	24814.35	−0.03	$^3P_0$ — 343°_1	
4029.023	5		24812.90	−0.06	17_3 — 425°_3	
4029.603	6		24809.32	−0.02	15_3 — 402°_3	
4029.922	3		24807.36			
4029.982	3		24807.00	−0.02	24_3 — 494°_3	
4030.844	1		24801.70	+0.15	28_6 — 531°_5	
4031.668	6		24796.62	−0.03	$^7P^\circ_3$ — 52_3	
4032.382	4		24792.23			
4032.622	3		24790.75			
4033.466	1 *b*		24785.56	+0.01	31_5 — 561°_4	
4034.744	2		24777.71	−0.07	20_2 — 457°_1	
4034.898	1 *b*		24776.77			
4035.356	12		24773.96	0.00	15_3 — 402°_4	
4036.227	2		24768.62	+0.02	19_3 — 445°_2	
4036.428	2		24767.38	−0.06	$^3P_2$ — 440°_3	
4036.520	2		24766.82	−0.01	$^3G_4$ — 411°_4	
4036.855	40	2	24764.77	−0.01	19_4 — 440°_3	(b)
4039.418	8		24749.05	−0.11	17_3 — 424°_4	
4039.854	12		24746.38	+0.02	18_3 — 437°_4	
4039.922	5		24745.97	−0.03	23_3 — 486°_4	
4040.588	10		24741.88	0.00	19_6 — 443°_6	
4040.80	3		24740.6	−0.04	22852_4 — 475°_3	

TABLE 3. *Observed and classified lines of* W I

Wavelength Å	Intensity		Wavenumber (cm⁻¹)		Classification	Zeeman effect
	Arc	Spark	Observed	o−c		
4041.08	2		24738.88	0.00	$26_2 - 516^\circ_3$	
4042.390	6		24730.86	+0.02	$14_2 - 397^\circ_2$	
4042.674	3		24729.12	−0.05	$19_4 - 439^\circ_4$	
4043.408	3		24724.63	−0.05	$24_2 - 495^\circ_3$	
4043.526	2		24723.91			
4043.894	8		24721.66	0.00	$^3P_2 - 439^\circ_2$	
4044.048	3		24720.72	0.00	$19826_5 - 445^\circ_5$	
4044.280	30		24719.30	0.00	$^7P^\circ_2 - 50949_1$	(0)
4045.404	5 *b*		24712.43	+0.03	$^3H_4 - 368^\circ_3$	
4045.594	100	10	24711.27	+0.04	$^7S_3 - 276^\circ_2$	Res
4046.702	25	2	24704.51	+0.02	$^3G_3 - 380^\circ_3$	
4046.98	1		24702.81	−0.04	$29853_4 - 545^\circ_3$	
4047.938	12	1	24696.96	−0.03	$^5D_1 - 263^\circ_2$	
4048.136	2		24695.75		$32_4 - 568^\circ_4$	
4048.320	5		24694.63	−0.04	$20_2 - 456^\circ_3$	
4048.854	5		24691.37			
4050.493	1		24681.38	+0.08	$28204_2 - 528^\circ_2$	
4051.300	3 *b*		24676.47	+0.04	$^7P^\circ_2 - 50906_1$	
4052.32	6		24670.26	+0.03	$14_2 - 396^\circ_3$	
4052.68	2 *b*		24668.07	+0.06	$19_4 - 439^\circ_5$	
4053.932	15	2	24660.45	+0.01	$14_2 - 396^\circ_1$	
4055.056	1		24653.61	+0.01	$23_6 - 481^\circ_5$	
4055.23	5		24652.56	0.00	$^3G_3 - 380^\circ_4$	
4055.642	4		24650.05	+0.02	$^3H_5 - 397^\circ_4$	
4056.181	2 *b*		24646.77	−0.11	$^5F^\circ_3 - 53_4$	
4056.459	2		24645.08	−0.01	$28347_3 - 529^\circ_4$	
4056.908	2		24642.36	+0.08	$27_4 - 518^\circ_4$	
4057.460	4		24639.01	−0.05	$^3P_2 - 438^\circ_1$	
4059.244	4		24628.18	−0.06	$24_2 - 494^\circ_3$	
4060.166	1	2 *s*	24622.58	+0.04	$28_5 - 528^\circ_6$	
4060.234	2		24622.17	−0.07	$276^\circ_2 - 52_3$	
4060.705	12		24619.32	−0.02	$19_3 - 444^\circ_3$	
4062.260	1		24609.9			
4064.580	4		24595.85	−0.03	$28347_3 - 529^\circ_3$	
4064.791	40	4	24594.57	−0.03	$19_4 - 438^\circ_3$	
4065.320	6		24591.37	+0.08	$^7F^\circ_4 - {}^7D_5$	
4065.992	5		24587.30	−0.03	$17_4 - 416^\circ_3$	
4066.910	8		24581.76	−0.03	$263^\circ_2 - 50949_1$	
4067.513	2		24578.11	−0.02	$13_2 - 383^\circ_1$	
4069.154	4		24568.20	−0.10	$20_2 - 455^\circ_3$	
4069.794	12	3	24564.34	−0.04	$19826_5 - 443^\circ_6$	
4069.950	80	8	24563.40	0.00	$^5D_3 - 293^\circ_2$	Res
4070.608	60	2	24559.42	−0.06	$^5D_1 - {}^7P^\circ_2$	
4070.890	1 *b*		24557.72			
4071.928	25		24551.46	−0.03	$15_3 - 400^\circ_2$	
4073.150	12		24544.10	−0.02	$^3H_5 - 396^\circ_5$	
4073.864	3		24539.80	−0.02	$19_3 - 443^\circ_2$	
4074.358	600	60	24536.82	0.00	$^7S_3 - {}^7P^\circ_3$	Res
4076.124	2		24526.19			
4077.043	5		24520.66	−0.02	$276^\circ_2 - 52183_2$	

TABLE 3. *Observed and classified lines of* W I

Wavelength Å	Intensity		Wavenumber (cm^{-1})		Classification	Zeeman effect
	Arc	Spark	Observed	o−c		
4078.119	6		24514.19	+0.05	$^7P^\circ_3$–52002$_3$	
4079.258	4		24507.35	−0.04	22852$_4$– 473$^\circ_4$	
4079.458	1		24506.15	0.00	28$_1$– 532$^\circ_1$	
4079.804	3		24504.08	+0.01	18$_3$– 434$^\circ_3$	
4080.166	1 *b*		24501.90			
4081.737	1		24492.46	−0.06	$^3G_4$– 409$^\circ_3$	
4082.054	3		24490.56	−0.10	18$_1$– 425$^\circ_1$	
4082.958	30	3	24485.14	+0.01	19$_4$– 437$^\circ_5$	(0)
4083.711	6		24480.62	−0.05	$^3G_4$– 409$^\circ_5$	
4085.044	2		24472.64			
4086.00	2		24466.91	+0.05	$^3P_1$– 377$^\circ_1$	
4086.525	3		24463.77			
4086.961	2		24461.16	−0.10	24$_3$– 490$^\circ_3$	
4087.388	4		24458.60	0.00	31$_5$– 558$^\circ_6$	
4087.729	1		24456.56	−0.09	18$_2$– 425$^\circ_1$	
4087.980	1		24455.06	−0.10	22476$_4$– 469$^\circ_4$	
4088.330	30	1	24452.97	0.00	$^5D_2$– 277$^\circ_1$	
4088.768	10		24450.35	−0.05	19535$_5$– 439$^\circ_4$	
4089.054	2 *b*		24448.64	−0.09	$^7P^\circ_3$– 51$_2$	
4089.380	8		24446.68	+0.02	$^7F^\circ_5$– e^5D_4	
4090.30	2		24441.2			
4090.636	6		24439.19	−0.01	20$_2$– 454$^\circ_2$	
4091.040	4		24436.77			
4091.212	3		24435.74			
4092.392	10 *b*		24428.70	+0.03	13$_2$– 382$^\circ_3$	
4093.134	10 *b*		24424.27			
4094.747	3		24414.65			
4095.693	15		24409.01	−0.01	$^3H_6$– 414$^\circ_6$	3
4095.992	2		24407.22	+0.06	23$_2$– 483$^\circ_1$	
4096.424	2 *b*		24404.65	−0.05	277$^\circ_1$–52183$_2$	
4096.756	1 *b*		24402.67			
4097.344	2 *b*		24399.18	+0.14	26$_2$– 512$^\circ_1$	
4097.664	10		24397.27	−0.03	18$_2$– 425$^\circ_3$	
4097.826	3		24396.30	−0.03	23$_3$– 483$^\circ_3$	
4098.028	2 *b*		24395.10	+0.02	$^7P^\circ_4$–52284$_3$	
4098.48	3		24392.4	−0.02	17$_4$– 414$^\circ_3$	
4099.016	10		24389.22	−0.02	19535$_5$– 439$^\circ_5$	
4100.334	2		24381.37	−0.03	28$_6$– 527$^\circ_5$	
4100.891	6		24378.07	−0.05	22476$_4$– 468$^\circ_5$	
4101.648	3		24373.57			
4101.845	8		24372.40			
4102.367	2 *b*		24369.30	−0.01	29479$_4$– 538$^\circ_4$	
4102.702	100	10	24367.31	0.00	$^5D_4$– 305$^\circ_3$	
4102.942	4		24365.88	+0.04	$^5D_2$– 291$^\circ_2$	
4103.118	6		24364.84	−0.08	23$_1$– 478$^\circ_1$	
4106.698	6		24343.60	−0.01	23$_2$– 483$^\circ_3$	
4107.816	5		24336.97	−0.02	$^5D_2$– 276$^\circ_2$	
4108.529	12		24332.75	−0.01	18$_2$– 424$^\circ_2$	
4109.746	30	3	24325.54	+0.02	$^3G_3$– 376$^\circ_3$	
4110.572	8		24320.66	−0.05	$^5S_2$– 426$^\circ_3$	

TABLE 3. *Observed and classified lines of* W I

Wavelength Å	Intensity		Wavenumber (cm^{-1})		Classification	Zeeman effect
	Arc	Spark	Observed	o−c		
4111.672	5		24314.15	−0.06	23_3 − 482°_2	
4111.815	25		24313.30	−0.01	$^5D_1$ − 259°_1	
4112.484	8		24309.35	−0.02	20_1 − 447°_1	
4114.19	1	2 *s*	24299.27	+0.06	28204_2 − 525°_2	
4114.821	6 *b*		24295.54	−0.04	$^7P^\circ_2$ − 50_2	
4115.585	12		24291.03	−0.05	$^3H_5$ − 393°_5	
4116.718	3		24284.35			
4118.052	25	3	24276.48	−0.01	18_3 − 432°_4	
4118.186	15	2	24275.69	−0.02	19_6 − 439°_5	
4118.246	5		24275.34	0.00	13_2 − 380°_3	
4118.976	6		24271.04			
4119.287	1 *b*	*b*	24269.21	+0.18	33_5 − 575°_5	
4120.22	1 *b*		24263.7	0.00	29853_4 − 541°_3	
4120.356	1 *b*		24262.9			
4120.854	15		24259.98	+0.03	15_3 − 397°_4	
4122.014	12		24253.15	0.00	18_3 − 432°_2	
4123.051	10		24247.05	+0.04	15_3 − 397°_2	
4124.164	2 *b*		24240.50	+0.03	23_3 − 481°_3	
4125.164	20	2	24234.63	+0.09	$^3G_4$ − 406°_3	
4125.325	8		24233.68	+0.02	$^5S_2$ − 425°_3	
4125.727	2		24231.32	+0.03	27_5 − 520°_5	
4126.803	30	3	24225.00	−0.02	$^3P_2$ − 434°_3	
4127.257	5		24222.34	0.00	19_4 − 434°_3	
4129.982	3		24206.36	0.00	19535_5 − 437°_5	
4130.539	1		24203.10	+0.10	28_5 − 524°_4	
4132.202	10		24193.35	+0.03	19_3 − 440°_3	
4132.472	3 *b*		24191.77			
4133.160	2 *b*		24187.74	−0.01	23_2 − 481°_3	
4133.388	8		24186.41	+0.01	15_3 − 396°_3	
4133.481	5		24185.87	+0.01	19535_5 − 437°_4	
4134.581	1		24179.43	−0.04	18_1 − 422°_1	
4136.348	5		24169.10	−0.02	$^5S_2$ − 424°_2	
4137.457	80	8	24162.62	+0.04	$^5D_2$ − $^7P^\circ_3$	
4138.018	40	4	24159.35	−0.02	19826_5 − 439°_4	
4138.304	15	2	24157.68	−0.05	19_3 − 439°_4	
4139.318	10	1	24151.76	0.00	$^3G_4$ − 405°_4	
4140.039	8		24147.56	+0.02	19_3 − 439°_2	
4140.400	8		24145.45	−0.01	18_2 − 422°_1	
4140.797	1		24143.13	+0.09	28898_2 − 530°_1	
4142.253	25	2	24134.65	−0.02	18_2 − 422°_3	
4142.693	2		24132.08			
4144.812	2		24119.75	+0.04	32_4 − 562°_4	
4145.160	25	1	24117.72	−0.02	$^3G_3$ − 374°_2	
4145.860	4		24113.65	0.00	$^7D^\circ_2$ − e^5D_2	
4145.947	10		24113.14	0.00	$^3H_4$ − 362°_5	
4147.385	2		24104.78	+0.02	28898_2 − 530°_2	
4148.516	3		24098.22	+0.01	19826_5 − 439°_5	
4149.074	3 *b*		24094.97			
4149.435	10		24092.88	+0.05	19_6 − 437°_5	
4149.737	6		24091.12	−0.01	17_4 − 411°_4	

TABLE 3. *Observed and classified lines of* W I

Wavelength Å	Intensity		Wavenumber (cm^{-1})		Classification	Zeeman effect
	Arc	Spark	Observed	o−c		
4151.822	2		24079.03	−0.01	22852_4 — 469°_4	
4152.182	2		24076.94	+0.03	27_4 — 512°_5	
4154.096	2		24065.84			
4154.664	20	2	24062.55	0.00	$^7F^\circ_0$ — $^7D_1$	(0)
4155.277	2*b*		24059.0			
4155.527	2*b*		24057.56			
4156.064	3*b*		24054.45			
4157.677	2		24045.09	−0.02	$^3G_4$ — 404°_5	
4158.822	2		24038.50	−0.04	23_3 — 479°_4	
4158.954	2		24037.73			
4159.609	4		24033.95			
4159.782	5		24032.95	0.00	17_3 — 417°_2	
4160.030	8	1	24031.52	0.00	20_2 — 450°_3	
4160.341	8	1	24029.72	+0.03	22476_4 — 465°_5	
4161.476	4		24023.17	+0.01	19_3 — 438°_3	
4163.914	3		24009.10	+0.04	29853_4 — 538°_5	
4164.398	2		24006.31	+0.01	27_5 — 518°_4	
4164.998	1		24002.85	+0.05	28_6 — 523°_5	
4165.152	4		24001.96	−0.04	22852_4 — 468°_5	
4166.139	10		23996.28	+0.03	13_2 — 377°_1	
4166.40	2		23994.78	+0.02	19_4 — 432°_4	
4166.676	2		23993.19	+0.03	17_3 — 416°_3	
4166.846	4		23992.21			
4167.002	2*b*		23991.31			
4168.652	12	4	23981.82	0.00	$^5S_2$ — 422°_1	
4169.996	4		23974.08	−0.02	$^3P_2$ — 432°_2	
4170.526	30	3	23971.04	+0.01	$^5S_2$ — 422°_3	
4170.820	1		23969.35			
4171.174	60	6	23967.32	+0.08	$^5D_3$ — $^7D^\circ_4$	
4171.415	2		23965.93			
4171.794	2		23963.75	−0.02	$^3P_2$ — 432°_1	
4172.934	2		23957.20	+0.08	31_5 — 553°_4	
4174.52	2*b*		23948.1	+0.01	$^5F^\circ_4$ — 55_5	
4175.988	5		23939.68	+0.02	20_1 — 443°_2	
4176.589	2		23936.24	+0.01	18_3 — 429°_4	
4177.822	8*b*		23929.18			
4178.054	2		23927.85			
4178.445	1		23925.61	−0.01	20_1 — 443°_1	
4179.366	2*b*		23920.33	−0.01	$^3H_4$ — 360°_4	
4180.232	10		23915.38	+0.05	19826_5 — 437°_5	
4181.388	5		23908.77	−0.01	22476_4 — 463°_3	
4182.305	2		23903.53	+0.05	$^3H_6$ — 409°_5	
4182.89	2		23900.18	−0.03	314°_4 — 55_4	
4183.655	10		23895.81	+0.02	18_1 — 419°_2	
4183.816	12	1	23894.90	+0.07	19826_5 — 437°_4	
4186.002	6		23882.41	0.00	18_1 — 419°_0	
4187.643	1*b*		23873.06	−0.09	299°_3 — 53_4	
4189.149	3*b*		23864.47			
4189.619	2		23861.80	+0.02	18_2 — 419°_2	
4189.788	1		23860.84	+0.10	28291_3 — 521°_2	

TABLE 3. *Observed and classified lines of* W I

Wavelength Å	Intensity		Wavenumber (cm⁻¹)		Classification	Zeeman effect
	Arc	Spark	Observed	o−c		
4189.960	1		23859.86	−0.02	28204_2— 520°_2	
4190.136	3 *b*		23858.85	−0.05	281°_1—52057_1	
4190.395	1 *b*		23857.38	+0.12	26_2— 507°_2	
4192.087	2		23847.75	+0.10	28_5— 520°_5	
4192.363	1		23846.2			
4192.578	1		23844.96			
4193.786	6		23838.09	+0.05	$^3G_4$— 402°_3	
4193.950	5		23837.16	+0.02	23_2— 478°_1	
4195.54	1		23828.1			
4195.840	1		23826.42	+0.08	28_5— 520°_4	
4197.044	1		23819.58			
4197.530	2		23816.83	+0.01	17_4— 409°_5	
4197.982	1 *b*		23814.26			
4198.57	1		23810.93	−0.15	28204_2— 520°_3	
4199.617	8		23805.00	+0.03	17_4— 409°_5	
4200.020	15		23802.71	+0.05	$^3G_4$— 402°_4	
4200.419	2		23800.45	−0.08	23_1— 472°_1	
4200.885	4		23797.81	+0.01	$^3G_3$— 371°_4	
4201.615	1		23793.68			
4203.165	1		23784.90			
4203.816	15	2	23781.21	0.00	$^3H_4$— 359°_3	
4203.957	2		23780.41			
4204.405	30	3	23777.88	+0.02	19_4— 430°_5	(0)
4204.724	2		23776.08			
4205.550	12		23771.41	+0.09	$^7D^\circ_1$— e^5D_0	
4206.164	2		23767.94	+0.04	28291_3— 520°_4	
4206.236	15		23767.53	+0.09	29_7— 532°_6	
4207.052	50	5	23762.92	−0.04	19_6— 434°_7	
4207.71	1		23759.2	−0.04	23_3— 476°_4	
4208.135	2		23756.81	+0.12	28_1— 524°_1	
4208.888	3	1	23752.56			
4209.50	2		23749.1			
4209.776	3		23747.55			
4210.185	5		23745.24	0.00	28_5— 519°_6	
4212.886	5	1	23730.02			
4214.056	4		23723.43	+0.03	28291_3— 520°_3	
4214.954	6		23718.37	−0.05	20_6— 438°_1	
4215.376	25		23716.00	+0.01	19535_5— 432°_4	
4215.548	2 *b*	3 *b*	23715.03	+0.10	29479_4— 531°_5	
4216.048	2 *b*	1	23712.22	+0.04	28347_3— 520°_4	
4216.797	2 *b*	1	23708.01	+0.05	24_3— 483°_2	
4218.552	15	2	23698.14	0.00	$^5S_2$— 419°_2	
4219.011	2		23695.57	−0.08	27_4— 509°_4	
4219.372	80	8	23693.54	+0.02	$^5D_4$— 299°_3	Res
4220.273	6	2	23688.48	−0.11	13_2— 374°_2	
				+0.09	28_6— 520°_5	
4220.534	5		23687.02	+0.02	19_3— 435°_2	
4221.717	6	1	23680.38	+0.08	27_4—50894°_3	
4222.045	20	2	23678.54	+0.03	$^3H_5$— 387°_4	
4223.978	4		23667.70	+0.02	28347_3— 520°_3	

TABLE 3. *Observed and classified lines of* W I

Wavelength Å	Intensity		Wavenumber (cm^{-1})		Classification	Zeeman effect
	Arc	Spark	Observed	o−c		
4224.763	20	2	23663.30	−0.06	23_3 — 475°_3	
4225.260	3 *b*		23660.52			
4225.627	3 *b*		23658.47			
4226.338	20	2	23654.49	−0.01	19_4 — 429°_4	
4226.503	4	1	23653.56	−0.01	22852_4 — 465°_5	
4226.915	25	2	23651.26	−0.04	18_1 — 417°_2	
4229.792	1		23635.17	+0.14	$^7P^\circ_3$ — e^5D_4	
4230.150	2 *h*		23633.17	−0.24	24_3 — 482°_2	
				+0.27	26_2 — 504°_2	
4231.320	8	1	23626.64	−0.04	18_3 — 426°_3	
4231.734	12	1	23624.33	−0.05	23_1 — 470°_2	
4231.938	4		23623.19	−0.05	27_5 — 514°_4	
4232.035	2	1	23622.64	−0.02	28_5 — 518°_4	
4232.996	20	2	23617.28	−0.01	18_2 — 417°_2	
4234.345	40	4	23609.76	0.00	19_4 — 428°_5	
4236.622	8	1	23597.07	+0.01	$^3P_1$ — 369°_2	
4237.487	2		23592.25	0.00	27_4 — 508°_5	
4240.140	15		23577.49	−0.01	18_2 — 416°_3	
4240.913	3		23573.19			
4241.445	100	10	23570.24	0.00	15_3 — 390°_2	
4243.350	8		23559.65	−0.02	24_3 — 481°_3	
4243.630	20		23558.10	−0.01	18_3 — 425°_4	
4244.088	1		23555.56	+0.04	$^3G_3$ — 369°_2	
4244.364	200	20	23554.03	+0.02	$^5D_4$ — $^7D^\circ_5$	
4245.557	10	1	23547.41	+0.03	20_1 — 439°_2	
4247.006	1		23539.37	−0.26	18_3 — 425°_3	
4248.852	5		23529.15	−0.03	24_2 — 483°_2	
4249.452	20	2	23525.83	+0.03	$^3G_3$ — 368°_3	
4250.812	10		23518.30			
4250.894	5		23517.84	−0.01	22_0 — 462°_1	
4251.880	5	1	23512.39	−0.06	23_3 — 474°_2	
4253.242	3	1	23504.86			
4254.052	12	1	23500.39	+0.02	18_1 — 415°_2	
4254.284	15	1	23499.10	+0.01	19535_5 — 430°_5	
4254.675	2		23496.94	−0.02	17_3 — 411°_4	
4255.594	3		23491.87	+0.01	29853_4 — 53345°_3	
4257.978	3		23478.72			
4258.458	10	1	23476.07	+0.01	17_4 — 405°_4	
4258.524	5		23475.71	−0.02	18_3 — 424°_4	
4258.626	1		23475.15	+0.06	18_3 — 424°_2	
4259.351	80	8	23471.16	+0.08	$^7F^\circ_2$ — e^7D_2	
4259.932	12	1	23467.95	+0.03	$^3H_6$ — 404°_5	
4260.130	2		23466.86	+0.02	$^7D^\circ_3$ — e^5D_3	
4260.287	30	3	23466.00	+0.06	$^7D^\circ_1$ — e^7D_2	
4260.511	3		23464.76	−0.02	20_1 — 438°_1	
4260.652	2		23463.99	−0.01	20_2 — 444°_3	
4260.86	2		23462.84	−0.02	333°_5 — 56_6	
4262.267	4	1	23455.10			
4263.304	50	5	23449.39	+0.08	$^7F^\circ_3$ — $^7D_3$	
4264.664	1		23441.91	−0.23	26_2 — 503°_3	

TABLE 3. *Observed and classified lines of* W I

Wavelength Å	Intensity		Wavenumber (cm^{-1})		Classification	Zeeman effect
	Arc	Spark	Observed	o−c		
4264.840	5	1	23440.94	+0.01	27_5— 512°_5	
4264.980	10	1	23440.17			
4266.538	20	2	23431.61	−0.05	23_3— 473°_3	
4266.822	3		23430.06	−0.05	23_3— 473°_4	
4267.745	6		23424.99	+0.03	19826_5— 432°_4	
4268.045	12	1	23423.34	+0.02	19_3— 432°_4	
4269.382	200	20	23416.01	+0.02	$^7S_3$— 263°_2	
4269.774	40	4	23413.86	0.00	$^5S_2$— 416°_3	
4270.900	10	1	23407.68	−0.03	23_3— 473°_2	
4271.228	4 *g*		23405.89			
4271.695	1		23403.33	−0.01	17_3— 411°_2	
4272.300	8	1	23400.01	+0.03	19_3— 432°_2	
4272.985	1 *b*		23396.26	−0.06	28204_2— 516°_3	
4273.210	2		23395.03	+0.03	29_7— 528°_6	
4273.356	5		23394.23			
4273.688	20	2	23392.41	−0.01	22476_4— 458°_4	
4273.850	5		23391.53			
4274.136	1 *b*		23389.96			
4274.548	100	10	23387.71	+0.03	$^7F^\circ_1$— $^7D_1$	
4274.932	10	2	23385.61	+0.05	19_6— 430°_5	
4275.142	6	1	23384.46	−0.02	20_2— 443°_2	
4275.486	50	5	23382.58	−0.01	18_2— 414°_3	
4275.800	6	1	23380.86	−0.03	24_2— 481°_3	
4276.016	20	1	23379.68	+0.02	14_2— 383°_1	
4276.740	60	6	23375.72	−0.01	19535_5— 429°_4	
4277.310	3		23372.60			
4277.703	3		23370.46	+0.02	20_2— 443°_1	
4277.898	4		23369.39	−0.02	17_4— 404°_5	
4278.405	12	1	23366.62	+0.02	$^3P_1$— 366°_2	
4280.280	1 *b b*		23356.39	+0.11	32_4—55492°_5	
4280.540	2		23354.97	−0.02	23_2— 473°_2	
4280.760	4	*g*	23353.77			
4281.210	4	*g*	23351.32	−0.11	23_1— 468°_2	
4281.898	3		23347.57	−0.06	$^3P_2$— 426°_3	
4282.040	2		23346.79			
4282.345	30	3	23345.13	+0.02	$^3H_4$— 355°_5	
4282.723	2	*g*	23343.07	−0.13	28_1— 520°_2	
4282.922	1		23341.98			
4283.180	1 *l*		23340.57	−0.02	29853_4— 531°_5	
4283.800	20	2	23337.20	+0.01	$^3H_4$— 354°_3	
4284.359	3		23334.15			
4284.964	25	3	23330.86	−0.13	19535_5— 428°_5	
				+0.02	22_6— 461°_1	
4286.008	30	5	23325.17	+0.03	$^3G_3$— 366°_2	
4286.208	6	1	23324.08	+0.02	26_2— 501°_3	
4286.982	2		23319.87	−0.06	$^3P_2$— 425°_1	
4287.914	1 *b*		23314.81	−0.09	28291_3—51606°_2	
4288.350	2		23312.44	−0.02	22476_4— 457°_5	
4290.138	10	1	23302.72	0.00	$^5S_2$— 415°_2	
4290.530	2		23300.59			

TABLE 3. *Observed and classified lines of* W I

Wavelength Å	Intensity		Wavenumber (cm⁻¹)		Classification	Zeeman effect
	Arc	Spark	Observed	o−c		
4291.502	3		23295.31	+0.15	30_2 — 536°_2	
4292.149	1		23291.80			
4292.730	4		23288.65	0.00	$^3G_4$ — 397°_4	
4293.110	2		23286.59	+0.04	276°_2–50949_1	
4293.280	2		23285.66			
4293.535	3		23284.28			
4294.097	30	5	23281.24	+0.02	$^3P_1$ — 365°_0	
4294.606	800	80	23278.48	0.00	$^7S_3$ — $^7P^\circ_2$	
4294.996	12	2	23276.36	−0.02	19_4 — 425°_4	
4295.683	6	1	23272.64	−0.11	23_2 — 472°_1	
4297.140	3		23264.75	+0.12	29853_4 — 531°_4	
4297.860	3 *b*		23260.85	+0.27	$^3P_2$ — 425°_3	
4298.410	10		23257.88	−0.02	19_4 — 425°_3	
4302.110	200	20	23237.88	−0.03	$^7S_3$ — $^7D^\circ_3$	
4302.897	4	*g*	23233.62	+0.16	$^7P^\circ_4$ — e^5D_4	
4303.528	3		23230.22	+0.02	14_2 — 382°_3	
4304.934	3		23222.63	−0.02	17_3 — 409°_3	
4305.318	3		23220.56			
4305.614	10	1	23218.96	+0.01	$^5S_2$ — 414°_3	
4306.325	4		23215.13	+0.03	$^3G_4$ — 396°_3	
4306.870	60	6	23212.19	+0.04	$^7F^\circ_4$ — $^7D_4$	
4307.638	50	5	23208.06	0.00	19826_5 — 430°_5	
4308.496	4		23203.43	−0.07	333°_5–56573_5	
4308.944	15	1	23201.02	+0.01	22476_4 — 456°_3	
4309.260	4 *b*		23199.32	−0.04	305°_3 — 53_4	
4309.864	8		23196.07	+0.03	$^3P_2$ — 424°_2	
4310.248	20	1	23194.00	0.00	19_4 — 424°_4	
4311.084	6		23189.50	+0.03	$^3H_5$ — 382°_4	
4311.290	3		23188.39			
4312.336	15	1	23182.77	+0.03	$^3G_4$ — 396°_5	
4314.424	2		23171.55			
4314.625	1		23170.47	−0.10	277°_1–50949_1	
4315.237	6		23167.18	−0.04	17_3 — 408°_2	
4315.486	3		23165.85			
4316.574	2		23160.01			
4316.802	20	1	23158.79	+0.11	23_1 — 466°_0	(0)
4317.650	2		23154.24			
4318.570	8	1	23149.30	−0.02	23_3 — 470°_2	
4318.760	4		23148.29			
4319.865	4		23142.37			
4320.479	3		23139.08	+0.05	29853_4 — 529°_4	
4320.985	3		23136.37			
4322.124	2		23130.27			
4322.740	12	1	23126.97	+0.01	17_4 — 402°_4	
4323.280	4		23124.09			
4326.960	4		23104.42	+0.03	26_2 — 499°_3	
4327.400	3		23102.07	+0.01	27_5 — 509°_6	
4328.408	2		23096.69	+0.04	13_2 — 368°_3	
4328.782	1 *b b*		23094.70			
4330.306	2		23086.57		281°_1–51285_0	

TABLE 3. *Observed and classified lines of* W I

Wavelength Å	Intensity		Wavenumber (cm^{-1})		Classification	Zeeman effect
	Arc	Spark	Observed	o−c		
4330.658	20	2	23084.69	−0.01	19826_5− 429°_4	
4330.967	30	3	23083.04	−0.02	19_3− 429°_4	
4331.620	2 *b*		23079.56			
4332.130	25	2	23076.85	−0.02	14_2− 380°_3	
4332.536	4		23074.68	+0.04	22476_4− 455°_3	
4333.760	2		23068.17			
4336.326	4 *b*		23054.52			
4337.630	3		23047.59			
4338.213	3		23044.49	−0.06	18_1− 411°_0	
4338.288	4		23044.09	+0.01	291°_3–52183_2	
4338.727	3		23041.76	+0.01	$^5D_2$− 263°_2	
4339.070	8	1	23039.94	−0.02	19826_5− 428°_5	
4339.446	15	1	23037.94	−0.04	20_2− 440°_3	
4340.270	2		23033.57			
4340.90	2 *b*		23030.22	−0.06	24_2− 478°_1	
4341.124	4		23029.04			
4341.61	3		23026.46			
4342.53	1		23021.58	−0.01	23_6− 465°_5	
4342.781	6	1	23020.25			
4343.533	2		23016.27	−0.03	22852_4− 458°_4	
4344.376	3		23011.80	+0.04	32_1− 553°_2	
4344.634	4		23010.43			
4344.963	8		23008.69	−0.05	$^3P_2$− 422°_1	
4345.828	20	1	23004.11	0.00	18_3− 419°_2	
4346.280	6		23001.72	−0.04	23_3− 469°_4	
4346.977	30	3	22998.03	+0.08	$^3P_2$− 422°_3	
4347.495	20	2	22995.29	+0.02	19_4− 422°_3	
4348.108	20	25 *s*	22992.05	−0.15	20_2− 439°_2	
4348.927	1		22987.72	+0.04	18_2− 411°_2	
4348.995	5		22987.36	0.00	291°_2–52183_2	
4351.097	2 *b*		22976.25			
4351.336	2 *b*		22975.00	+0.03	22476_4− 454°_5	
4352.110	2 *b*		22970.9			
4353.10	10	2	22965.68			
4353.29	8		22964.68	+0.01	17_3− 406°_3	
4354.72	6	1	22957.14	+0.02	29479_4− 524°_4	
4354.90	6	1	22956.19	−0.08	27_5− 508°_5	
4355.166	40	4	22954.79	−0.03	$^3H_4$− 351°_4	Res
4359.37	2		22932.66			
4359.663	3		22931.11	−0.08	$^3H_5$− 380°_4	
4361.066	10	1	22923.73	0.00	27_4− 501°_5	
4361.534	8	3 *s*	22921.28	+0.06	31_5− 543°_5	
4361.814	25	3	22919.80	−0.01	$^5D_4$− 291°_3	
4362.228	3		22917.63			
4362.670	3		22915.30	+0.07	19535_5− 424°_4	
4363.754	3		22909.61	+0.01	20_2− 438°_1	
4364.40	3		22906.22			
4364.778	40	8	22904.24	0.00	$^5D_2$− $^7P^\circ_2$	Res
4365.954	15	3	22898.07	+0.04	28_6− 512°_5	(0)
4366.073	20	3	22897.44	+0.01	18_3− 418°_4	(0)

TABLE 3. *Observed and classified lines of* W I

Wavelength Å	Intensity		Wavenumber (cm^{-1})		Classification	Zeeman effect
	Arc	Spark	Observed	o−c		
4366.346	6		22896.01	+0.02	13_2 — 366°_2	
4368.762	12	1	22883.35	−0.04	$^3P_1$ — 361°_1	
4369.045	10	1	22881.87	−0.02	17_3 — 405°_4	
4370.795	5		22872.71	−0.02	23_1 — 463°_2	
4371.732	10		22867.80	−0.02	20_2 — 438°_3	
4372.522	40	4	22863.67	0.00	$^5D_2$ — $^7D^\circ_3$	
4373.063	3 *b*		22860.84			
4377.460	1		22837.88	−0.04	26_2 — 496°_2	
4378.484	50	10	22832.54	+0.02	$^5D_3$ — 276°_2	Res
4379.048	2		22829.60	−0.14	34_4 — 571°_3	
4380.118	12	1	22824.02	−0.02	$^5S_2$ — 411°_2	
				−0.04	27_1 — 504°_2	
4381.862	5		22814.94			
4384.850	40	4	22799.39	0.00	15_3 — 382°_4	
4385.168	5		22797.74	−0.04	14_2 — 377°_1	
				+0.02	291°_3–51936_2	
4386.770	15	1	22789.41	−0.08	20_1 — 432°_1	
4387.450	2		22785.88	+0.01	22476_4 — 452°_4	
4389.837	20	2	22773.49	−0.02	19_3 — 426°_3	
4391.115	3		22766.87			
4392.510	1		22759.63	+0.01	18_3 — 417°_2	
4394.074	30	3	22751.53	−0.03	18_2 — 408°_2	
4394.510	3	1	22749.28	−0.03	24_3 — 473°_4	
4395.077	10		22746.34	−0.03	15_3 — 382°_3	
4397.518	3		22733.71	−0.03	$^3G_3$ — 360°_4	
4398.270	2 *b*		22729.83	+0.13	31_5 — 541°_4	
4398.698	1		22727.62			
4398.850	2		22726.83	−0.08	24_3 — 473°_2	
4399.194	1		22725.05	−0.01	$^3P_2$ — 419°_2	
4399.317	1		22724.42	−0.16	28347_3 — 510°_3	
4400.203	12	2	22719.85	+0.02	18_3 — 416°_3	
4400.850	2		22716.50			
4401.316	2		22714.10			
4402.652	3		22707.21			
4403.274	6		22704.00	−0.05	19535_5 — 422°_6	
4403.947	40	4	22700.53	−0.01	$^3H_6$ — 397°_7	7
4404.458	4		22697.89	−0.01	14_2 — 376°_3	
4405.024	3		22694.98	+0.01	23_3 — 466°_4	
4405.996	1	1	22689.97	+0.05	28204_2–50894°_3	
4406.390	8	1	22687.94	−0.01	18_1 — 407°_1	
4406.676	4		22686.47	+0.01	19_3 — 425°_3	
4406.88	2		22685.42			
4408.282	50	5	22678.20	0.00	$^7F^\circ_5$ — $^7D_5$	
4408.706	8		22676.02	−0.01	28_5 — 509°_4	
4409.946	2		22669.65			
4412.188	40	4	22658.13	+0.06	$^5D_2$ — 259°_1	
				+0.02	$^5D_3$ — $^7P^\circ_3$	
4413.006	5		22653.93	−0.01	18_2 — 407°_1	
4413.240	2		22652.73	+0.03	26_2 — 495°_3	
4413.860	4		22649.55	−0.05	23_1 — 461°_1	

TABLE 3. *Observed and classified lines of* W I

Wavelength Å	Intensity		Wavenumber (cm^{-1})		Classification	Zeeman effect
	Arc	Spark	Observed	o−c		
4415.075	25		22643.31	−0.04	$^5S_2$ — 409°$_3$	
4415.703	12		22640.09	0.00	22476°$_4$ — 451°$_4$	
4418.441	15	1	22626.06	+0.02	20°$_1$ — 430°$_0$	
4418.811	6		22624.17	−0.03	19826°$_5$ — 424°$_4$	
4419.247	12		22621.94	+0.02	19°$_3$ — 424°$_2$	
4420.463	40	4	22615.72	+0.02	19°$_4$ — 418°$_4$	
4420.998	20	2	22612.98	+0.03	17°$_4$ — 397°$_4$	
4421.836	15	3 *s*	22608.69	0.00	18°$_3$ — 417°$_2$	
4422.447	3		22605.57	+0.02	$^3H_6$ — 396°$_5$	
4423.507	2 *v*		22600.15	−0.07	22°$_6$ — 453°$_1$	
4423.769	20	3	22598.81	−0.04	22852°$_4$ — 454°$_5$	
4424.888	8		22593.10	+0.06	15°$_3$ — 380°$_3$	
4425.912	30	6	22587.87	−0.05	$^5S_2$ — 408°$_2$	
4427.366	8		22580.45	−0.01	29479°$_4$ — 520°$_4$	
4428.476	6		22574.79	+0.03	27°$_4$ — 497°$_4$	
4430.830	2		22562.8	+0.19	32°$_1$ — 549°$_1$	
4431.522	3		22559.28	+0.12	28°$_6$ — 509°$_6$	
4431.963	2		22557.03			
4432.175	10		22555.95	+0.07	33°$_5$ — 558°$_6$	
4433.482	1 *b*		22549.3	+0.29	18°$_2$ — 406°$_3$	
4433.634	2		22548.53			
4435.102	3 *b*		22541.07	−0.04	15°$_3$ — 380°$_4$	
4435.43	4 *b*		22539.4	0.00	17°$_4$ — 396°$_3$	
4435.733	10		22537.86	0.00	22476°$_4$ — 450°$_3$	
4436.898	40	4	22531.94	−0.01	$^7D_2^\circ$ — $^7D_3$	
4438.284	25	3	22524.91	−0.01	18°$_3$ — 414°$_3$	
4439.709	12		22517.68	−0.02	29°$_7$ — 519°$_6$	
4441.808	20	1	22507.04	0.00	17°$_4$ — 396°$_5$	
4442.443	3 *b*		22503.82	+0.18	33°$_5$ — 557°$_5$	
4444.066	4		22495.60	+0.04	20°$_2$ — 434°$_3$	
4444.440	6		22493.71	+0.08	$^7D_2^\circ$ — e^5D_1	
4445.143	30	3	22490.15	+0.03	14°$_2$ — 374°$_2$	
4447.047	1	*a*	22480.52	−0.05	$^3P_2$ — 417°$_2$	
4449.000	40	3	22470.65	+0.02	$^3H_4$ — 346°$_4$	
4450.340	20	2	22463.89	0.00	22476°$_4$ — 449°$_4$	
4452.016	4 *b*		22455.43	+0.05	23°$_3$ — 463°$_3$	
4453.608	2		22447.40	−0.06	23°$_1$ — 459°$_2$	
4455.458	20	2	22438.08	−0.02	19°$_4$ — 416°$_3$	
4456.096	15	2	22434.87	+0.03	27°$_5$ — 502°$_4$	
4458.086	20	2	22424.85	−0.01	$^3P_1$ — 357°$_2$	
4458.284	10		22423.86	+0.03	19°$_3$ — 422°$_3$	
4458.523	1 *b l*		22422.66	−0.04	27°$_4$ — 496°$_4$	
4460.486	40	4	22412.80	+0.02	13°$_2$ — 361°$_1$	
4462.514	8	1	22402.61	−0.05	23°$_2$ — 463°$_3$	
4463.498	12	1	22397.67	0.00	23°$_3$ — 463°$_2$	
4466.344	50	5	22383.40	0.00	$^3G_3$ — 357°$_2$	
4466.742	40	4	22381.40			
4467.68	3		22376.7	−0.08	29479°$_4$ — 518°$_4$	
4467.885	1		22375.68	+0.14	329°$_3$ — 55°$_4$	
4468.79	2		22371.14	−0.16	28347°$_3$ — 507°$_2$	

TABLE 3. *Observed and classified lines of* W I

Wavelength Å	Intensity		Wavenumber (cm^{-1})		Classification	Zeeman effect
	Arc	Spark	Observed	o−c		
4469.714	10		22366.52			
4472.514	8		22352.52	+0.01	$^3H_6$— 393°$_5$	
4474.03	15	1	22344.94	−0.01	23$_2$— 463°$_2$	
4475.64	4		22336.91	−0.02	19535$_5$— 418°$_4$	
4477.824	4	3 *b*	22326.01	+0.11	$^7D°_4$— e^5D_4	
4478.826	2		22321.02	+0.06	24$_3$— 469°$_4$	
4479.594	3 *b*		22317.19	+0.06	$^3G_4$— 387°$_4$	
4481.270	15	2	22308.84	+0.01	23$_2$— 462°$_1$	
4484.188	100	10	22294.33	−0.05	$^5D_1$— $^7D°_2$	
				+0.05	18$_2$— 404°$_1$	
4485.091	12 *c g*		22289.84	+0.10	24$_2$— 470°$_2$	
4485.476	4 *c*		22287.93	+0.18	27$_5$— 501°$_5$	
4487.156	4		22279.58	+0.20	30$_2$— 526°$_2$	
4489.010	25	1	22270.38	+0.03	299°$_3$—52183$_2$	
4490.302	2 *d*		22263.97	0.00	22852$_4$— 451°$_4$	
4492.298	15	1	22254.08	+0.08	17$_4$— 393°$_5$	
4493.958	20	4	22245.86	−0.01	$^3P_2$— 414°$_3$	
4494.177	1		22244.78	+0.14	20$_2$— 432°$_2$	
4494.497	50	5	22243.19	0.00	19$_4$— 414°$_3$	
4495.294	40	4	22239.25	+0.02	$^3H_5$— 373°$_5$	
4496.228	5	1	22234.63			
4497.674	5		22227.48	+0.05	29853$_4$— 520°$_5$	
4498.448	15	2	22223.66	+0.03	18$_3$— 411°$_4$	
4499.094	3		22220.46			
4501.103	3		22210.55	+0.05	26$_2$— 490°$_3$	
4502.590	4	*g*	22203.21			
4503.136	3		22200.52	+0.10	33$_5$—55492°$_5$	
4504.133	30	1	22195.60	+0.03	24$_3$— 468°$_2$	
4504.838	60	6	22192.13	0.00	$^3H_4$— 343°$_3$	
4509.300	4 *b*		22170.17			
4509.753	2		22167.95	+0.02	$^7P°_3$— e^5D_3	
4510.276	2		22165.38	0.00	13$_2$— 359°$_3$	
4511.301	3 *b*		22160.34			
4512.880	50	6	22152.58	+0.07	18$_2$— 402°$_3$	
4513.252	60	5	22150.76	+0.17	$^3G_3$— 354°$_3$	
				−0.18	19$_3$— 419°$_2$	
4514.284	5		22145.70	+0.05	20$_1$— 425°$_1$	
4515.860	4		22137.97	+0.03	23$_3$— 460°$_3$	
4516.620	2		22134.24			
4517.344	12	1	22130.70	+0.06	$^5S_2$— 404°$_1$	
4519.153	15	1	22121.83	+0.01	23$_2$— 461°$_1$	
4519.950	6 *b*		22117.94			
4522.200	5 *b*		22106.93			
4526.114	4		22087.82	+0.05	22852$_4$— 449°$_4$	
4528.443	2		22076.45	+0.02	$^3H_5$— 371°$_4$	
4529.740	20	1	22070.14	+0.06	22476$_4$— 445°$_5$	
4530.448	25	1	22066.69	+0.05	$^3H_4$— 342°$_3$	
4534.685	30	3	22046.07	+0.17	19826$_5$— 418°$_4$	
4535.031	30	3	22044.38	+0.12	19$_3$— 418°$_4$	
4535.389	2		22042.64			

TABLE 3. *Observed and classified lines of* W I

Wavelength Å	Intensity		Wavenumber (cm^{-1})		Classification	Zeeman effect
	Arc	Spark	Observed	o−c		
4536.636	40	4	22036.58	+0.10	28_6 — 504°_6	
4539.674	4		22021.84	+0.08	20_1 — 424°_2	
4540.279	5		22018.91	+0.13	17_3 — 397°_4	
4542.873	30	2	22006.33	+0.04	15_3 — 374°_2	
4543.245	8	1	22004.53	+0.07	$^3P_1$ — 353°_2	
4543.491	60	6	22003.34	+0.12	$^7F^\circ_2$ — $^7D_1$	
4544.545	10	1	21998.24	+0.16	$^7D^\circ_1$ — $^7D_1$	
4546.469	50	5	21988.93	+0.06	$^5S_2$ — 402°_3	
4549.510	6		21974.23	+0.13	27_4 — 491°_5	
4550.280	8		21970.51	+0.17	22476_4 — 444°_3	
4551.820	100	8	21963.08	0.00	333°_5 — 55_4	
				+0.08	$^3G_3$ — 353°_2	
4552.500	25	2	21959.80	+0.08	$^3H_4$ — 341°_4	
4553.639	6		21954.30	+0.05	13_2 — 357°_2	
4554.664	2		21949.36	+0.04	18_3 — 409°_3	
4555.297	4		21946.32			
4555.528	3		21945.20	−0.03	17_3 — 396°_3	
4556.190	4		21942.01	+0.11	19_4 — 411°_4	
4556.828	20	1	21938.94	−0.08	23_3 — 458°_4	
				+0.16	27_5 — 497°_4	
4558.943	12	1	21928.76	+0.09	18_1 — 400°_2	
4559.102	12	1	21928.00	+0.02	14_2 — 369°_2	
4560.474	4		21921.40			
4563.570	30	2	21906.53	+0.08	19_3 — 417°_2	
4564.048	10	1	21904.23	+0.12	28_5 — 501°_5	
4565.297	25	1	21898.24	+0.06	14_2 — 368°_3	
4566.031	1		21894.72	+0.06	18_2 — 400°_2	
4566.198	8		21893.92	+0.03	18_3 — 408°_2	
4567.566	12	1	21887.36			
4568.597	4		21882.42	−0.09	19535_5 — 414°_6	
4570.638	80	8	21872.66	+0.13	230°_3 — $^7D_2$	
4571.872	10	1	21866.75	+0.09	19_3 — 416°_3	
4575.352	2		21850.12			
4575.661	3		21848.64	+0.09	$^7P^\circ_2$ — e^5D_2	
4578.316	20	2	21835.97	+0.03	29_7 — 512°_7	
4579.688	25	1	21829.43	−0.01	328°_4 — 54_3	
4579.952	4		21828.17	+0.08	$^3G_4$ — 382°_4	
4581.635	3 *b*		21820.15	+0.21	28898_2 — 507°_2	
4584.244	3		21807.74			
4584.536	3		21806.35	−0.05	34_4 — 561°_3	
4585.624	3		21801.17			
4586.832	40	4	21795.43	+0.01	$^3P_0$ — 313°_1	
4588.734	60	6	21786.40	+0.06	$^7D^\circ_3$ — $^7D_4$	
4592.390	20	2	21769.05	+0.07	19_6 — 414°_6	
4592.566	15	1	21768.22	0.00	$^3G_3$ — 351°_4	
4592.907	1		21766.60	+0.24	$^7P^\circ_4$ — e^5D_3	
4599.940	40	6	21733.32	+0.09	$^7F^\circ_4$ — $^7D_3$	
4600.413	15	2	21731.09	+0.07	$^5S_2$ — 400°_2	
4603.270	4		21717.60	+0.18	33_5 — 550°_5	
4603.410	5		21716.94	+0.07	24_3 — 463°_2	

TABLE 3. *Observed and classified lines of* W I

Wavelength Å	Intensity		Wavenumber (cm⁻¹)		Classification	Zeeman effect
	Arc	Spark	Observed	o−c		
4606.998	4 *b*		21700.03	+0.05	329°_3— 54_3	
4607.565	6 *b*		21697.36	−0.16	14_2— 366°_2	
4608.816	8		21691.47	+0.13	18_3— 406°_3	
4609.886	25	3	21686.44	+0.09	15_3— 371°_4	
4612.987	5		21671.86	+0.10	19_3— 414°_3	
4613.296	40	4	21670.40	+0.05	$^5D_4$— $^7P^\circ_4$	
4613.886	2		21667.63	+0.04	19_4— 409°_3	
4614.830	6		21663.20	+0.07	19535_5— 411°_4	
4616.396	3		21655.85	+0.11	19_4— 409°_5	
4619.448	4 *c*		21641.55	+0.12	17_4— 387°_4	
4620.520	15	1	21636.53	+0.10	19535_5— 411°_6	
4622.266	2		21628.35			
4623.140	5		21624.26	+0.07	18_1— 397°_2	
4623.645	10	1	21621.90	+0.16	$^3G_4$— 380°_3	
4623.768	3		21621.32	+0.08	23_3— 455°_3	
4624.446	6		21618.16	−0.01	20_2— 426°_3	
4625.140	8		21614.91	+0.07	$^3P_2$— 408°_2	
4625.756	4		21612.03			
4626.730	3		21607.48			
4627.591	6		21603.47	−0.14	31_5— 529°_4	
4629.230	4		21595.81	+0.01	24_2— 463°_2	
4629.561	5 *b*		21594.27	+0.05	22852_4— 444°_3	
4630.139	2		21591.58	+0.10	19826_5— 414°_6	
4630.372	6		21590.49	+0.02	20_2— 425°_1	
4634.786	20	4	21569.93	+0.12	$^3G_4$— 380°_4	
4635.054	4		21568.68	+0.16	23_2— 455°_3	
4636.044	4		21564.07	+0.07	23_1— 450°_2	
4637.102	4	1	21559.15			
4637.857	8		21555.64	−0.03	293°_2—50949_1	
4638.251	2 *b*		21553.82	+0.03	18_1— 396°_1	
4639.46	4		21548.2	+0.22	322°_3— 53_4	
4640.270	8		21544.44	+0.12	22476_4— 440°_3	
4641.764	10		21537.50	+0.22	$^5D_3$— 263°_2	
				+0.10	20_1— 419°_0	
4642.530	40	2	21533.95	+0.10	13_2— 353°_2	
4643.116	10		21531.23	+0.11	20_2— 425°_3	
4643.446	2		21529.70	+0.13	18_2— 396°_3	
4644.880	5		21523.05	+0.15	19_6— 411°_6	
4645.72	1		21519.16			
4646.135	8		21517.24	+0.02	$^3P_2$— 407°_1	
4651.52	3		21492.33	+0.15	23_3— 454°_2	
4656.72	4		21468.33			
4657.034	4		21466.88	−0.02	31_5— 528°_6	
4657.416	40	2	21465.12	+0.12	$^7P^\circ_4$— $^7D_5$	
4659.867	60	6	21453.83	−0.07	$^5D_0$— $^7D^\circ_1$	
4661.235	8		21447.54	−0.03	22476_4— 439°_5	
4661.975	10		21444.13	−0.02	15_3— 369°_2	
4662.642	2		21441.07	+0.09	28347_3— 497°_4	
4662.94	6		21439.69	+0.23	23_2— 454°_2	
4665.760	4	3 *s*	21426.74	+0.20	$^5S_2$— 397°_2	

318-092 O-69—11

TABLE 3. *Observed and classified lines of* W I

Wavelength Å	Intensity		Wavenumber (cm^{-1})		Classification	Zeeman effect
	Arc	Spark	Observed	o−c		
4668.176	2		21415.64	−0.03	305°_{3}–52002_{3}	
4668.460	15		21414.34	−0.01	15_{3}— 368°_{3}	
4668.895	2		21412.35	+0.12	$^{3}P_{1}$— 347°_{1}	
				+0.06	$^{3}P_{2}$— 406°_{3}	
4671.626	8		21399.83	+0.06	$^{5}D_{3}$— $^{7}P^{\circ}_{2}$	
4672.553	2		21395.59			
4675.090	4		21383.98			
4676.623	20		21376.97	0.00	19535_{5}— 409°_{5}	
4676.93	2		21375.56			
4677.374	4		21373.54			
4677.690	20		21372.09	−0.01	19826_{5}— 411°_{4}	
4678.48	1		21368.48			
4679.04	8		21365.92	−0.01	$^{5}S_{2}$— 396°_{3}	
4680.509	80	8	21359.22	+0.02	$^{5}D_{3}$— $^{7}D^{\circ}_{3}$	
4681.182	5		21356.15	+0.01	$^{5}S_{2}$— 396°_{1}	
4682.558	6		21349.87	+0.07	$^{7}D^{\circ}_{5}$— $e^{5}D_{4}$	
4683.542	30	1	21345.39	−0.01	19826_{5}— 411°_{6}	
4686.00	1		21334.2			
4686.373	3		21332.49	+0.02	23_{3}— 452°_{4}	
4687.118	3		21329.10	+0.03	17_{3}— 390°_{2}	
4687.612	6		21326.86	+0.03	19_{4}— 405°_{4}	
4689.168	2		21319.78	+0.13	30_{2}–51693°_{2}	
4690.237	1		21314.92	−0.04	24_{2}— 461°_{1}	
4690.62	1		21313.18	+0.12	28204_{2}— 495°_{2}	
4691.55	5		21308.96	+0.05	26861_{2}— 481°_{3}	
4692.112	2		21306.40	+0.11	20_{1}— 417°_{2}	
4693.719	40	2	21299.11	+0.05	$^{7}F^{\circ}_{5}$— $^{7}D_{4}$	
4694.636	6		21294.95	+0.11	18_{3}— 402°_{3}	
4695.527	2		21290.90	−0.06	32_{1}— 536°_{2}	
4698.108	8		21279.21	−0.07	20_{2}— 422°_{1}	
4698.62	10		21276.89	+0.05	19_{3}— 411°_{2}	
4700.422	15		21268.73	−0.05	$^{5}D_{4}$— $^{7}P^{\circ}_{3}$	
4701.590	4		21263.45	+0.01	19_{6}— 409°_{5}	
4702.17	2		21260.83			
4702.47	10		21259.47	+0.01	18_{3}— 402°_{4}	
4705.64	1		21245.15			
4705.834	2		21244.27	+0.08	22476_{4}— 437°_{4}	
4706.16	8		21242.80	+0.03	$^{3}G_{4}$— 376°_{3}	
4709.58	2		21227.38			
4709.75	2		21226.61			
4710.32	6		21224.04	−0.04	27_{5}— 490°_{5}	
4711.173	12		21220.20	+0.02	19_{4}— 404°_{5}	
4712.486	15		21214.29	−0.02	14_{2}— 361°_{1}	
4713.355	2		21210.37	+0.08	299°_{3}— $e^{5}D_{4}$	
4713.51	2		21209.68	+0.10	32_{4}–53345°_{3}	
4713.852	5		21208.14	+0.06	$^{3}H_{4}$— 333°_{5}	
4714.507	5		21205.19	+0.02	$^{3}H_{5}$— 362°_{5}	
4716.864	8		21194.60	−0.02	$^{3}H_{6}$— 382°_{6}	
4718.618	8		21186.72	+0.03	23_{3}— 451°_{4}	
4720.392	10		21178.76	0.00	$^{3}P_{1}$— 344°_{2}	

TABLE 3. *Observed and classified lines of* W I

Wavelength Å	Intensity		Wavenumber (cm^{-1})		Classification	Zeeman effect
	Arc	Spark	Observed	o−c		
4723.076	2		21166.72	−0.02	28347_3— 495°_3	
4725.118	20	2	21157.57	+0.01	$^3P_2$— 404°_1	
4725.592	2		21155.45	−0.03	$^3P_0$— 306°_1	
4726.274	5		21152.40	+0.01	17_4— 382°_4	
4728.768	4		21141.24	−0.02	23_1— 445°_2	
4729.648	20	2	21137.31	+0.01	$^3G_3$— 344°_2	
4730.695	4		21132.63	+0.02	22852_4— 439°_4	
4731.027	2		21131.15			
4736.036	3		21108.80			
4736.95	2 *b*		21104.72	+0.20	342°_3— 55_4	
4737.86	2 *b*		21100.67	+0.30	18_1— 391°_1	
4738.152	4		21099.37	0.00	17_4— 382°_3	
4741.498	4		21084.48	+0.02	23_3— 450°_3	
4745.586	8 *b*		21066.32	−0.04	18_2— 391°_1	
4746.785	3 *b*		21061.00			
4747.964	2		21055.77	−0.04	29853_4— 509°_4	
4749.697	5		21048.09	+0.03	19535_5— 405°_4	
4749.909	1		21047.15	−0.11	17_3— 387°_4	
4751.363	6		21040.71	−0.01	19_3— 408°_2	
4752.200	8		21037.00	+0.01	18_3— 400°_2	
4752.584	8		21035.30	−0.04	$^3P_1$— 343°_1	
4753.388	6		21031.74	0.00	23_2— 450°_3	
4756.98	3		21015.86	+0.07	$^3P_2$— 402°_3	
4757.542	30	3	21013.38	0.00	$^7S_3$— $^7D^\circ_2$	
4757.781	8		21012.32	−0.05	$^3H_5$— 360°_4	
4758.197	10		21010.48	−0.01	23_3— 449°_4	
4759.340	2 *b*		21005.44	−0.08	$^3G_3$— 343°_3	
4760.714	3		20999.38			
4761.02	3		20998.03	−0.01	22852_4— 438°_3	
4765.63	2		20977.72	−0.01	19_4— 402°_4	
4767.782	8		20968.25	+0.05	29_7— 504°_6	
4768.057	3		20967.04	+0.05	14_2— 359°_3	
4770.724	3		20955.32	+0.15	$^7D^\circ_2$— $^7D_2$	
4772.492	8		20947.56	+0.14	18_1— 390°_2	
4773.89	15		20941.42	+0.01	19535_5— 404°_5	
4777.02	2		20927.70			
4780.29	2		20913.40	−0.01	18_2— 390°_2	
4780.50	6		20912.47	−0.01	23_1— 443°_2	
4783.694	2		20898.50	+0.06	23_1— 443°_1	
4784.72	1		20894.02	−0.09	17_4— 380°_4	
4787.206	2 *b l*		20883.17			
4787.925	10		20880.03	−0.01	$^3G_3$— 342°_3	
4788.421	10		20877.87	+0.02	$^3G_4$— 373°_5	
4792.806	2		20858.77	−0.03	$^7D^\circ_4$— e^5D_3	
4797.030	3		20840.40	−0.04	28_5— 490°_5	
4797.546	10		20838.16	−0.01	19_3— 406°_3	
4799.907	25	1	20827.91	+0.03	19_6— 404°_5	
4806.31	4 *b b l*		20800.17	−0.18	28347_3— 491°_4	
4807.380	20		20795.54	−0.08	$^3H_4$— 329°_3	
4809.642	3		20785.76			

TABLE 3. *Observed and classified lines of* W I

Wavelength Å	Intensity		Wavenumber (cm⁻¹)		Classification	Zeeman effect
	Arc	Spark	Observed	o−c		
4810.887	3		20780.38	+0.12	28291_3— 490°_3	
4812.58	5		20773.07	−0.05	$^3G_3$— 341°_4	
4816.105	6		20757.86	−0.08	$^3P_2$— 400°_2	
4816.845	8 *b*		20754.67	+0.26	23_2— 447°_1	
				−0.13	27_4— 479°_4	
4817.675	6		20751.10	−0.01	20_2— 417°_2	
4818.358	3		20748.16	−0.24	346°_4— 55_5	
4826.943	2		20711.26	−0.06	20_2— 416°_3	
4835.01	15		20676.70	+0.02	20_1— 411°_2	
4837.48	8		20666.14	−0.03	$^3H_4$— 328°_4	
				−0.06	23_3— 445°_2	
4843.810	400	20	20639.14	0.00	$^5D_2$— $^7D^\circ_2$	
4844.30	6		20637.05	+0.09	$^3P_1$— 339°_2	
				+0.03	27_4— 478°_5	
4847.754	8	*a*	20622.34	+0.05	15_3— 360°_4	
4848.724	3		20618.22	−0.08	28898°_2— 495°_2	
4853.831	5 *n*		20596.53	−0.05	20_0— 407°_1	
4854.082	40		20595.46	−0.04	$^3G_3$— 339°_2	
4858.596	12		20576.33	−0.05	13_2— 343°_3	
4860.774	4		20567.11	+0.04	17_4— 376°_3	
4861.84	3 *c*		20562.6			
4862.89	2		20558.16	−0.06	17_3— 382°_4	
4863.062	15		20557.43	+0.01	22476_4— 430°_5	
				−0.01	$^7D^\circ_4$— $^7D_5$	
4864.98	3 *c*		20549.33	+0.05	28_1— 492°_2	
4865.33	3		20547.85			
4866.55	3		20542.70			
4868.025	15		20536.47	−0.03	305°_3— e^5D_4	
4871.884	3 *b*		20520.21	+0.01	23_1— 439°_2	
4872.790	10 *b*		20516.39	−0.02	20_2— 414°_3	
4874.055	3 *b*		20511.07			
4875.424	8		20505.31	+0.11	17_3— 382°_3	
4876.690	6		20499.98	−0.12	26_2— 473°_3	
4878.28	20		20493.30	−0.01	18_1— 385°_0	
4879.686	4		20487.40	−0.03	$^7P^\circ_3$— $^7D_4$	
4880.713	8		20483.09	−0.09	15_3— 359°_3	
4882.122	2		20477.18			
4882.528	3		20475.47	−0.04	27_4— 476°_4	
4882.744	3		20474.57	−0.13	259°_1— e^5D_1	
4883.520	3		20471.31			
4884.541	4		20467.03	+0.01	31_5— 518°_4	
4885.225	5		20464.17	−0.05	23_2— 444°_3	
4886.191	2		20460.12	−0.08	291°_2— e^5D_3	
4886.899	200	20	20457.16	+0.01	$^5D_4$— $^7F^\circ_5$	
4887.770	4		20453.51	+0.05	$^3P_2$— 397°_2	
4888.371	20		20451.00	+0.10	13_2— 342°_3	
4890.273	25		20443.04	−0.01	$^3G_4$— 368°_3	
4890.602	1 *b*		20441.67	0.00	19_3— 402°_3	
4890.872	10		20440.54	−0.02	20_1— 408°_2	
4891.142	2		20439.41	−0.06	23_6— 439°_5	

TABLE 3. *Observed and classified lines of* W I

Wavelength Å	Intensity		Wavenumber (cm^{-1})		Classification	Zeeman effect
	Arc	Spark	Observed	o−c		
4891.621	10		20437.41	−0.01	23_3 — 443°_2	
4892.422	40		20434.06	0.00	22476_4 — 429°_4	
4893.165	3		20430.96	−0.02	29853_4 — 502°_4	
4896.518	2		20416.97			
4896.806	2		20415.77	−0.03	276°_2 — e^5D_2	
4897.718	1		20411.97	−0.26	$^3P_1$ — 347°_1	
4898.682	2		20407.95	+0.02	19826_5 — 402°_4	
4899.068	4		20406.34	+0.05	19_3 — 402°_4	
4901.033	2		20398.16	−0.04	22852_4 — 432°_4	
4902.073	2		20393.84	−0.07	26_2 — 472°_1	
4902.320	25		20392.81	−0.04	$^3P_2$ — 396°_3	
4902.950	20		20390.19	+0.02	19_4 — 396°_3	
4903.157	4		20389.32	0.00	22476_4 — 428°_5	
4904.32	3 *b b*	3 *l s*	20384.50	−0.20	23_2 — 443°_2	
				+0.30	28291_3 — 486°_4	
4904.67	1		20383.04	−0.02	$^3P_2$ — 396°_1	
4905.487	5		20379.64	+0.02	27_4 — 475°_3	
4908.894	3		20365.50	−0.07	318°_2—52183_2	
4910.744	20		20357.83	+0.02	19_4 — 396°_5	
4912.192	4		20351.82	−0.05	17_3 — 380°_3	
4913.113	3		20348.01			
4914.331	5		20342.97	+0.03	20_1 — 407°_1	
4916.178	30		20335.32	−0.06	14_2 — 353°_2	
4916.986	2		20331.98	−0.06	29853_4 — 501°_3	
4917.844	3		20328.44	−0.04	28347_3 — 486°_4	
4919.807	2		20320.33			
4920.802	1		20316.21			
4922.496	3		20309.22	−0.04	29479_4 — 497°_4	
4922.926	15		20307.45	+0.03	$^7D^\circ_3$ — $^7D_3$	
4924.561	15	*a*	20300.71	+0.05	$^3H_6$ — 373°_5	
4925.112	2 *b*		20298.44	0.00	362°_5—56573_5	
4926.711	6		20291.85	−0.13	28_6 — 486°_6	
4927.510	2		20288.56	−0.02	27_5 — 481°_5	
4931.551	50	1	20271.93	−0.02	15_3 — 357°_2	
4932.048	2		20269.90	+0.04	27_4 — 474°_3	
4932.777	4		20266.90	+0.05	$^7P^\circ_2$ — $^7D_3$	
4933.816	5		20262.63	−0.01	293°_2 — e^5D_3	
4934.542	2		20259.65	+0.09	32_4 — 523°_5	
4935.784	2		20254.55	+0.16	34_4 — 545°_3	
4936.74	2 *v*	1	20250.63			
4937.73	1		20246.57			
4939.26	2		20240.3	+0.13	318°_2—52057_1	
4940.09	4		20236.9	−0.02	20_6 — 404°_1	
4941.942	3		20229.31	−0.05	24_2 — 450°_2	
4943.21	2 *b*		20224.12			
4945.089	2 *b b*		20216.44	+0.10	351°_4 — 55_4	
4947.186	3		20207.87			
4948.587	10		20202.14	−0.01	17_4 — 373°_5	
4952.790	3		20185.00	+0.05	19535_5 — 397°_4	
4953.075	15		20183.84	+0.02	19_3 — 400°_2	

TABLE 3. *Observed and classified lines of* W I

Wavelength Å	Intensity		Wavenumber (cm^{-1})		Classification	Zeeman effect
	Arc	Spark	Observed	o−c		
4953.713	2		20181.24	−0.06	22852_4— 430°_5	
4956.61	2 *b*		20169.45			
4957.366	30		20166.37	+0.02	13_2— 339°_2	
4959.600	3		20157.29	+0.09	29479_4— 496°_4	
4960.432	1		20153.91			
4961.514	5		20149.52	+0.06	27_1— 478°_1	
4961.91	2		20147.90	−0.02	27_4— 473°_3	
4962.288	8		20146.37	0.00	27_4— 473°_4	
4967.685	4		20124.48	−0.03	22476_4— 426°_3	
4968.428	4		20121.47	−0.03	20_2— 411°_2	
4969.110	2		20118.71	−0.11	27_5— 479°_4	
4970.68	3		20112.36	−0.01	29853_4— 499°_3	
4972.56	30		20104.75	−0.02	19_4— 393°_5	
4974.024	2		20098.83			
4975.260	3		20093.84			
4976.00	4		20090.85	−0.07	23_3— 440°_3	
4976.333	10		20089.51	−0.03	18_2— 382°_3	
4977.253	15		20085.80	−0.06	$^7P^\circ_4$— $^7D_4$	
4977.706	4		20083.97	+0.01	31_5— 514°_4	
4979.840	50		20075.36	0.00	$^5S_2$— 383°_1	
4981.47	2		20068.79			
4981.88	2		20067.14	−0.04	28_1— 487°_1	
4982.593	200	4	20064.27	−0.03	$^5D_0$— $^7F^\circ_1$	
4983.529	15		20060.50	0.00	19_6— 397°_7	
4984.16	5		20057.96	+0.02	22852_4— 429°_4	
4984.698	20		20055.80	+0.06	18_3— 390°_2	
4986.92	80		20046.86	+0.02	15_5— 351°_4	
4987.330	3 *b*		20045.21	+0.07	23_3— 439°_2	
4988.050	3 *b*		20042.32			
4989.08	15		20038.18	−0.02	23_2— 440°_3	
4989.87	5		20035.01	−0.01	29479_4— 495°_3	
4990.82	1		20031.19			
4991.85	2		20027.06	+0.10	28291_3— 483°_2	
4992.374	4		20024.96	0.00	346°_4— 54_3	
4994.083	6		20018.11			
4995.29	20		20013.27	+0.07	22852_4— 428°_5	
5000.49	4		19992.46	+0.04	23_2— 439°_2	
5001.072	5		19990.13			
5002.79	12		19983.27	−0.01	20_1— 404°_1	
5003.933	2		19978.70	−0.11	28347_3— 483°_3	
5005.216	4		19973.58	+0.02	22476_4— 424°_4	
5005.392	6		19972.88	−0.02	17_3— 376°_3	
5006.150	60	6	19969.86	−0.01	$^5D_4$— $^7D^\circ_3$	
5007.221	8		19965.58	+0.07	19_6— 396°_5	
5008.110	4		19962.04	+0.06	313°_1–51285_0	
5009.874	4		19955.01			
5010.366	5 *b*		19953.05			
5011.454	3		19948.72			
5011.768	1		19947.47	−0.08	24_2— 447°_1	
5012.29	3 *b b*		19945.40	+0.22	322°_3— 52_2	

TABLE 3. *Observed and classified lines of* W I

Wavelength Å	Intensity		Wavenumber (cm^{-1})		Classification	Zeeman effect
	Arc	Spark	Observed	o−c		
5013.436	10		19940.83	−0.02	20_2— 409°_3	
5013.980	4		19938.67	+0.09	29479_4— 494°_3	
				−0.04	305°_3— 50_2	
5014.57	8		19936.32	+0.11	18_2— 380°_3	
5015.304	50	5	19933.41	+0.02	$^5D_3$— $^7F^\circ_4$	
5017.212	12		19925.83	−0.07	$^5S_2$— 382°_3	
5018.504	4		19920.69	−0.07	23_3— 438°_3	
5019.520	3		19916.66			
5021.324	5	2 *s*	19909.51	−0.31	23_2— 438°_1	
5022.496	5		19904.86	−0.08	28_5— 481°_5	
5023.423	2 *b*		19901.20			
5025.270	5		19893.88	−0.04	19826_5— 397°_4	
5025.684	6	5 *b*	19892.24	−0.04	19_3— 397°_4	
5027.44	5		19885.29	−0.09	20_2— 408°_2	
5028.934	20		19879.38	+0.04	19_3— 397°_2	
				+0.04	32_4— 520°_3	
				−0.04	281°_1— 48_2	
5029.112	6		19878.68	+0.01	28291_3— 481°_3	
5029.498	2 *b*		19877.15			
5031.813	15		19868.01	−0.03	23_2— 438°_3	
5034.364	2 *b*		19857.94	−0.06	28_6— 482°_7	
5035.75	4		19852.47	+0.05	341°_4— 53_5	
5035.998	5		19851.50	−0.05	15_3— 353°_2	
5039.028	10		19839.56	+0.03	27_5— 476°_4	
5040.360	60	2	19834.32	+0.04	$^3P_1$— 331°_2	
5041.41	3 *b*		19830.19			
5041.768	4 *b*		19828.78	−0.06	266°_0— e^5D_1	
5042.482	3		19825.97	−0.03	19535_5— 393°_5	
5044.32	20		19818.74	+0.01	19_3— 396°_3	
5044.908	4	*a*	19816.44			
5051.41	1 *c*		19790.93	+0.14	23_3— 437°_4	
5052.23	30		19787.72	−0.04	20_2— 407°_1	
5053.276	400	40	19783.62	+0.01	$^5D_1$— $^7D^\circ_1$	
5054.596	150	15	19778.46	−0.01	$^5D_1$— $^7F^\circ_2$	
5055.516	50	1	19774.86	+0.03	22476_4— 422°_3	
5056.094	4		19772.60	+0.03	$^5S_2$— 380°_3	
5056.50	2		19771.02			
5056.84	2		19769.68			
5057.45	2		19767.30	−0.05	17_4— 368°_3	
5058.006	30		19765.12	0.00	17_3— 374°_2	
5059.342	2		19759.90			
5062.08	2		19749.20			
5063.142	5		19745.07			
5063.638	8		19743.14	−0.01	14_2— 347°_1	
5064.807	5		19738.58			
5065.682	4		19735.17	−0.01	28_5— 479°_4	
5066.573	3		19731.70			
5067.19	2		19729.30			
5069.118	120	10	19721.80	+0.02	$^5D_2$— $^7F^\circ_3$	
5071.515	6		19712.47	0.00	19_6— 393°_5	

TABLE 3. *Observed and classified lines of* W I

Wavelength Å	Intensity		Wavenumber (cm⁻¹)		Classification	Zeeman effect
	Arc	Spark	Observed	o−c		
5071.735	150	10	19711.62	0.00	$^7F^\circ_6$ — $^7D_5$	
5072.504	3		19708.63	+0.03	29479_4 — 491°_5	
5077.010	10		19691.14	+0.01	18_1 — 377°_1	
5079.204	4		19682.63	−0.20	20_2 — 406°_3	
5079.922	3		19679.85	+0.03	22852_4 — 425°_4	
5080.72	10		19676.76	+0.02	28291_3 — 479°_4	
5082.00	3		19671.80			
5082.722	4		19669.01	−0.07	28_1 — 483°_1	
5083.142	4		19667.38	+0.07	27_1 — 473°_2	
5085.876	5 *b b*		19656.81	+0.02	15_3 — 351°_4	
5089.982	20		19640.96	−0.02	27_4 — 468°_5	
5093.92	2		19625.76	+0.17	313°_1 — 50949_1	
5094.173	6		19624.80			
5095.02	2 *c*		19621.55	−0.15	371°_4 — 56768_5	
5096.126	2		19617.28	−0.12	28_5 — 478°_5	
5096.50	2		19615.84	+0.10	28204_2 — 478°_1	
5098.25	2		19609.10	+0.08	$^3G_3$ — 329°_3	
5101.276	3 *b*		19597.47	+0.03	22852_4 — 424°_4	
5104.643	2		19584.55	−0.05	23_3 — 435°_2	
5104.885	1		19583.62	−0.04	20_1 — 400°_2	
5105.144	4		19582.62	−0.10	313°_1 — 50906_1	
5105.478	20	1	19581.34	0.00	$^7D^\circ_5$ — $^7D_5$	
5106.411	4		19577.76	−0.08	24_2 — 443°_2	
5107.78	5		19572.52			
5108.25	2		19570.72			
5110.36	15		19562.64	−0.03	$^3H_5$ — 346°_4	
5111.774	10		19557.23	−0.01	18_2 — 376°_3	
5113.90	3 *b b*		19549.1	−0.22	23_6 — 430°_5	
5114.59	3	3 *s*	19546.46	−0.13	34_4 — 538°_4	
5115.29	4		19543.78	+0.04	28_1 — 482°_0	
5117.612	20		19534.91	−0.06	19826_5 — 393°_5	
5118.418	8		19531.84	−0.04	23_2 — 435°_2	
5120.553	20		19523.70	−0.04	373°_5 — 56_6	
5123.625	1		19511.99	+0.13	$^3G_4$ — 359°_3	
5124.234	40		19509.67	−0.01	14_2 — 344°_2	
5125.32	1		19505.54			
5127.88	4 *c*		19495.80	+0.02	23_2 — 434°_3	
5128.49	20		19493.48	0.00	$^5S_2$ — 377°_1	
5128.836	6		19492.17	−0.03	19_4 — 387°_4	
5129.81	25		19488.47	−0.05	22_0 — 422°_1	
5130.114	50		19487.31	0.00	$^7D^\circ_2$ — $^7D_1$	
5131.318	10		19482.74			
5132.11	2 *c*		19479.72	+0.16	$^3G_3$ — 328°_4	
5133.11	20		19475.93			
5136.08	5 *b b*		19464.66	+0.08	32_4 — 516°_3	
5136.70	12		19462.34	−0.08	20_0 — 396°_1	
5137.63	3		19458.80	−0.08	373°_5 — 56768_5	
5137.798	6		19458.17	+0.03	28_6 — 478°_5	
5138.400	25		19455.88	−0.01	28_5 — 476°_4	
5141.248	12		19445.11	−0.07	17_3 — 371°_4	

TABLE 3. *Observed and classified lines of* W I

Wavelength Å	Intensity		Wavenumber (cm⁻¹)		Classification	Zeeman effect
	Arc	Spark	Observed	o−c		
5145.453	8		19429.22			
5145.774	25	4	19428.00	−0.10	20_2— 404°_1	
5147.72	3 *c*		19420.67	+0.03	329°_3— 52_4	
5148.727	6		19416.86	−0.13	31_5— 508°_5	
5149.765	3		19412.95			
5150.252	4		19411.11	−0.12	27_4— 466°_4	
5150.79	5		19409.09	+0.17	27_1— 470°_2	
5151.286	3		19407.22			
5153.555	40		19398.67	−0.04	22852_4— 422°_3	
5153.880	20		19397.45	0.00	28291_3— 476°_4	
5154.462	30		19395.26	0.00	22476_4— 418°_4	
5154.904	15		19393.60	0.00	$^5S_2$— 376°_3	
5156.722	4		19386.76			
5157.618	4		19383.39	+0.08	18_1— 374°_2	
5158.187	15		19381.25	+0.03	23_6— 428°_5	
5159.095	2		19377.84	−0.06	14_2— 343°_3	
5159.564	3		19376.08			
5160.00	5		19374.44	−0.09	24_3— 439°_4	
5160.322	4		19373.24			
5161.06	4		19370.46			
5162.146	8		19366.39	+0.13	14_2— 343°_1	
5162.874	4		19363.66	−0.01	13_2— 331°_2	
5163.48	4		19361.39			
5166.648	2		19349.52	+0.16	18_2— 374°_2	
5168.78	2 *b b*		19341.53	+0.03	346°_4— 53_5	
5170.65	2		19334.54			
5172.626	3		19327.15	−0.03	329°_3–52284_3	
5173.64	4		19323.36			
5174.31	5		19320.86	−0.06	23_3— 432°_4	
5175.732	6		19315.55	+0.10	32_1–51693°_2	
5177.76	8		19308.00	−0.12	28_5— 475°_6	
5179.51	10		19301.46	−0.10	28291_3— 475°_3	
5180.04	3		19299.49			
5180.57	1 *b*		19297.53	−0.05	23_3— 432°_2	
5181.94	5 *b*		19292.41	−0.14	27_4— 465°_5	
5182.30	3 *b*		19291.07			
5183.586	6		19286.29	−0.04	20_2— 402°_3	
5183.965	40	2	19284.88	−0.01	18_3— 382°_4	
5185.52	2		19279.10	−0.08	20_1— 397°_2	
5187.537	6		19271.60	+0.01	28898_2— 481°_3	
5188.867	10		19266.66	+0.06	$^3H_6$— 362°_5	
5189.516	3		19264.25	−0.13	373°_5–56573_5	
5192.705	40		19252.42	0.00	14_2— 342°_3	
5195.63	40	1	19241.58	−0.04	259°_1— e^5D_0	
5196.49	9		19238.40	+0.07	28204_2— 474°_2	
5198.28	5		19231.78	−0.09	18_3— 382°_3	
5199.96	2		19225.55	−0.07	329°_3— 52_2	
5201.44	4	1	19220.09	−0.13	29853_4— 490°_5	
5202.11	2		19217.63	−0.03	22476_4— 416°_3	
5203.25	10	2	19213.39	−0.04	19535_5— 387°_4	

TABLE 3. *Observed and classified lines of* W I

Wavelength Å	Intensity		Wavenumber (cm^{-1})		Classification	Zeeman effect
	Arc	Spark	Observed	o−c		
5204.52	12	3	19208.71	−0.07	20_1 − 396°_1	
5205.18	4		19206.30	−0.08	26_2 − 460°_3	
5206.18	12	3	19202.60	+0.03	19_3 − 390°_2	
5207.78	2		19196.70	−0.06	29479_4 − 486°_4	
5209.12	5		19191.76	−0.04	28291_3 − 474°_3	
5210.74	1		19185.78	−0.04	$^5S_2$ − 374°_2	
5212.34	3		19179.88	+0.01	13_2 − 329°_3	
5212.81	16	6	19178.17	−0.13	$^7D^\circ_4$ − $^7D_4$	
5214.175	12		19173.15	−0.03	17_3 − 368°_3	
5215.55	3		19168.09	0.00	17_4 − 362°_5	
5218.194	4		19158.38	−0.03	354°_3 − 54_3	
5218.432	10		19157.51	−0.03	28204_2 − 473°_3	
5219.22	3		19154.61	−0.16	32_4 − 512°_5	
5219.56	2		19153.37	−0.03	346°_4 − 53_4	
5220.354	4 *b*		19150.45	−0.20	28291_3 − 474°_2	
5224.27	4		19136.10	+0.02	28347_3 − 474°_3	
5224.657	250	25	19134.67	+0.01	$^5D_3$ − $^7D^\circ_2$	
5229.127	25		19118.29	−0.12	23_1 − 425°_1	
5230.246	2		19114.25			
5233.523	150		19102.26	−0.02	$^3P_2$ − 383°_1	
5239.092	4		19081.96	−0.08	27_5 − 469°_4	
5239.786	60		19079.43	−0.03	$^3P_1$ − 323°_0	
5240.782	15		19075.81	+0.05	$^3G_4$ − 355°_5	
5242.56	40		19069.34	−0.06	305°_3 − e^5D_3	
5242.98	250		19067.81	−0.03	$^3G_4$ − 354°_3	
5243.996	5 *b*		19064.11			
5245.686	4		19057.97	−0.05	362°_5 − 55_4	
5247.417	25		19051.70	−0.05	$^3H_5$ − 341°_4	
5249.045	3		19045.78	−0.13	28291_3 − 473°_2	
5250.131	1 *b b*		19041.84	+0.08	331°_2 − 52_2	
5250.406	12		19040.84	0.00	26_2 − 459°_2	
5254.542	100		19025.85	0.00	15_3 − 344°_2	
5255.396	120		19022.76	+0.01	22476_4 − 414°_3	
5259.342	300		19008.49	−0.02	$^7P^\circ_3$ − $^7D_3$	
5262.818	3		18995.93			
5263.215	100		18994.50	−0.08	23_1 − 424°_2	
5267.054	6		18980.66	0.00	23_3 − 429°_4	
5268.550	80		18975.27	−0.02	17_4 − 360°_4	
5269.326	100		18972.48	−0.04	17_3 − 366°_2	
5274.787	15		18952.83	+0.01	$^3P_2$ − 382°_3	
5275.529	150		18950.17	+0.03	19_4 − 382°_3	
5278.59	20		18939.18	−0.02	291°_3 − e^5D_2	
5279.81	5 *b*		18934.81			
5281.21	5		18929.79			
5282.646	4 *b*		18924.65			
5283.274	15		18922.40	0.00	19826_5 − 387°_4	
5283.732	4		18920.76	0.00	19_3 − 387°_4	
5284.077	5		18919.52			
5285.52	5		18914.35			
5287.017	3 *b*		18908.64			

TABLE 3. *Observed and classified lines of* W I

Wavelength Å	Intensity		Wavenumber (cm^{-1})		Classification	Zeeman effect
	Arc	Spark	Observed	o−c		
5288.505	3		18903.68	−0.12	24_3 — 435°_2	
5290.637	4		18896.06	+0.10	30_2 — 492°_2	
5290.774	15		18895.57	+0.01	31_5 — 502°_4	
5292.486	2		18889.46	0.00	$^3G_3$ — 322°_3	
5293.034	20		18887.50			
5294.449	5		18882.46	−0.02	291°_2 — e^5D_2	
5295.252	6		18879.59			
5296.462	20		18875.28	+0.08	28204_2 — 470°_2	
5298.585	8		18867.72	+0.02	24_3 — 434°_3	
5302.378	15		18854.22	+0.02	27_4 — 460°_3	
5305.939	12		18841.57	+0.03	22852_4 — 416°_3	
5307.459	15		18836.17	+0.01	17_4 — 359°_3	
5308.036	4		18834.12	+0.02	276°_2 — $^7D_3$	
5310.37	4		18825.85			
5311.353	20		18822.36	−0.06	27_5 — 466°_6	
				−0.06	29853_4 — 486°_4	
5311.64	1		18821.34	+0.01	18_1 — 369°_2	
5312.282	5		18819.07			
5313.124	6 *b*		18816.09	+0.04	26_2 — 456°_3	
5314.384	8 *b*		18811.63			
5316.037	5 *b*		18805.78			
5317.831	15		18799.43	−0.06	$^3P_2$ — 380°_3	
5318.862	40	1	18795.79	+0.01	276°_2 — e^5D_1	
5320.604	10		18789.64	−0.08	29_7 — 482°_7	
5321.282	3 *b*		18787.24	−0.08	18_2 — 369°_2	
5325.769	6 *b*		18771.41			
5326.575	1 *b*		18768.57	−0.02	15_3 — 342°_3	
5326.77	1		18767.89	−0.09	33_5 — 520°_4	
5327.052	4		18766.89	−0.04	380°_4—56768_5	
5329.711	5		18757.53	+0.01	18_2 — 368°_3	
5332.57	4 *b*		18747.47			
5336.23	3		18734.61			
5337.348	40		18730.69	+0.05	261°_3 — $^7D_2$	
5339.260	8		18723.98	−0.02	20_2 — 397°_2	
5339.940	10		18721.60	−0.05	28_1 — 474°_2	
5343.002	6		18710.87			
5344.84	5 *b*		18704.44			
5345.887	3 *b*		18700.77			
5346.193	4 *b*		18699.70	+0.13	18_3 — 376°_3	
5346.691	5		18697.96	+0.02	30_2 — 490°_3	
5348.058	5 *b*		18693.18			
5348.932	60	2	18690.13	+0.06	$^7P^\circ_2$ — $^7D_2$	
5349.854	8		18686.90	+0.02	33_5 — 519°_6	
5350.434	40		18684.88	−0.04	293°_2 — e^5D_2	
5351.892	30		18679.79	−0.01	277°_1 — e^5D_1	
5354.446	50		18670.88	+0.04	$^3P_0$ — 281°_1	
5355.25	25		18668.08	−0.03	19535_5 — 382°_6	
5356.601	20		18663.37	−0.02	20_2 — 396°_3	
5357.094	40		18661.65	−0.02	15_3 — 341°_4	
5358.32	25		18657.38	+0.11	27_1 — 463°_2	

TABLE 3. *Observed and classified lines of* W I

Wavelength Å	Intensity		Wavenumber (cm^{-1})		Classification	Zeeman effect
	Arc	Spark	Observed	o−c		
5361.41	15		18646.63	0.00	22852_4— 414°_3	
5362.864	12		18641.57	+0.13	34_4— 529°_3	
5363.337	5 *b*		18639.93	−0.03	28291_3— 469°_4	
5363.716	2		18638.61			
5365.085	2		18633.86			
5367.124	2 *b*		18626.78			
5368.014	5		18623.68	0.00	$^5S_2$— 369°_2	
5368.685	40	1	18621.36	0.00	28_5— 468°_5	
5369.534	1 *b*		18618.41	+0.02	23_2— 426°_3	
5370.004	4 *b*		18616.79	+0.01	24_3— 432°_2	
5371.967	2		18609.98			
5372.828	25		18607.00	+0.06	$^7P^\circ_4$— $^7D_3$	
5374.138	40	1	18602.47	+0.06	20_1— 390°_2	
				−0.07	23_3— 425°_4	
5374.418	15		18601.50			
5376.117	2 *b b*		18595.62			
5376.603	2 *b b*		18593.94	+0.06	$^5S_2$— 368°_3	
5377.488	3		18590.88	+0.01	18_1— 366°_2	
5379.438	10 *b*		18584.14	+0.08	23_3— 425°_3	
5381.992	10		18575.32	0.00	27_4— 457°_5	
5382.813	4 *b*		18572.49	+0.07	380°_4—56573_5	
5388.004	40	2	18554.59	+0.01	19_6— 382°_6	
5388.584	15	1	18552.59	+0.03	263°_2— $^7D_2$	
5389.661	3		18548.89			
5391.070	30		18544.04	−0.02	$^5D_4$— $^7F^\circ_4$	
5392.54	2		18539.0			
5392.78	4		18538.16			
5393.81	2		18534.62	−0.05	28_1— 472°_1	
5394.736	10		18531.44	+0.10	23_2— 425°_3	
5396.506	5		18525.36			
5397.020	25		18523.60	0.00	23_1— 419°_2	
5397.948	30	1	18520.41	+0.01	$^3P_2$— 377°_1	
5398.212	8		18519.51	−0.01	23_3— 424°_2	
5399.388	1		18515.47			
5399.602	5 *b*		18514.74	+0.17	28291_3— 468°_2	
5400.289	8		18512.36	0.00	26_2— 453°_1	
5400.936	15		18510.17	−0.05	23_1— 419°_0	
5402.296	3		18505.51	+0.02	18_1— 365°_0	
5402.628	1		18504.37	−0.14	34_4— 528°_3	
5404.322	25		18498.57	0.00	$^3H_6$— 355°_5	
5406.302	15		18491.79	0.00	18_3— 374°_2	
5408.136	1		18485.52			
5408.576	15		18484.02	−0.03	15_3— 339°_2	
5412.055	1 *b*		18472.14	+0.08	34_4— 527°_5	
5412.960	6		18469.05	−0.02	$^3G_3$— 318°_2	
5413.832	10		18466.07	−0.04	19535_5— 380°_4	
5414.826	1 *b*		18462.68	−0.10	28898_2— 473°_3	
5415.528	12		18460.29	−0.02	13_2— 322°_3	
5415.974	3		18458.77	+0.01	368°_3— 55_4	
5419.390	40		18447.14	−0.01	22476_4— 409°_3	

TABLE 3. *Observed and classified lines of* W I

Wavelength Å	Intensity		Wavenumber (cm^{-1})		Classification	Zeeman effect
	Arc	Spark	Observed	o−c		
5421.858	15		18438.74	−0.04	28_5— 466°_6	
5422.090	2		18437.95	−0.05	24_2— 432°_2	
5422.876	40		18435.28	−0.02	22476_4— 409°_5	
5423.21	1		18434.14	0.00	27_1— 461°_1	
5423.44	12		18433.36	0.00	19826_5— 382°_4	
5423.93	40		18431.70	−0.02	19_3— 382°_4	
5424.63	4		18429.32			
5424.91	2		18428.37			
5425.10	1		18427.72	+0.05	24_2— 432°_1	
5425.99	2		18424.70	+0.02	$^3H_4$— 305°_3	
5427.21	10		18420.56	+0.04	$^3P_2$— 376°_3	
5427.99	5		18417.91	+0.07	19_4— 380°_3	
5429.14	3		18414.01	+0.15	30_2— 487°_1	
5430.94	2		18407.91			
5433.256	6		18400.06	0.00	17_4— 355°_5	
5433.884	2		18397.93			
5435.032	100	5	18394.05	+0.01	$^5D_1$— $^7F^\circ_1$	
5435.59	30		18392.16	+0.02	17_4— 354°_3	
5435.75	4		18391.62	+0.01	28_5— 466°_4	
5437.637	2*b*		18385.23			
5438.852	8		18381.13	+0.01	17_3— 360°_4	
5439.568	15		18378.71	+0.01	19_3— 382°_3	
5440.05	25		18377.08	0.00	19826_5— 382°_6	
5441.11	8		18373.50			
5441.696	4		18371.52	0.00	29479_4— 478°_5	
5442.01	1		18370.46	+0.04	382°_6—56573_5	
5443.35	12		18365.94			
5446.126	5		18356.58	−0.01	28898_2— 472°_1	
5448.90	3		18347.23			
5449.454	2		18345.37	+0.03	22852_4— 411°_4	
5451.79	4		18337.51	+0.01	27_4— 455°_3	
5452.49	1		18335.15			
5456.58	30		18321.41	−0.02	23_3— 422°_3	
5457.92	12		18316.91	+0.02	29853_4— 481°_3	
5459.35	3*b*		18312.11			
5460.52	3*b*		18308.19			
5462.93	1		18300.11	0.00	$^3H_5$— 333°_5	
5464.45	3*b*		18295.02	+0.06	328°_4— e^5D_4	
5466.95	4		18286.66	−0.19	35499°_3— 53_4	
5467.53	12		18284.72	0.00	29853_4— 481°_5	
5468.60	1		18281.14			
5469.092	15		18279.49	−0.01	23_2— 422°_1	
				−0.03	28_6— 466°_6	
5469.70	2		18277.46	+0.01	28347_3— 466°_4	
5469.932	2		18276.69			
5471.02	2*b*		18273.05	+0.12	28_5— 465°_5	
5471.50	3		18271.45			
5472.314	6		18268.73	+0.02	23_2— 422°_3	
5475.110	30		18259.40	0.00	281°_1— e^5D_1	
5476.032	15		18256.33	−0.07	27_5— 461°_6	

TABLE 3. *Observed and classified lines of* W I

Wavelength Å	Intensity		Wavenumber (cm⁻¹)		Classification	Zeeman effect
	Arc	Spark	Observed	o−c		
5477.776	80		18250.51	+0.07	$^3P_0$ — 277°$_1$	
5478.656	3		18247.58	+0.14	31$_5$ — 496°$_4$	
5479.229	10		18245.68			
5480.617	15		18241.06			
5482.866	2		18233.57			
5483.276	2		18232.21	+0.21	27$_1$ — 459°$_2$	
5484.486	4		18228.19			
5485.312	2		18225.44	+0.07	19$_3$ — 380°$_3$	
5486.006	60		18223.14	+0.01	314°$_4$ — e^5D_3	
5487.766	40		18217.29	−0.02	$^5D_3$ — $^7F°_3$	
5488.466	6		18214.97			
5489.13	4	1	18212.77	+0.03	$^3P_2$ — 374°$_2$	
5489.96	20		18210.01	0.00	29479$_4$ — 476°$_4$	
5492.306	150	4	18202.23	+0.03	$^7D°_5$ — $^7D_4$	
5492.56	3		18201.39	+0.10	$^3G_4$ — 346°$_4$	
5492.908	4		18200.24	+0.06	20$_2$ — 391°$_1$	
5495.256	3		18192.46			
5496.234	30		18189.23	+0.06	22476$_4$ — 406°$_3$	
5498.622	12		18181.33	+0.07	28204$_2$ — 463°$_3$	
				+0.09	33$_5$ — 514°$_4$	
5500.490	75		18175.15	+0.07	19826$_5$ — 380°$_4$	
5500.996	10		18173.48	+0.04	19$_3$ — 380°$_4$	
5501.47	5		18171.91	+0.06	18$_3$ — 371°$_4$	
5503.44	100	2	18165.41	+0.21	14$_2$ — 331°$_2$	
				−0.06	299°$_3$ — e^5D_2	
				−0.15	329°$_3$ — e^5D_4	
5506.48	12		18155.38	+0.23	32$_1$ — 505°$_1$	
5508.474	4		18148.81	+0.11	32$_4$ — 502°$_4$	
5508.61	20		18148.36	+0.06	20$_1$ — 385°$_0$	
5512.81	1		18134.54	+0.14	34$_4$ — 524°$_4$	
5514.676	300	30	18128.41	+0.04	$^5D_2$ — $^7D°_1$	
5515.06	3		18127.14			
5515.20	2		18126.68			
5518.80	1*b*		18114.85	−0.11	29853$_4$ — 479°$_4$	
5519.135	2		18113.75	+0.01	339°$_2$ — 52$_1$	
5521.004	10		18107.62	−0.04	18$_1$ — 361°$_1$	
5525.276	1*b*		18093.62	+0.04	28291$_3$ — 463°$_3$	
5526.644	2*b*		18089.14			
5528.090	6		18084.41	+0.06	$^3G_3$ — 314°$_4$	
5531.384	30		18073.64	−0.01	18$_2$ — 361°$_1$	
5533.026	6		18068.28			
5537.289	3*b*		18054.37			
5537.722	10		18052.95	+0.03	19$_4$ — 373°$_5$	
5538.68	2		18049.83	+0.07	32$_4$ — 501°$_3$	
5539.482	6		18047.22	−0.01	20$_2$ — 390°$_2$	
5539.91	2		18045.83			
5542.368	2		18037.82	−0.04	28347$_3$ — 463°$_3$	
5542.94	1		18035.95	+0.08	28291$_3$ — 463°$_2$	
5548.078	3*b*		18019.26	−0.04	27$_5$ — 458°$_4$	
5550.319	4		18011.98			

TABLE 3. *Observed and classified lines of* W I

Wavelength Å	Intensity		Wavenumber (cm^{-1})		Classification	Zeeman effect
	Arc	Spark	Observed	o−c		
5551.012	5		18009.73	−0.04	17_4 − 351°_4	
5552.685	1		18004.31	−0.05	29479_4 − 474°_3	
5554.112	4 *b*		17999.68	−0.06	22476_4 − 404°_5	
5554.887	3		17997.17	−0.01	29853_4 − 478°_5	
5555.320	4		17995.77	−0.05	23_2 − 419°_2	
5559.764	4		17981.38	−0.02	14_2 − 329°_3	
5562.12	3		17973.77	+0.04	359°_3 − 53_3	
5563.97	4 *b*		17967.8			
5568.086	10		17954.51	−0.09	342°_3–52183_2	
5570.43	3		17946.96			
5571.99	2		17941.93	+0.07	23_3 − 418°_4	
5572.822	3		17939.25	−0.09	27_5 − 457°_5	
5575.812	4		17929.63	−0.02	18_3 − 369°_2	
5576.318	6		17928.01	+0.01	20_1 − 383°_1	
5577.945	1		17922.78	+0.01	$^3G_4$ − 343°_3	
5578.26	2		17921.76	−0.01	314°_4 − $^7D_5$	
5579.925	5		17916.42			
5584.00	3 *b*		17903.34	+0.08	24_3 − 425°_3	
5585.09	1		17899.86	+0.01	18_3 − 368°_3	
5588.12	2		17890.14	+0.02	19_4 − 371°_4	
5590.53	1		17882.43	+0.01	29479_4 − 473°_3	
5591.03	2		17880.83	−0.04	29479_4 − 473°_4	
5592.67	1		17875.58	+0.01	26_2 − 447°_1	
5593.56	10		17872.74	−0.02	28_5 − 461°_6	
5594.37	1		17870.15	+0.06	30_2 − 482°_2	
5601.818	1		17846.39	−0.01	19_3 − 376°_3	
5604.31	40		17838.46	+0.05	318°_2 − e^5D_3	
5605.20	3		17835.62	−0.05	29853_4 − 476°_4	
5608.134	5		17826.30	−0.03	18_2 − 359°_3	
5612.303	4		17813.05	0.00	22852_4 − 406°_3	
5615.16	2		17803.99	−0.06	23_3 − 417°_2	
5616.15	6		17800.85	+0.13	27_4 − 450°_3	
5617.05	5		17798.00	+0.03	17_3 − 354°_3	
5617.26	5		17797.33	+0.04	$^3G_4$ − 342°_3	
5618.74	2		17792.65	−0.02	22476_4 − 402°_3	
5623.97	2		17776.10	−0.04	28291_3 − 460°_3	
5624.58	6		17774.17	+0.02	19535_5 − 373°_5	
5629.67	8		17758.10	−0.09	$^3H_5$ − 328°_4	
5629.90	3		17757.38	+0.09	22476_4 − 402°_4	
5631.27	10	1	17753.06	−0.04	333°_5 − e^5D_4	
5631.94	20	2	17750.95	+0.06	$^3H_4$ − 299°_3	
5635.50	5		17739.73	−0.05	29853_4 − 475°_3	
5637.11	4		17734.66	+0.02	26_2 − 445°_2	
5639.64	5		17726.71	−0.04	27_4 − 449°_4	
5641.39	5		17721.21			
5642.03	6		17719.20	+0.06	$^5D_1$ − $^7F^\circ_0$	
5643.85	1		17713.49	−0.01	28_6 − 461°_6	
5644.47	5		17711.54	0.00	23_2 − 416°_3	
5647.02	3 *b*		17703.54	+0.02	27_1 − 453°_1	
5648.37	50	5	17699.31	+0.12	18_3 − 366°_2	
				−0.07	$^7D^\circ_4$ − $^7D_3$	

TABLE 3. *Observed and classified lines of* W I

Wavelength Å	Intensity		Wavenumber (cm^{-1})		Classification	Zeeman effect
	Arc	Spark	Observed	o−c		
5651.24	2		17690.32	−0.05	$^3G_4$ − 341°$_4$	
5652.41	2		17686.66	0.00	23$_6$ − 411°$_6$	
5654.10	3		17681.37	0.00	15$_3$ − 331°$_2$	
5657.00	3		17672.31	−0.05	23$_1$ − 411°$_0$	
5657.88	2		17669.56			
5660.07	6		17662.73	+0.04	$^5S_2$ − 359°$_3$	
5660.72	20	2	17660.70	+0.08	19$_6$ − 373°$_5$	
5663.30	3 *b*		17652.65	+0.01	32$_4$ − 497°$_4$	
5663.98	3		17650.53	−0.07	$^3P_2$ − 369°$_2$	
5664.33	8		17649.44	−0.06	23$_1$ − 411°$_2$	
5667.18	4		17640.57	−0.06	24$_3$ − 422°$_3$	
5670.56	1		17630.05	+0.03	29853$_4$ − 474°$_3$	
5673.53	5		17620.82	+0.02	$^3P_2$ − 368°$_3$	
5674.39	10	1	17618.15	+0.03	19$_4$ − 368°$_3$	
5675.37	5		17615.11	−0.01	18$_2$ − 357°$_2$	
5676.60	6		17611.29	−0.06	19535$_5$ − 371°$_4$	
5676.90	8		17610.36	−0.02	17$_3$ − 353°$_2$	
5678.90	4		17604.16			
5679.64	3		17601.87	+0.02	27$_5$ − 454°$_5$	
5680.08	4		17600.50	+0.10	23$_2$ − 415°$_2$	
5689.68	2		17570.81	+0.06	28$_1$ − 462°$_1$	
5690.13	3		17569.42	+0.07	23$_3$ − 414°$_3$	
5693.73	4 *b*		17558.31			
5694.56	3		17555.75	+0.05	28$_5$ − 457°$_5$	
5695.06	3		17554.21	+0.15	34$_4$ − 518°$_4$	
5697.79	10		17545.80	+0.03	13$_2$ − 313°$_1$	
5704.37	4		17525.56	−0.03	17$_4$ − 346°$_4$	
5705.71	5		17521.44	−0.06	28347$_3$ − 458°$_4$	
5707.29	1		17516.59	−0.04	23$_2$ − 414°$_3$	
5708.00	2		17514.41	+0.15	33$_5$ − 508°$_5$	
5709.05	4 *b*		17511.19	0.00	371°$_4$ − 54$_3$	
5712.47	3		17500.71	+0.13	32$_4$ − 496°$_4$	
5715.38	4		17491.80	+0.12	305°$_3$ − e^5D_2	
5718.18	2		17483.23	+0.11	19826$_5$ − 373°$_5$	
5721.10	2		17474.31			
5721.35	1		17473.55	+0.06	28204$_2$ − 456°$_3$	
5721.88	1		17471.93	+0.04	393°$_5$ − 56$_6$	
5723.05	8		17468.35	−0.03	259°$_1$ − $^7D_1$	
5724.54	1 *b*		17463.81	−0.06	347°$_1$ − 52183$_2$	
5726.43	2		17458.04			
5728.56	4		17451.55	+0.07	$^5S_2$ − 357°$_2$	
5735.09	50	5	17431.68	−0.05	$^7P°_3$ − $^7D_2$	
5738.87	3		17420.20	+0.06	$^3P_2$ − 366°$_2$	
5739.60	10		17417.99	−0.03	322°$_3$ − e^5D_3	
5740.06	2		17416.59	+0.04	22852$_4$ − 402°$_3$	
5741.12	4		17413.38	0.00	23$_1$ − 408°$_2$	
5747.27	8 *b*		17394.74	−0.04	306°$_1$ − e^5D_2	
5749.24	20		17388.78	−0.12	305°$_3$ − $^7D_4$	
5750.22	4		17385.82	+0.01	28291$_3$ − 456°$_3$	

TABLE 3. *Observed and classified lines of* W I

Wavelength Å	Intensity		Wavenumber (cm^{-1})		Classification	Zeeman effect
	Arc	Spark	Observed	o−c		
5751.37	2		17382.34	+0.03	18_2— 354°_3	
5752.65	3		17378.47	+0.07	32_4— 495°_3	
5753.34	4 *b*		17376.39	−0.05	$^3P_1$— 306°_1	
5753.85	6		17374.85			
5754.57	5		17372.67	−0.15	20_2— 383°_1	
5756.10	8		17368.06	−0.05	15_3— 328°_4	
5759.65	10		17357.35	−0.15	291°_3— $^7D_3$	
5763.40	3 *b*		17346.06	−0.06	20_1— 377°_1	
5767.76	2 *b*		17332.95	+0.01	27_4— 445°_5	
5768.74	2		17330.00	−0.09	28347_3— 456°_3	
5771.98	6		17320.28	−0.04	19826_5— 371°_4	
5773.48	5		17315.78	+0.02	23_1— 407°_1	
5784.76	3		17282.01	+0.06	32_4— 494°_3	
5789.81	4		17266.94	−0.03	27_5— 451°_4	
5791.33	3		17262.41	−0.05	291°_2— e^5D_1	
5791.80	1 *b*		17261.00	−0.06	24_3— 418°_4	
5792.34	1 *b*		17259.40	−0.04	28291_3— 455°_3	
5792.65	3 *b*		17258.47			
5793.06	10		17257.25	−0.07	276°_2— $^7D_2$	
5796.49	8		17247.04	−0.03	17_4— 343°_3	
5797.75	2		17243.29	+0.01	22476_4— 397°_4	
5799.51	5		17238.06	−0.02	$^3G_3$— 305°_3	
5801.13	1		17233.24	+0.04	27_4— 444°_3	
5803.04	3		17227.57			
5804.46	2		17223.36	0.00	20_2— 382°_3	
5804.85	40	4	17222.20	−0.01	$^7P^\circ_2$— $^7D_1$	
5806.05	3		17218.64	−0.03	$^5S_2$— 354°_3	
5806.24	6		17218.08	+0.02	28204_2— 454°_2	
5810.46	1		17205.57	−0.09	28898_2— 461°_1	
5814.14	2		17194.68	−0.04	18_2— 353°_2	
5815.36	1		17191.07	−0.19	374°_2— 54_3	
5818.57	1		17181.59	−0.01	28_1— 459°_2	
5821.00	4	1	17174.42	−0.02	23_3— 411°_2	
5822.13	1		17171.09	+0.09	34_4— 514°_4	
5822.60	10		17169.70	−0.03	22476_4— 396°_3	
5826.10	2		17159.39	+0.03	26861_2— 440°_3	
5832.26	5		17141.26	−0.08	277°_1— $^7D_2$	
5833.61	8		17137.29	−0.08	22476_4— 396°_5	
5835.94	1		17130.45	+0.07	28291_3— 454°_2	
5838.97	8		17121.56	−0.03	17_4— 342°_3	
5841.68	2		17113.62	+0.04	26_2— 439°_2	
5843.70	1 *b*		17107.71	−0.08	18_3— 360°_4	
5845.27	10	1	17103.11	−0.11	293°_2— $^7D_3$	
5848.81	2		17092.76			
5849.52	4		17090.68	−0.09	27_5— 449°_4	
5851.58	10	1	17084.67	−0.03	263°_2— $^7D_1$	
5854.39	5		17076.47	−0.01	19_3— 369°_2	
5856.61	6		17069.99	−0.04	20_2— 380°_3	
5857.70	2		17066.82	+0.09	27_1— 447°_1	
5858.22	4		17065.30	0.00	32_1— 494°_1	

318-092 O-69—12

TABLE 3. *Observed and classified lines of* W I

Wavelength Å	Intensity		Wavenumber (cm^{-1})		Classification	Zeeman effect
	Arc	Spark	Observed	o−c		
5860.42	1		17058.89	−0.06	28_6− 454°_5	
5862.75	1		17052.11	+0.13	32_4− 491°_5	
5864.16	1		17048.02	−0.10	397°_4–56768_5	
5864.63	12	1	17046.65	−0.03	19_3− 368°_3	
5866.02	1 *b*		17042.61	+0.07	368°_3− 53_3	
5867.46	1		17038.44	−0.02	20_1− 374°_2	
5870.03	4		17030.97	−0.11	$^5S_2$− 353°_2	
				−0.01	26_2− 438°_1	
5870.65	1		17029.17	+0.06	28_5− 452°_4	
5871.37	1		17027.08	+0.03	29479_4− 465°_5	
5871.64	4 *b*		17026.30	−0.02	281°_1− e^5D_0	
5874.22	6		17018.82	−0.04	19_4− 362°_5	
5875.69	5		17014.56	−0.11	17_4− 341°_4	
5876.28	2		17012.85	+0.11	369°_2− 53_3	
5879.44	1		17003.71	+0.19	28898_2− 459°_2	
5879.69	2		17002.99			
5880.21	10	1	17001.48	+0.02	341°_4− e^5D_4	
5882.82	1		16993.94	+0.19	23_3− 409°_3	
5883.17	2		16992.93	+0.09	33_5− 502°_4	
5883.48	2		16992.03			
5884.62	4		16988.74	+0.05	34_4− 512°_5	
5884.96	1		16987.76	+0.22	30_2− 473°_3	
5888.65	1		16977.12	−0.04	$^3H_4$− 291°_3	
5890.32	5		16972.30	−0.02	24_3− 415°_2	
5891.61	8		16968.59	−0.07	18_3− 359°_3	
5893.34	1		16963.61	+0.02	30_2− 473°_2	
5895.98	1		16956.01	−0.09	23_1− 404°_1	
5900.02	1		16944.40	−0.07	24_2− 417°_2	
5901.20	8		16941.01	−0.02	23_2− 409°_3	
5902.00	4		16938.72	−0.01	$^3G_4$− 333°_5	
5902.30	4		16937.85	−0.08	32_4− 490°_5	
5902.64	20		16936.88	−0.05	$^3P_2$− 361°_1	
5904.57	1		16931.34	−0.08	17_3− 346°_4	
5905.05	4		16929.97			
5906.52	2 *b*		16925.75	−0.05	27_1− 445°_2	
5906.76	2		16925.07			
5910.32	2		16914.87	−0.08	28347_3− 452°_4	
5913.39	5		16906.09	−0.05	29479_4− 463°_3	
5913.92	3		16904.57	−0.11	24_2− 416°_3	
5917.42	3 *b*		16894.57	+0.03	342°_3− e^5D_4	
5919.66	3 *b*		16888.18			
5920.60	4		16885.50	−0.10	23_2− 408°_2	
5921.05	3		16884.22	−0.11	22476_4− 393°_5	
5921.37	3		16883.31	−0.02	28_5− 451°_4	
5921.87	1		16881.88	+0.12	32_1− 492°_2	
5922.07	1		16881.31	−0.04	30_2− 472°_1	
5927.05	3		16867.13	−0.03	22852_4− 397°_4	
5928.58	10		16862.77	−0.07	22_0− 396°_1	
5928.93	1		16861.78	−0.06	28898_2− 457°_1	
5931.13	2		16855.52			

TABLE 3. *Observed and classified lines of* W I

Wavelength Å	Intensity		Wavenumber (cm^{-1})		Classification	Zeeman effect
	Arc	Spark	Observed	o−c		
5934.49	8		16845.98	−0.04	19_3— 366°_2	
5936.14	1		16841.30	−0.15	14_2— 318°_2	
5937.08	3		16838.63			
5940.89	10		16827.83	−0.15	$^5D_4$— $^7F^\circ_3$	
				−0.09	328°_4— e^5D_3	
5941.54	3		16825.99	−0.07	19_4— 360°_4	
5941.94	3		16824.86	−0.03	28291_3— 451°_4	
5947.08	8		16810.32	−0.02	28204_2— 450°_3	
5947.57	30		16808.93	0.00	13_2— 305°_3	
5948.19	3		16807.18	0.00	27_4— 440°_3	
5949.44	4		16803.65			
5953.96	8		16790.89	−0.05	20_2— 377°_1	
5956.19	10		16784.61	−0.07	17_3— 344°_2	
5958.23	1		16778.86	+0.13	28898_2— 456°_3	
5958.53	2		16778.01	0.00	15_3— 322°_3	
5960.83	15		16771.54	−0.05	27_4— 439°_4	
				+0.15	29853_4— 466°_4	
5964.48	3	5 *s*	16761.28	+0.03	22852_4— 396°_5	
5965.86	40	2	16757.39	−0.06	18_3— 357°_2	
5972.03	3		16740.09	0.00	19535_5— 362°_5	
5972.51	25		16738.74	−0.03	$^5D_2$— $^7F^\circ_1$	
5973.40	1		16736.25			
5973.56	2		16735.80	+0.03	23_3— 406°_3	
5976.65	8		16727.15	+0.01	28291_3— 450°_2	
5978.86	15		16720.96	+0.02	281°_1— $^7D_2$	
5980.95	2		16715.12			
5982.60	2		16710.51	+0.08	27_4— 439°_5	
5983.82	20		16707.11	−0.02	28_5— 449°_4	
5984.50	2 *b*		16705.21	+0.01	30_2— 470°_2	
5986.94	6		16698.40	−0.06	329°_3— e^5D_3	
5987.43	12 *b*		16697.03	+0.01	27_1— 443°_2	
				+0.07	27_5— 445°_5	
5989.59	10		16691.02	−0.04	20_2— 376°_3	
5990.11	5		16689.56	−0.05	$^3P_2$— 359°_3	
5991.07	3		16686.89	−0.04	19_4— 359°_3	
5992.15	1		16683.88	−0.17	354°_3—52183_2	
5992.46	8		16683.02	−0.03	23_2— 406°_3	
				+0.04	27_1— 443°_1	
5993.21	2 *b*		16680.93			
5996.20	2		16672.61			
5998.28	3		16666.83	−0.11	28347_3— 450°_3	
6001.02	2		16659.22			
6003.21	4		16653.14	+0.02	28_1— 453°_1	
6009.01	10		16637.07	+0.05	27_4— 438°_3	
6009.17	1		16636.63	+0.13	18_1— 347°_1	
6009.68	8		16635.21	−0.07	$^3H_4$— $^7D^\circ_4$	
6012.78	50	5	16626.64	+0.08	19_6— 362°_5	
6015.64	3 *b*		16618.73	−0.03	$^5D_3$— $^7F^\circ_2$	
6016.27	2		16616.99	+0.05	26_2— 434°_3	
6019.73	3		16607.44	+0.01	34_4— 509°_4	

TABLE 3. *Observed and classified lines of* W I

Wavelength Å	Intensity		Wavenumber (cm⁻¹)		Classification	Zeeman effect
	Arc	Spark	Observed	o−c		
6021.52	40		16602.52	+0.03	18_2— 347°_1	
6027.16	1		16586.97	−0.29	24_3— 411°_4	
6028.32	15		16583.78	+0.01	299°_3— $^7D_3$	
6029.84	5		16579.60	+0.06	31_5— 479°_4	
6030.64	2 *v*		16577.40			
6034.72	3 *b*		16566.19			
6035.42	4		16564.27	−0.02	$^3G_3$— 299°_3	
6037.31	3 *b*		16559.08			
6038.28	2		16556.42	−0.06	23_1— 400°_2	
6041.62	10		16547.27	−0.02	19535_5— 360°_4	
6043.31	25		16542.64	+0.01	314°_4— $^7D_4$	
6046.80	3		16533.09	+0.08	28204_2— 447°_1	
6048.87	2 *b*		16527.44	+0.02	17_3— 342°_3	
6049.25	1 *b*		16526.40	+0.13	$^3G_4$— 329°_3	
				−0.16	328°_4— $^7D_5$	
6049.92	12		16524.57	−0.07	18_3— 354°_3	
6053.17	2 *b*		16515.70			
6055.93	2		16508.17	−0.04	22852_4— 393°_5	
6057.41	5 *b*		16504.13	+0.10	34_4— 508°_5	
6061.29	1		16493.57	−0.07	24_3— 411°_2	
6065.08	15		16483.27	−0.01	20_2— 374°_2	
6066.88	4		16478.37	−0.03	$^3P_2$— 357°_2	
6067.64	10		16476.31	−0.01	20_1— 369°_2	
6077.70	1		16449.04	−0.02	19535_5— 362°_5	
6081.44	30		16438.92	+0.07	$^5S_2$— 347°_1	
6082.89	3		16435.00			
6083.88	4		16432.33	+0.08	30_2— 468°_2	
6092.38	5		16409.40	−0.02	22_0— 391°_1	
6094.75	5		16403.02	−0.01	18_1— 344°_2	
6107.42	10		16369.00	−0.02	18_2— 344°_2	
6111.66	15		16357.64	+0.02	15_3— 318°_2	
6115.52	12		16347.31	+0.01	14_2— 313°_1	
6119.39	4		16336.98	−0.07	18_3— 353°_2	
6128.25	20		16313.36	+0.04	28_5— 445°_5	
6129.60	3		16309.76	−0.06	29479_4— 457°_5	
6131.63	2		16304.36	−0.04	28291_3— 445°_2	
6131.79	1		16303.94	+0.05	23_3— 402°_4	
6133.19	4		16300.22	−0.03	31_5— 476°_4	
6138.36	1		16286.49	−0.06	23_2— 402°_3	
6141.04	1		16279.38			
6143.94	12		16271.70	−0.06	22476_4— 387°_4	
6146.52	1		16264.87	+0.11	27_4— 434°_3	
6147.23	3		16262.99	−0.04	17_4— 333°_5	
6148.15	2 *b*		16260.56	−0.13	318°_2— e^5D_2	
6151.81	1		16250.88	+0.05	19_4— 355°_5	
6153.72	2 *b*		16245.84	−0.02	20_1— 366°_2	
6154.87	6		16242.80	−0.02	28204_2— 444°_3	
				−0.08	17_3— 339°_2	
6161.43	8		16225.51	−0.09	18_2— 343°_1	
6162.70	1		16222.16	+0.02	27_1— 438°_1	

TABLE 3. *Observed and classified lines of* W I

Wavelength Å	Intensity		Wavenumber (cm⁻¹)		Classification	Zeeman effect
	Arc	Spark	Observed	o−c		
6165.70	1		16214.27	−0.09	$29853_4 - 460^\circ_3$	
6169.11	10		16205.31	−0.07	$^5S_2 - 344^\circ_2$	
6176.18	1		16186.76			
6179.66	3		16177.64			
6181.39	2		16173.11			
6186.24	15		16160.44	−0.04	$20_1 - 365^\circ_0$	
6187.57	5		16156.96	−0.02	$28_5 - 443^\circ_6$	
6188.73	3		16153.93	−0.13	$28_6 - 445^\circ_5$	
6193.23	10		16142.20	−0.07	$18_3 - 351^\circ_4$	
6195.78	1		16135.55	−0.06	$27_5 - 439^\circ_4$	
6195.96	10	2	16135.08	−0.06	$13_2 - 299^\circ_3$	
6196.36	10	1	16134.04	−0.13	$24_2 - 409^\circ_3$	
6198.19	2		16129.28	+0.01	$23_6 - 396^\circ_5$	
6203.51	20	1	16115.45	−0.04	$19_3 - 359^\circ_3$	
6216.65	3 *b*		16081.39	−0.03	$23_3 - 400^\circ_2$	
6219.36	2		16074.38	−0.07	$27_5 - 439^\circ_5$	
6220.31	2 *b*		16071.92	−0.08	$29479_4 - 455^\circ_3$	
6224.18	3		16061.93	−0.03	$^5S_2 - 343^\circ_1$	
6225.75	4		16057.88	−0.12	$^3P_2 - 353^\circ_2$	
6234.74	1 *b*		16034.73	+0.12	$32_4 - 481^\circ_3$	
6237.69	2		16027.14			
6239.27	2 *b*		16023.09			
6240.54	5		16019.82	−0.08	$28347_3 - 443^\circ_2$	
6241.94	4 *b*		16016.23	−0.06	$20_0 - 361^\circ_1$	
6243.10	2		16013.25			
6243.72	2		16011.66			
6245.79	8 *b*		16006.36	0.00	$351^\circ_4 - e^5D_4$	
6251.48	5		15991.79			
6253.63	6		15986.29			
6254.28	25		15984.63	−0.01	$333^\circ_5 - {}^7D_5$	
6258.88	5		15972.88	−0.02	$15_3 - 314^\circ_4$	
6259.11	4 *b*		15972.29	+0.10	$24_3 - 405^\circ_4$	
				−0.04	$29479_4 - 454^\circ_5$	
6269.28	4		15946.38			
6279.68	3 *b v*		15919.97			
6285.88	25		15904.27	−0.01	$19_3 - 357^\circ_2$	
6288.75	3		15897.01			
6289.10	2		15896.13			
6291.01	8		15891.30	−0.04	$20_2 - 368^\circ_3$	
6292.02	60	3	15888.75	+0.01	$^3P_1 - 291^\circ_2$	
6297.31	3		15875.41	+0.01	$28_1 - 445^\circ_2$	
6298.57	6		15872.23			
6302.96	1		15861.17	−0.06	$18_1 - 339^\circ_2$	
6303.21	20		15860.55	+0.01	$19_4 - 351^\circ_4$	
6304.03	3		15858.48	−0.05	$19_6 - 355^\circ_5$	
6308.50	10		15847.25	−0.03	$^3G_3 - 291^\circ_2$	
6309.71	2		15844.21	+0.01	$27_1 - 435^\circ_2$	
6313.15	2		15835.57	+0.06	$34_4 - 501^\circ_5$	
6314.32	3		15832.64	−0.04	$32_4 - 479^\circ_4$	
6319.24	8		15820.31	−0.03	$27_4 - 430^\circ_5$	

TABLE 3. *Observed and classified lines of* W I

Wavelength Å	Intensity		Wavenumber (cm^{-1})		Classification	Zeeman effect
	Arc	Spark	Observed	o−c		
6324.67	2*b*		15806.73	+0.02	$^3G_4$ — 322°$_3$	
6331.44	4		15789.83	−0.05	23°$_3$ — 397°$_4$	
6335.10	3		15780.71	−0.01	291°$_3$ — $^7D_2$	
6336.60	2		15776.97	+0.03	23°$_3$ — 397°$_2$	
6342.40	3		15762.54	−0.11	20°$_1$ — 361°$_1$	
6344.50	2		15757.33			
6346.66	2		15751.96	−0.01	28°$_5$ — 439°$_4$	
6351.68	2		15739.51	−0.04	26°$_2$ — 426°$_3$	
6352.51	4*b*		15737.46	−0.06	322°$_3$ — $^7D_4$	
6355.66	3		15729.66	−0.04	22476$_4$ — 382°$_3$	
6355.90	10		15729.06	−0.05	28291$_3$ — 440°$_3$	
6357.98	3		15723.92	−0.08	291°$_2$ — $^7D_2$	
6359.14	6		15721.05	−0.06	17°$_4$ — 328°$_4$	
6361.06	4		15716.31	−0.02	23°$_3$ — 396°$_3$	
6362.35	1		15713.12			
6363.79	1		15709.55			
6364.73	10		15707.24	−0.12	14°$_2$ — 306°$_1$	
6368.73	1		15697.38	+0.06	28898$_2$ — 445°$_2$	
6370.32	6		15693.46	−0.07	28291$_3$ — 439°$_4$	
6371.43	20		15690.73	+0.05	20°$_2$ — 366°$_2$	
6375.40	10		15680.96	−0.07	19826$_5$ — 355°$_5$	
6378.47	3		15673.41	+0.01	28347$_3$ — 440°$_3$	
				−0.07	277°$_1$ — $^7D_1$	
6379.29	3		15671.39	−0.07	19°$_3$ — 354°$_3$	
6382.49	8		15663.54	−0.04	$^5S_2$ — 339°$_2$	
				−0.07	23°$_2$ — 396°$_3$	
6384.72	8		15658.07	+0.02	18°$_3$ — 346°$_4$	
6386.47	20		15653.77	+0.05	23°$_2$ — 396°$_1$	
6387.13	4		15652.16	−0.02	27°$_4$ — 428°$_5$	
6389.39	2		15646.62	−0.02	28204$_2$ — 438°$_3$	
6393.07	4		15637.61	−0.20	28347$_3$ — 439°$_4$	
				+0.16	29479$_4$ — 451°$_4$	
				+0.10	353°$_2$ — 50949$_1$	
6395.20	1		15632.41	−0.17	28°$_1$ — 443°$_1$	
6397.30	3		15627.28			
6399.74	10		15621.32	−0.14	24°$_2$ — 404°$_1$	
6402.07	12		15615.63	−0.06	13°$_2$ — 293°$_2$	
6404.21	30		15610.41	−0.05	14°$_2$ — 305°$_3$	
6409.34	1		15597.91			
6415.03	1		15584.09			
6416.00	12		15581.73	−0.04	19535$_5$ — 351°$_4$	
6417.36	4		15578.43			
6418.22	2		15576.34	+0.03	22476$_4$ — 380°$_3$	
6418.69	3		15575.20	+0.01	23°$_1$ — 390°$_2$	
6425.42	10		15558.88	−0.08	28291$_3$ — 438°$_3$	
6426.12	4		15557.18	0.00	27°$_1$ — 432°$_2$	
6427.70	5		15553.36	−0.03	32°$_4$ — 476°$_4$	
6429.89	3		15548.07	+0.01	28898$_2$ — 444°$_3$	
6430.43	1		15546.76	+0.09	27°$_1$ — 432°$_1$	
6432.12	3		15542.68	−0.08	31°$_5$ — 469°$_4$	

TABLE 3. *Observed and classified lines of* W I

Wavelength Å	Intensity		Wavenumber (cm^{-1})		Classification	Zeeman effect
	Arc	Spark	Observed	o−c		
6435.24	8		15535.14	−0.08	$29479\,{}_4$— 450°_3	
6435.58	12		15534.32	−0.04	341°_4— e^5D_3	
6438.12	4		15528.19	−0.09	$30\,{}_2$— 459°_2	
6438.85	3		15526.43	+0.01	293°_2— $^7D_2$	
6439.70	15		15524.38	+0.04	$22476\,{}_4$— 380°_4	
6443.08	1		15516.24			
6443.95	2		15514.15			
6445.12	50		15511.33	+0.04	$18\,{}_3$— 344°_2	
6445.78	10		15509.74	−0.10	$29\,{}_7$— 449°_7	
6447.25	1		15506.20			
6448.25	6		15503.80			
6448.76	1		15502.57			
6449.93	3		15499.76			
6450.12	2		15499.30			
6450.76	1		15497.76			
6451.24	2		15496.61			
6456.61	7		15483.73	−0.15	$19\,{}_3$— 353°_2	
6458.35	10		15479.55	−0.13	$24\,{}_2$— 402°_3	
6461.78	5		15471.34			
6462.62	2		15469.32	−0.16	365°_0—$52057\,{}_1$	
6463.00	2 *b*		15468.42	−0.12	$28898\,{}_2$— 443°_2	
6464.13	18		15465.71	+0.06	$^3P_2$— 347°_1	
				−0.01	$31\,{}_5$— 468°_5	
6464.43	4		15465.00			
6468.86	2		15454.41	−0.09	$28898\,{}_2$— 443°_1	
6471.25	1		15448.70	+0.02	$^3G_3$— $^7D^\circ_4$	
6474.84	8		15440.13	−0.01	$17\,{}_3$— 331°_2	
6479.51	10		15429.00	+0.01	$28291\,{}_3$— 437°_4	
6480.19	4		15427.38	−0.06	342°_3— e^5D_3	
6484.09	25		15418.11	−0.02	$13\,{}_2$— 291°_2	
6487.38	2		15410.29	−0.11	368°_3— $52\,{}_3$	
6491.50	6		15400.50	−0.12	$24\,{}_3$— 400°_2	
				−0.16	$26\,{}_2$— 422°_1	
6494.75	6		15392.80	−0.08	$33\,{}_5$— 486°_6	
6499.96	5		15380.46	−0.14	369°_2— $52\,{}_3$	
6500.38	15		15379.47	−0.10	$18\,{}_3$— 343°_3	
6501.70	1		15376.34	+0.02	$19\,{}_4$— 346°_4	
6502.09	4		15375.42	+0.02	411°_4—$56573\,{}_5$	
6503.07	3		15373.10	−0.17	$28347\,{}_3$— 437°_4	
6506.26	6 *b*		15365.57			
6508.05	20		15361.34	+0.07	$13\,{}_2$— 291°_3	
6513.44	5		15348.63	+0.06	$28\,{}_6$— 437°_5	
6514.65	2		15345.78			
6515.44	3		15343.92			
6519.46	1		15334.46	−0.02	$34\,{}_4$— 496°_4	
6521.98	4		15328.53	−0.02	366°_2—$52002\,{}_3$	
6523.01	6		15326.11	−0.04	$^3H_4$— $^7P^\circ_3$	
6523.73	1		15324.42			
6526.15	12		15318.74	+0.06	$27\,{}_4$— 425°_4	
6526.66	1		15317.54			

TABLE 3. *Observed and classified lines of* W I

Wavelength Å	Intensity		Wavenumber (cm^{-1})		Classification	Zeeman effect
	Arc	Spark	Observed	o−c		
6529.66	4		15310.50	+0.04	$28204\,{}_{2}-\ 435^{\circ}_{2}$	
6532.39	25		15304.11	+0.01	$20\,{}_{1}-\ 357^{\circ}_{2}$	
6533.29	5		15302.00	+0.04	$343^{\circ}_{3}-\ e^{5}D_{3}$	
6534.03	8		15300.26	+0.04	$27\,{}_{4}-\ 425^{\circ}_{3}$	
6538.11	30		15290.72	+0.02	$19826\,{}_{5}-\ 351^{\circ}_{4}$	
6541.41	8		15283.00	−0.14	$31\,{}_{5}-\ 466^{\circ}_{6}$	
6544.89	2		15274.88			
6545.18	1		15274.20	+0.16	$28204\,{}_{2}-\ 434^{\circ}_{3}$	
6549.96	2		15263.05	+0.06	$29853\,{}_{4}-\ 451^{\circ}_{4}$	
				−0.09	$366^{\circ}_{2}-\ 51\,{}_{2}$	
6552.84	15		15256.34	−0.11	$17\,{}_{3}-\ 329^{\circ}_{3}$	
6553.83	8		15254.04	+0.05	$18\,{}_{3}-\ 342^{\circ}_{3}$	
6554.25	20		15253.06	+0.02	$281^{\circ}_{1}-\ 43\,{}_{1}$	
6561.43	1		15236.37	+0.07	$27\,{}_{4}-\ 424^{\circ}_{4}$	
6562.26	1		15234.44			
6562.89	8 *b*		15232.98	−0.02	$34\,{}_{4}-\ 493^{\circ}_{5}$	
6563.20	25		15232.26	+0.04	$^{3}P_{2}-\ 344^{\circ}_{2}$	
6567.32	7		15222.71	+0.07	$28291\,{}_{3}-\ 435^{\circ}_{2}$	
6567.79	15		15221.62	−0.22	$24\,{}_{2}-\ 400^{\circ}_{2}$	
6569.77	5		15217.03	−0.09	$357^{\circ}_{2}-50949\,{}_{1}$	
6571.81	3		15212.31	+0.01	$34\,{}_{4}-\ 495^{\circ}_{3}$	
6573.93	30		15207.40	−0.07	$20\,{}_{2}-\ 361^{\circ}_{1}$	
6577.08	1		15200.11	−0.14	$22852\,{}_{4}-\ 380^{\circ}_{3}$	
6578.27	4		15197.37	−0.03	$22476\,{}_{4}-\ 376^{\circ}_{3}$	
6579.77	1		15193.90			
6582.91	12		15186.66	+0.04	$28291\,{}_{3}-\ 434^{\circ}_{3}$	
6590.06	1		15170.18	0.00	$344^{\circ}_{2}-\ e^{5}D_{3}$	
6594.13	3		15160.82	−0.06	$29853\,{}_{4}-\ 450^{\circ}_{3}$	
6599.98	2		15147.38	+0.04	$328^{\circ}_{4}-\ {}^{7}D_{4}$	
6600.10	8		15147.10	−0.07	$18\,{}_{3}-\ 341^{\circ}_{4}$	
6602.37	1		15141.89			
6603.95	1		15138.27	−0.13	$371^{\circ}_{4}-\ 52\,{}_{3}$	
6605.46	2		15134.81	−0.01	$313^{\circ}_{1}-\ e^{5}D_{1}$	
6607.13	18		15130.99	−0.02	$17\,{}_{4}-\ 322^{\circ}_{3}$	
				−0.01	$28347\,{}_{3}-\ 434^{\circ}_{3}$	
6608.50	8		15127.85	−0.04	$368^{\circ}_{3}-52002\,{}_{3}$	
6609.05	18		15126.59	−0.04	$15\,{}_{3}-\ 305^{\circ}_{3}$	
6611.62	20		15120.71	−0.04	$329^{\circ}_{3}-\ e^{5}D_{2}$	
6612.24	2		15119.29			
6613.20	4 *b*		15117.10	−0.19	$31\,{}_{5}-\ 465^{\circ}_{5}$	
				+0.12	$26\,{}_{2}-\ 419^{\circ}_{2}$	
6613.90	2		15115.50	+0.04	$34\,{}_{4}-\ 494^{\circ}_{3}$	
6616.19	2		15110.27			
6620.64	10		15100.11	−0.06	$23\,{}_{3}-\ 390^{\circ}_{2}$	
6621.51	15		15098.13	+0.04	$369^{\circ}_{2}-52002\,{}_{3}$	
6621.74	20		15097.60	+0.01	$19535\,{}_{5}-\ 346^{\circ}_{4}$	
6622.42	8		15096.05	−0.09	$24\,{}_{5}-\ 397^{\circ}_{2}$	
6622.91	4		15094.93			
6626.00	4		15087.90			
6626.51	5		15086.73	−0.18	$29853\,{}_{4}-\ 449^{\circ}_{4}$	

TABLE 3. *Observed and classified lines of* W I

Wavelength Å	Intensity		Wavenumber (cm⁻¹)		Classification	Zeeman effect
	Arc	Spark	Observed	o−c		
6631.10	2*b*		15076.29	+0.03	28898_2— 439°_2	
6634.54	2		15068.47			
6635.04	6		15067.34	−0.10	29479_4— 445°_5	
6636.02	6		15065.11			
6636.49	4		15064.05	−0.08	32_1— 474°_2	
6636.68	10		15063.61	−0.16	402°_3— 55_4	
				−0.10	314°_4— $^7D_3$	
6638.97	4		15058.42	−0.13	18_1— 331°_2	
6639.56	1		15057.08			
6643.58	5		15047.97	−0.09	30_2— 454°_2	
6643.86	3		15047.34	−0.11	23_2— 390°_2	
6645.27	1		15044.14			
6648.12	2		15037.69	0.00	27_4— 422°_3	
6651.91	1		15029.12			
6652.37	1		15028.09			
6652.98	1		15026.71			
6653.96	10		15024.50	−0.04	18_2— 331°_2	
6654.44	5		15023.41	−0.05	28204_2— 432°_2	
				−0.03	346°_4— e^5D_3	
6656.54	12		15018.67	−0.13	28_6— 434°_7	
6656.84	1		15017.99	+0.03	329°_3— $^7D_4$	
6657.03	10*b*		15017.56	0.00	28_5— 432°_4	
6657.66	4		15016.15	−0.05	27_5— 428°_5	
6659.04	4		15013.03	−0.10	28204_2— 432°_1	
6659.36	1		15012.31			
6663.18	1		15003.70			
6663.61	1		15002.74			
6664.16	15		15001.50	−0.10	$^3G_4$— 314°_4	
6664.80	25		15000.06	−0.12	22_0— 377°_1	
6666.75	2*b*		14995.67			
6669.22	2		14990.12			
6671.59	1		14984.80			
6674.12	1		14979.11			
6675.97	15		14974.96	−0.08	$^3P_2$— 342°_3	
6677.17	15		14972.27	−0.09	19_4— 342°_3	
6678.42	80		14969.47	−0.08	18_3— 339°_2	
6679.28	2		14967.54	−0.16	29479_4— 444°_3	
6679.79	1		14966.40			
6682.60	12		14960.10	−0.05	20_2— 359°_3	
6682.90	1		14959.44	+0.05	32_1— 473°_2	
6693.08	30		14936.68	+0.01	14_2— 299°_3	
6696.32	3		14929.45	+0.01	29_7— 443°_6	
6701.81	4		14917.22	−0.14	24_2— 397°_2	
6705.68	4		14908.62			
6708.17	2		14903.08	+0.07	27_1— 425°_1	
6708.60	2		14902.13			
6709.24	4		14900.70	−0.12	23_1— 383°_1	
6710.57	3		14897.75			
6713.28	15		14891.74	−0.06	$^3P_1$— 281°_1	
6713.96	4		14890.23			

TABLE 3. *Observed and classified lines of* W I

Wavelength Å	Intensity		Wavenumber (cm^{-1})		Classification	Zeeman effect
	Arc	Spark	Observed	o−c		
6718.59	5		14879.97	−0.09	28347_3 − 432°_2	
6719.89	8		14877.09	−0.06	32_1 − 472°_1	
6725.18	15		14865.39	−0.05	19_4 − 341°_4	
6726.42	4		14862.64			
6729.15	4		14856.61	−0.09	404°_5 − 55_4	
6733.04	14		14848.04	0.00	362°_5 − e^5D_4	
6734.00	1		14845.92	+0.01	34_4 − 491°_4	
6740.08	12 *b*		14832.53	+0.05	22476_4 − 373°_5	
6744.36	1		14823.12			
6745.47	7		14820.67			
6746.56	15		14818.28	−0.08	23_3 − 387°_4	
6750.19	1		14810.31			
6752.67	1		14804.87	−0.05	19_3 − 346°_4	
6754.60	10		14800.64	−0.02	28_5 − 430°_5	
6755.75	4		14798.13			
6756.38	2		14796.75			
6756.78	1		14795.86	−0.04	32_4 − 469°_4	
6757.84	5 *b*		14793.54	+0.15	357°_2 − 50_2	
6764.45	15		14779.09	−0.03	27_1 − 424°_2	
6766.04	1		14775.62			
6767.78	8		14771.81	−0.03	34_4 − 490°_5	
6770.04	8		14766.88			
6778.33	10		14748.82	−0.12	20_2 − 357°_2	
6782.78	2 *b*		14739.15			
6787.69	1		14728.49			
6792.42	4		14718.23	−0.11	23_6 − 382°_6	
6792.98	10		14717.02	−0.10	31_5 − 461°_6	
				+0.12	374°_2 − 52_2	
6793.64	3		14715.58	−0.13	361°_1 − 50906_1	
6795.56	2		14711.44			
6796.34	6		14709.74			
6799.30	12		14703.34	−0.07	$^3H_5$ − $^7D^\circ_5$	
6804.08	10		14693.01	−0.09	29853_4 − 445°_5	
6805.31	25		14690.36	−0.14	$^3P_2$ − 339°_2	
6808.78	1		14682.87	+0.05	27_5 − 425°_4	
6811.38	12		14677.26	−0.04	28_5 − 429°_4	
6812.58	1		14674.69			
6814.92	20		14669.64	−0.04	22476_4 − 371°_4	
6816.24	12		14666.80			
6817.70	1		14663.66			
6819.89	4		14658.96			
6820.27	20		14658.13	−0.05	19_3 − 344°_2	
				+0.01	27_4 − 418°_4	
6825.92	1		14646.00			
6826.49	4		14644.78	−0.04	30_2 − 450°_2	
6828.43	20		14640.61	−0.06	318°_2 − e^5D_1	
6829.75	1		14637.78	−0.01	26_2 − 414°_3	
6832.19	8		14632.56	0.00	28_5 − 428°_5	
6838.63	8		14618.78	−0.08	28291_3 − 429°_4	
6840.08	8		14615.68	−0.05	28898_2 − 435°_2	

TABLE 3. *Observed and classified lines of* W I

Wavelength Å	Intensity		Wavenumber (cm^{-1})		Classification	Zeeman effect
	Arc	Spark	Observed	o−c		
6844.88	10		14605.43	−0.07	333°_5 — $^7D_4$	
6846.90	1		14601.12			
6847.25	12		14600.38	−0.06	27_5 — 424°_4	
6851.25	2		14591.85	+0.03	27_1 — 422°_1	
6852.84	2		14588.47			
6853.74	30		14586.54	−0.13	19535_5 — 341°_4	
6857.00	1 *b*		14579.61	−0.01	28898_2 — 434°_3	
6861.16	1		14570.77			
6862.07	5		14568.84			
6864.81	15		14563.03	−0.11	28347_3 — 429°_4	
6866.65	2		14559.12	+0.08	33_5 — 478°_5	
6871.13	1		14549.63			
6874.84	10		14541.78	+0.10	306°_1 — e^5D_0	
				+0.10	29479_4 — 440°_3	
6875.16	3		14541.10	−0.10	$^3G_3$ — $^7P^\circ_4$	
6876.01	20		14539.30	+0.04	351°_4 — e^5D_3	
6876.73	2		14537.78			
6877.23	1		14536.73	−0.11	17_3 — 322°_3	
6877.59	15		14535.97	+0.02	374°_2—52002_3	
6882.15	5		14526.33	−0.07	19_3 — 343°_3	
6887.03	5		14516.04	−0.09	20_2 — 354°_3	
6887.81	10		14514.40	−0.12	$^3H_4$ — $^7F^\circ_5$	
6891.43	4		14506.77			
6891.80	8		14506.00	−0.09	29479_4 — 439°_4	
6893.20	2		14503.05			
6900.54	12		14487.62			
6903.80	2 *b*		14480.78			
6904.20	3		14479.94	−0.08	31_5 — 458°_4	
6904.88	3		14478.52			
6906.73	3		14474.64			
6907.46	5		14473.11	−0.19	28_6 — 428°_5	
6908.29	20		14471.37	−0.03	$^3P_1$ — 277°_1	
6915.52	10		14456.24	−0.12	22852_4 — 373°_5	
6917.19	10		14452.75	−0.09	15_3 — 299°_3	
6920.97	20		14444.86	−0.07	29479_4 — 439°_5	
6926.65	1 *b*		14433.01			
6929.02	1 *b*		14428.08	+0.03	32_1 — 468°_2	
6934.23	30		14417.23	+0.01	14_2 — 293°_2	
6942.10	3		14400.89	−0.03	19_3 — 342°_3	
6942.56	3		14399.94	−0.12	31_5 — 457°_5	
6943.08	3 *b*		14398.86			
6943.68	12		14397.61	−0.07	22476_4 — 368°_3	
				+0.08	33_5 — 476°_4	
6944.00	3		14396.95	−0.04	28204_2 — 426°_3	
6952.55	2		14379.24			
6955.59	15		14372.96	−0.08	23_2 — 383°_1	
6956.32	1		14371.45	−0.07	29479_4 — 438°_3	
6956.84	10		14370.38	−0.05	32_4 — 465°_5	
6957.39	2		14369.24	−0.05	28204_2 — 425°_1	
6958.77	8		14366.39			

TABLE 3. *Observed and classified lines of* W I

Wavelength Å	Intensity		Wavenumber (cm^{-1})		Classification	Zeeman effect
	Arc	Spark	Observed	o−c		
6964.12	25		14355.36	−0.06	$^3P_1$ − 276°_2	
6964.96	4		14353.63			
6969.43	6		14344.42	−0.06	353°_2 − e^5D_3	
6971.64	15		14339.87			
6974.11	3		14334.79	−0.07	361°_1 − 50_2	
6974.89	4		14333.19	−0.01	305°_3 − $^7D_2$	
6977.29	5		14328.26	−0.28	20_2 − 353°_2	
6977.84	2		14327.13			
6978.47	3		14325.84	−0.06	17_4 − 314°_4	
6981.88	6		14318.84	−0.10	23_1 − 377°_1	
6984.27	40		14313.94	−0.02	$^3G_3$ − 276°_2	
6985.80	1		14310.80			
6989.27	15		14303.70	−0.03	18_1 − 323°_0	
6991.50	12		14299.14	−0.04	28_5 − 425°_4	
6991.84	1		14298.44			
6992.96	10		14296.15			
6993.27	30		14295.52	−0.12	19826_5 − 341°_4	
6993.65	4		14294.74	−0.02	27_1 − 419°_0	
6994.06	15		14293.90	−0.10	19_3 − 341°_4	
7001.56	2		14278.59			
7002.70	10		14276.26	−0.04	23_3 − 382°_3	
7009.68	8		14262.05	0.00	29479_4 − 437°_5	
7011.40	6		14258.55	−0.05	322°_3 − $^7D_3$	
7013.38	1		14254.53			
7014.52	3 *b*		14252.21			
7015.76	8		14249.70	−0.06	33_5 − 475°_6	
7016.22	8		14248.76	−0.02	368°_3 − e^5D_4	
7017.88	20		14245.39	−0.01	28204_2 − 424°_2	
7020.26	8		14240.56	−0.03	24_2 − 390°_2	
7027.89	5		14225.10			
7028.68	12		14223.50	−0.08	23_2 − 382°_3	
7030.50	10		14219.82	+0.16	14_2 − 291°_2	
7031.56	2		14217.67			
7031.99	3		14216.80	0.00	28_5 − 424°_4	
7032.38	4		14216.02			
7033.14	2		14214.48			
7033.32	3		14214.11			
7034.80	3		14211.12			
7043.94	4 *b*		14192.68			
7056.16	12		14168.11	−0.13	20_0 − 343°_1	
7056.59	3		14167.25	−0.09	29853_4 − 440°_3	
7058.73	10		14162.95	+0.01	14_2 − 291°_3	
				+0.07	377°_1 − 51_2	
7060.86	5		14158.68			
7061.04	10		14158.32	−0.04	28291_3 − 424°_4	
7061.36	12		14157.68	−0.04	28291_3 − 424°_2	
7061.76	2		14156.87	−0.02	354°_3 − e^5D_3	
7066.88	2 *b*		14146.62			
7067.49	2 *b*		14145.40			
7070.44	5		14139.49	−0.06	$^3G_3$ − $^7P^\circ_3$	

TABLE 3. *Observed and classified lines of* W I

Wavelength Å	Intensity		Wavenumber (cm^{-1})		Classification	Zeeman effect
	Arc	Spark	Observed	o−c		
7070.70	2		14138.98			
7071.45	3		14137.48	−0.08	24_3— 387°_4	
7071.81	2*b*		14136.75			
7073.78	1		14132.81			
7074.30	4		14131.78	+0.03	29853_4— 439°_4	
7075.01	2*b*		14130.36	+0.21	380°_3—52183_2	
7075.85	1		14128.68			
7076.75	2		14126.88			
7078.74	2		14122.91	−0.06	23_3— 380°_3	
7079.61	1		14121.18	0.00	18_2— 322°_3	
7081.21	1		14117.99			
7082.03	8*b*		14116.35	−0.03	19_3— 339°_2	
				−0.10	17_3— 318°_2	
7083.32	6		14113.78	−0.02	19_4— 333°_5	
7083.81	1		14112.80			
7088.99	1		14102.49	−0.15	28347_3— 424°_4	
7089.29	10		14101.90	−0.10	28347_3— 424°_2	
7091.96	1		14096.59			
7092.21	1		14096.09			
7100.52	2		14079.59			
7104.48	1		14071.75	+0.01	323°_0— e^5D_1	
7104.86	3		14070.99	−0.05	23_3— 380°_4	
7105.26	4		14070.20	−0.05	23_2— 380°_3	
7108.57	8		14063.65	0.00	27_1— 417°_2	
7109.16	1		14062.48	−0.09	31_5— 454°_5	
7109.34	6		14062.13	−0.06	26_2— 409°_3	
7111.18	10		14058.49	−0.09	293°_2— $^7D_1$	
7116.85	6		14047.29	−0.02	28204_2— 422°_3	
7118.19	2*b*		14044.64			
7127.05	10		14027.18	−0.06	$^3H_4$— $^7D^\circ_3$	
7128.71	2		14023.92			
7129.64	5		14022.09	−0.05	27_5— 418°_4	
7132.89	1		14015.70			
7133.23	3		14015.03			
7134.34	1		14012.85			
7137.50	8		14006.65	−0.11	26_2— 408°_2	
7138.04	3		14005.58	−0.04	28_5— 422°_6	
7140.52	40		14000.72	−0.07	13_2— 277°_1	
7142.40	2*b*		13997.04	−0.14	29853_4— 438°_3	
7147.00	3*b*		13988.03			
7148.92	10		13984.27	−0.05	27_4— 411°_4	
7149.55	8		13983.04	−0.03	18_3— 329°_3	
7150.90	1*b*		13980.40			
7151.20	1		13979.81			
7151.46	1		13979.30	+0.04	30_2— 443°_1	
7152.80	1		13976.69	−0.09	371°_4— e^5D_4	
				−0.13	382°_3—52183_2	
7155.30	1		13971.80			
7155.84	1		13970.75			
7156.36	1		13969.73			

TABLE 3. *Observed and classified lines of* W I

Wavelength Å	Intensity		Wavenumber (cm^{-1})		Classification	Zeeman effect
	Arc	Spark	Observed	o−c		
7161.59	5		13959.53	−0.10	28291_3— 422°_3	
7162.64	50		13957.49	−0.05	$^5S_2$— 322°_3	
7163.53	3		13955.75			
7166.90	10		13949.19	−0.16	32_1— 463°_2	
7173.38	5 *b*		13936.59			
7176.49	4		13930.55			
7179.85	10		13924.03	−0.05	357°_2— e^5D_3	
7183.83	4		13916.32			
7184.29	5		13915.42			
7184.77	12		13914.50	−0.10	20_1— 343°_1	
7185.70	2 *h*		13912.70	−0.02	27_1— 415°_2	
7187.56	6		13909.10	−0.04	26_2— 407°_1	
7191.33	20		13901.80	+0.06	313°_1— e^5D_0	
7195.68	4		13893.40			
7198.62	20		13887.72	−0.10	$^3P_2$— 331°_2	
				+0.01	29853_4— 437°_5	
7200.16	40		13884.75	−0.06	13_2— 276°_2	
7202.94	1		13879.40			
7204.36	1		13876.66			
7206.02	4		13873.46	−0.01	31_5— 452°_4	
7216.35	20		13853.60	−0.01	18_3— 328°_4	
7218.22	6 *b*		13850.01			
7219.18	2		13848.17			
7220.18	8		13846.26	−0.10	28_6— 422°_6	
7226.06	20		13834.99	−0.04	19535_5— 333°_5	
7230.38	1		13826.72			
7231.66	6		13824.27	−0.11	23_6— 373°_5	
7237.12	30		13813.84	−0.14	373°_5— e^5D_4	
7240.57	1		13807.26			
7242.20	4		13804.15	−0.06	26_2— 406°_3	
7245.21	12		13798.42	0.00	22476_4— 362°_5	
7245.88	1		13797.14			
7249.04	1		13791.13	−0.03	23_2— 377°_1	
7256.40	2		13777.14			
7259.30	4		13771.64	−0.04	29479_4— 432°_4	
7267.91	5 *b*		13755.33			
7269.97	4 *b*		13751.42			
7273.94	8		13743.92	−0.08	23_3— 376°_3	
7274.47	30		13742.92	+0.07	382°_4—52002_3	
7278.24	100		13735.80	−0.03	15_3— 291°_2	
				−0.08	343°_1— e^5D_2	
7279.68	1		13733.08	−0.08	32_4— 458°_4	
7280.44	10		13731.65	−0.08	17_3— 314°_4	
7282.70	10 *b*		13727.39	+0.08	$^3H_5$— $^7D^\circ_4$	
7282.98	10 *b*		13726.86			
7285.81	60		13721.53	+0.03	19_6— 333°_5	
7288.48	1		13716.50			
7291.74	8 *b*		13710.37	−0.03	13_2— $^7P^\circ_3$	
7291.97	6 *b*		13709.94	−0.07	27_4— 409°_3	
7295.16	8		13703.94	−0.08	$^3P_2$— 329°_3	

TABLE 3. *Observed and classified lines of* W I

Wavelength Å	Intensity		Wavenumber (cm^{-1})		Classification	Zeeman effect
	Arc	Spark	Observed	o−c		
7296.11	5		13702.16	−0.07	28898_2 − 426°_3	
7296.55	80		13701.33	−0.01	19_4 − 329°_3	
7296.87	15		13700.73	−0.06	18_2 − 318°_2	
7298.25	18		13698.14	−0.02	27_4 − 409°_5	
7301.89	1		13691.31	+0.03	23_2 − 376°_3	
7308.43	3		13679.05	−0.06	15_3 − 291°_3	
7309.14	1		13677.74			
7310.27	3		13675.62			
7310.91	3		13674.42	−0.11	28898_2 − 425°_1	
7313.00	4		13670.51			
7318.95	1		13659.40			
7322.29	3		13653.17	−0.03	32_4 − 457°_5	
7324.79	2		13648.50	−0.02	24_3 − 382°_4	
7325.68	1		13646.85	+0.05	30_2 − 440°_3	
7334.93	1		13629.64			
7337.49	3		13624.89	−0.03	29853_4 − 434°_3	
7340.42	2		13619.45			
7344.49	2*b*		13611.90			
7347.91	12		13605.56	−0.06	22476_4 − 360°_4	
7351.35	3		13599.20			
7355.00	8		13592.45	−0.01	344°_2 − e^5D_2	
7361.69	6		13580.10	+0.04	28291_3 − 418°_4	
7363.73	1		13576.34			
7365.16	8		13573.70	−0.04	360°_4 − e^5D_3	
7366.32	2*b*		13571.56			
7368.48	10		13567.58	−0.14	27_5 − 414°_6	
7372.90	1		13559.45			
7377.25	2		13551.45	−0.04	31_5 − 449°_4	
7381.31	15		13544.00	0.00	19826_5 − 333°_5	
7384.12	8*b*		13538.84	−0.20	329°_3 − $^7D_3$	
7385.08	60		13537.08	−0.07	$^5S_2$ − 318°_2	
7385.62	4		13536.10	−0.12	23_3 − 374°_2	
7386.35	1		13534.76	−0.06	31_5 − 449°_6	
7386.56	2		13534.38			
7389.02	6		13529.87	−0.06	28204_2 − 417°_2	
7390.12	1		13527.85			
7392.05	3		13524.32	−0.02	28347_3 − 418°_4	
7410.82	2		13490.06	−0.08	28204_2 − 416°_3	
7416.29	1		13480.11			
7416.64	1		13479.47	−0.16	17_4 − 305°_3	
7429.10	5		13456.87	−0.03	27_1 − 411°_0	
7431.78	2		13452.02	−0.01	27_4 − 406°_3	
7433.40	3		13449.09	−0.05	23_1 − 369°_2	
				+0.03	376°_3 − e^5D_4	
7437.19	8		13442.23	+0.06	24_3 − 380°_3	
				−0.02	28291_3 − 417°_2	
7439.45	8		13438.15			
7448.21	6*b*		13422.35	+0.05	22852_4 − 362°_5	
7451.39	15		13416.62	−0.09	22_0 − 361°_1	
				−0.10	24_2 − 382°_3	

TABLE 3. *Observed and classified lines of* W I

Wavelength Å	Intensity		Wavenumber (cm^{-1})		Classification	Zeeman effect
	Arc	Spark	Observed	o−c		
7452.08	2 *b*		13415.38	0.00	$32\,{}^{\circ}_{4}$ — $455\,{}^{\circ}_{3}$	
7456.37	10		13407.66	−0.05	$26\,{}^{\circ}_{2}$ — $402\,{}^{\circ}_{3}$	
7459.27	12		13402.45	−0.01	$28291\,{}^{\circ}_{3}$ — $416\,{}^{\circ}_{3}$	
7462.19	4		13397.20	−0.14	$29853\,{}^{\circ}_{4}$ — $432\,{}^{\circ}_{4}$	
7466.11	5		13390.17	−0.07	$24\,{}^{\circ}_{3}$ — $380\,{}^{\circ}_{4}$	
7467.74	2		13387.25	−0.04	$34\,{}^{\circ}_{4}$ — $476\,{}^{\circ}_{4}$	
7468.22	8		13386.39	−0.14	$28347\,{}^{\circ}_{3}$ — $417\,{}^{\circ}_{2}$	
7470.41	7		13382.46	+0.06	$32\,{}^{\circ}_{1}$ — $457\,{}^{\circ}_{1}$	
7471.56	15		13380.40	−0.02	$33\,{}^{\circ}_{5}$ — $466\,{}^{\circ}_{6}$	
7473.90	1		13376.21			
7483.35	30		13359.32	−0.10	$20\,{}^{\circ}_{2}$ — $343\,{}^{\circ}_{1}$	
7489.50	4		13348.35	+0.01	$27\,{}^{\circ}_{5}$ — $411\,{}^{\circ}_{4}$	
7493.08	3		13341.98	−0.05	$^{3}G\,{}^{\circ}_{4}$ — $^{7}D\,{}^{\circ}_{5}$	
7497.96	2		13333.30	+0.05	$33\,{}^{\circ}_{5}$ — $466\,{}^{\circ}_{4}$	
7504.13	40		13322.33	−0.03	$^{3}P\,{}^{\circ}_{1}$ — $266\,{}^{\circ}_{0}$	
7504.59	2		13321.51	−0.13	$27\,{}^{\circ}_{5}$ — $411\,{}^{\circ}_{6}$	
7507.21	1		13316.86	−0.06	$331\,{}^{\circ}_{2}$ — $e^{5}D\,{}_{1}$	
7507.88	6		13315.68	−0.03	$32\,{}^{\circ}_{4}$ — $454\,{}^{\circ}_{5}$	
7509.00	40		13313.68	−0.02	$19\,{}^{\circ}_{3}$ — $331\,{}^{\circ}_{2}$	
7515.08	1		13302.91			
7520.66	20		13293.05	−0.06	$19535\,{}^{\circ}_{5}$ — $328\,{}^{\circ}_{4}$	
7521.59	6		13291.40	+0.08	$28291\,{}^{\circ}_{3}$ — $415\,{}^{\circ}_{2}$	
				0.00	$34\,{}^{\circ}_{4}$ — $475\,{}^{\circ}_{3}$	
7525.54	1		13284.42			
7532.38	1		13272.36	−0.02	$360\,{}^{\circ}_{4}$ — $^{7}D\,{}_{5}$	
7537.45	50		13263.44	−0.07	$18\,{}^{\circ}_{3}$ — $322\,{}^{\circ}_{3}$	
				+0.05	$24\,{}^{\circ}_{2}$ — $380\,{}^{\circ}_{3}$	
7537.95	10		13262.56	−0.04	$27\,{}^{\circ}_{4}$ — $404\,{}^{\circ}_{5}$	
7542.89	4 *b*		13253.87			
7543.46	1 *b*		13252.86			
7550.48	40		13240.54	−0.11	$18\,{}^{\circ}_{1}$ — $313\,{}^{\circ}_{1}$	
7556.57	1		13229.87			
7561.68	3		13220.94			
7563.00	2		13218.62	−0.06	$23\,{}^{\circ}_{1}$ — $366\,{}^{\circ}_{2}$	
7564.38	4		13216.21	−0.07	$23\,{}^{\circ}_{3}$ — $371\,{}^{\circ}_{4}$	
7569.36	2		13207.52	−0.03	$28291\,{}^{\circ}_{3}$ — $414\,{}^{\circ}_{3}$	
7569.92	80		13206.54	−0.10	$18\,{}^{\circ}_{2}$ — $313\,{}^{\circ}_{1}$	
7574.84	2		13197.96	+0.04	$27\,{}^{\circ}_{1}$ — $408\,{}^{\circ}_{2}$	
7576.81	1		13194.53			
7581.93	1		13185.62			
7582.17	1		13185.20			
7582.88	50		13183.97	−0.11	$28\,{}^{\circ}_{5}$ — $414\,{}^{\circ}_{6}$	
7590.55	1		13170.65			
7595.37	2		13162.29			
7598.06	1		13157.63	−0.05	$31\,{}^{\circ}_{5}$ — $445\,{}^{\circ}_{5}$	
7600.78	10 *b*		13152.92	−0.03	$390\,{}^{\circ}_{2}$ — $52183\,{}_{2}$	
7601.48	15		13151.71	−0.12	$28347\,{}^{\circ}_{3}$ — $414\,{}^{\circ}_{3}$	
7606.85	1		13142.43			
7607.97	3		13140.49	+0.01	$30\,{}^{\circ}_{2}$ — $435\,{}^{\circ}_{2}$	
7612.18	50		13133.22	−0.08	$23\,{}^{\circ}_{1}$ — $365\,{}^{\circ}_{0}$	

TABLE 3. *Observed and classified lines of* W I

Wavelength Å	Intensity		Wavenumber (cm^{-1})		Classification	Zeeman effect
	Arc	Spark	Observed	o−c		
7614.15	150		13129.83	−0.07	19_3 — 329°_3	
7626.06	2		13109.32			
7627.94	3 *b*		13106.09			
7628.90	8		13104.44	+0.06	30_2 — 434°_3	
7630.24	10		13102.14	−0.07	318°_2 — $^7D_2$	
7631.29	40		13100.34	+0.04	27_1 — 407°_1	
7631.88	3		13099.32			
7637.57	2		13089.57			
7637.91	2		13088.98			
7641.04	3		13083.62			
7642.34	3		13081.40	−0.21	422°_3 — 55_4	
7643.41	20		13079.56	−0.02	362°_5 — $^7D_5$	
7644.09	3 *b*		13078.40			
7653.63	30		13062.10	−0.08	27_5 — 409°_5	
7654.81	80		13060.09	−0.09	$^3P_1$ — 263°_2	
7656.48	2		13057.23	+0.15	29853_4 — 429°_4	
7657.48	10		13055.54	+0.01	27_4 — 402°_3	
7657.94	1		13054.75			
7658.80	4		13053.28	−0.02	29479_4 — 425°_4	
7664.88	200		13042.93	−0.07	$^5S_2$ — 313°_1	
7666.95	2		13039.41			
7669.72	1		13034.70	−0.12	29479_4 — 425°_3	
7672.29	15		13030.33	−0.06	22476_4 — 355°_5	
7675.61	20		13024.70	−0.12	28_6 — 414°_6	
7676.98	6		13022.38	−0.09	22476_4 — 354°_3	
7678.57	6		13019.68			
7679.18	40		13018.64	−0.08	$^3G_3$ — 263°_2	
7680.12	1		13017.05			
7681.30	4		13015.05			
7688.97	80		13002.06	−0.02	19826_5 — 328°_4	
7689.97	25		13000.37	−0.07	19_3 — 328°_4	
7692.80	6		12995.59	−0.01	32_1 — 453°_1	
7693.90	4		12993.73			
7694.36	3		12992.96	−0.11	409°_3 — 53_3	
7696.04	2		12990.12			
7698.00	10		12986.81			
7699.48	20		12984.32	+0.02	24_2 — 377°_1	
7701.01	40		12981.74	−0.04	19_4 — 322°_3	
7701.54	1		12980.84	+0.01	32_4 — 451°_4	
7702.63	2 *b*		12979.01			
7704.00	1 *b*		12976.70			
7705.58	6		12974.04	−0.04	23_3 — 369°_2	
7706.80	5 *b*		12971.98	−0.02	390°_2—52183_2	
7711.08	1		12964.78			
7721.49	2 *b*		12947.30			
7722.06	12		12946.35			
7723.34	12		12944.20	−0.08	23_3 — 368°_3	
7726.81	4		12938.39			
7727.07	20		12937.96	−0.04	28_5 — 411°_6	
7729.36	2		12934.12			

318-092 O-69—13

TABLE 3. *Observed and classified lines of* W I

Wavelength Å	Intensity		Wavenumber (cm^{-1})		Classification	Zeeman effect
	Arc	Spark	Observed	o−c		
7732.06	4		12929.61	−0.01	383°_1 — 51_0	
7736.29	8		12922.54	−0.13	$^3P_1$ — $^7P^\circ_2$	
7746.08	20		12906.20	−0.06	28291_3 — 411°_4	
7747.07	3		12904.56			
7749.65	6		12900.26	−0.06	28204_2 — 411°_2	
7754.92	6		12891.49	−0.07	23_2 — 368°_3	
7758.58	20		12885.41	−0.05	17_3 — 305°_3	
7761.16	40		12881.13	−0.08	$^3G_3$ — $^7P^\circ_2$	
7761.61	1		12880.38			
7771.65	6		12863.74	0.00	382°_4 — e^5D_4	
7772.52	8		12862.30	−0.06	28_1 — 415°_2	
7774.68	10		12858.73	−0.03	351°_4 — $^7D_4$	
7776.73	30		12855.34	−0.08	24_3 — 374°_2	
7777.81	6		12853.55	+0.09	30_2 — 432°_2	
7779.71	5		12850.41	−0.13	28347_3 — 411°_4	
7782.77	12		12845.36	−0.02	26_2 — 397°_2	
7784.15	100		12843.08	−0.04	18_3 — 318°_2	
7785.65	3		12840.61	−0.03	$^3G_3$ — $^7D^\circ_3$	
7790.13	5		12833.23			
7793.33	4		12827.96			
7797.57	5		12820.98			
7798.39	6		12819.63	−0.12	$^3H_5$ — $^7P^\circ_4$	
7799.64	1		12817.58			
7801.60	8		12814.36	−0.04	33_5 — 461°_6	
7802.65	2		12812.63	−0.01	28291_3 — 411°_2	
7805.87	2		12807.35			
7806.81	8		12805.81	−0.03	17_4 — 299°_3	
7808.96	60		12802.28	−0.04	14_2 — 277°_1	
7812.44	7		12796.58			
7819.14	1		12785.61			
7819.67	7		12784.75	−0.02	26_2 — 396°_3	
7820.28	2		12783.75			
7823.82	40		12777.96	−0.12	29_7 — 422°_6	
7825.64	3		12774.99	+0.01	26_2 — 396°_1	
7826.86	3		12773.00			
7827.42	15		12772.09	−0.10	29479_4 — 422°_3	
7835.82	12		12758.40			
7836.78	5		12756.83	−0.09	28347_3 — 411°_2	
7838.84	4		12753.48	−0.16	391°_1 — 51_2	
7839.50	12		12752.41			
7844.95	7		12743.55	−0.07	23_3 — 366°_2	
7846.33	5*b*		12741.31			
7849.93	2		12735.46	−0.01	23_1 — 361°_1	
7863.47	60		12713.54	0.00	20_1 — 331°_2	
7867.04	50		12707.77	−0.04	$^3G_4$ — 291°_3	
7877.51	15		12690.88	−0.02	23_2 — 366°_2	
7878.48	5		12689.31			
7880.40	70		12686.22	−0.12	14_2 — 276°_2	
7883.16	10		12681.78	−0.04	322°_3 — $^7D_2$	
7884.96	7		12678.88	−0.08	29853_4 — 425°_4	

TABLE 3. *Observed and classified lines of* W I

Wavelength Å	Intensity		Wavenumber (cm^{-1})		Classification	Zeeman effect
	Arc	Spark	Observed	o−c		
7885.25	6		12678.42	−0.12	28_5 — 409°_5	
7886.48	80		12676.44	−0.06	$^3P_1$ — 259°_1	
7892.81	5		12666.28	−0.05	17_4 — $^7D^\circ_5$	
7894.08	2		12664.24	+0.04	28204_2 — 408°_2	
7894.61	2		12663.39			
7896.48	6		12660.39	−0.09	29853_4 — 425°_3	
7901.83	3*b*		12651.82			
7905.30	40		12646.26	−0.09	22852_4 — 354°_3	
7906.37	1		12644.55			
7909.21	40		12640.01	−0.09	22476_4 — 351°_4	
7912.64	8		12634.53	−0.03	$^3H_6$ — $^7F^\circ_6$	
7914.31	15		12631.87	−0.08	28291_3 — 409°_3	
7917.64	5		12626.55	−0.07	27_5 — 404°_5	
7918.27	2		12625.55			
7934.00	6		12600.52	+0.05	28898_2 — 414°_3	
7940.92	120		12589.54	−0.03	13_2 — 263°_2	
7947.45	7		12579.19	+0.02	354°_3 — e^5D_2	
7948.12	3*b*		12578.13			
7949.17	5		12576.47	−0.05	28291_3 — 408°_2	
7953.03	2		12570.36			
7955.41	25		12566.61	+0.03	28204_2 — 407°_1	
7957.06	40		12564.00	−0.07	$^3P_2$ — 318°_2	
7965.76	5		12550.28	−0.08	383°_1 — 50906_1	
7967.14	20		12548.10			
7968.15	2		12546.51	−0.07	396°_1 — 52183_2	
7975.38	10		12535.14	−0.03	31_5 — 439°_5	
7977.18	2		12532.31			
7979.54	1		12528.60			
7981.08	1		12526.19			
7985.51	12		12519.24	−0.04	28_6 — 409°_5	
7985.91	2		12518.61			
7988.72	10		12514.21	−0.03	339°_2 — e^5D_1	
7990.20	4		12511.89	−0.04	14_2 — $^7P^\circ_3$	
7991.62	25		12509.67	−0.01	371°_4 — e^5D_3	
7992.89	2		12507.68			
7993.87	4		12506.15	+0.01	27_4 — 397°_4	
7998.74	2		12498.53			
8017.19	120		12469.77	−0.03	18_2 — 305°_3	
8022.40	20		12461.67	+0.02	28204_2 — 406°_3	
8024.52	6		12458.38	−0.02	18_3 — 314°_4	
8028.62	1		12452.02	−0.04	13_2 — $^7P^\circ_2$	
8037.22	1		12438.69			
8039.04	1		12435.88			
8043.11	1		12429.58	−0.09	15_3 — $^7P^\circ_4$	
8054.89	30		12411.41	−0.08	13_2 — $^7D^\circ_3$	
8055.64	120		12410.25	−0.09	19_3 — 322°_3	
8057.13	10		12407.96			
8058.15	20		12406.38	−0.12	28_1 — 411°_0	
8060.38	60		12402.95	−0.11	$^5S_2$ — 306°_1	
8061.78	2*b*		12400.80			

TABLE 3. *Observed and classified lines of* W I

Wavelength Å	Intensity		Wavenumber (cm^{-1})		Classification	Zeeman effect
	Arc	Spark	Observed	o−c		
8064.83	5		12396.11			
8072.09	1		12384.96			
8076.41	2		12378.34			
8078.58	2 *b*		12375.01	+0.07	341°_{4} — $^{7}D_{3}$	
8079.26	5		12373.97	0.00	28291_{3} — 406°_{3}	
8084.54	12		12365.89	−0.04	$^{3}G_{4}$ — $^{7}D^{\circ}_{4}$	
8091.14	30		12355.80	−0.04	396°_{3}–52002_{3}	
8093.44	15		12352.29	0.00	31_{5} — 437°_{5}	
8100.80	1		12341.07	+0.05	27_{1} — 400°_{2}	
8101.05	1		12340.69			
8106.88	5		12331.81	+0.02	31_{5} — 437°_{4}	
8111.86	3		12324.24			
8112.70	10		12322.96	−0.05	34_{4} — 466°_{4}	
8115.85	8		12318.18	−0.07	28347_{3} — 406°_{3}	
8122.63	1		12307.90			
8123.82	150		12306.10	−0.06	$^{5}S_{2}$ — 305°_{3}	
8125.08	1		12304.19			
8125.47	10		12303.60			
8127.78	5		12300.10	−0.12	396°_{1}–51936_{2}	
8128.76	4		12298.62			
8132.35	15		12293.19	−0.09	24_{3} — 369°_{2}	
8136.26	2 *b*		12287.28			
8136.98	1		12286.20	+0.06	445°_{5} — 56_{6}	
8137.38	8		12285.59			
8137.96	1		12284.72			
8139.57	30		12282.28	−0.01	397°_{4}–52002_{3}	
8143.19	60		12276.82	−0.12	23_{1} — 357°_{2}	
8145.58	1		12273.22	−0.04	400°_{2}–52284_{3}	
8146.35	1		12272.06			
8149.33	1		12267.58			
8150.86	1		12265.27			
8151.80	1		12263.86			
8160.80	5		12250.33			
8161.04	1		12249.97			
8161.44	5		12249.37			
8165.72	30		12242.95	−0.03	28_{5} — 404°_{5}	
8175.02	1		12229.02			
8180.26	1		12221.19			
8181.34	1		12219.58			
8186.69	12		12211.59	−0.08	17_{3} — 299°_{3}	
8188.61	1		12208.73			
8189.36	15		12207.61	−0.08	23_{2} — 361°_{1}	
8190.74	2		12205.55			
8192.80	3		12202.48	−0.03	15_{3} — 276°_{2}	
8210.22	50		12176.60	−0.07	19_{4} — 314°_{4}	
8215.08	1		12169.39			
8215.52	5		12168.74	+0.13	26861_{2}–39030°_{2}	
8222.52	1		12158.38	+0.02	20_{2} — 331°_{2}	
8226.73	1		12152.16	−0.06	23_{3} — 360°_{4}	
8229.81	4		12147.61	+0.09	28_{1} — 408°_{2}	

TABLE 3. *Observed and classified lines of* W I

Wavelength Å	Intensity		Wavenumber (cm^{-1})		Classification	Zeeman effect
	Arc	Spark	Observed	o−c		
8230.25	1		12146.96			
8234.99	8		12139.97	+0.03	30_2— 425°_3	
8242.81	3 *b*		12128.45	−0.05	313°_1— $^7D_1$	
8248.90	3 *b*		12119.50			
8251.89	1		12115.11			
8252.38	8		12114.39	−0.05	24_2— 369°_2	
8260.68	12		12102.22	+0.06	418°_4— 53_5	
8263.42	2 *b*		12098.20			
8265.50	15		12095.16			
8268.09	1		12091.37			
8269.02	2		12090.01			
8270.47	1		12087.89			
8272.74	10		12084.57	−0.13	24_2— 368°_3	
8273.36	8		12083.67	−0.05	28_6— 404°_5	
8278.44	1		12076.25			
8282.85	5		12069.82	−0.10	$^3P_2$— 313°_1	
8283.20	1		12069.31			
8283.50	2		12068.88			
8286.05	10		12065.16	+0.01	28204_2— 402°_3	
8287.72	8		12062.73	−0.09	24_3— 366°_2	
8289.01	1		12060.85			
8290.44	10		12058.77			
8292.64	1		12055.57			
8294.39	1 *b*		12053.03			
8294.79	1		12052.45			
8296.02	2		12050.66	−0.13	402°_4—52284_3	
8299.56	8		12045.52	0.00	373°_5— $^7D_5$	
8301.18	1		12043.17			
8306.12	3		12036.01			
8308.83	6		12032.08	−0.03	17_4— 291°_3	
8311.63	25		12028.03	−0.07	15_3— $^7P^\circ_3$	
8312.66	1		12026.54			
8313.64	1		12025.12			
8313.80	1		12024.89	+0.02	28898_2— 409°_3	
8317.14	15		12020.06	−0.05	29479_4— 414°_3	
8322.05	50		12012.97	−0.12	23_3— 359°_3	
8329.37	1		12002.41			
8330.70	1 *h*		12000.50			
8336.00	1		11992.87			
8336.50	1		11992.14			
8338.08	120		11989.87	−0.08	19_3— 318°_2	
8339.07	4		11988.45			
8343.61	6		11981.93	−0.03	376°_3— e^5D_3	
8344.08	1		11981.25			
8346.72	5		11977.46	+0.01	28291_3— 402°_3	
8348.81	50		11974.46	−0.10	20_2— 329°_3	
8350.24	15		11972.41	−0.03	344°_2— e^5D_1	
8354.60	5		11966.17	+0.03	27_1— 396°_1	
8357.32	1		11962.27	+0.01	329°_3— $^7D_2$	
8358.72	75		11960.27	−0.10	23_2— 359°_3	

TABLE 3. *Observed and classified lines of* W I

Wavelength Å	Intensity		Wavenumber (cm^{-1})		Classification	Zeeman effect
	Arc	Spark	Observed	o−c		
8359.85	20		11958.65	−0.07	20_1— 323°_0	
8364.78	1*h*		11951.60			
8367.97	1		11947.05			
8368.27	6		11946.62			
8369.06	20		11945.49	−0.06	22_0— 347°_1	
8382.94	30		11925.71	−0.13	$^3P_0$— $^7D^\circ_1$	
8385.81	2		11921.63	−0.12	28347_3— 402°_3	
8387.87	1*h*		11918.70			
8389.46	1		11916.44			
8390.39	10		11915.12			
8398.18	1		11904.07			
8399.59	2		11902.07			
8401.08	6		11899.96			
8402.60	40		11897.81	−0.09	19535_5— 314°_4	
8403.30	1		11896.82			
8404.28	1*b*		11895.43			
8405.86	5		11893.20	−0.04	360°_4— $^7D_4$	
8409.44	8		11888.13	+0.03	30_2— 422°_1	
8417.13	40		11877.27	−0.13	22476_4— 343°_3	
				−0.04	30_2— 422°_3	
8421.01	3		11871.80	−0.02	28898_2— 407°_1	
8422.20	4		11870.12	−0.04	27_5— 397°_4	
8423.15	1		11868.78			
8428.10	1		11861.81			
8431.95	20		11856.40	−0.14	23_1— 353°_2	
8433.12	1		11854.75			
8434.88	1		11852.28			
8436.90	3		11849.44	−0.03	32_4— 439°_4	
8449.01	4		11832.46			
8466.97	1		11807.36	+0.06	28204_2— 400°_2	
8470.08	4		11803.02			
8470.53	5		11802.39			
8470.95	15		11801.81	−0.07	23_3— 357°_2	
8475.14	40		11795.97	−0.04	18_2— 299°_3	
8486.81	20		11779.75	−0.05	22852_4— 346°_4	
8495.07	15		11768.30	+0.02	402°_4—52002_3	
8495.70	8		11767.43			
8496.70	1		11766.04	+0.06	34_4— 460°_3	
8497.42	4		11765.05			
8498.00	1		11764.24	−0.01	27_5— 396°_5	
8499.51	12		11762.15	+0.02	393°_5— e^5D_4	
8506.97	30		11751.84	−0.08	22476_4— 342°_3	
8508.93	4		11749.13	−0.03	23_2— 357°_2	
8509.43	1		11748.44			
8515.40	25		11740.20			
8516.34	20		11738.91	−0.06	347°_1— e^5D_1	
8518.87	4		11735.42			
8522.08	3		11731.00			
8527.98	8		11722.89	−0.11	391°_1—50906_1	
8530.99	15		11718.75	−0.07	29479_4— 411°_4	

TABLE 3. *Observed and classified lines of* W I

Wavelength Å	Intensity		Wavenumber (cm^{-1})		Classification	Zeeman effect
	Arc	Spark	Observed	o−c		
8533.77	2		11714.93	+0.03	32_4− 438°_3	
8537.07	2		11710.40	−0.06	29_7− 411°_6	
8537.77	1		11709.44			
8542.90	3		11702.41			
8543.51	1		11701.58			
8550.37	8		11692.19	−0.03	17_3− 293°_2	
8551.86	1		11690.15	−0.08	17_4− 287°_4	
8566.61	1		11670.02			
8571.16	4		11663.83	−0.07	28347_3− 400°_2	
8571.80	1		11662.96			
8574.70	2		11659.01			
8577.69	5		11654.95	+0.03	380°_4− e^5D_3	
8577.95	2		11654.60			
8584.51	2		11645.69	−0.08	29853_4− 414°_3	
8585.11	300		11644.88	−0.12	22476_4− 341°_4	
				−0.14	31_5− 430°_5	
8587.43	1		11641.73			
8592.85	1		11634.39	+0.04	318°_2− $^7D_1$	
8593.94	3		11632.91	−0.06	449°_4−56573_5	
8594.42	120		11632.26	−0.11	$^5S_2$− 299°_3	
				+0.16	33_5− 449°_6	
8613.27	50		11606.80	−0.07	19826_5− 314°_4	
8614.50	30		11605.15	−0.08	19_3− 314°_4	
8615.02	3		11604.45	+0.03	30_2− 419°_2	
8616.12	1		11602.96	−0.03	380°_3− e^5D_3	
8619.49	2		11598.43			
8621.14	1		11596.21			
8626.00	10		11589.68			
8628.04	1		11586.94			
8640.12	1		11570.74			
8640.59	3		11570.11			
8641.42	25		11569.00	−0.07	23_3− 354°_3	
8641.75	20		11568.55	−0.11	22_0− 343°_1	
8651.92	1		11554.96			
8654.77	2		11551.15			
8660.29	1		11543.79			
8662.53	1		11540.80			
8673.93	2		11525.63	−0.09	404°_1−51936_2	
8676.93	6		11521.65	−0.01	31_5− 429°_4	
8680.98	5		11516.27	−0.08	23_2− 354°_3	
8683.59	1		11512.81	+0.09	27_1− 391°_1	
8684.86	6		11511.13	−0.08	27_5− 393°_5	
8686.40	8		11509.09	0.00	396°_5− e^5D_4	
8691.03	1 *b*		11502.96			
8692.38	5		11501.17	−0.11	22852_4− 343°_3	
8697.32	4		11494.64	−0.02	17_3− 291°_2	
8697.70	1		11494.14	−0.06	26_2− 383°_1	
8698.35	8		11493.28			
8703.45	2		11486.54	+0.08	28_5− 397°_4	
8710.77	12		11476.89	−0.03	31_5− 428°_5	

TABLE 3. *Observed and classified lines of* W I

Wavelength Å	Intensity		Wavenumber (cm⁻¹)		Classification	Zeeman effect
	Arc	Spark	Observed	o−c		
8714.98	4		11471.34			
8723.90	1		11459.62			
8731.48	1		11449.67	+0.01	382°_3 — e^5D_3	
8732.93	3		11447.77			
8737.18	1		11442.20	−0.01	28204_2 — 396°_3	
8740.47	25		11437.89	−0.05	17_3 — 291°_3	
8744.60	15		11432.49	+0.07	28204_2 — 396°_1	
8746.63	40		11429.84	−0.14	$^3P_2$ — 306°_1	
8754.76	10		11419.22	+0.04	405°_4—52002_3	
8766.00	4		11404.58	−0.04	366°_2 — e^5D_2	
8767.08	1		11403.17	−0.01	397°_4 — e^5D_4	
8772.12	1		11396.62	−0.02	382°_4 — e^5D_3	
8776.42	8		11391.04	−0.06	14_2 — 263°_2	
8777.43	12		11389.73	−0.06	20_1 — 318°_2	
8784.47	6		11380.60	−0.01	28_5 — 396°_5	
8786.31	1		11378.22			
8788.24	4		11375.72	−0.08	22852_4 — 342°_3	
8791.89	1		11370.99			
8800.39	1		11360.01			
8821.37	5		11333.00	−0.08	$^3P_2$ — 305°_3	
8823.42	7		11330.36	−0.04	19_4 — 305°_3	
8834.34	1		11316.36			
8838.86	1		11310.57	0.00	18_1 — 293°_2	
8865.53	10		11276.55	−0.01	18_2 — 293°_2	
8871.62	8		11268.80	−0.08	22852_4 — 341°_4	
8875.20	1 *b*		11264.25			
8882.52	1 *b*		11254.97			
8883.66	5		11253.53	−0.06	14_2 — 262°_2	
8909.14	1		11221.35			
8914.99	1		11213.98			
8915.83	8		11212.93	−0.09	14_2 — $^7D^\circ_3$	
8922.98	5		11203.94	−0.02	368°_3 — e^5D_2	
8936.80	5		11186.62	−0.08	23_3 — 351°_4	
8946.76	1		11174.16	0.00	369°_2 — e^5D_2	
8947.10	1		11173.74			
8966.47	3		11149.60	−0.01	34_4 — 454°_5	
8977.15	1		11136.34	+0.06	32_1 — 435°_2	
8981.39	20		11131.08			
8984.25	6		11127.54	−0.03	28_5 — 393°_5	
8989.52	2		11121.01			
8992.09	6 *b*		11117.83			
8996.08	6		11112.90	−0.11	18_1 — 291°_2	
				−0.02	$^5S_2$ — 293°_2	
9005.61	1		11101.14	−0.04	368°_3 — $^7D_4$	
9007.55	1		11098.75	+0.13	33_5 — 443°_6	
9009.73	1		11096.06	0.00	17_3 — 287°_4	
9010.34	1		11095.32	+0.04	382°_4 — $^7D_5$	
9017.84	1		11086.09			
9018.33	1		11085.48			
9023.80	1		11078.76	−0.24	18_2 — 291°_2	

TABLE 3. *Observed and classified lines of* W I

Wavelength Å	Intensity		Wavenumber (cm⁻¹)		Classification	Zeeman effect
	Arc	Spark	Observed	o−c		
9041.53	0		11057.04	+0.24	$^3G_4$— $^7P^\circ_3$	
9050.80	1		11045.72	+0.14	27_4— 382°_4	
9069.98	5		11022.36	+0.08	18_2— 291°_3	
9082.33	3		11007.37	−0.05	14_2— 259°_1	
9083.90	2		11005.47			
9090.86	2		10997.04	−0.06	29479_4— 404°_5	
9110.83	10		10972.94			
9114.72	1		10968.25	−0.06	28_6— 393°_5	
9139.70	5		10938.28	−0.06	18_3— 299°_3	
9157.89	1		10916.55			
9158.90	20		10915.35	−0.01	$^5S_2$— 291°_2	
9161.47	6		10912.28	−0.04	26_2— 377°_1	
9165.38	4		10907.63	+0.03	387°_4— e^5D_3	
9165.78	1		10907.15	−0.12	15_3— 263°_2	
9167.00	4		10905.70	+0.04	27_1— 385°_0	
9169.77	2		10902.41			
9175.52	2		10895.58	−0.06	20_1— 313°_1	
9177.39	7		10893.36	0.00	22476_4— 333°_5	
9181.75	4		10888.18	−0.09	24_3— 354°_3	
9182.46	1		10887.34			
9203.07	0		10862.96			
9203.80	3		10862.10			
9206.78	3		10858.58	−0.06	$^5S_2$— 291°_3	
9214.14	2		10849.91	−0.07	31_5— 422°_6	
9227.14	2		10834.62	+0.01	20_2— 318°_2	
9234.42	5		10826.08	+0.03	28204_2— 390°_2	
9246.28	3 *b*		10812.19	0.00	29853_4— 406°_3	
9253.21	1		10804.10			
9262.88	1		10792.82			
9265.32	2		10789.98			
9267.65	3		10787.26	−0.04	27_4— 380°_4	
9270.69	1		10783.72			
9282.81	7		10769.64	−0.12	15_3— 262°_2	
9292.09	5		10758.89	−0.07	19_3— 305°_3	
9317.84	5 *b*		10729.16	−0.03	15_3— 261°_3	
9320.32	7		10726.30	−0.04	357°_2— e^5D_1	
9341.08	1		10702.46			
9342.76	4		10700.54	+0.02	346°_4— 55_4	
9353.72	2		10688.00			
9379.00	5		10659.19	−0.10	$^3P_2$— 299°_3	
9381.36	30		10656.51	−0.10	19_4— 299°_3	
9389.99	3		10646.72	0.00	404°_5— e^5D_4	
9399.03	1		10636.48	−0.08	440°_3— 54_3	
9402.58	1		10632.46			
9485.24	1		10539.80	−0.27	405°_4— e^5D_4	
9505.62	2 *b*		10517.21	−0.03	22852_4— 333°_5	
9507.62	2		10515.00	0.00	28_5— 387°_4	
9512.85	2		10509.21			
9515.88	5		10505.87	−0.03	24_3— 351°_4	
				−0.02	347°_1— e^5D_0	

TABLE 3. *Observed and classified lines of* W I

Wavelength Å	Intensity		Wavenumber (cm^{-1})		Classification	Zeeman effect
	Arc	Spark	Observed	o−c		
9518.50	1		10502.98	+0.16	414°_{3}— 52_{3}	
9529.67	1		10490.67			
9531.25	7		10488.93			
9538.58	20		10480.87	−0.03	22476_{4}— 329°_{3}	
9590.74	1		10423.86	−0.14	23_{3}— 343°_{3}	
9595.35	3		10418.86	−0.03	18_{3}— 293°_{2}	
9615.88	1		10396.61	+0.03	30_{2}— 407°_{1}	
9632.98	1		10378.16			
9639.47	1		10371.17			
9668.13	1		10340.43	−0.03	20_{2}— 313°_{1}	
9707.53	1		10298.46	−0.06	23_{3}— 342°_{3}	
9726.08	2		10278.82			
9728.03	2		10276.76			
9736.31	1		10268.02	+0.21	361°_{1}— $e^{5}D_{1}$	
9747.98	4		10255.72	−0.02	20_{1}— 306°_{1}	
9755.27	2		10248.06	0.00	29_{7}— 397°_{7}	
9757.51	5		10245.71			
9764.61	6		10238.26	−0.07	19535_{5}— $^{7}D^{\circ}_{5}$	
9778.95	0		10223.24			
9780.79	4		10221.32	−0.01	18_{3}— 291°_{2}	
9809.43	12		10191.48	−0.12	23_{3}— 341°_{4}	
9813.74	10		10187.00	+0.04	13_{2}— $^{7}D^{\circ}_{2}$	
9833.12	0		10166.92	−0.17	29479_{4}— 396°_{3}	
9835.20	10		10164.78	+0.17	18_{3}— 291°_{3}	
9847.80	1		10151.77	+0.13	28204_{2}— 383°_{1}	
9859.46	3		10139.76	−0.08	$^{3}P_{2}$— 293°_{2}	
9874.07	8		10124.76	−0.04	19_{6}— $^{7}D^{\circ}_{5}$	
9908.53	0		10089.55			
9912.76	3		10085.24	+0.07	19_{3}— 299°_{3}	
9915.98	10		10081.97	−0.09	18_{2}— 281°_{1}	
9928.10	5		10069.66			
9944.44	6		10053.12			
9963.75	0		10033.63	+0.38	422°_{3}—52284_{3}	
9968.85	2		10028.50			
9983.22	2		10014.06	+0.08	23_{3}— 339°_{2}	
10000.66	1		9996.60			
10002.65	15		9994.61	+0.09	19_{6}— $^{7}F^{\circ}_{6}$	
10021.50	2		9975.81			
10050.31	4		9947.22	−0.08	19826_{5}— $^{7}D^{\circ}_{5}$	
10079.52	1		9918.39	−0.03	$^{5}S_{2}$— 281°_{1}	
10101.67	1		9896.64			
10103.91	2		9894.44			
10115.52	3		9883.09	+0.21	19_{4}— 291°_{3}	
10126.93	2		9871.96	+0.02	382°_{3}— $e^{5}D_{2}$	
10140.54	1		9858.71	−0.07	28347_{3}— 382°_{3}	
10217.38	0		9784.56	−0.04	366°_{2}— $e^{5}D_{1}$	
10241.63	4		9761.40	+0.06	22476_{4}— 322°_{3}	
10306.04	0		9700.39	−0.13	20_{2}— 306°_{1}	
10347.27	3		9661.74	+0.08	18_{2}— 277°_{1}	
10409.77	2		9603.73	+0.11	20_{2}— 305°_{3}	

TABLE 3. *Observed and classified lines of* W I

Wavelength Å	Intensity		Wavenumber (cm^{-1})		Classification	Zeeman effect
	Arc	Spark	Observed	o−c		
10450.97	1		9565.87	+0.15	$19_3 - 293^\circ_2$	
10477.97	0		9541.22	+0.22	$19_4 - {}^7D^\circ_4$	

(Paper 72A6–522)

JOURNAL OF RESEARCH of the National Bureau of Standards—A. Physics and Chemistry
Vol. 72A, No. 6, November–December 1968

Theoretical Interpretation of the Even Levels in the First Spectrum of Tungsten*

Y. Shadmi and E. Caspi****

(August 2, 1968)

The calculated even levels of W I up to the height of about 40,000 cm^{-1}, which is the height of the ground level of the d^6 configuration, are reported. Fifty-seven observed levels are fitted to them, with a mean error of 100 cm^{-1}. L–S coupling and configuration assignments are usually meaningless because of a very strong spin-orbit interaction and configuration interaction. For every level, the largest squared L–S coupling components of its eigenvector are reported, as well as observed and calculated g-values.

Key Words: Atomic spectrum, W I; energy levels, W I; spectrum of tungsten; tungsten; W I.

Laun has published a list of new levels belonging to The W I spectrum [1].[1] He was kind enough to send us his list of even levels prior to their publication. He thought it desirable to have theoretical names for these new levels, as well as for the previously observed levels already published in Moore's book [2]. For a detailed history of their investigation, the reader is referred to AEL [2].

About seven years ago, one of the authors of the present paper (Y. S.) performed theoretical calculations of the configurations of the type $(5d+6s)^n$ for all the first spectra of the platinum group. The interaction between the three above-mentioned configurations and the spin-orbit interaction, which are both very strong in the platinum group, were included in the Hamiltonian. In these calculations, the analogous interaction parameters of the various spectra, as well as the differences between the centers of the three configurations, were expressed by interpolation formulas. This enabled us to include in our calculations the d^n configurations (which are the highest ones) within the spectra of Hf I, Ta I and W I, in which levels belonging to configurations of this type are not experimentally known. For a more detailed description of the above-mentioned approximations and of the interpolative method, the reader is referred to analogous papers on the iron and palladium groups [3, 4, 5].

During the past several years, we tried to improve the above-mentioned calculations on the first spectra of the platinum group by adding to their Hamiltonians various effective-interactions which had been successfully used in the iron group. It turned out, that in the platinum group, these new corrections did not improve the approximation.

In order to investigate the validity and interpretation of the new observed levels of W I, we simply used for the interaction parameters the interpolative values which we had obtained in our above mentioned previous calculations, and diagonalized the numerical energy matrix of W I obtained in this way. We used the derivatives of its renewed diagonalization ("Diag. 1") for least-squares calculations in which we tried to fit all the observed levels with the calculated ones. Since the d^6 configuration is completely unknown, we determined its interaction parameters by forcing them into a linear progression with the analogous parameters of the d^4s^2 and d^5s configurations. The difference between the additive parameters of d^6 and d^5s (A − A′), which was extrapolated from the first spectra on the right-hand side of W I, was fixed. The results of our calculations are as follows: Out of 38 even levels of W I lower than 40,000 cm^{-1} reported in AEL [2], we were able to fit 37 to the calculated ones. Out of the 24 levels now reported by Laun, we could fit 23 levels to our calculated ones. Thus the total number of observed levels fitted to the calculated ones is 60. The level 22852.84 with $J=5$ reported in AEL and the level 30155.90 with $J=1$, now reported by Laun cannot be fitted to any calculated level.[2] Three observed levels can be fitted to calculated ones, only with rather large deviations. These are the level 27670.48 with $J=1$, and the levels 28204.20 and 30374.20, both with $J=2$. For details, the reader is referred to table 2. In the first least-squares calculation ("L.S. 1a"), in which the three above mentioned levels were included, the mean error was ± 143 cm^{-1}. In the second least-

*An invited paper. This paper was partially supported by the National Bureau of Standards, Washington, D.C.
**Present address: The Hebrew University of Jerusalem.
[1] Figures in brackets indicate the literature references at the end of this paper.
[2] We were glad to hear that Dr. Laun, to whom we had sent a preprint of our paper prior to its publication, has now decided to exclude these two levels from his new list of observed levels.

squares calculation ("L.S. 1b"), where these levels were not included, the mean error was reduced to ± 102 cm^{-1}. Unfortunately, our present calculation is not good enough to enable us to make a final decision regarding the reality of these three observed levels. It is well known that in the first spectra of the platinum group, there are more even configurations which are not much higher than the d^n configurations, which can perturb the relatively higher levels of the configurations $d^{n-1}s$. In the case of W I, the additional perturbations are probably due to configurations having one $7s$ electron, and perhaps configurations having one $6d$ or two $6p$ electrons. Thus, we believe that for some of the levels whose heights approach 30,000 cm^{-1}, and, of course, for many higher ones, the predictions of our present approximation may be inaccurate. In order to achieve convergence, the parameters of L.S. 1b were used for an additional diagonalization, which was followed by a least-squares calculation ("L.S. 2"). Also in L.S. 2, the three above mentioned problematic levels were not included, and the mean error was ± 100 cm^{-1}.

The results of the present calculation are reported in two tables. In table 1, we give the values obtained for the various interaction parameters. The symbols used for these parameters are the usual ones (see, for example, references [3, 4, 5]). Analogous parameters of the configurations d^4s^2, d^5s and d^6, are designated by the same letter double primed, single primed, and unprimed, respectively. The values given in the column "Diag. 1" are the interpolated values used in the first diagonalization. It is worthwhile noticing that the values obtained for the parameters in the least-squares calculations, and which were determined by the observed material of W I, assumed numerical values rather close to the interpolative ones (which were determined by the observed material of all the first spectra of the Pt group).

TABLE 1. W I $(5d+6s)^6$—*Parameters of the various stages of the calculation*

	Diag. 1	L.S. 1a	L.S. 1b	L.S. 2
A″	17210	17442 ± 395	17186 ± 291	17152 ± 286
A′–A″	15430	15361 ± 451	16096 ± 345	16190 ± 340
A–A′	14310	Fixed	Fixed	Fixed
B″	485	499 ± 9	490 ± 7	489 ± 7
B′	440	436 ± 10	451 ± 8	451 ± 7
B	395	Prog.	Prog.	Prog.
C″	1843	1867 ± 30	1878 ± 21	1880 ± 21
C′	1735	1736 ± 30	1710 ± 22	1707 ± 20
C	1627	Prog.	Prog.	Prog.
G	2650	2747 ± 30	2731 ± 21	2743 ± 24
H	475	483 ± 7	476 ± 6	475 ± 6
α	39	38 ± 3	39 ± 2	39 ± 2
ζ''	2080	2114 ± 29	2108 ± 21	2104 ± 20
ζ'	1875	1853 ± 46	1889 ± 35	1888 ± 34
ζ	1670	Prog.	Prog.	Prog.
Mean error	.....	± 143	± 102	± 100

Notes:
1. The symbols for the parameters as given in the first column are the usual ones. For their detailed definition, see, for example, Refs. 3, 4, and 5.
2. The abbreviation "Prog." denotes that the value of that parameter was determined by forcing it into a linear progression with the analogous parameters of the two lower configurations.

In table 2, observed and calculated energy levels and g values are given. The calculated energy levels are those obtained in L.S. 2. The three levels not included in this L.S. calculation are given in brackets, and so are their deviations. For $J=0$, 1, 2, 3 and 4, we reported only those calculated levels which are lower than the ^{5}D of d^6 and this ^{5}D itself. For higher J numbers, we reported the levels up to the height of 40,000 cm^{-1}.

In the column "assignment," we gave the con-

TABLE 2. W I—*Observed and calculated energy levels*

Assignment	J	Obs.	Calc.	O–C	Obs. g	Calc. g
69% d^4s^2 ^{5}D	0	0.00	−99	99		
d^4s^2[47% ^{3}P + 24% ^{5}D + 19% ^{1}S]	0	9528.07	9480	48		
60% d^4s^2 ^{1}S	0	20174.20	20086	88		
85% d^5s(^{4}D)^{5}D	0	22773.78	22872	−98		
[55% d^5(^{4}P)s + 31% d^4s^2]^{3}P	0		29106			
[43% d^4s^2 + 32% d^5s + 13% d^6]^{3}P	0		35204			
[34% d^5s + 24% d^4s^2][42% ^{1}S + 17% ^{3}P] + 23% d^6 ^{5}D	0		40939			
62% d^6 ^{5}D	0		41888			
84% d^4s^2 ^{5}D	1	1670.30	1697	−27	1.51	1.498
67% d^4s^2 ^{3}P	1	13307.06	13405	−98	1.32	1.303
[46% d^4s^2 + 21% d^5s]^{3}D	1	18082.80	18095	−12	0.7	0.784
65% d^5s(^{4}P)^{5}P	1	20427.81	20407	21	2.1	2.100
d^5s[56% (^{4}D)^{5}D + 28% (^{4}P)^{5}P]	1	23455.02	23541	−86		1.720
74% d^5s(^{4}F)^{5}F	1	(27670.48)	28123	(−453)		0.210
[41% d^5(^{4}P)s + 37% d^4s^2]^{3}P	1	28720.88	28877	−156		1.395
d^5s[56% (^{2}D)^{3}D + 18% (^{2}D)^{3}D]	1	32378.40	32443	−65		0.539
43% d^5s (^{4}D)^{3}D + 25% d^4s^2 ^{3}P	1		32639			0.871
34% d^5s(^{2}D)^{3}D + [28% d^5(^{4}P)s + 17% d^4s^2]^{3}P	1		35756			1.058
91% d^5s(^{2}S)^{3}S	1		37538			1.973
85% d^6 ^{5}D	1		41269			1.488
88% d^4s^2 ^{5}D	2	3325.53	3382	−57	1.48	1.485
d^4s^2[33% ^{3}F + 28% ^{3}D + 9% ^{3}P] + d^5s[10% ^{3}D + 5% ^{3}P]	2	13777.70	13708	70	1.09	1.042
d^4s^2[46% ^{3}F + 12% ^{3}P + 11% ^{3}D]	2	14976.21	15058	−82	1.06	0.982

TABLE 2. W I—*Observed and calculated energy levels*—Continued

Assignment	J	Obs.	Calc.	O–C	Obs. g	Calc. g
d^5s[57% $(^4G)^5G$ + 12% $(^2F)^3F$] + 15% $d^4s^2\ ^3P$	2	18116.84	18240	−123	1.08	0.724
d^5s[52% $(^6S)^5S$ + 21% $(^4P)^5P$] + 10% $d^4s^2\ ^3D$	2	18280.48	18385	−105	1.43	1.759
23% $d^4s^2\ ^3P$ + d^5s[20% $(^4G)^5G$ + 12% $(^4P)^5P$]	2	19253.58	19283	−30	1.18	1.214
24% $d^4s^2\ ^3P$ + d^5s[23% $(^6S)^5S$ + 16% $(^4P)^5P$ + 14% $(^4D)^5D$]	2	20983.06	21031	−48		1.582
d^5s[41% $(^4D)^5D$ + 37% $(^4P)^5P$]	2	23982.80	24028	−45		1.562
d^4s^2[36% ^1D + 26% ^3P + 14% ^3F]	2	24789.66	24799	−9		1.123
[22% $d^5(^2F)s$ + 13% $d^4s^2]^3F$ + [16% d^4s^2 + 10% $d^5s]^3P$ + 10% $d^5s(^2D)^1D$	2	26861.64	26844	18		1.029
62% $d^5s(^4F)^5F$	2	(28204.20)	28576	(−372)		1.025
d^4s^2[28% ^1D + 26% ^3P] + d^5s[11% $(^4F)^5F$ + 11% $(^2F)^3F$]	2	28898.96	28790	109		1.129
d^4s^2[19% ^3F + 15% ^3P] + d^5s[13% ^3P + 13% ^3D]	2	(30374.20)	29840	(534)		1.127
d^5s[28% $(^4D)^3D$ + 24% ^3F + 23% $(^2D)^3D$]	2		31037			1.057
d^5s[33% $(^2D)^3D$ + 28% $(^2F)^3F$ + 14% $(^2D)^3D$]	2		34341			0.963
d^5s[24% $(^4P)^3P$ + 23% $(^2F)^3F$] + 16% $d^4s^2\ ^3F$	2		35128			1.079
d^5s[28% ^3F + 25% $(^2D)^1D$ + 19% $(^4D)^3D$] + 11% $d^4s^2\ ^3F$	2		35753			0.919
29% $d^4s^2\ ^1D$ + d^5s[26% $(^2D)^1D$ + 20% ^3D + 10% ^3F]	2		37463			1.033
61% $d^6\ ^5D$	2		40340			1.334
94% $d^5s(^6S)^7S$	3	2951.29	2833	118	1.98	1.978
85% $d^4s^2\ ^5D$	3	4830.00	4836	−6	1.50	1.475
d^4s^2[49% ^3G + 23% ^3F]	3	13348.54	13424	−76	0.92	0.942
[36% d^4s^2 + 20% $d^5(^2D)s]^3D$ + 14% $d^4s^2\ ^3F$	3	15459.99	15405	55	1.17	1.256
d^4s^2[52% ^3F + 23% ^3G]	3	17701.14	17736	−35	1.02	1.020
61% $d^5s(^4G)^5G$	3	18974.47	18994	−20	1.06	1.089
d^5s[36% $(^4P)^5P$ + 23% $(^4G)^5G$ + 19% $(^4D)^5D$]	3	19827.67	19759	69	1.28	1.400
d^5s[43% $(^4D)^5D$ + 29% $(^4P)^5P$]	3	23930.08	23870	60		1.488
48% $d^4s^2\ ^1F$ + 16% $d^5s(^2F)^1F$	3	24610.90	24741	−130		1.034
d^5s[36% $(^2F)^3F$ + 16% $(^4G)^3G$] + 15% $d^4s^2\ ^1F$	3	28291.88	28196	96		1.060
d^5s[56% $(^4F)^5F$ + 12% $(^2F)^3F$]	3	28347.60	28454	−106		1.173
d^5s[26% $(^4G)^3G$ + 13% $(^2F)^1F$ + 12% $(^2F)^3F$] + 25% $d^4s^2\ ^3F$	3		29409			1.035
d^5s[22% ^3G + 16% $(^2D)^3D$ + 15% $(^2F)^3F$] + 14% $d^4s^2\ ^3F$	3		31996			1.060
d^5s[52% ^3G + 22% $(^2D)^3D$]	3		32821			1.008
d^5s[50% $(^4D)^3D$ + 16% ^3F + 14% ^3G]	3		33675			1.178
d^5s[32% $(^2F)^3F$ + 30% $(^2G)^3G$ + 16% ^3D]	3		34566			1.030
d^5s[42% $(^2F)^1F$ + 19% $(^2D)^3D$ + 18% ^3F]	3		37143			1.072
d^5s[39% $(^2F)^3F$ + 16% $(^4D)^3D$] + 25% $d^4s^2\ ^3F$	3		38562			1.174
82% $d^6\ ^5D$	3		39911			1.452
77% $d^4s^2\ ^5D$	4	6219.33	6105	114	1.49	1.452
d^4s^2[42% ^3H + 19% ^3G + 15% ^1G + 11% ^3F]	4	12161.95	12162	0	0.99	0.995
d^4s^2[48% ^3G + 19% ^3H + 16% ^1G]	4	16431.28	16567	−136	1.02	1.010
d^4s^2[43% ^3F + 22% ^3H + 11% ^1G]	4	17107.02	17043	64	1.19	1.117
82% $d^5s(^4G)^5G$	4	19256.23	19275	−19	1.20	1.179
61% $d^5s(^4D)^5D$	4	22476.68	22442	35	1.48	1.414
d^4s^2[38% ^1G + 16% ^3F + 12% ^3H]	4	22852.80	22826	27		1.077
d^5s[37% $(^2F)^3F$ + 33% $(^4F)^5F$] + 10% $d^4s^2\ ^3F$	4	27213.82	27114	100		1.241
d^4s^2[34% ^3F + 9% ^1G] + d^5s[17% $(^4F)^5F$ + 11% $(^2F)^3F$]	4	29479.32	29453	26		1.230
d^5s[33% $(^4G)^3G$ + 20% $(^4F)^5F$ + 19% $(^2H)^3H$]	4	29853.66	29813	41		1.081
d^5s[35% $(^4G)^3G$ + 10% $(^2G)^1G$] + d^4s^2[16% ^1G + 11% ^3F]	4	32135.94	31902	234		1.070
25% $d^4s^2\ ^1G$ + d^5s[22% $(^2H)^3H$ + 21% $(^2F)^3F$]	4		33421			1.036
d^5s[31% ^3G + 20% $(^2F)^3F$ + 15% $(^4F)^5F$]	4	34302.04	34159	143		1.147
d^5s[46% $(^2G)^3G$ + 40% $(^2H)^3H$]	4		35219			0.970
[41% d^5s + 17% $d^4s^2]^3F$ + 22% $d^6\ ^5D$	4		37030			1.284
61% $d^6\ ^5D$	4		38229			1.405
61% $d^4s^2\ ^3H$	5	15069.94	15124	−54	1.05	1.097
46% $d^5s(^4G)^5G$ + d^4s^2[22% ^3G + 18% ^3H]	5	19535.04	19391	144	1.21	1.203
48% $d^5s(^4G)^5G$ + d^4s^2[24% ^3G + 20% ^3H]	5	19826.04	20035	−209	1.20	1.198
66% $d^5s(^2I)^3I$	5	27849.80	27755	95		0.933
75% $d^5s(^4F)^5F$	5	28233.44	28273	−40		1.338
d^5s[58% $(^4G)^3G$ + 20% $(^2I)^3I$]	5	31389.08	31256	133		1.114
d^5s[37% $(^2G)^3G$ + 28% $(^2H)^3H$ + 12% $(^2H)^1H$]	5	33291.80	33352	−60		1.146
d^5s[44% $(^2H)^3H$ + 42% $(^2G)^3G$]	5		36364			1.117
80% $d^4s^2\ ^3H$	6	17008.50	16983	26	1.4	1.138
92% $d^5s(^4G)^5G$	6	19648.56	19599	50	1.32	1.318
78% $d^4s^2\ ^1I$	6	23484.78	23424	61		1.033
80% $d^5s(^2I)^3I$	6	28392.72	28482	−89		1.054
d^5s[46% $(^2I)^3I$ + 34% $(^2H)^3H$ + 16% $(^2I)^3I$]	6		33276			1.069
d^5s[50% $(^2I)^3I$ + 42% $(^2H)^3H$]	6		37206			1.078
$d^5s(^2I)^3I$	7	29460.98	29588	−127		1.143

figuration and term-assignment of each level, when these quantum numbers are meaningful. Unfortunately, in the W I spectrum, we have a case of typical intermediate-coupling and strong configuration interaction as well. In many cases, the eigenvectors do not have one dominant $L-S$ coupling component. In these cases, the assignment column gives the largest squared components of the eigenvector. For some levels belonging to the d^5s configuration, we report the term assignment without specifying the parent-term. This is done in cases where various parent-terms are mixed.

It is worthwhile mentioning that, in most cases, the assignments given by Laporte and Mack [6] to the even levels up to the approximate height of 20,000 cm^{-1} coincide with the L–S assignments of the largest squared components of the corresponding calculated eigenvector as reported in table 2.

The second author of the present paper (E. C.) is now doing research on configuration-interaction in the platinum group spectra. We hope that in these calculations we shall be able to take into account more interacting configurations. Only then, shall we be able to make a final decision as to the reality of the observed levels which seem doubtful according to the present calculation. Then, we shall probably also have reliable predictions for higher even levels.

References

[1] Laun, Donald D., and Corliss, C. H., J. Res. NBS 72A (Phys. and Chem.) No. 6609 (1968).

[2] Moore, C. E., "Atomic Energy Levels", NBS Circular 467, Vol. **III** (1958).

[3] Racah, G., and Shadmi, Y., Bull. Res. Council Israel **8F,** No. 1, 15, (1959).

[4] Shadmi, Y., Bull. Res. Council Israel, **9F,** No. 4, 141 (1961).

[5] Shadmi, Y., J. Res. NBS **70A** (Phys. and Chem.) No. 5, 435 (1966).

[6] Laporte, O., and Mack, J. E., Phys. Rev. **63,** 246 (1943).

(Paper 72A6–523)

JOURNAL OF RESEARCH of the National Bureau of Standards—A. Physics and Chemistry
Vol. 72A, No. 6, November–December 1968

Stable Carbon Isotope Ratio Measurements With a Gas Density Meter

S. P. Wasik and W. Tsang

Institute for Materials Research, National Bureau of Standards, Washington, D.C. 20234

(June 27, 1968)

A method is presented for measuring C^{13}/C^{12} isotope ratio of organic compounds by burning the material in a stream of normal CO_2, separating the combustion products by gas chromatography and sequentially measuring the density of the enriched CO_2 peak with a gas density meter. Data are presented for the analysis of enriched ethyl acetate from 15 to 1 percent enrichment. The method is applicable for other stable isotope analysis.

Key Words: Carbon-13; carbon dioxide; ethyl acetate; gas chromatography; gas density meter; isotope ratios.

1. Introduction

Several years ago, Liberti, Conti, and Crescezzi [1][1] and Phillips and Timms [2] made molecular weight determinations using a gas density meter [3]. The latter investigators found that with nitrogen as both the carrier and reference gases, molecular weights up to 150 could be determined to an accuracy of 1 percent. The present study can be considered to be an extension of these earlier investigations. Primary attention will be devoted to the measurement of the molecular weight of a substance, carbon dioxide, to the highest possible precision. This will permit the determination of the isotopic composition or C^{13}/C^{12} ratios of enriched samples of numerous organic compounds.

When a sample of gas density ρ and volume v is swept into the gas density meter, the integral response (peak area A) of the detector can be written as

$$A = kv(\rho - \rho') \tag{1}$$

where k is a cell constant and ρ' is the density of the carrier and reference gases. Since the latter is known, a direct determination of the density of the sample can be made. Its molecular weight can then be determined from the perfect gas law or some other appropriate equation of state. In this study carbon dioxide is used as the carrier and reference gas. An enriched sample of a volatile compound is completely burned and the density of the newly formed carbon dioxide is compared to that of the normal gas. In this mode of operation full advantage is taken of the fact that the gas density meter is a differential detector. A signal will be generated only when enriched carbon dioxide is passing through the detector.

2. Experimental Procedure

A schematic drawing of the flow system and the gas density meter is given in figure 1. The procedure was as follows: (a) injection of enriched samples, (b) its combustion at 730 °C as it passed through a 6-in (0.20 in i.d.) long stainless steel column packed with 40–60 mesh copper oxide, (c) separation of the combustion products, principally carbon dioxide and water, by a 4 ft silica gel column (coated with 2 percent ethyl-hexasebacate), and (d) density determination in the gas density meter. The test substance used was enriched ethyl acetate. Analyses were carried out with the original mixture as well as various samples diluted with normal ethyl acetate. The sample size ranged from 10 to 25 μl. Freshly ground wire copper oxide sieved to 40–60 mesh was found to give the optimum conditions for combustion. A finer mesh gave more efficient combustion but the resulting pressure drop across the columns was found to be too great. Under the present conditions combustion to carbon dioxide was always over 99 percent complete. Methane which was the principal minor product was completely eluted before the appearance of the $C^{13}O_2$ peak. After about 70 μl of the ethyl acetate

[1] Figures in brackets indicate the literature references at the end of this paper.

318-092 O-69—14

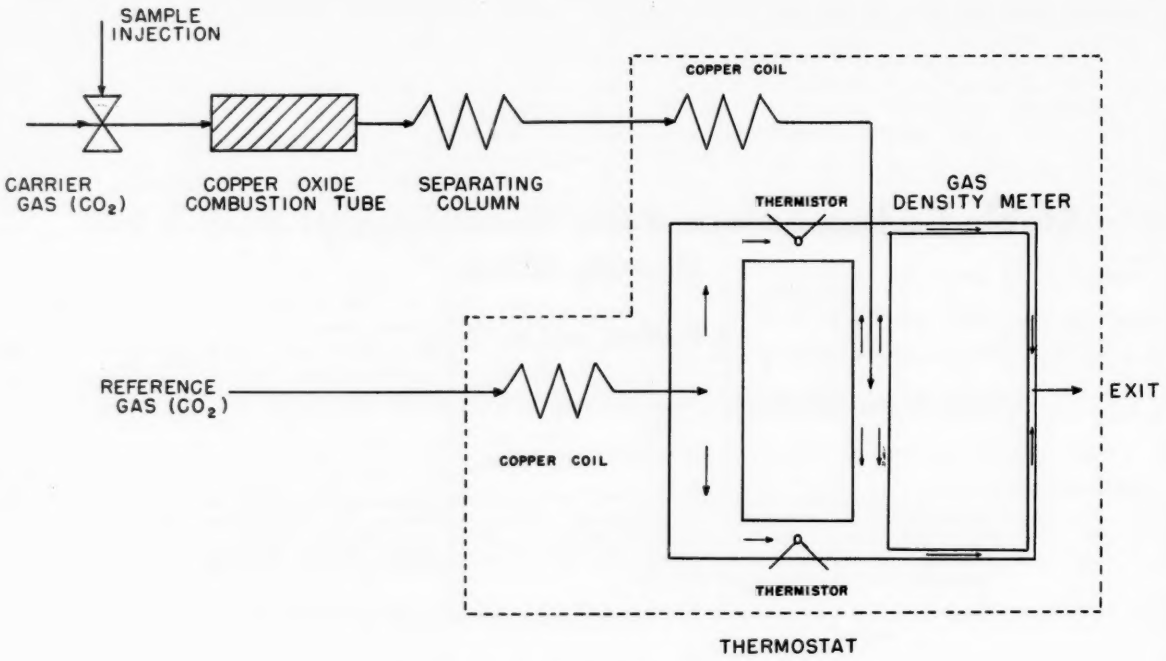

FIGURE 1. *Flow system and gas density meter.*

was burned ethane and ethylene appeared as combustion products and the copper oxide had to be renewed.

The gas density meter was essentially a copy of the one designed by Nerheim [4]. Two 10-ft 1/4-in o.d. copper coils immediately preceding the meter permitted the carrier and reference gases to equilibrate to thermostatic temperature. The density meter and thermostating coils were immersed in a 25-gal oil bath. Better results were obtained when the bath temperature was allowed to drift rather than attempting to regulate it. The temperature change was approximately 0.01° per hour. A one-liter tank down stream from the meter effectively isolated the detector from atmospheric disturbances. All experiments were carried out at two atmospheres pressure, with the detector at approximately 25 °C. Two sets of matched thermistors were tried out as the sensing elements, Fenwal G 112 (8000 Ω)[2] and Fenwal G 128 (100,000 Ω). The former when amplified (5 X) by a Honeywell deviation amplifier had about the same sensitivity as the 100,000 Ω thermistors but with a somewhat lower noise level. The thermistors formed adjacent arms of a standard Wheatstone bridge circuit [5] with the operating current at 5 mA for the 8000 Ω thermistors and 1 mA for the 100,000 Ω thermistors. Detector response was displayed on a 1μV full scale potentiometer recorder (Leeds and Northrop Speedomax) with adjustable speed. The chart speed and attenuation were adjusted so that the area of the recorded peaks could be copies on a 8×17-in Xerox paper. The peak areas were determined as the average weight of three cutouts of the peak. The reproducibility of the weight of a cutout of the same peak was about 1.0 percent. The weight of each peak was approximately 13 g. The carbon dioxide used in these experiments was "Coleman Grade" from the Matheson Company. The flow rates were about 50 cm³/min for the carrier gas and 100 cm³/min for the reference gas.

The gas density meter was calibrated by recording the response of the detector to the passage of known volumes v_A (at 2 atm and 25 K) of argon. The latter was injected into the system immediately before and after a $C^{13}O_2$ determination. The cell constant k' was determined using the equation

$$k' = A[v_A(M_A - M_{CO_2}/Z)^{-1} \quad (2)$$

where M_A is the molecular weight of argon, M_{CO_2} the molecular weight of carbon dioxide (in natural abundance), A the average weight of the Xerox cutouts, and Z the compressibility of carbon dioxide at 2 atm and 25 °C. This relationship is similar to that of eq (1) except that the molecular weight dependence is now explicitly given. It is a mark of the sen-

[2] Certain commercial materials and equipment are identified in this paper in order to specify adequately the experimental procedure. In no case does such identification imply recommendation or endorsement by the National Bureau of Standards, nor does it imply that the material or equipment identified is necessarily the best available for the purpose.

sitivity of the density meter that failure to take the compressibility factor (0.990) [6] into account would have resulted in an error of 10 percent in the isotope ratio determinations. It was not necessary to consider the compressibility of argon since by the time the 100–200 μl sample reached the detector it was highly diluted and behaved as a perfect gas. This assumes no interaction between argon and carbon dioxide. From the cell constant and the peak area A' of the enriched CO_2, the molecular weight increment was calculated from the expression

$$\Delta M_{CO_2}=\frac{ZA'}{k'}\left[\frac{4ZRTv_l d\left(1+\frac{\Delta M}{M}\right)}{PM\left(1+\frac{\Delta M}{M}\right)}\right]^{-1}=\frac{A'PM}{4k'RTv_l d}$$

where v_l is the volume of enriched ethyl acetate injected into the system, $d\left(1+\frac{\Delta M}{M}\right)$ the liquid density of the enriched ethyl acetate, M its molecular weight, and P and T the pressure and temperature at which experiments were carried out (2 atm and 25 °C). The factor of 4 takes into account the number of carbon atoms in ethyl acetate. The absolute ratio of carbon-13 to carbon-12 was calculated from the relation

$$C^{13}/C^{12}=\Delta M_{CO_2}+0.0111.$$

The last number represented the natural abundance [7].

3. Results and Discussion

A typical chromatogram of a 1 percent enriched sample is shown in figure 2. This signal is a direct measure of the density difference between the enriched and normal carbon dioxide. On the basis of the observed peak height and base line noise, it can be concluded that the minimum detectable isotopic enrichment ($S/N=2$) is about 0.02 percent. This is equivalent to a molecular weight difference of 0.0002 g/mol. Sensitivity can probably be improved with the injection of larger samples. The experimental results are summarized in table 1. The uncertainty limits for each individual run should not exceed 6 percent. This arises from estimated uncertainties in area measurement, in the volume of the injected liquid sample and the determination of the cell constant. It can be seen from table 1 that practically all the data fall within this limit. The larger error at the 3.17 percent enrichment is probably due to a dilution error. This is supported by the good reproducibility of the three determinations carried out at this enrichment. Peak height measurements also gave good values for isotope enrichment, providing the same sample size was used each time. A typical calibration plot is given in figure 3. The main deficiency of such a procedure is the necessity for calibration with known enriched samples.

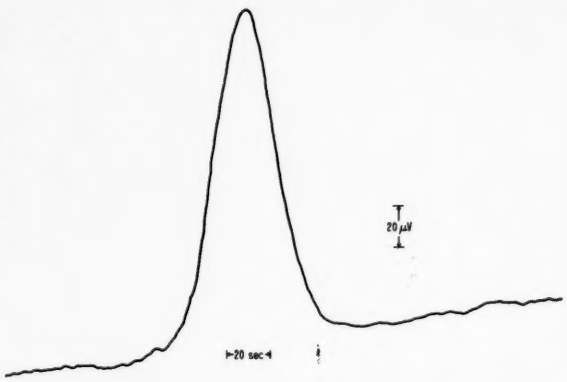

FIGURE 2. *Chromatogram of 1 percent enriched* $C^{13}O_2$.

Isotope ratios are usually determined using a mass spectrometer. The sensitivity limits are governed by the cracking pattern and the presence of the various natural occurring isotopes. It is estimated [8] that for carbon dioxide a typical commercial analytical instrument will have uncertainty limits of between 0.05 to 0.10 percent enrichment. On this basis, it is

TABLE 1. *Gas density analysis of* C^{13} *content* CO_2 *produced by burning enriched ethyl acetate*

% C^{13} (abs.) natural abundance	Volume of sample (liquid ethyl acetate)μl	Observed change in average molecular weight ΔM	% C^{13} cal. from ΔM
16.08[a]	7	0.1457	15.67[c]
16.08	7	.1458	15.68
16.08	10	.1466	15.76
16.08	10	.1511	16.21
16.08	10	.1532	16.42
16.08	10	.1511	16.21
16.08	10	.1548	16.51
16.08	10	.1508	16.18
			16.08 + 0.25[e]
8.59[b]	10	.0727	8.37
6.092[b]	7	.04899	5.999
6.092	7	.04905	6.005
			6.002 ± 0.003
5.385[b]	10	.04283	5.383
5.385	10	.04219	5.319
			5.351 ± 0.03
3.599[b]	10	.0235	3.45
3.599	10	.0234	3.44
			3.445 ± 0.005
3.17[b]	25	.0180	2.90[c, d]
3.17	10	.0177	2.87
3.17	10	.0176	2.86
			2.88 ± .02
2.324[b]	10	.01202	2.302
2.324	10	.0123	2.332
			2.317 ± .02
1.45[b]	10	.00345	1.445

[a] Enrichment in material as reported by supplier.
[b] Enriched ethyl acetate (16.08%) diluted with normal ethyl acetate.
[c] The estimated uncertainty in the numbers in this column, based on the various parts of the experimental procedure is 6 percent.
[d] Dilution technique used here is believed to be an important source of error.
[e] Standard deviation.

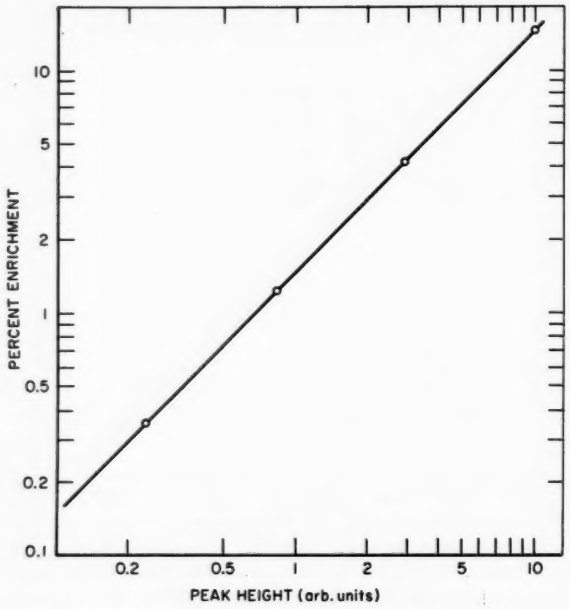

FIGURE 3. *Calibration of percent enrichment versus peak heights.*

clear that the sensitivity of the gas density meter is sufficient for it to be employed in routine determinations of isotope ratios. The chief attraction of such a procedure in comparison with mass spectrometric determinations is the low capital cost for gas density determinations. Practically all the equipment used in these studies is on hand in any gas chromatographic laboratory. The experimental procedure is exactly the same as that used in routine chromatographic analysis and thus extremely simple and straight forward.

Although the present study is only concerned with the determination of carbon-13/carbon-12 ratios in ethyl acetate, it is quite clear that with the present set-up practically any organic compound could have been used. Ethyl acetate was selected as the test substance solely for its ready availability and convenience of handling. Furthermore flow systems similar to that given here can probably also be set up to determine oxygen-18/oxygen-16 [9] and nitrogen-15/nitrogen-14 [10] ratios. Due to the great difference in their thermal conductivities deuterium/hydrogen ratios can probably be determined most accurately using thermal conductivity detectors. With regard to the lower hydrocarbons, such as methane and ethane where there may be combustion problems or for that matter any gaseous compounds, the best procedure would be to discard the burner completely and to use as the carrier and reference gases the normal versions of the substance whose isotope ratio is to be determined. This should have the added benefit of increasing sensitivity.

Finally, the unique capabilities of the gas density meter as a chromatographic detector in experiments similar to the type described here deserve wider appreciation. When the carrier gas has physical and chemical properties similar to that of the solute or such cases where there are high concentration of detectable material ultrasensitive ionization detectors will respond mainly to the carrier gas and may approach saturation. This is not usually encountered in normal chromatography, but may occur in vacancy chromatography or when a volatile substrate is used. Thermal conductivity detectors which have about the same sensitivity as the gas density meter become unpredictable in mixtures of components having roughly the same conductivity. Calibration of the gas density on the other hand is independent of the molecular constitution of the species studied, which is, in sharp contrast to the behavior of other classes of detectors. It is foreseeable that there will be an increased use for the gas density meter in the future as a gas chromatographic detector and for other physical chemical experiments.

4. References

[1] Liberti, A., Conti, L., and Crescenzi, V., Nature **178,** 1067 (1956).
[2] Phillips, C. S. G., and Timms, P. L., J. Chromatog. **5,** 131 (1961).
[3] Littlewood, A. B., Gas Chromatography, p. 351 (Academic Press, New York, 1962).
[4] Nerheim, A. G., Anal. Chem. **35,** 1641 (1963).
[5] Kieselbach, R., Anal. Chem. **32,** 1749 (1960).
[6] Van Huff, N. E., Houghton, G., and Corell, J., J. Chem. Eng. Data **8,** 336 (1963).
[7] Cherdyntsev, V. V., Abundance of Chemical Elements (Univ. of Chicago Press, 1961).
[8] Hughes, E. E., National Bureau of Standards, Washington, D.C. (personal communication).
[9] Oita, I. J., and Conway, H. S., Anal. Chem. **26,** 600 (1954).
[10] Glascock, R. F., Isotopic Gas Analysis For Biochemists, p. 199. (Academic Press, Inc., New York, 1954).

(Paper 72A6–524)

JOURNAL OF RESEARCH of the National Bureau of Standards—A. Physics and Chemistry
Vol. 72A, No. 6, November–December 1968

The Single Crystal Spectrum of Hexakis(imidazole)nickel(II)Nitrate

Curt W. Reimann

Institute for Materials Research, National Bureau of Standards, Washington, D.C. 20234

(July 16, 1968)

The crystal spectrum of hexakis(imidazole)nickel(II)nitrate from 7000 cm^{-1} to 30,000 cm^{-1} at liquid nitrogen temperature has been measured. Three spin-allowed and three spin-forbidden bands in this spectrum were assigned on the basis of octahedral ligand field symmetry. These assignments are compared with those made in several related materials. Important differences and similarities in spectral detail and their bearing on assignments in other strong field nickel(II) complexes, are discussed.

Key Words: Crystal spectrum; hexakis(imidazole)nickel(II)nitrate; octahedral nickel(II); spin-forbidden bands.

1. Introduction

The visible spectra of nickel(II) complexes are characterized by spin-allowed and by relatively weaker spin-forbidden bands. In octahedral ligand fields three spin-allowed bands may be observed from which estimates can be made of the ligand field strength parameter, Dq, and of the interelectronic repulsion parameter, B. These parameters can then be utilized to estimate the energies of all octahedral ligand field states which arise from the terms of the free nickel(II) ion. One difficulty with nickel(II) spectra which has led to conflicting assignments arises from the proximity of the ^1E_g(D) and ^3T_2g(F) energy levels. Transitions from the ^3A_2g(F) ground state to the ^1E_g(D) and ^3T_2g(F) levels often result in two overlapping bands. As the value of Dq is derived from the energy of the $^3A_2g(F) \rightarrow {}^3T_2g(F)$ transition, the proper assignment is required for a consistent interpretation. In a recent study Robinson, Curry and Busch [1][1] measured solution spectra of some strong field nickel(II) complexes ($Dq \sim 1000$–1300 cm^{-1}). The spectral region from 10000–14000 cm^{-1} showed that the $^3A_2g(F) \rightarrow {}^1Eg(D)$ transition "passes through" the $^3A_2g(F) \rightarrow {}^3T_2g(F)$ transition from the high to the low energy side with increasing ligand field strength. This type of comparison of related spectra is an especially useful guide in the interpretation of spectra in which some bands are not observable or are obscured by stronger bands. Palmer and Piper [2], for example, assigned the energy levels in $Ni(bipyridine)_3^{++}$ with the aid of the analysis reported by Robinson, Curry and Busch [1].

Although many solution spectra of nickel(II) in strong octahedral ligand fields have been reported, relatively few single crystal studies have been carried out. The principal advantages of the single crystal studies are derived from the fact that the spectra of species of known structure can be investigated at reduced temperatures. The improved resolution at low temperature may reveal the presence of band splittings and of spin-forbidden bands. Neither of these features may be evident in the solution spectra but both are of great importance in analyses which attempt to relate intensity distribution with molecular symmetry.

As part of a program in the investigation of the structural and spectroscopic properties of coordination compounds of transition metal ions single crystals were grown of hexakis(imidazole)nickel(II)nitrate, $(C_3H_4N_2)_6Ni(NO_3)_2$. A preliminary spectrum from 7000 cm^{-1}–31000 cm^{-1} was found to be free from the charge transfer or ligand absorption bands which frequently mask the much less intense d—d bands. The x-ray structure determination of $(C_3H_4N_2)_6Ni(NO_3)_2$

[1] Figures in brackets indicate the literature references at the end of this paper.

has recently been completed and the coordination polyhedron has been shown to be a very slightly distorted octahedron [3]. In this paper the room temperature and liquid nitrogen temperature spectra of $(C_3H_4N_2)_6Ni(NO_3)_2$ are reported and an assignment is made of three spin-forbidden and three spin-allowed bands observed in these spectra. Finally, the spectral data for $(C_3H_4N_2)_6Ni(NO_3)_2$ as well as those for several related complexes are considered with regard to their bearing on assignments in general cases.

2. Experimental Procedure

Crystals of $(C_3H_4N_2)_6Ni(NO_3)_2$ were grown from stoichiometric aqueous solutions of $Ni(NO_3)_2$ and imidazole. Preliminary x-ray studies showed that these crystals are trigonal, space group $R\bar{3}$. The crystal data based upon hexagonal indexing is as follows: $a=b=12.353\pm0.001$ Å, $C=14.803\pm0.002$ Å (where the error limits indicate standard deviations), of the individual measurements, to reflect their spread; or standard errors of preceding numbers to show how freely they are determined; $\rho_o=1.51$ g cm^{-3}, $\rho_c=1.505$ g cm^{-3}, $z=3$. The complete x-ray structure determination showed that the complex cation consists of the nickel ion and six imidazole rings coordinated through the pyridine type (=N) nitrogen atom. The nickel ion lies on a three-fold axis and a center of symmetry ($\bar{3}$ site symmetry) and is, therefore, equidistant (2.13 Å) from six nitrogen atoms. The six nitrogen atoms describe a slightly distorted octahedron. The actual configuration of the coordinating nitrogen atoms may be described as resulting from a 0.04 Å compression along one of the three-fold axes of a regular octahedron.

Spectroscopic measurements were performed on a recording spectrophotometer (Cary 14). Low temperature measurements were carried out in a cold finger type silica Dewar with liquid nitrogen as coolant.

The single crystal spectrum of $(C_3H_4N_2)_6Ni(NO_3)_2$ at room temperature and at liquid nitrogen temperature is shown in figure 1. The spectrum consists of three symmetrical bands which occur at 11,100 cm^{-1}, 18,150 cm^{-1}, and at 28,700 cm^{-1} at liquid nitrogen temperature. A weak shoulder is observed near 13,300 cm^{-1} and a broad weak band occurs near 24,000 cm^{-1}. A very weak and narrower band appears at 22,500 cm^{-1}.

3. Assignment of Spectrum

The nickel(II) ion has eight $3d$ electrons which permits the free ion terms ^3F, ^3P, ^1D, ^1G, and ^1S. In crystalline fields of octahedral symmetry the sevenfold degeneracy of the ^3F free ion ground term is partially removed and the $^3A_2g(F)$, $^3T_2g(F)$, and $^3T_1g(F)$ crystal field states arise. The ^3P free ion term remains unsplit in an octahedral field ($^3T_1g(P)$). The remaining free ion terms, ^1D, ^1G, and ^1S become the crystal field states $^1Eg(D)$, $^1T_2g(D)$, $^1A_1g(G)+{}^1T_1g(G)+{}^1Eg(G)+{}^1T_2g(G)$ and $^1A_1g(S)$ respectively.

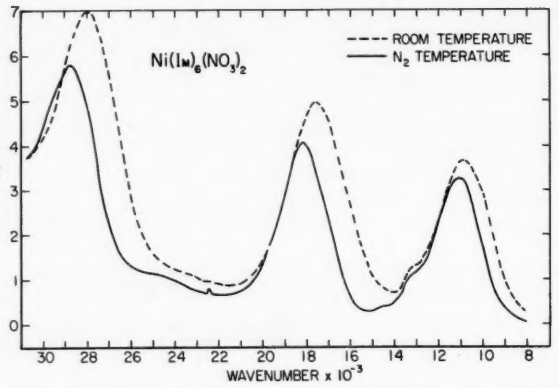

FIGURE 1. *The single crystal spectrum of* $(C_3H_4N_2)_6Ni(NO_3)_2$ *at room temperature and at liquid nitrogen temperature.*

The three broad bands observed in $(C_3H_4N_2)_6Ni(NO_3)_2$ at 11,100 cm^{-1}, 18,150 cm^{-1}, and 28,700 cm^{-1} are readily identified with the three spin-allowed transitions. The 11,100 cm^{-1} band corresponds to a $^3A_2g(F)\rightarrow{}^3T_2g(F)$ transition while the 18,150 cm^{-1} and 28,700 cm^{-1} bands are assigned to the $^3A_2g(F)\rightarrow{}^3T_1g(F)$ and $^3A_2g(F)\rightarrow{}^3T_1g(P)$ transitions. The separation between the $^3A_2g(F)$ and $^3T_2g(F)$ states is equal to 10 Dq where Dq is the parameter which is a measure of the ligand field strength. Thus, Dq for $(C_3H_4N_2)_6Ni(NO_3)_2$ is 1110 cm^{-1}. The interelectronic repulsion parameter, B, can be computed from the energies of the $^3A_2g(F)\rightarrow{}^3T_1g(F)$ and $^3A_2g(F)\rightarrow{}^3T_1g(P)$ transitions and from the value of Dq [4]. The computed value of B, 745 cm^{-1}, represents a reduction from the free ion value by about 25%. The Liehr-Ballhausen energy level diagram for the $3d^8$ system [5] can now be used to aid in the assignment of the three observed spin-forbidden bands. The low intensity shoulder near 13,400 cm^{-1} is assigned to the $^3A_2g(F)\rightarrow{}^1Eg(D)$ transition. A relatively sharp weak band at $\sim$ 22,500 cm^{-1} is assigned to the $^3A_2g(F)\rightarrow{}^1A_1g(G)$ transition and a much broader weak band observed at $\sim$ 24,000 cm^{-1} is assigned to the $^3A_2g(F)\rightarrow{}^1T_2g(D)$ transition. The last two assignments are supported by the breadth of the bands as well as by their energies. The breadths differ as a consequence of the fact that the upper states have different dependencies upon Dq. Thus, the $^1A_1g(G)$ level, being less sensitive to changes in Dq, is considerably less vibrationally broadened. The remaining possible spin-forbidden band in the spectral region studied, $^3A_2g(F)\rightarrow{}^1T_1g(G)$, is expected to lie just below the more intense and broader $^3A_2g(F)\rightarrow{}^1T_1g(P)$ band. It was not observed. A summary of the assignments for $(C_3H_4N_2)_6Ni(NO_3)_2$ is given in table 1.

4. Discussion

The assignment of energy levels from 7000 cm^{-1} to 30,000 cm^{-1} in the spectrum of $(C_3H_4N_2)_6Ni(NO_3)_2$

TABLE 1. *Transition energies and assignments of observed bands*

11,100 cm^{-1}	$^3A_2g(F) \rightarrow {}^3T_2g(F)$
13,400	$\rightarrow {}^1Eg(D)$
18,150	$\rightarrow {}^3T_1g(F)$
22,500	$\rightarrow {}^1A_1g(G)$
24,000	$\rightarrow {}^1T_2g(D)$
28,700	$\rightarrow {}^3T_1g(P)$

allows a comparison with the results of several recent studies of nickel(II) complexes. In this analysis significant differences and similarities in assignments, intensities and transition energies between $(C_3H_4N_2)_6Ni(NO_3)_2$ and each related spectrum will be discussed in terms of molecular symmetry. Finally the results of this analysis will be summarized to aid in making assignments in general cases.

The single crystal spectrum of $Ni(NH_3)_4(NCS)_2$ reported by Hare and Ballhausen [6] offers a close comparison with the spectrum of $(C_3H_4N_2)_6Ni(NO_3)_2$ because NCS and NH_3 occupy adjacent positions in the spectrochemical series and the ligand field at the nickel(II) ion in $Ni(NH_3)_4(NCS)_2$ is also very nearly octahedral. The similarity in structure between $Ni(NH_3)_4(NCS)_2$ and $(C_3H_4N_2)_6Ni(NO_3)_2$ is reflected in the similarity in their spectra. For example, the transition identified as $^3A_2g(F) \rightarrow {}^1Eg(D)$ occurs in both spectra near 13,000 cm^{-1}. More significantly, the intensity with which this transition occurs in both spectra compared with that of the adjacent $^3A_2g(F) \rightarrow {}^3T_2g(F)$ transition is consistent with its assignment as a spin-forbidden band. In addition, the energies and relative intensities of the spin-allowed bands in these spectra are quite similar. The spectrum of $Ni(NH_3)_4(NO_2)_2$ reported by Hare and Ballhausen [6], on the other hand, differs markedly from those compared above. In the 11–14,000 cm^{-1} region, the spectrum of $Ni(NH_3)_4(NO_2)_2$ (in both polarization directions) has a broad band with a shorter wavelength shoulder of comparable intensity. The band corresponding to the $^3A_2g(F) \rightarrow {}^3T_1g(F)$ transition occurs about 2000 cm^{-1} higher and with greater relative intensity than the corresponding transitions in $Ni(NH_3)_4(NCS)_2$ and $(C_3H_4N_2)_6Ni(NO_3)_2$ and the band corresponding to the $^3A_2g(F) \rightarrow {}^3T_1g(P)$ transition in $Ni(NH_3)_4(NO_2)_2$ was too intense to be observed.

Robinson, Curry, and Busch [1] recorded the spectra of a series of nickel-strong field ligand complexes to determine the relative behavior of the neighboring $^3A_2g(F) \rightarrow {}^1Eg(D)$ and $^3A_2g(F) \rightarrow {}^3T_2g(F)$ transitions as a function of ligand field strength. In each spectrum one band of an overlapping pair of bands was assigned to the $^3A_2g(F) \rightarrow {}^1Eg(D)$ transition and the other to the $^3A_2g(F) \rightarrow {}^3T_2g(F)$ transition. An analysis of these assignments indicated that for small Dq the $^1Eg(D)$ level lies above the $^3T_2g(F)$ while for large Dq the reverse obtains. From this analysis a band crossover point at $Dq \sim 1200$ cm^{-1} was estimated. In all spectra utilized in the Robinson et al. [1] analysis the overlapping bands have comparable intensity. In the spectrum of $Ni(NH_3)_4(NCS)_2$ and of $(C_3H_4N_2)_6Ni(NO_3)_2$, however, the $^3A_2g(F) \rightarrow {}^1Eg(D)$ transition not only appeared with a very small fraction of the intensity of the $^3A_2g(F) \rightarrow {}^3T_2g(F)$ transition but also at ~ 1200 cm^{-1} higher energy than in the most closely comparable solution spectra used in the Robinson et al. [1] analysis. Thus, the single crystal studies would seem to indicate that a band crossover occurs significantly above $Dq = 1200$ cm^{-1}.

Palmer and Piper [2] investigated the single crystal spectra of $Ni(bipyridine)_3^{++}$ which they interpreted on the basis of trigonal symmetry. A sharp band near 21,000 cm^{-1} was assigned as the $^3A_2g(F) \rightarrow {}^1A_1g(G)$ transition which occurs at $\sim 22{,}500$ cm^{-1} in $(C_3H_4N_2)_6Ni(NO_3)_2$. A shoulder which was observed near 23,000 cm^{-1} in $Ni(bipyridine)_3^{++}$ was assigned by Palmer and Piper as a ligand transition because of its estimated small breadth. However, the occurrence of a weak band near 24,000 cm^{-1} in $(C_3H_4N_2)_6Ni(NO_3)_2$ suggests that the 23,000 cm^{-1} band in $Ni(bipyridine)_3^{++}$ may be ascribed to a d-d transition ($^3A_2g(F) \rightarrow {}^1T_2g(D)$). The two bands near 12,000 cm^{-1} in $Ni(bipyridine)_3^{++}$ were assigned by comparison with the spectral data reported by Robinson et al. [1]. The lower energy band was assigned as the $^3A_2g(F) \rightarrow {}^1Eg(D)$ transition.

A summary of the assignments made in the aforementioned spectra shows that the intensity of the band assigned to the spin-forbidden $^3A_2g(F) \rightarrow {}^1Eg(D)$ transition varies over a wide range with respect to that of the spin-allowed $^3A_2g(F) \rightarrow {}^3T_2g(F)$ transition. In the general case, then, when these adjacent bands appear with comparable intensity, an assignment cannot be made on the basis of intensity alone. Nor are these transitions necessarily distinguishable by their relative energies as this has been shown to depend upon Dq. These observations illustrate how the problem of assignments in the region from 10 to 14,000 cm^{-1} is bound up with the problem of intensity distribution. Of the spectra recorded in the studies cited, only $(C_3H_4N_2)_6Ni(NO_3)_2$ and $Ni(NH_3)_4(NCS)_2$ are in conformity with the octahedral model and, as indicated above, they have similar intensity distributions. The single crystal spectrum of $Ni(NH_3)_4(NO_2)_2$ differs in essential detail from these but has been intrepreted successfully on the basis of tetragonal symmetry. The remaining spectra, when considered together, indicate that the $^1Eg(D)$ level lies below $^3T_2g(F)$ for $Dq > 1200$. As already noted, however, in the spectra in which the intensity of the $^3A_2g(F) \rightarrow {}^1Eg(D)$ transition is consistent with its assignment as a spin-forbidden band, it occurs ~ 1200 cm^{-1} higher than in spectra for which a relatively high intensity $^3A_2g(F) \rightarrow {}^1Eg(D)$ transition has been assigned. These wide variations in spectral characteristics of apparently structurally related compounds are difficult to ascribe to variations in singlet-triplet mixing alone. Rather it appears that another factor, the presence of lower symmetry components in the ligand field of the metal ion, is of greater significance. The importance of ligand field components with lower than octahedral symmetry lies in the fact that these components must split the ^3T octahedral states and thereby redistribute the intensity associated with spin-allowed transitions. If the departure from octahedral symmetry is not

large, additional energy levels will appear in the 10 to 14,000 cm^{-1} region. If such levels are identified exclusively with $^3A_2g(F) \rightarrow {}^3T_2g(F)$ transitions, a consistent account in terms of the ligand field theory cannot be given. In such cases the detailed crystal structure must be determined so that an interpretation can be made in terms of the detailed molecular symmetry.

5. References

[1] Robinson, M. A., Curry, J. D., and Busch, D. H., Inorg. Chem. **2,** 1178 (1963).

[2] Palmer, R. A., and Piper, T. S., Inorg. Chem. **5,** 864 (1966).

[3] Santoro, A., Mighell, A. D., Zocchi, M., and Reimann, C. W., Acta. Cryst., in press.

[4] Bostrup, O., Jorgensen, C. K., Acta. Chem. Scand. **11,** 1223 (1957).

[5] Liehr, A. D., and Ballhausen, C. J., Ann. Phys. (N.Y.), **6,** 134 (1959).

[6] Hare, C. R., and Ballhausen, C. J., J. Chem. Phys. **40,** 792 (1964).

(Paper 72A6–525)

JOURNAL OF RESEARCH of the National Bureau of Standards—A. Physics and Chemistry
Vol. 72A, No. 6, November–December 1968

Crystalline *alpha* and *beta* Forms of 3-O-α-D-Glucopyranosyl-D-arabinopyranose

Horace S. Isbell,* Harriet L. Frush, and J. D. Moyer**

Institute for Materials Research, National Bureau of Standards, Washington, D.C. 20234

(July 30, 1968)

Crystalline 3-*O*-α-D-glucopyranosyl-α-D-arabinopyranose monohydrate, mp 120 to 121 °C, and 3-*O*-α-D-glucopyranosyl-β-D-arabinopyranose, mp 155 to 157 °C, were prepared from a sirup obtained by the Ruff degradation of calcium maltobionate. For the *alpha* monohydrate, $[\alpha]_D^{20} = +16.7 \times 10^{-0.024t} - 9.6 \times 10^{-0.098t} + 46.6$, and for the anhydrous *beta* form, $[\alpha]_D^{20} = -25.6 \times 10^{-0.025t} - 9.4 \times 10^{-0.097t} + 49.2$. The structure of the sugar was established by converting it into maltose.

Treatment of the *alpha* form with pyridine–acetic anhydride gave a heptaacetate, mp 127 to 128 °C, $[\alpha]_D^{20} + 62.4°$ (*c* 2.5, chloroform). The *beta* form gave a heptaacetate, mp 194.5 – 195.5° C, $[\alpha]_D^{20} + 13.4°$ (*c* 2.5, chloroform).

Key Words: Anomeric sugars; calcium maltobionate; 3-*O*-α-D-glucopyranosyl-D-arabinopyranose; maltose-*1*-^{14}C; mutarotation of 3-*O*-α-D-glucopyranosyl-D-arabinopyranose; Ruff

1. Introduction

3-*O*-α-D-Glucopyranosyl-D-arabinose was required for the synthesis of maltose-*1*-^{14}C [1][1] and recently for a study of the behavior of sugars in alkaline solutions [2]. Products purported to be 3-*O*-α-D-glucopyranosyl-D-arabinose had been reported by Zemplén [3] and Gakhokidze [4]. Zemplén's product, a sirup obtained by degradation of octa-*O*-acetylmaltobiononitrile, was amorphous, and had an equilibrium rotation of + 72°. Gakhokidze's compound (mp 172 °C, equilibrium rotation + 16.5°) was obtained by ozonolysis of hexa-*O*-acetylmaltal.

In view of the discrepancy in the properties of the two products, preparation of the compound from calcium maltobionate was undertaken by the degradation method of Ruff [5] as modified by Hockett and Hudson [6]. After several months, our sirupy product yielded crystals (I) that, when purified, proved to be a monohydrate of the expected 3-*O*-α-D-glucopyranosyl-D-arabinose; mp 120 to 121 °C; $[\alpha]_D^{20} + 53.7 \rightarrow + 46.6°$ ($56.8 \rightarrow + 49.3°$, anhydrous basis). Its structure was proved by converting it to maltose [1].

In an attempt to obtain an anomeric modification of the sugar, the hydrate was recrystallized from ethyl alcohol. The crystals that formed in the course of several days had variable compositions and contained alcohol of crystallization. However, two recrystallizations of these crystals from methanol yielded an anhydrous form (II); mp 155 to 157 °C; $[\alpha]_D^{20} + 14.2 \rightarrow + 49.2°$.

It is now established that 3-*O*-α-D-glucopyranosyl-D-arabinose has an equilibrium rotation of + 49.2°, and that neither Zemplén's product, $[\alpha]_D = +72°$, nor Gakhokidze's compound, $[\alpha]_D = +16.2°$, was the purported compound.

2. Assignment of Anomeric Configuration

The mutarotation of I (see fig. 1) shows a striking similarity to the complex mutarotations of α-L-arabinopyranose, β-D-galactopyranose, and D-*glycero*-β-D-*galacto*-heptopyranose [7]. Similarly, the mutarotation of II (see fig. 2) is in qualitative agreement with the mutarotations of β-L-arabinopyranose, α-D-galactopyranose, D-*glycero*-α-D-*galacto*-heptopyranose, and D-*glycero*-α-L-*galacto*-heptopyranose. As in the curves representing the mutarotations of α- and β-L-arabinose and related sugars, the deviation from linearity in the first portion presumably arises from a rapid pyranose-furanose interconversion, and the linear portion from a slower α-β-pyranose anomerization. The character of the mutarotations supports the conclusion that the monohydrate (I) is an α-D-pyranose, and the anhydrous form (II) is a β-D-pyranose. However, the dif-

*Present address: Chemistry Department, American University, Washington, D.C. 20016.
**Present address: W. R. Grace Company, Clarksville, Md. 21029.
[1] Figures in brackets indicate the literature references at the end of this paper.

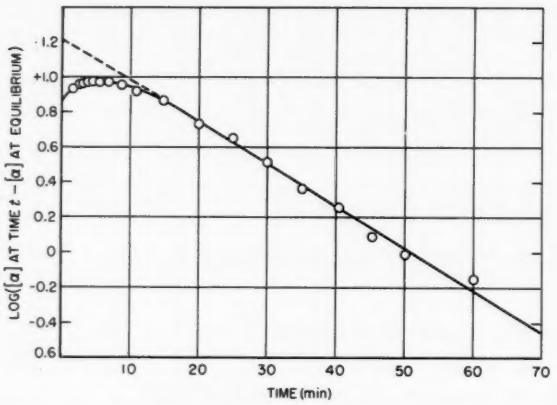

FIGURE 1. *Mutarotation of* 3-O-α-D-*glucopyranosyl-*α-D-*arabinopyranose in water at 20 °C.*

ference between the initial molecular rotations, Hudson's 2A, is only + 13,290, compared with + 16,950 for the anomeric forms of D-arabinopyranose [8].

The anomeric assignments are further substantiated by low-temperature acetylation of the sugars with pyridine and acetic anhydride. Under the acetylation conditions used, little anomeric change occurs, and the configuration of the main product is the same as that of the parent sugar. Compound I yielded principally a heptaacetate of $[\alpha]_D^{20} + 62.4°$, whereas II gave a heptaacetate of $[\alpha]_D^{20} + 13.4°$. The difference between the molecular rotations of the two heptaacetates (+31,720) is in good agreement with the difference (−33,400) that Hudson and Dale found for the tetraacetates of L-arabinopyranose [9].

3. Experimental Details

3.1. 3-O-α-D-Glucopyranosyl-α-D-arabinopyranose Monohydrate (I)

Calcium maltobionate was prepared from maltose by electrolytic oxidation in the presence of calcium carbonate and calcium bromide [10]. The amorphous calcium maltobionate was degraded as follows. A stirred mixture of 5 g of barium acetate monohydrate, 3.1 g of hydrated ferric sulfate [$Fe_2(SO_4)_3 \cdot ca\ 6H_2O$], and 100 g of calcium maltobionate in 500 ml of water was heated almost to boiling, cooled to 35 °C, and treated with 30 ml of 30-percent hydrogen peroxide. Completion of the ensuing reaction (during which the temperature rose to 50 °C) was indicated by the darkening of the solution. The reaction mixture was then cooled to 40 °C, and re-treated with 30 ml of the hydrogen peroxide. When the solution had again darkened, about 10 g of a decolorizing carbon was added, and the suspension was filtered. The filtrate was concentrated under vacuum to a sirup (n_D^{20} 1.46, or about 70 percent total solids); then 200 ml of methanol was slowly added with vigorous stirring. The resulting precipitate was filtered off, washed with two 100-ml portions of methanol, and discarded. The alcoholic filtrate and washings were combined and evaporated to a thick sirup. This sirup was diluted with 200 ml of methanol, and isopropyl alcohol was added to the incipient separation of a second liquid phase. The salts that precipitated were filtered off, thoroughly washed with methanol, and discarded. The filtrate and washings were combined, and concentrated under vacuum to a thin sirup, which was then diluted with water and passed through a column containing 100 ml of mixed cation- and anion-exchange resins. (A test with a conductivity meter showed that the effluent was substantially free from ionic impurities.) The effluent was concentrated under vacuum to a thick sirup, which was diluted with several volumes of methanol, and kept over calcium chloride in a desiccator.

The first crystals of I (17.6 g, 18.3%) formed only after several months (but their use in the nucleation of other syrupy preparations readily caused crystallization). After two recrystallizations from water, plus methanol to incipient turbidity, the compound contained 1 molecule of water of crystallization per molecule; mp 120 to 121 °C; $[\alpha]_D^{20} + 53.7 \rightarrow + 46.6°$ (*c* 4, water).

Anal.: Calc. for $C_{11}H_{20}O_{10} \cdot H_2O$: C, 40.0; H, 6.7. Found: C, 40.0; H, 6.7.

A solution of 0.4 g of I in 10 ml of water saturated with carbon dioxide showed a complex mutarotation. The data, analyzed by the method of Isbell and Pigman [11], follow the equation

$$[\alpha]_D^{20} = + 16.7 \times 10^{-0.024t} - 9.6 \times 10^{-0.098t} + 46.6,$$

in which time (t) is expressed in minutes. The data are presented graphically in figure 1.

3.2. 3-O-α-D-Glucopyranosyl-β-D-arabinopyranose (II)

A finely powdered sample of I (7 g) was dissolved in 700 ml of boiling, absolute ethyl alcohol, and the solution was boiled for 15 min, cooled to 25 °C, and kept at room temperature for one day and in a refrigerator for three days. The resulting crystalline product (apparently a mixture of an ethyl alcoholate and the anhydrous sugar) was twice recrystallized from methanol with the addition of isopropyl alcohol; mp 155 to 157 °C; $[\alpha]_D^{20} + 14.2 \rightarrow + 49.2°$ (*c* 4, water).

Anal.: Calc. for $C_{11}H_{20}O_{10}$: C, 42.3; H, 6.4. Found: C, 42.4; H, 6.5.

A solution of 0.4 g of II in 10 ml of water saturated with carbon dioxide exhibited the complex mutarotation expressed by the equation

$$[\alpha]_D^{20} = - 25.6 \times 10^{-0.025t} - 9.4 \times 10^{-0.097t} + 49.2.$$

The data are presented graphically in figure 2.

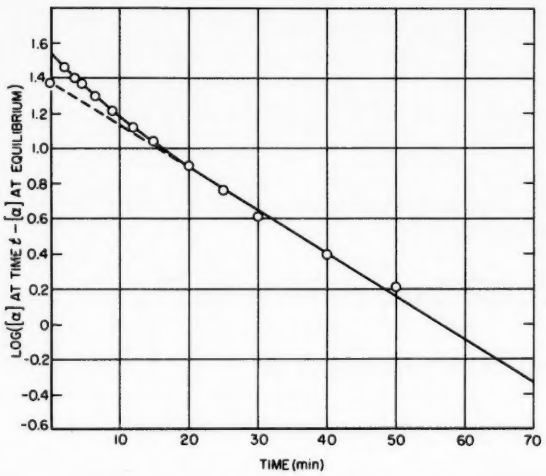

FIGURE 2. *Mutarotation of* 3-O-α-D-*glucopyranosyl-*β-D-*arabinopyranose in water at 20 °C.*

3.3. Hepta-O-acetyl-3-O-α-D-glupyranosyl-α-D-arabinopyranose

One gram of I was added, with mechanical stirring, to 20 ml of 1:1 (v/v) pyridine-acetic anhydride precooled in an ice-salt mixture. After being kept for 18 hr at 0 °C and 4 hr at room temperature, the mixture was poured into 400 ml of ice-water and stirred for 2 hr. The resulting crystals (0.9 g) were separated by filtration. The filtrate was extracted with chloroform, and the extract, after concentration, gave a second crop of crystals (0.8 g). The two crops were combined and recrystallized three times from ethyl alcohol by addition of water; yield, 1.3 g (67%); mp 127–128 °C; $[\alpha]_D^{20}+62.4°$ (*c* 2.5, chloroform).

Anal.: Calc. for $C_{25}H_{34}O_{17}$: C, 49.5; H, 5.6. Found: C, 49.5; H, 5.7.

3.4. Hepta-O-acetyl-3-O-α-D-glycopyranosyl-β-D-arabinopyranose

A sample of finely powdered II (0.84 g) was acetylated in the manner described for the acetylation of I. The crude crystalline compound (1.15 g) was recrystallized three times from ethyl alcohol; mp 194.5–195.5 °C; $[\alpha]_D^{20}+13.4°$ (*c* 2.5, chloroform).

Anal.: Calc. for $C_{25}H_{34}O_{17}$: C, 49.5; H, 5.6. Found: C, 49.3; H, 5.6.

4. References

[1] Isbell, H. S., and Schaffer, R., J. Am. Chem. Soc. **78,** 1887 (1956).
[2] Isbell, H. S., and Frush, H. L., Abstracts Papers, Am. Chem. Soc. Meeting **155,** C25 (1968).
[3] Zemplén, G., Ber. **60,** 1555 (1927).
[4] Gakhokidze, A. M., Zhur. Obschchei Khim. **18,** 60 (1948); Chem. Abstracts **42,** 4948 (1948).
[5] Ruff, O., and Ollendorf, G., Ber. **33,** 1798 (1900).
[6] Hockett, R. C., and Hudson, C. S., J. Am. Chem. Soc. **56,** 1632 (1934).
[7] Isbell, H. S., J. Res. NBS **18,** 505 (1937)RP990.
[8] Montgomery, E. M., and Hudson, C. S., J. Am. Chem. Soc. **56,** 2074 (1934). (See footnote 7.)
[9] Hudson, C. S., and Dale, J. K., J. Am. Chem. Soc. **40,** 992 (1918).
[10] Isbell, H. S., and Frush, H. L., BS J. Res. **6,** 1145 (1931)RP328.
[11] Isbell, H. S., and Pigman, W. W., J. Res. NBS **18,** 141 (1937) RP969.

(Paper 72A6–526)

JOURNAL OF RESEARCH of the National Bureau of Standards—A. Physics and Chemistry
Vol. 72A, No. 6, November–December 1968

Preparation and Solubility of Hydroxyapatite

E. C. Moreno,* T. M. Gregory,* and W. E. Brown*

Institute for Basic Standards, National Bureau of Standards, Washington, D.C. 20234

(August 2, 1968)

Two portions of a synthetic hydroxyapatite (HA), $Ca_5OH(PO_4)_3$, fully characterized by x-ray, infrared, petrographic, and chemical analyses, were heated at 1,000 °C in air and steam atmospheres, respectively. Solubility isotherms for these two samples in the system $Ca(OH)_2$-H_3PO_4-H_2O were determined in the *p*H range 5 to 7 by equilibrating the solids with dilute H_3PO_4 solutions. Both samples of HA dissolved stoichiometrically. The activity products $(Ca^{++})^5(OH^-)(PO_4^{\equiv})^3$ and their standard errors—obtained by a least squares adjustment of the measurements (Ca and P concentrations and *p*H of the saturated solutions) subject to the conditions of electroneutrality, constancy of the activity product, and stoichiometric dissolution—were $3.7_3 \pm 0.5 \times 10^{-58}$ for the steam-heated HA and $2.5_1 \pm 0.4 \times 10^{-55}$ for the air-heated HA. Allowance was made in the calculations for the presence of the ion pairs $[CaHPO_4]^0$ and $[CaH_2PO_4]^+$. The higher solubility product for the air-heated HA is ascribed either to a change in the heat of formation brought about by partial dehydration or to a state of fine subdivision resulting from a disproportionation reaction. The solubility product constants were used to calculate the points of intersection (i.e., singular points) of the two HA solubility isotherms with the isotherms of $CaHPO_4 \cdot 2H_2O$ and $CaHPO_4$; it was found that the *p*H's of the singular points for the air-heated HA were a full unit higher than those of the steam-heated preparation. Conditions are described for the precipitation of HA crystals suitable for solubility measurements.

Key Words: Apatite; hydroxyapatite; calcium phosphates; solubility; solubility isotherms; solubility product.

1. Introduction

Hydroxyapatite (HA), $Ca_5OH(PO_4)_3$, has wide biological and industrial importance. Its physicochemical properties, in particular solubility and detailed crystallographic structure, are directly related to the mineralization processes in biological systems. The various reports in the literature on solubility of HA are contradictory. Clark [1],[1] on the basis of precipitation and dissolution experiments, concluded that HA has a definite solubility product. Thermodynamic functions for HA (from which a solubility product constant can be calculated) have also been reported [2, 3, 4]. Other reports [5–8], however, claim that systems saturated with respect to HA do not conform to the principle of a solubility product constant based on the stoichiometry of the salt. Among the models that have been advanced to explain the apparent anomalous behavior of HA in aqueous solutions, those advocating formation of complexes on the surface of the solid [5, 8] have received considerable attention. These models implicitly assume that equilibrium between the solid and the liquid phases is not achieved with the crystalline portion of the HA, but instead with surface layers having quite different chemical composition from that of the bulk of the solid. Furthermore, the composition of such layers has been assumed to be constant over a wide range of calcium, phosphorus, and hydrogen concentrations in the liquid phase.

At least part of the problem in the interpretation of data on solubility of HA is related to the difficulty in preparing pure samples of this compound. So far, the best crystals have been obtained by hydrothermal methods, but the yields are small, the equipment is relatively expensive and the product may contain extraneous phases such as β-calcium pyrophosphate and/or β-tricalcium phosphate. Direct precipitation methods usually yield very finely divided

*Research Associates from the American Dental Association of the National Bureau of Standards, Washington, D.C. 20234.

This investigation was supported in part by Research Grants DE–01819 and DE–02659 to the American Dental Association from the National Institute of Dental Research and is part of the dental research program conducted by the National Bureau of Standards, in cooperation with the Council on Dental Research of the American Dental Association; the National Institute of Dental Research; the Army Dental Corps; the Aerospace Medical Division, USAF School of Aerospace Medicine; and the Veterans Administration.

[1] Figures in brackets indicate the literature references at the end of this paper.

products, often without the stoichiometric composition of HA. A particularly serious difficulty is contamination by precipitation of the more acid calcium phosphates, among which octacalcium phosphate (OCP), $Ca_8H_2(PO_4)_6 \cdot 5H_2O$ and its decomposition products are the most difficult to eliminate.

The purposes of this work were (a) to devise a simple method for preparation of HA that would yield sufficiently large and pure crystals so that an unambigious characterization would be possible, (b) to learn whether this compound behaves as a normal chemical compound with unique thermodynamic properties when equilibrated with aqueous solutions, and (c) to establish its solubility isotherm and solubility product constant at 25 °C.

2. Experimental Methods and Procedures

In the method of preparation outlined here, the possibility of OCP precipitation is minimized by the use of relatively high temperature and pH. However, pH values higher than 10 are avoided because they seem to favor the formation of very finely divided precipitates. Other conditions are (a) slow addition of reagents to reduce continuous nucleation, (b) high ionic strength and the presence of acetate ions (a Ca complexing agent) to increase the solubility of HA, and thus to favor formation of larger crystals, (c) use of a large reaction vessel to perform the precipitation without sacrificing yields, and (d) special precautions to avoid contamination with carbonate from the atmosphere or reagents (ammonia was used to control the pH instead of NaOH or KOH because the alkali hydroxides are difficult to obtain free of carbonate contamination).

2.1. Preparation of HA

Freshly boiled distilled water and chemically pure salts were used to prepare 2.5 liter of 7.25×10^{-2} *M* $(NH_4)_2HPO_4$ solution and 2.5 liter of 13.33×10^{-2} *M* $Ca(NO_3)_2 \cdot 4H_2O$ solution; their pH's were adjusted with ammonia gas to 8.5–9. These solutions were stored in borosilicate glass bottles vented through ascarite tubes.

The reaction vessel was a 22-l, 3-neck, borosilicate glass flask. A 4-ft condenser was attached to one neck; transfer of reagents and materials was done through the other two necks. The top of the condenser was connected by a glass tube to a 6-l, 3-neck flask containing 3 liters of 10 *N* NaOH solution; a check valve permitting outward flow of gases was connected to one neck and a tube, extending into the NaOH solution and acting as a relief valve, entered through the third neck. The reactant solutions were introduced into the large vessel by a peristaltic pump at a rate of 100 ml/hr. Ammonia gas was passed through an ascarite tower and then bubbled through water before entering the reaction vessel. Samples were withdrawn through a tube that extended to the bottom of the reaction vessel for petrographic examination of the solid and pH determination of the liquid.

Initially, 9 l of *N* ammonium acetate solution were boiled in the reaction vessel for about 12 hr to remove CO_2; then ammonia gas was passed in until the pH reached a value between 8.5 and 9, and the pumping of the phosphate and calcium solutions was started, maintaining vigorous boiling. The pH was maintained between 8.5 and 9.5 (measured at room temperature) by an adequate flow of NH_3 until the total volume of the solutions was pumped into the reaction vessel; then the flow of NH_3 was discontinued but boiling was continued for about 3 hr. The solid was allowed to settle, the supernatant liquid was withdrawn, about 9 l of boiled distilled water were introduced and the mixture was boiled for about 2 hr. This washing operation was repeated as was deemed necessary to remove the soluble salts (usually five times). Further washing was done by decantation, using boiled distilled water and short settling periods so as to discard as much as possible the finest fraction of the precipitate. Precautions to avoid contamination by atmospheric CO_2 were taken during all these operations. The suspension was then filtered and the solid was dried at 150 °C for 48 hr. As explained in section 3, a portion of this sample was heated at 1,000 °C in air and another portion was heated at the same temperature in steam at one atmosphere.

2.2. Equilibrations

Equilibrations were made in glass-stoppered bottles, each of which contained 5g of HA and 120 ml of a phosphoric acid solution, by slowly rotating end-over-end in a water bath at 25 ± 0.1 °C. After two weeks, the suspension was transferred to a thermostated saturator, described in an earlier publication [9], in which the pH of the clear filtered solution was measured. Samples of this solution were taken for calcium and phosphorous analyses. Standardization of the pH-meter (with claimed relative accuracy of ± 0.0037 pH units) was made with certified NBS buffer standards [10].

Phosphoric acid solutions used in the equilibrations were prepared from doubly crystallized $2H_3PO_4 \cdot H_2O$ and freshly boiled conductance water. The molarities of the final solutions were determined by chemical analyses.

2.3. Calcium and Phosphorus Determinations

Calcium was determined colorimetrically by the indirect technique described by Banerjee et al. [11]. Phosphorus was determined using the vanadomolybdate reagent of Brabson et al. [12]. In both analyses, samples were compared directly with blanks and standards in a double-beam spectrophotometer.

The analytical errors estimated for the measurements reported here were: pH, ± 0.009 units; calcium ± 2.5 percent; and phosphorus, ± 1.5 percent of the amounts analyzed.

3. Characterization of the Solid

The HA was characterized by petrographic, gas-adsorption, chemical, infrared and x-ray methods.

Under the petrographic microscope, the crystals appeared as masses of birefringent, irregularly shaped equant particles up to 5 μm in diameter. Present, also, was a minor fraction of thin needles up to 10 μm in length. The mean index of refraction (white radiation, 25 °C) was 1.636 with a standard error of ± 0.002. The material was petrographically homogeneous, both the equant particles up to 5 μm in diameter. Present, also, HA. The mean index is lower than the indexes usually given for HA prepared hydrothermally, $N_\epsilon = 1.644$ and $N_\omega = 1.651$ [37], but this appears to be a characteristic of precipitated HA. The treatments at 1,000 °C did not change the mean indexes significantly.

The surface area determined by the BET procedure,[2] using nitrogen as the adsorbate, yielded a surface area of 6 m^2/g. Although this area is 5 to 10 times larger than that expected from microscopic examination, the agreement is reasonable considering the uncertainties inherent to the two methods.

Chemical analyses yielded $18.22 \pm .27$ percent P and 39.63 ± 0.99 percent Ca, the indicated errors being calculated on the basis of the estimated standard errors of the analytical procedures employed. These values compare with the theoretical values 18.50 percent P and 39.89 percent Ca for HA.

The infrared spectrum displayed all the bands characteristic of well-crystallized HA [14]. Small bands in the regions of 1410 and 1640 cm^{-1} indicated slight contamination with carbonate and moisture, respectively. Analysis by the Warburg method yielded 0.04 percent CO_2.

The x-ray diffraction pattern was sharp and characteristic of that for pure HA [13]. No extraneous peaks were found.

Although the above methods to characterize the HA did not reveal the presence of extraneous phases, when a sample of the HA was heated to 1,000 °C for 24 hr, the infrared spectrum showed small peaks in the region 920 to 1,200 cm^{-1}. These peaks indicate the presence of β-$Ca_3(PO_4)_2$ [14], which presumably formed on heating from a contaminant, an acid calcium phosphate.

A portion of the HA, therefore, was heated at 1,000 °C for 6 days in room atmosphere to anneal the crystals, to drive off carbon dioxide and moisture, and to convert the less basic calcium phosphate into β-$Ca_3(PO_4)_2$. Following the heat treatment, the sample was extracted with 2×10^{-3} M H_3PO_4 to remove the β-$Ca_3(PO_4)_2$. Approximately 10 percent of the sample was dissolved by this treatment.

Another portion of the HA was subjected to the same heat treatment but in the presence of one atmosphere of water vapor, and then extracted with the H_3PO_4 solution.

The infrared spectra of the heated samples were very similar, both corresponding to pure HA [14] but the height of the peak at 3,570 cm^{-1} was considerably greater for the steam-heated sample, indicating either a more uniform environment for the OH^- group in this sample or actually a higher content of OH^- in the crystals.

Another sample of HA, referred to here as "as prepared" was synthesized according to the method described above, but it was not subjected to high temperature treatment.

4. Calculation of Solubility Product Constants

The solubility product constants,

$$K_{sp} = (Ca^{++})^5(OH^-)(PO_4^{\equiv})^3$$

where parentheses denote ionic activities, were calculated by a procedure very similar to the one described elsewhere [9]. The values are listed in tables 1, 2, and 5. However, it was recognized that the best values to be derived from such data must take into account more completely the propagation of errors and the proper weight of the measurements. A more refined method was devised, therefore, for these calculations which entails the simultaneous adjustment of the weighted observables—i.e., calcium and phosphorus concentrations and pH's in the various equilibrated solutions plus the initial concentration of H_3PO_4—and the determination of a parameter which yields best estimates of K_{sp}. The main features of the method follow the general least-squares adjustment discussed by Deming [15] and they are similar to those recently presented by Wentworth et al. [16] for the calculation of complexing constants using spectrophotometric data. However, for the present work, two or three condition functions were used instead of one. A detailed account of the method will be given elsewhere [17]. It suffices here to give the three condition functions used in this investigation, based on electroneutrality, the solubility product for HA, and congruency in the dissolution of the solid, respectively,

$$2[M-\tau] + \frac{(H^+)}{f_{H^+}} + R\tau - \frac{K_w}{(H^+)f_{OH^-}} - \frac{[P-\tau]Q_1}{Q_2} = O \quad (1)$$

$$[M-\tau]^5 f_{Ca^{++}}^5 \left[\frac{K_3(P-\tau)}{(H^+)Q_2}\right]^3 \frac{K_w}{(H^+)} - S = O \quad (2)$$

$$\frac{[M]}{P-P_0} - \frac{5}{3} = O \quad (3)$$

in which M and P are the total molar concentrations of Ca and P in solution, respectively; (H^+) is the activity of the hydrogen ion; f is the molar activity coefficient of the subscripted species; K_w and K_3

[2] Measurement made by Dr. W. V. Loebenstein, NBS.

are the dissociation constants of water and the third ionization constant of H_3PO_4, respectively; P_0 is the initial molar concentration of H_3PO_4; S is the parameter to be calculated, its value being the best estimate of K_{sp}; the fraction 5/3 is the theoretical Ca/P ratio in HA; τ is the total molar concentration of Ca or P present as the ion pairs $[CaHPO_4]^\circ$ and $[CaH_2PO_4]^+$ [9] and it is defined, as are the quantities L, Q_1, Q_2, and R, by the expressions,

$$\tau = (1/2\ M + 1/2\ P + L) - \sqrt{(1/2\ M + 1/2\ P + L)^2 - MP} \quad (4)$$

$$L = \frac{Q_2}{2f_{Ca^{++}}\left[K_x + \frac{K_y(H^+)}{K_2 f_{H_2PO_4^-}}\right]} \quad (5)$$

$$Q_1 = \frac{(H^+)}{K_2 f_{H_2PO_4^-}} + \frac{2}{f_{HPO_4^=}} + \frac{3K_3}{(H^+) f_{PO_4^{\equiv}}} \quad (6)$$

$$Q_2 = \frac{(H^+)^2}{K_1 K_2} + \frac{(H^+)}{K_2 f_{H_2PO_4^-}} + \frac{1}{f_{HPO_4^=}} + \frac{K_3}{(H^+) f_{PO_4^{\equiv}}} \quad (7)$$

$$R = \frac{1}{1 + \frac{K_x K_2 f_{H_2PO_4^-}}{K_y (H^+)}}. \quad (8)$$

In eqs (4–8), K_1 and K_2 are the first and second ionization constants of H_3PO_4, respectively, and K_x and K_y are the association constants for the ion-pairs $[CaHPO_4]^\circ$ and $[CaH_2PO_4]^+$. A list of the numerical values for the various constants used in this investigation is given in the appendix.

The three condition functions, eqs (1–3), were used to obtain the best estimates of K_{sp} for the preheated hydroxyapatites (in air and steam). Condition (3), defining stoichiometric dissolution, was excluded for the calculations with HA "as prepared" because phosphate was adsorbed in some of these equilibrations, as explained in section 5.1.

Equation (4) was obtained from the simultaneous solution of eqs (9) and (10) which describe the equilibria involved in the formation of ion pairs. Calling X the concentration of $[CaHPO_4]^\circ$ and Y that of $[CaH_2PO_4]^+$,

$$X = \frac{K_x[M-\tau][P-\tau] f_{Ca^{++}}}{Q_2 f_x} \quad (9)$$

$$Y = \frac{K_y[M-\tau][P-\tau] f_{Ca^{++}} (H^+)}{Q_2 K_2 f_y} \quad (10)$$

in which f_x and f_y are the activity coefficients for the species $[CaHPO_4]^\circ$ and $[CaH_2PO_4]^+$, respectively.

The ionic strength, μ, was defined in these calculations by

$$\mu = 2[M-\tau] + 1/2\left[\frac{(H^+)}{f_{H^+}} + \frac{K_w}{(H^+) f_{OH^-}} + R\tau + \frac{(P-\tau)Q_3}{Q_2}\right] \quad (11)$$

in which

$$Q_3 = \frac{(H^+)}{K_2 f_{H_2PO_4^-}} + \frac{4}{f_{HPO_4^=}} + \frac{9K_3}{(H^+) f_{PO_4^{\equiv}}}. \quad (12)$$

The values for the ionic activity coefficients were calculated by the use of the Debye-Hückel theory using the distances of the closet approach given in the appendix. The iterative procedure, starting with unitary activity coefficients, reported in previous publications [9, 18] was used for these calculations. The activity coefficients f_x and $f_{H_3PO_4}$ were taken to be unity, and it was assumed that $f_y = f_{H_2PO_4^-}$.

5. Results

5.1. Solubility of HA

The experimental results for the steam-heated and air-heated preparations are given in tables 1 and 2, respectively, along with the values of K_{sp} calculated from these results using the activity product that appears as the leading term in eq (2). The spread in K_{sp} in each table is acceptably low even though the average K_{sp} for the steam-heated material, table 1, is three orders of magnitude less than that for the air-heated material, table 2. The other tests that can be applied to these data—apparent electroneutrality unbalance, stoichiometry of the dissolution reaction, and smoothness of the plots of Ca or P versus pH—also show deviations which are within the anticipated experimental errors, thus vouching for the validity of the results. In tables 3 and 4 are given the adjusted values for the three observables, Ca, P, and pH, and the adjusted values of K_{sp}, electroneutrality and the ratio Ca/P of the dissolution reactions. It is clear that the adjustments in the Ca, P, and pH values are within their anticipated experimental errors. The fact that these adjustments are small is further confirmation of the internal consistency of the data. We believe that the best estimate of the two K_{sp}'s obtained by the adjustment procedure (tables 3 and 4), which weights the experimental measurements according to their errors, constitute better values for the solubility products than the simple unweighted mean values, given in tables 1 and 2.

TABLE 1. *Solubility of steam-heated* HA, *unadjusted quantities*

Initial $[H_3PO_4]$ $M \times 10^3$	Composition of saturated solution			Ca/P Dissol. Reac.	$K_{sp} \times 10^{55}$
	pH	[P] $M \times 10^3$	[Ca] $M \times 10^3$		
4.17	5.04_9	6.19	3.16	1.56	3.7_0
2.00	5.40_0	2.94	1.49	1.58	5.1_4
1.00	5.69_0	1.50	0.79	1.59	5.2_1
1.00	5.74_7	1.48	.78	1.64	9.7_1
0.30	6.22_1	0.46	.25	1.50	2.9_9
				Avg. 1.57 ± 0.02[a]	$5.3_8 \pm 2.6_2$[a]

[a] Standard errors in the means.

TABLE 2. *Solubility of air-heated* HA, *unadjusted quantities*

Initial $[H_3PO_4]$ $M \times 10^3$	Composition of saturated solution			Ca/P Dissol. Reac.	$K_{sp} \times 10^{55}$
	pH	[P] $M \times 10^3$	[Ca] $M \times 10^3$		
2.04	5.76_8	3.02	1.62	1.65	2.5_7
1.98	5.79_0	3.00	1.57	1.53	3.1_3
0.99	6.11_9	1.39	0.76	1.90	2.3_6
1.01	6.12_8	1.46	.83	1.85	4.1_3
1.01	6.13_0	1.51	.84	1.70	5.6_2
0.50	6.40_6	0.75	.49	1.95	3.8_2
.10	7.07_1	.19	.15	1.60	3.6_0
.05	7.36_2	.11	.09	1.62	2.2_7
				Avg. 1.72 ± 0.02[a]	$3.4_1 \pm 0.1$[a]

[a] Standard errors in the means.

TABLE 3. *Solubility of steam-heated* HA, *adjusted quantities*

Initial $[H_3PO_4]$ $M \times 10^3$	Composition of saturated solution			Ca/p Dissol. Reac.	r[a]	Ionic strength $\mu \times 10^3$	Apparent charge imbalance $M \times 10^6$	K_{sp} $\times 10^{58}$
	pH	[P] $M \times 10^3$	[Ca] $M \times 10^3$					
4.28	5.05_7	6.13	3.10	1.68	0.03_6	9.10	0.0	3.7_3
2.00	5.38_9	2.89	1.47	1.67	$.02_4$	4.40	−.1	3.9_2
1.02	5.69_2	1.48	0.77	1.67	$.01_7$	2.32	.0	3.9_2
1.00	5.72_0	1.45	.75	1.67	$.01_6$	2.28	−.3	5.3_1
0.31	6.23_6	0.46	.25	1.68	$.01_2$	0.80	.0	3.8_5
							$S = 3.7_3 \pm 0.4_8$[b]	

[a] Fraction of Ca present as ion pairs.
[b] Standard error from least-squares adjustment.

TABLE 4. *Solubility of air-heated* HA, *adjusted quantities*

Initial $[H_3PO_4]$ $M \times 10^3$	Composition of saturated solution			Ca/P Dissol. Reac.	r[a]	Ionic strength $\mu \times 10^3$	Apparent charge imbalance $M \times 10^6$	K_{sp} $\times 10^{55}$
	pH	[P] $M \times 10^3$	[Ca] $M \times 10^3$					
2.06	5.77_2	3.02	1.59	1.67	0.03_1	4.75	0.0	2.5_1
2.02	5.78_5	2.94	1.55	1.68	$.03_1$	4.64	−.1	2.5_7
0.96	6.11_3	1.42	0.78	1.69	$.02_7$	2.39	.0	2.5_2
.99	6.10_2	1.47	.81	1.68	$.02_8$	2.48	−.2	2.8_0
1.00	6.10_8	1.49	.82	1.67	$.02_8$	2.52	−.5	3.2_6
0.50	6.40_0	0.77	.44	1.68	$.02_4$	1.42	.0	2.6_6
.11	7.08_8	.19	.14	1.68	$.01_7$	0.48	.0	2.6_2
.05	7.39_3	.11	.09	1.67	$.01_4$	0.33	.0	2.5_3
							$S = 2.5_1 \pm 0.3_7$[b]	

[a] Fraction of Ca present as ion pairs.
[b] Standard error from least-squares adjustment.

The large difference between the two K_{sp} values (tables 3 and 4) probably relates to structural changes induced by the heat treatments, as discussed later.

Also listed in tables 3 and 4 are the values for ionic strength and the fraction, r, of Ca present in the form of ion pairs given by τ/M. The gradual increase in r with decreasing pH relates to the increase in Ca and P concentrations, and is mostly the result of an increase in the concentration of the ion-pair $[CaH_2PO_4]^+$.

Results of the solubility experiments for the "as prepared" HA are shown in table 5. The large variation in the K_{sp} values in table 5 is believed to relate to the presence of other calcium phosphates less basic than HA; evidence for this type of contamination is presented in section 3. The data also suggest the presence of an anion foreign to the system $Ca(OH)_2$-H_3PO_4-H_2O as evidenced by an apparent positive electroneutrality unbalance which is far beyond experimental error for the three treatments with pH's above 6. This may have been caused by carbonate since the infrared spectrum showed small $CO_3^=$ peaks.

TABLE 5. *Solubility of "as prepared"* HA, *unadjusted quantities*

Initial $[H_3PO_4]$ $M \times 10^3$	Final solution composition			$K_{sp} \times 10^{58}$
	pH	[P] $M \times 10^3$	[Ca] $M \times 10^3$	
7.82	4.74_9	10.17	5.11	0.8_4
3.05	5.26_9	3.43	1.67	1.5_4
0.49	6.60_2	0.23	0.16	11.9_4
.20	7.05_1	.06	.10	10.9_4
.05	7.45_6	.03	.11	251.2

Interpretation of the data in table 5 is further complicated by sorption phenomena; for example the phosphorus concentrations in the solutions for the last three entries of table 5 are less than the initial H_3PO_4 concentrations. A systematic study of this type of surface phenomenon with finely divided HA has been reported elsewhere [20]. Although some of the K_{sp} values in table 5 are in the range of those given in table 1 for the steam-heated HA, the three at the higher pH's are abnormally large. Furthermore, the calculated adjustments of the measurements, not shown here, were so large as to invalidate the least squares procedure. As a result, little weight is given to the set of data in table 5. They give some confirmation in the low pH range of the results obtained for the steam-heated HA and they illustrate how the solutions can be made supersaturated in the high pH range by the presence of calcium phosphates less basic than HA.

The phosphorus concentrations of the solutions saturated with respect to the preheated HA's, tables 1 and 2, are plotted against their corresponding pH's in figure 1. Similar plots for solutions saturated with respect to $CaHPO_4 \cdot 2H_2O$ (DCPD) [17, 18] and $CaHPO_4$ (DCPA) [19] at 25 °C are also shown in the same figure. The HA curves were extrapolated (dotted lines) to meet the intersection points A, B, C, and D in figure 1. These four points correspond to singular points between the preheated HA's and DCPD or DCPA. The chemical compositions of the solutions at the singular points were calculated by solving eq (13) for (H^+) through a method of successive approximations,

$$\frac{2(H^+)^2 K_{DC} K}{f_{Ca^{++}}} + \frac{(H^+)}{f_{H^+}} + \frac{R K_x K_{DC}}{1-R} - \frac{Q_1}{(H^+)^2 K} - \frac{K_w}{(H^+) f_{OH^-}} = 0 \qquad (13)$$

318-092 O-69—15

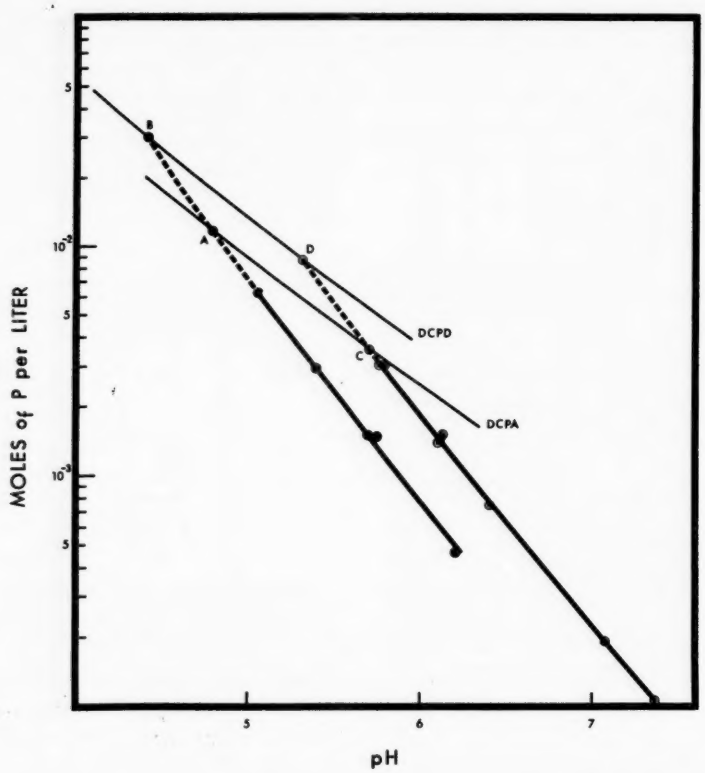

FIGURE 1. *Solubility isotherms of steam-heated HA, full circles, and air-heated HA, open circles, at 25 °C.*

The two lighter curves are the isotherms of $CaHPO_4 \cdot 2H_2O$ [17], DCPD, and $CaHPO_4$ [19], DCPA. Compositions of the calculated singular points A, B, C, and D are given in table 6.

in which K_{DC} represents the solubility product constant for either DCPD or DCPA, as the case may be, and K is defined by

$$K=\left[\frac{K_{sp}}{K_3^3 K_{ic} K_{DC}^5}\right]^{1/2} \tag{14}$$

The value for (H^+) obtained from eq (13) was then used to obtain the numerical value of τ since, for saturation with respect to either DCPD or DCPA,

$$\tau=\frac{K_x K_{DC}}{1-R}. \tag{15}$$

The concentrations of calcium and phosphorus are obtained from eqs (16) and (17), respectively.

$$M=\frac{(H^+)^2 K_{DC} K}{f_{Ca^{++}}}+\tau \tag{16}$$

$$P=\frac{Q_2}{(H^+)^2 K}+\tau. \tag{17}$$

The chemical compositions of the solutions at the four singular points, calculated in the foregoing fashion, are given in table 6. Considerably higher concentrations of Ca and P (and lower pH's) are found at the singular points of the preheated HA's with DCPD than at the corresponding singular points with DCPA; the same pattern is observed for the fractions of Ca present as ion pairs (r in the table). These results are a consequence of the higher solubility of DCPD [17, 18] relative to the anhydrous salt at 25 °C [19]. The most striking differences in the compositions at the singular points, however, are brought about by the solubility of the HA itself. Thus, a full pH unit difference exists between the singular points of air-heated and steam-heated HA with either of the two dicalcium phosphates; changes in calcium and phosphorus concentrations by factors of about 3.5 and 4, respectively, parallel this pH difference. If, as it is apparent from the present results, the solubility of HA depends upon the previous history of the sample, it is nearly impossible to predict the composition of singular points between a precipitated HA and other calcium phosphates without fully characterizing the solubility properties of the HA involved.

TABLE 6. *Solution compositions at singular points*

Solid phases	pH	[P] $M \times 10^3$	[Ca] $M \times 10^3$	r[a]
DCPD + HA (air)	5.31_5	8.64	4.43	0.05_4
DCPD + HA (steam)	4.41_6	30.21	15.09	$.10_9$
DCPA + HA (air)	5.70_1	3.53	1.85	$.03_8$
DCPA + HA (steam)	4.79_1	11.54	5.80	$.05_8$

[a] Fraction of Ca present as ion pairs.

Although the weight loss in our sample was not measured, slight weight losses have been reported [22] in the range 1,000 to 1,100 °C for synthetic HA samples heated gradually from 25 to 1,200 °C; these losses occurred without alteration in the x-ray patterns. Also, it has been reported [23] that at 1,200 °C in air, disproportionation of HA into tricalcium phosphate and tetracalcium phosphate occurs according to the reaction,

$$2Ca_5OH(PO_4)_3 \rightarrow 2\,\alpha\text{-}Ca_3(PO_4)_2 + Ca_4O(PO_4)_2 + H_2O. \quad (18)$$

The x-ray powder diffraction pattern of the air-heated sample was the same as that of HA, but it is impossible to rule out a partial disproportionation.

In view of the foregoing considerations, there are two explanations for the higher solubility of the air-heated HA: (1) Reversal of the disproportionation reaction [18] when the sample is returned to an aqueous system might yield very finely divided HA with an unusually high solubility because of surface energy contribution, or (2) loss of OH^- ions by dehydration during heating of the solid, without destruction of the HA lattice, might yield crystals with higher free energy. Evidently, the process responsible for the increased solubility is not readily reversible, since otherwise the values for the K_{sp} of the two preparations would have been the same. Therefore, the equilibria attained with the air-heated HA must have been metastable relative to the more stable form of HA. This would require that the rate of dissolution of the air-heated HA was higher than the rate of precipitation of the more stable salt.

The K_{sp} values for the two kinds of preheated apatites correspond to a difference of about 16 kJ/mol (3.9 kcal/mol) in the standard free energies of formation. If it were assumed that the standard heat of formation is the same for both compounds, the observed difference in free energy would correspond to about 59 J/mol K (14 cal/mol K) less entropy in the air-heated apatite than in the steam-heated salt. This difference appears too large to be associated with a change in entropy resulting from vacancies or ordering. For this reason it is believed that the difference in solubility is mostly related to a difference in their heat contents.

6. Discussion

6.1. Solubility of HA

The solubility data given in tables 1 and 2 for the two preheated HA samples are consistent with stoichiometric dissolution represented by the reaction $Ca_5OH(PO_4)_3 \rightleftarrows 5Ca^{++} + OH^- + 3PO_4^{\equiv}$. It is believed that saturation conditions were obtained in the two-week equilibrations as evidenced by the smooth curves obtained in the plots of calcium concentration versus pH (fig. 1), calcium concentration versus phosphorus concentration (not shown in this paper), and a reasonable constancy in the ionic activity product for HA. The success of the adjustment procedure described in section 4 is additional evidence that the parameters S, tables 3 and 4, are valid solubility product constants for the preheated hydroxyapatites.

The higher solubility product constant obtained for the HA heated in air, relative to the product obtained for the sample heated in steam, is most probably due to structural changes induced by the thermal treatment. Such changes might relate in part to the statistically disordered structure of HA described by Kay et al. [21], originating from small displacements of the OH^- groups from the mirror planes in the space group $P6_3/m$. If this were purely an entropy effect, such disorder would tend to stabilize the lattice; the steam-heated sample, therefore, would have to be the disordered one. However, it is difficult to see why heating HA in air would induce more order in the OH^- groups than would be obtained by heating in steam. A more likely explanation is that heating in air results in loss of OH^- groups by partial dehydration of the HA. Indeed, the infrared spectra tend to substantiate this alternative. Whereas the half width of the peak at 3,570 cm^{-1} corresponding to the OH^- stretching mode, was essentially the same for both preheated hydroxyapatites, its height for the steam-heated HA was almost twice that of the air-heated HA.

6.2. Singular Points

A system of two solid phases in equilibrium with an aqueous phase in the ternary system $Ca(OH)_2$-H_3PO_4-H_2O is characterized by zero degrees of freedom (under conditions of constant temperature and pressure). Such singular points are important in solubility diagrams because they correspond to points where there is a change in the relative stability of the two solid phases. Thus, with reference to table 6, in saturated solutions with pH's below 4.33, DCPD is more stable than the steam-heated HA; in solutions with pH's above 4.33, steam-heated HA is more stable than DCPD. The greater solubility of the air-heated HA has the effect of increasing the pH of the singular points with the dicalcium phosphates by about one pH unit relative to those with steam-heated HA. If an apatite comparable to the air-heated HA were formed in oral environments, its greater solubility would extend the stability ranges of the two dicalcium phosphates to conditions which occur in saliva in vivo.

In the concentration ranges covered by the present experiments, the degree of ion-pair formation varied from about 1.4 percent (at the highest pH) to about 3.4 percent (at the lowest pH) of the total calcium concentration. In view of the uncertainty, both theoretical and experimental in these calculations for nonsymmetrical electrolytes, the formation of ion-pairs in the experimental segments of the solubility isotherms for HA is not considered significant. However, in more acid solutions, such as those of the calculated singular points, the ion-pair formation does become significant.

6.3. Stoichiometry and Potential Diagrams

The stoichiometry of a solid calcium phosphate equilibrated with aqueous solutions is easily revealed by the use of "potential diagrams" [24, 25, 26]. These are solubility diagrams in which the coordinates are functions of the chemical potentials of the components, $Ca(OH)_2$ and H_3PO_4, in solution. For example, if the quantity $-\log (Ca^{++})(OH^-)^2$ is plotted against $-\log (H^+)^3(PO_4^{\equiv})$, the saturation condition is defined by a straight line and the absolute value of its slope corresponds to the reciprocal of the Ca/P ratio in the solid. This kind of diagram is illustrated in figure 2 with calculations based on the data for the two preheated apatites (tables 1 and 2). Similar calculations were made with data from other investigators and these are plotted in the same diagram. The slopes and their standard errors, of the regression lines for the air-heated and steam-heated apatites shown in figure 2 correspond to apparent Ca/P ratios of 1.69 and 1.68 with standard errors of 0.02 and 0.07, respectively. These ratios agree with the theoretical ratio for HA, 1.67, and the ratio, 1.68 obtained by chemical analysis of the untreated solid. In view of these facts, the relatively low value obtained for the Ca/P ratio in the dissolution reaction, 1.57, of the steam-heated preparation, table 1, must be ascribed to experimental errors. It is to be noted that the Ca/P ratio calculated from dissolution involves a difference between two experimental measurements.

6.4. Comparison With Reported Data

Clark [1] reported a value of 57.75 as his best estimate of pK_{sp} (the negative logarithm of K_{sp}) of HA at 25 °C. (The actual value he reported, 115.5, is based on the formula $Ca_{10}(OH)_2(PO_4)_6$ rather than the formula $Ca_5OH(PO_4)_3$ used here.) His systems consisted of HA precipitated by mixing dilute solutions of $Ca(OH)_2$ and H_3PO_4 at 90 °C; he kept the resulting suspensions at that temperature for 120 hr and reequilibrated them at 25 °C for 90 hr. The K_{sp} corresponding to his pK_{sp} value of 57.75 is 1.78×10^{-58}, which is in good agreement with the value 3.73×10^{-58} reported here for the steam-heated HA. The individual values reported by Clark range from 0.53×10^{-58} to 7.59×10^{-58}. Even though Clark's data, as plotted in the chemical potential diagram, figure 2, have some scatter, it is apparent that they approximate closely the same line as our data for the steam-heated HA. The same author observed that equilibrations made at 25 °C with HA precipitated at 40 °C resulted in large apparent supersaturations with respect to the

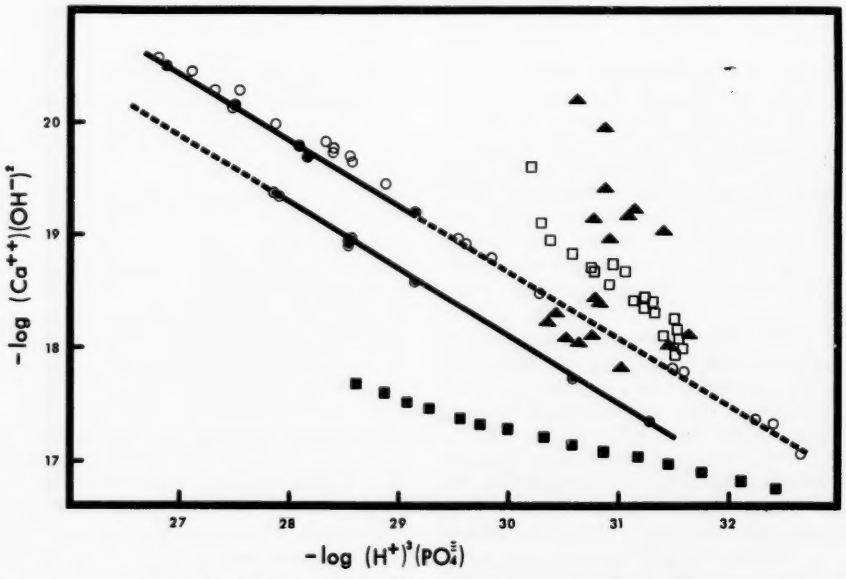

FIGURE 2. *Potential plot, calcium hydroxide versus phosphoric acid.*
●, steam-heated HA; ⊙, air-heated HA; ○, data from Clark [1]; ▲, data from Levinskas and Neuman [31]; □, data from Rootare et al. [5] at 25 °C; ■, data from Rootare et al. [5] at 40 °C.

values for K_{sp} given above. In light of present knowledge, one would expect that those precipitates contained some of the more acid calcium phosphate which are more soluble than HA. Thus, the more reliable of Clark's results agree with those reported here for steam-heated HA. We consider it significant that such good agreement was obtained between materials prepared by precipitation from aqueous systems and a material subjected to annealing at 1,000 °C in a steam atmosphere. This suggests that the K_{sp} value obtained for the steam-heated material is characteristic of any well-crystallized HA.

A solubility product constant for HA was calculated from the following thermodynamic quantities: $\Delta H_f^\circ = -13{,}439$ kJ/mol ($-3{,}212$ kcal/mol) reported by Smirnova et al. [2] for HA which had also been heated at 1,000 °C in the presence of steam; $S^\circ = 780.7$ J/mol K (186.6 cal/mol K) reported by Egan and Wakefield [4] for another HA treated in a similar way, and standard entropies of formation of the elements and standard free energies of formation of ions reported in NBS Publications [27, 28]. The product thus obtained, based on the formula $Ca_5OH(PO_4)_3$, is of the order 10^{-57}.

This result, too, is considered to be in good agreement with the order of magnitude given here, 10^{-58}, for the steam-heated apatite, considering the uncertainties in some of the thermodynamic quantities used and the great effect that small variations in these quantities have on the K_{sp} calculated in this fashion.

The foregoing results are not in agreement with those of Levinskas [29], Levinskas and Neuman [6], and Neuman and Neuman [7] who concluded that synthetic preparations of HA equilibrated in aqueous solutions do not obey the solubility-product constant principle. One of the hydroxyapatites (L-apatite) most extensively studied by these authors was a commercial preparation of fine particle size, 68 m^2/g. The large surface areas of their materials could introduce difficulties in the interpretation of solubility studies. However neither theoretically [30] nor experimentally [20] do sorption phenomena invalidate the application of the solubility product constant to systems equilibrated with HA. It should be pointed out that the sample of HA (L-apatite) used by Neuman and co-workers had a refractive index of 1.605 [5] which is much too low for a well-crystallized HA; in addition, their preparation was contaminated with calcite, contained 0.28 percent sulfate and 0.8 percent CO_2 [5]. No history is given for the synthesis of L-apatite, but the analytical results clearly show the heterogeneity of the sample. Under these circumstances, reactions other than simple dissolution and precipitation of HA are to be expected, and their involved kinetics is a burden for sound interpretations of solubility studies. The adoption of the ion-activity product $(Ca^{++})(HPO_4^=)$ to characterize HA systems, as suggested by Neuman and co-workers [7, 29] cannot be justified on theoretical bases [30]. Our recalculation of their data [31] plotted in figure 2 shows that the points are widely scattered, do not define a single line, and cannot be used to derive a reliable K_{sp} for a solid of any Ca/P ratio.

Rootare, Deitz, and Carpenter [5] reported results on solubility studies done with several commercial and laboratory-prepared samples. They observed wide variations in the calculated ion-activity products for HA; these were explained by postulating formation of a surface complex according to the reactions,

$$Ca_{10}(PO_4)_6(OH)_2 + 6H_2O \rightleftarrows 4Ca_2(HPO_4)(OH)_2] + 2Ca^{++} + 2HPO_4^= \quad (19)$$

$$Ca_2(HPO_4)(OH)_2 \rightleftarrows 2Ca^{++} + HPO_4^= + 2OH^- \quad (20)$$

It is true, as they claim, that the ionic product calculated according to eq (20) showed less variability (pK values from 24.6 to 26.8) than those calculated for HA on the basis of the formula unit $Ca_{10}(OH)_2(PO_4)_6$ (pK from 108 to 120). However, the mechanism postulated by Rootare et al. is open to the following criticisms: (a) Although the composition of the HA surface does not have to conform necessarily to the stoichiometry of the bulk solid, there is no a priori reason to postulate that certain surface compositions will prevent equilibrium with the crystalline HA lattice [30]; (b) It is highly improbable that the surface of HA equilibrated in aqueous solutions has a definite composition independent of the composition of the aqueous medium [20]; (c) If a definite composition is ascribed to the "surface complex" and the solubility product principle is applied according to its stoichiometry, it is mandatory that such species be considered as another solid phase (i.e., has constant molar free energy and stoichiometry [30]); then, in the light of eqs (19) and (20), the system would have zero degrees of freedom (in the system $Ca(OH)_2$-H_3PO_4-H_2O) under fixed temperature and pressure [30] so that the solution composition could not vary as observed by them; (d) It can be easily shown that the equilibrium conditions [19] and [20], as given by Rootare et al., also imply equilibrium with respect to the HA solid phase; (e) Of the 12 samples used by Rootare et al., only four were petrographically homogeneous [5]; the rest were contaminated with calcite varying from traces to about 1 percent, with sulfate varying from 0.006 to 0.29 percent and, with the exception of two, all the samples contained carbonate in significant amounts; only the four samples prepared in the laboratory showed a refractive index approaching the one expected for well-crystallized HA; one of the latter, P–20, probably contained less basic calcium phosphates as evidenced by a Ca/P ratio of 1.583 and the report by Gee [32] that pyrophosphate was formed upon heating it at 600 °C for 60 hr.

The results reported by Rootare et al. [5] form two distinct populations when plotted in figure 2. The regression line for the points at 25 °C (the point 30.20, 19.61 excluded) has a slope of -0.778, which would correspond to a ratio of Ca/P = 1.28 in the solid phase.

The points from treatments at 40 °C appear to define two lines with slopes -0.309 and -0.211 which would correspond to Ca/P ratios of 3.24 and 4.74 in the solid. If equilibrium with respect to $Ca_2(HPO_4)(OH)_2$ had been established, as claimed by Rootare et al. [5], lines with slope of -0.5 (Ca/P = 2) should have been defined by their data in the potential plot. The fact that their data define two or three Ca/P ratios, none of which correspond to their postulated surface complex, along with the other criticisms listed above, argue very strongly against the existence of the surface complex hypothesized by them. LaMer [8] reexamined the data of Rootare et al. [5] and came to the conclusion that the product, $(Ca^{++})(HPO_4^{=})$ showed the least variation. However, for the reasons given above, this is not an adequate basis for any conclusions regarding the nature of the equilibrating solid phase.

In the light of the foregoing results and discussion we conclude that our samples of preheated HA did equilibrate according to the stoichiometry of HA and according to the usual solubility product principles, that the steam-heated HA yielded a solubility constant usable as a frame of reference for well-crystallized HA, and that most of the difficulties reported in the literature on this matter relate to contamination of the solid and lack of equilibrium between the solution and the solid.

7. Appendix

Ionic activity coefficients were calculated from the extension of the Debye-Hückel limiting law,

$$\log f_i = -\frac{AZ_i^2\sqrt{\mu}}{1+\mathrm{Ba}_i\sqrt{\mu}}. \qquad (21)$$

The values used [33] for the temperature-dependent constants A and B were 0.5092 and 0.3286×10^8, respectively; those for the parameters a_i [34] were Ca^{++}, 6×10^{-8} cm; $H_2PO_4^-$, $HPO_4^=$, and $PO_4^{\equiv}$, 4×10^{-8} cm; H^+, 9×10^{-8} cm; and OH^-, 3.5×10^{-8} cm.

The values used for the three ionization constants of H_3PO_4 were K_1, $7.10_8\times10^{-3}$ [35]; K_2, $6.31_8\times10^{-8}$ [36]; K_3, 4.73×10^{-13} [37]; and for K_w, 1.012×10^{-14} [38]. The association constants used in this paper are defined by

$$K_x = \frac{[CaHPO_4]^\circ}{(Ca^{++})(HPO_4^{=})} \qquad K_y = \frac{(CaH_2PO_4^+)}{(Ca^{++})(H_2PO_4^-)}$$

with values [17] K_x, 244.0; and K_y, 8.20.

The points in the potential plot (fig. 2) corresponding to the data of Rootare et al. [5], at 40 °C were calculated using the following constants: K_1, $5.99_6\times10^{-3}$ [35]; K_2, $6.60_7\times10^{-8}$ [36]; K_3, $7.58_6\times10^{-13}$ [39]; K_w, 2.936×10^{-14} [38]; A, eq (21), 0.524_1 [33]; and B, 0.3318×10^8 [33].

8. References

[1] Clark, J. S., Can. J. Chem. **33,** 1696 (1955).
[2] Smirnova, F. G., Illarionov, V. V., and Vol'fkovich, S. I., Russian J. Inorg. Chem. **7,** 920 (1962).
[3] Jacques, J. K., J. Chem. Soc. 3820 (1963).
[4] Egan, E. P., Jr., Wakefield, Z. T., and Elmore, K. L., J. Am. Chem. Soc. **73,** 5579 (1951).
[5] Rootare, H. M., Deitz, V. R., and Carpenter, F. G., J. Colloid Sci. **17,** 179 (1962).
[6] Levinskas, G. J., and Neuman, W. F., J. Phys. Chem. **59,** 164 (1955).
[7] Neuman, W. F., and Neuman, M. W., The Chemical Dynamics of Bone Mineral, p. 30 (University of Chicago Press, Chicago, Ill., 1958).
[8] LaMer, V. K., J. Phys. Chem. **66,** 973 (1962).
[9] Moreno, E. C., Gregory, T. M., and Brown, W. E., J. Res. NBS **70A** (Phys. and Chem.) No. 6, 545 (1966).
[10] Bates, R. G., J. Res. NBS **66A** (Phys. and Chem.) No. 2, 179 (1962).
[11] Banerjee, D. K., Budke, C. C., and Miller, F. D., Anal. Chem. **33,** 418 (1961).
[12] Brabson, J. A., Dunn, R. L., Epps, E. A., Jr., Hoffman, W. M., and Jacob, K. D., J.A.O.A.C. **41,** 517 (1958).
[13] ASTM Powder diffraction file, Card No. 9-432.
[14] Fowler, B. O., Moreno, E. C., and Brown, W. E., Arch. Oral Biol. **11,** 477 (1966).
[15] Deming, W. E., Statistical Adjustment of Data (John Wiley & Sons, Inc., New York, 1943).
[16] Wentworth, W. E., Hirsch, W., and Chen, E., J. Phys. Chem. **71,** 218 (1967).
[17] Gregory, T. M., Moreno, E. C., and Brown, W. E. (Abstract), Internat. Assoc. Dental Res., 45th General Meeting, Washington, D.C. (1967).
[18] Moreno, E. C., Brown, W. E., and Osborn, G., Soil Sci. Soc. Amer. Proc. **24,** 94 (1960).
[19] McDowell, H., Ph. D. Thesis, Howard University, Washington, D.C. (1967).
[20] Avnimelech, Y., Moreno, E. C., and Brown, W. E. (Abstract), Internat. Assoc. Dental Res., 45th General Meeting, Washington, D.C. (1967).
[21] Kay, M. I., Young, R. A., and Posner, A. S. Nature **204,** 1050 (1964).
[22] Egan, E. P., Jr., Wakefield, Z. T., and Elmore, K. L., J. Am. Chem. Soc. **72,** 2418 (1950).
[23] Bredig, M. A., Franck, H. H., and Füldner, H., Z. Elecktrochem. **39,** 959 (1933).
[24] Aslyng, H. C., Royal Vet. and Agric. Coll. Copenhagen, Denmark, Yearbook Reprint, pp. 1–50 (1954).
[25] Moreno, E. C., Lindsay, W. L., and Osborn, G., Soil Sci. **90,** 59 (1960).
[26] MacGregor, J., and Brown, W. E., Nature **205,** 359 (1965).
[27] National Bureau of Standards. Selected Values of Chemical Thermodynamic Properties, Circ. 500 (1952).
[28] National Bureau of Standards. Technical Note 270–1 (1965) and Technical Note 270–2 (1966).
[29] Levinskas, G. J., Ph. D. Thesis, University of Rochester, New York (1953).
[30] Brown, W. E., Moreno, E. C., and Gregory, T. M., Thermodynamics of hydroxyapatite solubility. In preparation.
[31] Table 2 of reference 6.
[32] Gee, A., Proc. Third Tech. Session on Bone Char. p. 337 (1953).
[33] Manov, G. G., Bates, R. G., Hamer, W. J., and Acree, S. F., J. Am. Chem. Soc. **65,** 1765 (1943).
[34] Kielland, J., J. Am. Chem. Soc. **59,** 1675 (1937).
[35] Bates, R. G., J. Res. NBS **47,** 127 (1951) RP2236.
[36] Bates, R. G., and Acree, S. F., J. Res. NBS **34,** 373 (1945) RP1648.
[37] Tennessee Valley Authority. Chem. Eng. Report No. 8 (1950).
[38] Harned, H. S., and Owen, B. B., The physical chemistry of electrolytic solutions, p. 645 (equation 15–3–7a), (Reinhold Publishing Corporation, New York, 1958).
[39] Bjerrum, N., and Unmack, A., Kgl. Danske Videnskab. Selskab., Math-fys. Medd. **9,** 5 (1929).

(Paper 72A6–527)

JOURNAL OF RESEARCH of the National Bureau of Standards—A. Physics and Chemistry
Vol. 72A, No. 6, November–December 1968

High Temperature Dehydroxylation of Apatitic Phosphates

T. Negas and R. S. Roth

Institute for Basic Standards, National Bureau of Standards, Washington, D.C. 20234

(August 7, 1968)

$Sr_{10}P_6O_{24}(OH)_2$, (Hex. $a=9.765$ Å, $c=7.280$ Å), and $Ba_{10}P_6O_{24}(OH)_2$, (Hex. $a=10.177$ Å, $c=7.731$ Å), undergo cell parameter contractions at elevated temperatures in air. These can be correlated with progressive dehydroxylation, although neither can be completely dehydrated. $Pb_{10}P_6O_{24}(OH)_2$, (Hex. $a=9.878$ Å, $c=7.432$ Å), also does not completely dehydrate in air.

A new apatite-like strontium phosphate, (Hex. $a=9.872$ Å, $c=7.199$ Å), was prepared at elevated temperatures in vacuum.

Key Words: Apatite, dehydroxylation, high temperature, phosphates, x-ray diffraction.

1. Introduction

The existence of the so-called oxyapatites, has been a subject of much controversy. Associated is the problem concerning the existence and nature of phases produced from the dehydroxylation of hydroxyapatite. The general cell content formula for hydroxyapatite is

$$A_{10}B_6O_{24}(OH)_2, \text{ space group } P6_3/m$$

where A is a large cation distributed in 7- and 9-fold sites [1][1] and B a small cation in tetrahedral coordination. Ideally, each $(OH)^-$ is shared by three A ions. Dehydroxylation or substitution by O^{-2} for $(OH)^-$ may result in the formation of true oxyapatites in a number of ways.

If two O^{-2} anions replace the two $(OH)^-$ groups excess negative charge results. This necessitates either a valence change in the A or B cation sites or a change in the ratio of the constituents with the appearance of additional phases. Such compounds as $Sr_{10}Cr_6^{5+}O_{24}(OH)_2$ and $Ba_{10}Cr_6^{5+}O_{24}(OH)_2$ have oxyapatite counterparts which appear to be $Sr_{10}Cr_4^{5+}Cr_2^{6+}O_{24}O_2$ and $Ba_{10}Cr_4^{5+}Cr_2^{6+}O_{24}O_2$ [2]. The hydroxyapatites $Sr_4La_6Si_6O_{24}(OH)_2$ and $Na_2La_8Si_6O_{24}(OH)_2$ dehydrate to oxyapatites according to:

$$8Sr_4La_6Si_6O_{24}(OH)_2 \xrightarrow{1100\ ^\circ C} 6Sr_2La_8Si_6O_{24}O_2 + 10Sr_2SiO_4 + 2SiO_2 + 8H_2O(g)$$

and

$$9Na_2La_8Si_6O_{24}(OH)_2 \xrightarrow{1100\ ^\circ C} 8NaLa_9Si_6O_{24}O_2 + (5Na_2O:6SiO_2)_{glass} + 9H_2O(g)$$

respectively [3]. Unit cell dimensions of all of the above oxyapatites are substantially different from those of their correspondingly related hydroxyapatites.

Theoretically, when the aforementioned mechanisms cannot operate, charge neutrality can be accomplished by the substitution of only one O^{-2} for two $(OH)^-$. Such a mechanism creates vacancies in half the available positions, an unacceptable condition to some workers [4, 5]. Nevertheless, such compounds as $Ba_{10}P_6O_{24}(OH_2)$, $Pb_{10}P_6O_{24}(OH)_2$, and $Sr_{10}P_6O_{24}(OH)_2$ have been reported to have $A_{10}B_6O_{24}O$ type oxy-analogs [6, 7, 8]. This paper deals with this class of hydroxyapatites and the question concerning the existence of oxy-analogs.

Recently, Kreidler and Hummel [8] reported that they synthesized $Sr_{10}P_6O_{24}O$ by the dehydroxylation of $Sr_{10}P_6O_{24}(OH)_2$ above 1400 °C in air and at 1400 °C in vacuum. From phase equilibria considerations they reasoned that a series of solid solutions exists between the hydroxy and oxyapatite having the general formula

$$Sr_{10}P_6O_{24}(OH)_{2-2x}O_xV_x$$

where $O \leqq X \leqq 1$ and V = a vacancy. Furthermore, x-ray powder patterns of $Sr_{10}P_6O_{24}(OH)_2$, synthesized below 1400 °C, and $Sr_{10}P_6O_{24}O$ were said to be identical. This latter interpretation seemed untenable considering the gross "defectiveness" of the oxyapatite phase. The writers have reinvestigated in detail the behavior of $Sr_{10}P_6O_{24}(OH)_2$ at elevated temperatures and extended the interpretation of these results to data obtained for barium-phosphorus and lead-phosphorus analogs.

[1] Figures in brackets indicate the literature references at the end of this paper.

2. Experimental Procedure

Starting materials of $Sr_{10}P_6O_{24}(OH)_2$ and $Ba_{10}P_6O_{24}(OH)_2$ were prepared in air by heating pressed pellets of the appropriate carbonate and $NH_4H_2PO_4$ (10:6 molar ratio mixture) from room temperature to 300 °C, then at 600 °C and 900 °C with intermediate grinding and pressing.[2] To avoid reaction of the alkaline earths, particularly barium, with platinum, syntheses were carried out on gold. The 900 °C Sr-apatite starting material was not effervesecent in HCl. The 900 °C Ba-apatite, however, was weakly effervescent indicating either retention of carbonate as a structural component or free unreacted $BaCO_3$. Specimens heated above 1000 °C were not effervescent in HCl. Portions of each apatite batch were mixed with distilled water, sealed in platinum capsules and reheated at 300 °C for five days in a Morey bomb. X-ray powder patterns of the phases produced in such a hydrothermal manner are identical to those synthesized in air. The strontium apatite was heated at 100 °C intervals in open gold envelopes (below 1000 °C) or platinum tubes (> 1000 °C), using small portions of the apatite previously synthesized in air. Above 1100 °C, the barium apatite could not be investigated using platinum tubes because of reaction with the metal. Instead, thin pressed wafers of the starting material were placed on two strands of fine platinum wire wrapped around an alumina dish and heated in this suspended manner.

Lead-phosphorous apatite was prepared in air and hydrothermally by the procedures described above except that the monoxide was used as the large cation source.

Specimens were heated in a platinum-wound tube-type horizontal furnace and cooled by rapid withdrawal. A number of heat treatments were made in vacuum using a modified quench furnace.

Phase analysis was accomplished predominantly by x-ray powder diffraction at room temperature using Ni-filtered copper radiation and $\frac{1}{4}$ deg 2θ per minute diffractometer scanning rate. Parameters may be considered to be accurate to ± 2 in the last decimal place listed. Supporting data were obtained by gravimetric measurements and nuclear magnetic resonance. Specimens for NMR examination were immediately transferred from the furnace to evacuated vycor tubes and sealed against contamination from atmospheric moisture.

3. Results and Discussion

3.1. $Sr_{10}P_6O_{24}(OH)_2$

The x-ray powder patterns of hydrothermal and low temperature (< 900 °C) "in air" apatite are identical and can be completely indexed on the basis of an hexagonal cell having $a = 9.765$ Å and $c = 7.280$ Å. On this basis, the 900 °C phase was considered fully hydroxylated and used as a compositional reference point for further experiments. With increasing temperature, commencing near 1000 °C, (fig. 1), unit-cell parameters continuously contract, reaching values of $a = 9.724$ Å and $c = 7.263$ Å at 1600 °C. Pertinent experimental data are given in table 1. The compound *does not* decompose with complete loss of H_2O at a fixed temperature as does, for example, $Sr_{10}Cr_6O_{24}(OH)_2$[2].

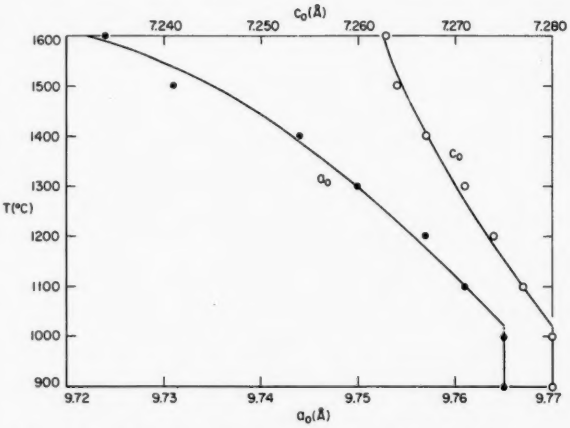

FIGURE 1. *Unit-cell parameter changes of strontium-phosphorus apatite as a function of the temperature of heating in air.*

Kreidler and Hummel [8] apparently failed to observe this unit cell contraction [3] but on reasonable thermodynamic grounds concluded that $Sr_{10}P_6O_{24}(OH)_2$ dehydroxylates in air with increasing temperature until above 1400 °C $Sr_{10}P_6O_{24}O$ exists. As shown in figure 1, cell contraction continues beyond 1400 °C and parameters *do not* attain constant values as would be expected if total dehydroxylation to $Sr_{10}P_6O_{24}O$ occurs. This suggests that even above 1400 °C a partially hydroxylated phase exists. A specimen of $Sr_{10}P_6O_{24}(OH)_2$, heated 40 hr at 1500 °C lost weight and then after reheating for 50 hr on gold at 900 °C regained weight suggesting the composition of the phase at 1500 °C to be

$$Sr_{10}P_6O_{24}(OH)_{0.74}O_{0.63}V_{0.63}$$

after compensation for loss of P_2O_5 at the higher temperature. Furthermore, NMR data unequivocably established the presence of protons in a specimen heated only at 1500 °C.

[2] Infrared absorption analysis indicated the presence of about 0.2 percent and 0.5 percent carbonate in the starting Sr- and Ba-apatites, respectively. Personal communication, Dr. Bruce Fowler, National Institutes of Health.

[3] After the completion of this manuscript, the writers received data from the dissertation of Kreidler (Ph.D. Thesis, The Pennsylvania State University, 1967). Cell contraction was observed with a conversion of hydroxy- to oxy-apatite in air at 1510 ± 15 °C.

TABLE 1. *Experimental Data for the Dehydroxylation of Phosphates*

T (°C)	Time (hrs)	a (Å)	c (Å)	Comments
Strontium-Phosphorus Apatite *				
800	100	9.765	7.280	
900	100	9.765	7.280	NMR **
300	120	9.765	7.280	Hydrothermally prepared.
1000	70	9.765	7.280	
1100	70	9.761	7.277	
1200	40	9.757	7.274	
1300	70	9.750	7.271	
1400	30	9.744	7.267	
1500	2, 20, 40	9.731	7.264	NMR **
1600	1	9.724	7.263	
900	5	9.765	7.280	Reversed from 1500 °C.
900	50	9.765	7.280	Reversed from 1500 °C; $Sr_{10}P_6O_{24}(OH)_{0.74}O_{0.63}V_{0.63}$ from weight loss and regain.
900	17	9.765	7.280	Reversed from 1400 °C.
1400	68	9.744	7.267	Reheat of 1500 °C specimen.
1500	2	9.731	7.264	Reheat of hydrothermal specimen.
1500	4	9.731	7.264	Initially a 3:1 mixture of $Sr_3(PO_4)_2$ and $SrCO_3$.
1100	70	9.84 9.72	7.21 7.26	Vacuum, 10^{-2} torr; two phases.
1250	113	9.729	7.240	Vacuum, 2×10^{-2} torr.
1270	70	9.872	7.199	Vacuum, 7×10^{-3} torr.
1275	110	9.872	7.199	Vacuum, 10^{-2} torr.
1350	115	9.728	7.240	Vacuum, 2×10^{-2} torr; NMR.**
1500	15	9.726	7.246	Vacuum; 3.8×10^{-4} torr, $Sr_4P_2O_9$ present; NMR analysis.
950	310	9.827	7.234	Reheat of 1270 °C, 7×10^{-3} torr material in air.
Barium-Phosphorus Apatite*				
700	96	10.177	7.731	
900	120	10.177	7.731	NMR.**
300	120	10.177	7.731	Hydrothermally prepared.
1000	50	10.175	7.728	
1200	20	10.170	7.719	
1300	20	10.164	7.714	
1400	48	10.157	7.705	
1500	20	10.148	7.696	
1500	20	10.148	7.696	NMR.**
1600	2	10.153	7.696	Partly melted?
900	5	10.177	7.731	Reheat of 1500 °C specimen.
900	16	10.177	7.731	Reheat of 1400 °C specimen.
Lead-Phosphorus Apatite*				
300	120	9.878	7.432	Hydrothermally prepared.
700	65	9.825	7.421	Reheat of hydrothermal specimen; $Pb_{10}P_6O_{24}(OH)_{0.26}O_{0.87}V_{0.87}$ by weight loss.
900	50	9.825	7.421	
925	75	9.825	7.421	Reheat of 700 °C specimen; NMR.**
1000		9.825	7.421	Melted and slow cooled to 950 °C in ½ hr.

*Unless otherwise indicated, heat treatments were made in air using starting material synthesized in air at 900 °C.

**NMR analysis indicated the presence of protons.

A number of questions naturally arise at this point. Do the curves shown in figure 1 represent equilibrium conditions, i.e., for each temperature at a fixed partial pressure of H_2O does there exist a stable anion deficient apatite characterized by specific unit cell parameters, or can the data be equally interpreted as being the manifestation of a kinetic problem in which $Sr_{10}P_6O_{24}(OH)_2$ converts very sluggishly, yet with increasing rate with increased temperature, to $Sr_{10}P_6O_{24}O$ through a series of defect states? If at each temperature there does exist an equilibrium phase characterized by a specific ratio of $(OH)^-:O^{-2}$: vacancies with unique cell parameters, a thermodynamically possible situation, are the anions and vacancies statistically disordered resulting in a true nonstoichiometric solid solution?

Specimens, generally, were heated for periods up to 100 hr to insure sufficient time to attain reproducible results. For example, specimens held 2 hr, 20 hr, and 40 hr at 1500 °C yielded apatite phases with identical cell parameters. The 20 hr 1500 °C specimen, held 68 hr at 1400 °C, and the 100 hr 900 °C specimen, held directly at 1400 °C for 30 hr, yielded identical cell parameters. A 3:1 molar mixture of $Sr_3(PO_4)_2$ and $SrCO_3$ was heated directly at 1500 °C for 4 hr and, although it did not react completely to a single phase within this time, the predominant phase was apatite with cell dimensions identical to those previously observed at 1500 °C. High temperature phases are readily reversed by reheating at lower temperatures, as shown in table 1.

The reversibility of the process shows that a kinetic problem is not involved, however, the nature of the anion vacancy is not revealed. Thus, the best interpretation of the behavior of $Sr_{10}P_6O_{24}(OH)_2$ at elevated temperatures is that increasing dehydroxylation occurs with increasing temperature and is associated with unit cell contraction. Regardless of the true nature of the high temperature phase, a completely dehydroxylated $Sr_{10}P_6O_{24}O$ definitely was not found in air.

A number of experiments, made in vacuum, also provide some interesting observations concerning the dehydroxylation of $Sr_{10}P_6O_{24}(OH)_2$. A specimen heated 70 hr at 1100 °C and 10^{-2} torr clearly showed two phases, one having cell dimensions quite similar to the 1600 °C in air phase, the other $a=9.84$ Å and $c=7.21$ Å. The diffuseness of the powder pattern precluded a more precise calculation of cell parameters. Another specimen held 110 hr at 1275 °C and 10^{-2} torr consisted of an apatite-like single phase whose pattern could be completely indexed on the basis of a hexagonal cell with $a=9.872$ Å and $c=7.199$ Å. The compound was again prepared at 1270 °C, 70 hr and 7×10^{-3} torr. Portions of the powder pattern of this new phase are compared to those of the 900 °C and 1500 °C in air apatite phases in figure 2.

Considering the trend established in the "in-air" experiments, that the cell contracts with hydroxyl loss, this new phase is unusual because of its rather large a and quite small c. When heated in air at 950 °C, the compound apparently reacts with atmospheric moisture very sluggishly and a contracts and c expands toward the values of the fully hydroxylated apatite. Unfortunately, the nature of this new phase could not be investigated in detail because of difficulty in the preparation of sufficiently large quantities of material for gravimetric experiments and NMR analysis.[4] Whether or not it represents a true, ordered, $Sr_{10}P_6O_{24}O$ oxyapatite must await single crystal structure analyses. Kreidler and Hummel [8] reported the synthesis of strontium-phosphorus oxyapatite in vacuum at 1400 °C but did not detect x-ray changes. Their

[4] This compound was found to be $(OH)^-$ and $(CO_3)^=$ free by infrared absorption. Personal communication, Dr. Bruce Fowler, National Institutes of Health.

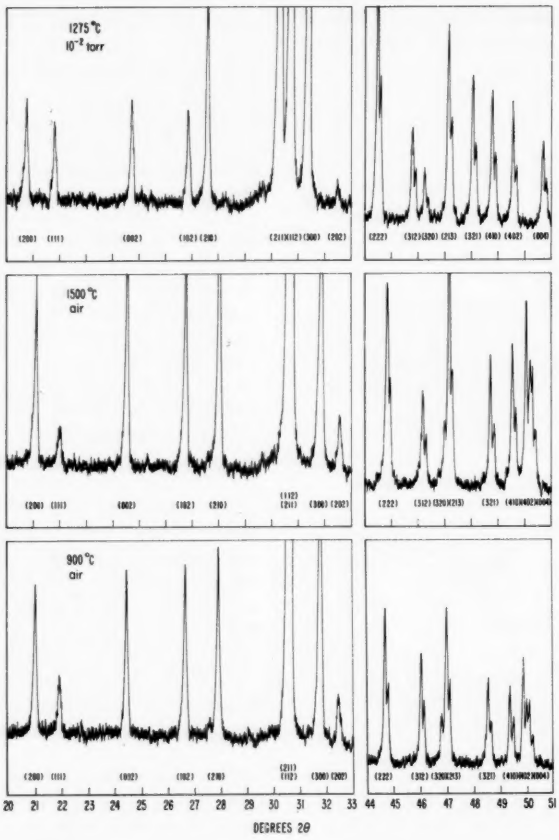

FIGURE 2. *Comparison of portions of the powder patterns of* $Sr_{10}P_6O_{24}(OH)_2$, *(bottom)—as prepared at 900 °C in air; (middle)—after heating at 1500 °C; (top)—heated at 1275 °C and* 10^{-2} *torr.*

inability to observe this phase may have been due to insufficient equilibration times and/or poor vacuum. In this study, approximately 1 g specimens heated between 1250 and 1500 °C from 15 to 113 hr and less than 2×10^{-2} torr (see table 1) yielded apatite phases with powder patterns similar in appearance to the air apatites. Analysis by NMR indicated that even these phases contain protons. Although their powder patterns are not exceedingly sharp, the cell parameters indicate an expansion of a and contraction of c. Smaller specimens yield the new phase although a vacuum less than 10^{-2} torr and temperatures greater than 1100 °C are necessary.

In view of the results obtained on vacuum heated specimens another question can be raised concerning the nature of the products of high temperature in air experiments. Are the results shown in figure 1 a manifestation of stable or only metastable equilibrium? The answer to this question can only be decided after considerable experimentation with vacuum prepared starting material.

3.2. $Ba_{10}P_6O_{24}(OH)_2$ and $Pb_{10}P_6O_{24}(OH)_2$

A few attempts were made to correlate the high temperature "in-air" behavior of barium and lead-phosphorus apatites with that of strontium. Experimental data are given in table 1.

Hydrothermal and low temperature (700 to 900 °C) specimens of barium-phosphorus apatite are identical, with $a = 10.177$ Å and $c = 7.731$ Å. From just above 900 to 1500 °C, as shown in figure 3, cell parameters contract continuously with increasing temperature suggesting dehydroxylation as in the case of strontium. Some structural carbonate, however, may be present and the curve may represent, in reality, hydroxyl and carbonate loss. Phases can be easily reversed by reheating at lower temperatures. The 1600 °C apatite has $a = 10.153$ Å and $c = 7.696$ Å. These values do not lie on the extrapolation of the a and c curves to 1600 °C. The fact that specimens at 1600 °C show partial melting and discoloration which may be due to reaction with platinum may explain this apparent anomaly.

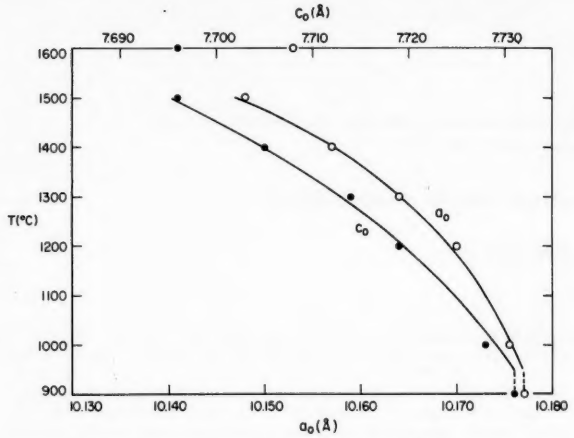

FIGURE 3. *Unit-cell parameter changes of barium-phosphorus apatite as a function of the temperature of heating in air.*

Alternatively, the slight increase in a at 1600 °C may reflect the same tendency observed in the strontium-phosphorus apatite heated in vacuum. Regardless of the cause, a completely dehydroxylated barium oxyapatite does not appear to exist in air. For example, NMR analysis of a specimen held at 1500 °C for 20 hr definitely established the presence of protons.

Hydrothermal and "in-air" lead-phosphorus apatites are not identical. The former has $a=9.878$ Å and $c=7.432$ Å while the latter has $a=9.825$ Å and $c=7.421$ Å. Merker and Wondratscheck [7, 9] reported a doubling of the c-axis for this compound. The powder patterns made in this study do not, and perhaps cannot, reveal this doubling. A specimen of the hydrothermal apatite heated in air at 700 °C for 65 hr gave weight loss data suggesting the formula

$$Pb_{10}P_6O_{24}(OH)_{0.26}O_{0.87}V_{0.87}.$$

NMR analysis of this material reheated at 925 °C for 75 hr also indicated that the phase was not totally deficient in protons. These data conflict with past reports [6, 8] regarding the synthesis of a completely dehydroxylated $Pb_{10}P_6O_{24}O$ type oxyapatite.

The "in-air" lead apatite does not show a progressive contraction of parameters with increase in temperature. In fact, crystals grown by slow cooling of the melt from 1000 to 950 °C yield powder patterns indistinguishable from lower temperature material. Significant, however, is the cell contraction of the hydrothermal apatite when partly dehydroxylated by heating in air.

4. Summary

Strontium and barium-phosphorus hydroxyapatites undergo cell parameter contractions at elevated temperatures in air. These can be correlated with progressive dehydroxylation according to

$$M_{10}P_6O_{24}(OH)_{2-2x}O_xV_x.$$

Neither, however, form the limiting $M_{10}P_6O_{24}O$ type oxyapatite in air as complete dehydroxylation does not occur. The possibility exists that such a phase can be formed at elevated temperatures in vacuo. The unit-cell dimensions of a new strontium-phosphate phase herein reported may represent those of the fully dehydroxylated apatite.

Dehydroxylation of lead-phosphorus hydroxyapatite in air does not produce a true oxyapatite but rather one which is still partially hydrated.

The writers wish to thank Thomas Farrar, National Bureau of Standards, for conducting the NMR analyses.

5. References

[1] Posner, A. S., Perloff, A., and Diorio, A. F., Acta Cryst. **11,** 308–309 (1958).
[2] Negas, T., to be published.
[3] Ito, J., to be published.
[4] McConnell, D., Am. Mineralogist **23,** 1–19 (1938).
[5] McConnell, D., Arch. Oral Biol. **10,** 421–431 (1965).
[6] Balz, W., Dissertation, T. H. Karlsruhe, 1961.
[7] Merker, V. L., and Wondratschek, H., Z. Anorg. Allgen Chem. **306,** 25–29 (1960).
[8] Kreidler, E. R., and Hummel, F. A., Inorg. Chem. **6,** 884–891 (1967).
[9] Wondratschek, H., Neues Jahrb. Mineral. Abhand. **99,** 113–160 (1963).

(Paper 72A6–528)

JOURNAL OF RESEARCH of the National Bureau of Standards—A. Physics and Chemistry
Vol. 72A, No. 6, November–December 1968

Publications of the National Bureau of Standards*

Selected Abstracts

Brady, E. L., *Editor*, **Status report National Standard Reference Data System, Aptil 1968,** *Tech. Note 448 (June 1968) 70 cents.*
This report summarizes the status of activities of the NBS Office of Standard Reference Data as of April 1968. It provides a detailed review of the data compilation activities within the seven broad categories of the technical scope of the program: (1) nuclear data, (2) atomic and molecular data, (3) solid state data, (4) thermodynamic and transport data, (5) chemical kinetics, (6) colloid and surface properties, and (7) mechanical properties. Progress in data systems design and development and in information services are reviewed. Certain problem areas of the program are identified. The appendix includes: (1) a listing of information and data centers associated with the Office of Standard Reference Data, (2) publications of the National Standard Reference Data System, and (3) a listing of organizations, groups, or individuals compiling or evaluating data.

Key Words: Nuclear data; atomic and molecular data; solid state data, thermodynamic and transport properties; chemical kinetics; colloid and surface properties; mechanical properties; data systems design and development; information services; standard reference data.

Kessler, K. G., Passaglia, E., Winogradoff, N. N., **Research on laser standards and materials at the National Bureau of Standards,** *Tech. Note 449 (June 1968), 30 cents.*
A brief report is presented on research in the areas of laser standards and laser materials now in progress at the National Bureau of Standards. Included are the measurement of the power and energy output of lasers, their near and far field patterns and their optical properties. The physical and chemical properties of laser materials are studied in an attempt to relate such properties to the operating characteristics of lasers.

Key Words: Holography; laser energy; laser materials; laser power; laser radiometry; laser standards; laser transitions; modulation of lasers; near and far field patterns; optical properties.

Mason, H. L., *Editor*, **Calibration and test services of the National Bureau of Standards,** *Spec. Publ. 250, 1968 edition (May 1968), $1.75 (Supersedes Misc. Publ. 250, 1965 edition).*
This publication contains a descriptive listing, item by item, of most of the test and calibration work done at the National Bureau of Standards with the respective fees. The content is fully indexed providing easy access to data on specific measurement services. Included also is information about the Bureau's organization and statutory functions, the procedures for requesting tests, and the reports issued thereon. Throughout the text various other publications are mentioned which form a bibliography in measurement techniques. This publication supersedes Miscellaneous Publication 250–1965 Edition, and is incorporated by reference in the Federal Register.

Key Words: Calibration services; fees for testing; test fee schedule; test procedures.

Rosenberg, S. J., **Nickel and its alloys,** *Mono. 106 (May 1968), $1.25 (Supersedes Circular 592).*
This monograph reviews available information on the production, properties, and uses of high-purity and commercial forms of nickel, and on the properties and applications of its important alloys, both ferrous and nonferrous. It is a revision of National Bureau of Standards Circular 592, issued in 1958.

Key Words: Alloys; corrosion-resisting alloys; copper-nickel alloys; electroplating; electrical resistance alloys; heat resisting alloys; magnetic alloys; maraging steels; nickel; stainless steels; steels.

Tipson, R. S., **Infrared spectroscopy of carbohydrates, a review of the literature,** *Mono. 110 (June 1968), 30 cents.*
A survey has been made of the literature on the infrared spectroscopy of carbohydrates, in order to assemble and systematize information in this field. The Monograph discusses principles and instrumentation, sampling techniques, comparison of samples, and the interpretation of the spectra, particularly as regards functional groups of carbohydrates and their derivatives, correlations for the fingerprint region and beyond, and conformational studies. In addition, examples are discussed of the use of infrared spectra for qualitative and quantitative purposes and in the determination of structure. Special techniques are briefly described, including use of plane-polarized radiation, the technique of attenuated total reflection, and Raman spectra.

Key Words: Analysis; carbohydrates; conformations; infrared spectra; spectrometry; structure.

Bates, R. G., *Editor*, **Electrochemical Analysis Section: Summary of activities July 1967 to June 1968,** *Tech. Note 453 (July 1968), 55 cents.*
This survey of the activities of the Electrochemical Analysis Section, Analytical Chemistry Division, covers the period July 1967 to June 1968. An attempt is made to summarize a year's progress on the technical projects of the Section in such a way as to stress the program and capabilities of the organizational unit as a whole. Brief summaries of several lines of work underway are given. The review describes briefly new equipment and facilities acquired during the year. A major effort devoted to acidity measurements has led to new pH standards and new reference solutions for pD in heavy water. Solvent effects on acid-base phenomena in mixed solvents have shed some light on the factors, including solvent structure, governing ion-solvent interactions. A start was made on the study of ion-specific electrodes and the establishment of standard scales for ionic activity. Equilibrium data for hydrochloric acid in 92.41 wt. percent ethanol and for the ionization of carbonic acid in heavy water have been obtained. The establishment of conductance standards for oceanographic research was begun. The survey concludes with lists of the members of the Section staff, publications and manuscripts produced during the year, talks given by the staff, and committee assignments.

Key Words: Acidity; analysis; conductance measurements; electrochemical analysis; electrochemistry of solutions; ionic activity; ion-selective electrodes; pD measurements; pH measurements; medium effects; solvent effects.

Beam, A. E., Hilsenrath, J., **PRECISE: A multiple precision version of omnitab,** *Tech. Note 446 (June 1968), 55 cents.*
This users manual describes PRECISE—a completely assembled interpretive program for the IBM 7090/7094 which enables the user to carry out arithmetic operations and function generation in multiple precision (accuracy to 28 significant figures). PRECISE oper-

ates as a sub-monitor under the IBSYS or DC–IBSYS monitor systems. Appendixes describe how jobs are set up to be run under the PRECISE sub-monitor, and how the system may be expanded to include new subroutines. The program, which responds to instructions in the form of plain English sentences or contractions thereof, has provision for handling numbers out of the normal 7090/7094 range. It handles numbers as large as 10 to the 10 to the 9 power. Other features of the program include: free-field input; a work-sheet of 7,500 cells (3×2500 computer words) which can be dimensioned by the user at run time (75 rows by 100 columns, 300 rows by 25 columns, (etc.); solution of systems of linear equations in as many as 85 unknowns; flexible formatting; tape handling facility; and row and column sums. A description of the UOM Multiple Precision Package (SHARE Dist. No. 3081) is included as an appendix.

Key Words: Elementary functions; equation solver; double precision; linear equation solver; magnetic tape utility program; multiple-precision computing; multiple-precision programming; PRECISE; triple-precision; user's manual.

Moore, C. E., Merrill, P. W., **Partial Grotrian diagrams of astrophysical interest,** *NSRDS–NBS 23 (June 1968), 55 cents.*
This publication is a reprint of Appendix A of the book by Paul W. Merrill entitled, "Lines of the Chemical Elements in Astronomical Spectra" (Carnegie Inst. Wash. Publ. 610, 1956). It contains partial Grotrian Diagrams of selected spectra of astrophysical interest, which give wavelengths, multiplet numbers and key letters for the transitions shown. The diagrams are accompanied by tabular keys in which the key letters indicate related lines in spectra similar in structure to those illustrated in the diagrams. There are 39 diagrams of spectra between hydrogen and nickel and tabular keys for 90 spectra between lithium and rhenium.

Key Words: Atomic spectra; partial Grotrian diagrams; Grotrian diagrams.

Mosburg, E. R., Jr., Lojko, M. S., **Solution of the Abel integral transform for a cylindrical luminous region with optical distortions at its boundary,** *Tech. Note 368 (July 12, 1968), 25 cents.*
The use of orthogonal polynomial expansions in the calculation of the Abel integral transform is discussed. Particular attention is directed to the effects of optical and instrumental distortions when the luminous region is contained by a cylindrical glass tube. An easily calculable solution of the Abel integral is presented which reduces the effect of such distortions by employing a weighting function which has a maximum at the center and vanishes at the boundary. This approach results in a more accurate solution of the Abel integral transform in the case where significant optical and instrumental distortions are present near the boundary of the luminous region.

Key Words: Abel transform; Abel inversion; plasma diagnostics; emissivity profile; radiance profile.

Newman, M., **Matrix representations of groups,** *AMS60 (July 1968), 60 cents.*
The theory of group representations is presented from the matrix standpoint. Many special representations are worked out in detail, and there are appendices on the elements of the theory of algebraic numbers.

Key Words: Algebraic numbers; groups; matrices; representations.

Passaglia, E., *Editor,* **Research on high temperature materials at the National Bureau of Standards,** *Tech. Note 447 (July 1968), 20 cents.*
The National Bureau of Standards, with support from the Advanced Research Projects Agency of the Department of Defense, has begun a program on High Temperature Materials. This program includes projects on properties of high temperature materials, projects on their preparation, and others designed to explain basic phenomena limiting the use of materials at high temperatures. A summary of the progress in this program is given here.

Key Words: High temperature materials; materials properties.

Roder, H. M., McCarty, R. D., Johnson, V. J., **Saturated liquid densities of oxygen, nitrogen, argon, and parahydrogen,** *Tech. Note 361 (Jan. 31, 1968), 50 cents.*
Integrated tables of pressure, volume, and temperature for the saturated liquid, from the triple point to the critical point, of oxygen, nitrogen, argon, and parahydrogen are presented. The tables include entries of integral values of temperature in both Kelvin and Rankine, and integral values of pressure in both atmospheres and psia. Volumes and densities in three different units and a density ratio are tabulated for each entry. Estimates of the uncertainty of the tabulated data are given.

Key Words: Pressure; volume; density; temperature; saturated liquid; oxygen; nitrogen; argon; parahydrogen; uncertainties.

Schwendeman, R. H., **Tables for the rigid asymmetric rotor: Transformation coefficients from symmetric to asymmetric bases and expectation values of P_z^2, P_z^4, and P_z^6,** *NSRDS–NBS12 (June 1968), 60 cents.*
Tables of computed quantities associated with the rigid asymmetric rotor are presented. The first group of tables gives transformation coefficients from symmetric to asymmetric rotor bases. These coefficients permit the eigenfunctions of the asymmetric rotor to be written in terms of symmetric-rotor eigenfunctions. In Part II the angular-momentum expectation values (P_z^2), (P_z^4), and (P_z^6) are tabulated. In both sets of tables values are given at intervals of 0.1 in the asymmetry parameter κ and for $J \leqq 15$. The tabulated quantities find use in the analysis of microwave rotational spectra and the rotational fine structure in vibrational and electronic band spectra.

Key Words: Angular momentum; asymmetric rotor; eigenfunction; microwave spectra; rotational spectrum; transformation coefficients.

Alley, C. O., Bender, P. L., **Information obtainable from laser range measurements to a lunar corner reflector,** *Book, IAU–IUGG Symposium No. 32 on Continental Drift, Secular Motion of the Pole and the Rotation of the Earth* **32,** *86–90 (Reidel Publ. Co., Dordrecht, The Netherlands, 1968).*
It has been proposed to the U.S. National Aeronautics and Space Administration that optical retro-reflector packages be placed on the lunar surface under either the Surveyor or Apollo Programs. Methods for measuring the range to the reflectors with an expected accuracy of 15 cm have been presented. The new technique is briefly discussed, and an analysis of the determination of geocentric longitude is given, indicating a potential uncertainty of 0.25×10^{-3} seconds of time.

Key Words: Laser; lunar distance; surveyor.

Astin, A. V., **Standards of measurement,** *Sci. Am.* **218,** *No. 6, 50–62 (June 1968).*
Virtually all measurements made in science and technology depend upon the four independent standards for length, mass, time, and temperature. This article traces the development of standards for these four quantities, with emphasis on recent advances that make possible greater measurement accuracy in science and industry. The possibilities for achieving even greater accuracy in measuring the four basic quantities are discussed.

Key Words: Measurement accuracy; physical measurement; physical standards; standards for science.

Astin, A. V., **Voluntary standardization and the government (fifty years of cooperation),** *Mag. Stds.* **39,** *No. 6, 167–172 (June 1968).*
A half-century of progress in cooperative development of voluntary national standards for science and technology is reviewed. Beginning with the 1919 reorganization of the American Engineering Standards Committee and Secretary of Commerce Herbert Hoover's "crusade for standardization," the article traces the growth of government and non-government agency teamwork to the present era in which some 500 national organizations collaborate in standardization on the basis of consensus and continuing review and modernization.

Key Words: Voluntary standardization; government/non-government cooperation; safety codes; standards of quality; simplified practice recommendations; performance standards.

Breen, D. R., Keller, R. A., **Intramolecular energy transfer between triplet states of weakly interacting chromophores. I. Compounds in which the chromophores are separated by a series of methylene groups,** *J. Am. Chem. Soc.* **90,** *No. 8, 1935–1940 (Apr. 10, 1968).*
The intramolecular transfer of triplet excitation energy from the donor chromophor (phthalimide and carbazole) to the acceptor chromophor (naphthalene) was studied when the chromophors were separated by methylene groups. In all cases, complete transfer of triplet excitation energy occurred. New absorption and emission bands not characteristic of either chromophor were observed and were attributed to charge transfer absorption and emission.

Key Words: Triplet states; energy transfer; phosphorescence; fluorescence.

Brown, R. L., Brennen, W., **Spin-relaxation effects on the EPR spectrum of gaseous nitrogen atoms,** *J. Chem. Phys.* **47,** *No. 11, 4697–4705 (Dec. 1, 1967).*
Experimental evidence is presented which indicates that N atoms produced in a flow system by a microwave discharge through purified N_2 have a "spin-lattice" relaxation time T_1 of the order of 25 msec. In a fast flow system, the residence time of the atoms in the EPR magnet can easily be shorter than this. As a result, atoms which are generated outside of the magnet may arrive at the microwave cavity before they have had time to reach their equilibrium magnetization. Addition to the discharged gas of as little as 10 p.p.m. O_2 (which did not affect the N atom concentration) decreased the spin relaxation time, and led to increases as great as 7-fold in the N atom EPR signal. Because of the long relaxation time it was necessary to work at the low microwave power level of 0.006 μW to avoid saturation effects. Power saturation was governed primarily by the rate at which unsaturated atoms entered the cavity and not by collision relaxation processes. Interpretation of the effects of O_2 addition in terms of a two level spin model allowed us to estimate a value of $\sim 1.5 \times 10^{-15}$ cm^2 for the spin exchange cross section for N–O_2 collisions. Several qualitative observations regarding the nitrogen pink afterglow, electron production, and the effects of NO addition are also reported.

Key Words: Electron paramagnetic resonance; flow system kinetics; nitrogen atoms; spin exchange cross sections; spin relaxation time.

Butterfield, M. A., **Optical character recognition as an archival tool,** *Proc. A Pioneer Presentation of a National Symposium on the Impact of Automation and Documentation, Denver, Colo., Apr. 27–29, 1967, pp. 101–118 (1968).*
The exponential growth of technology and records in our Third Industrial Revolution will require librarians and archivists to adopt mechanized and automated techniques to overcome problems of volume. A suggest input mechanization technique is Optical Character Recognition (OCR). The history and growth of OCR is presented along with current status and specific uses. Typical user experiences are described. Bibliography.

Key Words: Optical Character Recognition; OCR History and growth; OCR Applications; OCR Bibliography; OCR as a Library Tool; OCR as an Archival Tool.

Cooper, M. J., **Comments on the scaling-law equation of state,** *Phys. Rev.* **168,** *No. 1, 183–184 (Apr. 5, 1968).*
A generalization of Kadanoff's scaling arguments is shown to provide a functional equation whose solution is a two-parameter power-law form for the equation of state.

Key Words: Critical indices; equation of state; scaling-laws.

Costrell, L., **Standard nuclear instrument modules,** *(Adopted by AEC Committee on Nuclear Instrument Modules January 1968), AEC Report TID–20893 (Rev. 2), (Superintendent of Documents, Government Printing Office, Washington, D.C., 1968, 25 cents.)*
The interchangeability problem posed by the advent of modular instrumentation has been alleviated by the development of a standard Nuclear Instrument Module (NIM) system by the AEC Committee on Nuclear Instrument Modules. The Committee held its first meeting on March 17, 1964. The completed specifications were issued in July 1964 and laboratory utilization and industry exhibit of the NIM system began in November 1964. Acceptance by the laboratories and by the nuclear instrument industry has been so rapid and so overwhelming that it is estimated that NIM instruments constituted over two-thirds of the total modular nuclear instrument production in the U.S. in 1966 and between 85% and 95% in 1967. Since all necessary components are available, other fields and other industries can readily adopt the system.

Key Words: Instrument; interchangeability; modules; nuclear; standard.

Coyle, T. D., Cooper, J., Ritter, J. J., **Preparation and some reactions of difluoroborane,** *Inorg. Chem.* **7,** *No. 5, 1014–1020 (May 1968).*

Difluoroborane is produced by the direct interaction of boron trifluoride with diborane in the gas phase at 100 °C or above. Pyrolysis of BF_3–B_2H_6 mixtures at 250 °C for periods of 30 minutes to one hour, followed by rapid quenching, yields HBF_2–BF_3 mixtures free of B_2H_6. An alternative, synthetically useful route is the reaction of $HB(OCH_2)_2$ with excess BF_3. Difluoroborane undergoes rapid H–F exchange with boron trifluoride and H–D exchange with deuterated diborane, but does not exchange boron with diborane. Addition of difluoroborane to propene and isobutene yields *n*-propyldifluoroborane and isobutyldifluoroborane, respectively. Reactions with fluoroethylenes give boron trifluoride, ethylfluoroboranes and less highly-fluorinated olefins.

Key Words: Difluoroborane; boron; fluoride; hydride; isotope exchange; organoboron compounds; hydroboration.

Coyle, T. D., Ritter, J. J., **Reactions of diboron tetrahalides with some unsaturated organometallic compounds,** *J. Organometallic Chem.* **12,** *269–280 (1968).*
Tetrachloro- and tetrafluorodiborane(4) add to the double bond in a number of vinyl derivatives of boron, carbon, silicon, germanium, and tin to form 1,2-bis(dihaloboryl)ethyl derivatives. Most of the compounds are stable *in vacuo* at temperatures in excess of 150 °C. Tetrachlorodiborane(4) undergoes addition considerably more readily than does tetrafluorodiborane(4). Relative rates of addition have been determined and shown to be markedly dependent on the nature of the substituent on the vinyl group.

Key Words: Tetrachlorodiborane(4); tetrafluorodiborane(4); boron subhalides; organometallic compounds; addition reactions; boron.

Dehl, R. E., **Broadline NMR study of H_2O and D_2O in oriented rayon fibers,** *J. Chem. Phys.* **48,** *No. 2, 831–835 (Jan. 15, 1968).*
The broadline NMR spectra of H_2O and D_2O absorbed in parallel fibers of highly crystalline rayon have been found to consist of two lines, whose separation depends upon the angle between the fiber axis and the magnetic field. The D_2O splitting, resulting from quadrupole pertubation of the nuclear Zeeman levels, was about ten times greater than the H_2O splitting, produced by direct nuclear dipole-dipole interaction. Two models for the partial orientation of water molecules are discussed, (I) in which the molecules rotate about a fixed axis, and (II) in which the molecules reorient rapidly about all possible axes, but maintain a small resultant projection, along the fiber axis. Model I is shown to be incorrect for the rayon fibers, on the basis of the combined H_2O and D_2O results; Model II, however, appears to be applicable not only to rayon but to other examples of partially oriented water as well.

Key Words: Broadline NMR; H_2O; D_2O; rayon fibers, oriented water; dipole-dipole interaction; quadrupole-field gradient interaction.

DeVoe, J. R., Spijkerman, J. J., **Mössbauer spectrometry,** *Anal. Chem.* **40,** *No 5, 472R–489R (Apr. 1968).*
A review of the literature on chemical applications of Mössbauer Spectroscopy for 1966 and 1967 is presented. This is done primarily with a table of pertinent information on compounds and techniques. New developments in the field are also presented.

Key Words: Review; literature; chemical applications; Mössbauer spectroscopy.

Dickson, P. F., Jones, M. C., **Infrared spectral reflectances of metals at low temperatures,** *Cryogenics* **8,** *No. 1, 24–29 (Feb. 1968).*
Experimental results of infrared spectral reflectances of ten pure metals and one alloy system at low temperatures are reviewed. Reflectances are in many cases calculated from published optical constants or obtained from absorptance measurements. Comparisons with room temperature measurements are made where possible and some observations regarding the effect of sample preparation technique and surface oxidation are made.

Key Words: Compilation; cryogenic; infrared; metals; reflectance.

Fatiadi, A. J., **Formation of arylazocyclohexene derivatives on acylation of certain inosose phenylhydrozones,** *Carbohydrate Res.* **7,** *89–94 (1968).*
It has been found that acetylation of *myo*-inosose-2 phenylhydrazone with acetic anhydride in the presence of pyridine at room temperature products 1-phenylazo-1-cyclohexene-DL-*ido*-3,4,5,6-tetrol tetraacetate (β-elimination product) instead of the phenylhydrozone derivative reported. In contrast, acylation with propionyl anhydride and pyridine gives the phenylhydrozone pentapropionate. However, acylations of DL-*epi*-inosose-2 phenylhydrazone at 0 to 5 °C with acetic or propionic anhydrides give the corresponding pentaacylated phenylhydrazones.

Key Words: Acylation; arylazoethylenes; inosose phenylhydrazones.

Gray, V. E., Cadoff, B. C., **Survey of techniques for evaluating effects of weathering on plastics,** *Appl. Polymer Symp.* **4,** *85–95 (1967).*
This paper surveys those physical and chemical test methods that could be applied in the prediction of the performance of plastics under outdoor exposure.
Techniques to measure appearance, strength, and flexibility are reviewed. Color changes alone, although widely used, are shown to be an insufficient measure of weathering.
The more sensitive spectroscopic and chemical test methods that have been found to measure oxidation and hydrolysis products in polymeric materials are examined for usefulness in quantitatively measuring plastic degradation. The methods reviewed are used to determine carbonyl, carboxyl, peroxidic, and hydroxyl groups.

Key Words: Color and gloss measurements; colorimetric analysis; infrared analysis; oxidation; plastics; ultraviolet analysis; weathering.

Hall, L. H., Spijkerman, J. J., Lambert, J. L., **Preparation and coordination studies of the complex acid, dihydrogen diethylenetriamine-pentaacetatoferrate (III) dihydrate, and several of its metal (I) salts,** *J. Am. Chem. Soc.* **90,** *No. 8, 2044–2048 (April 10, 1968).*
The coordination numbers of the central metal ion which exists in iron (III) chelated with diethylenetriaminepentaacetic acid, H_5DTPA have been investigated by the following methods: (a) infrared spectroscopy, (b) magnetic susceptibility, (c) Mössbauer spectroscopy, (d) photodecomposition and (e) thermogravimetric analysis. The iron (III) DTPA complexes were found to exist in three different forms in the solid phase; the complex acid, the mono-salt and the di-salt. All three forms were found to be high spin complexes. The complex acid $H_2FeDTPA \cdot 2H_2O$ was shown to have a coordination number of six around the central metal atom. The mono-ammonium salt, $NH_4HFeDTPA \cdot 1H_2O$ was found to be seven coordinated. However, the di-alkali metal salts $M_2FeDTPA \cdot nH_2O$ were found to have a coordination number of eight around the central atom but one of the iron (III) carboxylate bonds is different than the remaining four.
The cation in the salt of the complex interacts with the metal *d*-orbitals, and appears to decrease the size of the metal *d*-orbitals, which results in a concentration of the *d*-electron density nearer the nucleus.

Key Words: Preparation; coordination; $M_2FeDTPA$; infrared spectroscopy; magnetic susceptibility; Mössbauer spectroscopy; photodecomposition; thermogravimetric analysis.

Keller, R. A., **Intramolecular energy transfer between triplet states of weakly interacting chromophores. II. Compounds in which the chromophores are perpendicular to each other,** *J. Am. Chem. Soc.* **90,** *No. 8, 1940–1944 (Apr. 10, 1968).*
The intramolecular energy transfer properties of the following two molecules were investigated at 77 °K. The spiro linkage holds the two chromophores perpendicular to each other. Complete transfer of both singlet and triplet excitation energy to the chromophor with the lowest excited state of a particular multiplicity was observed for both of these molecules. No absorption or emission bands were observed which could not be attributed to one of the chromophors.

Key Words: Energy transfer; TRIPLET STATES; Phosphorescence; Fluorescence.

Kneissl, G. J., Richmond, J. C., Wiebelt, J. A., **A laser source integrating sphere for the measurement of directional hemispherical reflectance at high temperatures** (*Proc. Thermophysics Specialist Conf. of AIAA, New Orleans, La., Apr. 17–20, 1967), Book, Thermophysics of Spacecraft and Planetary Bodies, Chapt. 1, Radiation Properties of Solids and their Measurement,* **20,** *177–202 (Academic Press Inc., New York, N.Y., Dec. 1967).*
The purpose of this research was to evaluate the high-temperature spectral emittance of refractory metals and ceramics by measuring their reflectance very accurately at high temperatures. An integrating sphere was used to measure the directional, hemispherical reflectance at temperatures up to 2000 °K. The accuracy of the measurement was practically independent of the directional distribution of the reflected flux, which made it possible to measure accurately any material of any surface texture. The source used for this instrument was an He-Ne CW laser operated at 0.6328, 1.15 and 3.39 μm. A narrow bandpass filter, whose peak transmittance coincided with the lasing wavelength, was placed in front of the detector to increase the signal-to-noise ratio. Since conventional sphere coatings could not be used for this high-temperature integrating sphere, a new sphere coating had to be developed. This coating exhibits a high reflectance at all three wavelengths in question, is a very good diffuser, possesses good mechanical properties, and can be used in a low-pressure system. Preliminary data are shown for materials such as graphite, tungsten, and thorium oxide.

Key Words: Reflectance; integrating sphere; high temperature reflectance; sodium chloride coating; laser; thoria; tungsten; graphite.

Larsen, N. T., **50 microdegree temperature controller,** *Rev. Sci. Instr.* **39,** *No. 1, 1–12 (Jan. 1968).*
A temperature controller has been developed using a platinum resistance thermometer in a bridge with inductively coupled ratio arms. It is capable of maintaining water bath temperatures constant to within ± 25 microdegrees Celsius for 24 hours in an environment varying as much as ± 1.5 °C at any temperature from 18 °C to 28 °C. The sensitivity of the controller approaches the theoretical limitation imposed by Johnson noise. The design makes possible control dials which are direct-reading in °C.

Key Words: Temperature control; controller.

Little, J. L., Mooers, C. N., **Standards for user procedures and data formats in automated information systems and networks,** *AFIPS Conf. Proc. Spring Joint Computer Conf., Atlantic City, N.J., Apr. 30–May 2, 1968, 32, 89–94 (Thompson Book Co., Washington, D.C., 1968).*
In the brave new world of the publicly accessible "on-line" computers and automated information systems, users are finding a rapidly growing chaos of incompatible control languages and methods of operation. Almost every automated system has been provided with a different language and method. The resulting chaos promises effectively to destroy much of the potential value of nationwide networks of such information systems. The community of users—and potential users—of such systems are the ones most seriously affected. In order to remedy this intolerable situation, the users must initiate immediate action to introduce standards for user control methods and languages which will permit easy and compatible utilization of automated information systems. This paper is devoted to an examination of twelve elementary logical functions for user control, and suggested keyboard assignment for these functions is reported.

Key Words: Data formats; automated systems; automated networks; information system; standards; user procedures information networks; time-sharing computers; on-line systems reactive typewriters; distributed data base; retrieval.

Lundgren, F. A., Nargolwalla, S. S., **Use of a dual sample-biaxial rotating assembly with a pneumatic tube transfer system for high precision 14-MeV neutron activation analysis,** *Anal. Chem.* **40,** *No. 4, 672–677 (Apr. 1968).*
Imprecision in 14-MeV Neutron activation analysis is primarily due to nonhomogeneity and anisotropy in the usable neutron flux. This fact is considerably magnified in analyses pertaining to short-lived radioactivity such as in the determination of oxygen by $^{16}O(n,p)^{16}N$ reaction.
A design for a variable-speed dual sample rotating assembly is described. This assembly allows reproducible placement of pneumatically injected samples and permits both sample and standard to be exposed to an identical neutron flux as a result of biaxial rotation. The analytical precision, which is now most often limited by the total number of counts accumulated, is about 10 times better than that which most standard normalization techniques can provide. The system permits the analyst to determine both neutron and gamma attenuation in dense samples.
This irradiation assembly is currently being utilized for the accurate and precise determination of oxygen in NBS Standard Reference Materials.

Key Words: Activation analysis; precision; accuracy; oxygen; sample rotator; design; 14 MeV neutrons.

Mahler, R. J., James, L. W., **Nuclear electric hexadecapole-phonon interaction** (*Proc. XIV Colloque Ampere, Sept. 6–11, 1966, Ljubljana, Yugoslavia*), *Book, Magnetic Resonance and Relaxation, Ed. R. Blinc, pp. 938–945 (North-Holland Publ. Co., Amsterdam, The Netherland, 1967).*
A nucleus with spin 5/2 or larger may possess an electric hexadecapole as well as an electric quadrupole moment. These electric moments can interact with the lattice to yield a static shift in the nuclear energy levels, or with the lattice vibrations (phonons) to produce transitions between the nuclear energy levels.
One can show theoretically that the hexadecapole interaction can give rise to $\Delta m = \pm 1$, 2, 3, and 4 nuclear transitions, but experimentally the $\Delta m = \pm 1$ and 2 transitions would be masked by the much larger quadrupole interactions. Since a $\Delta m = \pm 3$ or 4 nuclear transition gives rise to a net change in the nuclear magnetization, pulsed NMR techniques are ideally suited to observe these interactions.
A theoretical expression for the hexadecapole-phonon interactions is derived, and the experimental procedure used to observe the interactions is discussed. Results of these and related experiments are given.

Key Words: Hexadecapole; phonon-nuclear interactions; ultrasonically induced transitions; angular dependence; hexadecapole transitions; saturation factor.

Margoshes, M., Scribner, B. F., **Emission spectrometry,** *Anal. Chem.* **40,** *No. 5, 223R-246R (Apr. 1968).*
A review is given of emission spectrometry and flame emission, atomic absorption, and atomic fluorescence spectrometry for the years 1966–67. Emphasis is placed on analytical applications, but some theoretical papers are included. The major subjects included are books and reviews; spectral descriptions and classifications; instrumentation; standards, samples, calibration, and calculation; excitation sources; flame emission, absorption, and fluorescence; trace analysis; lasers and microanalysis; and other applications. Six hundred and seventy-six references are listed.

Key Words: Atomic absorption spectrometry; atomic fluorescence spectrometry; emission spectrometry; flame photometry; isotopic analysis; microanalysis; review.

Nargolwalla, S. S., Crambes, M. R., DeVoe, J. R., **A technique for the evaluation of systematic errors in the activation analysis for oxygen with 14-MeV neutrons,** *Anal. Chem.* **40,** *No. 4, 666–671 (Apr. 1968).*
In comparative 14-MeV neutron activation analysis of oxygen, the neutron and gamma ray attenuation differences in the sample and standard introduce systematic errors. A quantitative evaluation of these attenuation processes in a wide range of matrices and for three sample diameters is given.
The experimentally determined correction factor, in each case, shows an exponential dependence on the calculated difference between the appropriate attenuation coefficients for sample and standard. Over the range of sample diameters tested, the slope of each calibration line is linearly dependent on the sample diameter. For comparable diameters, the magnitude of the slope for neutron attenuation is approximately ten times greater than for gamma attenuation. These calibration lines are used to predict attenuation correction factors for the determination of oxygen in other matrices. Some typical analyses of Standard Reference Materials, corrected for attenuation, illustrate the high degree of accuracy and precision obtained.

Key Words: Neutron and gamma-ray attenuation; correction factors; 14-MeV activation analysis; oxygen; removal cross section; systematic errors.

Oppenheim, I., Shuler, K. E., Weiss, G. H., **On the decay of initial correlations in stochastic processes,** *J. Chem. Phys.* **46,** *No. 10, 4100–4111 (May 15, 1967).*
We study the relaxation of a noninteracting, initially correlated many particle system in contact with an infinite reservoir. We use the master equation to study the time development of the r-particle distribution function $P_r(\mathbf{n}; t)$ and assume that the relaxation process is Markovian. We study the decay of the correlations by investigating the time development of the r-particle Ursell functions, $U_r(\mathbf{n}; t)$. We show that the correlation function $U_r(\mathbf{n}; t)$ goes to zero much more rapidly with time than the r-particle distribution function approaches its equilibrium value $P_r(\mathbf{n}; \infty) = \prod_{i=1}^{r} P(n_i; \infty)$. The exact forms of the relaxation of $P_r(\mathbf{n}; t)$ and $U_r(\mathbf{n}; t)$ depend upon the eigenvalue spectrum of the transition rate matrix of the master equation. The general theory is developed and then applied to a number of examples.

Key Words: Eigenvalue spectrum; initial correlation; r-particle Ursell functions; stochastic process.

Pichanick, F. M. J., Simpson, J. A., **Resonances in the total cross sections for metastable excitation of noble gases by electron impact,** *Phys. Rev.* **168,** *No. 1, 64–70 (Apr. 5, 1968).*
Total cross sections for excitation by electron impact of metastable states in the noble gases helium, neon, argon, krypton, and xenon have been measured as a function of impact energies. A 180° spherical monochromator was used to obtain incident beams of electrons with energy resolutions between 0.035 eV and 0.050 eV. Metastable atoms were detected in the scattering chamber by electron ejection from a metal surface. The detector was biased negatively to repel scattered electrons, and was electrostatically shielded from the incident electron beam. The cross sections were measured for impact energies up to 5 eV above the metastable thresholds. Several narrow resonances associated with negative ion states were observed, and where possible their shapes and positions on the energy scale were compared with similar results obtained by different techniques.

Key Words: Cross sections; electron impact; excitation; helium; metastable.

Radford, H. E., Evenson, K. M., **Paramagnetic resonance spectrum of metastable (^{2}D) atomic nitrogen,** *Phys. Rev.* **168,** *No. 1, 70–74 (Apr. 5, 1968).*
The paramagnetic resonance spectrum of free metastable (^{2}D) nitrogen atoms has been observed in the flowing products of an electric discharge in nitrogen-helium gas mixture. An analysis of the Zeeman effect and hyperfine structure yields the following values for the atomic g-factors and radial integrals: $g_j(^2D_{3/2}) = 1.20036 \pm 0.00001$; $g_j(^2D_{3/2}) = 0.79949 \pm 0.00002$; $\langle r_l^{-3} \rangle = (20.21 \pm 0.02) \times 10^{24}$ cm^{-3}; $\langle r_s^{-3} \rangle = (22.22 \pm 0.02) \times 10^{24}$ cm^{-3}. The ^{2}D fine structure separation is found to be -8.69 ± 0.02 cm^{-1}. Evidence is found of a small electric quadrupole hyperfine structure interaction.

318-092 O - 69 - 16

Key Words: Electron paramagnetic resonance; metastable atomic nitrogen; electric discharge Zeeman spectroscopy; *g*-factors; fine structure separation.

Reimann, C. W., Zocchi, M., **The structure of the trinuclear cation bis-[μ-(tri-1,2,4-triazolo-N^1,N^2)-triquonickel]**, *Chem. Commun.* **5**, *272 (Mar. 6, 1968)*.
The complex bis[triaquo tri μ(1,2,4 triazolo(-N_1-N_2))nickel]nickel hexanitrate dihydrate has been prepared and the crystal structure was determined by single crystal X-ray diffraction techniques. This complex crystallizes in the monoclinic system with $a = 14.261$, $b = 11.745$, $c = 14.948$Å, $\beta = 127.9°$, space group $P2_1/c$, $\rho_0 = 1.85$ g cm^{-3}, $\rho_c = 1.84$ g cm^{-3} and $z = 2$.
The bis[triaquo tri μ(1,2,4 triazolo(-N_1-N_2))nickel]nickel cation was found to contain three colinear nickel atoms with the central nickel atom bridged to the terminal nickel atoms by three 1,2,4 triazole rings. The Ni-Ni separation was found to be 3.73Å. The coordination about each nickel atom is octahedral. The octahedral coordination of the terminal nickel atoms is completed by three molecules of water.

Key Words: Bis[triaquo tri μ(1,2,4 triazolo(-N_1-N_2))nickel]nickel; crystal structure; trinuclear complex.

Shuler, K. E., **Microscopic and macroscopic approach to chemical rate processes** (*Proc. 7th AGARD Colloquium, Oslo, Norway, May 16–20, 1966*), *Book, Recent Advances in Aerothermochemistry, Ed. I. Glassman, 1, No. 12, 1–21 (Technical Editing and Reproduction Ltd., London, England, 1967)*.
Chemical rate processes, like all other transport processes, can be considered on two levels—the molecular one and the statistical one. On the molecular (microscopic) level one is concerned with binary (or higher order) collisions between single atoms and/or molecules. Such elementary processes can best be studied through the scattering of the reactant species in atomic and molecular beams. The quantity of interest is the reactive scattering cross section; the theoretical approach involves the quantum theory of scattering. On the statistical (macroscopic) level one is concerned with the interactions of an ensemble of atoms and molecules characterized by their velocity and internal energy distribution functions. The experimental quantity of interest is now the rate coefficient; the theoretical approach involves the derivation and solution of the appropriate macroscopic transport equation in terms of the (microscopic) scattering cross sections and the distribution functions of reactants and products. In this paper, we will discuss these two approaches to the study of rate processes and their connection.

Key Words: Chemical kinetics; scattering theory; transport processes; rate theory; cross sections; trajectory calculations.

Spijkerman, J. J., Hall, H. L., Lambert, J. L., **Coordination studies by Mössbauer spectroscopy of some metal(I) salts of the complex acid, hydrogen aquoethylenediaminetetraacetatoferrate (III)**, *J. Am. Chem. Soc.* **90**, *No. 8, 2039–2043 (Apr. 10, 1968)*.
The coordination numbers of the central metal ion that exist when iron(III) is chelated with ethylenediaminetetraacetic acid, H_4EDTA, have been investigated by the following methods: (a) infrared spectroscopy, (b) magnetic susceptibility, (c) Mössbauer spectroscopy, (d) photodecomposition and (e) thermogravimetric analysis.
The iron(III) EDTA complexes were found to exist in two different forms in the solid phase, the complex acid and its M^{+1} salt. Both forms were found to be high spin complexes. The complex acid, $HFe(OH_2)EDTA$, was found to be six coordinate; however, the M^{+1} salts, $MFe(OH_2)EDTA \cdot nH_2O$, were found to have a coordination number of seven around the central metal ion.
An interesting effect, ascribed to the influence of the cation in the salts of these complexes, was also observed. It is believed that this effect arises either from an interaction of the cation with the metal *d*-orbitals or with one of the carboxylate groups or both. Each interaction appears to result in a decrease of the size of the metal *d*-orbitals of the central metal ion. This results in a concentration of the *d*-electron density nearer the nucleus.

Key Words: Coordination studies; Mössbauer spectroscopy; magnetic susceptibility; hydrogen aquoethylenediaminetetraacetatoferrate(III) infrared spectroscopy; photodecomposition; thermogravimetric analysis; $MFe(OH_2)EDTA \cdot nH_2O$.

Swanson, N., Powell, C. J., **Excitation of L-shell electrons in Al and Al_2O_3 by 20-keV electrons**, *Phys. Rev.* **167**, *No. 3, 592–600 (Mar. 15, 1968)*.
The energy loss distributions of ≈ 20 keV electrons transmitted through 210 to 575 Å thick specimens of Al and Al_2O_3 have been measured at zero scattering angle. Two types of Al_2O_3 were used: film of the γ-phase and amorphous films prepared by anodization. Loss spectra were obtained for an energy loss range of zero to 160 eV, in which structure due to L-shell excitation in Al and Al_2O_3 was observed. The positions of the absorption edges and of the peaks on the high-energy loss side of each edge agreed well with recent X-ray absorption measurements. Slightly different structure for the two forms of Al_2O_3 was found near the edge, as recently found by X-ray absorption. From the observed intensities, values of oscillator strengths, mass absorption coefficients and electron scattering cross sections have been derived for each material up to ≈ 85 eV beyond the absorption edge. The Al results are in good agreement with recent X-ray measurements and are consistent with the Al_2O_3 data. The similarity in the electron energy loss and X-ray absorption measurements are consistent with the equality of the longitudinal and transverse dielectric constants [$\epsilon(\omega)$] and the expectation that in this energy loss region $\mathrm{Im}(\epsilon)$ equals $-\mathrm{Im}(1/\epsilon)$ to a good approximation.

Key Words: Aluminum; amorphous Al_2O_3; cross sections; electron energy loss spectra; L-shell electrons; oscillator strengths; X-ray mass absorption coefficients; γ-Al_2O_3.

Acquista, N., Schoen, L. J., Lide, D. R., Jr., **Infrared spectrum of the matrix-isolated OH radical**, *J. Chem. Phys.* **48**, *No. 4, 1534–1536 (Feb. 15, 1968)*.
Infrared absorption in the region of 3450 cm^{-1} has been observed in water-rare gas matrices subjected to vacuum ultraviolet photolysis at 20.4 and 4.2 °K. The splittings and isotope frequency ratios obtained from H_2O^{16}-D_2O^{16}, H_2O^{16}-H_2O^{18} and D_2O^{16}-D_2O^{18} mixtures lead to the assignment of these spectra to trapped OH radicals. No evidence for rotational motion of OH is found in these experiments.

Key Words: Infrared; photolysis; radical; matrix; isotope; doublet.

Ambrose, J. R., Kruger, J., **The stress-corrosion of Ti and Ti-8Al-1Mo-1V in methanol vapour**, *Corrosion Sci.* **8**, *119–124 (1968)*.
An investigation into the stress corrosion cracking of titanium and titanium 8Al-1Mo-1V in methanol has shown that failure will occur in the methanol vapor phase with times to failure being at least an order of magnitude shorter than previously reported. Those effects which significantly altered time to failure were system volume, metal surface condition, and environment composition.
It has been reported that titanium, as well as several of its alloys, is susceptible to stress corrosion cracking (SCC) at room temperature in a methanol-chloride ion solution. Recent publications have also demonstrated the susceptibility of various alloys to SCC in a liquid methanol system with no detectable chloride ion concentration. The purpose of this communication is to report methanol vapor cracking of titanium and titanium 8-1-1 alloy, with a time to failure being at least an order of magnitude less than that in liquid methanol or methanol solutions.

Key Words: Methanol; stress corrosion; titanium; titanium 8-1-1; vapor phase failure.

Bates, R. G., **Standardization of acidity measurements. Extension of the pH concept to mixed solvents and heavy water**, *Anal. Chem.* **40**, *28A–38A (May 1968)*.
The modern concept of the operational pH value is examined in detail. Procedures by which the NBS pH scale (based on conventional hydrogen ion activity) was established are reviewed, and it is shown how those same methods and concepts can be extended to set up useful scales for acidity in nonaqueous and mixed solvent systems (using the unit pH*) and in heavy water (using the unit pD). The availability, in the form of standard reference materials, of two new pH standards and three new pD standards is announced.

Key Words: Acidity scales; deuterium oxide; nonaqueous media; pD; pH; pH*; pH concept; standards for acidity.

Billick, I. H., Dishon, M., Weiss, G. H., Yphantis, D. A., **Numerical solutions of the Lamm equation. IV. Rotor slowing experiments,** *Biopolymers* **5,** *1021–1028 (1967).*
This paper presents the results of a numerical solution of the Lamm equation for rotor slowing specified by $\omega^2 = \omega_0^2 \exp(-\lambda\tau)$, for parameters relevant for equilibrium experiments. It is shown that in the two component system it is theoretically possible to deduce s/D from measurements of the difference of concentration across the cell with rotor slowing, provided that the time at which the difference reaches a maximum is known.

Key Words: Lamm equation; ultracentrifugation; sedimentation equilibrium; rotor slowing; numerical solutions; molecular weight.

Billick, I. H., Schulz, M., Weiss, G. H., **Quasi-equilibrium sedimentation experiments with rotor deceleration,** *J. Phys. Chem.* **71,** *No. 8, 2496–2502 (July 1967).*
This paper presents an analysis of the rectangular approximation to the Lamm equation suitable for analyzing experiments with variable rotor speeds. The theory is applied to the case specified by deceleration described by $\omega^2 = \omega_0^2 \exp(-\lambda\tau)$. It is shown that s/D for a two component system can be determined experimentally by a measurement of concentration difference across the cell at a specified time after the beginning of the experiment. The resulting experiment offers the possibility of considerable savings in time over conventional sedimentation equilibrium experiments. Another experiment, involving a quasi-equilibrium state is analyzed. It is found that the rate of approach to the quasi-equilibrium state is slower than the rate of approach to equilibrium for conventional sedimentation equilibrium experiments under comparable conditions.

Key Words: Equilibrium sedimentation; Lamm equation; rotor deceleration; ultracentrifugation.

Bollacasa, D., Goldman, D. T., **Importance of upscattering in the calculation of neutron spectra,** *Proc. Intern. Atomic Energy Agency Symp. Neutron Thermalization and Reactor Spectra, Ann Arbor, Michigan, July 17–21, 1967, 1, 537–554 (IAEA, Vienna, Austria, Jan. 1968).*
A study has been made of the effect of raising the thermal energy cutoff higher than .625 eV. In most neutron thermalization calculations, the assumption is made that there is no upscattering above .625 eV. This may be a poor assumption especially for moderator models with chemically bound hydrogen even at room temperature. In the study, a thermal cutoff energy of 3.06 eV was chosen. This done because the upscattering above this energy is small and this energy corresponds to that of a group in a slowing down program used in the calculations. Neutron spectra and group averaged cross sections were computed and the inadequacy of a thermal cutoff of .625 eV was manifested by comparisons between calculations at these energy cutoffs. A discontinuity can be observed in joining the thermal and epithermal fluxes at .625 eV, while the joining is smooth at 3.06 eV. This provides the possibility of directly normalizing the thermal neutron source to the slowing down density from the epithermal energy region. Thus, neutron spectra in the thermal and epithermal energy regions can be calculated in one process. Comparison were made in group constants with no upscattering included between .625 eV and 3.06 and with upscattering included up to 3.06 eV. Differences up to 9% were observed. These effects could become significant in the calculation of criticality factors if large resonances were present or if systems with large metal-to-water ratios were considered. A spectrum calculation for a SHA (a homogeneous assembly) fuel element was compared to a measurement made of its asymptotic spectrum. Even though the agreement between calculation and experiment was not exact, the calculated spectrum closely matched the measured spectrum above .625 eV.

Key Words: Neutron; reactor spectrum; scattering; group averaging; cross sections; slowing down density; and epithermal energy.

Branscomb, L. M., **The role of atomic collision processes in astrophysics,** *Book, The Physics of Electronic and Atomic Collisions: Invited Papers from the Fifth International Conference, Leningrad, U.S.S.R., July 17–23, 1967, Ed. L. M. Branscomb, pp. 12–31 (Joint Institute for Laboratory Astrophysics, University of Colorado, Boulder, Colorado, 1968).*
This paper is the manuscript of a lecture in which the importance of atomic collision processes in the field of astronomy is summarized. The paper deals primarily with the formation of stellar spectra, particularly from the sun, as well as problems of low density astrophysics such as the interstellar medium and planetary nebulae.

Key Words: Review atomic collision processes astrophysics.

Brenner, A., Metzger, W. H., Jr., **Determination of the composition of complexes and their instability constants by calorimetry III. The complex in fused sodium molybdate and molybdenum trioxide,** *J. Electrochem. Soc.* **115,** *No. 3, 258–261 Mar. 1968).*
A method of determining the composition of complexes in solution and their instability constants, which is based on the measurement of the partial molal heat effect developed when a small increment of each salt is added in turn to a series of mixtures covering the range of composition from 0 to 100%, has been applied to the molten Na_2MoO_4–MoO_3 system at 800 °C. The data show that one complex is formed consisting of one molecule of Na_2MoO_4 and two molecules of MoO_3. The instability constant was approximately unity and the complex was between 50% and 75% dissociated.

Key Words: Complex salts; calorimetry; fused salts; sodium molybdate-molybdenum trioxide system; partial molal heat effect; composition of complex salts, determination of.

Caldwell, B. P., **Kubelka-Munk coefficients from transmittance,** *J. Opt. Soc. Am.* **58,** *No. 6, 755–758 (June 1968).*
A simplified method is described for the exact computation of Kubelka-Munk coefficients from internal transmittance measurements of two specimens of the same material where one specimen is twice as thick as the other. Equations are derived for determining the scattering coefficient S, the absorption coefficient K, the Kubelka parameters a and b, the internal transmittance τ_i, the reflectance of an infinitely thick specimen ρ_∞, and the reflectance of a specimen with an ideal black background ρ_0. Graphs are given to estimate the range of error in ρ_∞, S, and K as a function of estimated measurement errors in transmittance.

Key Words: Scattering; absorption; Kubelka-Munk coefficients; optical constants.

Chang, S. S., Bestul, A. B., **Heat capacities for atactic polystyrene of narrow molecular weight distribution to 360 °K,** *J. Polymer Sci.* **6,** *Part A-2, 849–860 (1968).*
Precise heat capacity values to better than 0.1% of the values are reported over the temperature range from 10° to 360 °K for a narrow molecular weight distribution atactic polystyrene sample taken from the same stock from which National Bureau of Standards Standard Sample 705 Narrow Molecular Weight Distribution Polystyrene was established. Data are reported for the sample as received and after an annealing procedure. At temperatures below about 60 °K a systematic difference comparable with the limits of experimental precision appears between the values obtained for the present sample in the as received and in the annealed conditions, although at higher temperatures the values for the two did not show any systematic difference beyond the limits of precision of the measurements. At temperatures above 100 °K previously published values for atactic polystyrene samples of various molecular weight distributions and for isotactic polystyrene agree within about 0.5% of the values from this investigation. At temperatures below 100 °K significant heat capacity differences appear, especially between values for the atactic and the isotactic isomers, and even between atactic samples of different molecular weight distribution.

Key Words: Atactic polystryene; narrow molecular weight distribution; precise heat capacities; heat capacity calorimetry; enthalpy increment; entropy increment, glass, glass transformation; annealed sample; literature values.

Childs, G. E., Hanley, H. J. M., **Applicability of dilute gas transport property tables to real gases,** *Cryogenics* **8,** *No. 2, 94–97 (Apr. 1968).*

The pressure range for which published "dilute" or "low pressure" transport property tables may be used is experimentally defined. The method is based on the fact that, in a well defined temperature range, transport properties can be computed from kinetic theory expressions. The method is general but specific examples are given for neon, argon, krypton, xenon, oxygen, and nitrogen.

Key Words: Transport properties; viscosity; dilute gas; low pressure; mean-free-path; dilute limit; validity range.

Cohen, M. I., Blunt, R. F., **Optical properties of $SrTiO_3$ in the region of the absorption edge,** *Phys. Rev.* **168,** *No. 3, 929–933 (Apr. 15, 1968).*
The absorption coefficient, reflectivity, and electroreflectance of $SrTiO_3$ in the neighborhood of the fundamental absorption edge are reported. The absorption coefficient shows an exponential rise with incident energy (Urbach rule) over five orders of magnitude. Its logarithm has a slope of $1/kT$. The data indicate that the band gap of $SrTiO_3$ is about 3.4 eV. Additional results for reduced $SrTiO_3$ show that Redfield's model for an exponential edge is not applicable to this material. The reflectivity indicates structure in the region of 3.4 eV and the electroreflectance shows appreciable signal from 2.5 to 5.0 eV with some structure near 3.4 eV. The electroreflectance signal appears to be due to some process other than the Franz-Keldysh effect. It could be due to a shift or splitting in the major oscillator (4.4 eV), responsible for the refractive index, with induced lattice polarization.

Key Words: Absorption coefficient; band structure; electroreflectance; optical properties; perovskite; reflectivity; strontium titanate.

Cooper, M. J., Mountain, R. D., **Interpretation of relaxation times in the "electric-field effect on critical opalescence,"** *J. Chem. Phys.* **48,** *No. 3, 1064–1066 (Feb. 1, 1968).*
The relaxation time characterizing the response of concentration fluctuations in a binary mixture to the application of an electric field is related to the free relaxation of concentration fluctuations. Examination of light scattered by such systems in the vicinity of the critical mixing point indicates that the change in the turbidity of the fluid with time *cannot* be related to the diffusion coefficient as simply as is the change in the intensity with time of the light scattered through a given angle which is related to the diffusion coefficient D and change in the wavevector k by a factor $\exp(-2Dk^2t)$.

Key Words: Relaxation time; binary mixture; critical opalescence; concentration fluctuations; electric field effect and light scattering.

Corliss, E. L. R., Burnett, E. D., Kobal, M. T., Bassin, M. A., **The relative importance of frequency distortion and changes in time constants in the intelligibility of speech,** *IEEE Trans. Audio Electroacoustics* **AU-16,** *No. 1, 36–39 (Mar. 1968).*
A recording technique developed by E. D. Burnett permitted changes to be made in the relative proportions of intermodulation and harmonic distortion introduced by squaring the input signal. This process was achieved by sending equal parts of the signal through a squaring device, and through a 90-degree phase dividing network followed by a squaring device, and combining the squared outputs. Coupling this procedure with the time-changing features inherent in the sound recording process, we were able to set up a sequence of intelligibility tests whose scores provided solutions to sets of simultaneous equations involving the variables of frequency doubling, frequency halving, and doubling and halving transition times. It was possible to set up an over-specified series of tests, so that more than one solution could be derived from the experiments. Lowering of the characteristic frequency proved to have the most serious effect upon intelligibility. The next most serious was stretching the transition times. Doubling the frequency by second-harmonic distortion was considerably less damaging, though still significant. Reducing the transition times to half their initial values proved relatively trivial.

Key Words: Speech communication; sound reproduction; telephony; perception of speech; speech intelligibility; measures of speech quality.

Corliss, E. L. R., Burnett, E. D., Stimson, H. F., **Polyacusis, a hearing anomaly,** *J. Acoust. Soc. Am.* **43,** *No. 6, 1231–1236 (June 1968).*
A previously unrecognized anomaly of pitch was discovered by Dr. H. F. Stimson while testing his hearing. Signals above 3500 Hz did not produce the same pitch in each ear; the right ear's sensation was that of a sound at a lower frequency, for which he also had normal pitch perception. Between 3700 Hz and 5200 Hz the pitch perceived in the right ear was independent of the frequency of the stimulus. As intensity was raised, additional pitches appeared, and for an intense sound a chord was heard whose constituents were not harmonically related. Stimson can match these anomalous pitches with sinusoidal stimuli of the appropriate lower frequency within about 2%; part of this variation is a change of pitch with intensity. Tones in his normal pitch range having a pronounced overtone structure are perceived as multiple. Overtones falling in the anomalous range give rise to the anomalous pitch. This would indicate a Fourier type of analysis before pitch recognition. Beats are not excited by interference between the pitches evoked by signals in the anomalous range and those heard normally. Loudness studies show signal powers to be additive. Tone masking and loudness summation experiments yield data suggesting that the pitch recognition mechanism lies in that part of the auditory system in which loudness is perceived, i.e., beyond the cochlea.

Kew Words: Hearing; pitch perception; diplacusis; physiology of hearing; masking; theories of hearing; hearing loss.

Dickson, R. W., Anderson, R. C., **Temperature dependence of the elastic moduli of $91Y_2O_3 + 9ThO_2$ from 25° to 1100° C,** *J. Am. Ceram. Soc.* **51,** *No. 4, 233 (Apr. 1968).*
Young's modulus and the shear modulus of pore-free, transparent yttria sintered with thoria ($90\ Y_2O_3 + 10\ ThO_3$) were determined from 25 °C to 1100 °C. Poisson's ratio was calculated and shows a slight increase with increasing temperature.

Key Words: Young's modulus; shear modulus; Poisson's ratio; yttria; elastic moduli; porosity.

Eisenhart, C., **Expression of uncertainties of final results,** *Science* **160,** *No. 3833, 1201–1204 (June 14, 1968).*
The terms used to describe the precision and accuracy of measurements are defined and discussed. Specific rules are recommended for expressing the uncertainty of a reported value for four cases distinguished according to the relative magnitudes of the imprecision and the likely systematic error of the measurement process employed. Examples of recommended forms of uncertainty statements are given.

Key Words: Accuracy; calibrations; expression of uncertainty; measurements; precision; standard error; systematic error; uncertainty.

Eisenhauer, C., **Gamma radiation fluxes near a ground-air interface using an image source technique,** *Nucl. Sci. Engr.* **32,** *166–177 (1968).*
Calculations are made of the radiation flux of gamma rays which have originated from a point isotropic source and have been singly scattered in the air lying beyond a plane interface. Calculations are made in the limit that the source-detector separation distance is small compared to a mean free path in air. These results are interpreted in terms of an image source. The results, combined with earlier calculations of the radiation flux reflected from a condensed medium, such as ground, predict the effect of the ground-air interface on radiation fluxes in air near the interface. The results are extrapolated to source-detector separation of the order of a mean free path by using infinite medium buildup factors. Comparisons with experiment show that the model produces results which are in qualitative agreement with experiment.

Key Words: Interface; air-scatter; gamma rays; image source; single scatter; shielding; buildup factor.

Flynn, D. R., O'Hagan, M. E., **Measurements of the thermal conductivity and electrical resistivity of platinum from 100 °C to 900 °C,** *Engelhard Ind. Tech. Bull.* **VIII,** *No. 4, 117–147 (Mar. 1968).*

Measurements have been made of the thermal conductivity and the electrical resistivity of commercial grade platinum (99.98% pure) in the temperature range 100 to 900 °C. The measurements have been made with a view to providing accurate data on the thermal conductivity of platinum to serve as a basis for establishing platinum as a thermal conductivity standard reference material. Two methods of measuring the thermal conductivity have been employed, one an electrical method and the other a non-electrical method. In the electrical method, a direct current passed through a necked-down portion of the specimen and the thermal conductivity was determined in terms of the temperature and electrical potential distribution in the necked-down region. The second method was of the absolute guarded longitudinal heat flow type. The experiment was designed to permit measurements by both methods in the same apparatus and on the same specimen thereby providing as direct a comparison as possible between the methods. The data given by the two methods agree within experimental error and show the thermal conductivity of platinum to be a smoothly increasing function of temperature in the measured range. Additional measurements on samples of differing purities are necessary before platinum could be adopted as a thermal conductivity reference material.

Key Words: Conductivity; electrical conductivity; electrical resistivity; heat conductivity; Lorenz function; platinum; reference material; resistivity; standard; thermal conductivity.

Franklin, A. D., **Born model calculation of defect energies in CaF_2,** *J. Phys. Chem. Solids* **29,** *823–841 (1968).*
A general formulation of the Born model as applied to the calculation of the energies to form point defects in ionic crystals is given, and then specialized to vacancies and interstitials of both kinds in CaF_2. After examination of the effects produced by several factors in the calculation, "best values" are chosen for the formation energies. These are used to compute the energies to form anion Frenkel pairs (2.7 ± 0.4 eV/pair), Cation Frenkel pairs (7.5 ± 0.8 eV/pair), and Schottky trios (5.1 ± 0.7 eV/trio). The results are in reasonable agreement with Ure's experimental results, which indicate that anion Frenkel pairs are the equilibrium defects in CaF_2, with a formation energy of 2.8 eV.

Key Words: Born model calculation; calcium fluoride; energies of formation; Frenkel pairs; interstitials; ionic crystals; point defects; Schottky pairs; vacancies.

Halford, D., **A general mechanical model for $|f|^\alpha$ spectral density random noise with special reference to flicker noise $1/|f|$,** *Proc. IEEE* **56,** *No. 3, 251–258 (Mar. 1968).*
Any class of reasonable time-dependent perturbations occurring at random, under certain internal constraints, generates random noise having a spectral density varying as $|f|^\alpha$ over an arbitrarily large range of spectral frequency f only for $-2 \leq \alpha \leq 0$. A class is the set of all perturbations which are equivalent under some individual independent scaling of amplitude, scaling of time, and translation of time. A subclass is characterized by $P(\tau)$ and $A^2(\tau)$. $P(\tau)$ is the lifetime probability density. $A^2(\tau)$ is a mean square amplitude of perturbations having lifetime τ. For a given class, $|f|^{\alpha_\infty}$ and $|f|^{\alpha_0}$ are the frequency-smoothed laws in the limits of infinite and zero frequencies, respectively. Any reasonable perturbation has $\alpha_\infty \leq -2$ and $\alpha_0 \geq 0$. To generate random noise having an $|f|^\alpha$ law over an arbitrarily large range of f from a subclass chosen from any class characterized by α_∞ and α_0, it is necessary that $\alpha_\infty \leq \alpha \leq \alpha_0$. For $\alpha_\infty < \alpha < \alpha_0$, it is necessary and sufficient that such subclasses satisfy the condition, $P(\tau)A^2(\tau) \approx B\tau^{-\alpha-3}$ with B constant, over a suitable range of τ, and that $P(\tau)A^2(\tau)$ not be larger than $B\tau^{-\alpha-3}$ outside the range. This general mechanical model is of immediate value in the formulation and criticism of specific physical models of $|f|^\alpha$ noise, including flicker noise, and in computer simulation of $|f|^\alpha$ noise.

Key Words: Noise; spectral density; flicker noise; random noise; noise model; reasonable perturbations; mechanical model; low frequency noise; noise simulation; precision measurements; modulation noise; $1/f$ noise.

Hamer, W. J., **Using standard cells,** *Meas. Data* **1,** *No. 6, 64–67 (Nov.–Dec. 1967).*
This paper contains information on effects of temperature, pressure, electric current, light, shock, and vibration on standard cells. The paper also includes some information on the temperature range for which standard cells can be used and some information on their life.

Key Words: Early types of standard cells; life of standard cells; standard cells; temperature coefficient of standard cells.

Heydemann, P. L. M., **An ultrasonic pressure gage,** *J. Basic Eng.* **89,** *No. 3, 551–553 (Sept. 1967).*
The transit time of short ultrasonic pulses in solid rods is used to measure pressures throughout the fluid range. Self-excited regenerating circuits are used. Measurements to 3500 bar with an uncertainty of 0.3 bar and to 20 kb with an uncertainty of 2 bar are reported. Further improvements, temperature compensation, and stability are discussed.

Key Words: Fluid range; measure pressures; pressure gages; pressure-sensitive components; regenerating circuits; transit time; ultrasonic pulses.

Kuriyama, M., **Dynamical calculation of the x-ray diffraction profile from a distorted crystal,** *J. Appl. Phys.* **39,** *No. 4, 2162–2163 (Mar. 1968).*
A dynamical line-shape calculation for a distorted, parallel-sided crystal is given for the Laue geometry. The scattering amplitude previously formulated by the author is demonstrated to be indeed valid for an arbitrarily large distortion.

Key Words: X-ray diffraction; line broadening; scattering amplitude; lattice sum; absorption; distortion; theory; perfect crystal.

Maki, A. G., Thibault, R., **Analysis of some perturbations in the ν_4 band of methyl chloride,** *J. Chem. Phys.* **48,** *No. 5, 2163–2167 (Mar. 1, 1968).*
The ν_4 band of CH_3Cl has been analyzed in detail. It is found that there is a weak but important, vibrational resonance between ν_4^1 and $3\nu_6^1$. The resonance is quantitatively taken into account in order to determine the unperturbed rotational constants for both ν_4^1 and $3\nu_6^1$. Both chlorine isotopes are resolved and treated separately. The interaction parameter is found to be given by 3.519 $(\pm 0.006)^* + 0.028\ ks$ $(\pm 0.003)^*$ cm^{-1}. The k dependent term is evidently due to a Coriolis-like interaction which is also possible between ν_4^1 (E) and $3\nu_6^1$ (E).
* Three times computed standard errors.

Key Words: Infrared; methyl chloride; spectra; perturbations; vibrational resonance; absorption spectra.

Manning, J. R., **Correlation factors for diffusion of vacancies in binary alloys** (*Proc. Subconference on Lattice Defects, Honolulu, Hawaii, Sept. 1965*), *Book, Lattice Defects and Their Interactions, Ed. R. R. Hasiguti, pp. 269–289 (Gordon and Breach, New York, N.Y., 1967).*
A vacancy in a pure cubic crystal follows a random walk. In a binary alloy however, a vacancy usually has a higher jump frequency when exchanging with one type of atom than with the other. As a result, a vacancy in a binary alloy does not follow a random walk. Partial correlation factors f_v^A and f_v^B can be defined for vacancy jumps with A and B atoms, respectively. Then, the correlation factor for diffusion of vacancies is given by the weighted average $f_v = (w_A N_A f_v^A + w_B N_B f_v^B)/(w_A N_A + w_B N_B)$, where w_A, w_B are vacancy jump frequencies for exchange with A and B atoms, while N_A, N_B are the mole fractions of A and B atoms. The partial correlation factors also enter into the equations for the vacancy flux in a Kirkendall shift experiment, but in a different combination than that for f_v. Consideration of this flux and the theory of correlated walks in a driving force allows f_v^A, f_v^B, and f_v to be calculated. Experimental applications are considered.

Key Words: Binary alloys; correlation factors; diffusion; Kirkendall shift; thermodynamic equations for diffusion; vacancies; calculations.

Milligan, D. E., Jacox, M. E., **Matrix-isolation study of the reaction of atomic and molecular fluorine with carbon**

atoms. The infrared spectra of normal and ^{13}C-substituted CF_2 and CF_3, *J. Chem. Phys.* **48,** *No. 5, 2265–2271 (Mar. 1, 1968).*
Carbon atoms, resulting from the photolysis of cyanogen azide, are found to react with molecular fluorine in an argon matrix at 14 °K to produce CF_2. The use of carbon-13 has led to confirmation of the previous assignment of features at 1073 and 1191 cm^{-1} to $^{13}CF_2$ present in natural abundance. Using recent structural data on CF_2 and the $^{12}CF_2$ and $^{13}CF_2$ frequencies, it has been possible to calculate the complete valence force potential of CF_2. Values of the potential constants are compared with those of the related species NF_2 and CF_2. When the sample is subjected to radiation of wavelengths effective in photolyzing F_2, CF_3 is also produced. Sufficient yields of both $^{12}CF_3$ and $^{13}CF_3$ have been obtained for observation of all four vibrational fundamentals. Data have been fitted to a four-constant valence force potential. Agreement is most satisfactory for a C_{3v} structure with a deviation of 13° from planarity. Using this structure, the thermodynamic properties of CF_3 have been estimated.

Key Words: C atom reaction; $^{12}CF_2$; $^{13}CF_2$; $^{12}CF_3$; $^{13}CF_3$; F atom reaction; F_2 reaction; force constants; free radical; infrared spectrum; matrix isolation; NF_2; photolysis, thermodynamic properties; ultraviolet spectrum.

Rosenstock, H. M., **Theory of mass spectra—A general review,** *(Proc. Conf. on Mass Spectrometry, Berlin, Germany, Sept. 1967), Book, Advances in Mass Spectrometry* **4,** *523–545 (The Institute of Petroleum, London, England, 1968).*
In this paper we shall discuss developments in the theory of mass spectra since 1961. At that time an appraisal of the status of theory was presented, the main conclusions of which were as follows:
1. Quasi-equilibrium theory can reasonably account for the general features of mass spectra.
2. Quantiative disagreement between theory and experiment was in larege measure due to poor mathematical approximations made in enumerating densities of states of reactants and activated complexes.
3. Non-equilibrium or non-equilibration effects were difficult to predict *a priori*, but some meaningful tests could be made by designing experiments to study the effects of different initial preparation on the subsequent kinetic behaviour of ions.
Since the publication of these conclusions, considerable work has been done on enumeration of states, calculation of mass spectra and breakdown curves, detailed energization and fragmentation mechanisms, behaviour of metastable transitions, initial preparation effects, and quantum-mechanical theory of ion decomposition. These subjects will be discussed in detail below.

Key Words: Franck-Condon factors; theory of mass spectra; unimolecular dissociation.

Rush, J. J., Flowtow, H. E., **Vibration spectra of vanadium hydride in three crystal phases by inelastic neutron scattering,** *J. Chem. Phys.* **48,** *No. 8, 3795–3804 (Apr. 15, 1968).*
The vibration spectra of vanadium hydride in three crystal phases have been investigated by the energy-gain scattering of cold neutrons. The measured spectra are generally split into two broad bands above and below about 300 cm^{-1}, which are primarily associated with optical hydrogen vibrations and metal-atom vibrations, respectively. Pseudo-frequency distributions for the hydrogen vibrations were derived from the measured neutron spectra. These indicate broad optical vibration bands peaked at 970 ± 50 and ~ 1400 cm^{-1} in the α (bcc) phase, 440 ± 20, 970 and ~ 1400 cm^{-1} in the β (bct) phase and ~ 1300 cm^{-1} in the γ (fcc) phase. The width of the 440 cm^{-1} band increases with hydrogen concentration, possibly due to hydrogen-hydrogen interactions. The "metal-atom" vibration spectra also show changes in peak positions and widths as the distribution of phases is changed. The changes in the neutron spectra with temperature and as a function of composition between $VH_{0.20}$ and $VH_{1.71}$ correlate quite well with the previously measured phase diagram.
A comparison of the present results with neutron spectra for hydrides with known hydrogen positions suggests that in the α phase hydrogens only occupy tetrahedral-type sites, while in the β phase both octahedral and tetrahedral sites are occupied. The results for $VH_{1.40}$ and $VH_{1.71}$ indicate that in the γ phase the hydrogens occupy regular tetrahedral sites corresponding to the fluorine positions in a CaF_2-type structure.

Key Words: Vanadium hydride; metal hydride; neutron inelastic scattering; vibration spectra; hydrogen vibration; frequency distribution; hydrogen positions; phase transformation; and crystal structure.

Saunders, J. B., **Precision measurements,** *Book, Advanced Optical Techniques, Capt. 1, pp. 3–22 (North-Holland Publ. Co., Amsterdam, The Netherlands, 1967).*
This paper contains methods and instrumentation for making precision measurements in a limited field of optical engineering. The fundamentals of all the included material has been published previously. The subjects that have been covered here are: refractive indices, wavelength measurement, testing of optical surfaces, surface plate testing, temperature measurement by optical methods, expansion measurements, lens and mirror testing, and the measurement of double stars.

Key Words: Expansion measurements; lens and mirror testing; measurement of double stars; optical engineering; optical surfaces; precision measurements; refractive indices; surface plate testing; wavelength measurement.

Schneider, W. E., Garvey, J. A., **Procedures for determining the spectral responsivity of an infrared radiometer,** *Appl. Opt.* **7,** *No. 6, 1141–1148 (June 1968).*
With the increasing number of commercial radiometers employing rather varied and sophisticated optical designs, the determination of the spectral responsivity of these radiometers has accordingly become more involved. A joint National Bureau of Standards-U.S. Army calibration of an infrared radiometer was conducted at the White Sands Missile Range facility. The radiometer chosen for the measurements employed an uncooled PbS detector with an 8 inch Cassegrainian optical system. The selection of this particular type of instrument permitted two methods of measurement (each employing different standards and techniques) to be investigated. The methods of calibration and the uncertainties associated with each method are described and the application of the responsivity values to field measurements is discussed. The agreement of the spectral responsivity values as determined by each method is within the estimated uncertainty computed for each procedure.

Key Words: Infrared radiometers; calibration techniques; radiometry; radiometric standards; spectral responsivity.

Sengers, J. M. H. L., **On the determination of virial coefficients from PVT data,** *Proc. 4th Symp. Thermophysical Properties, University of Maryland, College Park, Md., Apr. 1–4, 1968, pp. 37–44 (American Society of Mechanical Engineers, New York, N.Y., 1968).*
In calculating coefficients of a power series expansion from experimental data, several factors besides experimental precision affect the standard error of these coefficients. Using the principles of statistical analysis, the effects of the factors: interval size, extrapolation, number, relative weight and distribution of experimental points have been studied by high-speed computer experiments.
For gas PVT data a density expansion is possible and approximate theoretical knowledge of the first five virials is available. This enables formulation of experimental conditions—other than improved precision—leading to decreased standard error in one or more of the first four virials.

Key Words: Virial coefficients; density expansion; PVT; statistical analysis, gas thermometry; power series coefficients.

Sengers, J. M. H. L., Vicentini-Missoni, M., **Thermodynamic anomalies near the gas-liquid critical point,** *Proc. 4th Symp. Thermophysical Properties, University of Maryland, College Park, Md., Apr. 1–4, 1968, pp. 79–86 (American Society of Mechanical Engineers, New York, N.Y., 1968).*
Thermodynamic anomalies near the gas-liquid critical point are more correctly described by the Ising model theory of the ferromagnet and the lattice gas than by van der Waals-type theories. The inherent symmetries and the critical anomalies of the lattice gas are discussed using the proper variables, namely chemical potential, density and temperature. Part of the lattice gas symmetries are shown to be retained in the real gas if the same variables are used. The range of validity and some of the properties of a non-

analytic equation-of-state in these variables, recently proposed by Widom, Kadanoff, and Griffiths and representing successfully PVT data and density vs height isotherms in the critical region, are discussed.

Key Words: Thermodynamic anomalies; critical region; lattice gas; scaling law; chemical potential; specific heat; vapor pressure.

Smit, J., Ogburn, F., Bechtoldt, C. J., **Multiple twin structures in electrodeposited silver dendrites,** *J. Electrochem. Soc.* **115,** *No. 4, 372–374 (Apr. 1968).*
Silver dendrites, formed by electrocrystallization from aqueous solution were examined for twinning using optical goniometric, x-ray diffraction and metallographic techniques. The dendrites, in every case, were found to be twinned with a maximum of eight orientations in twin relation in a single dendrite. The growth axis of the dendrites was observed to be in the < 110 direction. Dominant facets were found to be (111) planes on the 110 zone of the growth axis.

Key Words: Silver; electrocrystallization; dendrites; twinning; x-ray diffraction; faceting.

Stern, K. H., **Ion diffusion into fused silica from molden salts,** *J. Phys. Chem.* **72,** *No. 6, 2256–2259 (June 1968).*
Compositional changes of fused silica containing a few ppm impurities resulting from immersion of the glass in molten salts were studied. At 570 °C immersion in AgCl and AgBr results in 1:1 exchange of Ag^+ with Na^+ (glass). At 890° immersion in NaCl, KCl, and AgCl, respectively, increases the ionic concentration in Na^+, K^+, and Ag^+ above the initial total ($Na^+ + K^+ + Li^+$). Cl^- diffusion is virtually absent. Possible interpretations of these results are presented.

Key Words: Ion exchange; glass; molten salts.

Stern, K. H., **Membrane potentials and ion selectivity of fused silica in molten salts,** *J. Phys. Chem.* **72,** *No. 6, 1963–1975 (June 1968).*
The effect of alkali metal cations on membrane potentials at the molten salt-fused silica interface has been studied using the concentration cell Ag|AgCl, M_1Cl, M_2Cl . . . |glass|M_1Cl, M_2Cl . . ., AgCl|Ag where M_1, M_2 . . . are alkali metal cations and several types of fused silica and Vycor. The ion exchange theory is more appropriate for the interpretation of the data than the liquid junction theory, but the application of the theory requires detailed data on ion exchange and ionic mobility in fused silica which are not yet available.
The effect of anions on the membrane potential was studied with the cell M|MCl, NaCl|fused silica|MBr, NaBr|M where M = Ag, Tl, and Pb. The results for the three metals are quite analogous. The emf of the cells could be calculated by straightforward thermodynamic methods, without the assumption of specific anion-glass interactions. The emf measurement of these cells at low sodium halide concentration can also serve as an analytical tool for sodium determinations down to 10^{-3} mole %, but not lower.

Key Words: Membrane potentials; ion selectivity; fused silica; molten salts.

Swartzendruber, L. J., Bennett, L. H., **Hyperfine field distributions in $(ZrCo_2)$ $(ZrFe_2)_{1-}$ alloys,** *J. Appl. Phys.* **39,** *No. 2, Part II, 1323–1324 (Feb. 1, 1968).*
Mössbauer effect measurements in the cubic Laves phase pseudobinary magnetic alloys $(ZrCo_2)_x(ZrFe_2)_{1-x}$ yield complex spectra. Magnetization curves on these alloys have been previously reported. $ZrFe_2$, with a saturation moment at 4 °K of about 1.6 μ_B per Fe atom and a Brillouin type magnetization curve, displays a Mössbauer spectrum consisting of two six line patterns, each with a hyperfine field of about 200 kOe. ZrFeCo has been reported to show only a quadrupole splitting at 78 °K, although this is well below the Curie temperature. We have observed resolved hyperfine splitting in this composition at 78 °K and at 4 °K. The magnetization curves in $(ZrCo_2)_x(ZrFe_2)_{1-x}$ for $x = 0.2$, 0.4, 0.5 and 0.6 imply magnetic moment distributions. The Mössbauer spectra for these alloys show hyperfine field distributions that are strong functions of temperature over a wide range below the Curie temperatures.

Key Words: Mössbauer effect; zirconium; iron; cobalt; hyperfine fields; alloys.

Swartzendruber, L. J., Bennett, L. H., **Line profiles in the nuclear magnetic resonance and Mössbauer effect of $TiFe_{1-x}Co_x$ alloys,** *J. Appl. Phys.* **39,** *No. 5, 2215–2220 (Apr. 1968).*
The ^{57}Fe Mössbauer effect (ME) and the ^{59}Co nuclear magnetic resonance (NMR) have been investigated as a function of alloy concentration, temperature and stoichiometry in $TiFe_{1-x}Co_x$ alloys over most of the range $0 \leq X \leq 1$. At room temperature, in carefully prepared samples, a single narrow ^{57}Fe ME line was observed for all values of x. This line broadened only slightly at low temperatures although the magnetic properties of these alloys would have led one to expect a larger broadening at certain compositions. The ^{59}Co NMR line width was relatively narrow for x close to 0 or 1 and was a strong function of x as well as of magnetic field. The intermediate compositions displayed resolved satellite structures. Annealing reduced both the ME and NMR linewidths. Deviations from stoichiometry and internal oxidation were readily observable from their effect on the ME line profile. Both the ME and NMR results are consistent with a CsCl structure over the entire composition range. The NMR results indicate a lack of ordering on the Co, Fe sublattice.

Key Words: Intermetallic compounds; Mössbauer effect; nuclear magnetic resonance; line structure; Ti; Fe; Co; internal oxidation.

Swartzendruber, L. J.. Bennett, L. H., **Mössbauer line structure in "non-magnetic" Cu-Fe and Cu-Ni-Fe alloys,** *Physics Letters* **27A,** *141–142 (1968).*
The high temperature ^{57}Fe Mössbauer effect residual line structure in Cu-rich Cu-Fe and Cu-Ni-Fe alloys is reinterpreted as being of magnetic origin, rather than arising from quadrupole interactions or lack of solubility.

Key Words: Alloys; copper; iron; local moments; magnetism; Mössbauer effect; nickel.

Sze, W. C., **Comparator for calibration of inductive voltage dividers from 1 to 10 kHz,** *ISA Trans.* **6,** *No. 4, 263–267 (Oct. 1967).*
A high accuracy comparator is described for measuring the relative deviations in voltage ratios and phase angles of inductive voltage dividers. The new technique overcomes several inherent limitations of the existing comparison methods. The balance is accomplished by utilizing special shielded transformers and a resistance-capacitance network for in-phase and quadrature voltage injections. The measurements are accurate to within 1×10^{-7} of input in the frequency range from 1 to 10 kHz. Resolution is better than 2×10^{-10}.

Key Words: Calibration; comparator; high permeability core; inductive voltage divider; phase angle; R-C network; shielded transformer; toroidal core; voltage divider; voltage ratio.

Tighe, N. J., Hyman, A., **Transmission electron microscopy of alumina ceramics** *(Proc. Intern. Symp. Anisotropy in Single-Crystal Refractory Compounds, Dayton, Ohio, June 13–15, 1967), Book, Anisotropy in Single-Crystal Refractory Compounds, Ed. F. W. Vahldiek and S. A. Mersol, 2, 121–136 (Plenum Press Inc., New York, N.Y., 1968). Watson, R. E., Bennett, L. H., Freeman, A. J., Origin of solvent Knight shifts in alloys, Phys. Rev. Letters* **20,** *No. 13, 653–656 (Mar. 25, 1968).*
Transmission electron microscopic studies have been carried out on two samples of sintered alumina having different density (3.99g/cm³ and 3.78g/cm³), composition and grain size. Specimens were thinned by an ionic-bombardment method which preserved the grain boundaries and allowed observation of relatively large areas. The sample of nearly full density Al_2O_3 had very few dislocations or small angle boundaries. It did have grains of second phase material (spinel) and these grains contained faults. The sample of lower density, had many small angle boundaries, pores and extensive dislocation networks. A number of the networks were composed of dislocations with Burgers vectors: $1/3\langle 11\bar{2}0\rangle$ and $1/3\langle 10\bar{1}1\rangle$.

Key Words: Alumina; defects; dislocations; polycrystalline Al_2O_3; electron microscopy; ionic bombardment.

Wiederhorn, S. M., Shorb, A. M., Moses, R. L., **Critical analysis of the theory of the double cantilever method of measuring fracture-surface energies,** *J. Appl. Phys.* **39,** *No. 3, 1569–1572 (Feb. 15, 1968).*

This paper presents a critical discussion of the double cantilever method of measuring fracture surface energies. It was found that the equation developed by Gillis and Gilman is valid for crack lengths greater than 1.5 times the crack arm height. The constants in this equation were evaluated and were found to be practically independent of the elastic constants of the material for which they were evaluated, suggesting the equation could be used on any material. The Gilman and Gillis approach to the double cantilever problem was found to be consistent with the approach used by Gross and Srawley.

Key Words: Cleavage; crack propagation; elasticity; fracture; fracture energy; surface energy.

Yakowitz, H., **Evaluation of specimen preparation and the use of standards in electron probe microanalysis,** *Am Soc. Testing Mater. Spec. Tech. Publ.* **430,** *Fifty Years of Progress in Metallographic Techniques, 383–408 (1968).*

The magnitudes of systematic and statistical errors in electron probe microanalysis due to faulty sample preparation are discussed theoretically and experimentally. It is shown that these errors increase as the energy of the X-ray line being monitored decreases and also as the X-ray emergence angle decreases. Specific samples are chosen to illustrate various preparation problems in metallurgy, petrography and biology. Generalizing from these, certain useful instrumental adjuncts can be listed; these adjuncts tend to allow the effects of the sample surface on the analysis to be controlled more rigorously. Several conductive coatings commonly used are evaluated in terms of electron and optical transparency, adherence, X-ray attenuation, and thermal and electrical conductivity. Finally, a brief survey of standards employed in electron probe microanalysis is made. Situations for which non-elemental standards are required are outlined. The choice of standards for various types of work is discussed.

Key Words: Specimen preparation; electron microprobe; metallography; petrography; microprobe standards.

Other NBS Publications

J. Res. NBS 72B (Math. Sci.), No. 3 (July–Sept. 1968).

Interaction in multidimensional contingency tables: An information theoretical approach. H. H. Ku and S. Kullback.

On the coupling of longitudinal and transverse waves in a linear three-element viscoelastic string subjected to transverse impact. J. C. Smith and J. T. Fong.

Allocating service periods to minimize delay time. W. A. Horn.

The second orthogonality conditions in the theory of proper and improper rotations. I. Derivation of the conditions and of their main consequences. H. Gelman.

Thickness and connectivity in graphs. A. M. Hobbs and J. W. Grossman.

J. Res. NBS 72C (Eng. and Instr.), No. 3 (July–Sept. 1968).

Gas density balance design considerations. E. C. Creitz.

Standard mismatch—the production of controlled small reflections in waveguides. L. Lewin.

Viscoelastic behavior of dental amalgam. P. L. Oglesby, G. Dickson, M. L. Rodriguez, R. M. Davenport, and W. T. Sweeney.

The steady-state creep behavior of dental amalgam. G. Dickson, P. Oglesby, and R. Davenport.

Adams, J. W., Desch, R. F., Experimental confirmation of barretter substitution error, IEEE Trans. Microwave Theory Tech. **MTT-16,** No. 3, 201–202 (Mar. 1968).

Bennett, J. A., To avoid fatigue failures, pay attention to details, Current Engr. Pract. **9,** 12–16 (Sept. 1966).

Bleicher, M. N., Knopp, M. I., Lattice points in a sphere, Acta Arith. **X,** 369–376 (1965).

Branscomb, L. M., Twenty years of physics: atoms, molecules and electrons, Phys. Today **21,** No. 5, 36–39 (May 1968).

Cornell, R. G., Speckman, J. A., Estimation for a simple exponential model, Biometrics **23,** No. 4, 717–737 (Dec. 1967).

Cornog, J. R., Bryan, H. L., Jr., Manual and machine-assisted search methods used in examining patent applications in the transistor art, Proc. Natl. Electronics Conf., Chicago, Ill., Oct. 25–27, 1965, **XXI,** 672–677 (1965).

Crumlish, J. D., Wirth, G. F., A preliminary study of engineering seismology benefits, Environmental Science Services Administration, Coast and Geodetic Survey (Superintendent of Documents, Government Printing Office, Washington, D.C. 20402, Aug. 1967, 35 cents).

Cushen, W. E., Systems engineering—Where did it come from . . . where will it go? Consulting Engr. **30,** No. 3, 130–134 (Mar. 1968).

Cuthill, J. R., McAlister, A. J., Williams, M. L., Soft x-ray spectroscopy of alloys: TiNi and the Ni-Al system, J. Appl. Phys. **39,** No. 5, 2204–2208 (Apr. 1968).

deMain, P. A. D., Marron, B. A., The SOLID SYSTEM. I. A method for organizing and searching files (Proc. Third Annual Colloquium on Information Retrieval, Philadelphia, Pa., May 12–13, 1966), Book, Information Retrieval, A Critical View, Ed. G. Schecter, pp. 243–282 (Thompson Book Co., Washington, D.C., 1967).

DeSimone, D. V., Education for innovation, IEEE Spectrum **5,** No. 1, 83–90 (Jan. 1968).

Dibeler, V. H., Walker, J. A., Mass spectrometric study of the photoionization of small polyatomic molecules (Proc. Conf. on Mass Spectrometry, Berlin, Germany, Sept. 1967), Book, Advances in Mass Spectrometry **4,** 767–780 (The Institute of Petroleum, London, England, 1968).

Dick, C. E., Marella, A. B., Miller, W. C., A simple beam positioning system for low energy electrons, Nucl. Instr. Methods **60,** 346–348 (1968).

Durst, R. A., Fluoride microanalysis by linear null-point potentiometry, Anal. Chem. **40,** No. 6, 931–935 (May 1968).

Durst, R. A., May, E. L., Taylor, J. K., Improved technique for the microdetermination of silver by linear null-point potentiometry, Anal. Chem. **40,** No. 6, 977–978 (May 1968).

Eisenhart, C., Gauss, C. F., International Encyclopedia of the Social Sciences **6,** 74–81 (The Macmillan Company and The Free Press, New York, N.Y., 1968).

Fell, H., Mather, J., Barely faithful algebras, Math. Monthly **72,** No. 9, 1001–1003 (Nov. 1965).

Fraction, G. F., Tauber, S. J., Walker, J. C., Connection tables from Wiswesser line notation: A partial algorithm, Proc. Wiswesser Line Notation Meeting of the Army Chemical Information and Data Systems Program, Edgewood Arsenal, Watertown, N.J., Oct. 6–7, 1966, Edgewood Arsenal Spec. Publ. EASP-400-8, pp. 139–197 (Jan. 1968).

Goldman, A. J., Nemhauser, G. L., A transport improvement problem transformable to a best-path problem, Transportation Sci. **1,** No. 4, 295–307 (Nov. 1967).

Hall, L. A., A bibliography of thermophysical properties of methane from 0 to 300 °K, Tech. Note 367 (May 1968), 60 cents.

Hamer, W. J., Battery, electric, Encyclopedia Americana **3,** 357–363 (1967).

Hamer, W. J., Wood, R. E., Electrolytic conductivity and electrode processes, Handbook of Physics, Second Ed., Ed. E. U. Condon and H. Odishaw, Part. 4. Electricity and Magnetism, Chap. 9, pp. 4–146—4–171 (McGraw-Hill Book Co., New York, N.Y., 1967).

Hammond, H. K., III, Phototube response evaluation, Appl. Opt. **7,** No. 5, 985 (May 1968).

Harvey, M. E., Precision temperature-controlled water bath, Rev. Sci. Instr. **39,** No. 1, 13–18 (Jan. 1968).

Hayward, R. W., Nuclear electromagnetic radiation, Handbook of Physics, Second ed., Ed. E. U. Condon and H. Odishaw, Part 9. Nuclear Physics, Chapt. **6,** pp. 9–172—9–194 (McGraw-Hill Book Co., New York, N.Y., 1967).

Horiuti, J., Miyahara, K., Hydrogenation of ethylene on metallic catalysts, NSRDS13 (June 1968), $1.00.

Huget, E. F., Brauer, G. M., Loebenstein, W. V., Apparent heats of wetting and heats of reaction of the components of tooth structure and synthetic fluorapatite, J. Dental Res. **47,** No. 2, 291–301 (Apr. 1968).

Hutchinson, J. M. R., Naas, C. R., Walker, D. H., Mann, W. B., Backscattering of alpha particles from thick metal backings as a

function of atomic weight, Intern. J. Appl. Radiation Isotopes **19,** 517–522 (June 1968).

Ives, L. K., Ruff, A. W., Jr., Studies of the effect of annealing on extended dislocation nodes in silver-tin alloys, Phys. Stat. Sol. **27,** 117–123 (1968).

Jensen, M. W., The Fair Packaging and Labelling Act of 1966—its history and its implementation, Monthly Rev. J. Inst. Weights Measures Admin. **76,** No. 4, 3–6 (Apr. 1968).

Johannesen, R. B., Relative signs of NMR coupling constants and isotope shifts in ammonium ions, J. Chem. Phys. **48,** No. 3, 1414–1415 (Feb. 1, 1968).

Judd, D. B., Color vision and colorimtery, Handbook of Physics, Second Ed., Ed. E. U. Condon and H. Odishaw, Part 6. Optics, Chapt. 4, pp. 6–65—6–77 (McGraw-Hill Book Co., New York, N.Y., 1967).

Kokoszka, G. F., Brinckman, F. E., Electron paramagnetic resonance studies of phosphorus-containing reactive intermediates, Chem. Commun. **7,** 349–350 (Apr. 10, 1968).

Mackay, D. R., Editor, Editorial format for Product Standards, PS0–67 (July 1968), 10 cents.

Marron, B. A., deMaine, P. A. D., Automatic Data Compression, Commun. ACM **10,** No. 11, 711–715 (Nov. 1967).

Marvin, R. S., Twenty years of rheology, Phys. Today (20th Anniversary Edition) **21,** No. 5, 52–53 (May 1968).

Mattis, R. L., Phillips, W. E., Bullis, W. M., Measurement and interpretation of carrier lifetime in silicon and germanium, Tech. Rept. AFML–TR–68–81 (Air Force Materials Laboratory, Air Force Systems Command, Wright-Patterson Air Force Base, Ohio, July 1968).

Melmed, A. J., Field emission shadow microscopy, Apol. Phys. Letters **12,** No. 3, 100–102 (Feb. 1, 1968).

Menke, J. L., Schrack, R. A., Feeble field feeler, Nucl. Instr. Methods **57,** 158–159 (1967).

Moore-Sitterly, C. E., Commission 14—Fundamental spectroscopic data report of meetings, 23 and 25 August 1967, Trans. Intern. Astron. Union **13B,** 87–91 (1968).

Newman, M., Pairs of matrices generating discrete free groups and free products, Mich. Math. J. **15,** 155–160 (1968).

Osgood, C. F., A method in diophantine approximation (II), Acta Arith. **XIII,** 383–393 (1968).

Page, C. H., Electronic circuits, Handbook of Physics, Second Ed., Ed. E. U. Condon and H. Odishaw, Part 4. Electricity and Magnetism, Chap. 4, pp. 4–45—4–52 (McGraw-Hill Book Co., New York, N.Y., 1967).

Schafft, H. A., Needham, S. G., A bibliography on methods for the measurement of inhomogeneities in semiconductors (1953–1967), Tech. Note 445 (May 1968), 35 cents.

Sengers, J. V., Sengers, J. M. H. L., The critical region, Chem. Eng. News **46,** No. 25, 104–118 (June 10, 1968).

Swindells, J. F., Thermometry and pyrometry, Handbook of Physics, Second Ed., Ed. E. U. Condon and H. Odishaw, Part 5, Heat and Thermodynamics, Chapt. 3, pp. 5–34—5–44 (McGraw-Hill Book Co., New York, N.Y., 1967).

Youden, W. J., Statistical design of experiments, Handbook of Physics, Second Ed., Ed. E. U. Condon and H. Odishaw, Part 1. Mathematics, Chapt. 13, pp. 1–198—1–201 (McGraw-Hill Book Co., New York, N.Y., 1967).

**Publications for which a price is indicated are available by purchase from the Superintendent of Documents, U.S. Government Printing Office, Washington, D.C. 20402 (foreign postage, one-fourth additional). The NBS non-periodical series are also available from the Clearinghouse for Federal Scientific and Technical Information, Springfield, Va. 22151. Reprints from outside journals and the NBS Journal of Research may often be obtained directly from the authors.*

JOURNAL OF RESEARCH of the National Bureau of Standards—A. Physics and Chemistry
Vol. 72A, No. 6, November–December 1968

Index to Volume 72A
January to December 1968

A

Page

Abramowitz, S., Acquista, N., Levin, I. W., Infrared matrix spectra of lithium fluoride... 487
—, *Levin, I. W.*, Force field for SiF_4... 247
Absolute isotopic abundance ratios of common, equal-atom, and radiogenic lead isotopic standards... 261
Absolute ratios... 261
Absorption... 309
Absorption spectra... 39, 149
Abstraction... 49
Abundance... 261
Acquista, N., Abramowitz, S., Levin, I. W., Infrared matrix spectra of lithium fluoride... 487
Activation energy...
Activity coefficient... 239
Adaptation... 309
Air pollutants... 39
Al-10 percent Si alloy... 269
Alloys... 19
Ammonia... 207
Annealing... 425
Anomeric sugars...
Anthraquinone-1,5-dicarboxylic acid... 39
Apatite...
Apatitic...
Aprotic solvents... 309
Archival record film... 251
Armstrong, G. T., Churney, K. L., Studies in bomb calorimetry. A new determination of the energy of combustion of benzoic acid in terms of electrical units... 453
—, *Domalski, E. S.*, The heat of formation of boron carbide... 133
—, *King, R. C.*, Constant pressure flame calorimetry with fluorine II. The heat of formation of oxygen difluoride... 113
Aromatic hydrocarbons... 351
Atomic hydrogen... 521
Atomic spectra... 295,
Atomic spectrum...

B

β and T corrections... 505
Band contour... 247
Bates, R. C., Schindler, P., Robinson, R. A., Solubility of tris(hydroxymethyl)aminomethane in water-methanol solvent mixtures and medium effects in the dissociation of the protonated base... 141
Beams... 521
Beer's law... 309
BeH... 85
Bennett, H. S., Electric fields produced by a charge density in ionic crystals... 475
—, Electrostatic potentials and their spatial derivatives about point defect in ionic crystals... 471
Benesch, W., Krupenie, P. H., Electronic transition moment integrals for first ionization of CO and the A–X transition in CO^+. Some limitations on the use of the r-centroid approximation... 495
Benzoic acid... 453
Beryllium difluoride... 75
Beryllium oxide... 75
Blemish due to aging... 251
Blemish formation in processed film... 251
Bomb calorimeter... 133, 453
Bomb calorimetry... 453
Bond energy (O–F)... 113
Boron carbide... 133
Boron trifluoride... 133
Boyd, M. E., Larsen, S. Y., Plumb, H., Second virial coefficient of He^4 in the temperature range from 2 to 20 °K... 155
Brillouin scattering... 95
Brower, W. S., Khanna, R. K., Guscot, B. R., Lippincott, E. R., Laser induced Raman spectra of some tungstates and molybdates... 81
Brown, W. E., Moreno, E. C., Gregory, T. M., Preparation and solubility of hydroxyapatite...
Bozman, W. R., Corliss, C. H., Tech, J. L., Energy levels and classified lines in the first spectrum of technetium (Tc I)...

C

C_2F_6... 479
C_3F_8... 479
C_4F_{10}... 479
CF_3Br... 479
CF_3Cl... 479
CF_3H... 479
CF_3I... 479
CF_4... 479
Ca, Mg phosphate... 425
CaF_2... 471, 475
Calcium chloride... 239
Calcium maltobinate...
Calcium phosphates...
Calibration of the nickel dimethylglyoxine spectral shift at pressures to 20 kilobars for use in spectroscopic measurement... 149
Carbon–13...
Carbon dioxide...
Carbon tetrafluoride... 133
Caspi, E., Shadmi, Y., Theoretical interpretation of the even levels in the first spectrum of tungsten...
Catanzaro, E. J., Murphy, T. J., Shields, W. R., Garner, E. L., Absolute isotopic abundance ratios of common, equal-atom, and radiogenic lead isotopic standards... 261
Charge-transfer...
Chemical interdiffusion... 157
Chromatic adaptation... 309
Churney, K. L., Armstrong, G. T., Studies in bomb calorimetry. A new determination of the energy of combustion of benzoic acid in terms of electrical units... 453
Classical ionic lattice theory... 471
Classification lines, V IV and V V... 295
CO_+... 495
CO^+... 495
Collision integrals... 359
Colloidal silver... 251
Color vision... 309
Concentration... 309
Cones... 309
Configurations $3d^n4p$... 505
Configurations $3d^n4p$ in doubly ionized atoms of the iron group... 505
Constant pressure flame calorimetry with fluorine II. The heat of formation of oxygen difluoride... 113
Coriolis constant... 247
Corliss, C. H., Bozman, W. R., Tech, J. L., Energy levels and classified lines in the first spectrum of technetium (Tc I)...
—, *Laun, D. D.*, The first spectrum of tungsten (W I)...
Correlation energy... 85
Coulometers... 435
Covington, A. K., Robinson, R. A., The thermodynamics of the ternary system: water-potassium chloride-calcium chloride at 25 °C... 239
Cox, D. M., Long, R. L., Jr., Smith, S. J., Electron impact excitation of hydrogen Lyman-α radiation... 521
Crystal spectrum...
Crystal symmetry... 231
Crystalline *alpha* and *beta* forms of 3-*O*-α-D-glucopyranosyl-D-arabinopyranose...
Curve shape... 309

D

Davis, H. W., Calibration of the nickel dimethylglyoxime spectral shift at pressures to 20 kilobars for use in spectroscopic measurement... 149
Dehydroxylation...
Density fluctuations in fluids having an internal degree of freedom... 95
Density fluctuations in liquids... 95
Dextran... 49
Dextrin... 49
Diamond-anvil cell... 149
Dibeler, V. H., Krauss, M., Walker, J. A., Mass spectrometric study of photoionization. X. Hydrogen chloride and methyl halides... 281
Dickinson calorimeter... 453
Diffusion... 359
Diffusion rates in inorganic nuclear materials... 157
Dihydroxy-perylenequinones... 39
Dilatometry... 467
Dipole shell coefficient... 475
Dissociation... 27, 281
Dissociation constant... 141
Dissociation energy... 85
Domalski, E. S., Armstrong, G. T., The heat of formation of boron carbide... 133
Double salt... 351
Dragoo, A. L., Diffusion rates in inorganic nuclear materials... 157

E

Eby, R. K., Martin, G. M., Effect of low pressures on the room temperature transitions of polytetrafluoroethylene... 467

Page

Effect of low pressures on the room temperature transitions of polytetrafluoroethylene... 467
Effect of oxide additions on the polymorphism of tantalum pentoxide (system Ta_2O_5-TiO_2)... 175
Efimenko, J., A mass spectrometric study of the BeO-BeF_2 system at high temperatures... 75
Elastic collisions... 91
Electric fields... 475
Electric fields produced by a charge density in ionic crystals... 475
Electrical calibration... 453
Electron impact excitation... 521
Electron impact excitation of hydrogen Lyman-α radiation... 521
Electron probe microanalyzer... 269
Electron spin resonance spectra of polymer radicals in aqueous solution... 49
Electronic transition moment integrals... 495
Electronic transition moment integrals for first ionization of CO and A–X transition in CO^+. Some limitations on the use of the *r*-centroid approximation... 495
Electrostatic potential... 471
Electrostatic potentials and their spatial derivatives about point defects in ionic crystals... 471
Energies... 281
Energy levels... 505,
Energy levels and classified lines in the first spectrum of technetium (Tc I)...
Energy levels, W I...
Energy transfer...
Energy surface...
Enthalpy... 467
Entropy... 467
Equilibrium... 27
Equivalent sites... 231
Ethyl acetate...
Experimental... 521

F

Faraday... 435
Fatiadi, A. J., Periodic acid, a novel oxidant of polycyclic aromatic hydrocarbons... 341
—, Preparation and purification of some oxidation products of perylene... 39
Fiber composites... 269
First spectrum of tungsten (W I)...
Flame calorimetry... 113
Florin, R. E., Sicilio, F., Wall, L. A., Electron spin resonance spectra of polymer radicals in aqueous solution... 49
Flow calorimetry... 113
Fluorine... 113
Force field... 247, 487
Force field for SiF_4... 247
Fourth and fifth spectra of vanadium (V IV and V V)... 295
Franck-Condon factors... 495
Franck-Condon principle... 495
Free radicals... 49
Frush, H. L., Isbell, H. S., Moyer, D. J., Crystalline *alpha* and *beta* forms of 3-*O*-α-D-glucopyranosyl-D-arabinopyranose...

G

Galvanic cell with a low emf-temperature coefficient... 351
Galvanic cell with low temperature... 351
Galvanic cells... 351
Garner, E. L., Catanzaro, E. J., Murphy, T. J., Shields, W. R., Absolute isotopic abundance ratios of common, equal-atom, and radiogenic lead isotopic standards... 261
Gas chromatography...
Gas density...
Germania glass... 425
3-*O*-α-D-Glucopyranosyl-D-arabinopyranose...
Grain-boundary diffusion... 157
Gregory, T. M., Moreno, E. C., Brown, W. E., Preparation and solubility of hydroxyapatite...
Guscott, B. R., Khanna, R. K., Brower, W. S., Lippincott, E. R., Laser induced Raman spectra of some tungstates and molybdates... 81

H

$H_2(X^1\Sigma_g^+)$...
Haar, L., Thermodynamic properties of ammonia as an ideal gas... 207
Hahn, H., Yakowitz, H., Jenkins, W. D., Role of nickel in Al-10 percent Si composites containing nickel-coated sapphire whiskers... 269
Hamer, W. J., Resume of values of the Faraday... 435
—, *Roberts, G. N.*, A galvanic cell with a low emf-temperature coefficient... 351
Hartree-Fock...
HCl... 281
He^4... 155
Heat of combustion... 133, 453
Heat of formation... 113, 133
Heat of formation of boron carbide... 133
Heat of reaction... 113
Heats of formation... 479
Helical molecule... 467
Hexakis(imidazole)nickel(II)nitrate...
High luminance... 309
High pressure measurement... 149
High temperature...
High temperature dehydroxylation of apatitic phosphates...
High temperatures... 75
High vacuum... 521
Howett, G. L., Variation of absorptance-curve shape with changes in pigment concentrations... 309
Hydrogen fluoride (aqueous)... 113
Hydrothermal synthesis... 359
Hydroxyapatite...
Hydroxyl... 49

I

Page

Ideal gas... 207
Iglesias, L., The fourth and fifth spectra of vanadium (V IV and V V)... 295
Inclusions in silver coulometers... 435
Index of refraction... 425
Infrared... 39, 247, 487
Infrared matrix spectra of lithium fluoride... 487
Inorganic synthesis... 425
Interaction energy surfaces for $Li(2^2S)$ and $Li(2^2P)$ with H_2...
Interaction parameters... 505
Intermetallic compounds... 1, 11, 19
Intrinsic diffusion... 157
Ionization... 281
Ionization energies... 479
Iron group... 505
Isbell, H. W., Frush, H. L., Moyer, J. D., Crystalline *alpha* and *beta* forms of 3-*O*-α-D-glucopyranosyl-D-arabinopyranose...
Isopiestic measurements... 239
Isotope ratios...
Isotopic shift... 247
Isotopic standards... 261
Ito, J., Synthesis of cerite... 355

J

Jenkins, W. D., Yakowitz, H., Hahn, H., Role of nickel in Al–10 percent Si composites containing nickel-coated sapphire whiskers... 269
Jump rates... 231
Jump rates for point defects in special positions held by a trapping center of noncubic symmetry... 231

K

Khanna, R. K., Brower, W. S., Guscott, B. R., Lippincott, E. R., Laser induced Raman spectra of some tungstates and molybdates... 81
King, R. C., Armstrong, G. T., Constant pressure flame calorimetry with fluorine II. The heat of formation of oxygen difluoride... 113
Klein, M., Smith, F. J., Tables of collision integrals for the (*m*, 6) potential function for 10 values of *m*... 359
Krauss, M., Interaction energy surfaces for $Li(2^2S)$ and $Li(2^2P)$ with H_2...
—, *Walker, J. A., Dibeler, V. H.*, Mass spectrometric study of photoionization. S. Hydrogen chloride and methyl halides... 281
Krupenie, P. J., Benesch, W., Electronic transition moment integrals for first ionization of CO and the A-X transition in CO^+. Some limitations on the use of the *r*-centroid approximation... 495

L

Larsen, S. Y., Boyd, M. E., Plumb, H., Second virial coefficient of He^4 in the temperature range from 2 to 20 °K... 155
Lattice constants... 187
Lattice diffusion... 157
Lattice Distortion... 471
Laun, D. D., Corliss, C. H., The first spectrum of tungsten (W I)...
Lead... 261
Levin, I. W., Abramowitz, S., Force field for SiF_4... 247
—, —, *Acquista, N.*, Infrared matrix spectra of lithium fluoride... 487
$Li(2^2P)$...
$Li(2^2S)$...
LiH... 85
Lippincott, E. R., Khanna, R. K., Brower, W. S., Guscott, B. R., Laser induced Raman spectra of some tungstates and molybdates... 81
Lithium fluoride dimer... 487
Ln_2O-PdO systems... 27
Ln_2O_3 : PdO compounds... 27
Long, R. L., Jr., Cox. D. M., Smith, S. J., Electron impact excitation of hydrogen Lyman-α radiation... 521
Low pressure... 467
Low temperature... 155, 247, 487
Lyman-α... 521

M

Macedo, P. B., Napolitano, A., Spectrum of relaxation times in GeO_2 glass... 425
Malonic acid... 341
Maltose-1-^{14}C...
Martin, G. M., Eby, R. K., Effect of low pressures on the room temperature transitions of polytetrafluoroethylene... 467
Mass spectrometric... 479
Mass spectrometric study of the BeO-BeF_2 system at high temperatures... 75
Mass spectrometric study of photoionization. X. Hydrogen chloride and methyl halides... 281
Mass spectrometric study of the photoionization of some fluorocarbons and trifluoromethyl halides... 479
Mass spectrometry... 75, 281
Matrix... 487
Matrix-whiskers bonding... 269
McDaniel, C. L., Schneider, S. J., Phase relations between palladium oxide and the rare earth sesquioxides in air... 27
Medium effect... 141
Metameric matches... 309
Methanol-water solvents... 141
Meter...
Microfilm... 251
Microfilm storage cartons... 251
Mineral chemistry... 355
Mixed salt solutions... 239
Molecular orbital... 85
Molybdates... 81

Page

Moreno, E. C., Gregory, T. M., Brown, W. E., Preparation and solubility of hydroxyapatite
Mountain, R. D., Density fluctuations in fluids having an internal degree of freedom 95
Moyer, J. D., Isbell, H. S., Frush, H. L., Crystalline *alpha* and *beta* forms of 3-*O*-α-D-glucopyranosyl-D-arabinopyranose
Mullen, L. R., Park, J. J., Reactions of uranium and the platinide elements. III. The uranium-iridium system 19
Murphy, T. J., Catanzaro, E. J., Shields, W. R., Garner, E. L., Absolute isotopic abundance ratios of common, equal-atom, and radiogenic lead isotopic standards 261
Mutarotation of 3-*O*-α-D-glucopyranosyl-D-arabinopyranose

N

NaCl 471, 475
Napolitano, A., Macedo, P. B., Spectrum of relaxation times in GeO_2 glass 425
Negas, T., Roth, R. S., High temperature dehydroxylation of apatitic phosphates
Ni coated sapphire whiskers 269
Nickel dimethylglyoxime 149
Noutary, C. J., Mass spectrometric study of the photoionization of some fluorocarbons and trifluoromethyl halides 479

O

Octahedral nickel(II)
Optical metallography 269
Osmotic coefficient 239
4-Oxo-4*H*-benz/*de*/anthrocene-7,8-dicarboxylic anhydride 39
Oxygen 113
Oxygen difluoride 113

P

Park, J. J., Reactions of uranium with the platinide elements. I. The uranium-ruthenium system 1
—, Reactions of uranium and the platinide elements. II. The uranium-rhodium system 11
—, *Lyle, L. R.*, Reactions of uranium and the platinide elements. III. The uranium-iridium system 19
Peak intensity 187
Peiser, H. S., Wachtman, J. B., Jr., Jump rates for point defects in special positions held by a trapping center of noncubic symmetry 231
Periodic acid 341
Periodic acid, a novel oxidant of polycyclic aromatic hydrocarbons 341
Permanent record film 251
Peroxides 251
Perylene 39
Perylenequinones 39
Phase diagram 1, 11, 19, 467
Phase equilibrai 175
Phase relations 27
Phase relations between palladium oxide and the rare earth sesquioxides in air 27
Phosphates
Photoionization 479
Photo-oxidation products of perylene 39
Photopigment 309
Physical constants 187
Pigment 309
Plumb, H., Boyd, M. E., Larsen, S. Y., Second virial coefficient of He^4 in the temperature range from 2 to 20 °K 155
Point defect 471
Point defects 231
Polarization 475
Polyacrylic 49
Polycyclic aromatic hydrocarbons 39
Polyethylene imine 49
Polyethylene oxide 49
Polymer degradation 49
Polymethacrylic acid 49
Polymorphism 175
Polypropylene oxide 49
Polytetrafluoroethylene 133, 467
Polyvinyl alcohol 49
Pope, C. I., Blemish formation in processed microfilm 251
Positronium 91
Potassium chloride 239
Potential 359
Potential energy curve 85
Preparation and purification of some oxidation products of perylene 39
Preparation solubility of hydroxyapatite
Procedures and errors 453
Pyrene radical 341

Q

Quinones 341

R

Raman spectra 81
Rare-earth silicate 355
Rayleigh scattering 95
Reaction calorimetry 113
Reaction enthalpy 75
Reaction mechanism 341
Reactions of uranium with the platinide elements. I. The uranium-ruthenium system 1
Reactions of uranium and the platinide elements. II. The uranium-rhodium system 11
Reactions of uranium and the platinide elements. III. The uranium-iridium system 19
Reiman, C. W., The single crystal spectrum of hexakis(imidazole)nickel(II)nitrate

Page

Relaxation 231
Relaxation times 425
Resonance state
Résume of values of the Faraday 435
Roberts, G. N., Hamer, W. J., A galvanic cell with a low emf-temperature coefficient 351
Robinson, R. A., Covington, A. K., The thermodynamics of the ternary system: water-potassium chloride-calcium chloride at 25 °K 239
—, *Schindler, P., Bates, R. G.*, Solubility of tris(hydroxymethyl)aminomethane in water-methanol solvent mixtures and medium effects in the dissociation of the protonated base 141
Role of nickel in Al-10 percent Si composites containing nickel-coated sapphire whiskers 269
Roth, C., The configurations $3d^8rp$ in doubly ionized atoms of the iron group 505
Roth, R. S., Negas, T., High temperature dehydroxylation of apatitic phosphates
—, *Waring, J. L.*, Effect of oxide additions on the polymorphism of tantalum pentoxide (system Ta_2O_5-TiO_2) 175
Ruff degradation
Ruthenium 1

S

Sanders, W., Krauss, M., Valence-only correlation in LiH and BeH^{--} 85
Sapphire whiskers 269
Sauder, W. C., Thermalization by elastic collisions: Positronium in a rare gas moderator 91
Schindler, P., Robinson, R. A., Bates, R. G., Solubility of tris(hydroxymethyl)aminomethane in water-methanol solvent mixtures and medium effects in the dissociation of the protonated base 141
Schneider, S. J., McDaniel, C. L., Phase relations between palladium oxide and the rare earth sesquioxides in air 27
Second virial 155
Second virial coefficient of He^4 in the temperature range from 2 to 20 °K 155
Self-diffusion 157
Shadmi, Y., Caspi, E., Theoretical interpretation of the even levels in the first spectrum of tungsten
Shields, W. R., Catanzaro, E. J., Murphy, T. J., Garner, E. L., Absolute isotopic abundance ratios of common, equal-atom, and radiogenic lead isotopic standards 261
Sicilio, F., Florin, R. E., Wall, L. A., Electron spin resonance spectra of polymer radicals in aqueous solution 49
SiF_4 247
Single crystal spectrum of hexakis(imidazole)nickel(II)nitrate
Smith, F. J., Klein, M., Tables of collision integrals for the (*m* 6) potential function for 10 values of *m* 359
Smith, S. J., Long, R. L., Jr., Cox, D. M., Electron impact excitation of hydrogen Lyman-α radiation 521
Sodium metaperiodate 341
Solubility 1, 11, 141,
Solubility of tris(hydroxymethyl)aminomethane in water-methanol solvent mixtures and medium effects in the dissociation of the protonated base 141
Solubility isotherms
Solubility product
Spatially extended defects 475
Spectra, V IV and V V 295
Spectral distribution of scattered light 95
Spectral line profiles 187
Spectrum of relaxation times in GeO_2 glass 425
Spectrum of technetium
Spectrum of tungsten
Spectroscopy
Spin-forbidden bands
Stable carbon isotope ratio measurements with a gas density meter
Standard cells 351
Starch 49
Statistical error analysis 187
Structural relaxation 95
Studies in bomb calorimetry. A new determination of the energy of combustion of benzoic acid in terms of electrical units 453, 75
Sublimation enthalpy
Sugars
Synthesis of cerite 355

T

Tables of collision integrals for the (*m*, 6) potential function for 10 values of *m* 359
Tantalum pentoxide 175
Tc I
Tech, J. L., Bozman, W. R., Corliss, C. H., Energy levels and classified lines in the first spectrum of technetium (Tc I)
Technetium
Terms, V IV and V V 295
Theoretical interpretation of the even levels in the first spectrum of tungsten
Thermal conductivity 359
Thermal diffusion 359
Thermal expansion 425
Thermal relaxation 95
Thermalization 91
Thermalization by elastic collisions: Positronium in a rare gas moderator 91
Thermodynamic functions 207
Thermodynamic properties of ammonia as an ideal gas 207
Thermodynamics of the ternary system: water-potassium chloride-calcium chloride at 25 °C 239
Thin layer chromatograms 39
Third spectra 505
Thomsen, J. S., Yap, F. Y., Effect of statistical counting errors on wavelength criteria for x-ray spectra 187
Titanium dioxide 175
Tsang, W., Wasik, S. P., Stable carbon isotope ratio measurement with a gas density meter
Tracer, diffusion 157
Transition probabilities 495

Page

Transitions 467
Transport properties 359
Trapping center 231
Triple point 467
Tris(hydroxymethyl)aminomethane 141
Tungstates 81
Tungsten .....
Two relaxation model 425

U

Ultraviolet 39
Uranium 1, 19
Uranium-iridium 19

V

Vacuum ultraviolet 479
Vacuum ultraviolet spectroscopy 281
Valency-only correlation in LiH and BeH+ 85
Values of Faraday 435
Vanadium, the fourth and fifth spectra 295
Vapor pressure 239
Variation of absorptance-curve shape with changes in pigment concentrations 309
Vibrational assignment 487
Viscosity 359, 425
Visible absorption system 39
Vision 309
Volume viscosity 95

W

Page

W I .....
Wachtman, J. B., Jr., Peiser, H. S., Jump rates for point defects in special positions held by a trapping center of noncubic symmetry 231
Walker, J. A., Krauss, M., Dibeler, V. H., Mass spectrometric study of photoionization. X. Hydrogen chloride and methyl halides 281
Wall, L. A., Florin, R. E., Sicilio, F., Electron spin resonance spectra of polymer radicals in aqueous solution 49
Waring, J. L., Roth, R. S., Effect of oxide additions on the polymorphism of tantalum pentoxide (system Ta_2O_5-TiO_2) 175
Wasik, S. P., Tsang, W., Stable carbon isotope ratio measurement with a gas density meter .....
Water 113
Wavelengths .....

X

X-ray diffraction .....
X-ray line shapes 187
X-ray powder analysis 355
X-ray spectra 187
X-ray wavelength criteria 187

Y

Yakowitz, H., Jenkins, W. D., Hahn, H., Role of nickel Al-10 percent Si composites containing nickel-coated sapphire whiskers 269
Yap, F. Y., Thomsen, J. S., Effect of statistical counting errors on wavelength criteria for x-ray spectra 187

U.S. Government Printing Office : 1968 OL—318-092

Errata to recent paper entitled

Studies in Bomb Calorimetry. A New Determination of the Energy of Combustion of Benzoic Acid in Terms of Electrical Units

Authors: K. L. Churney and G. T. Armstrong
Journal of Research of the National Bureau of Standards
Section A, Physics and Chemistry, Vol. 72A, No. 5, Oct.–Nov. 1968

In this title, abstract, and elsewhere in the paper occurs the phrase "determination of the energy of combustion of benzoic acid in terms of electrical units." Strictly speaking, this phrase should be construed as "determination of the energy of combustion of benzoic acid in SI units by comparison with electrical energy measurements." This is to avoid implication that the joule is essentially an electrical unit.

UNITED STATES
GOVERNMENT PRINTING OFFICE
DIVISION OF PUBLIC DOCUMENTS
WASHINGTON, D.C. 20402

OFFICIAL BUSINESS

POSTAGE AND FEES PAID
U.S. GOVERNMENT PRINTING OFFICE

JOURNAL OF RESEARCH of the National Bureau of Standards Vol. 72A, No. 6 November–December 1968
A. Physics and Chemistry

Contents

	Page
Interaction energy surfaces for Li(2^2S) and Li(2^2P) with H_2. M. Krauss.	553
Energy levels and classified lines in the first spectrum of technetium (Tc I). W. R. Bozman, C. H. Corliss, and J. L. Tech.	559
The first spectrum of tungsten (W I). Donald D. Laun and C. H. Corliss.	609
Theoretical interpretation of the even levels in the first spectrum of tungsten. Y. Shadmi and E. Caspi.	757
Stable carbon isotope ratio measurement with a gas density meter. S. P. Wasik and W. Tsang.	761
The single crystal spectrum of hexakis(imidazole)nickel(II) nitrate. Curt W. Reimann.	765
Crystalline alpha and beta forms of 3-*O*-α-D-glucopyranosyl-D-arabinopyranose. Horace S. Isbell, Harriet L. Frush, and J. D. Moyer.	769
Preparation and solubility of hydroxyapatite. E. C. Moreno, T. M. Gregory, and W. E. Brown.	773
High temperature dehydroxylation of apatitic phosphates. T. Negas and R. S. Roth.	783
Publications of the National Bureau of Standards.	789
Index to volume 72A, January to December 1968.	803

Library of Congress Catalog Card Number: 62–37039

For sale by the Superintendent of Documents, U.S. Government Printing Office, Washington, D.C. 20402. Price $1 (single copy). Subscription price: $6 a year; $1.25 additional for foreign mailing.
UNITED STATES GOVERNMENT PRINTING OFFICE, WASHINGTON : 1968